

**Sommerfeld corrections in
neutralino dark matter pair-annihilations
and relic abundance in the general MSSM**

Dissertation

vorgelegt von

Charlotte Hellmann

Betreuer: Prof. Dr. Martin Beneke

Lehrstuhl für Theoretische Elementarteilchenphysik T31

Fakultät für Physik
der Technischen Universität München



TECHNISCHE UNIVERSITÄT MÜNCHEN

Lehrstuhl für Theoretische Elementarteilchenphysik T31

Sommerfeld corrections in neutralino dark matter
pair-annihilations and relic abundance in the general MSSM

Anna Charlotte Hellmann

Vollständiger Abdruck der von der Fakultät für Physik
der Technischen Universität München zur Erlangung des akademischen Grades eines

Doktors der Naturwissenschaften

genehmigten Dissertation.

Vorsitzender: Univ.-Prof. Dr. Lothar Oberauer
Prüfer der Dissertation: 1. Univ.-Prof. Dr. Martin Beneke
2. Univ.-Prof. Dr. Alejandro Ibarra
3. Univ.-Prof. Dr. Michael Klasen,
Westfälische Wilhelms-Universität Münster
(nur schriftliche Beurteilung)

Die Dissertation wurde am 03.12.2014 bei der Technischen Universität München
eingereicht und durch die Fakultät für Physik
am 13.02.2015 angenommen.

Abstract

It is intriguing that the observed dark matter abundance in our Universe can be explained rather naturally as thermal relic of a weakly interacting massive particle. Probably the most popular such particle dark matter candidate is the lightest neutralino in the Minimal Supersymmetric Standard Model (MSSM). In this thesis we study the impact of Sommerfeld enhancements on the neutralino relic abundance calculation for heavy neutralino dark matter in the general MSSM including co-annihilations of further nearly mass-degenerate neutralino and chargino states. To this end we develop an effective field theory that systematically resums the enhanced radiative corrections to pair-annihilation rates of slowly moving neutralinos and charginos. The framework is applied to heavy wino- and higgsino-like scenarios and models interpolating between these cases.

Zusammenfassung

Die in unserem Universum beobachtete Dunkelmaterie kann in natürlicher Weise als thermisches Relikt eines schwach wechselwirkenden massiven Teilchens erklärt werden. Ein solcher vielversprechender Dunkelmaterie-Teilchenkandidat ist das leichteste Neutralino im Minimalen Supersymmetrischen Standardmodell (MSSM). In der vorliegenden Arbeit wird der Einfluss der Sommerfeld-Verstärkung auf die Neutralino Reliktdichte für schwere Neutralino Dunkelmaterie-Kandidaten im allgemeinen MSSM und unter Einbeziehung von Co-Annihilationseffekten weiterer näherungsweise massenentarteter Neutralino- und Chargino-Spezies untersucht. Dazu wird eine effektive Theorie entwickelt, die überhöhte Strahlungskorrekturen in Paar-Annihilationen langsamer Neutralinos und Charginos resumiert. Der Formalismus wird auf Wino- und Higgsino-artige Szenarien angewandt, sowie auf Modelle, die zwischen diesen Fällen extrapolieren.

Contents

1	Introduction	5
2	Sommerfeld enhancements in a toy scenario	13
2.1	The origin of the enhancement	14
2.2	An enhancement formula for a N -state model	18
2.3	$N = 1$ state models with Coulomb and Yukawa potential interactions . .	31
2.3.1	One-state model with Coulomb potential	33
2.3.2	One-state model with Yukawa potential	35
2.4	A two-state model with off-diagonal interactions	39
3	Relic abundance calculation	47
3.1	The Boltzmann equation	47
3.2	Co-annihilations	52
3.3	Thermally averaged annihilation cross sections	56
4	The neutralino and chargino sector in the MSSM	59
4.1	Motivations for supersymmetry and basic ideas	59
4.2	The MSSM: field content and parameters	62
4.3	The neutralino and chargino sector	65
4.4	MSSM spectrum generation	69
5	Effective theory description of neutralino pair annihilations	71
5.1	The Lagrangian in the effective theory	71
5.2	χ^0/χ^\pm pair-annihilations in the NRMSSM	75
5.2.1	Basis of dimension-6 operators in $\delta\mathcal{L}_{\text{ann}}$	77
5.2.2	Basis of dimension-8 operators in $\delta\mathcal{L}_{\text{ann}}$	80
6	The hard annihilation reactions	83
6.1	Matching calculation & Master formula	84
6.1.1	Matching condition	84
6.1.2	Expansion in momenta and mass differences in $\delta\mathcal{L}_{\text{ann}}$	86
6.1.3	Unitary vs Feynman gauge	90
6.1.4	A master formula for the Wilson coefficients	91

6.2	Numerical comparison:	
	Tree-level annihilation rates	95
6.2.1	$\chi_1^+ \chi_1^+ \rightarrow W^+ W^+$ and $\chi_1^+ \chi_1^- \rightarrow W^+ W^-$	99
6.2.2	The S -wave dominated processes $\chi_1^0 \chi_1^+ \rightarrow t\bar{b}, u\bar{d}$	100
6.2.3	The P -wave dominated reaction $\chi_2^+ \chi_2^- \rightarrow h^0 h^0$	102
6.2.4	The off-diagonal $\chi_1^+ \chi_1^- \rightarrow W^+ W^- \rightarrow \chi_2^+ \chi_2^-$ rate	104
6.2.5	Annihilation cross sections of “hydrogen-like” $\chi\chi$ states	106
6.3	Application of the analytic results at $\mathcal{O}(v_{\text{rel}}^2)$:	
	A pure-wino NRMSSM sample calculation	107
6.3.1	Coupling factors	108
6.3.2	Kinematic factors	111
6.3.3	Exclusive pure-wino NRMSSM co-annihilation rates	114
7	Long-range potential interactions	119
7.1	NRMSSM potentials: Matching calculation	119
7.2	Matrix representation of NRMSSM potentials	126
7.2.1	The two possible bases of $\chi\chi$ states in the NRMSSM	127
7.2.2	Pure-wino NRMSSM potential & annihilation matrices	130
8	Sommerfeld enhancement	133
8.1	Sommerfeld-corrected annihilation rates	134
8.2	NR matrix-elements & the Schrödinger equation	139
8.3	Sommerfeld factors in the method-1 and 2 bases	146
8.4	Solution of the Schrödinger equation: improved method	147
8.5	Second-derivative operators	154
8.6	Approximate treatment of heavy channels	156
9	Benchmark models in the general MSSM	163
9.1	Wino-like χ_1^0	164
9.2	Higgsino-like χ_1^0	172
9.3	Light scenario	179
9.4	Higgsino-to-wino trajectory	182
9.5	Mixed wino-higgsino χ_1^0	190
10	Conclusions	197
A	Absorptive parts of Wilson coefficients of dimension-6 and 8 operators in $\delta\mathcal{L}_{\text{ann}}$	201
A.1	Coupling factors	202
A.1.1	Coupling factor construction	202
A.1.2	(Axial-)vector and (pseudo-)scalar MSSM vertex factors	205
A.1.3	Example: construction of $c_{n,i_1 V}^{(\alpha)}$ in $\chi_{e_1}^- \chi_{e_2}^+ \rightarrow W^+ G^- \rightarrow \chi_{e_4}^0 \chi_{e_3}^0$	209
A.2	Kinematic factors at leading order	210
A.2.1	Kinematic factors for $X_A X_B = VV$	212

A.2.2	Kinematic factors for $X_A X_B = VS$	214
A.2.3	Kinematic factors for $X_A X_B = SS$	216
A.2.4	Kinematic factors for $X_A X_B = ff$	217
A.2.5	Kinematic factors for $X_A X_B = \eta\bar{\eta}$	220
A.3	Kinematic factors at $\mathcal{O}(v^2)$	221
A.3.1	P -wave kinematic factors for $X_A X_B = VV$	222
A.3.2	P -wave kinematic factors for $X_A X_B = VS$	226
A.3.3	P -wave kinematic factors for $X_A X_B = SS$	230
A.3.4	P -wave kinematic factors for $X_A X_B = ff$	233
A.3.5	P -wave kinematic factors for $X_A X_B = \eta\bar{\eta}$	236
B	Explicit expressions for the MSSM potentials in \mathcal{L}_{pot}	239
C	Equivalence between method-1 and method-2	241

Chapter 1

Introduction

The existence of a cold dark matter (DM) component in our Universe is by now well established by various observations and at all experimentally accessible scales, ranging from the size of galaxies to galaxy clusters and large scale structures up to the largest observable scales associated with the cosmic microwave background radiation (CMB) [1]. For instance, the fact that galactic rotation curves become approximately constant and do not decrease with increasing distance from the galactic centre is explained by the presence of halos of non-luminous and non-absorbing – hence dark – matter. Similar observations and explanations in terms of dark matter exist for galaxy clusters. The most accurate determination of the present cold dark matter density $\Omega_{\text{cdm}}h^2$ is related to cosmological precision measurements and has reached percent level accuracy: from a combination of PLANCK, WMAP, baryon acoustic oscillation (BAO) and high resolution CMB data, a value of

$$\Omega_{\text{cdm}}h^2 = 0.1187 \pm 0.0017 \quad (1.1)$$

is obtained [2], where h denotes the Hubble constant in units of $100 \text{ km} / (\text{sMpc})$.

In spite of evidence for its existence, the nature and origin of the cold dark matter component are still unknown. The Standard Model (SM) of particle physics that has been tested extensively by experiments and that describes so far successfully the microscopic interactions of the constituents associated with ordinary matter (quarks, gluons, leptons, neutrinos, the photon, the electroweak gauge bosons and the SM Higgs boson) [1], provides no particle dark matter candidate. This in turn is one of the few empirical evidences that the SM cannot be the fundamental theory of nature. Assuming that dark matter has particle nature, possible extensions of the SM should therefore involve a particle dark matter candidate that is stable or at least sufficiently long lived on cosmic timescales. Furthermore this particle candidate may not interact with photons nor take part in strong interactions, otherwise dark matter would be visible or it would have been found in rare isotopes [3, 4].

It is intriguing that the origin of the observed cosmic cold dark matter abundance can be explained rather naturally through thermal production and subsequent freeze-out of a particle with weak interaction strength and a TeV scale mass, a so called

weakly interacting massive particle (WIMP) [3,4]. This might indicate that new physics at the TeV scale, which is needed to address certain formal issues in the SM such as the stability of the electroweak scale, is also associated with a cosmic dark matter constituent, thereby connecting problems related to the smallest and largest observable scales. The explanation of the cosmic cold dark matter abundance in terms of a cold relic implies that the corresponding freeze-out process in the early Universe takes place at temperatures when the DM particles become non-relativistic. An accurate determination of the relic density considers also the presence and freeze-out of those further species in the early Universe, that are close-in-mass and interact with the DM candidate. The central ingredients in the relic abundance calculation are the pair-annihilation rates of the DM and additional nearly mass-degenerate particles. Given that the DM particles have typical non-relativistic velocities $v \sim 0.2c$ around freeze-out, the corresponding tree-level co-annihilation cross sections can be expanded according to

$$\sigma_{\text{ann}} v_{\text{rel}} = a + b v_{\text{rel}}^2 + \mathcal{O}(v_{\text{rel}}^4), \quad (1.2)$$

where $v_{\text{rel}} = |\vec{v}_1 - \vec{v}_2|$ is the relative velocity of the two annihilating particles in their centre-of-mass frame. Referring to tree-level rates and keeping only the first two terms in the expansion is often a good approximation in the relic abundance calculation.

In the simple freeze-out scenario DM pair-annihilation reactions eventually cease when the DM number density is sufficiently diluted due to the expansion of the Universe. However, pair-annihilation reactions can restart when DM eventually accumulates in the present Universe due to gravitational interactions. Corresponding regions with a DM over-density can be galactic centres, but also the sun potentially has a sufficient gravitational potential to attract, capture and amass DM particles. The DM pair-annihilation reactions occurring today in these regions are described by the same annihilation rates (1.2) as in the early Universe. Since the typical velocities of the annihilating particles today are however much smaller, $v \sim 10^{-3}c$, it is often enough to consider the leading order term a in the non-relativistic expansion of the corresponding annihilation cross sections.

Certainly one of the most studied and probably best motivated DM candidates is the lightest neutralino (χ_1^0) in the Minimal Supersymmetric Standard Model (MSSM) [3,4], a supersymmetric extension of the SM. There exist several codes that allow for the calculation of the χ_1^0 relic density in the general MSSM, currently relying on tree-level annihilation rates and taking co-annihilation reactions with further supersymmetric particles close in mass with the χ_1^0 into account [5,6]. The calculated relic density of a viable χ_1^0 dark matter candidate should at least not exceed the observed $\Omega_{\text{cdm}} h^2$ value. The latter allows for the possibility that the cosmic dark matter is constituted by several particle species, each contributing a certain portion to the total dark matter abundance. From the requirement that the χ_1^0 explains all observed cosmic dark matter in terms of a thermal χ_1^0 relic, stringent constraints on the MSSM parameter space can be derived [7,8].

The actual identification of a particle dark matter candidate with the cosmic constituent relies on the complementarity of different experimental search strategies; for corresponding investigations related to the χ_1^0 DM candidate see for instance the recent

publications [9, 10]. The aforementioned pair-annihilation reactions in the galactic centre or the sun would produce indirect signals of dark matter particles, revealing themselves in cosmic or gamma ray signatures or neutrino fluxes, looked for with corresponding space or ground-based telescopes. Direct detection experiments are searching for signals from scattering reactions of DM particles off terrestrial detector materials. To assign (future) signals from indirect and direct detection experiments to a certain candidate, this particle should ideally be produced directly at a particle collider such as the Large Hadron Collider (LHC) at CERN, which would allow to determine – or at least narrow down – some of its properties as for instance its mass and spin. Let us mention here that in the past several experimental collaborations working on direct and indirect DM detection have reported the observation of signals, which they claimed could not be explained by known backgrounds or other astrophysical sources and which therefore could be assigned to dark matter. However the explanation as dark matter signals in none of these cases is definitely confirmed and former DM indications could later often be attributed to underestimated background or detector effects.

In this thesis we focus on the neutralino relic abundance calculation and improve its accuracy by systematically resumming a certain class of radiative corrections to the relevant neutralino and chargino co-annihilation cross sections. Indeed, given the experimental percent level accuracy on $\Omega_{\text{cdm}}h^2$, (1.1), it seems desirable to include radiative corrections to the co-annihilation rates, which enter the relic abundance calculation as a central ingredient and are currently afflicted with the largest uncertainties. Two different approaches in refining the determination of the co-annihilation rates of the χ_1^0 and further close-in-mass MSSM states can be distinguished. On the one hand, next-to-leading order corrections to the co-annihilation rates are calculated in fixed order perturbation theory in the general MSSM. The determination of the complete next-to-leading order SUSY QCD corrections in neutralino and chargino pair-annihilations, including co-annihilations with possibly nearly mass-degenerate sfermion states has been finalised recently [11–15]. Moreover, the first steps in the calculation of the full next-to-leading order electroweak corrections have been carried out [16–18]. On the other hand there exists a class of radiative corrections that can be enhanced in non-relativistic neutralino co-annihilation reactions and eventually requires systematic resummation up to all orders in perturbation theory. This situation generically arises in theories that allow for light mediator exchange between heavy non-relativistic DM particles prior to their annihilation. The light mediator exchanges give rise to long-range potential interactions that distort the incoming DM particles’ wave-functions away from plane waves, such that their annihilation probability becomes larger. In terms of Feynman diagrams, the effect is associated with amplitudes that exhibit ladder-like exchanges of the mediators between the co-annihilating non-relativistic DM particles before the latter actually pair-annihilate. Each loop in the corresponding diagrams involves a contribution that scales as $g^2 m_{\text{DM}}/m_\phi$, where g denotes the respective coupling, m_ϕ the mediator mass and m_{DM} refers to the DM mass scale. For sufficiently light mediator masses, $m_\phi \ll m_{\text{DM}}$, these terms are unsuppressed and eventually lead, after systematic resummation, to the so-called Sommerfeld enhancement of the corresponding annihilation rate. In the MSSM

with χ_1^0 dark matter candidate the mutual exchange of electroweak gauge bosons, and to a lesser extend light Higgs bosons, causes the Sommerfeld enhancement in heavy neutralino pair-annihilations. Sommerfeld enhancements are associated with the non-relativistic nature of the pair-annihilating particles. They are typically the stronger the smaller the velocities of the particles. Consequently the relevance of the Sommerfeld enhancement effect for χ_1^0 DM has first been pointed out in context of gamma ray signatures from χ_1^0 pair-annihilations in the galactic centre today [19,20], where the authors considered the simplified scenarios of pure wino and pure higgsino χ_1^0 states. Although the enhancement effect is much milder during χ_1^0 freeze-out because of the larger mean velocities ($v \sim 0.2c$) it was found in [20] that its impact on the relic density can be significant for pure wino χ_1^0 DM. Subsequently, the Sommerfeld enhancement effect in the MSSM has been studied extensively both in application to indirect detection and the χ_1^0 relic abundance calculation [21–27], where these analyses mainly referred to the limiting scenarios of wino- or higgsino-like χ_1^0 or even pure wino and pure higgsino χ_1^0 models. In addition, in [28] Sommerfeld enhancements were investigated in context of “minimal dark matter” models that resemble the MSSM in the limits of pure wino and pure higgsino DM. In addition to MSSM related studies, there have been several investigations on the Sommerfeld enhancement effect in generic dark matter models. In particular, the measurement of an anomalous positron excess by the PAMELA experiment in 2008 has triggered several investigations on Sommerfeld enhancements in generic dark matter models, where the effect was considered as a means to boost the DM annihilation rates in the present Universe while at the same time providing electroweak scale cross sections during freeze-out due to much milder enhancement factors at larger velocities [29].

In this thesis we address Sommerfeld enhancement effects in co-annihilation reactions of nearly mass-degenerate neutralinos and charginos in the general MSSM, extending previous work on the subject in several important aspects. With the term “general MSSM” we imply that our calculations allow an application to any generic R-parity conserving MSSM scenario. In particular, the χ_1^0 can be an arbitrary admixture of the electroweak gaugino and higgsino gauge-eigenstates, away from the strict wino and higgsino limits. Further important improvements or extensions to existing investigations in the literature are the following:

- We use an effective theory framework to describe the pair-annihilation reactions of non-relativistic and nearly mass-degenerate neutralino and chargino pairs, similar to the NRQCD approach to heavy quarkonium annihilations in [30]. An important difference to the latter QCD case is the fact that we deal with several nearly mass-degenerate scattering states $\chi_{e_a}\chi_{e_b}$. The exchange of electroweak gauge or light Higgs bosons prior to the short-distance annihilation allows for potential scattering transitions from an initially incoming pair $\chi_i\chi_j$ to another such nearly mass-degenerate two-particle state. In the effective theory we therefore encounter diagonal as well as off-diagonal potential interactions. These are of Coulomb-type for photon exchange (which corresponds to a purely diagonal potential scattering reaction) but are Yukawa-like in case of electroweak gauge boson and Higgs exchange. We determine analytic expressions for all (off-) diagonal potential inter-

actions at leading-order in the non-relativistic expansion.

- The effective field theory approach by construction provides a factorisation between the long-range and short-distance contributions to the co-annihilation rates. The total pair-annihilation cross section of an incoming $\chi_i\chi_j$ pair is related to the absorptive part of the forward scattering amplitude $\chi_i\chi_j \rightarrow \dots \rightarrow \chi_{e_1}\chi_{e_2} \rightarrow \sum X_A X_B \rightarrow \chi_{e_4}\chi_{e_3} \rightarrow \dots \chi_i\chi_j$, where $X_A X_B$ denotes a pair of SM or light Higgs particles. Due to the presence of off-diagonal potential interactions $\chi_{e_a}\chi_{e_b} \rightarrow \chi_{e_c}\chi_{e_d}$, changing the nature of the incoming two-particle state prior to annihilation, the short-distance annihilations encoded in reactions $\chi_{e_1}\chi_{e_2} \rightarrow \sum X_A X_B \rightarrow \chi_{e_4}\chi_{e_3}$ are generically associated with off-diagonal processes as well, where the $\chi_{e_1}\chi_{e_2}$ pair is not necessarily identical to the $\chi_{e_4}\chi_{e_3}$ pair. Off-diagonal annihilation rates were only known in the pure wino and higgsino limits and at leading order in the non-relativistic expansion. They have not been considered previously in applications to the generic MSSM. We derive purely analytical results for all (off-) diagonal short-distance annihilation rates. In the effective theory they are encoded in the absorptive parts of Wilson coefficients and are automatically partial-wave separated. We determine not only the leading order S -wave contributions, but also calculate P -wave and next-to-next-to-leading order S -wave terms associated with the term b in (1.2).
- The determination of the Sommerfeld enhancement factors for an incoming $\chi_i\chi_j$ state in a certain partial-wave configuration requires the solution of a matrix Schrödinger equation involving matrix-valued potentials that refer to corresponding (off-) diagonal potential scattering reactions. As we allow the neutralino and chargino states in the effective theory to exhibit small mass differences, there will be potential transitions to kinematically closed two-particle channels. If the mass splittings between the incoming and the closed channels become larger, numerical instabilities arise in the solution of the Schrödinger equation. We discuss a novel method based on an appropriate reformulation of the Schrödinger problem that solves this issue.
- The Sommerfeld factors depend on the partial wave state of the annihilating pair. Consequently, the consistent determination of the Sommerfeld-enhanced annihilation rates requires a partial wave separation of the short-distance annihilation rates. In particular the P - and next-to-next-to-leading order S -wave contributions to the coefficient b in (1.2) have to be known separately. Within the effective theory we obtain such partial wave separation by construction.

A number of limitations of our framework has to be mentioned. The formalism in its current form does not allow to cover resonant s -channel annihilations in the short-distance rates, as the process is no longer short-distance in this case. Moreover we cannot consider MSSM scenarios where co-annihilations of sfermion states are relevant in the χ_1^0 relic abundance calculation, since this would require the determination of corresponding

potentials and short-distance annihilation rates in the effective theory. Although conceptually straightforward, this is beyond the scope of this thesis. Both the cases of resonant s -channel annihilations and co-annihilations with nearly mass-degenerate sfermion states require a certain degree of tuning between mass parameters in the MSSM spectrum. In that sense such scenarios are less generic than models with mass degeneracies between neutralino and chargino states, which naturally occur for heavy χ_1^0 with a mass of several hundred GeV up to some TeV, since in these cases the neutralino and chargino states arrange in approximate electroweak multiplets. In addition to the above restrictions we do neither include the effect of running couplings nor thermal effects throughout. Concerning thermal effects in Sommerfeld-enhanced rates, the temperature dependence of the gauge boson masses has been considered in [22, 28]. Pair-annihilation processes of non-relativistic neutralino and chargino states involve the two well-separated scales associated with the particle masses on the one hand and with the non-relativistic kinetic energies on the other hand. The running of couplings can therefore in principle be relevant, but is not considered here.

The thesis is based on and in certain points extends the four publications [31–34]. Its outline is as follows. As the rigorous analysis of Sommerfeld enhancements in χ_1^0 pair-annihilation reactions in the general MSSM requires a large portion on formal preparations before an analysis of viable generic MSSM scenarios can be performed, we prepend with Chap. 2 an introduction to the Sommerfeld enhancement by establishing an advanced guess formula for the corresponding enhancement factors and analysing enhancement effects in several simplified toy models. This allows to familiarise with the Sommerfeld effect and to estimate the order of magnitude of enhancements that can be expected in the later application to the neutralino and chargino sector of the MSSM. A review on the relic abundance calculation for generic particle dark matter is subsequently given in Chap. 3. The discussion of problems in the SM and an introduction to the MSSM is the content of Chap. 4, where we additionally discuss the neutralino and chargino sector of the MSSM in view of its properties relevant for our further analyses. The main part of the thesis is contained in Chaps. 5–8, where we discuss the construction of the effective field theory designed to describe pair-annihilation reactions of non-relativistic nearly mass-degenerate neutralino and chargino pairs. We start in Chap. 5 with the discussion of the relevant terms in the effective theory Lagrangian. Chap. 6 then comprises the extensive discussion of the analytic determination of the Wilson coefficients of four-fermion operators in the effective theory encoding the hard neutralino and chargino pair-annihilation rates. In addition we describe the numerical and analytical comparison of our results with data from numerical codes providing corresponding tree-level annihilation rates as well as with known analytic expressions in the literature. The terms in the effective theory Lagrangian associated with potential interactions between non-relativistic neutralino and chargino states, eventually causing the Sommerfeld enhancements, are determined in Chap. 7. With the prerequisites of the preceding chapters at hand we can finally give in Chap. 8 the rigorous derivation of Sommerfeld enhancements in the effective theory: we refine the advanced-guess Sommerfeld enhancement formula from Chap. 2

and provide an expression for the non-relativistic expansion of neutralino and chargino co-annihilation cross sections including Sommerfeld enhancements and taking P - and next-to-next-to-leading order S -wave effects in the short-distance annihilation rates into account. Further we present the novel method in the solution of matrix Schrödinger equations that is free from numerical instabilities. In addition, we introduce a method that allows to treat effects from very heavy neutralino and chargino states perturbatively in the co-annihilation rates of the nearly mass-degenerate neutralinos and charginos. The application of the developed formalism to the χ_1^0 relic abundance calculation in several popular MSSM benchmark models is contained in Chap. 9. Here we analyse in detail the underlying physics effects in each step of the corresponding calculations, illustrating the general use of the developed effective field theory set-up. In Chap. 10 we summarise and draw our conclusions. Appendices A, B and C, contain results or further details on specific parts of the calculation.

Chapter 2

Sommerfeld enhancements in a toy scenario

This chapter contains a first introduction to the Sommerfeld enhancement effect. A rigorous derivation of the enhancement within the non-relativistic effective field-theory approach is postponed to Chapter 8, after the required formalism has been developed and the ingredients for the study of non-relativistic neutralino (co-) annihilations in the general MSSM within this framework have been calculated. As most of the preliminary work needed for this study is rather technical, we decide to first consider here strongly simplified but clear and intuitive toy scenarios. These scenarios allow to introduce the effect and motivate the need for the involved calculations within the MSSM. To this end the pair-annihilation reaction of non-relativistic fermions in the presence of gauge interactions starting from relativistic perturbation theory is considered in Sec. 2.1, and the situations requiring a resummation of so-called ladder diagrams up to all orders are discussed. Based on heuristic arguments we can then give in Sec. 2.2 a generic expression for the enhancement of annihilation rates in the presence of long-range potentials, expressed in terms of two-particle scattering wave-functions and short-distance annihilation rates, in a model with several nearly mass-degenerate two-particle states in the presence of (off-) diagonal potential interactions.¹ This formula is then brought into a simple form useful for further numeric studies. With this formula at hand we recap the properties of the enhancement in toy scenarios with one two-particle state with Coulomb- or Yukawa-potential interactions. Subsequently, the case of a two-state model with small mass splitting between the states and off-diagonal (real-symmetric) potential interactions is studied. The purpose of these toy-models is to emphasise the importance of a precise knowledge of the mass splittings between the annihilating states and the form of the potentials to a rigorous study of Sommerfeld enhancements. In addition it provides us with an estimate on the order of magnitude, that we can expect from the enhancements.

¹We will see in Chap. 8 that the correct Sommerfeld enhancement formula derived therein differs slightly from the advanced-guess expression presented here, and that the latter provides correct results for the enhancement only, if the potentials in the corresponding Schrödinger equations are symmetric.

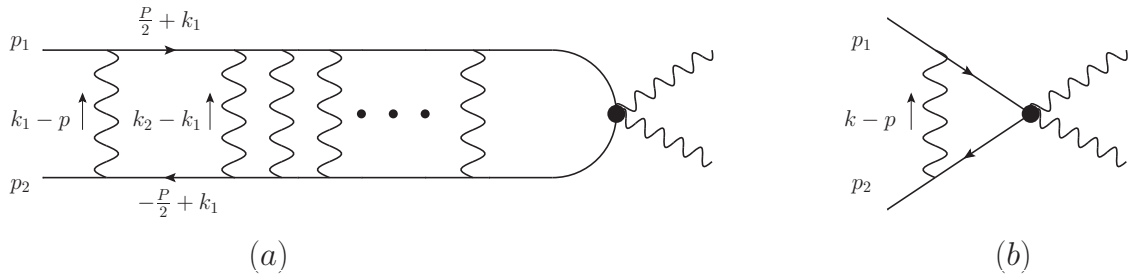


Figure 2.1: (a): Ladder diagram with an arbitrary number of mutual exchanges of a very light or massless particle (wavy propagators) between the two heavy particles (solid propagators) prior to their hard annihilation reaction (fat vertex). Similarly, such ladder diagrams exist in the production reaction of the heavy particle pair. (b): One-loop amplitude, that is part of the class of ladder diagrams in (a). We choose the centre-of-mass system of the reaction and refer to the case of non-relativistic external momenta $p_{1,2}$ in the text. 'Canonical' routing of the momenta in the loop is indicated, where k_i or k denotes a loop-momentum. $p_{1,2} = P/2 \pm p$, with $P^\mu = (2M_\chi + E, \vec{0})^\mu$ and $p^\mu = (0, \vec{p})^\mu$.

2.1 The origin of the enhancement

The Sommerfeld enhancement effect is related to a threshold singularity in pair-annihilation or pair-production reactions of heavy non-relativistic particles, that allow for mutual exchange of massless or very light (as compared to the heavy particle mass scale) mediators. In the regime of small particle velocities, $v \ll 1$, usual relativistic perturbation theory, relying on an expansion in the couplings α of the theory, breaks down, implying that a certain class of diagrams has to be resummed to all orders. The consistent resummation of such contributions leads to an enhanced production- or annihilation-rate.

The set of diagrams which exhibit a singular behaviour at threshold ($v \rightarrow 0$) is given by the class of ladder diagrams shown in Fig. 2.1 (a).² A full result for the corresponding multi-loop integrals is in general not known. However, instead of a direct calculation of each such diagram, the threshold expansion method [35] is conveniently used. The latter is appropriate to separate contributions to a (multi-) loop-integral, that are associated with different scaling of the loop-momenta, according to the given energy scales of the problem. Relying on this method, the dominant contributions to each ladder diagram can be identified and only those are subsequently taken into account in the resummation. In such a way a rearrangement of the perturbative expansion, applicable in the case $\alpha/v \sim 1$, is possible, leading us to an effective field theory description of the non-relativistic pair-annihilation reaction. The explicit construction of such an effective theory for non-relativistic neutralino dark matter pair-annihilation processes will

²Singular behaviour (a so called Coulomb singularity) is obtained for massless mediator exchange. In case of a very light mediator, the ladder diagrams are strongly enhanced and require resummation, but they are finite at threshold.

be discussed in Chapters 5-7. Here we want to get a better insight into the origin of the threshold singularity and gain a qualitative understanding how to deal with it by applying the threshold expansion method.

Consider the annihilation reaction of a particle anti-particle pair $\chi\bar{\chi}$ of non-relativistic Dirac-fermions with individual mass M_χ in its centre-of-mass frame. Following [35], determine the large and small scales characterising the process: the non-relativistic kinetic energy $E \sim M_\chi v^2$, the non-relativistic momentum $M_\chi v$ and the mass scale M_χ , where $M_\chi v^2 \ll M_\chi v \ll M_\chi$. The loop-momentum in a diagram contributing to the annihilation amplitude can then be distinguished to be either

$$\begin{aligned}
\text{hard:} & \quad k_0 \sim M_\chi, \quad \vec{k} \sim M_\chi, \\
\text{soft:} & \quad k_0 \sim M_\chi v, \quad \vec{k} \sim M_\chi v, \\
\text{potential:} & \quad k_0 \sim M_\chi v^2, \quad \vec{k} \sim M_\chi v, \\
\text{ultra-soft:} & \quad k_0 \sim M_\chi v^2, \quad \vec{k} \sim M_\chi v^2,
\end{aligned} \tag{2.1}$$

where this classification implies a certain 'canonical' assignment of the routing of the momenta in a given loop-diagram. For an explicit example, consider the 1-loop diagram (b) in Fig. 2.1, where a (massless) gauge boson is exchanged between the χ and $\bar{\chi}$ prior to the annihilation (hence assuming, that the two particles $\chi, \bar{\chi}$ are oppositely charged under an $U(1)$ gauge group). As regards the proper annihilation, denoted with the fat vertex, the details on the particular interaction and the number of produced final state particles are not important here for the moment. (We will specify later the two-particle final-states we are interested in, see Sec. 5. In any case the final-state masses are assumed to be considerably lighter than M_χ .)

Subject to the specific 'canonical' assignment of the momentum flow in Fig. 2.1 (b), the expression for the amplitude is of the form

$$\mathcal{A} \sim g^2 M_\chi^2 \int [dk] \frac{1}{\left(\left(\frac{P}{2} + k\right)^2 - M_\chi^2 + i0\right) \left(\left(\frac{P}{2} - k\right)^2 - M_\chi^2 + i0\right) (k-p)^2}. \tag{2.2}$$

On the right hand side, we have factored out the mass-dimension full factor M_χ^2 associated with the amplitude's numerator and then dropped the remaining dimensionless Dirac-structure, which is unimportant to our qualitative discussion. In addition we kept the factor g^2 in the numerator, where g denotes the gauge coupling of the $\chi, \bar{\chi}$ states to the gauge boson. For the external momenta $p_{1,2} = P/2 \pm p$ with $P^\mu = (2M_\chi + E, \vec{0})^\mu$, $p^\mu = (0, \vec{p})^\mu$ is used, where $E \sim M_\chi v^2$ and $|\vec{p}| \sim M_\chi v$. Finally, $[dk]$ denotes the integration measure. In four space-time dimensions³ it reads $[dk] = d^4k/(2\pi)^4 = dk^0 d^3\vec{k}/(2\pi)^4$. We can now easily estimate the scaling of contributions to the threshold expansion of (2.2).

³The original amplitude obtained from Fig. 2.1 (b) is both UV- and IR-divergent, requiring regularisation of the 1-loop integral. Note that the right hand side of (2.2) is only UV-finite because we have dropped the numerator structures of the original amplitude: the numerator of the full 1-loop amplitude in Fig. 2.1 (b) contributes two powers of the loop-momentum in the UV, such that a logarithmic UV-divergence results by power-counting. To properly treat the UV- and IR divergencies it is conve-

For the region of hard loop-momenta, the integration measure scales as $[dk] \sim M_\chi^4$, and consequently, using (2.1),

$$\mathcal{A}^{\text{hard}} \sim g^2 . \quad (2.3)$$

This indicates, that the contribution from the hard region gives rise to an ordinary radiative correction to the $\chi\bar{\chi}$ annihilation vertex. By direct calculation it can be shown that the contributions to the threshold expansion of (2.2) from the soft and ultra-soft region vanish. Therefore we do not explore the scaling of the different terms in (2.2) in these regions here. For potential scaling of loop-momentum k we obtain $[dk] \sim M_\chi^4 v^5$. Further both the denominators of the heavy fermion propagators as well as the denominator of the gauge boson propagator in (2.2) scale as $M_\chi^2 v^2$ in the potential region, see (2.5) and (2.6) below, such that

$$\mathcal{A}^{\text{potential}} \sim \frac{g^2}{v} . \quad (2.4)$$

The behaviour proportional to $1/v$ implies, that the potential contribution to the threshold expansion will dominate and gives rise to the (Coulomb) singularity for $v \rightarrow 0$.

Being more explicit, the threshold expansion method prescribes, that in each region the integrand of (2.2) is expanded in those parameters, which are small in that region, and subsequently, that integration over the loop momentum is carried out (over the entire loop integration domain⁴). In the potential region, this prescription implies at first an expansion of the propagators in the small $k_0 \sim M_\chi v^2$, with the effect that the denominators in (2.2) are replaced by

$$\frac{1}{\left(\left(\frac{E}{2} \pm k\right)^2 - M_\chi^2 + i0\right)} \longrightarrow \frac{1}{2 M_\chi \left(E/2 \pm k_0 - \frac{\vec{k}^2}{2M_\chi} + i0\right)} , \quad (2.5)$$

$$\frac{1}{(k-p)^2} \longrightarrow - \frac{1}{(\vec{k} - \vec{p})^2} . \quad (2.6)$$

nient to use dimensional regularisation. In this case the integration measure is $[dk] \rightarrow \tilde{\mu}^{2\epsilon} d^d k / (2\pi)^d = 1/(4\pi)^2 e^{\epsilon\gamma_E} d^d k / (\pi)^{d/2}$, with $d = 4 - 2\epsilon$. Here $\tilde{\mu} = \sqrt{e^{\epsilon\gamma_E}/(4\pi)} \mu$ with $\gamma_E = 0.577216\dots$ is used and μ denotes the renormalisation scale. We are not interested in the exact calculation of the amplitude but rather in the scaling behaviour of contributions from a certain region of the loop-momentum as specified in (2.1). To this end we want to apply simple power counting arguments. This is however not easily done in dimensional regularisation, as (2.1) distinguishes time and spatial components of the four-momentum in four space-time dimensions, and the scaling of the measure $[dk]$ referring to d -dimensional k is not clear in this case. Focusing on the scaling behaviour of different contributions to the amplitude it is sufficient to consider $[dk] = d^4 k / (2\pi)^4$ in the following and to assume that UV- and IR-divergencies are appropriately regulated.

⁴The point, why this is possible is non-trivial and it requires the use of dimensional regularisation. A rough, simple argument, why the integration of the loop momentum in each region can be extended to the entire domain, reads as follows: After expansion in the small parameters according to the considered region, the contributions to the integrand from other than that region give rise to scaleless integrals. These vanish when dimensional regularisation is used.

In the potential region, the gauge boson propagator hence gives rise to a non-local in space but instantaneous interaction between the two heavy fermions: the Fourier-transform of the right hand side of (2.6) leads to the familiar Coulomb potential $V(r) \propto 1/r$. Here, the variable r refers to the relative distance of the two fermions in configuration space. Proceeding in the determination of the potential region contribution to (2.2), using the right hand side expressions in (2.5), (2.6), the k_0 integration can now be carried out easily, using contour integration methods. Note, that the two poles at $k_0 = \pm(\vec{k}^2/2M_\chi - E/2 - i0)$ from the heavy fermion propagators pinch the k_0 integration contour in the region of potential \vec{k} , consequently leading to the $1/v$ threshold singularity as already anticipated in (2.4). The threshold singularity of the integral (2.2), originating from the region of potential loop momenta, is therefore associated with the two internal fermion propagators going simultaneously on-shell.

Moving now to a multi-loop ladder diagram as depicted in Fig. 2.1 (a), each single loop integral is dominated by the $1/v$ proportional contribution from the respective potential loop-momentum region. This eventually requires resummation of the $1/v^n$ proportional potential region contributions to the n -ladder diagram up to all orders n in perturbation theory. It is worth to mention, that no n -loop diagrams other than ladders and from each loop-integral no region other than the potential loop-momentum region will give rise to $1/v^n$ enhanced terms: as seen for the 1-loop case above, each $1/v$ singularity is associated with two heavy fermion propagator poles pinching the respective k_0 loop-momentum contour in the potential region, when the internal fermion propagators go simultaneously on-shell. This can only happen for ladders and, for example is not possible, if two ladder rungs are crossed.

Finally let us discuss the case of massive mediator exchange, by assigning a mass $m_\phi \ll M_\chi$ to the gauge boson exchanged between the heavy fermion propagators in Fig. 2.1 (a) and (b).⁵ This introduces an additional scale to the integrand of the 1-loop amplitude in (2.2). As m_ϕ is assumed to be sufficiently lighter than M_χ , our conclusions on the contribution from the hard loop-momentum region, (2.3), are unchanged. For small loop momenta however, the additional scale becomes relevant: the heavy fermion propagators can still be expanded in the small quantity k_0^2 , leaving us with the same expression (2.5) as before. In the next step of calculating the contribution to the expansion of the 1-loop amplitude we will perform the k_0 integration, picking the pole from one heavy fermion propagator. This implies $k_0 \sim \vec{k}^2/M_\chi \ll |\vec{k}|$. Hence the expansion of the gauge boson propagator becomes $-1/((\vec{k} - \vec{p})^2 + m_\phi^2)$ instead. The Fourier transform of the latter gives rise to a Yukawa potential interaction $V(r) \propto \exp(-m_\phi r)/r$ between the two heavy fermions. Using the above expression as well as (2.5), we can now carry out the k_0 integration using contour methods as before. Thereafter we are left with a \vec{k} -integration over an integrand, that contains not only the scale $M_\chi v$, but m_ϕ as well. While in the $m_\phi = 0$ case, the only left-over scale in the \vec{k} -integration was $M_\chi v$ (as anticipated in the potential scaling rule for \vec{k} , (2.1)), we can now distinguish the cases

⁵We are only interested in the case of $m_\phi < M_\chi$. Otherwise, the gauge boson exchange between the fermions would reduce to a contact interaction.

$m_\phi \ll M_\chi v$, $m_\phi \gg M_\chi v$ and $m_\phi \sim M_\chi v$. The \vec{k} integral will be dominated by the respective larger scale. For $m_\phi \ll M_\chi v$ the mediator mass m_ϕ becomes irrelevant, and we expect to recover the previously obtained $1/v$ enhanced result for the contribution to the 1-loop amplitude (2.4). If instead $m_\phi \gg M_\chi v$, the \vec{k} -integration will be dominated by the scale $\vec{k} \sim m_\phi$. From simple power counting, we then obtain in this case ($\vec{k} \sim m_\phi \ll M_\phi$) the following contribution to the threshold expansion of (2.2)

$$\mathcal{A}^{\text{small}} \sim g^2 \frac{1}{m_\phi/M_\chi} . \quad (2.7)$$

Note that we do not refer to the contribution as 'potential' but use the (a bit vague) term 'small', as the \vec{k} -integration is not dominated by potential $\vec{k} \sim M_\chi v$ but 'small' $\vec{k} \sim m_\phi$ momenta here. Obviously, for a sufficiently light mediator, $m_\phi \ll M_\chi$, the simple estimate (2.7) predicts an enhanced contribution to the expansion of the amplitude as well, which implies the need for resummation of the respective contributions to ladder diagrams up to all orders. However, no threshold singularity is obtained for $v \rightarrow 0$ as in (2.4). Rather the ratio m_ϕ/M_χ acts as an infrared cut-off, setting a maximal size for a possible enhancement. We will see later, that our naive arguments leading to (2.7) correctly predict a saturation of the enhancement of the (resummed) annihilation amplitude in the $v \rightarrow 0$ case if $m_\phi > 0$. There are however resonance effects, considerably enhancing the $\mathcal{A}^{\text{small}}$ contribution with respect to the naive expectation (2.7). These are associated with particular values of the coupling strength g and the masses m_ϕ and M_χ and cannot be captured in our simple discussion here. Their effect will be discussed in Sec. 2.3.2.

In both the cases of either a small or a vanishing mediator mass, we have seen that certain contributions to the threshold expansion of ladder diagrams are enhanced and require resummation of the dominant contributions to all orders. The contributions are associated with the internal fermion propagators being (close to) on-shell states, while the mutual gauge boson exchanges become instantaneous long-range interactions, describing potential scattering reactions of the fermion pair. The need for resummation indicates that these potential interactions cannot be treated perturbatively any longer, requiring a rearrangement of the perturbative expansion. We enter in the construction of a corresponding effective field theory in later chapters. Now that we have qualitatively discussed the origin of the enhancement in non-relativistic pair-annihilation reactions, we will proceed with the derivation of an enhancement formula for a non-relativistic particles' pair-annihilation rate, given potential interactions from light mediator exchange prior to their actual annihilation.

2.2 An enhancement formula for a N -state model

Let us consider a set of N nearly mass-degenerate two-particle states $(\chi\chi)_I$, $I = 1, \dots, N$, in their common centre-of-mass system. The pairs $(\chi\chi)_I$ are built from a collection of one-particle states χ_i , such that all $(\chi\chi)_I$ states in the set share the same conserved

charges. The relative velocities in each $(\chi\chi)_I$ system are assumed to be non-relativistic and (potential) scattering reactions shall allow for transitions $(\chi\chi)_I \rightarrow (\chi\chi)_J$. This implies that the mass splittings $\delta M_J = M_J - M_1$ between the lightest state $(\chi\chi)_1$ and the remaining $(\chi\chi)_J$ in the set must not be too large; in case of larger mass splittings δM_J a heavier $(\chi\chi)_J$ state cannot be created on-shell in $(\chi\chi)_1 \rightarrow (\chi\chi)_J$ scattering given a non-relativistic initial state. In the reverse reaction, with a non-relativistic on-shell initial state $(\chi\chi)_J$, the final $(\chi\chi)_1$ state would be characterised by velocities outside the non-relativistic regime. Further we assume the presence of (“diagonal”) long-range potential interactions between the two constituents χ_i, χ_j of each pair $(\chi\chi)_I$, accounting for $(\chi\chi)_I \rightarrow (\chi\chi)_I$ scattering, as well as off-diagonal potential interactions that cause scattering transitions $(\chi\chi)_I \rightarrow (\chi\chi)_J$ with $I \neq J$. We restrict the discussion to spherically symmetric potentials, where the latter only depend on the relative radial coordinate in the $(\chi\chi)_I$ systems. Arranging the N states $(\chi\chi)_I$ in a vector, the potential interactions can be encoded in a $N \times N$ potential matrix with in general non-vanishing off-diagonals. The potential matrix has to be hermitian, but it is not necessarily real-symmetric.⁶

In application to co-annihilation reactions of non-relativistic neutralinos and charginos, sets of $(\chi\chi)_I$ states are obtained in the following way: at first all possible two-particle pairs $\chi\chi$ are built from the individual χ_i^0 and χ_j^\pm states. The resulting pairs are then arranged according to the two-particle states’ electric charge. Hence there are five different charge-sectors, characterised by neutral, single-positive, single-negative, double-positive or double-negative electric charge. Out of each charge-sector the set of those pairs is singled out, that have a sufficiently small mass splitting to the $\chi_1^0\chi_1^0$ pair. As far as co-annihilation processes to non-relativistic $\chi_1^0\chi_1^0$ annihilations are concerned, the such defined sets contain all those two-particle states, that have to be taken into account in non-relativistic χ^0/χ^\pm co-annihilation reactions relevant within the determination of the χ_1^0 relic abundance. The calculation of the potential matrices associated with the different charge-sectors will be the subject of Chapter 7. For the time being we refer to the generic case of N nearly mass-degenerate non-relativistic two-particle states $(\chi\chi)_I$ and leave the application to neutralino and chargino pairs for later.

A diagrammatic picture for the $(\chi\chi)_I$ annihilation reactions that we want to describe is given in Fig. 2.2. In the schematic diagram for the annihilation amplitude (and its complex conjugate) depicted in the first line of Fig. 2.2, the potential interactions, that are active between the non-relativistic $(\chi\chi)_I$ pairs’ constituents, are indicated by the grey rectangle. The hard annihilation process is denoted by a point-like interaction. This implicitly assumes factorisation between the long-range potential interactions, associated with the non-relativistic kinetic energies in the $(\chi\chi)_I$ system, and the actual

⁶Subject of Chapters 5 and 7, the potentials in our effective field theory description of non-relativistic neutralino and chargino co-annihilation reactions are derived from interactions in the underlying full theory, the MSSM. As a consequence of the hermiticity of the MSSM’s interaction Lagrangian, the potential matrix is hermitian as well. Due to complex coupling factors in the general MSSM, off-diagonal potentials can then be associated with complex couplings as well, such that we have to account for hermitian and not necessarily real-symmetric potential matrices in the general case.

$$\begin{aligned}
& \int dP_{S_{X_A X_B}} \left(\left((\chi\chi)_I \right. \right. \left. \left. \begin{array}{c} \text{---} \boxed{\text{wavy}} \text{---} \dots \text{---} \boxed{\text{wavy}} \text{---} (\chi\chi)_J \\ \text{---} \boxed{\text{wavy}} \text{---} \dots \text{---} \boxed{\text{wavy}} \text{---} (\chi\chi)_J \end{array} \right. \right. \left. \left. \begin{array}{c} \text{---} \text{---} \text{---} \\ \text{---} \text{---} \text{---} \end{array} \right) \begin{array}{c} X_A \\ X_B \end{array} \right) \left(\dots \right)^* \\
& = 2 \Im \left(\left((\chi\chi)_I \right. \right. \left. \left. \begin{array}{c} \text{---} \boxed{\text{wavy}} \text{---} \dots \text{---} \boxed{\text{wavy}} \text{---} (\chi\chi)_{J'} \\ \text{---} \boxed{\text{wavy}} \text{---} \dots \text{---} \boxed{\text{wavy}} \text{---} (\chi\chi)_{J'} \end{array} \right. \right. \left. \left. \begin{array}{c} \text{---} \text{---} \text{---} \\ \text{---} \text{---} \text{---} \end{array} \right) \begin{array}{c} X_A \\ X_B \end{array} \right) \left(\left((\chi\chi)_J \right. \right. \left. \left. \begin{array}{c} \text{---} \boxed{\text{wavy}} \text{---} \dots \text{---} \boxed{\text{wavy}} \text{---} (\chi\chi)_I \\ \text{---} \boxed{\text{wavy}} \text{---} \dots \text{---} \boxed{\text{wavy}} \text{---} (\chi\chi)_I \end{array} \right. \right. \left. \left. \begin{array}{c} \text{---} \text{---} \text{---} \\ \text{---} \text{---} \text{---} \end{array} \right) \begin{array}{c} X_A \\ X_B \end{array} \right)
\end{aligned}$$

Figure 2.2: Diagrammatic picture of the annihilation reactions of a non-relativistic $(\chi\chi)_I$ pair into a two-particle $X_A X_B$ final state in the presence of long-range potential interactions (wavy propagators contained in the grey boxes). Generically, the potential scattering reactions allow for transitions $(\chi\chi)_I \rightarrow (\chi\chi)_J$, to all accessible additional non-relativistic states $(\chi\chi)_J$. The proper hard annihilation process is depicted by a single vertex.

short-distance annihilation reaction, which is characterised by the mass scale M_I of the annihilating $(\chi\chi)_I$ pair. The long-range potential interactions cannot be treated perturbatively. This implies that the well-known approach in relativistic quantum field theory fails, where the individual incoming single-particle states, that subsequently take part in perturbatively treated local interactions, are associated with asymptotically free plane-wave functions. Instead, the non-perturbative nature of the potential interactions requires the consideration of an incoming two-particle scattering wave-function corresponding to the incoming $(\chi\chi)_I$ pair, where this wave-function is a scattering solution to a multi-state Schrödinger equation involving the $N \times N$ potential matrix. It is convenient to use the optical theorem at the amplitude level to relate the annihilation cross section to the imaginary part of the forward scattering amplitude, as done in the second line of Fig. 2.2. The physical picture is then as follows: an incoming two-particle wave-function associated with the incoming $(\chi\chi)_I$ state gets distorted away from the free plane-wave solution due to the presence of the potential interactions. In particular, off-diagonal potential interactions cause transitions to any accessible nearly mass-degenerate state $(\chi\chi)_J$. This implies that the actual hard annihilation reaction, which is to very good approximation described by a local interaction, can proceed from any of these $(\chi\chi)_J$ states reached by prior (off-) diagonal potential scattering. Referring to the formulation in terms of the imaginary part of the forward scattering amplitude, the hard annihilation reaction is hence encoded in an annihilation matrix, that exhibits diagonal as well as off-diagonal entries as a consequence of the off-diagonal potential interactions. Diagonal annihilation matrix entries encode the absorptive part of the perturbative $(\chi\chi)_J \rightarrow (\chi\chi)_J$ reactions, while off-diagonals refer to the absorptive part of perturbative $(\chi\chi)_J \rightarrow (\chi\chi)_{J'}$ scattering with $J \neq J'$.

While a rigorous derivation of the relation among the annihilation amplitude and the two-particle scattering wave function as well as a sound derivation of the quantity referred to as annihilation matrix is postponed to later chapters, the above discussion allows us to guess the expression for the Sommerfeld enhancement factor, that describes the enhancement (suppression) of the annihilation cross section due to attractive (repulsive) long-range potential interactions, which cannot be treated perturbatively:

$$S = \frac{\psi_J^{(I)*}(r=0) \tilde{\Gamma}_{JJ'} \psi_{J'}^{(I)}(r=0)}{\psi_{0J}^{(I)*}(r=0) \tilde{\Gamma}_{JJ'} \psi_{0J'}^{(I)}(r=0)}. \quad (2.8)$$

We have introduced the matrix $\tilde{\Gamma}$, that encodes physics related to the hard perturbative annihilation rates. The N -component vector wave-function $\vec{\psi}^{(I)}$ refers to a solution of the Schrödinger equation

$$\left(-\frac{\vec{\partial}^2}{2\mu_I} \mathbf{1} + V(r) \right) \vec{\psi}^{(I)}(\vec{r}) = E \vec{\psi}^{(I)}(\vec{r}) \quad (2.9)$$

where μ_I denotes the reduced mass associated with the incoming $(\chi\chi)_I$ pair and E indicates a certain available non-relativistic kinetic energy. $\vec{\psi}_0^{(I)}$ gives the corresponding solution for the free case, in absence of long-range potential interactions. The potential matrix V encodes (off-) diagonal potential interactions, that are assumed to depend on the radial variable r only and to vanish for $r \rightarrow \infty$ at least as $1/r$. In addition, the diagonal entries of V also incorporate effects from the constant mass splittings $\delta M_I = M_I - M$ between the N two-particle states $(\chi\chi)_I$ to a certain mass scale M . Because the potential interactions vanish for $r \rightarrow \infty$, the potential matrix becomes diagonal in this limit,

$$V_{IJ}(r \rightarrow \infty) \rightarrow \delta M_I \delta_{IJ}. \quad (2.10)$$

In particular, these entries are present in the equation for the free wave-function $\vec{\psi}_0^{(I)}$. The mass scale M in the definition of $\delta M_I = M_I - M$ can but does not need to be chosen as the mass of the lightest state $(\chi\chi)_1$ out of the N -state set. In any case, however, it has to be chosen close to the lightest state's mass to ensure the non-relativistic nature of the set-up. Imagine for example the case of the single positive-charged sector in neutralino-chargino co-annihilations. Here it could prove useful to choose M as $2m_{\chi_1^0}$, the mass of the lightest neutral state $\chi_1^0\chi_1^0$ and not the (typically only slightly) larger mass $m_{\chi_1^0} + m_{\chi_1^+}$ of the lightest state in the single-charged sector. In this case, the energy E in the single-charged sector's Schrödinger equations will refer to the kinetic energy available for the $\chi_1^0\chi_1^0$ state, $E = m_{\chi_1^0}v^2$ with v the velocity of each χ_1^0 in the centre-of-mass of the two-particle system. The non-vanishing mass splittings contained in the diagonals of the single-charged sector's potential matrices then correct to the actually available kinetic energy for each single-charged $(\chi\chi)_I$ channel. Using such a convention for all charge sectors in χ^0/χ^\pm (co-) annihilation reactions, the same kinetic energy $E = m_\chi v^2$ will

appear in all Schrödinger equations of the different charge-sectors. We will adapt this convention later and hence anticipate here the identification $E = m_\chi v^2$ for the kinetic energy in the Schrödinger equation (2.9). Keep in mind, that (2.9) applies to the relative coordinate \vec{r} in the $(\chi\chi)_I$ system and we have used $r = |\vec{r}|$. Let us first approximate (2.9) by replacing the reduced mass μ_I of the given incoming pair $(\chi\chi)_I$ by the reduced mass $\mu \equiv m_\chi/2$, typically referring to the lightest state $(\chi\chi)_1$ out of the N state set. In the application to neutralino and chargino co-annihilations, m_χ will denote the mass of the lightest neutralino χ_1^0 . After this replacement, we arrive at a Schrödinger equation

$$\left(-\frac{\vec{\partial}^2}{m_\chi} \mathbf{1} + V(r) \right) \vec{\psi}^{(I)}(\vec{r}) = m_\chi v^2 \vec{\psi}^{(I)}(\vec{r}). \quad (2.11)$$

This equation applies now to any of the possible N incoming states $(\chi\chi)_I$. The difference of (2.11) with respect to (2.9) due to the replacement of the reduced mass is a higher order effect, counting as a correction $\delta M_J m_\chi v^2 \sim (m_\chi v^2)^2$, as the mass splittings in the N -state set are of order of the available non-relativistic kinetic energies.

According to the scattering reaction with incoming $(\chi\chi)_I$ state, that we want to describe, the vector-function $\vec{\psi}^{(I)}$ ($\vec{\psi}_0^{(I)}$) has to be a scattering solution with the following asymptotic behaviour

$$\psi_J^{(I)}(r \rightarrow \infty) \rightarrow c_{JI} e^{ik_J z} + f_{JI}(\theta, \phi) \frac{e^{ik_J r}}{r}, \quad (2.12)$$

describing an incoming plane wave propagating along the z -direction and an outgoing scattered spherical wave.⁷ The coefficients c_{JI} should be identified with δ_{JI} , if a pure incoming $(\chi\chi)_I$ state is described, but for notational clarity, keeping track of different contributions, it is convenient to consider the more general case with arbitrary c_{JI} first and restrict to $c_{JI} = \delta_{JI}$ later. The coefficients $f_{JI}(\theta, \phi)$ characterise the outgoing scattered spherical wave and due to the off-diagonal potentials they are in general not proportional to δ_{JI} . Recall, that the determination of the enhancement (or suppression)

⁷ The asymptotic form (2.12) applies in case of radial potential interactions vanishing faster than $1/r$ in the limit $r \rightarrow \infty$. This holds for Yukawa potentials, arising from massive mediator exchange, which is – besides Coulomb interactions from photon exchange – the relevant potential interaction in application to χ^0/χ^\pm pair annihilations. For Coulomb potentials (2.12) does however not apply. In our case Coulomb potentials can arise from photon exchange only, which implies that the $1/r$ potentials exclusively arise on the diagonal of the potential matrix $V(r)$, when written in the two-particle mass-eigenstate basis. For large values of r the matrix $V(r)$ will then always be diagonal, containing Coulomb potential contributions as well as constant δM_J terms only: $V_{IJ}(r \gg 0) \rightarrow (\delta M_I + \alpha_{II}/r) \delta_{IJ}$, with r chosen large enough, such that all contributions from the shorter-ranged (Yukawa) potentials are negligible. Accounting for Coulomb potentials, the $\exp(ik_J z)$ factor in (2.12) should be replaced by the incoming wave-function in presence of the Coulomb potential in the JJ component of $V(r)$. In addition, within the expression for the spherically outgoing scattered wave in (2.12) one has to replace $\exp(ik_J r)$ by $\exp\left(ik_J r + \frac{m_\chi \alpha_{JJ}}{2k_J} \ln(2k_J r)\right)$. As the derivation taking Coulomb potentials on the diagonals of $V(r)$ into account is completely analogous to the short-range potential case, and in particular leads to the same result for the enhancement factor, we will for clarity refer to the asymptotic behaviour (2.12) in the following.

in presence of attractive (repulsive) potential interactions via (2.8) requires the knowledge of the scattering solutions $\vec{\psi}^{(I)}$ and $\vec{\psi}_0^{(I)}$ close to the origin $r \sim 0$, where the short-distance annihilation takes place. Hence we describe next, how these scattering wave-functions can be determined.

Following the standard procedure, $\vec{\psi}^{(I)}$, $\vec{\psi}_0^{(I)}$ are obtained as linear combinations from a set of basis solutions to (2.11), such that the asymptotic behaviour in (2.12) is matched. The spherical symmetry of the individual potential interactions suggests to perform a separation of variables and construct $\vec{\psi}$ from

$$\vec{\psi}^{(I)} = \sum_l P_l(\cos \theta) \vec{R}_l^{(J)}(r) A_l^{(I)} \quad (2.13)$$

where $\vec{R}_l^{(J)}(r)$ denotes a set of basis solutions to the radial Schrödinger equation for the l th partial wave,

$$-\frac{1}{m_\chi r^2} \frac{d}{dr} \left(r^2 \frac{d\vec{R}_l(r)}{dr} \right) + V(r) \vec{R}_l(r) + \frac{1}{m_\chi r^2} l(l+1) \vec{R}_l(r) = m_\chi v^2 \vec{R}_l. \quad (2.14)$$

The $A_l^{(I)}$ denote the coefficients to the basis solutions $\vec{R}_l^{(J)}$ that give the specific scattering solutions $\vec{\psi}^{(I)}$. A sum over the index J is implied. Finally P_l denotes the l th Legendre polynomial and we have hence already taken advantage of the azimuthal symmetry of the scattering configurations of interest. The free scattering solutions $\vec{\psi}_0^{(I)}$ can be built in a similar way, replacing $\vec{R}_l^{(J)}$ by $\vec{R}_{0l}^{(J)}$ as well as $A_l^{(I)}$ by $A_{0l}^{(I)}$ in (2.13). The radial functions $\vec{R}_{0l}^{(J)}$ are then obtained as solutions to (2.14), with the potential matrix $V(r)$ replaced by the constant diagonal matrix $V(r \rightarrow \infty)$, (2.10), containing only the mass splittings. There exist $2N$ linearly independent solutions to (2.14) out of which N are irregular at the origin, hence restricting us to the set of N regular solutions. The asymptotic behaviour of the J th component of the regular linearly independent solutions $\vec{R}^{(I)}$, $I = 1, \dots, N$, is given by

$$R_{lJ}^{(I)}(r \rightarrow \infty) \rightarrow \frac{1}{r} (n_l)_{JI} \sin \left(k_J r - \frac{l\pi}{2} + (\delta_l)_{JI} \right), \quad (2.15)$$

with constant coefficients $(n_l)_{JI}$ and scattering phases $(\delta_l)_{JI}$.⁸ Further, we have defined

⁸ Taking Coulomb potentials on the diagonal of the potential matrix $V(r)$ into account, the asymptotic behaviour of the basis solutions $\vec{R}_l^{(I)}$ reads

$$R_{lJ}^{(I)}(r \rightarrow \infty) \rightarrow \frac{1}{r} (n_l)_{JI} \sin \left(k_J r - \frac{l\pi}{2} + \frac{m_\chi \alpha_{JJ}}{2k_J} \ln(2k_J r) + (\delta_l)_{JI} \right),$$

with constant coefficients $(n_l)_{JI}$ and scattering phases $(\delta_l)_{JI}$ as before. The r and k_J dependent term $\frac{m_\chi \alpha_{JJ}}{2k_J} \ln(2k_J r)$, appearing as additional argument inside the sine, accounts for the presence of a long range Coulomb potential $-\alpha_{JJ}/r$ in the JJ component of $V(r)$. Note that the modifications on the asymptotic behaviour of the scattering solutions $\psi_J^{(I)}(r \rightarrow \infty)$ in (2.12) when including Coulomb-potentials consist in the introduction of the same type of additional contributions, namely factors $\exp \left(\pm i \left(\frac{m_\chi \alpha_{JJ}}{2k_J} \ln(2k_J r) \right) \right)$, modifying the (terms in the partial-wave expansion of the) incoming plane wave $\exp(ik_J z)$ as well as the outgoing scattered spherical wave $\propto \exp(ik_J r)/r$, see footnote 7.

$$k_J = \sqrt{m_\chi(m_\chi v^2 + i\epsilon - V_{JJ}(r \rightarrow \infty))} = \sqrt{m_\chi(m_\chi v^2 + i\epsilon - \delta M_J)}. \quad (2.16)$$

With the $+i\epsilon$ prescription we implement our convention $\sqrt{-1} = +i$. For completeness and due to the slightly increased complexity in case of the matrix-valued Schrödinger equation with its vector solutions, we write here the well known procedure to determine the scattering wave functions in terms of the basis of partial-wave solutions in (2.13). This is done in close analogy to [36]. In particular we adopt a similar notation as used in this reference.

On the one hand side, using the expansion of the plane wave $e^{ik_J z}$ in terms of spherical waves, (2.12) can be rewritten as

$$\begin{aligned} \psi_J^{(I)}(r \rightarrow \infty) \rightarrow & \frac{e^{ik_J r}}{r} \left(\frac{c_{JI}}{2ik_J} \sum_l (2l+1) P_l(\cos \theta) + f_{JI}(\theta, \phi) \right) \\ & - \frac{e^{-ik_J r}}{r} \frac{c_{JI}}{2ik_J} \sum_l (-1)^l (2l+1) P_l(\cos \theta). \end{aligned} \quad (2.17)$$

On the other hand, starting from (2.13)

$$\begin{aligned} \psi_J^{(I)}(r \rightarrow \infty) \rightarrow & \frac{e^{ik_J r}}{r} \left(\frac{1}{2i} \sum_l (-i)^l P_l(\cos \theta) e^{i(\delta_l)_{JJ'}} (n_l)_{JJ'} A_{lJ'}^{(I)} \right) \\ & - \frac{e^{-ik_J r}}{r} \left(\frac{1}{2i} \sum_l i^l P_l(\cos \theta) e^{-i(\delta_l)_{JJ'}} (n_l)_{JJ'} A_{lJ'}^{(I)} \right). \end{aligned} \quad (2.18)$$

It is convenient to establish a matrix-notation here, introducing $N \times N$ matrices ψ and R_l , that contain the scattering and regular (l th partial-wave) radial solutions in their columns, respectively:

$$\psi_{JI}(r) = \psi_J^{(I)}(r), \quad R_{lJI}(r) = R_{lJ}^{(I)}(r). \quad (2.19)$$

Similarly, a constant coefficient matrix A_l is built, with components $A_{lJI} = A_{lJ}^{(I)}$. Eventually, introducing the matrix M_l with components

$$(M_l)_{JJ'} = (n_l)_{JJ'} e^{-i(\delta_l)_{JJ'}}, \quad (2.20)$$

we derive from the comparison of the respective second lines in (2.17) and (2.18) the expression for the coefficient matrix

$$A_{lJI} = i^l (2l+1) (M_l^{-1})_{JJ'} \frac{c_{JI}}{k_{J'}}. \quad (2.21)$$

M_l^{-1} encodes normalisations and scattering phases of the basis solutions, while the normalisation of the scattering solutions for $r \rightarrow \infty$ is assured by the dependence on the

coefficients c_{JI} . It is worth to note, that (2.21) as well as all following steps in our derivation hold in exactly the same form for the case including Coulomb potential interactions on the diagonal of the potential matrix $V(r)$, where in this case the normalisations and scattering phases encoded in M_l^{-1} have to be extracted from the asymptotic behaviour of the corresponding basis solutions $R_{lJ}^{(I)}(r \rightarrow \infty)$ as given in footnote 8.

The scattering wave-functions at the origin that appear in our guessed form (2.8) of the Sommerfeld enhancement factor are now obtained from the columns of the matrix ψ in the appropriate limit

$$\psi_J^{(I)}(r \rightarrow 0) = \psi_{JI}(r \rightarrow 0) = \sum_l P_l(\cos \theta) R_{lJJ'}(r \rightarrow 0) A_{lJI} . \quad (2.22)$$

Consequently the next step is the determination of $R_l(r \rightarrow 0)$. From the l th partial-wave radial Schrödinger equation (2.14), the behaviour $R_l(r \rightarrow 0) \propto r^l$ is inferred, supposing, that the long-range potentials in V grow less strongly than $1/r^2$ for $r \rightarrow 0$. As we will consider Coulomb and Yukawa potential interactions, this condition is fulfilled in our case. The usual ansatz $R_l(r) = \chi_l(r)/r$ allows to rewrite the radial Schrödinger equation for the matrix-valued function $\chi_l(r)$

$$\frac{d^2}{dr^2} \chi_l(r) = \left(\frac{l(l+1)}{r^2} + m_\chi (V(r) - m_\chi v^2 \mathbf{1}) \right) \chi_l(r) , \quad (2.23)$$

and the leading terms in the expansion of matrix $R_l(r)$ around $r = 0$ can be expressed in terms of the $(l+1)$ th derivative of χ_l ,

$$R_l(r \rightarrow 0) = r^l \frac{\chi_l^{(l+1)}(r=0)}{(l+1)!} + \mathcal{O}(r^{l+1}) . \quad (2.24)$$

Analytic solutions to (2.23) can be found for the free case (where $V(r)$ is given by the constant diagonal-matrix $V(r \rightarrow \infty)$, (2.10)) as well as for a 1-state model with long-range Coulomb potential interactions. Already for the case of a Yukawa potential in a 1-state model, the equation has to be solved numerically. In the free case, relevant for the determination of the denominator expression in the Sommerfeld enhancement formula (2.8), the radial Schrödinger equation (2.23) can be rewritten to

$$r^2 \frac{d^2}{dr^2} \chi_{0lJI}(r) + r^2 k_J^2 \chi_{0lJI}(r) - l(l+1) \chi_{0lJI}(r) = 0 . \quad (2.25)$$

There is no summation over the index J in (2.25), such that a system of N decoupled equations is obtained. The free vector basis-solutions in the radial coordinate, encoded in the columns of matrix χ_{0l} , can hence be chosen as $\vec{\chi}_{0l}^{(I)J} = \chi_{0lJI} = \delta_{JI} \tilde{\chi}_{0l}$, where $\tilde{\chi}_{0l}$ denotes an ordinary, one-dimensional and in general complex valued wave-function. Using the ansatz $\tilde{\chi}_{0l} = \sqrt{r} \tilde{J}_{0l}$ in (2.25), a Bessel differential equation for the function \tilde{J}_{0l} results,

$$x_J^2 \frac{d^2}{dx_J^2} \tilde{J}_{0l}(x_J) + x_J \frac{d}{dx_J} \tilde{J}_{0l}(x_J) + \left(x_J^2 - (l + \frac{1}{2})^2 \right) \tilde{J}_{0l}(x_J) = 0 , \quad (2.26)$$

with $x_J = k_J r$ and no summation over J . A generic solution to (2.26) is found as linear combination of Bessel functions of the first and second kind, $J_{l+1/2}(x_J)$ and $Y_{l+1/2}(x_J)$. As the scattering wave-function has to be regular at $x_J = 0$, though, only $\tilde{J}_{0l}(x_J) = J_{l+1/2}(x_J)$ is considered. Hence the N basis solutions encoded in the matrix χ_{0l} can be expressed in terms of

$$\chi_{0lJI}(r) = \delta_{JI} \tilde{c}_J \sqrt{r} J_{l+1/2}(k_J r) , \quad (2.27)$$

where \tilde{c}_J is an arbitrarily chosen normalisation constant to the l th basis solution. Obviously, the dependence on \tilde{c}_J finally has to cancel out, when the free scattering solutions are constructed. From the known asymptotic behaviour of the Bessel functions we obtain for $r \rightarrow \infty$

$$\begin{aligned} R_{0lJI}(r \rightarrow \infty) &= \frac{\chi_{0lJI}(r \rightarrow \infty)}{r} \\ &\rightarrow \frac{1}{r} \delta_{JI} \tilde{c}_J \sqrt{\frac{2}{\pi k_J}} \sin\left(k_J r - \frac{l\pi}{2}\right) + \mathcal{O}\left(\frac{1}{k_J r^{3/2}}\right) , \end{aligned} \quad (2.28)$$

as well as in the limit $r \rightarrow 0$

$$R_{0lJI}(r \rightarrow 0) \rightarrow \delta_{JI} r^l \tilde{c}_J \frac{(k_J/2)^{l+1/2}}{\Gamma(l+3/2)} + \mathcal{O}(r^{l+2}) . \quad (2.29)$$

Comparing to (2.15), the constant normalisation coefficients $(n_l)_{JI}$ hence read in the free case $(n_{0l})_{JI} = \delta_{JI} \tilde{c}_J \sqrt{2/\pi k_J}$, and all scattering phases vanish, $(\delta_{0l})_{JI} = 0$. Consequently (using $(M_{0l}^{-1})_{JJ'} = \delta_{JJ'}/\tilde{c}_J \sqrt{\pi k_J/2}$) the free case's coefficient matrix (2.21) reads

$$A_{0lJI} = i^l (2l+1) \frac{\delta_{JJ'}}{\tilde{c}_J} \sqrt{\frac{\pi k_J}{2}} \frac{c_{JJ'}}{k_{J'}} = i^l (2l+1) \sqrt{\frac{\pi}{2 k_J}} \frac{c_{JI}}{\tilde{c}_J} . \quad (2.30)$$

After simple algebraic manipulations, the free scattering solutions for $r \rightarrow 0$ are finally obtained from

$$\begin{aligned} \psi_{0JI}(r \rightarrow 0) &= \sum_l P_l(\cos \theta) R_{0lJJ'}(r \rightarrow 0) A_{lJ'I} \\ &\rightarrow \sum_l P_l(\cos \theta) r^l i^l \frac{2l+1}{(2l+1)!!} k_J^l c_{JI} . \end{aligned} \quad (2.31)$$

Let us suppose that for the interacting case with a generic potential matrix V , including (off-) diagonal long-range potential interactions, a matrix χ_l of solutions has been determined numerically from (2.23), subject to certain initial conditions, and the $(l+1)$ th derivative $\chi_l^{(l+1)}$ is known as well. Then the scattering solutions for $r \rightarrow 0$ can be generically expressed in terms of

$$\psi_{JI}(r \rightarrow 0) = \sum_l P_l(\cos \theta) r^l i^l \frac{2l+1}{(l+1)!} [\chi_l^{(l+1)}(r=0)]_{JJ'} (M_l^{(-1)})_{J'I} C_{I'I} \quad (2.32)$$

where we have introduced the matrix C , that encodes the initial conditions (2.12) for the incoming plane-wave part of the scattering solutions, $C_{I'I} = c_{I'I}/k_{I'}$.

Similar to the partial-wave decomposition (2.13) of the (free) scattering solutions contained in $\psi(r)$ and $\psi_0(r)$, also the short-distance annihilation process can be arranged in a partial-wave expansion. In the formulation of the guessed enhancement factor in (2.8), with the configuration-space scattering wave-functions to the left and right of the quantity $\tilde{\Gamma}$, such a partial-wave expansion of the latter annihilation matrix expression involves spatial derivatives acting on the wave-functions to its left and right. Written in radial coordinates, the l th partial-wave contribution in particular involves the l th derivatives with respect to the radial variable r , acting on ψ^* and ψ in (2.8), respectively. This allows us to refine the first guess of the formula for the Sommerfeld enhancement factor. The enhancement of the l th partial-wave annihilation rate of the incoming scattering state (described by an incoming plane wave $c_{JI} \exp(ik_J z)$, that gets subsequently distorted by (off-) diagonal long-range potential interactions) with respect to the corresponding perturbative l th partial-wave rate is given by

$$S_l^I = \frac{\psi_{JI}^*(r=0) \tilde{\Gamma}_{JJ'} \psi_{J'I}(r=0) |_{l\text{-wave}}}{\psi_{0JI}^*(r=0) \tilde{\Gamma}_{JJ'} \psi_{0J'I}(r=0) |_{l\text{-wave}}} \\ = \left(\frac{(2l+1)!!}{(l+1)!} \right)^2 \frac{\left[[\chi_l^{(l+1)}(r=0)] M_l^{-1} C \right]^\dagger \cdot \Gamma_l \cdot \left[\chi_l^{(l+1)}(r=0) M_l^{-1} C \right]_{II}}{[k_J^l c_{JI}]^* \Gamma_{lJJ'} [k_{J'}^l c_{J'I}]} . \quad (2.33)$$

To describe the case of a pure incoming state $(\chi\chi)_I$, the identification $c_{JI} = \delta_{JI}$, implying $C_{I'I} = \delta_{I'I}/k_I$ for the matrix C in the numerator above has to be made. (2.33) makes use of the $r \rightarrow 0$ behaviour of the (free) scattering solutions contained in ψ_0 and ψ as given in (2.31) and (2.32). The quantity Γ_l denotes the constant coefficient matrix encoding the hard (off-) diagonal l -wave annihilation process, that is obtained from the corresponding appropriate partial-wave expansion of the perturbative $(\chi\chi)_I \rightarrow (\chi\chi)_J$ amplitudes' absorptive part.

To make use of (2.33) as it stands the combination of normalisation coefficients $(n_l)_{JI}$ and scattering phases $(\delta_l)_{JI}$ encoded in the matrix M_l , (2.20), has to be known. They can in principle be extracted from the asymptotic form of the numerically determined solutions χ_l , but a separate precise determination, especially of the scattering phases, is very hard. Fortunately, the product of matrices $[\chi_l^{(l+1)}(r=0)] M_l^{-1}$ is related to quantities, that can be determined in an easier way. As a consequence, we will finally reformulate (2.33) in an even simpler form. To this purpose, let us consider the matrix $\chi_l(r)$ introduced earlier, containing the regular, linear independent solution vectors to the radial Schrödinger equation (2.23) in its columns. Following (2.24) and (2.15), the asymptotic behaviour, that we have assigned (in absence of Coulomb potential interactions) is

$$\chi_{lJI}(r \rightarrow 0) \longrightarrow r^{l+1} \frac{[\chi_l^{(l+1)}(r=0)]_{JI}}{(l+1)!} + \mathcal{O}(r^{l+2}) , \quad (2.34)$$

$$\chi_{lJI}(r \rightarrow \infty) \longrightarrow (n_l)_{JI} \sin(k_J r - \frac{l\pi}{2}) + (\delta_l)_{JI} . \quad (2.35)$$

The overall normalisation of the basis solution contained in χ_l is fixed by yet to define initial conditions. A convenient choice in particular for numeric solutions is related to conditions on χ_l in the $r \rightarrow 0$ limit: by assigning appropriate values to $\chi_l^{(l+1)}(r=0)$ the $r \rightarrow 0$ behaviour of the regular solutions (2.34) is fixed. For the time being we can leave the question of the initial condition for the regular solutions open and come back to this point later. In addition to the matrix χ_l let $\eta_l(r)$ be the matrix with the irregular solutions to (2.23) with the asymptotic form

$$\eta_{JI}(r \rightarrow 0) \longrightarrow \delta_{JI} r^{-l}, \quad (2.36)$$

$$\eta_{JI}(r \rightarrow \infty) \longrightarrow T_{lJI} e^{-ik_J r}, \quad (2.37)$$

such that the irregular solutions asymptotically correspond to purely incoming spherical waves.⁹ T_l denotes a hermitian coefficient matrix with in general non-vanishing off-diagonal entries. The normalisation of the basis solutions in η_l is fixed by the initial condition that is implicit in (2.36). Due to the hermiticity of the potential matrix $V^\dagger(r) = V(r)$, the Schrödinger equation is hermitian itself, such that the matrices χ_l^\dagger and η_l^\dagger are solutions to the hermitian conjugate radial Schrödinger equation

$$\frac{d^2}{dr^2} \xi_l^\dagger = \xi_l^\dagger \left[\frac{l(l+1)}{r^2} + m_\chi (V(r) - m_\chi v^2 \mathbf{1}) \right], \quad (2.38)$$

with $\xi_l = \chi_l, \eta_l$. As a direct consequence it is easily seen that the generalisation of the Wronskian,

$$W_l(r) = \eta_l^\dagger \cdot \left(\frac{d}{dr} \chi_l \right) - \left(\frac{d}{dr} \eta_l^\dagger \right) \cdot \chi_l \quad (2.39)$$

is constant in r , $d/dr W(r) = 0$.¹⁰ We can hence equate

$$W_l(r=0)_{JI} = \frac{2l+1}{(l+1)!} \left[\chi_l^{(l+1)}(r=0) \right]_{JI}, \quad (2.40)$$

with

$$W_l(r \rightarrow \infty)_{JI} = i^l T_{lJI}^\dagger k_{I'} (M_l)_{I'I}. \quad (2.41)$$

This allows to obtain the relation

$$\left[[\chi_l^{(l+1)}(r=0)] M_l^{-1} \right]_{JI} = i^l \frac{(l+1)!}{2l+1} T_{lJI}^\dagger k_I. \quad (2.42)$$

⁹Coulomb potential interactions from photon exchange on the diagonal of the potential matrix $V(r)$ change the asymptotic behaviour for $r \rightarrow \infty$ in (2.35) and (2.37). In both cases we have to replace k_{Jr} by $k_{Jr} + m_\chi \alpha_{JJ} / 2k_J \ln(2k_{Jr})$ (also see footnotes 7 and 8).

¹⁰Note that (2.39) is a generalisation of the expression W_l considered in [36]. In this reference the potential matrix was considered to be real-symmetric, such that the transpose of the matrix η , η^T , appears in the corresponding expression W_l defined therein, instead of the hermitian conjugate η^\dagger . Due to the generic hermiticity property of the Schrödinger equation, the definition of W_l with hermitian conjugates, (2.39), looks more natural even in the case with real-symmetric potentials.

Our final expression for the enhancement in the annihilation of the l th partial-wave component, (2.33), subject to an incoming $(\chi\chi)_I$ state, hence assumes the following compact form

$$S_l^I = ((2l - 1)!!)^2 \frac{[T_l \cdot \Gamma_l \cdot T_l^\dagger]_{II}}{k_I^{2l} \Gamma_{lII}}, \quad (2.43)$$

where we use the double factorial $(2l - 1)!! = \prod_{i=1}^{l-1} (2i + 1)$. Note that k_I is always real, as it corresponds to the momentum of the particles in the incoming scattering state $(\chi\chi)_I$. Equation (2.43) is consistent with the corresponding result in [36], although T^* appears in the reference's formula instead of T as in (2.43). However, [36] considered different irregular solutions, with asymptotically outgoing (instead of incoming, (2.37)) spherical wave behaviour, while the formulation of the corresponding generalisation of the Wronskian W_l referred to the transposed instead of the hermitian conjugate of the irregular-solution matrix (see footnote 10). The definition of matrix T in (2.37) hence agrees with T^* in [36].

Thanks to the constant Wronskian W_l , the matrix T_l , related to the irregular l th partial-wave solutions, can be calculated from the regular solutions contained in χ_l only. Without making use of the asymptotic form of the regular solutions in (2.35), we obtain

$$\begin{aligned} W_l(r \rightarrow \infty)_{JI} &\longrightarrow T_l^\dagger{}_{JJ'} e^{ik_{J'r}} \left(\frac{d}{dr} \chi_{lJ'I}(r) - ik_{J'} \chi_{lJ'I}(r) \right) \Big|_{r \rightarrow \infty} \\ &= [T_l^\dagger \cdot U_l(r \rightarrow \infty)]_{JI}, \end{aligned} \quad (2.44)$$

where the matrix $U_l(r)$ is defined by the first line above,¹¹

$$U_{lJI}(r) = e^{ik_{Jr}} \left(\frac{d}{dr} \chi_{lJI}(r) - ik_J \chi_{lJI}(r) \right). \quad (2.45)$$

It is now convenient to choose the initial condition for the regular solutions such that $[\chi_l^{(l+1)}(r=0)]_{JI} = (l+1)!/(2l+1) \delta_{JI}$, which implies $W_l(r=0)_{JI} = \delta_{JI}$, the matrix T_l in (2.43) is obtained from

$$T_l^\dagger = U_l^{-1}(r \rightarrow \infty). \quad (2.46)$$

As a check of (2.43) let us consider the free-case, where we should reproduce $S_l^I = 1$. We could either directly determine the irregular solutions for the free case or calculate T_l from (2.46). Choosing the latter option, we consider the free regular solutions $\chi_{0lJI}(r)$ in (2.27), with normalisation

$$c_{lJ} = \sqrt{\frac{2}{\pi}} (2l - 1)!! \frac{1}{k_J^{l+1/2}}, \quad (2.47)$$

¹¹Note that the exponential factor $\exp(ik_{Jr})$ in both (2.44) and (2.45) should be replaced by $\exp(i(k_{Jr} + m_\chi \alpha_{JJ}/2k_J \ln(2k_{Jr}))$, when Coulomb potential interactions from photon exchange on the diagonal of potential matrix $V(r)$ are taken into account (see footnotes 7 and 8).

such that the correct $r \rightarrow 0$ behaviour $[\chi_l^{(l+1)}(r=0)]_{JI} = (l+1)!/(2l+1) \delta_{JI}$ is obtained. Building $U_{lJI}(r)$ as in (2.45), we obtain

$$T_{0lJI}^\dagger = U_{0lJI}^{-1}(r \rightarrow \infty) = \frac{(-i)^l k_J^l}{(2l-1)!!} \delta_{JI}, \quad (2.48)$$

such that

$$\left[T_{0l} \cdot \Gamma_l \cdot T_{0l}^\dagger \right]_{II} = T_{0lIJ} \Gamma_{lJJ'} T_{0lIJ'}^* = \left(\frac{1}{(2l-1)!!} \right)^2 k_I^{2l} \Gamma_{lII}. \quad (2.49)$$

Taken together with the prefactor and denominator in (2.43), we consistently recover $S_l^I = 1$ for the free case.

In generic practical applications, where the Schrödinger equation (2.23) generally has to be solved with numerical methods, the strategy in the determination of S_l^I is as follows:

- (1) Determine the matrix χ_l , containing in its columns the N regular basis solutions to (2.23), subject to the initial conditions

$$[\chi_l(r = \hat{r})]_{JI} = \hat{r}^{l+1} \frac{\delta_{JI}}{2l+1}. \quad (2.50)$$

\hat{r} has to be chosen close to zero, such that the solutions will obey $[\chi_l^{(l+1)}(r=0)]_{JI} = (l+1)!/(2l+1) \delta_{JI}$, which we imposed above in order to have $W_{lJI}(r) = \delta_{JI}$.

- (2) With the matrix χ_l known, build the matrix $U_l(r)$, (2.45). To catch the asymptotic constant behaviour of $U_l(r)$, a large enough r_∞ has to be chosen in order to determine the constant matrix T_l^\dagger from (2.46).
- (3) Supposing the annihilation matrix Γ_l , encoding the perturbative (off-) diagonal annihilation rates of the l th partial-wave states is known, calculate the enhancement factor S_l^I for the incoming $(\chi\chi)_I$ pair from (2.43).

There are numerical issues related to the solutions of the Schrödinger equation for a multi-state system, that are delicate and require application of sophisticated methods. We discuss the origin of the numerical problems and describe an improved method for the numerical determination of the Sommerfeld enhancement factors, that solves the issue, when applying the formalism developed here to multi-state systems of χ^0/χ^\pm pairs. The technical details of this improved method are postponed to Chap. 8.4, although the data tables for the plots presented throughout the thesis rely on the improved version. In this chapter we will continue with simple one- and two-state toy models, in order to illustrate the Sommerfeld effect and to make ourselves familiar with generic properties of the enhancement in presence of Coulomb or Yukawa potentials.

2.3 $N = 1$ state models with Coulomb and Yukawa potential interactions

Before we enter a brief discussion on the well known enhancement due to Coulomb and Yukawa potential interactions in models with only one single $\chi\chi$ state, let us first deduce the general form of the $N = 1$ state enhancement factor S_l from the generic N -state system expressions (2.33) and (2.43). Starting from (2.33), the enhancement factor for the single $\chi\chi$ state case reduces to

$$S_l = \left(\frac{(2l+1)!!}{(l+1)!} \right)^2 \frac{|\chi_l^{(l+1)}(r=0)/n_l|^2}{k^{2l+2}} = \left(\frac{(2l+1)!!}{l!} \right)^2 \frac{|R_l^{(l)}(r=0)/n_l|^2}{k^{2l+2}}, \quad (2.51)$$

with $R_l(r) = \chi_l(r)/r$ as usual. $\chi_l(r)$ is now the solution to the single state radial Schrödinger equation as obtained from (2.23) for $N = 1$. The asymptotic behaviour of χ_l and R_l follows from (2.35), (2.34) and (2.15), (2.24), respectively. n_l denotes the normalisation of the regular solution $\chi_l(r)$ in the $r \rightarrow \infty$ limit. The linearity of the Schrödinger equation allows us to deliberately rescale any solution $\chi_l \rightarrow \tilde{\chi}_l = \tilde{c}\chi_l$, with a constant factor \tilde{c} , implying $n_l \rightarrow \tilde{n}_l = \tilde{c}n_l$. The effect of such a rescaling will in particular cancel in the enhancement formula (2.51).¹² The quantity k is given by $k = m_\chi v$, with m_χ twice the reduced mass of the two-particle state, and v half the (asymptotically free) incoming $\chi\chi$ state's relative velocity. If the $\chi\chi$ state is built from equal mass constituents, m_χ obviously agrees with the corresponding single particle mass and v gives the modulus of the single particle velocity subject to the asymptotically free incoming states. Just as the k_J in the N -state case, k hence generically indicates the modulus of each single particle's momentum in the centre-of-mass of the (asymptotic) incoming $\chi\chi$ system. It is interesting to note, that the dependence on the scattering phases δ_l cancels in the $N = 1$ state Sommerfeld factor, (2.51), as opposed to the generic N -state case, where each component $\chi_{lJI}(r)$ of the matrix encoding the regular radial solutions can come with a different phase in its $r \rightarrow \infty$ behaviour. In general, the matrix product in (2.33) will imply no cancellation of scattering phases. Further note, that the l -wave enhancement factor S_l in the one-state case, (2.51), only relies on the potential interaction and is independent of the hard annihilation rate. This no longer holds true in the general multi-state case, where a generic annihilation matrix Γ_{IJ} with non-vanishing off-diagonals encodes the short-distance annihilation part of the full process: while the denominator of S_l^I , (2.33) or (2.43), is proportional to the perturbative hard l -wave annihilation rate of the $(\chi\chi)_I$ state, encoded in Γ_{lII} , the numerator, to the contrary, will generally contain terms involving the hard (off-) diagonal l -wave rates $\Gamma_{lJJ'}$ of any states $(\chi\chi)_J$, $(\chi\chi)_{J'}$ accessible from the initial $(\chi\chi)_I$ by potential scattering.

Imposing an asymptotic normalisation $n_l = \sqrt{2/\pi}$ on the radial solution χ_l , we recover in (2.51) the l -wave enhancement formula that can be inferred from the results

¹²Note that the same argument applies to a global rescaling of the matrices χ_l and R_l in the N -state case.

presented in [37] (see Eq. (3.11) and (5.1) therein). The author of [38] independently derived an equivalent result for the l -wave enhancement in a single state system (see Eq. (21) therein), which we reproduce by selecting the regular solution $\chi_l(r)$ with normalisation $n_l = 1/k$ for $r \rightarrow \infty$.

Another equivalent form of the single $\chi\chi$ state enhancement factor S_l derives from (2.43),

$$S_l = ((2l - 1)!!)^2 \frac{|T_l|^2}{k^{2l}}, \quad (2.52)$$

where T_l denotes the normalisation of the irregular solution $\eta_l(r \rightarrow \infty) \rightarrow T_l \exp(-ikr)$, with $\eta_l(r \rightarrow 0) \rightarrow r^{-l}$. T_l can either be determined directly from solving for η_l , or, equivalently, from the $r \rightarrow \infty$ behaviour of the regular solution χ_l (with $\chi_l(r \rightarrow 0) \rightarrow 1/(2l + 1)r^{l+1}$) as given by the relations (2.45) and (2.46).

Unless it happens to be suppressed, the perturbative leading order S -wave $\chi\chi$ annihilation-rate constitutes the dominant contribution to the total annihilation rate of non-relativistic $\chi\chi$ pairs. Consequently the leading order S -wave enhancement associated with $S_{l=0}$ has been studied extensively in the recent literature, while higher partial waves were in first approximation legitimately neglected as higher-order effect (with the perturbative l -wave rate scaling with a factor v^{2l} , with v the non-relativistic velocity of each incoming χ particle). The authors of [29] discuss the case of $l = 0$ wave enhancement for a single $\chi\chi$ state and give the corresponding $S_{l=0}$ factor subject to a regular solutions with $\chi_{l=0}(r \rightarrow \infty) \rightarrow \sin(kr + \delta_l)$, implying $n_{l=0} = 1$ in (2.51). The same expression can be found in [39]. $S_{l=0}$ written in terms of irregular solutions $\rho_{l=0}$ with $\rho_{l=0}(r \rightarrow \infty) \propto \exp(ikr)$ is given in [29] and [40]. The enhancement is said to be $S_{l=0} = |\rho_{l=0}(r \rightarrow \infty)|^2 / |\rho_{l=0}(r = 0)|^2$. This is in agreement with (2.52). First note, that our initial condition on the irregular solution $\eta_{l=0}(r)$, implies $\eta_{l=0}(r = 0) = 1$. Hence (2.52) for $l = 0$ is equivalent to $S_{l=0} = |\eta(r \rightarrow \infty)|^2 / |\eta(r = 0)|^2$. As it should be, any rescaling of the irregular solution $\eta_{l=0}(r) \rightarrow \tilde{c}\eta_{l=0}(r)$ will hence leave the enhancement factor unchanged. From the $r \rightarrow \infty$ behaviour, we obtain $\eta_{l=0}^*(r) \propto \rho_{l=0}(r)$, such that finally the same $l = 0$ enhancement factor expression as given in [29] and [40] results.

Let us conclude with the remark that recent literature on the Sommerfeld enhancement for one-state $\chi\chi$ dark-matter systems focused on Yukawa potential interactions, which in particular applies to the references [29, 39, 40] above. This is of course related to the fact that the dark matter candidate has to be both electric and colour neutral, excluding Coulomb potential interactions from photon or gluon exchange. Assuming the dark-matter candidate together with a mediator – which causes potential interactions in the non-relativistic $\chi\chi$ system – to be part of a dark sector, also here the most general ansatz is to consider a massive mediator giving rise to a Yukawa potential. The enhancement due to a Yukawa potential exhibits additional so called zero-energy resonances, that can lead to even stronger enhancements compared to the Coulomb case. In the next two subsections we will discuss the characteristics of the enhancement from Coulomb and Yukawa potentials in the single $\chi\chi$ -state case.

2.3.1 One-state model with Coulomb potential

$\chi\chi$ scattering in a Coulomb potential is among the few cases that allow to derive an exact analytic expression for the enhancement factors S_l . Let us sketch the steps, familiar from quantum mechanics, that lead to the determination of the regular partial-wave solutions $\chi_l(r)$ to the corresponding radial Schrödinger equation,

$$\frac{d^2}{dr^2} \chi_l(r) = \left(\frac{l(l+1)}{r^2} - m_\chi \frac{\alpha}{r} - k^2 \right) \chi_l(r), \quad (2.53)$$

which finally allow to determine the Coulomb l -wave enhancement factor. Positive (negative) $\alpha = g^2/4\pi$ in (2.53), with g the coupling responsible for the Coulomb potential interaction, refers to the case of an attractive (repulsive) potential. We will apply (2.52), by extracting the constant factor T_l from the asymptotic $r \rightarrow \infty$ behaviour of the regular solutions $\chi_l(r)$ with $\chi_l(r \rightarrow 0) \rightarrow 1/(2l+1)r^{l+1}$. In order to determine $\chi_l(r)$ we make the well-known ansatz

$$\chi_l(r) = c r^{l+1} e^{ikr} \omega_l(r), \quad (2.54)$$

with constant c to be determined such that the above imposed $\chi_l(r \rightarrow 0)$ behaviour is matched. The function $\omega_l(r)$ interpolates between the $r \rightarrow 0$ and $r \rightarrow \infty$ behaviour of the solution $\chi_l(r)$, that is described by the r^{l+1} term and the outgoing spherical wave $\exp(ikr)$, respectively. The resulting differential equation for $\omega_l(r)$ can be written as Kummer differential equation for $w_l(z)$,

$$z \omega_l'' + (2l+2-z) \omega_l'(z) - \left(l+1 - i \frac{m_\chi \alpha}{2k} \right) \omega_l(z) = 0, \quad (2.55)$$

with $z = -2ikr$. The solutions regular at $r = 0$ are the confluent hyper-geometric functions ${}_1F_1(l+1 - im_\chi \alpha/2k, 2l+2, -2ikr)$. Choosing the right $r \rightarrow 0$ normalisation, we find the regular solutions to (2.53) as

$$\chi_l(r) = \frac{1}{2l+1} r^{l+1} e^{ikr} {}_1F_1(l+1 - im_\chi \alpha/2k, 2l+2, -2ikr). \quad (2.56)$$

In order to extract T_l we need the asymptotic $r \rightarrow \infty$ behaviour of the confluent hyper-geometric functions. The latter is found from

$${}_1F_1(a, b, |z| \rightarrow \infty) = \frac{\Gamma(b)}{|\Gamma(a)|} \left(e^{i\eta} (-z)^{-a} + e^{-i\eta+z} z^{a-b} \right), \quad (2.57)$$

with η defined as $\Gamma(a) = e^{i\eta} |\Gamma(a)|$. After some algebraic manipulations, this allows us to obtain

$$\chi_l(r \rightarrow \infty) = \frac{(2l)! e^{-\pi m_\chi \alpha/4k}}{2^l k^{l+1} \Gamma(l+1 - \frac{im_\chi \alpha}{2k})} \sin \left(kr - \frac{l\pi}{2} + \frac{m_\chi \alpha}{2k} \ln(2kr) + \eta \right). \quad (2.58)$$

Hence, following (2.45) with the appropriate replacement of the factor $\exp(ik_j r)$ by $\exp[i(kr + m_\chi \alpha / 2k \ln(2kr))]$ for the Coulomb case,

$$\begin{aligned} U_l(r) &= e^{i(kr + \frac{m_\chi \alpha}{2k} \ln(2kr))} \left(\frac{d}{dr} \chi_l(r) - ik \chi_l(r) \right) \\ &= \frac{i^l e^{i\eta} (2l)! e^{-\pi m_\chi \alpha / 4k}}{2^l k^l \Gamma(l + 1 - \frac{im_\chi \alpha}{2k})} + \mathcal{O}\left(\frac{1}{r}\right), \end{aligned} \quad (2.59)$$

such that for the one-state case we obtain from (2.52), with $T^\dagger = T^* = U^{-1}(r \rightarrow \infty)$,

$$\begin{aligned} S_l &= 2^{2l} \left(\frac{(2l-1)!!}{(2l)!} \right)^2 \left| \Gamma\left(l + 1 - \frac{im_\chi \alpha}{2k}\right) \right|^2 e^{\pi m_\chi \alpha / 2k} \\ &= \frac{\pi \alpha / v}{1 - e^{-\pi \alpha / v}} \prod_{j=1}^l \left(1 + \frac{(\alpha/v)^2}{4j^2} \right). \end{aligned} \quad (2.60)$$

In the last step we have used $\Gamma(x+1) = x\Gamma(x)$, the property $\Gamma(x^*) = \Gamma(x)^*$ and the relation $\Gamma(1+ix)\Gamma(1-ix) = \pi x / \sinh(\pi x)$ for real x . Finally, $k = m_\chi v$ allowed us to express the Coulomb l -wave enhancement factor in terms of the fraction α/v only.

In the limit $v \gg |\alpha|$ we have $S_l \rightarrow 1$ for both the attractive ($\alpha > 0$) and repulsive ($\alpha < 0$) case, as expected. For the attractive case, for very low velocities $v \ll \alpha$, the enhancement factor scales as $S_l \rightarrow \pi(\alpha/v)^{2l+1} / (2^{2l} l!^2)$. In the leading order S -wave ($l = 0$) case we hence recover the familiar $\pi\alpha/v$ behaviour of the Coulomb enhancement for $v/\alpha \ll 1$. Since the perturbative l -wave annihilation rate $\sigma_l^0 v_{\text{rel}}$ has a velocity dependence proportional to v^{2l} , the corresponding Sommerfeld enhanced rate $\sigma_l v_{\text{rel}} = S_l \sigma_l^0 v_{\text{rel}}$ exhibits a $1/v$ velocity dependence for $v/\alpha \rightarrow 0$, which is in particular the same for all l -waves. Higher Sommerfeld enhanced l -wave rates are however suppressed by the constant factor $1/l!^2 (\alpha/2)^{2l}$, that arises in the product $v^{2l} S_l \rightarrow \pi\alpha/v \times 1/l!^2 (\alpha/2)^{2l}$. For $v/\alpha \rightarrow 0$, the enhanced leading order S -wave rate will hence dominate the annihilation and higher l -waves can be safely neglected. As long as moderate velocities are considered, for example $v \sim 1/3$ as around freeze-out of a cold dark-matter candidate, the v^2 proportional perturbative P -wave rate possibly gives corrections to the leading perturbative S -wave rate at the level of some percent. Since in the attractive case the enhancement factor S_l , (2.60), obviously increases with increasing l , P -wave enhancements should consequently be considered in an accurate percent level calculation of annihilation rates, where the particle velocities are of order $\mathcal{O}(0.1)$. This provides us with the motivation to study the effect of Sommerfeld enhancements on neutralino and chargino (co-) annihilation rates including P - and up to $\mathcal{O}(v^2)$ S -wave enhancements in application to the χ_1^0 relic abundance calculation.

To conclude, consider the repulsive case ($\alpha < 0$). In the $v/|\alpha| \rightarrow 0$ limit, we obtain the familiar exponential suppression $S_l \propto \exp(-\pi|\alpha|/v)$, resulting from the need to penetrate the Coulomb barrier. Besides the exponential suppression, the $l > 0$ wave rates will be in addition reduced with respect to the $l = 0$ case by the same constant $1/l!^2 (\alpha/2)^{2l}$ factor as in the attractive case.

2.3.2 One-state model with Yukawa potential

In the case of a Yukawa potential $V(r) = -\alpha \exp(-m_\phi r)/r$, with $\alpha > 0$ ($\alpha < 0$) referring to an attractive (repulsive) interaction, the mediator mass m_ϕ gives an additional parameter in the Schrödinger equation and causes the potential to be short-ranged (in the sense that it vanishes faster for $r \rightarrow \infty$ as $\propto 1/r^{-1}$ due to the exponential suppression factor). We will restrict to the more interesting attractive case $\alpha > 0$ throughout this section, as we are primarily interested in the enhancement rather than the suppression of annihilation rates.¹³ After rescaling the radial coordinate r in the one-state Schrödinger equation by a factor αm_χ , the latter contains the two dimensionless parameters

$$\epsilon_v = \frac{v}{\alpha}, \quad \epsilon_\phi = \frac{m_\phi}{\alpha m_\chi}, \quad (2.61)$$

only. m_χ denotes the common mass of the particles χ , that build up the $\chi\chi$ one-state system under consideration and v is the single-particle velocity in the centre-of-mass frame. From the discussion in Sec. 2.1 we can expect two regions in the $\epsilon_v - \epsilon_\phi$ plane with different characteristics of the enhancement $S_l(\epsilon_v, \epsilon_\phi)$. Considering the momentum-space propagator of the t - or u -channel exchanged mediator in the potential region, $1/(\vec{k}^2 + m_\phi^2) \sim 1/(m_\chi^2 v^2 + m_\phi^2)$, we can neglect the mediator mass as long as $m_\phi \ll m_\chi v$. This condition is equivalent to $\epsilon_\phi \ll \epsilon_v$, and in the corresponding region the enhancement is expected to be Coulomb-like. On the other hand, for $m_\chi v \ll m_\phi$, but still $m_\phi \ll m_\chi$, the potential derived from the mediator exchange becomes constant, leading to a velocity independent enhancement in the region $\epsilon_v \ll \epsilon_\phi$. There is an additional effect in the $\epsilon_v < \epsilon_\phi$ region leading to extra sizable enhancements, that is specific to finite range potentials: the presence of so called “zero-energy resonances”. There exists a finite number of bound states for a finite range potential. By varying the dimensions of such a potential – in case of the one-state Yukawa potential encoded in the parameter ϵ_ϕ – one can arrange for a bound state with zero-energy. If such a zero-energy bound state exists, the scattering of an incoming state with single-particle velocity v close to zero becomes resonant. Such a behaviour, leading to strong resonant enhancements, is familiar from quantum mechanical scattering, for example scattering at an attractive potential well. The resonant enhancement can be already strong, if a loose, but not exactly zero-energy bound state exists in the spectrum of the system.

Although the Schrödinger equation for the Yukawa potential has to be solved numerically, an analytic approximation can be obtained by replacing the Yukawa by the so called Hulthén potential [38]. This allows to get some insight into the enhancement especially in the resonance region. The Hulthén potential shows the same short- and long-distance behaviour as the Yukawa potential and is of the form

$$V_H(r) = -\frac{\alpha \delta e^{-\delta r}}{1 - e^{-\delta r}}. \quad (2.62)$$

¹³As a side-remark note that the case of suppression of annihilation rates due to repulsive potentials will arise in the MSSM application in the double charged sector of $\chi^\pm \chi^\pm$ systems. This effect, though, turns out to play a sub-dominant role in the χ_1^0 relic abundance calculation, which constitutes our major concern in this work.

The parameter δ should be chosen such, that the Yukawa potential case with $V(r) = -\alpha \exp(-m_\phi r)/r$ is mimicked with sufficient accuracy. A convenient criterion fixing δ can be obtained from the Lippmann-Schwinger equations, which determine the radial solutions $R_l(r) = \chi_l(r)/r$ in presence of the Yukawa or Hulthén potential as a series in the corresponding potential interaction. Relying on this criterion, δ is fixed in [38] by the condition that the radial solutions $R_l(r)$ in presence of the Yukawa and Hulthén potential interactions agree to first order in α in the $\epsilon_v \rightarrow 0$ limit. This implies $\int_0^\infty dr r V(r) = \int_0^\infty dr r V_H(r)$ and yields $\delta = \pi^2 m_\phi/6$. The Hulthén approximation to the Yukawa potential case becomes worse for finite kinetic energy ($\epsilon_v > 0$). Yet, as we will see below, imposing the above matching criterion that fits the parameter δ , the analytic Sommerfeld enhancement expression obtained for the Hulthén approximation reproduces the numeric result in the Yukawa case with $\epsilon_v > 0$ within $\sim 10\%$ accuracy. The $l = 0$ enhancement formula derived from [38] and quoted for example in [36, 40] reads

$$S_{l=0}^{\text{Hul}} = \frac{\pi}{\epsilon_v} \frac{\sinh\left(\frac{2\pi\epsilon_v}{\tilde{\epsilon}_\phi}\right)}{\cosh\left(\frac{2\pi\epsilon_v}{\tilde{\epsilon}_\phi}\right) - \cos\left(2\pi\sqrt{\frac{1}{\tilde{\epsilon}_\phi} - \frac{\epsilon_v^2}{\tilde{\epsilon}_\phi^2}}\right)}, \quad (2.63)$$

where we have defined $\tilde{\epsilon}_\phi = \pi^2/6 \epsilon_\phi$. A similar expression for $l > 0$ waves is obtained easily from [38], adding additional factors to the $S_{l=0}^{\text{Hul}}$ term above. As the agreement between this Hulthén potential approximation to the Yukawa case becomes worse for higher partial waves we do not give the expressions here. For a discussion on the poorer agreement see [38]. From (2.63) we can see, that for an attractive potential ($\alpha > 0$) and $\epsilon_v \ll \epsilon_\phi$, resonances arise in the S -wave case if

$$m_\phi = \frac{6\alpha}{\pi^2 n^2} m_\chi, \quad n = 1, 2, \dots \quad (2.64)$$

A similar relation holds for the higher ($l > 0$) partial waves, with n above replaced by $n = l + 1, l + 2, \dots$. This is a specific feature of the Hulthén potential and does in particular not hold for the Yukawa potential case. In the latter case the resonance positions of different l -waves do not coincide.¹⁴ For m_ϕ given by (2.64), the enhancement $S_{l=0}^{\text{Hul}}$ in the small v region is given by

$$S_{l=0}^{\text{Hul}}(\epsilon_v \rightarrow 0, \epsilon_\phi = 6/\pi n^2) \rightarrow \frac{\pi^2 \alpha m_\phi}{6 v^2 m_\chi}, \quad (2.65)$$

hence scaling as v^{-2} , which gives rise to a much stronger enhancement compared to the Coulomb v^{-1} behaviour.¹⁵ Note that despite the resonance positions being shifted in case of the Yukawa potential, the on-resonance v^{-2} scaling in (2.65) also applies to the Yukawa case.

We exemplify the features of the S -wave Sommerfeld enhancement in presence of Yukawa and Hulthén potentials in Fig. 2.3 and Fig. 2.4. The ϵ_v -dependence of the

¹⁴It was argued in [38], that due to the non-coincidence of resonance positions of different l -waves in a Yukawa potential a process could be dominated by a higher than $l = 0$ partial wave, if taking place on a resonance of a $l > 0$ partial wave.

¹⁵The v^{-2} scaling of $S_l(\epsilon_v, \epsilon_\phi)$ at a resonance is generic also for the $l > 0$ partial waves.

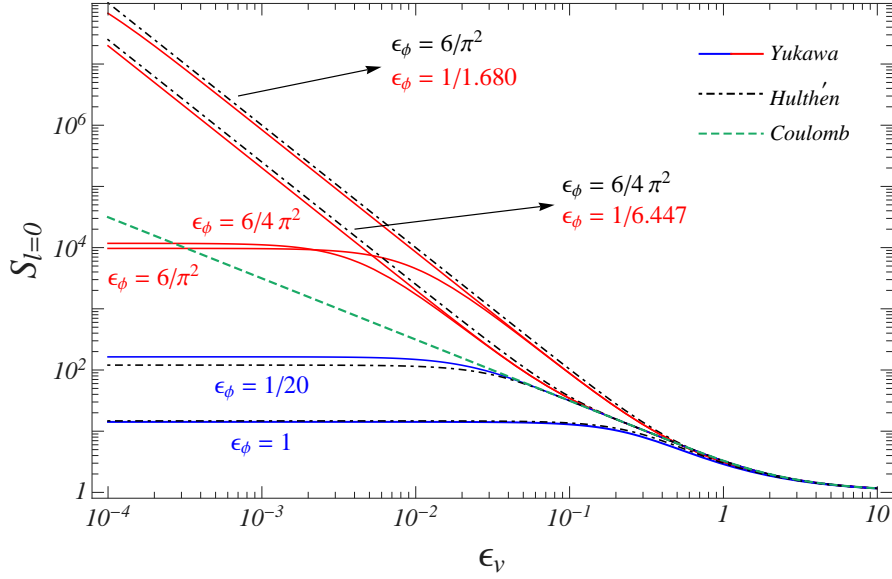


Figure 2.3: The S -wave Sommerfeld enhancement factor as a function of $\epsilon_v = v/\alpha$ for several fixed values of $\epsilon_\phi = m_\phi/(\alpha m_\chi)$. Solid curves refer to a Yukawa model with non-resonant enhancement (two lower-most curves with $\epsilon_\phi = 1, 1/20$) and resonant enhancement due to a zero-energy (two upper-most, $\epsilon_\phi = 1/1.680, 1/6.447$) or loosely (two middle curves, $\epsilon_\phi = 6/4\pi^2, 6/\pi^2$) bound state in the spectrum. Dot-dashed black curves give the enhancement as obtained from the Hulthén potential approximation. The dashed green line represents the Coulomb enhancement behaviour.

enhancement factor $S_{l=0}(\epsilon_v, \epsilon_\phi)$ for selected ϵ_ϕ values is shown in Fig. 2.3. While all solid curves refer to a numeric solution for one-state Yukawa potentials characterised by the corresponding ϵ_ϕ , we show in addition the $l = 0$ enhancement factor as obtained for the Coulomb potential from (2.60) (dashed curve) as well as $S_{l=0}^{\text{Hul}}(\epsilon_v)$ from (2.63) (dot-dashed curves). First note that for $\epsilon_v > \epsilon_\phi$ all Yukawa and Hulthén potential enhancement factors $S_{l=0}(\epsilon_v)$ expectedly follow the Coulomb enhancement behaviour. Around $\epsilon_v \sim \epsilon_\phi$ a transition region is found, that connects to a specific $S_{l=0}(\epsilon_v)$ behaviour for $\epsilon_v < \epsilon_\phi$. Let us first consider the two cases $\epsilon_\phi = 1$ (lowest lying solid/dot-dashed curve) and $\epsilon_\phi = 1/20$ (second-to-lowest lying solid/dot-dashed curve). Here the $\epsilon_v < \epsilon_\phi$ region shows a non-resonant, constant enhancement pattern for both the Yukawa and Hulthén potentials. Such a behaviour was already inferred from the discussion of massive mediator exchange in Sec. 2.1. It is worth to note, that the enhancement saturates and in particular never surpasses the value obtained for the Coulomb case. The analytic Hulthén potential approximation is found to reproduce the numerically obtained enhancement for the Yukawa potential within 10%. The remaining solid curves illustrate the case of resonant enhancements, caused by zero-energy or loose bound states in the spectrum of the corresponding Yukawa π model. The values of ϵ_ϕ for the uppermost solid curve

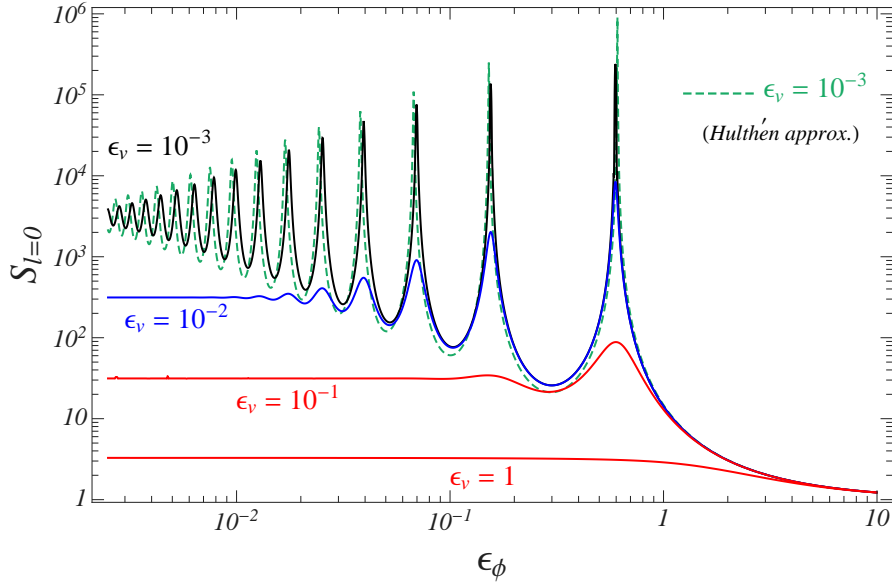


Figure 2.4: The S -wave enhancement factor in a one-state Yukawa model (solid lines) as a function of $\epsilon_\phi = m_\phi/(\alpha m_\chi)$ for selected constant values of $\epsilon_v = v/\alpha$. The dashed curve gives the approximate enhancement factor as obtained from a Hulthén potential with constant $\epsilon_v = 10^{-3}$.

($\epsilon_\phi = 1/1.680$) as well as the second solid curve from above ($\epsilon_\phi = 1/6.447$) are taken from [41] and correspond to the numerically determined first two critical values, that imply the existence of a $l = 0$ zero-energy bound state in the spectrum of the Yukawa model. The corresponding dot-dashed curves, following closely the Yukawa cases, correspond to the $S_{l=0}^{\text{Hul}}$ solutions with $\epsilon_\phi = 6/\pi^2 \approx 1/1.645$ and $\epsilon_\phi = 6/4\pi^2 \approx 1/6.580$, respectively. The latter correspond to the first two ϵ_ϕ values that are associated with a zero energy bound state in the Hulthén potential, see (2.64). The Hulthén approximation hence predicts the ϵ_ϕ associated with zero-energy resonances within an accuracy of 2% in both cases considered here. The two solid curves with $\epsilon_\phi = 6/\pi^2$ and $\epsilon_\phi = 6/4\pi^2$ that follow the above-discussed Yukawa-potential resonance curves for $\epsilon_v > 3 \cdot 10^{-2}$, but approach a constant enhancement for smaller values of ϵ_v correspond to Yukawa potentials with loose but not exactly zero-energy bound states. The fact that the enhancement factors for these two cases approach values $S_{l=0}(\epsilon_v \rightarrow 0)$ of the same order of magnitude is purely accidental. Generically, small variation of ϵ_ϕ around a resonance value, implying the presence of a loosely-bound state, will give rise to significantly different constant values $S_{l=0}(\epsilon_v \rightarrow 0)$. As can be seen from Fig. 2.3, the presence of loosely-bound states can lead to enhancements, that are several orders of magnitude stronger as compared to the non-resonant case. Depending on the considered value of the velocity it can even be stronger than in the Coulomb case, as a consequence of the v^{-2} proportionality of the resonant enhancement. This latter v^{-2} scaling-behaviour holds for the loosely-

bound states in the $\epsilon_v < \epsilon_\phi$ regime as long as the kinetic energy of the scattering state is significantly larger compared to the loosely-bound state's binding energy; the latter state can then be effectively considered as zero-energy bound state. Finally note that despite the formal v^{-2} divergence of the resonant enhancement (2.65) as $v \rightarrow 0$, the physical enhancement is finite on resonance due to the finite width of the zero-energy two-particle bound state. The latter width is however not taken into account in the quantum mechanical treatment of the scattering process that we have applied here.

The $l = 0$ wave enhancement factor for a Yukawa-model as a function of ϵ_ϕ is shown in Fig. 2.4, where we have fixed $\epsilon_v = 1, 10^{-1}, 10^{-2}, 10^{-3}$. The emergence of resonances for $\epsilon_\phi > \epsilon_v$ at specific ϵ_ϕ values is apparent. The first two resonance positions are found at $\epsilon_\phi = 1/1.680$ and $1/6.447$ in agreement with [41]. For $\epsilon_\phi < \epsilon_v$, resonances are expectedly absent in Fig. 2.4 and with further decreasing ϵ_ϕ the enhancement factor matches the Coulomb one for the corresponding ϵ_v value. For comparison, the enhancement factor as obtained for a Hulthén potential with $\epsilon_v = 10^{-3}$ is shown in addition (dashed curve). While the approximation agrees with the Yukawa case at the level of a few percent around the first resonances, we find, that it reproduces the latter at the 10% level only for smaller ϵ_ϕ values, in agreement with the results in [38, 40].

2.4 A two-state model with off-diagonal interactions

The next straightforward step in increasing the complexity of our toy-models implies considering more two-particle states $(\chi\chi)_I$. Another direction would be to change the number of potentials in the one-state case, allowing several mediators with different masses as well as different coupling strength to the constituents of the single $\chi\chi$ pair. Such kind of investigations have been carried out in [42] or [43]. We pursue the first option and consider the case of a two-state system with states $(\chi\chi)_I$, $I = 1, 2$, that take part in purely off-diagonal potential interactions through exchange of one single massive mediator with mass m_ϕ . The two states shall exhibit a small mass difference, $\delta M_2 = M_2 - M_1 > 0$, where M_I denotes the mass of the state $(\chi\chi)_I$. A very comprehensive study of the enhancements arising for the lighter two-particle state $(\chi\chi)_1$ in such an inelastic two-state model, including approximate analytic formulae, can be found in [36]. Here we will present results for the Sommerfeld enhancement obtained from numerically solving the Schrödinger equation for the coupled two-state system, highlighting the qualitative features of the enhancement. For an elaborate discussion including approximate analytical results the reader is referred to [36].

We assume that written in the mass-eigenstate basis of the two two-particle states $(\chi\chi)_1, (\chi\chi)_2$, the potential matrix $V(r)$ has the following form,

$$V(r) = \begin{pmatrix} 0 & -\frac{\alpha}{r} e^{-m_\phi r} \\ -\frac{\alpha}{r} e^{-m_\phi r} & \delta M_2 \end{pmatrix}. \quad (2.66)$$

It is convenient to use the dimensionless quantities $\epsilon_v = v/\alpha$ and $\epsilon_\phi = m_\phi/\alpha m_\chi$, as given in (2.61). m_χ denotes twice the reduced mass of the lighter state $(\chi\chi)_1$. (In

most applications m_χ is hence the mass of the single-particle constituents in $(\chi\chi)_1$.) In addition we introduce the new parameter $\epsilon_\delta = \sqrt{\delta M_2/\alpha^2 m_\chi}$, associated with the mass splitting in the two-state system.

The potential matrix (2.66) in this purely inelastic two-state system resembles the leading order 1S_0 -wave potential in the neutral sector of pair-annihilating wino-like χ_1^0 dark-matter. The latter neutral sector features the two nearly mass-degenerate two-particle states $\chi_1^0\chi_1^0, \chi_1^+\chi_1^-$. Off-diagonal potential scattering $\chi_1^0\chi_1^0 \rightarrow \chi_1^+\chi_1^-$ and $\chi_1^+\chi_1^- \rightarrow \chi_1^0\chi_1^0$ is mediated by W -exchange. For heavy χ_1^0, χ_1^\pm particles, $m_\chi \sim \mathcal{O}(\text{TeV})$, the mass splitting between the neutral two-particle states in the decoupling limit is given by $\delta M_2^{\text{wino}} \sim 300 \text{ MeV}$, independent of the wino-masses (as well as of the (decoupled) residual SUSY spectrum). The features of gaugino- as well as higgsino-like χ_1^0 dark-matter, including mass splittings, will be discussed in detail in later chapters. For the time being note that purely off-diagonal potential scattering generically arises for two-particle states built from one single Majorana fermion state (as for example the $\chi_i^0\chi_i^0$ states in the MSSM), if the potential interactions are mediated by gauge bosons; Majorana fermions cannot carry conserved charges, implying purely off-diagonal potential $(\chi\chi)_I \rightarrow (\chi\chi)_{J \neq I}$ scattering reactions to accessible nearly mass-degenerate states $(\chi\chi)_{J \neq I}$. In that sense the ansatz (2.66) for the potential interactions is generic for a two $\chi\chi$ -state system, with the lighter state, $(\chi\chi)_1$, built from a Majorana dark-matter candidate. The above reasoning pertaining to purely off-diagonal potential scattering does however not apply to $(\chi\chi)_I$ states built from Dirac fermions, as for example $\chi_1^+\chi_1^-$ in the system of neutral wino-states. The major difference between (2.66) and the 1S_0 potential interactions in the neutral sector of pair-annihilating non-relativistic winos is hence the fact, that the $\chi_1^+\chi_1^-$ state allows for diagonal potential interactions mediated by photon- and Z -exchange. These potentials will then appear in the $(2, 2)$ component of the corresponding potential matrix, in addition to the mass splitting δM_2 as in (2.66).

In the generic case, there exists no r -independent diagonalisation of the two-state Schrödinger equation over the complete range of r , given the potential matrix $V(r)$ in (2.66). Depending on the actual magnitude of the parameters ϵ_ϕ and ϵ_δ , there will be two regions, where the potential interaction $-\alpha/r \exp(-m_\phi r)$ dominates over the mass splitting and vice versa, separated by a transition region, where both the interaction and the mass splitting are of the same order.

It is instructive to first consider in a bit more detail the leading order S -wave Sommerfeld enhancement for both states $(\chi\chi)_{I=1,2}$ in case of vanishing mass splitting, $\epsilon_\delta = 0$, as in this case an r -independent diagonalisation of the two-state Schrödinger equation is possible and we can in addition gain some insight into the relevance of off-diagonal annihilation rates in the determination of S_l^I . Let us rewrite the Schrödinger equation for the matrix valued function $\chi_l(r)$ in the following form

$$\frac{d^2}{dx^2} \chi_l(x) = \begin{pmatrix} \frac{l(l+1)}{x^2} - \epsilon_v^2 & -\frac{e^{-\epsilon_\phi x}}{x} \\ -\frac{e^{-\epsilon_\phi x}}{x} & \frac{l(l+1)}{x^2} - \epsilon_v^2 + \epsilon_\delta^2 \end{pmatrix} \chi_l(x), \quad (2.67)$$

where we have introduced the rescaled radial coordinate $x = \alpha m_\chi r$, and ϵ_δ should

be set to 0 for the time being. The eigenvalues and the corresponding r -independent eigenvectors of the matrix multiplying $\chi_l(x)$ on the r.h.s. in (2.67) read

$$\lambda_l^\pm = \frac{l(l+1)}{x^2} - \epsilon_v^2 \pm \frac{\alpha e^{-\epsilon x}}{x}, \quad \psi^\pm = \frac{1}{\sqrt{2}} \begin{pmatrix} \mp 1 \\ 1 \end{pmatrix}. \quad (2.68)$$

In order to determine the l -wave Sommerfeld enhancement in annihilation reactions of incoming states $(\chi\chi)_{I=1,2}$ via (2.43), we have to determine the asymptotic $x \rightarrow \infty$ behaviour of the irregular solutions encoded in the matrix valued function $\eta_l(x)$, subject to the initial condition $\eta_{l=0,II}(x \rightarrow 0) \rightarrow \delta_{II} x^{-l}$. In the S -wave case, in particular, $\eta_{l=0}(x)$ can be obtained from

$$\eta_{l=0}(x) = \frac{1}{2} \begin{pmatrix} \phi^-(x) + \phi^+(x) & \phi^-(x) - \phi^+(x) \\ \phi^-(x) - \phi^+(x) & \phi^-(x) + \phi^+(x) \end{pmatrix}, \quad (2.69)$$

where $\phi^\pm(x)$ denote scalar (irregular) wave-functions, solving $d^2/dx^2 \phi^\pm(x) = \lambda_{l=0}^\pm \phi^\pm(x)$, subject to the initial conditions $\phi^\pm(x=0) = 1$. The columns of $\eta_{l=0}(x)$ above then encode those suitable linear combinations of the basis solutions $\phi^\pm(x) \psi^\pm$ to (2.67), that ensure the correct $\eta_{l=0}(x=0) = \mathbf{1}$ behaviour. It is important to note, that $\phi^+(x)$ is a solution to a single channel Schrödinger equation with repulsive Yukawa potential interaction, while $\phi^-(x)$ denotes a solution to a single channel Schrödinger equation with attractive Yukawa potential, see the λ_l^\pm expressions in (2.68). As for the time being we have imposed zero mass splitting, $\epsilon_\delta = 0$, in our toy-model, the parameters k_I , (2.16), are both given by $k_{I=1,2} = m_\chi v$. Hence we encounter just a global phase factor $\exp(-i\epsilon_v x)$ in the asymptotic behaviour $\eta_{l=0,II}(x \rightarrow \infty) \rightarrow e^{-i\epsilon_v x} T_{l=0,II}$.¹⁶ The latter phase will in particular cancel when building $S_{l=0}$. In the $\epsilon_\delta = 0$ case, the S -wave enhancement in our two-state toy-model can hence be determined from

$$S_{l=0}^I = \frac{\left[\eta_{l=0}(\infty) \cdot \Gamma_{l=0} \cdot \eta_{l=0}^\dagger(\infty) \right]_{II}}{\Gamma_{l=0,II}}, \quad (2.70)$$

with $\eta_{l=0}(\infty)$ obtained from (2.69). The generalisation of this expression to the $l > 0$ case by an appropriate rescaling of (2.70) by the factor $((2l-1)!!)^2/k^{2l}$ (see (2.43)) and the substitution of $\eta_{l=0}(x)$ by the suitably determined $\eta_{l>0}(x)$ in analogy to (2.69) is straightforward.

In the final step we have to specify the annihilation matrix $\Gamma_{l=0}$ in (2.70). Let us first consider the case, where $\Gamma_{l=0}$ is given by a 2×2 matrix with all entries being identical. The overall normalisation of the annihilation matrix cancels when building the ratio of

¹⁶The asymptotic form $\eta_{l=0,II}(x \rightarrow \infty) \rightarrow e^{-i\epsilon_v x} T_{l=0,II}$ with outgoing spherical wave $\exp(-i\epsilon_v x)$ applies to the matrix-valued irregular solution $\eta_{l=0}(x)$ considered as a function of the rescaled coordinate $x = \alpha m_\chi r$: note $kr = \epsilon_v x$. The constant normalisation coefficients $T_{l=0,II}$ are unchanged under the rescaling of the radial coordinate.

the enhanced to the tree-level rate as encoded in the ($l = 0$ wave) Sommerfeld factor (2.70), and we find for both mass-degenerate states $(\chi\chi)_{I=1,2}$

$$S_{l=0}^{I=1,2} = |\phi^-(\infty)|^2. \quad (2.71)$$

Recall that $\phi^-(x)$ corresponds to the irregular single $(\chi\chi)$ -state $l = 0$ scattering wavefunction for an attractive Yukawa potential ($V(r) = -\alpha/r \exp(-m_\phi r)$), with appropriate normalisation $\phi^-(x \rightarrow 0) \rightarrow 1$. Consequently, (2.71) just gives the ordinary single $\chi\chi$ -state S -wave Sommerfeld enhancement, see the introduction to Sec. 2.3. The enhancement of both the $(\chi\chi)_{I=1,2}$ annihilation rates is hence simply described by the enhancement discussed in Sec. 2.3.2. Neglecting the presence of off-diagonal annihilation rates encoded in the off-diagonal entries of $\Gamma_{l=0}$ and accordingly choosing $\Gamma_{l=0} \propto \mathbf{1}$ in our toy-scenario, the result for the S -wave enhancement would instead be

$$S_{l=0}^{I=1,2} (\Gamma \propto \mathbf{1}) = \frac{1}{2} \left(|\phi^-(\infty)|^2 + |\phi^+(\infty)|^2 \right). \quad (2.72)$$

Thus the result is given by one half the enhancement factor for the (single $\chi\chi$ state) attractive Yukawa potential case summed with one half the suppression factor obtained for the corresponding repulsive Yukawa potential case. The latter suppression factor will range between 0 and 1, such that in any case the S -wave enhancement $S_{l=0}^{I=1,2}$ would be underestimated when neglecting off-diagonal rates, (2.72) as opposed to the actual ‘full’ result (2.71). For sufficiently large enhancements ($|\phi^-(\infty)|^2 \gg 1$) in particular, (2.72) strongly underestimates the actual enhancement, the maximal error being a factor of deviation $\lesssim 2$. This is illustrated in the left-hand plot of Fig. 2.5, where the enhancement factors calculated from (2.71) (solid curves) and obtained from (2.72) (dotted curves), for two different choices of ϵ_ϕ are shown. Note for comparison, that the solid curves have already been presented, among others, in Fig. 2.3.

Once the annihilation matrix entries $\Gamma_{l=0, JJ'}$ come with different weights, the enhancement factors $S_{l=0}^I$ for the mass-degenerate states $(\chi\chi)_{I=1,2}$ will obviously no longer coincide. In such a generic case, the enhancements $S_{l=0}^{I=1,2}$ can be generally expressed in terms of linear combinations of products of the attractive and repulsive potential’s solutions $\phi^\pm(\infty)$. For example, let us consider

$$\Gamma_{l=0} \propto \begin{pmatrix} 1 & 2 \\ 2 & 4 \end{pmatrix}, \quad (2.73)$$

implying that the $(\chi\chi)_1$ state has a four times smaller tree-level annihilation rate compared to $(\chi\chi)_2$. For the S -wave enhancements we obtain in this case

$$S_{l=0}^{I=1} = \frac{1}{4} |3\phi^-(\infty) - \phi^+(\infty)|^2, \quad S_{l=0}^{I=2} = \frac{1}{16} |3\phi^-(\infty) + \phi^+(\infty)|^2. \quad (2.74)$$

The enhancement for $(\chi\chi)_1$ will hence always be larger than in case (2.71), where all $\Gamma_{l=0}$ entries were assumed to be identical. The reverse statement applies to $(\chi\chi)_2$: the

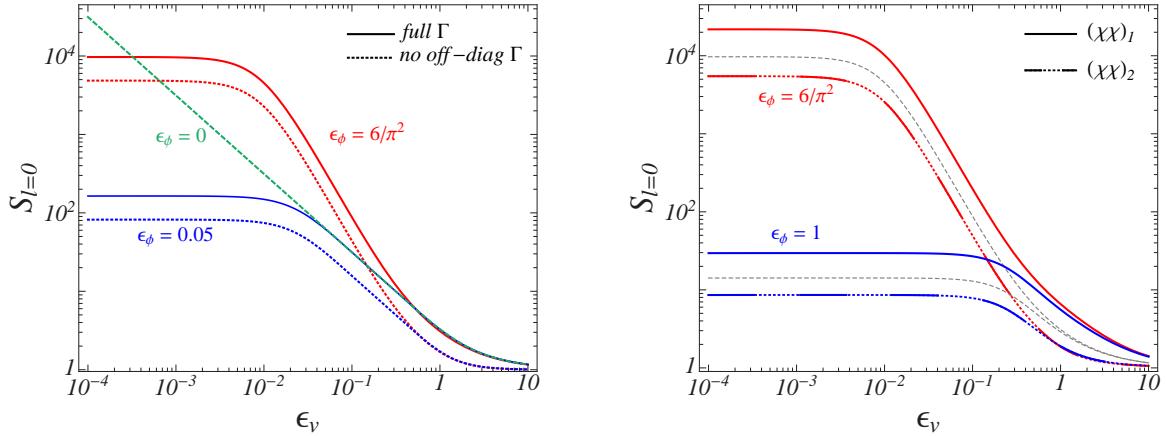


Figure 2.5: *Left plot*: Examples for the effect of neglecting off-diagonal entries in the annihilation matrices. The S -wave enhancement in the $\epsilon_\delta = 0$ case for matrices $\Gamma_{l=0}$ with all entries being identical (solid lines) is compared to the case, where the off-diagonal entries of $\Gamma_{l=0}$ are neglected (dotted curves). Enhancements are the same for both states $(\chi\chi)_{I=1,2}$. Apart from the results obtained for $\epsilon_\phi = 0.05$ (lower two (blue) curves) and the close-to-(first) resonance case $\epsilon_\phi = 6/\pi^2$ (upper two (red) curves), the enhancement for Coulomb potential interactions ($\epsilon_\phi = 0$) taking the full $\Gamma_{l=0}$ into account is shown in addition. Also see Fig. 2.3. *Right plot*: S -wave enhancement for the mass-degenerate states $(\chi\chi)_1$ (solid lines) and $(\chi\chi)_2$ (dot-dashed curves) in case of annihilation matrix $\Gamma_{l=0}$ given in (2.73). The lower (blue) curves refer to $\epsilon_\phi = 1$, the upper (red) to $\epsilon_\phi = 6/\pi^2$. As a reference, the corresponding enhancements obtained for matrices $\Gamma_{l=0}$ with identical entries are given by the dashed (grey) lines lying in between the curves for $(\chi\chi)_I$ and $(\chi\chi)_2$, respectively.

enhancement given in (2.74) is (slightly) smaller compared to (2.71). For sample values of ϵ_ϕ this is illustrated in the right-hand plot of Fig. 2.5.

The actual expressions for both potential and annihilation matrices depend on the interactions in the underlying model and have to be determined in a matching procedure from the full (high-energy) theory, which for the case of the χ^0/χ^\pm sector in the MSSM is the subject of later chapters. Here it is worth to note, that given the potential matrix (2.66) even with in general non-vanishing ϵ_δ , the assumption of an annihilation matrix Γ_l with all entries being identical is in fact the most consistent choice, if only gauge interactions causing both potential scattering and annihilation reactions are assumed, and both states $(\chi\chi)_{I=1,2}$ are built from Majorana fermions. This statement will be confirmed when discussing potential scattering and annihilation reactions in the sub-sector of the two neutral higgsino two-particle states $\chi_1^0\chi_1^0$ and $\chi_2^0\chi_2^0$. Note however, that the neutral sector of higgsino-type two-particle states $(\chi\chi)_I$ consists in total of four nearly mass degenerate states, such that the results in our two-state toy-model cannot be directly related to the neutral higgsino-sector.

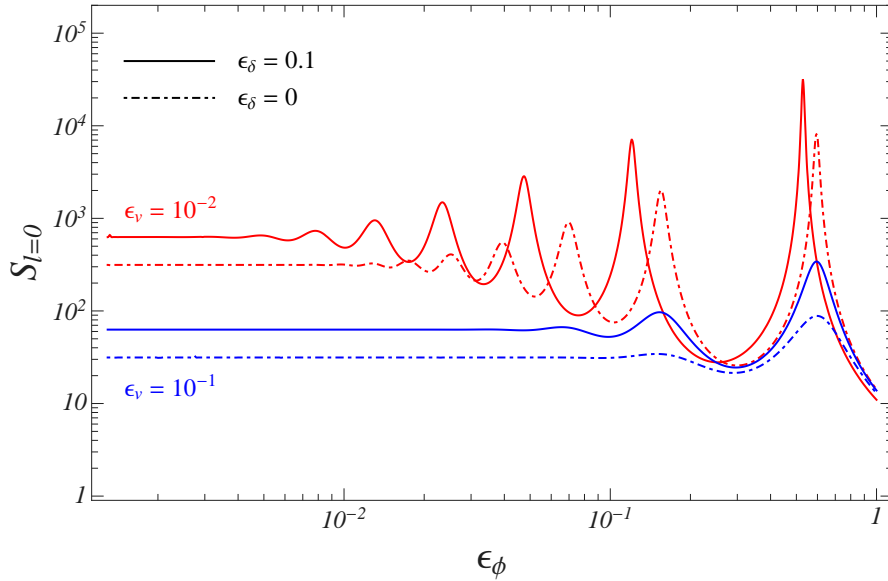


Figure 2.6: S -wave enhancement of the (lighter) $(\chi\chi)_1$ state in the two-state toy-model discussed in the text as a function of ϵ_ϕ . Solid lines refer to a finite mass splitting between the lighter and heavier state $(\chi\chi)_{I=1,2}$ with $\epsilon_\delta = 0.1$. Dot-dashed curves give the $\epsilon_\delta = 0$ case familiar from Fig. 2.4. The two upper (red) curves correspond to $\epsilon_v = 10^{-2}$, while the two lower (blue) curves refer to $\epsilon_v = 10^{-1}$.

Let us now consider the two-state toy-model with finite ϵ_δ . As regards the annihilation part, we choose a matrix Γ_l with all entries being identical, which agrees with the situation considered as application in [36] after the derivation of generically applicable analytic approximate formulae. Fig. 2.6 exemplifies the behaviour of the S -wave enhancement for the lighter $(\chi\chi)_1$ state as a function of the parameter ϵ_ϕ for two different choices of the velocity, for the case of vanishing mass splitting $\epsilon_\delta = 0$ as well as $\epsilon_\delta = 0.1$. The two lower (blue) curves give the case of $\epsilon_v = 0.1$, the upper two (red) refer to $\epsilon_v = 0.01$. First consider the case of the upper two curves. Here the uppermost solid line represents the case $\epsilon_v = 0.01$ and $\epsilon_\delta = 0.1$, hence referring to a situation below the excitation threshold for the second state $(\chi\chi)_2$. The next lower lying dot-dashed curve refers to the familiar $\epsilon_\delta = 0$ situation. In this latter case, for $\epsilon_\phi < \epsilon_v$, we are in the non-resonant enhancement region, and $S_{l=0}$ saturates at the Coulomb-enhancement value $S_{l=0} = \pi/\epsilon_v$, as already seen in Fig. 2.4. Such a saturation in the $\epsilon_\phi < \epsilon_v$ regime is also observed for the uppermost curve, while here the enhancement (corresponding to the below-threshold case, as $\epsilon_v \ll \epsilon_\delta$) is found to be roughly two times larger, $S_{l=0} \approx 2\pi/\epsilon_v$. This is in agreement with the findings in [36], where an increase of the non-resonant enhancement in the below-threshold case by a factor of about two has also been derived directly from the analytic approximation. Now let us come to the region of resonant enhancement, still referring to the upper two curves with $\epsilon_v = 0.01$. It can be seen from

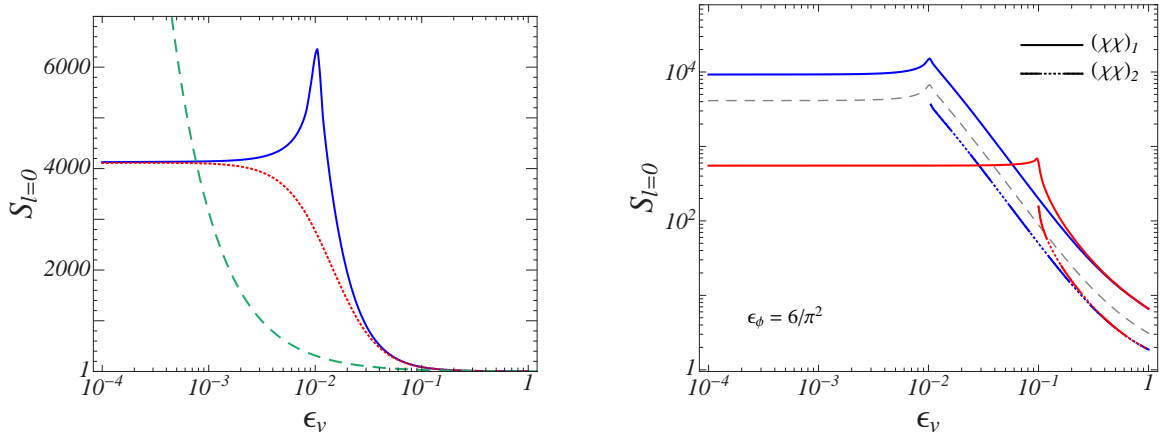


Figure 2.7: *Left plot*: Example for the possible behaviour $S_{l=0}^{I=1}(\epsilon_v)$ around the threshold region for on-shell excitation of the heavier $(\chi\chi)_2$ state. The solid (blue) curve gives the behaviour for $\epsilon_\delta = 0.01$ and $\epsilon_\phi = 6/\pi^2$. The dotted (red) curve gives a corresponding behaviour for zero mass-splitting ($\epsilon_\delta = 0$) and $\epsilon_\phi = 0.61474$, with the same asymptotics for ϵ_v far below and above the threshold region. For comparison, the Coulomb enhancement for zero mass-splitting is shown in addition (dashed, green curve). The results have been obtained for $\Gamma_{l=0}$ with all entries identical. *Right plot*: Enhancements as a function of ϵ_v for both states, given an annihilation matrix of the form (2.73) and $\epsilon_\phi = 6/\pi^2$. $\epsilon_\delta = 0.01$ (upper, blue curves) and $\epsilon_\delta = 0.1$ (lower, red curves) have been chosen. The solid (dot-dashed) curves correspond to the lighter (heavier) $(\chi\chi)_I$ state. For comparison, the dashed (grey) curve illustrates the case of $\Gamma_{l=0}$ with identical entries and $\epsilon_\delta = 0.01$, $\epsilon_\phi = 6/\pi^2$. Above threshold, in the latter case, the enhancement of the $(\chi\chi)_2$ state agrees with the $(\chi\chi)_1$ state's enhancement.

Fig. 2.6 that the position of the resonances in ϵ_ϕ for finite ϵ_δ is shifted downwards to smaller values with respect to the $\epsilon_\delta = 0$ case. Furthermore, the smaller the resonant ϵ_ϕ value, the larger the downwards shift relative to the resonance position. Moreover, the height of each resonance turns out to be larger by a factor of about four in the below-threshold $\epsilon_\delta = 0.1$ situation compared to the corresponding $\epsilon_\delta = 0$ case. Again, in [36], both these observations are correctly predicted from the analytic results. The two lower (blue) curves in Fig. 2.6 correspond to $\epsilon_v = 0.1$ and $\epsilon_\delta = 0.1$ (upper solid line) – directly at threshold for on-shell production of the heavier state $(\chi\chi)_2$ – as well as the zero mass-splitting case (lowermost, dot-dashed curve). In the regime of non-resonant enhancement $S_{l=0}(\epsilon_v = \epsilon_\delta)$ is found to be about two times larger than the corresponding value π/ϵ_v for $\epsilon_\delta = 0$. Contrary to the previously discussed below threshold case, however, here we do not observe any significant shift of the resonance positions in ϵ_ϕ compared to the $\epsilon_\delta = 0$ situation.

To close the discussion of the two-state toy-model, the left plot in Fig. 2.7 shows the enhancement of the lighter state $(\chi\chi)_1$ as a function of ϵ_v for $\epsilon_\delta = 0.01$ and $\epsilon_\phi = 6/\pi^2$

(≈ 0.607927) (solid, blue curve) and $\epsilon_\delta = 0$, $\epsilon_\phi = 0.614747$ (dotted, red curve). In the $\epsilon_\delta > 0$ case, $S_{l=0}^{I=1}$ is a non-monotonic function of ϵ_v , showing a ‘spike’ at threshold for on-shell production of $(\chi\chi)_2$. This behaviour is a threshold effect, which occurs here on top of resonant enhancement due to a loosely-bound state in the spectrum of the theory. The purely resonant enhancement in the $\epsilon_\delta = 0$ case is illustrated by the dotted (red) curve. The chosen ϵ_ϕ values for both curves are slightly different, reflecting the fact that resonance positions are shifted downwards for finite ϵ_δ values. For comparison and to highlight the fact, that the ϵ_ϕ values are associated with resonant enhancement, the dashed (green) curve gives the Coulomb enhancement in the case of zero mass-splitting. As regards the $\epsilon_\delta > 0$ case, the enhancement around threshold is found to be less than twice as large as the saturated enhancement for $\epsilon_v \rightarrow 0$; see [36] for an analytic estimate of this factor. It is argued in [36] that in any case the ratio of $S(\epsilon_v = \epsilon_\delta)/S(\epsilon_v = 0)$ should be bounded by two from above.

In the right-hand plot of Fig. 2.7 we show the enhancement factors for both states $(\chi\chi)_{I=1,2}$ for an annihilation-matrix with non-identical entries of the form (2.73). Although the annihilation rate of the heavier state is a factor of four larger than the corresponding rate of the lighter state, the enhancements of the former state are found to be a factor of about four smaller compared to $(\chi\chi)_1$. For comparison, the enhancement for an annihilation matrix with all entries identical and fixing $\epsilon_\delta = 0.01$, $\epsilon_\phi = 6/\pi^2$ is shown in addition (dashed, grey curve). In the latter case, $S_{l=0}^{I=1}(\epsilon_v)$ is found to agree with $S_{l=0}^{I=2}(\epsilon_v)$ above threshold.

Chapter 3

Relic abundance calculation

In this chapter we present the formalism needed for the determination of the relic abundance of a weakly interacting massive particle χ_1 . We start with a brief qualitative discussion of the phenomenon of freeze-out of the χ_1 's annihilation reactions in course of the Universe's expansion in Sec. 3.1. The description is subsequently quantified by introducing an (integrated) form of the Boltzmann equation, appropriate to describe the evolution of particle number densities in the expanding Universe. In Sec. 3.2 the setting is generalised to include the case of co-annihilations of several nearly mass degenerate species $\chi_i, i=1, \dots, N$. In addition a convenient form of the Boltzmann equation is derived that treats the decrease of the number densities due to the expansion of the Universe implicitly. A single-integral formula for the thermally averaged annihilation rate $\langle \sigma_{\text{eff}} v \rangle$ that enters the Boltzmann equation as central ingredient is finally given in Sec. 3.3. The formula involves the individual annihilation rates $\sigma_{ij}v$ of all co-annihilating pairs $\chi_i\chi_j$. In Chapters 6 – 8 we determine explicit expressions for the rates $\sigma_{ij}v$ in χ^0/χ^\pm co-annihilations including Sommerfeld enhancements. On the one hand this chapter is therefore a self-contained short review of the dark matter relic abundance calculation. On the other hand all necessary formulae are provided that allow a direct calculation of the χ_1^0 relic abundance including Sommerfeld enhancements, provided the (Sommerfeld-enhanced) rates $\sigma_{ij}v$ are known.

3.1 The Boltzmann equation

The standard explanation for the origin of a particle species in our present Universe starts from the assumption of its thermal production in the very early Universe. This implies that in these early times the species should have been in both chemical and kinetic equilibrium with the further particle constituents of the early Universe's thermal plasma. Such equilibrium state requires rapid annihilation and creation processes of the particle species as well as effective scattering reactions with the further particles present. Note that in general, in this picture, the early Universe's thermal plasma is assumed to be constituted by the particle species of the Standard Model as well as possibly additional species occurring in extensions of the SM. The expansion of the

Universe, which can conveniently be associated with the expansion rate given by the Hubble parameter H ($H(t) = \frac{d}{dt}R(t)/R(t)$, where $R(t)$ denotes the scale factor as a function of time), runs contrary to the processes that allow the maintenance of thermal equilibrium: it dilutes the actual number densities of the species. As a consequence interaction processes will become rare, finally leading to the fact that – depending on the strength of the interaction rates – a certain species will no longer stay in equilibrium with the others. Its annihilation and creation reactions stop more or less suddenly (“freeze out”) such that its particle number eventually stays constant (“freezes in”), giving rise to the thermal relic abundance observable today.¹ As a very rough criterion this happens when the Universe’s expansion rate H starts to dominate over the total annihilation rate Γ of the species, $H \gtrsim \Gamma$. Depending on the average thermal velocity of the species during freeze-out, non-relativistic ($v \ll 1$) or (semi-)relativistic ($v \lesssim 1$), one distinguishes cold or warm/hot thermal dark matter. The neutralino dark matter candidate χ_1^0 that we consider in this work is a cold thermal dark matter candidate; its freeze-out should have occurred for thermal bath temperatures around $T \sim m_{\chi_1^0}/20$. Therefore we focus here on the case of heavy cold dark matter candidates.

The first quantitative studies of the freeze-out process of a heavy particle species focused on a possible heavy neutrino relic. They were performed in the late 1970s by Lee and Weinberg [44] as well as independently by other authors and led to a lower bound on the mass of a heavy neutrino species, today referred to as the “Lee-Weinberg bound”. Since that time the theoretical description, relying on Boltzmann equations for the particle number densities in the expanding Universe, has been subsequently refined. Both improved analytical approximations and numerical solution methods have been applied [45–47] and a consistent treatment of co-annihilations in the (roughly) simultaneous freeze-out process of several (nearly) mass-degenerate heavy species has been given [48]. In addition the case of resonant annihilation reactions has been addressed [48] and the annihilation rates entering the Boltzmann equations of the non-relativistic particles can be consistently calculated including relativistic corrections, beyond the strict non-relativistic approximation [49]. Regarding the solution of the Boltzmann equation and the necessary input related to the thermodynamics in the expanding Universe, the determination of the thermal relic abundance of a particle species, which represents a viable dark matter candidate, has become a standard calculation. It is implemented in several computer codes, such as `DarkSUSY` [5] and `micrOMEGAS` [6]. The dominant uncertainties in the determination of the final abundance are currently associated with the annihilation rates entering the Boltzmann equations. These rates are an input from the particle physics model that provides the respective particle dark matter candidate. While the publicly available codes currently rely on tree-level annihilation rates, we aim

¹In the Universe today annihilation reactions of a species that underwent freeze-out in earlier times can start again. This may happen if due to gravitational attraction regions with a high number density of the particular species have formed, such as for example in the halo of galaxies, in galactic centres or possibly also in the Sun. If the particle dark matter hypothesis is true, dark matter pair-annihilation reactions should occur in these regions, giving rise to indirect detection signals in terms of cosmic rays or gamma ray lines. For an introduction to indirect dark matter searches see for example [3, 4].

to study the impact of Sommerfeld-enhanced cross sections on the predicted relic abundance. To this end we have developed a code that allows for the determination of the χ_1^0 dark matter relic abundance including Sommerfeld enhancements. We come back to the calculation of the rates in later chapters and proceed in this section with the derivation of the relevant generic formulae needed in the relic abundance determination. Our following discussion is mainly based on the textbook [50] as well as on the articles [3] and the more recent [4], which provide a nice review of the freeze-out of weakly interacting massive particles.

The Boltzmann equation describes the evolution of the phase space distribution $f(p^\mu, x^\mu)$ of a particle species and can be expressed as

$$\hat{\mathbf{L}}[f(p^\mu, x^\mu)] = \hat{\mathbf{C}}[f(p^\mu, x^\mu)] . \quad (3.1)$$

Let us in particular refer to the distribution function and corresponding Boltzmann equation of particle species χ_1 in the following. In the expanding Universe the left-hand side of (3.1) contains the covariant relativistic form of the Liouville operator acting on $f(p^\mu, x^\mu)$. The right-hand side is the collision term associated with all particle scatterings as well as annihilation or creation reactions, that change the distribution function $f(p^\mu, x^\mu)$ of species χ_1 . Under the assumption of a homogeneous and isotropic Universe described by the Friedman-Robertson-Walker metric, any phase space distribution function depends only on time and energy, $f(E = p^0, t)$, and the Liouville operator becomes

$$\hat{\mathbf{L}}[f(E, t)] = E \frac{\partial}{\partial t} f(E, t) - H(t) \vec{p}^2 \frac{\partial}{\partial E} f(E, t) . \quad (3.2)$$

$H(t)$ denotes the Hubble parameter. Instead of $f(E, t)$, we will be interested in the evolution of the particle number density

$$n(t) = g \int \frac{d^3 \vec{p}}{(2\pi)^3} f(E, t) , \quad (3.3)$$

with g the particle's internal (spin) degree of freedom. Dividing the Boltzmann equation by E and integrating over the three-momentum finally leads to the integral form

$$\frac{dn}{dt} + 3 H(t) n = g \int \frac{d^3 \vec{p}}{(2\pi)^3} \frac{1}{E} \hat{\mathbf{C}}[f(E, t)] . \quad (3.4)$$

After the momentum integration only those contributions to the collision term survive that change the actual number of χ_1 particles. These are related to annihilation and creation reactions involving species χ_1 . As in general $2 \rightarrow 2$ reactions will be most important in the thermal plasma, the relevant annihilation and creation processes are given by $\chi_1 \chi_1 \rightarrow X_A X_B$ and $X_A X_B \rightarrow \chi_1 \chi_1$ reactions. X_A, X_B denote any other particle species present in the thermal bath that undergo interactions with species χ_1 . Here we have implicitly assumed that the χ_1 is its own anti-particle, such that the only $2 \rightarrow 2$ reactions changing the number of χ_1 s present in the thermal bath are $\chi_1 \chi_1 \leftrightarrow X_A X_B$

processes (provided that the χ_1 is stable or at least sufficiently long-lived and interactions $\chi_1\chi_i \leftrightarrow X_A X_B$ with other species χ_i changing the χ_1 number are irrelevant). This applies if the χ_1 is a real scalar or Majorana fermion, while in case of a charged scalar or Dirac fermion, $\chi_1\bar{\chi}_1 \leftrightarrow X_A X_B$ processes involving the anti-particle $\bar{\chi}_1$ have to be considered. There is one subtle point in the former case, which is related to symmetry factors and the number of χ_1 s created or annihilated per $\chi_1\chi_1 \leftrightarrow X_A X_B$ reaction. In each $\chi_1\chi_1 \leftrightarrow X_A X_B$ process the number of χ_1 s is changed by two, such that one might expect a factor of 2 in front of the collision term on the right-hand side of (3.4). However, in the collision term a symmetry factor of 1/2 has to be taken into account when the momentum integration over the two identical particles in the (initial or final) $\chi_1\chi_1$ state is performed, such that these two factors, both related to identical particle states, eventually cancel each other out. In the following we take the cancellation of these two factors for granted and therefore write neither of the two explicitly. Note that although (elastic) scattering $\chi_1 X_A \rightarrow \chi_1 X_B$ with the thermal bath constituents $X_{A,B}$ (assumed to be in thermal equilibrium during χ_1 freeze-out) does not contribute to the momentum integrated right-hand side in (3.4), it plays an important role in maintaining species χ_1 in kinetic equilibrium² even after it is chemically decoupled from the thermal plasma [45]. We come back to this important feature later in this chapter. Altogether, the reactions $\chi_1\chi_1 \leftrightarrow X_A X_B$ determine the collision term in the following way:

$$\begin{aligned}
& g \int \frac{d^3\vec{p}}{(2\pi)^3} \frac{1}{E} \hat{\mathbf{C}}[f(E, t)] \\
\supset & - \sum_{\text{spins}} \int \frac{d^3\vec{p}}{2E(2\pi)^3} \frac{d^3\vec{p}'}{2E'(2\pi)^3} \frac{d^3\vec{p}_A}{2E_A(2\pi)^3} \frac{d^3\vec{p}_B}{2E_B(2\pi)^3} \times (2\pi)^4 \delta^{(4)}(p + p' - p_A - p_B) \\
& \times \left(f(E, t)f(E', t) |\mathcal{A}_{\chi_1\chi_1 \rightarrow X_A X_B}|^2 - f_A(E_A, t)f_B(E_B, t) |\mathcal{A}_{X_A X_B \rightarrow \chi_1\chi_1}|^2 \right). \quad (3.5)
\end{aligned}$$

A rigorous derivation of this expression³ can be addressed within thermal field theory. From heuristic arguments the origin of the different terms is however clear: the squared amplitudes $|\mathcal{A}_{\chi_1\chi_1 \rightarrow X_A X_B}|^2$ and $|\mathcal{A}_{X_A X_B \rightarrow \chi_1\chi_1}|^2$ describe the quantum mechanical transition probabilities of reactions $\chi_1\chi_1 \rightarrow X_A X_B$ and $X_A X_B \rightarrow \chi_1\chi_1$ and generically depend on the four-momenta of the four particles taking place in the scattering reaction. To obtain the transition rates, a phase space integration of the final state particles has to be performed and a summation over the spins of all involved particles has to be carried out. Subsequently each of these transition rates is weighted by the product of the incoming particles' statistical distributions ($f(E, t)f(E', t) \equiv f_{\chi_1}(E, t)f_{\chi_1}(E', t)$ or $f_A(E_A, t)f_B(E_B, t)$) and finally integrated over the initial state momenta.

²We assume the presence of such interactions, keeping the χ_1 close to kinetic equilibrium, throughout. Several authors have studied the effect of kinetic decoupling of the χ_1 that occurs after chemical decoupling if $\chi_1 X_A \rightarrow \chi_1 X_B$ reactions cease to maintain species χ_1 in kinetic equilibrium, see for example [40, 51, 52].

³Note that we have already dropped Fermi blocking and Bose stimulated emission factors in (3.5) (for a corresponding discussion see for example [50]).

To proceed let us assume that apart from χ_1 all thermal bath species X are in thermal equilibrium throughout the time within which we track the evolution of the χ_1 number density. Consequently the phase space distribution $f_X(E, t)$ of such species in the cosmic comoving frame, where the plasma is at rest as a whole, is given by the thermal equilibrium distribution

$$f_{X, \text{eq}}(E, t) = \frac{1}{\exp(E/T) + \eta_X}, \quad (3.6)$$

where η_X is 1 (-1) if X is of fermionic (bosonic) nature. Note that we have dropped the chemical potential μ_X of species X . This is in general a good approximation for the early Universe, as the chemical potential μ_X is generically much smaller than the energies E at the temperatures of interest to us: Energies in on-shell reactions $\chi_1\chi_1 \leftrightarrow X_A X_B$ of non-relativistic χ_1 particles will be characterised by the scale $2m_{\chi_1}$ (up to corrections of the order of the non-relativistic kinetic energy), which for a heavy cold dark matter candidate is at least of the order of some hundred GeV to some TeV. Further, in the χ_1 freeze-out process only temperatures $T \lesssim m_{\chi_1}/20$ are relevant. In this case the exact expression (3.6) can be replaced in very good approximation by a Maxwell-Boltzmann distribution, $f_{X, \text{eq}}(E, t) \simeq e^{-E/T}$, such that from energy conservation, $E + E' = E_A + E_B$, the relation

$$f_{A, \text{eq}}(E_A, t) f_{B, \text{eq}}(E_B, t) = f_{\text{eq}}(E, t) f_{\text{eq}}(E', t) \quad (3.7)$$

is obtained. The phase space integration related to the species X_A and X_B in (3.5) can now be performed independently of f_A and f_B . With the definition of the Lorentz invariant cross section we arrive at the relation

$$\begin{aligned} \sum_{\text{spins}} \int \frac{d^3\vec{p}_A}{2E_A(2\pi)^3} \frac{d^3\vec{p}_B}{2E_B(2\pi)^3} \times (2\pi)^4 \delta^{(4)}(p + p' - p_A - p_B) |\mathcal{A}_{\chi_1\chi_1 \rightarrow X_A X_B}|^2 \\ = 4 g g' \sqrt{(p \cdot p')^2 - m_{\chi_1}^2 m_{\chi_1}^2} \sigma_{\chi_1\chi_1 \rightarrow X_A X_B}. \end{aligned} \quad (3.8)$$

g, g' denote the spin factors (internal degrees of freedom) of the two χ_1 initial state particles. As first argued in [49], unitarity ensures that when replacing $|\mathcal{A}_{\chi_1\chi_1 \rightarrow X_A X_B}|^2$ in the integrand on the left-hand side by $|\mathcal{A}_{X_A X_B \rightarrow \chi_1\chi_1}|^2$, the same right-hand side expression as in (3.8) results. Summing over all possible states $X_A X_B$, the collision term then simplifies to

$$\begin{aligned} g \int \frac{d^3\vec{p}}{(2\pi)^3} \frac{1}{E} \hat{\mathbf{C}}[f(E, t)] = \\ -g \int \frac{d^3\vec{p}}{(2\pi)^3} g' \int \frac{d^3\vec{p}'}{(2\pi)^3} \left[f(E, t) f(E', t) - f_{\text{eq}}(E, t) f_{\text{eq}}(E', t) \right] \times (\sigma_{\chi_1\chi_1} v). \end{aligned} \quad (3.9)$$

$\sigma_{\chi_1\chi_1} \equiv \sigma_{\chi_1\chi_1 \rightarrow \sum X_A X_B}$ denotes the total annihilation cross section for $\chi_1\chi_1$ pair annihilations and v is the Møller velocity defined as [49]

$$v = \frac{\sqrt{(p \cdot p')^2 - m_{\chi_1}^4}}{E E'}. \quad (3.10)$$

Note that the Møller velocity v coincides with the relative velocity v_{rel} for anti-collinear collisions $\vec{p}' \propto \vec{p}$.

In the next step, the distribution functions $f(E, t)$ and $f(E', t)$ in (3.9) are approximated by a momentum independent factor times the (chemical and kinetical) thermal equilibrium Maxwell-Boltzmann distribution, that is $f(E, t) = \alpha(t) f_{\text{eq}}(E, t)$ with $f_{\text{eq}}(E, t) = e^{-E/T}$. The proportionality factor $\alpha(t)$ may depend (through its time dependence) on the temperature of the thermal bath, but is independent of the particle's energy. As argued in [45], this approximation holds if two conditions are fulfilled. First, the temperature of the thermal bath is already well below the mass scale of the species χ_1 , $T \ll m_{\chi_1}$, such that the Maxwell-Boltzmann distribution gives a good approximation to the equilibrium distribution. Second, scattering reactions $\chi_1 X_A \rightarrow \chi_1 X_B$ with the thermal plasma constituents $X_{A,B}$ have to be rapid and effective enough to maintain species χ_1 in kinetic equilibrium. In this case the momentum dependence of the distribution function stays close to its equilibrium functional dependence and the proportionality factor $\alpha(t)$ is momentum independent in very good approximation, see the corresponding discussion in [45]. Under these assumptions, (3.9) can finally be cast in the form

$$g \int \frac{d^3 \vec{p}}{(2\pi)^3} \frac{1}{E} \hat{C}[f(E, t)] = -\langle \sigma v \rangle (n^2 - n_{\text{eq}}^2), \quad (3.11)$$

with the thermally averaged total annihilation cross section

$$\langle \sigma v \rangle = \frac{1}{n_{\text{eq}}^2} g \int \frac{d^3 \vec{p}}{(2\pi)^3} g' \int \frac{d^3 \vec{p}'}{(2\pi)^3} (\sigma_{\chi_1 \chi_1} v) f_{\text{eq}}(E, t) f_{\text{eq}}(E', t). \quad (3.12)$$

n_{eq} denotes the equilibrium number density obtained from the Maxwell-Boltzmann distribution $f_{\text{eq}}(E, t)$ using (3.3). Finally, from (3.4) and (3.11), the familiar expression for the Boltzmann equation in the expanding Universe

$$\frac{d}{dt} n = 3H(t)n - \langle \sigma_{\chi_1 \chi_1} v \rangle (n^2 - n_{\text{eq}}^2) \quad (3.13)$$

is obtained. The first term on the right-hand side accounts for the dilution of the number density due to the Universe's expansion and the second term accounts for the particle physics processes that change the number of particles χ_1 .

3.2 Co-annihilations

In Sec. 3.1 we discussed the single χ_1 species freeze-out process, which is quantified by the evolution of the χ_1 number density governed by a Boltzmann equation. In the derivation of the central equation (3.13) it is implicitly assumed, that the remaining constituents of the thermal bath (generically denoted with $X_{A,B}$) are in chemical and kinetical equilibrium at least until the χ_1 annihilation reactions are completely frozen out. However, this does not apply if in addition to the χ_1 there are further slightly

heavier species χ_i , $i > 1$, present, that have comparable interaction strength and interact with the χ_1 . Being only slightly heavier, the species χ_i will be roughly as abundant as the χ_1 as long as chemical equilibrium holds.⁴ Given interaction rates of similar strength, the freeze-out of species χ_i and χ_1 will take place around the same time. In particular the evolution of the number densities n_i will affect the n_1 evolution due to coupled Boltzmann equations. This effect of co-annihilations has first been addressed in [48], where a consistent formalism to treat co-annihilations in the relic abundance calculation of species χ_1 has been given, applicable to the limit of strictly non-relativistic co-annihilation rates. Using the exact relativistic formulae for the annihilation rates in the single species freeze-out from [49], [53] subsequently provided a formalism that allows to include exact co-annihilation rates in dark matter relic abundance calculations, which in [53] was applied to the χ_1^0 relic abundance calculation in the MSSM.

Our application in Chap. 9 is the relic density calculation of $\mathcal{O}(\text{TeV})$ scale χ_1^0 dark matter in the MSSM. In this case co-annihilation processes with further neutralino and chargino species occur generically. A TeV-scale χ_1^0 that reproduces the observed cold dark matter as thermal relic has to be either wino- or higgsino-like, or a mixed wino-higgsino state. In these cases mass degeneracies between the χ_1^0 and at least its corresponding chargino partner χ_1^\pm at $\mathcal{O}(\text{GeV})$ or below are generic, making the consideration of co-annihilations in the relic abundance calculation necessary.⁵ Following [48,53] we therefore generalise the derivation from Sec. 3.1 here to include the effect of co-annihilations.

Consider a set of N nearly mass degenerate species χ_i , $i = 1, \dots, N$, ordered according to their increasing masses m_i ($m_j \leq m_k$ for $j < k$). The lightest species χ_1 is the dark matter candidate. Further the existence of a conserved multiplicative quantum number is assumed, in which all species χ_i shall differ from the SM particles. The latter guarantees the stability of the dark matter candidate χ_1 . Within the R-parity conserving MSSM considered in Chap. 9 R-parity takes exactly the role of this additional multiplicative quantum number. In the following $X_{A,B}$ denote SM particle species and it is assumed that these species are in chemical equilibrium throughout the freeze-out of co-annihilation reactions of the χ_i . The following processes can then change the number of species χ_i :

$$\chi_i \chi_j \leftrightarrow X_A X_B , \quad (3.14)$$

$$\chi_i X_A \leftrightarrow \chi_j X_B , \quad (3.15)$$

$$\chi_i \leftrightarrow \chi_j X_A X_B , \quad j < i . \quad (3.16)$$

Decay processes (3.16) imply that all species $\chi_{i>1}$ will eventually decay into the lightest

⁴Generically at temperature T , the equilibrium number density $n_{i,\text{eq}}$ of a heavier species χ_i will be suppressed relative to the density $n_{1,\text{eq}}$ of the (non-relativistic) species χ_1 by a Boltzmann factor $e^{-(m_i-m_1)/T}$, where m_i (m_1) is the mass of species χ_i (χ_1). See the end of Sec. 3.3 for a discussion on the origin of such Boltzmann suppression factor. For small mass splittings $\delta m_i = m_i - m_1 \ll T$ the number densities $n_{i,\text{eq}}$ and $n_{1,\text{eq}}$ are therefore of the same order.

⁵In addition to the rather natural mass degeneracies in the χ^0/χ^\pm sector for TeV-scale χ_1^0 dark matter scenarios, there are viable χ_1^0 dark matter models where co-annihilations with nearly mass-degenerate third generation sfermions (the \tilde{t}_1 or $\tilde{\tau}_1$) allow to reproduce the experimentally observed dark matter density. We focus here on χ^0/χ^\pm co-annihilations and exclude the case of additional mass degeneracies of the χ_1^0 with sfermion or Higgs states in the MSSM from our analysis.

and stable χ_1 , such that the number density of the latter today is determined from the sum over the number densities n_i of all χ_i species, $n = \sum_{i=1,\dots,N} n_i$. While annihilation and creation reactions (3.14) affect the total number density n of all χ_i species, the decay and inverse decay processes (3.16) cannot change n . Finally scattering reactions (3.15) affect neither n nor n_i , but are important to keep the individual χ_i close to kinetic equilibrium even after the species have chemically decoupled. With these preliminaries the Boltzmann equation corresponding to (3.13), that describes the evolution of the summed number density $n = \sum_{i=1,\dots,N} n_i$, takes the form

$$\frac{d}{dt} n = -3H(t)n - \sum_{i,j} \langle \sigma_{\chi_i \chi_j} v_{ij} \rangle (n_i n_j - n_{i,\text{eq}} n_{j,\text{eq}}) . \quad (3.17)$$

The $\chi_i \chi_j$ annihilation cross section $\sigma_{\chi_i \chi_j}$ is defined by an obvious generalisation of (3.8) and similarly the Lorentz-invariant Møller velocity v_{ij} derives from (3.10),

$$v_{ij} = \frac{\sqrt{(p_i \cdot p_j)^2 - m_{\chi_i}^2 m_{\chi_j}^2}}{E_i E_j} . \quad (3.18)$$

Note that the sum in (3.17) separately runs over $i, j = 1, \dots, N$. Under the assumption of rapid scattering reactions (3.15) with the SM thermal plasma it is argued in [53] that these processes ensure, that the ratio of particle number density n_i to the total particle number density n remains close to the corresponding ratio of equilibrium quantities,

$$\frac{n_i}{n} \simeq \frac{n_{i,\text{eq}}}{n_{\text{eq}}} . \quad (3.19)$$

This allows the following rewriting of the Boltzmann equation:

$$\frac{d}{dt} n = -3H(t)n - \langle \sigma_{\text{eff}} v \rangle (n^2 - n_{\text{eq}}^2) , \quad (3.20)$$

with the thermally averaged effective annihilation cross section

$$\langle \sigma_{\text{eff}} v \rangle = \sum_{i,j} \langle \sigma_{\chi_i \chi_j} v_{ij} \rangle \frac{n_{i,\text{eq}} n_{j,\text{eq}}}{n_{\text{eq}}^2} . \quad (3.21)$$

(3.20) is the generalisation of (3.13) that properly includes co-annihilations. Instead of n it is more convenient to consider the evolution of the yield Y ,

$$Y = \frac{n}{s} , \quad (3.22)$$

where s denotes the total entropy density, as this allows to tread the dilution effect from the Universe's expansion implicitly. Assuming the absence of entropy production, the total entropy per comoving volume element, $S = sR^3$, remains constant and the change

of number and entropy density due to the expansion is the same, namely $ds/dt = -3Hs$. From (3.20) we then obtain the Boltzmann equation for the yield,

$$\frac{d}{dt} Y = -s \langle \sigma_{\text{eff}} v \rangle (Y^2 - Y_{\text{eq}}^2) . \quad (3.23)$$

Instead of its time evolution it is more useful to consider the change of Y with the temperature T of the Universe's thermal bath. This temperature is associated with the bath of thermal photons in the Universe throughout its evolution. In particular, introducing the dimensionless inverse scaled temperature $x = m_{\chi_1}/T$ and noting that in absence of entropy production

$$\frac{dx}{dt} = \frac{x^2}{m_{\chi_1}} 3 H s \frac{dT}{ds} \quad (3.24)$$

we obtain

$$\frac{d}{dx} Y = - \frac{m_{\chi_1}}{3 H x^2} \frac{ds}{dT} \langle \sigma_{\text{eff}} v \rangle (Y^2 - Y_{\text{eq}}^2) . \quad (3.25)$$

In order to determine the change of the entropy density with the thermal bath temperature, ds/dT , consider the Friedmann equation

$$H^2 = \frac{8\pi G_N}{3} \rho , \quad (3.26)$$

where G_N is the gravitational constant. Freeze-out of the heavy species χ_i will take place during the radiation-dominated epoch, such that the energy density ρ on the right-hand side is dominated by relativistic degrees of freedom. It is therefore convenient to parametrise the total energy density ρ as well as the total entropy density s by

$$\rho = \frac{\pi^2}{30} g_{\text{eff}}(T) T^4 , \quad s = \frac{2\pi^2}{45} h_{\text{eff}}(T) T^3 . \quad (3.27)$$

g_{eff} and h_{eff} denote the effective degrees of freedom associated with the energy and entropy density in the thermal bath [49]. From (3.27) the change of s with T is obtained. (3.26) together with the parametrisation of ρ in (3.27) finally allows to relate the Hubble parameter H to the thermal bath temperature, such that the Boltzmann equation can be rewritten to

$$\begin{aligned} \frac{d}{dx} Y &= - \sqrt{\frac{\pi}{45 G_N}} g_*^{1/2} \frac{m_{\chi_1}}{x^2} \langle \sigma_{\text{eff}} v \rangle (Y^2 - Y_{\text{eq}}^2) \\ &= - \frac{2\sqrt{10}\pi m_{\text{Pl}}}{15} g_*^{1/2} \frac{m_{\chi_1}}{x^2} \langle \sigma_{\text{eff}} v \rangle (Y^2 - Y_{\text{eq}}^2) . \end{aligned} \quad (3.28)$$

In the last step we have introduced the reduced Planck mass m_{Pl} related to G_N via $m_{\text{Pl}} = (8\pi G_N)^{-1/2}$, with the numeric value $m_{\text{Pl}} = 2.42888 \cdot 10^{18} \text{ GeV}$. The temperature dependent parameter $g_*^{1/2}$ in (3.28) is defined as

$$g_*^{1/2} = \frac{h_{\text{eff}}}{\sqrt{g_{\text{eff}}}} \left(1 + \frac{T}{3 h_{\text{eff}}} \frac{d}{dT} h_{\text{eff}} \right) . \quad (3.29)$$

Under the three assumptions that first essentially only the SM species contribute to h_{eff} and g_{eff} at temperatures of interest,⁶ that second all these species behave as an ideal gas and that third no entropy is produced, simple analytic approximations to h_{eff} and g_{eff} can be given, see [49]. In a more accurate treatment the QCD quark-hadron phase transition has to be taken into account [54]. The numerical results for h_{eff} , g_{eff} and hence $g_*^{1/2}$ from such more involved calculations are tabulated and publicly available (for example they are provided with the codes `DarkSUSY` [5] and `micrOMEGAS` [6]). When numerically solving the Boltzmann equation to determine the χ_1^0 relic abundance in some popular MSSM scenarios in Chap. 9, we access these tabulated values of h_{eff} , g_{eff} and $g_*^{1/2}$. The equilibrium yield in (3.28) is given by

$$Y_{\text{eq}} = \frac{45}{4\pi^4} \frac{x^2}{h_{\text{eff}}} \sum_i g_i \frac{m_i}{m_{\chi_1}} K_2 \left(x \frac{m_i}{m_{\chi_1}} \right), \quad (3.30)$$

with K_2 the modified Bessel function of the second kind of order 2, and is obtained upon integration of equilibrium Maxwell-Boltzmann distributions for the species χ_i and division by the total entropy density s in (3.27).

The Boltzmann equation (3.28) is the central expression in this section. For temperatures $x \lesssim 1$ ($T \gtrsim m_{\chi_1}$) all species χ_i should still have been in chemical equilibrium with the plasma, which provides the boundary condition $Y(x=1) = Y_{\text{eq}}(x=1)$ for the numerical integration of (3.28). To determine the yield Y_0 associated with the number density of the stable species χ_1 today, the integration has to be carried out starting from $x=1$ to today, $x_0 = m_{\chi_1}/T_0 \sim \mathcal{O}(10^{10})$ (given a TeV scale species χ_1 and temperature $T_0 = 2.725 K = 2.34823 \cdot 10^{-13} \text{ GeV}$ of the photon background radiation today). As we will see in Chap. 9, a value $x_0 \sim 10^8$ is typically sufficient for practical purposes in the numerical solution. From Y_0 the relic abundance is finally obtained as

$$\Omega_{\chi_1} h^2 = \frac{\rho_{\chi_1}}{\rho_{\text{cr}}} h^2 = \frac{m_{\chi_1} s_0 Y_0}{\rho_{\text{cr}}} h^2. \quad (3.31)$$

s_0 denotes the entropy density today and can be determined from (3.27). The corresponding $h_{\text{eff}}(T_0)$ is essentially given by the photon and neutrino degrees of freedom, associated with the photon and neutrino background radiation today, $h_{\text{eff}}(T_0) = 3.9139$. The critical energy density ρ_{cr} is given by $\rho_{\text{cr}} = 3H_0/8\pi G_N$ where H_0 denotes the Hubble parameter today. It takes the numerical value $\rho_{\text{cr}} = 1.05368 \times 10^{-5} h^2 \text{ GeV cm}^{-3}$.

3.3 Thermally averaged annihilation cross sections

In order to finally solve the Boltzmann equation (3.28), an explicit expression of the thermally averaged effective annihilation rate $\langle \sigma_{\text{eff}} v \rangle$ defined in (3.21) is needed. In [49], where the case of one particle species χ_1 was considered, a single-integral formula for

⁶For the relic abundance calculation of a dark matter candidate with a freeze-out temperature of some 10 – 100 GeV, this is certainly fulfilled.

$\langle \sigma_{\text{eff}} v \rangle$ in terms of Lorentz invariant quantities was derived. Subsequently the expression was generalised to include co-annihilations in [53]. The starting point in the derivation of the single-integral formula for $\langle \sigma_{\text{eff}} v \rangle$ is the defining equation (3.21), with the thermal averages $\langle \sigma_{ij} v_{ij} \rangle$ of the individual rates performed in the cosmic comoving frame where the plasma is at rest as a whole. In this case the phase space distribution functions $f_{i,\text{eq}}$ that enter the thermally averaged rates $\langle \sigma_{ij} v_{ij} \rangle$ and number densities $n_{i,\text{eq}}$ are given by Bose-Einstein or Fermi-Dirac distributions (3.6). As already used in Sec. 3.1 and 3.2, both distributions are well approximated by Maxwell-Boltzmann distributions $f_{i,\text{eq}} = e^{-E_i/T}$ for temperatures $T \leq m_{\chi_1}/20$, that are relevant in the co-annihilating χ_i s freeze-out. Starting from (3.21) we can therefore write

$$\langle \sigma_{\text{eff}} v \rangle = \frac{1}{n_{\text{eq}}^2} \sum_{i,j} g_i g_j \int \frac{d^3 \vec{p}_i}{(2\pi)^3} \int \frac{d^3 \vec{p}_j}{(2\pi)^3} \sigma_{ij} v_{ij} e^{-(E_i+E_j)/T}, \quad (3.32)$$

with the total equilibrium number density of the co-annihilating species $\chi_{i=1,\dots,N}$ given by $n_{\text{eq}} = \sum_{i=1}^N n_{i,\text{eq}}$, and

$$n_{i,\text{eq}} = g_i \int \frac{d^3 \vec{p}_i}{(2\pi)^3} e^{-E_i/T} = \frac{T}{2\pi^2} g_i m_i^2 K_2(m_i/T). \quad (3.33)$$

g_i denotes the internal degrees of freedom of species χ_i . Note that the individual particle energies E_i, E_j in (3.32) explicitly refer to the cosmic comoving frame, while the cross sections σ_{ij} and the Møller velocities v_{ij} by definition are Lorentz invariant quantities. After a convenient change of variables following [49, 53], (3.32) can be simplified to the sum of single-integral expressions

$$\langle \sigma_{\text{eff}} v \rangle = \frac{1}{n_{\text{eq}}^2} \sum_{i,j} \frac{g_i g_j}{8\pi^4} T \int_{(m_i+m_j)^2}^{\infty} ds \sqrt{s} p_{ij}^2 \sigma_{ij} K_1(\sqrt{s}/T), \quad (3.34)$$

with K_1 the modified Bessel function of the second kind of order 1. The integration variable s is the Lorentz-invariant centre-of-mass energy $s = (p_i + p_j)^2$ in the individual $\chi_i \chi_j$ pair-annihilation reaction, where $p_{i,j}$ denote the 4-momenta of the annihilating particles. Finally, p_{ij} is the modulus of the individual particles' momenta in the centre-of-mass frame of the $\chi_i \chi_j$ annihilation reaction. Expressed in terms of Lorentz invariant quantities it reads

$$p_{ij} = \sqrt{\frac{(p_i \cdot p_j)^2 - m_i^2 m_j^2}{s}} = \frac{1}{\sqrt{s}} \sqrt{\frac{s^2}{4} - \frac{s}{2}(m_i^2 + m_j^2) + \frac{(m_i^2 - m_j^2)^2}{4}}. \quad (3.35)$$

While [53] now proceeds by interchanging summation and integration in (3.34) and introduces an effective rate given by the sum over the individual integrands related to the pairs $\chi_i \chi_j$, we follow a slightly different way and consider each integral in (3.34) separately. In Chap. 6 and 8 we determine the product $\sigma_{ij} v_{\text{rel}} \equiv \sigma_{ij} v_{\text{rel},ij}$ of the annihilation cross section σ_{ij} times the relative velocity $v_{\text{rel},ij}$ in the centre-of-mass frame of

the annihilation reaction, rather than the separate cross sections σ_{ij} . The centre-of-mass frame relative velocity of the $\chi_i\chi_j$ pair expressed in terms of Lorentz invariant quantities is given by

$$v_{\text{rel},ij} = p_{ij} \sqrt{s} \frac{4s}{s^2 - (m_i^2 - m_j^2)^2} . \quad (3.36)$$

Note that $v_{\text{rel},ij}$ coincides with the Møller velocity v_{ij} in any frame where the two particles χ_i, χ_j move collinearly. Our final result for the thermally averaged effective annihilation cross section that enters the Boltzmann equation (3.28) and involves the individual rates $\sigma_{ij}v_{\text{rel}}$ therefore reads

$$\langle \sigma_{\text{eff}} v \rangle = \frac{1}{n_{\text{eq}}^2} \sum_{i,j} \frac{g_i g_j}{8\pi^4} T \int_{(m_i+m_j)^2}^{\infty} ds p_{ij} (\sigma_{ij} v_{\text{rel}}) \frac{s^2 - (m_i^2 - m_j^2)^2}{4s} K_1(\sqrt{s}/T) . \quad (3.37)$$

In application of the presented formalism to the χ_1^0 relic abundance calculation in the MSSM in Sec. 9 we generically take all co-annihilating neutralino and chargino species in $\langle \sigma_{\text{eff}} v \rangle$ into account. Note however that the contribution from a heavy channel $\chi_i\chi_j$ is typically suppressed by a factor proportional to $e^{-(m_i+m_j-2m_1)/T}$ with respect to the contribution from the lightest state $\chi_1\chi_1$. This (Boltzmann) suppression arises from the asymptotic expansion of the Bessel function K_1 in the integrand for large $\sqrt{s}/T \gg 2m_1/T \gg 1$ for temperatures $T \leq m_1/20$ relevant in the cold dark matter relic abundance calculation. We determine all neutralino/chargino co-annihilation rates $\sigma_{ij}v_{\text{rel}}$ entering (3.37) in a non-relativistic (partial-wave) expansion, including $\mathcal{O}(v_{\text{rel}}^2)$ corrections to the hard annihilation reactions in Chap. 6. The effect of Sommerfeld-enhanced co-annihilation rates on the calculated χ_1^0 relic abundance is the particular phenomenological focus of this thesis. Consequently Sommerfeld enhancements on the hard rates of all those $\chi_i\chi_j$ pairs that can be produced on-shell from reactions $\chi_1\chi_1 \rightarrow \chi_i\chi_j$ of non-relativistic $\chi_1\chi_1$ states are included in the calculation of $\langle \sigma_{\text{eff}} v \rangle$ in our final analyses in Chap. 9. Before we can enter the detailed study of some popular MSSM benchmark models we introduce the framework needed for the calculation of Sommerfeld-enhanced rates $\sigma_{ij}v_{\text{rel}}$ in the next chapters. We finally come back to the relic abundance calculation and apply the formulae derived here in Chap. 9.

Chapter 4

The neutralino and chargino sector in the MSSM

In this chapter we discuss the neutralino and chargino sector of the MSSM – in particular the corresponding mass spectrum – in view of its properties relevant to our investigation of Sommerfeld enhancements and the neutralino relic abundance calculation. However before focusing on this subject we preprend in Sec. 4.1 a short discussion on problems of the Standard Model of particle physics, followed by a basic introduction to supersymmetry that possibly may help to solve or to change for better the aforementioned issues. Subsequently an overview on the field content and parameters in the general MSSM is given in Sec. 4.2. With the background of the preceding sections we finally concentrate in Sec. 4.3 on the neutralino and chargino sector of the MSSM. We conclude in Sec. 4.4 with some remarks on the generation of MSSM spectra to be analysed in view of Sommerfeld enhancement effects in neutralino and chargino co-annihilations in Chap. 9, emphasising the fact that a sound analysis requires the knowledge of the neutralino and chargino masses and mixing matrices from on-shell renormalisation at one-loop level.

4.1 Motivations for supersymmetry and basic ideas

The Standard Model of particle physics provides the successful theoretical framework to describe elementary interactions of the microscopic constituents associated with ‘ordinary’ matter – the six quark species, six lepton species, eight gluons, the electroweak gauge bosons W^\pm and Z , the photon and the Standard Model Higgs boson – up to energy scales currently testable at experiments [1].¹ The largest such energy scale reached at present is the scale of maximally 8 TeV centre-of-mass energy in pp -collisions during the first run of the Large Hadron Collider (LHC) at CERN. In 2012 the collaborations ATLAS and CMS running the two multi-purpose detectors at the LHC had announced the discovery of a spin-0 particle with the properties of the long sought-after Higgs boson,

¹We use the term ‘ordinary’ matter to distinguish it from the Universe’s cold dark matter component, whose elementary constituent (or constituents) – if dark matter has particle nature – is unknown.

the last of the particle constituents of the Standard Model that had not been observed experimentally before.² Further, no significant deviation of observed particle production rates from the SM prediction has so far been found at the colliders running at the high energy frontier.³

In spite of these successful tests the Standard Model is incomplete as it does not include gravitational interactions and is therefore considered to be the low energy effective theory of a more fundamental theory of nature that governs the physics at the Planck scale, where gravitational effects eventually become relevant. Several other problems related to both experimental observations and theoretical aspects of the Standard Model suggest or directly imply that the Standard Model cannot be the fundamental theory of microscopic interactions. For instance it is observed experimentally that contrary to the description in the Standard Model the three neutrino species are not massless but must have masses in the range of some eV. Similarly, the measurement of the anomalous magnetic moment of the muon does not match the Standard Model prediction. In addition there also are more formal issues that require an appropriate extension of the theory. The probably most important ones are the so called ‘hierarchy problem’ and the non-unification of running SM gauge couplings within the theory. Another severe problem is the lack of a dark matter particle candidate. We briefly sketch the latter three issues in the following.

The hierarchy problem is associated with the nowadays widely believed ansatz that the Standard Model is an effective theory, which is valid up to a certain energy scale where new physics effects will arise. This scale does not have to coincide with the $\mathcal{O}(10^{19})$ GeV Planck scale but can lie in the energy range in between the electroweak scale at $\mathcal{O}(10^2)$ GeV (typically associated with the Higgs field vacuum expectation value $v \approx 246$ GeV) and the Planck scale. The hierarchy problem can be formulated as the question how to obtain a scale v that is much smaller than the high energy scale denoting the range of validity of the effective theory. In the perturbative renormalisation of the SM Higgs mass, quantum corrections arise that are quadratic in the cut-off of the effective theory. To obtain the experimentally measured value of the Higgs boson mass $m_H = 125.7 \pm 0.4$ GeV [1] a sufficiently fine-tuned cancellation between the bare Higgs mass parameter and the quantum corrections has to take place. The hierarchy problem here manifests itself as a “fine-tuning” or naturalness problem, as the bare mass parameter of the Higgs field and the quantum corrections have to cancel each other over several orders of magnitude to give the experimentally measured $\mathcal{O}(10^2)$ GeV Higgs mass.

Relying on corresponding renormalisation group equations in the Standard Model it is found that the scale dependent Standard Model gauge couplings almost (but not

²The spin of the discovered particle, its CP properties and the signal strength in experimentally observed decay channels are so far consistent with an interpretation of the new state in terms of a Standard Model Higgs boson, see the corresponding section in [1] and references therein.

³Until 2011 the $p\bar{p}$ -collider Tevatron at Fermilab was running at maximally 1.96 TeV centre-of-mass energy. The LHC at CERN reached maximally 8 TeV centre-of-mass energy in run I while in run II, scheduled for 2015, it shall operate at 14 TeV centre-of-mass energy. Data from the second LHC run will hopefully allow to get a deeper insights into the mechanism of electroweak symmetry breaking and the role that the discovered Higgs boson plays in this context.

exactly) meet at some high energy scale between 10^{12} GeV to 10^{18} GeV. This could be a hint that the Standard Model gauge group is actually embedded into a larger gauge group, for instance $SU(5)$, with only one coupling constant [55]. The larger gauge group is associated with the so called grand unification scale, below which it is spontaneously broken to the Standard Model gauge group $SU(3)_C \times SU(2)_L \times U(1)_Y$. Above the grand unification scale the symmetry associated with the larger gauge group is however restored. The effects of the new physics that become relevant close to the grand unification scale modify the running of the Standard Model gauge couplings such that an exact unification of these couplings can take place, thus the notion grand unification of gauge couplings.

We have noted before that various observations exist which imply the existence of a cold dark matter component in the Universe. They range from the scale of galaxies to galaxy clusters, large scale structures and finally the largest observable scales associated with the cosmic microwave background radiation. While the nature and origin of the observed dark matter component can be rather naturally explained in terms of a thermal relic as discussed in Chap. 3, the Standard Model does not provide a suitable particle candidate. The fact that the calculated thermal relic density of a weakly interacting massive particle with $\mathcal{O}(1 \text{ TeV})$ mass and weak interaction strength matches the order of magnitude of the observed cold dark matter abundance seems to indicate that new physics, which addresses not only the problem of a missing dark matter candidate but potentially also further problems of the Standard Model, could be related to the TeV scale.

Several theories have been proposed that solve or amend the problems encountered in the Standard Model. Probably one of the best motivated and certainly most studied ideas is the concept of a supersymmetric extension of the Standard Model [1, 56–59]. Supersymmetry (SUSY) generalises the concept of symmetries in quantum field theories by connecting bosonic and fermionic degrees of freedom. Due to formal aspects it is thus an attractive idea. Supersymmetric transformations are space-time transformations: the Poincaré algebra is extended to include fermionic generators. When acting on a particle state, these fermionic generators transform a bosonic state into a fermionic one, and vice versa, by changing the spin in units of one-half. The full symmetry of a model is given as direct product of the supersymmetry group and possible inner symmetry groups. Consequently the states are classified by the irreducible representations of the supersymmetry algebra, called supermultiplets, and the irreducible representations of the possible additional inner symmetries. Each supermultiplet must be characterised by the same number of bosonic and fermionic degrees of freedom. Further, as supersymmetry transformations commute with the inner symmetries, the bosonic and fermionic constituents of the supermultiplet have to transform in the same representation with respect to the inner symmetries. This implies that in a supersymmetric extension of the Standard Model new particles have to be introduced to form appropriate supermultiplets together with the Standard Model species. As long as supersymmetry is unbroken the supersymmetric partners of the Standard Model species would be mass-degenerate with

the latter.⁴ As these superpartners have not been observed experimentally supersymmetry must be broken. We comment on possible breaking mechanisms in Sec. 4.2 in context of the Minimal Supersymmetric Standard Model. Let us note that in minimal supersymmetric extensions of the Standard Model only one fermionic supersymmetry generator is considered ($N = 1$), such that each Standard Model particle gets exactly one supersymmetric partner. In extended supersymmetric models more than one fermionic generator appears in the supersymmetry algebra ($N > 1$).

Supersymmetric theories, in particular the mechanism that breaks the mass degeneracies between the Standard Model particles and their supersymmetric partners, introduce new energy scales that can provide a solution or mitigation to the hierarchy problem. In particular, a solution of the fine-tuning problem is possible due to the fact that the new particles give additional contributions to the radiative corrections to the Higgs mass. Because contributions from a bosonic and a fermionic loop (related to particles within the same supermultiplet) come with a relative minus sign, the quadratic divergencies can compensate each other. Such cancellation however works only as long as the superpartners are not heavier than $\mathcal{O}(\text{TeV})$. Otherwise the hierarchy problem is reintroduced. The presence of the superpartners also changes the renormalisation group running of the gauge couplings discussed above, such that a unification of the gauge couplings at some high energy scale becomes possible. Finally – and for our purposes most importantly – some of the additional particles in supersymmetric theories that enlarge the number of particle species considered in the Standard Model are viable dark matter candidates.

Let us further point out that a supersymmetric model can eventually be extended to include gravity by promoting to local supersymmetry transformations, where the resulting non-renormalisable theory is called supergravity theory [60].

4.2 The MSSM: field content and parameters

The Minimal Supersymmetric Standard Model is a $N = 1$ supersymmetric theory based on the Standard Model gauge group $\mathcal{G}_{\text{SM}} = SU(3)_C \times SU(2)_L \times U(1)_Y$. The field content of the Standard Model is extended by adding appropriate fermionic and bosonic partner fields. Several reviews and textbooks on the construction and the properties of the MSSM exist, see for example [1, 56–59] and references therein. In the calculation of MSSM neutralino and chargino co-annihilation rates in later chapters, we refer to the notation and conventions established in the two review articles [56] and [61], where the latter reference focuses on the MSSM Higgs sector. In addition we rely on the set of MSSM Feynman rules collected in [62]. All the three latter references use the same conventions. The following brief summary on the MSSM field content is based on [62].

⁴The operator P^2 , square of the 4-momentum operator P^μ that appears as one of the bosonic generators in the supersymmetry algebra, is a Casimir operator of the algebra. This implies that – as long as supersymmetry is unbroken – all states in one supermultiplet have equal mass. Note that the operator W^2 associated with the spin of particle states is a Casimir operator of the Poincaré but not of the supersymmetry algebra. Consequently, the supersymmetry multiplets contain states with different spin.

The MSSM involves three gauge supermultiplets. Each of these transforms under \mathcal{G}_{SM} with respect to the adjoint representation in one of the factors $SU(3)_C$, $SU(2)_L$ and $U(1)_Y$ and with respect to the trivial representation in the other two. The Standard Model gauge fields in the corresponding multiplets are accompanied by two-component Weyl spinor fields. For instance, the first gauge multiplet refers to $U(1)_Y$ and contains the gauge field B_μ accompanied by the two component Weyl spinor field λ_B , the bino. Accordingly, the second gauge supermultiplet is related to the weak isospin $SU(2)_L$, comprising the three corresponding gauge fields $W_\mu^{i=1,2,3}$ together with the three Weyl spinors $\lambda_W^{i=1,2,3}$ named winos. The third multiplet is associated with the gauge group $SU(3)_C$ and includes the eight QCD gauge fields, the gluons, together with the eight fermionic partners, the gluinos.

The Standard Model fermions arrange in so called chiral supermultiplets. Their corresponding superpartners are complex scalar fields, referred to as sfermions. For instance the left-handed quarks of the first family that come in the $SU(2)_L$ doublet $\Psi_Q^{I=1} = (u_L, d_L)$ are accompanied by the $SU(2)_L$ doublet $Q^{I=1} = (\tilde{u}_L, \tilde{d}_L)$ containing the two complex scalar fields \tilde{u}_L and \tilde{d}_L .

In the Standard Model one $SU(2)_L$ Higgs doublet allows to give masses to the Standard Model fermions. In case of the down-type quarks or the leptons (e, μ, τ) , the relevant interaction terms that provide the mass terms after electroweak symmetry breaking are Yukawa interactions involving the Higgs field. The corresponding Yukawa interactions of the up-type quarks contain the complex conjugate Higgs field. In the MSSM the respective Yukawa interactions follow from the superpotential and cannot involve the complex conjugate of the Higgs fields, see for instance [62]. Therefore two Higgs doublets with opposite hypercharges are needed in the MSSM to eventually generate the Standard Model fermion masses. These two $SU(2)_L$ Higgs doublets arrange in two different chiral supermultiplets with corresponding Weyl fermion fields called higgsinos. After electroweak symmetry breaking the higgsinos mix with the bino and wino states to form the electrically neutral neutralino and the charged chargino mass eigenstates. We postpone the discussion of the neutralino/chargino sector of the MSSM to Sec. 4.3.

Certain terms in the MSSM Lagrangian are gauge invariant and allowed by supersymmetry but imply baryon (B) and lepton (L) number violation which in turn would lead to proton decay. The presence of such terms can be forbidden by imposing an additional global symmetry of the model, the so called R -parity [63]

$$R = (-1)^{L+3B+2s} , \quad (4.1)$$

where s denotes the spin of the respective species. With this definition the Standard Model particles have R -parity $+1$ while for the superpartners $R = -1$. For instance, all states in a chiral supermultiplet involving Standard Model leptons have lepton number $L = 1$ and baryon number $B = 0$; as for fermionic states $2s = 1$ the lepton states in the supermultiplet are characterised by $R = +1$, while for the corresponding bosonic slepton states $2s = 0$ which leads to $R = -1$. As a simple consequence of this symmetry we obtain the stability of the lightest supersymmetric particle (LSP). It further implies that all heavier supersymmetric particles will eventually decay into the LSP. It is worth to

note that R -parity realises the type of symmetry that we have imposed in the derivation of the relic abundance including co-annihilations in Sec. 3.2, implying that only processes of the type (3.14)–(3.16) between SM species $X_{A,B}$ and superpartners $\chi_{i,j}$ can take place. Consequently, if the LSP is electrically neutral and colourless, it constitutes a promising cold dark matter candidate, possibly explaining the observed abundance in terms of a thermal relic.

We have noted in Sec. 4.1 that the non-observation of superpartners that are mass-degenerate to the SM species implies that supersymmetry has to be broken. As supersymmetry is a continuous space-time symmetry it can be broken either explicitly or spontaneously. While the SUSY breaking mechanism is not yet understood on a fundamental level, it is known that supersymmetry very likely can only be broken by new fields and interactions not contained within the MSSM. In a qualitative picture for the breaking mechanism, new fields are introduced that reside in a “hidden” sector and communicate the breaking through a weak interaction to the “visible” MSSM sector. Possible options for such communication of the SUSY breaking discussed in the literature are gauge mediated supersymmetry breaking (GMSB) [64–67], anomaly mediated supersymmetry breaking (AMSB) where the gaugino masses are radiatively generated at one-loop [68], or supergravity models where the breaking is mediated through (gravitational) interactions associated with the Planck scale. In all these cases the interactions between the “hidden” sector and the MSSM effectively generate additional and explicitly SUSY breaking terms in the MSSM Lagrangian. The ignorance of the SUSY breaking mechanism can thus be parametrised in the MSSM by introducing such explicitly supersymmetry breaking terms. The corresponding supersymmetry breaking (mass) parameters may not be larger than a few TeV and the additional terms in the Lagrangian have to be “soft” supersymmetry breaking [69], in order to prevent that quadratic divergences are introduced in the theory, which would spoil the solution of the hierarchy problem.

Four different classes of soft breaking terms can be distinguished [69]. At first the class of mass terms for the scalar fields in the MSSM, comprising the Higgs fields and the sfermions. Second, gaugino mass terms introducing the bino (M_1), wino (M_2) and gluino (M_3) mass parameters. Next, terms involving trilinear couplings of the scalar fields in the MSSM that correspond to the Yukawa terms generated in the superpotential. Finally there is a further class of terms with trilinear interactions involving the charge conjugated Higgs fields that are called “non-analytic” terms. In our application to neutralino and chargino co-annihilation rates in the MSSM, these “non-analytic” terms do not arise and are thus irrelevant for our purposes. Moreover, they are often not considered as they are absent in most supersymmetry breaking scenarios.

After elimination of unphysical degrees of freedom, the MSSM Lagrangian including the most general form of soft breaking terms contains 105 new mass parameters, phases and mixing angles in addition to the 19 free parameters in the Standard Model [57]. This number of free parameters can be significantly reduced taking experimental constraints associated with the non-observation of flavour changing neutral currents and CP violation beyond the Standard Model into account; a corresponding discussion can, for example, be found in [57]. A further reduction can be obtained if relations among the

parameters are imposed, which are typically related to a certain supersymmetry breaking mechanism. For instance in minimal supergravity models (mSUGRA), first proposed in [70,71], only the five parameters $\{m_0, M_{1/2}, A_0, \text{sgn}(\mu), \tan\beta\}$ have to be fixed,⁵ where m_0 denotes the universal mass term for scalars and $M_{1/2}$ the universal mass term for gauginos at some high energy scale Λ_X . The parameter A_0 is the universal trilinear coupling at Λ_X and the parameter μ is related to the Higgs sector, similar to $\tan\beta = v_2/v_1$, the ratio of the vacuum expectation values of the two Higgs doublets. Through renormalisation group evolution of the parameters from the scale Λ_X down to the electroweak scale the spectrum of supersymmetric states at the latter low scale is then obtained. It is worth to stress that our results on neutralino and chargino co-annihilation rates presented in later chapters apply to the general R -parity conserving MSSM and are not restricted to specific constrained MSSM scenarios.

There are dedicated searches for supersymmetric particles at the LHC. However a signature pointing to production and subsequent decay of SUSY particles has not (yet) been found. Rather, the lower bounds for the masses of coloured supersymmetric states could already be pushed to the TeV scale – although these predictions involve a certain model dependency and the analyses of the data are often performed within simplified MSSM scenarios. Lower bounds on masses of colour-neutral SUSY states are somewhat softer, for instance in the range of some 10 GeV for the lightest neutralino and around 100 GeV for the lightest chargino, where these bounds mainly derive from data of the experiments at the e^+e^- -collider LEP that do not suffer from the enormous QCD background as corresponding LHC data. For a review and discussion on the status of the searches as well as corresponding tables see for example [1].

4.3 The neutralino and chargino sector

After electroweak symmetry breaking $SU(2)_L \times U(1)_Y \rightarrow U(1)_{\text{em}}$ the gauge eigenstates bino (λ_B), the three winos ($\lambda_W^{I=1,2,3}$) and the four higgsinos⁶ $\Psi_{H_1}^1, \Psi_{H_1}^2, \Psi_{H_2}^1$ and $\Psi_{H_2}^2$ mix to form four neutralino ($\chi_{i=1,\dots,4}^0$) and two chargino ($\chi_{j=1,2}^\pm$) mass eigenstates. The mixing arises through the gaugino-higgsino Higgs coupling implying that off-diagonal terms in the neutralino and chargino mass matrices are proportional to the vacuum expectation values v_1 and v_2 of the Higgs fields. The neutralino mass term $\mathcal{L}_{m_{\chi^0}}$ written in the basis of the neutral two-component Weyl spinor fields with $\tilde{\psi}^0 = (-i\lambda_B, -i\lambda_W^3, \Psi_{H_1}^1, \Psi_{H_2}^2)$ reads

$$\mathcal{L}_{m_{\chi^0}} = -\frac{1}{2} \tilde{\psi}^{0T} M_{\chi^0} \tilde{\psi}^0 + \text{h.c.}, \quad (4.2)$$

⁵In addition to these five parameters the gravitino mass parameter $m_{3/2}$ has to be given. It can be treated as additional independent parameter in which case the supergravity model is referred to as constrained minimal supersymmetric extension of the Standard Model (CMSSM). Although the notion mSUGRA and CMSSM are often used interchangeably, theories denoted as mSUGRA models originally involved the additional constraint $m_{3/2} = m_0$. See [1] for more details and references.

⁶The higgsinos arrange in the two $SU(2)_L$ gauge doublets $\Psi_{H_{i=1,2}} = (\Psi_{H_{i=1,2}}^1, \Psi_{H_{i=1,2}}^2)$. Regarding the position of the sub- and superscript indices specifying the doublets and their respective components, our notation here differs from the one in [62].

where the neutralino mass matrix M_{χ^0} at tree-level is given by

$$M_{\chi^0} = \begin{pmatrix} M_1 & 0 & -M_Z \cos \beta \sin \theta_W & M_Z \sin \beta \sin \theta_W \\ 0 & M_2 & M_Z \cos \beta \cos \theta_W & -M_Z \sin \beta \cos \theta_W \\ -M_Z \cos \beta \sin \theta_W & M_Z \cos \beta \cos \theta_W & 0 & -\mu \\ M_Z \sin \beta \sin \theta_W & -M_Z \sin \beta \cos \theta_W & -\mu & 0 \end{pmatrix}. \quad (4.3)$$

Here we have used tree-level relations among the Z -boson mass M_Z and the Higgs field vacuum expectation values $v_{1,2}$ to express the v_i -proportional off-diagonals of M_{χ^0} in terms of M_Z , the electroweak mixing angle θ_W and the ratio $\tan \beta = v_2/v_1$. Let us recall from Sec. 4.2 that the terms involving the gaugino mass parameters M_1 and M_2 are part of the soft supersymmetry breaking terms in the MSSM Lagrangian. The higgsino mass term proportional to the parameter μ arises from the superpotential and is thus associated with the supersymmetry conserving part of the MSSM. We adopt the conventions in [62] and diagonalise the neutralino mass matrix by means of the neutralino mixing matrix Z_N defined by

$$Z_N^T M_{\chi^0} Z_N = \begin{pmatrix} m_{\chi_1^0} & & & \\ & m_{\chi_2^0} & & \\ & & m_{\chi_3^0} & \\ & & & m_{\chi_4^0} \end{pmatrix}. \quad (4.4)$$

The two-component Weyl spinors κ_i^0 in the mass eigenstate basis $\tilde{\kappa}^0 = (\kappa_1^0, \kappa_2^0, \kappa_3^0, \kappa_4^0)$, with $\tilde{\kappa}^0 = Z_N^\dagger \tilde{\psi}^0$, are arranged into four four-component Majorana spinors $\chi_i^0 = (\kappa_i^0, \bar{\kappa}_i^0)$. Let us note that Z_N shall be defined such that $|m_{\chi_i^0}| < |m_{\chi_j^0}|$ for $i < j$. After diagonalisation of M_{χ^0} one or several neutralino mass eigenvalues $m_{\chi_i^0}$ can be negative. Positive neutralino mass parameters can be easily obtained through an appropriate redefinition of the corresponding fields and mass parameters. We comment on this case in context of the calculation of hard neutralino and chargino co-annihilation rates in Sec. 6.1.4. It is worth to stress already here that our effective field theory setup developed in later chapters relies on the positiveness of all neutralino and chargino mass parameters that are part of the effective theory.

In case of the chargino sector the four two-component spinors $\lambda_W^1, \lambda_W^2, \Psi_{H_1}^2$ and $\Psi_{H_2}^1$ have to combine to form the two four-component Dirac fermion fields χ_j^\pm . With the definition $\lambda_W^\pm = 1/\sqrt{2}(\lambda_W^1 \mp i\lambda_W^2)$ the chargino mass term $\mathcal{L}_{m_{\chi^\pm}}$ takes the form

$$\mathcal{L}_{m_{\chi^\pm}} = -\tilde{\psi}^{-T} M_{\chi^\pm} \tilde{\psi}^+ + \text{h.c.}, \quad (4.5)$$

where $\tilde{\psi}^+ = (-i\lambda_W^+, \Psi_{H_2}^1)$ and $\tilde{\psi}^- = (-i\lambda_W^-, \Psi_{H_1}^2)$ as well as

$$M_{\chi^\pm} = \begin{pmatrix} M_2 & \sqrt{2}M_W \sin \beta \\ \sqrt{2}M_W \cos \beta & \mu \end{pmatrix}. \quad (4.6)$$

According to [62] we define the chargino mixing matrices Z_\pm by

$$Z_-^T M_{\chi^+} Z_+ = \begin{pmatrix} m_{\chi_1^+} & \\ & m_{\chi_2^+} \end{pmatrix}, \quad (4.7)$$

where Z_{\pm} can be determined such that the chargino mass eigenvalues are positive and $m_{\chi_1^+} < m_{\chi_2^+}$. The four two-component Weyl spinors $\kappa_{i=1,2}^{\pm}$ in the mass eigenstate bases $\tilde{\kappa}^{\pm} = (\kappa_1^{\pm}, \kappa_2^{\pm})$ are related to the gauge eigenstates $\tilde{\psi}^{\pm}$ by $\tilde{\kappa}^{\pm} = Z^{\pm \dagger} \tilde{\psi}^{\pm}$. Eventually, the two four-component Dirac fermion fields χ_i^{\pm} associated with the physical chargino states χ_i^{\pm} are built from the Weyl spinor fields κ_i^{\pm} via $\chi_i^{\pm} = (\kappa_i^{\pm}, \bar{\kappa}_i^{\mp})$.

Typically, the neutralino and chargino mass matrices are diagonalised numerically. However exact analytic solutions exist in the literature [72, 73]. In addition some insight can be gained from an analytic perturbative diagonalisation of the mass matrices in the case $M_{W,Z} \ll |M_1|, |M_2|, |\mu|$. To this end we assume the gaugino parameters M_1 and M_2 to be real positive, while μ can be either real positive or negative. Concerning the chargino sector it is most convenient to consider the product $M_{\chi^+}^{\dagger} M_{\chi^+}$ ($M_{\chi^+} M_{\chi^+}^{\dagger}$) from which the squared mass eigenvalues $m_{\chi_i^+}^2$ and the mixing matrix Z_+ (Z_-) can be obtained. From a straightforward calculation under the additional assumption $M_{W,Z}^2 \ll |M_{1,2}^2 \pm \mu^2|$ the following expressions for the physical (positive) neutralino masses are obtained at second order in the perturbative diagonalisation procedure:

$$\begin{aligned}
m_{\chi_1^0} &= M_1 + \frac{\sin^2 \theta_W^2 M_Z^2 (M_1 + \mu \sin 2\beta)}{M_1^2 - \mu^2} + \dots, \\
m_{\chi_2^0} &= M_2 + \frac{\cos^2 \theta_W^2 M_Z^2 (M_2 + \mu \sin 2\beta)}{M_2^2 - \mu^2} + \dots, \\
m_{\chi_3^0} &= |\mu| + \text{sgn}(\mu) \frac{M_Z^2 (1 - \sin 2\beta) (\cos^2 \theta_W^2 (M_1 + \mu) + \sin^2 \theta_W^2 (M_2 + \mu))}{2(M_1 + \mu)(M_2 + \mu)} + \dots, \\
m_{\chi_4^0} &= |\mu| + \text{sgn}(\mu) \frac{M_Z^2 (1 + \sin 2\beta) (\cos^2 \theta_W^2 (\mu - M_1) + \sin^2 \theta_W^2 (\mu - M_2))}{2(\mu - M_1)(\mu - M_2)} + \dots. \quad (4.8)
\end{aligned}$$

Similarly, the chargino masses including second order terms in the perturbative diagonalisation read

$$\begin{aligned}
m_{\chi_1^+} &= M_2 + \frac{M_W^2 (M_2 + \mu \sin 2\beta)}{M_2^2 - \mu^2} + \dots, \\
m_{\chi_2^+} &= |\mu| + \text{sgn}(\mu) \frac{M_W^2 (\mu + M_2 \sin 2\beta)}{\mu^2 - M_2^2} + \dots. \quad (4.9)
\end{aligned}$$

The masses in (4.8) and (4.9) are not necessarily given in increasing mass order; depending on the actual values or the specific hierarchy that is attributed to the gaugino masses and the μ parameter, the subscript labels i and j on the above $m_{\chi_i^0}$ and $m_{\chi_j^+}$ may need to be rearranged. We further note that after diagonalisation either the third or fourth neutralino mass eigenstate comes with a negative sign whereas we give the physical positive masses $m_{\chi_3^0}$ and $m_{\chi_4^0}$ above. A similar reasoning applies to the mass $m_{\chi_2^+}$ of the second chargino state. Eqs. (4.8) and (4.9) agree with the results first derived in [74]. For corresponding expressions for the mixing matrices we refer the reader to this reference.⁷

⁷The correspondence between the unitary mixing matrices Z_N, Z^{\pm} and the corresponding expressions N and V, U used in [74] reads $N = Z_N^{\dagger}$, $V = Z^{+\dagger}$ and $U = Z^{-\dagger}$.

Let us however note here that under the aforementioned assumptions the neutralino and chargino states are expectedly rather pure gaugino or higgsino states. From the above expressions the masses of the wino-like neutralino χ_2^0 and its chargino partner χ_1^\pm , both associated with the wino mass parameter M_2 , are found to be identical at second order in the expansion. A $\mathcal{O}(m_Z^4/M_1\mu^2)$ splitting between these two masses is found by systematically extending the expansion to fourth order. Therefore we can generically expect that the splitting between the masses of wino-like states determined from tree-level mass matrices will be particularly small for $M_{W,Z} \ll M_{\text{SUSY}}$. The situation is different in case of higgsino-like states. Let us assume the hierarchy $M_{W,Z} \ll |\mu| \ll M_1, M_2$. In this case the following mass splittings between the states in the sector of higgsino-like particles are derived from (4.8, 4.9),⁸

$$\begin{aligned} m_{\chi_2^+} - m_{\chi_4^0} &\simeq \text{sgn}(\mu) \left(\frac{M_Z^2 \cos^2 \theta_W}{2 M_2} (1 - \sin 2\beta) + \frac{M_Z^2 \sin^2 \theta_W}{2 M_1} (1 + \sin 2\beta) \right), \\ m_{\chi_3^0} - m_{\chi_2^+} &\simeq \text{sgn}(\mu) \left(\frac{M_Z^2 \cos^2 \theta_W}{2 M_2} (1 + \sin 2\beta) + \frac{M_Z^2 \sin^2 \theta_W}{2 M_1} (1 - \sin 2\beta) \right), \end{aligned} \quad (4.10)$$

which are of order $\mathcal{O}(M_Z^2/M_{1,2})$ but can be small if the gaugino masses are heavy compared to the electroweak scale. We infer from (4.10) that in case of positive (negative) μ the χ_4^0 (χ_3^0) is the lightest of the higgsino-like neutralino and chargino states. Further, the chargino state χ_2^+ in any case constitutes the next-to-lightest of the three states χ_3^0, χ_4^0 and χ_2^+ .

There are cases where the precise knowledge of the mass splittings between the neutralino and chargino states is essential. This in particular applies to the processes considered in this thesis: as exemplified in the two $\chi\chi$ -state toy-model in Sec. 2.4, Sommerfeld enhancements sensitively depend on the mass splittings between the non-relativistic two-particle states that undergo (off-) diagonal long-range interactions prior to the actual short-distance annihilation reaction. Furthermore, mass splittings between (nearly mass-degenerate) co-annihilating species have a significant impact on the relic abundance calculation discussed in Chap. 3, as they give rise to Boltzmann suppression factors multiplying the individual co-annihilation rates that enter the thermally averaged effective annihilation rate $\langle\sigma_{\text{eff}}v\rangle$, see the discussion in connection with (3.37). Accordingly, a precise knowledge of the χ^0/χ^\pm mass splittings is required in both the accurate determination of Sommerfeld-enhanced neutralino and chargino co-annihilation rates and the subsequent χ_1^0 relic abundance calculation. It turns out that the particularly small tree-level mass splitting between the wino-like neutralino and chargino states noted above is actually dominated by one-loop corrections. Under the assumption of $M_{W,Z} < M_2 \ll M_1, |\mu|$ these radiative corrections can be almost entirely attributed to gauge boson loops and the one-loop dominated mass splitting becomes rather model independent in this case; numerically it is found to be approximately 160 MeV [75]. While

⁸Although the imposed hierarchy with $|\mu| \ll M_{1,2}$ would imply a relabelling of the masses to arrange them in increasing mass order, we avoid such relabelling with respect to (4.8, 4.9) here for the sake of clarity.

the mass splitting between higgsino-like states is tree-level dominated, one-loop corrections are found to give sizable – either positive or negative – corrections to the splitting in addition [76–78]. Moreover we aim at investigating scenarios where the neutralino and chargino mass eigenstates are given by strongly mixed gaugino and higgsino gauge eigenstates, such that more than just two or three nearly mass degenerate χ^0/χ^\pm states occur in the spectrum. A sound investigation of Sommerfeld enhancements in neutralino and chargino annihilation reactions therefore typically requires the knowledge of the χ^0/χ^\pm spectrum at one-loop level beyond the strict wino- and higgsino limits. Analytic formulae for and an investigation on the impact of the one-loop (on-shell) corrections to the neutralino/chargino masses can be found for instance in [75–80]. Recently the issue of a suitable choice of renormalisation conditions in the on-shell renormalisation scheme applicable to cases with strong mixing between the gauge eigenstates has been addressed in [81]. In addition, the analysis has been extended to the complex MSSM, see [82–85].

4.4 MSSM spectrum generation

The formalism that we present in this thesis allows to describe Sommerfeld-enhanced neutralino and chargino pair-annihilation rates within generic R-parity conserving MSSM scenarios, including the most general form of flavor mixing in the squark and slepton sector. As an input we require a MSSM spectrum that can be obtained with publicly available MSSM spectrum generators, for example [86–88], where the parameters M_1 , M_2 and μ among other required SUSY parameter inputs have to be specified. In constrained MSSM scenarios, as for instance models with grand unification of gauge couplings, certain relations among the input SUSY parameters are assumed. We would like to stress that our setup is not restricted to such cases, but allows to analyse Sommerfeld enhancements in χ^0 , χ^\pm co-annihilations in the most general MSSM models.

Generically we require for our calculations a (slha formatted) MSSM spectrum including mass parameters, mixing matrices and angles, typically provided as output of a MSSM spectrum calculator. At the end of the previous section we have noted the importance of a precise knowledge of neutralino and chargino masses beyond tree-level. However the publicly available spectrum calculators do currently not provide corresponding one-loop spectra. Moreover, parameters are usually provided in the $\overline{\text{DR}}$ -scheme, whereas a rigorous analysis of Sommerfeld-enhanced χ^0 and χ^\pm co-annihilation processes in a given model should refer to the on-shell mass spectrum of the neutralino and chargino states. Results on the one-loop on-shell renormalized χ^0/χ^\pm sector of the MSSM are available [82–85], but have not yet been implemented in public spectrum generators. For our analysis of benchmark models discussed in Chap. 9, we have therefore been provided by MSSM spectra with one-loop on-shell renormalised neutralino and chargino masses and mixing matrices by a member of the collaboration [83, 84].

Chapter 5

Effective theory description of neutralino pair annihilations

The effective theory framework that we introduce in this chapter allows to systematically address radiative corrections to pair-annihilation reactions of non-relativistic particle pairs built from neutralino and chargino states. In particular it provides the basis for a rigorous study of Sommerfeld-enhanced co-annihilation rates in the general MSSM, where the latter are obtained from forward scattering matrix elements of χ^0/χ^\pm two-particle states that can be calculated within the effective theory. Notably, no advanced guess, as in Chap. 2, concerning the relation among perturbative cross sections and corresponding enhancement factors will be necessary: in the effective theory the relation arises naturally from matrix elements. We start with the introduction of the effective theory Lagrangian in Sec. 5.1. Subsequently we give in Sec. 5.2 a detailed discussion on how χ^0/χ^\pm pair-annihilation reactions are described within the effective theory. The essential ingredients in this context are four-fermion operators in $\delta\mathcal{L}_{\text{ann}}$, a part of the Lagrangian of the effective theory. In the subsections Sec. 5.2.1 and Sec. 5.2.2 we provide explicit expressions for the dimension-6 and dimension-8 four-fermion operators in $\delta\mathcal{L}_{\text{ann}}$, which allow to determine the hard pair-annihilation rates of non-relativistic neutralinos and charginos including $\mathcal{O}(v_{\text{rel}}^2)$ corrections in an expansion in the relative velocity.

5.1 The Lagrangian in the effective theory

In order to describe the kinematics and interactions of neutralinos and charginos moving at small velocities, we set up a non-relativistic effective theory (EFT), the non-relativistic MSSM (NRMSSM), that contains only nearly on-shell non-relativistic neutralino and chargino modes. Since eventually we are interested in the calculation of the χ_1^0 relic abundance including χ^0/χ^\pm co-annihilations, the neutralinos and charginos described in the EFT approach are those whose masses are nearly degenerate with the mass m_{LSP} of the lightest neutralino. Effects from virtual modes, which are off-shell by an amount larger than $(m_{\text{LSP}}v)^2$, as well as effects from higher mass MSSM modes are encoded in the Wilson coefficients of (higher-dimensional) EFT operators. As we will see below, the

NRMSSM set-up allows to calculate inclusive pair-annihilation rates of non-relativistic χ^0/χ^\pm states, including their mutual interaction through gauge and light Higgs boson exchange, in a systematic expansion in coupling constants and velocity.

Our EFT ansatz is inspired by the NRQCD approach to describe inclusive annihilation reactions of heavy quarkonia from [30], extending the framework in basically two aspects. First, we account for several nearly mass-degenerate non-relativistic species in the NRMSSM instead for only one heavy non-relativistic quark Q together with its anti-particle \bar{Q} , as in [30]. Second, in addition to Coulomb-type potential interactions related to massless gauge boson exchange between the non-relativistic neutralino and chargino states, we consider the case of Yukawa-like potentials, which originate from the exchange of massive gauge bosons or light MSSM Higgses.

The effective Lagrangian of the NRMSSM reads

$$\mathcal{L}^{\text{NRMSSM}} = \mathcal{L}_{\text{kin}} + \mathcal{L}_{\text{pot}} + \delta\mathcal{L}_{\text{ann}} + \text{higher order terms} , \quad (5.1)$$

where the parts denoted with 'higher order terms' are not relevant to us in the calculation of χ^0/χ^\pm co-annihilation rates including Sommerfeld enhancements. In the following we discuss the components \mathcal{L}_{kin} and \mathcal{L}_{pot} in turn. The third important part in the NRMSSM Lagrangian, $\delta\mathcal{L}_{\text{ann}}$, is discussed in detail in Sec. 5.2.

The kinetic part of the Lagrangian, \mathcal{L}_{kin} , collects the terms bilinear in the two-component spinor fields ξ_i and $\psi_j = \eta_j, \zeta_j$, that represent the non-relativistic neutralinos (χ_i^0) and charginos (χ_j^-, χ_j^+), respectively. For $n_0 \leq 4$ non-relativistic neutralino species and $n_+ \leq 2$ non-relativistic chargino species the kinetic part of the NRMSSM Lagrangian is given by

$$\begin{aligned} \mathcal{L}_{\text{kin}} = & \sum_{i=1}^{n_0} \xi_i^\dagger \left(i\partial_t - (m_i - m_{\text{LSP}}) + \frac{\vec{\partial}^2}{2m_{\text{LSP}}} \right) \xi_i \\ & + \sum_{\psi=\eta,\zeta} \sum_{j=1}^{n_+} \psi_j^\dagger \left(i\partial_t - (m_j - m_{\text{LSP}}) + \frac{\vec{\partial}^2}{2m_{\text{LSP}}} \right) \psi_j . \end{aligned} \quad (5.2)$$

It is important to note that the mass parameters (m_i, m_j) of all non-relativistic neutralino and chargino fields in $\mathcal{L}^{\text{NRMSSM}}$ have to be positive. This requirement derives from the fact that the effective Lagrangian is obtained by extracting the high-energy fluctuations, of the order of the mass scale m_{LSP} and larger, from the corresponding relativistic fields. From this procedure we obtain for instance the mass difference terms $m_i - m_{\text{LSP}}$ and $m_j - m_{\text{LSP}}$ for all species other than the χ_1^0 (in which case the difference trivially vanishes) in (5.2). If the mass parameter for a non-relativistic species in $\mathcal{L}^{\text{NRMSSM}}$ was negative, the mass difference $m_i - m_{\text{LSP}}$ would give a $\mathcal{O}(m_{\text{LSP}})$ term in \mathcal{L}_{kin} , opposed to the canonical $\mathcal{O}(m_{\text{LSP}}v^2)$ scaling of the remaining terms in the kinetic part of the NRMSSM Lagrangian. This then indicates that the parametrisation used to relate the relativistic and non-relativistic fields for the species with negative mass parameter is not appropriate. In case that for a given MSSM spectrum one or several neutralino or chargino mass parameters are negative, suitable redefinitions of the fields and mass parameters have to

be performed to arrive at a spectrum with positive masses in the χ^0/χ^\pm sector. We come back to this point in connection with explicit expressions – in terms of MSSM parameters – for the Wilson coefficients encoding the hard annihilation reactions in the effective theory in Sec. 6.1.4. At this point we also present appropriate field rotations which transform to a spectrum with positive neutralino and chargino mass parameters. Finally note that the mass differences between the χ_i^0/χ_j^\pm species that are part of the NRMSSM have to be much smaller than the scale m_{LSP} to ensure the convergence of the effective theory. In particular, the effective theory relies on a systematic expansion not only in the non-relativistic velocity of the χ_i^0/χ_j^\pm states but also in the mass differences between the two-particle states involved in $\chi_i\chi_j \rightarrow \chi_l\chi_k$ scattering reactions. This manifests itself in the basis of dimension-8 operators in Sec. 5.2.2 and is discussed extensively in context of the MSSM matching calculation in Sec. 6.1.2.

Our EFT setup with one reference mass scale, m_{LSP} , is suited for the description of (neutralino) dark matter annihilation processes in the present Universe as well as for the computation of dark matter co-annihilation reactions with further nearly mass-degenerate neutralinos and charginos in the context of the relic abundance calculation. However, the EFT framework can easily be extended to the case where the non-relativistic particle species are (nearly) mass-degenerate with respect to two distinct scales $m_{\text{ref}}^{(1,2)}$, with $m_{\text{ref}}^{(1)} \ll m_{\text{ref}}^{(2)}$. In that case the mass differences ($m_k - m_{\text{LSP}}$) in (5.2) have to be replaced by $m_k - m_{\text{ref},k}$, where each $m_{\text{ref},k}$ is given by one of the scales $m_{\text{ref}}^{(1,2)}$. In this way an entirety of hydrogen-like two-particle states can be described, which are built from a set of light, nearly mass-degenerate and another set of heavy, nearly mass-degenerate particles. Our results for the hard tree-level annihilation rates in the effective theory that we discuss in detail in Chap. 6, cover both the cases of a set of particles nearly mass-degenerate with the neutralino LSP and a set of non-relativistic hydrogen-like neutralino and chargino systems. In particular we exemplify later in Sec. 6.2.5 the application of our results to tree-level annihilation reactions of two hydrogen-like χ^0/χ^\pm two-particle systems.

The term \mathcal{L}_{pot} in (5.2) summarises instantaneous but spatially non-local interactions between the non-relativistic two-particle states $\chi_{e_1}\chi_{e_2}$ and $\chi_{e_4}\chi_{e_3}$ that arise through exchange of Standard Model gauge bosons and Higgs particles. The two-particle states $\chi_{e_1}\chi_{e_2}$ and $\chi_{e_4}\chi_{e_3}$ are built from all possible non-relativistic neutralino and chargino species $\chi_{e_i} = \chi_{e_i}^0, \chi_{e_i}^\pm$ contained in the effective theory. Generically, the individual contributions to \mathcal{L}_{pot} are given by four-fermion operators whose matching coefficients are Yukawa- and Coulomb potentials that depend on the relative distance $\vec{r} = \vec{x}_1 - \vec{x}_2$ ($r \equiv |\vec{r}|$) in the respective two-body systems:

$$\mathcal{L}_{\text{pot}} = - \sum_{\chi\chi \rightarrow \chi\chi} \int d^3\vec{r} V_{\{e_1e_2\}\{e_4e_3\}}^{\chi\chi \rightarrow \chi\chi}(r) \chi_{e_4}^\dagger(t, \vec{x}_1) \chi_{e_3}^\dagger(t, \vec{x}_1 + \vec{r}) \chi_{e_1}(t, \vec{x}_1) \chi_{e_2}(t, \vec{x}_1 + \vec{r}) . \quad (5.3)$$

The sum ranges over all neutral, single-charged and double-charged $\chi_{e_1}\chi_{e_2} \rightarrow \chi_{e_4}\chi_{e_3}$ reactions, which are collected in Tab. 5.1. To obtain the explicit form of all possible

neutral reactions	single-charged reactions	double-charged reactions
$\chi^0\chi^0 \rightarrow \chi^0\chi^0$	$\chi^0\chi^+ \rightarrow \chi^0\chi^+$	$\chi^+\chi^+ \rightarrow \chi^+\chi^+$
$\chi^0\chi^0 \rightarrow \chi^-\chi^+$	$\chi^-\chi^0 \rightarrow \chi^-\chi^0$	$\chi^-\chi^- \rightarrow \chi^-\chi^-$
$\chi^-\chi^+ \rightarrow \chi^0\chi^0$		
$\chi^-\chi^+ \rightarrow \chi^-\chi^+$		

Table 5.1: Collection of all $\chi_{e_1}\chi_{e_2} \rightarrow \chi_{e_4}\chi_{e_3}$ scattering reactions that we account for in the terms \mathcal{L}_{pot} and $\delta\mathcal{L}_{\text{ann}}$ of the NRMSSM Lagrangian. The labels e_i on the fields χ_{e_i} are suppressed in the above table. If χ_{e_i} represents a field $\chi_{e_i}^0$, the label e_i can range over $e_i = 1, \dots, n_0$, whereas $e_i = 1, \dots, n_+$ for the case of a $\chi_{e_i}^\pm$ field.

four-fermion operators in (5.3), one has to replace – in all possible ways compatible with charge conservation – the generic field symbols χ_{e_i} by the (two-component spinor) fields ξ_{e_i}, η_{e_i} and ζ_{e_i} , related to the NRMSSM $\chi_{e_i}^0, \chi_{e_i}^-$ and $\chi_{e_i}^+$ species. In this way all possible $\chi_{e_1}\chi_{e_2} \rightarrow \chi_{e_4}\chi_{e_3}$ scattering reactions between χ^0/χ^\pm two-particle pairs, built from the NRMSSM χ_i^0, χ_j^\pm states, are obtained and accounted for in (5.3). The super- and subscript labels on the potentials $V_{\{e_1e_2\}\{e_4e_3\}}^{\chi\chi \rightarrow \chi\chi}(r)$ then specify the neutralino or chargino species ($\chi_{e_i}^0, \chi_{e_i}^\pm$) in the individual scattering reaction described by the corresponding four-fermion operator.

In this thesis we restrict to leading-order potential interactions, in which case the potentials depend only on the spin of the two-particle states, that is thus conserved. The generic form of the leading-order potentials therefore reads

$$V_{\{e_1e_2\}\{e_4e_3\}}^{\chi\chi \rightarrow \chi\chi}(r) = \left(A_{e_1e_2e_4e_3} \delta_{\alpha_4\alpha_1} \delta_{\alpha_3\alpha_2} + B_{e_1e_2e_4e_3} (\vec{S}^2)_{\alpha_4\alpha_1, \alpha_3\alpha_2} \right) \frac{e^{-m_\phi r}}{r}, \quad (5.4)$$

where m_ϕ denotes the mediator mass, *i.e.* in our application the mass of the exchanged SM gauge boson or MSSM Higgs particle. While we have suppressed the spin indices α_i that are contracted with the corresponding spin indices of the field operators χ_{e_i} in (5.3), we write them explicitly in (5.4). The total spin operator \vec{S} is constructed from the individual spin-operators related to the particles interacting at space-points \vec{x}_1 and \vec{x}_2 , respectively: $\vec{S}_{\alpha_4\alpha_1, \alpha_3\alpha_2} = \vec{\sigma}_{\alpha_4\alpha_1}/2 \delta_{\alpha_3\alpha_2} + \delta_{\alpha_4\alpha_1} \vec{\sigma}_{\alpha_3\alpha_2}/2 \equiv 1/2 (\vec{\sigma} \otimes \mathbf{1} + \mathbf{1} \otimes \vec{\sigma})$. The four-fermion operators contained in $\delta\mathcal{L}_{\text{ann}}$ that we consider in Sec. 5.2 and that describe the hard pair-annihilation reactions in the NRMSSM, by construction provide a decomposition of the annihilating $\chi\chi$ -states according to their ${}^{2S+1}L_J$ partial-wave configuration with defined total spin $s = 0, 1$. It is therefore convenient to drop the spin indices in the potentials and to replace the spin-operator \vec{S}^2 that acts on the operators corresponding to the states $\chi_{e_1}\chi_{e_2}$ and $\chi_{e_4}\chi_{e_3}$, by its eigenvalue $s(s+1) = 2s$ for $s = 0, 1$.

Details on the calculation of the Coulomb- and Yukawa-type potentials in \mathcal{L}_{pot} from the underlying MSSM interactions at leading order in the non-relativistic relative velocity v_{rel} in the $\chi\chi$ systems and at lowest non-vanishing order, $\mathcal{O}(g_i^2)$, in the coupling expansion, where g_i are the generic $SU(2)_L \times U(1)_Y$ gauge couplings, are given in Sec. 7.

Regarding the short-distance annihilation reactions in the effective theory, to be discussed in the next section and in Chap. 6, we take up to $\mathcal{O}(v_{\text{rel}}^2)$ corrections in the velocity expansion in the effective theory into account, while we work at lowest non-vanishing order, $\mathcal{O}(g_i^4)$, in the expansion in the couplings.

5.2 χ^0/χ^\pm pair-annihilations in the NRMSSM

Within the NRMSSM, we aim to describe neutralino and chargino pair-annihilation processes into two-particle final states of Standard Model and (light) Higgs particles, which are not non-relativistic. The theory will contain effects from virtual and higher-mass Higgs and SUSY particle modes as well, encoded in the EFT operator coefficients and parameters. Let us note that the framework presented here is not suited to study s -channel resonance-enhanced rates when accounting at the same time for Sommerfeld enhancements.¹ For this reason we have to choose models without s -channel resonant enhancement for our analysis of Sommerfeld enhancements in neutralino and chargino co-annihilation rates in Chap. 9. Finally, we exclude the case of accidental mass degeneracies of further SUSY particles with the set of non-relativistic neutralinos and charginos. An extension of the effective theory framework to include sfermion or Higgs states that are nearly mass-degenerate with the χ^0/χ^\pm species in the NRMSSM and can therefore have an impact on the χ_1^0 relic density through co-annihilation effects is straightforward but beyond the scope of this thesis.

The hard pair-annihilation reactions of heavy non-relativistic neutralinos and charginos produce SM and light Higgs particle final states that are not described within the non-relativistic effective theory, as these final states are characterised by velocities outside the non-relativistic regime. However, since the hard inclusive pair-annihilation processes take place within distances of order $1/m_{\text{LSP}}$, we can incorporate the short-distance annihilation rates of non-relativistic neutralinos and charginos in the effective theory through the absorptive part of Wilson coefficients of local four-fermion operators in $\delta\mathcal{L}_{\text{ann}}$, following the approach of [30]. The full annihilation rates in the non-relativistic effective theory are then given by the absorptive part of the matrix elements of these four-fermion operators. While the matrix elements of the operators themselves may encode long-distance effects, giving rise to Sommerfeld enhancements, the contribution to the hard annihilation reaction factors out in the form of the Wilson coefficient.

Let us see in more detail how this formalism is applied to our case: In contrast

¹As regards the short-distance (tree-level) annihilation rates, results for the specific case of resonant s -channel annihilation reactions can be obtained from our analytic expressions for the Wilson coefficients in $\delta\mathcal{L}_{\text{ann}}$ (collected in Appendix A) by adding a resonance width to the corresponding s -channel propagator. This is because the hard rates result from an on-shell matching involving an expansion around the mass scale set by the annihilating particle states (see Sec. 6.1). However, the treatment of both Sommerfeld enhancements and resonant s -channel annihilation requires that the corresponding s -channel propagator is expanded around the mass scale set by the initially incoming two-particle state instead of the actually annihilating states. A proper treatment of s -channel resonances in Sommerfeld-enhanced annihilation rates is therefore more involved and requires modifications of our set-up.

$$\begin{aligned}
\sigma_{ij} |\vec{v}_i - \vec{v}_j| &= \int d\text{PS}_{AB} \left(\sum_{e_1, e_2} \left(\begin{array}{c} i \\ \text{---} \\ \text{---} \\ j \end{array} \right) \begin{array}{c} e_1 \\ \text{---} \\ \text{---} \\ e_2 \end{array} \begin{array}{c} X_A \\ \text{---} \\ \text{---} \\ X_B \end{array} \right) \left(\sum_{e_3, e_4} \left(\begin{array}{c} i \\ \text{---} \\ \text{---} \\ j \end{array} \right) \begin{array}{c} e_4 \\ \text{---} \\ \text{---} \\ e_3 \end{array} \begin{array}{c} X_A \\ \text{---} \\ \text{---} \\ X_B \end{array} \right)^* \\
&= 2 \Im \left(\sum_{e_1, \dots, e_4} \left(\begin{array}{c} i \\ \text{---} \\ \text{---} \\ j \end{array} \right) \begin{array}{c} e_1 \\ \text{---} \\ \text{---} \\ e_2 \end{array} \begin{array}{c} X_A \\ \text{---} \\ \text{---} \\ X_B \end{array} \begin{array}{c} e_4 \\ \text{---} \\ \text{---} \\ e_3 \end{array} \begin{array}{c} i \\ \text{---} \\ \text{---} \\ j \end{array} \right)
\end{aligned}$$

Figure 5.1: Diagrammatic picture for the relation among the annihilation amplitude and the absorptive part of the corresponding forward scattering amplitude in presence of long-range potential interactions. The latter interactions are indicated by the grey-coloured oval.

to the application to quarkonium annihilation in QCD [30], we are going to describe annihilations of scattering states instead of bound states and allow for more than one non-relativistic particle species. The latter allows for the possibility that (long-range) potential interactions lead to transitions from the initially incoming two-particle state $\chi_i \chi_j$ to another nearly on-shell non-relativistic two-particle state $\chi_{e_1} \chi_{e_2}$ prior to the hard annihilation reaction.² A diagrammatic picture for a $\chi_i \chi_j$ pair-annihilation reaction of non-relativistic χ^0/χ^\pm states is given in Fig. 5.1, where the presence of (off-) diagonal potential scattering reactions is indicated with the grey-coloured oval.³ As we have already noted in Sec. 2, unitarity allows to relate the phase space integrated product of annihilation amplitudes $\chi_i \chi_j \rightarrow X_A X_B$ in the first line of Fig. 5.1 to the absorptive part of the forward scattering amplitude $\chi_i \chi_j \rightarrow \chi_i \chi_j$ depicted in the second line, where in our application $X_A X_B$ generically denotes a pair of SM and light Higgs particles. While the annihilation amplitudes in the first line of Fig. 5.1 involve the not non-relativistic final state particle pairs $X_A X_B$ that cannot be described in the effective theory, the $\chi_i \chi_j \rightarrow \chi_i \chi_j$ forward scattering amplitude in the second line can be expressed in the NRMSSM in terms of matrix elements of the four-fermion operators in $\delta\mathcal{L}_{\text{ann}}$. The inclusive spin-averaged annihilation cross section is then obtained in the effective theory as

$$\sigma^{\chi_i \chi_j \rightarrow \sum X_A X_B} v_{\text{rel}} = \left(\frac{1}{4} \sum_{s_i, s_j} \right) 2 \Im \langle \chi_i \chi_j | \delta\mathcal{L}_{\text{ann}} | \chi_i \chi_j \rangle, \quad (5.5)$$

²In the following we use the term ‘off-diagonal’ to denote $\chi_{e_1} \chi_{e_2} \rightarrow \chi_{e_4} \chi_{e_3}$ scattering reactions, where the incoming ($\chi_{e_1} \chi_{e_2}$) and outgoing ($\chi_{e_4} \chi_{e_3}$) particle pairs are not the same, while reactions $\chi_{e_1} \chi_{e_2} \rightarrow \chi_{e_1} \chi_{e_2}$ are termed ‘diagonal’.

³Fig. 5.1 basically agrees with Fig. 2.2 discussed in Chap. 2. While in the latter chapter we introduced to the Sommerfeld effect by using heuristic arguments, the effective field theory framework that we establish here provides the basis for a rigorous derivation and subsequent analysis of Sommerfeld enhancements in χ^0/χ^\pm pair-annihilation reactions.

with $v_{\text{rel}} = |\vec{v}_i - \vec{v}_j|$ the relative velocity of the annihilating particles in the centre-of-mass frame. The matrix elements⁴ of the four-fermion operators in $\delta\mathcal{L}_{\text{ann}}$ account for the (off-) diagonal long-range potential interactions between the non-relativistic $\chi\chi$ pairs prior to annihilation, which causes the Sommerfeld effect. The information on the hard annihilation reactions into all accessible $X_A X_B$ final states is contained in the Wilson coefficients of the operators, implying that the factorisation of long-range and short-distance effects becomes manifest in the effective theory. Due to the presence of the off-diagonal long-range potential interactions, the hard annihilation reactions, encoded in the Wilson coefficients, are determined by the absorptive part of $\chi_{e_1}\chi_{e_2} \rightarrow \chi_{e_4}\chi_{e_3}$ amplitudes, as can be seen in the second line of Fig. 5.1. It is worth to stress that the $\chi_{e_1}\chi_{e_2}$ particle pair is not necessarily equal to the $\chi_{e_4}\chi_{e_3}$ pair, such that apart from true forward scattering reactions $\chi_{e_1}\chi_{e_2} \rightarrow \chi_{e_1}\chi_{e_2}$, we encounter off-diagonal hard $\chi_{e_1}\chi_{e_2} \rightarrow \chi_{e_4}\chi_{e_3}$ reactions as well.

In the following subsections we discuss the terms in $\delta\mathcal{L}_{\text{ann}}$ that describe the absorptive part of hard $\chi_{e_1}\chi_{e_2} \rightarrow \chi_{e_4}\chi_{e_3}$ scattering reactions in the effective theory including $\mathcal{O}(v_{\text{rel}}^2)$ corrections. The dimension-6 four-fermion operators given in Sec. 5.2.1 provide the leading, $\mathcal{O}(v_{\text{rel}}^0)$, terms in the non-relativistic expansion of hard (off-) diagonal χ^0/χ^\pm pair-annihilations rates. Dimension-8 four fermion operators in Sec. 5.2.2, related to P - and next-to-next-to-leading order S -wave reactions, then allow to give the corresponding $\mathcal{O}(v_{\text{rel}}^2)$ corrections in the velocity expansion. We give the explicit expressions of four-fermion operators in $\delta\mathcal{L}_{\text{ann}}$ and discuss generic properties of the corresponding Wilson coefficients. The actual determination of these Wilson coefficients, at lowest non-vanishing order in the expansion in coupling factors, from a MSSM matching calculation is postponed to Sec. 6.1. Note that the lowest non-vanishing order in the coupling expansion, $\mathcal{O}(\alpha_i^2)$, where $\alpha_i = g_i^2/4\pi$, corresponds to tree-level annihilation processes. In this case the annihilation rates can be given separately for every exclusive SM or Higgs two-particle final state $X_A X_B$, since the tree-level processes are free from infrared divergencies. In higher orders in the couplings the formalism applies to the inclusive annihilation cross section [30] or to suitably defined infrared-safe final states.

5.2.1 Basis of dimension-6 operators in $\delta\mathcal{L}_{\text{ann}}$

The leading-order contributions in $\delta\mathcal{L}_{\text{ann}}$ are given by dimension-6 four-fermion operators. For instance, the specific dimension-6 four-fermion operator that encodes scattering of a non-relativistic incoming neutralino pair $\chi_1^0\chi_1^0$ in an 1S_0 partial-wave state into an outgoing $\chi_1^0\chi_1^0$ state in the same 1S_0 partial-wave configuration is given by

$$\delta\mathcal{L}_{\text{ann}}^{d=6} \supset \frac{1}{4} f_{\{\{11\}\{\{11\}\}}^{\chi^0\chi^0 \rightarrow \chi^0\chi^0}}(^1S_0) \xi_1^\dagger \xi_1^c \xi_1^{c\dagger} \xi_1, \quad (5.6)$$

⁴In order to make contact with the commonly used notation in quarkonium annihilation, we abuse notation when writing in (5.5) the matrix element of $\delta\mathcal{L}_{\text{ann}}$ instead of the corresponding forward scattering amplitude. Written properly, the matrix element on the right-hand side in (5.5) should involve the position-space integration over the interaction Lagrangian, $\int d^4x \delta\mathcal{L}_{\text{ann}}(x)$, which implies that an additional factor $(2\pi)^4 \delta^{(4)}(p_{\text{final}} - p_{\text{initial}})$ arises when evaluating the matrix element. This factors should however not be included in the relation (5.5).

where the spinor ξ^c is the charge conjugate of ξ , $\xi^c = -i\sigma^2 \xi^*$, and σ^2 specifies the second Pauli matrix. Note that $\xi_1^{c\dagger} \xi_1$ represents the Lorentz invariant bilinear built from the non-relativistic particle field ξ_1 , which destroys the incoming state of two identical χ_1^0 particles. The factor $1/4$ is a normalisation factor which compensates the symmetry factors arising from the number of identical contractions in the tree-level $\chi_1^0 \chi_1^0 \rightarrow \chi_1^0 \chi_1^0$ matrix element. The symbol $f_{\{11\}\{11\}}^{\chi^0 \chi^0 \rightarrow \chi^0 \chi^0}(^1S_0)$ denotes the Wilson coefficient corresponding to the dimension-6 operator. We can generalise the above expression to include all possible spin-0 and spin-1 S -wave four-fermion operators at leading order in the non-relativistic expansion. Written in a compact form, the contribution of dimension-6 operators in $\delta\mathcal{L}_{\text{ann}}$ reads

$$\delta\mathcal{L}_{\text{ann}}^{d=6} = \sum_{\chi\chi \rightarrow \chi\chi} \sum_{s=0,1} \frac{1}{4} f_{\{e_1 e_2\}\{e_4 e_3\}}^{\chi\chi \rightarrow \chi\chi} (^{2s+1}S_J) \mathcal{O}_{\{e_4 e_3\}\{e_2 e_1\}}^{\chi\chi \rightarrow \chi\chi} (^{2s+1}S_J), \quad (5.7)$$

where $J = s$ for the case of S -wave operators considered here. The first sum, taken over all non-relativistic $2 \rightarrow 2$ neutralino and chargino scattering processes $\chi\chi \rightarrow \chi\chi$, implies the consideration of neutral scattering reactions as well as single-charged and double-charged processes. The $\chi\chi \rightarrow \chi\chi$ reactions that we take into account involve the same $\chi\chi$ states as in the potential scattering transitions discussed in Sec. 5.1 and therefore are as well summarised in Tab. 5.1. The spin of the incoming and outgoing two-particle states can be either $s = 0$ or $s = 1$, such that the terms in the above Lagrangian $\delta\mathcal{L}_{\text{ann}}^{d=6}$ describe 1S_0 and 3S_1 partial-wave scattering reactions. The $f_{\{e_1 e_2\}\{e_4 e_3\}}^{\chi\chi \rightarrow \chi\chi} (^{2s+1}S_J)$ denote the Wilson coefficients that correspond to the four-fermion operators $\mathcal{O}_{\{e_4 e_3\}\{e_2 e_1\}}^{\chi\chi \rightarrow \chi\chi} (^{2s+1}S_J)$. The indices e_1 and e_2 (e_3 and e_4) refer to the neutralino or chargino species of the incoming (outgoing) particles, and take the values 1 to n_0 for neutralino species and 1 to n_+ for chargino species. Note that the order of the labels e_i on the Wilson coefficients and the operators is not accidental in (5.7). The labels on the operators are given in the order, in which the field operators with label e_i occur in the operator. In case of the corresponding Wilson coefficients, the indices refer to the actual scattering reaction $\chi_{e_1} \chi_{e_2} \rightarrow \chi_{e_4} \chi_{e_3}$ that is described by the operators. The basis of dimension-6 operators is given in Tab. 5.2. Each χ in the labels $\chi\chi \rightarrow \chi\chi$ of the operators and Wilson coefficients in (5.7) should indicate the particular particle species χ^0 and χ^\pm , whose $\chi_{e_1} \chi_{e_2} \rightarrow \chi_{e_4} \chi_{e_3}$ scattering reaction is described, see Tab. 5.1. Further note, that a summation over the indices e_i is implicit in (5.7). The normalisation factor $1/4$ in (5.7) ensures that the tree-level transition matrix element for 1S_0 -wave scattering is given by

$$\begin{aligned} \langle \chi_l \chi_k | & \int d^4x \sum_{\chi\chi \rightarrow \chi\chi} \frac{1}{4} f_{\{e_1 e_2\}\{e_4 e_3\}}^{\chi\chi \rightarrow \chi\chi} (^1S_0) \mathcal{O}_{\{e_4 e_3\}\{e_2 e_1\}}^{\chi\chi \rightarrow \chi\chi} (^1S_0)(x) | \chi_i \chi_j \rangle |_{\text{tree}} \\ & = (2\pi)^4 \delta^{(4)}(p_{\text{in}} - p_{\text{out}}) 2 f_{\{ij\}\{lk\}}^{\chi\chi \rightarrow \chi\chi} (^1S_0) \end{aligned} \quad (5.8)$$

for all $\chi_i \chi_j \rightarrow \chi_l \chi_k$ reactions at leading order in the non-relativistic effective theory. In (5.8) we have assumed that the incoming and outgoing two-particle states $\chi_i \chi_j$ and $\chi_l \chi_k$ both reside in an 1S_0 -wave configuration with normalised spin state $\frac{1}{\sqrt{2}}(|\uparrow\downarrow\rangle - |\downarrow\uparrow\rangle)$.

$\chi_{e_1}\chi_{e_2} \rightarrow \chi_{e_4}\chi_{e_3}$	$\mathcal{O}_{\{e_4e_3\}\{e_2e_1\}}^{\chi\chi\rightarrow\chi\chi} (^1S_0)$	$\mathcal{O}_{\{e_4e_3\}\{e_2e_1\}}^{\chi\chi\rightarrow\chi\chi} (^3S_1)$
$\chi^0\chi^0 \rightarrow \chi^0\chi^0$	$\xi_{e_4}^\dagger \xi_{e_3}^c \xi_{e_2}^{c\dagger} \xi_{e_1}$	$\xi_{e_4}^\dagger \vec{\sigma} \xi_{e_3}^c \xi_{e_2}^{c\dagger} \vec{\sigma} \xi_{e_1}$
$\chi^0\chi^0 \rightarrow \chi^-\chi^+$	$\eta_{e_4}^\dagger \zeta_{e_3}^c \xi_{e_2}^{c\dagger} \xi_{e_1}$	$\eta_{e_4}^\dagger \vec{\sigma} \zeta_{e_3}^c \xi_{e_2}^{c\dagger} \vec{\sigma} \xi_{e_1}$
$\chi^-\chi^+ \rightarrow \chi^0\chi^0$	$\xi_{e_4}^\dagger \xi_{e_3}^c \zeta_{e_2}^{c\dagger} \eta_{e_1}$	$\xi_{e_4}^\dagger \vec{\sigma} \xi_{e_3}^c \zeta_{e_2}^{c\dagger} \vec{\sigma} \eta_{e_1}$
$\chi^-\chi^+ \rightarrow \chi^-\chi^+$	$\eta_{e_4}^\dagger \zeta_{e_3}^c \zeta_{e_2}^{c\dagger} \eta_{e_1}$	$\eta_{e_4}^\dagger \vec{\sigma} \zeta_{e_3}^c \zeta_{e_2}^{c\dagger} \vec{\sigma} \eta_{e_1}$
$\chi^0\chi^+ \rightarrow \chi^0\chi^+$	$\xi_{e_4}^\dagger \zeta_{e_3}^c \zeta_{e_2}^{c\dagger} \xi_{e_1}$	$\xi_{e_4}^\dagger \vec{\sigma} \zeta_{e_3}^c \zeta_{e_2}^{c\dagger} \vec{\sigma} \xi_{e_1}$
$\chi^-\chi^0 \rightarrow \chi^-\chi^0$	$\eta_{e_4}^\dagger \xi_{e_3}^c \xi_{e_2}^{c\dagger} \eta_{e_1}$	$\eta_{e_4}^\dagger \vec{\sigma} \xi_{e_3}^c \xi_{e_2}^{c\dagger} \vec{\sigma} \eta_{e_1}$
$\chi^+\chi^+ \rightarrow \chi^+\chi^+$	$\zeta_{e_4}^\dagger \zeta_{e_3}^c \zeta_{e_2}^{c\dagger} \zeta_{e_1}$	$\zeta_{e_4}^\dagger \vec{\sigma} \zeta_{e_3}^c \zeta_{e_2}^{c\dagger} \vec{\sigma} \zeta_{e_1}$
$\chi^-\chi^- \rightarrow \chi^-\chi^-$	$\eta_{e_4}^\dagger \eta_{e_3}^c \eta_{e_2}^{c\dagger} \eta_{e_1}$	$\eta_{e_4}^\dagger \vec{\sigma} \eta_{e_3}^c \eta_{e_2}^{c\dagger} \vec{\sigma} \eta_{e_1}$

Table 5.2: Four-fermion operators for leading-order S -wave $\chi_{e_1}\chi_{e_2} \rightarrow \chi_{e_4}\chi_{e_3}$ transitions. The indices $e_i, i = 1, \dots, 4$ on the χ -fields are suppressed in the first column. In addition to the specified operators there are redundant ones, which are obtained by interchanging the field-operator symbols ξ, η or ζ (but not the labels) at the first and second and/or the third and fourth position in the operator $\mathcal{O}^{\chi\chi\rightarrow\chi\chi}$. For example, for 1S_0 $\chi^0\chi^+ \rightarrow \chi^0\chi^+$ operators one of the three classes of field-interchanged operators is given by the 1S_0 $\chi^+\chi^0 \rightarrow \chi^+\chi^0$ operators $\zeta_{e_4}^\dagger \xi_{e_3}^c \xi_{e_2}^{c\dagger} \zeta_{e_1}$.

A similar relation for the tree-level transition matrix element of 3S_1 -wave scattering in the effective theory holds for all $\chi_i\chi_j \rightarrow \chi_l\chi_k$ reactions. Note that in order to derive (5.8) one has to take into account relations among Wilson coefficients of different operators, which will be deduced in the next paragraph.

There are redundancies in $\delta\mathcal{L}_{\text{ann}}^{d=6}$, (5.7), as several operators can describe one specific scattering reaction with a χ_{e_1} and a χ_{e_2} (χ_{e_4} and χ_{e_3}) particle in the initial (final) state. This redundancy is associated with operators that arise from interchanging the single-particle field operators at the first and second and/or third and fourth position in a given $\mathcal{O}^{\chi\chi\rightarrow\chi\chi}$. The corresponding Wilson coefficients are related to each other, as they encode the same information on a given specific scattering reaction. Consequently, the redundancy manifests itself in symmetry relations among the Wilson coefficients under exchange of the labels $e_1 \leftrightarrow e_2$ and/or $e_4 \leftrightarrow e_3$. These relations read

$$\begin{aligned}
f_{\{e_2e_1\}\{e_4e_3\}}^{\chi_{e_2}\chi_{e_1} \rightarrow \chi_{e_4}\chi_{e_3}} ({}^{2s+1}S_J) &= \eta_s f_{\{e_1e_2\}\{e_4e_3\}}^{\chi_{e_1}\chi_{e_2} \rightarrow \chi_{e_4}\chi_{e_3}} ({}^{2s+1}S_J) , \\
f_{\{e_1e_2\}\{e_3e_4\}}^{\chi_{e_1}\chi_{e_2} \rightarrow \chi_{e_3}\chi_{e_4}} ({}^{2s+1}S_J) &= \eta_s f_{\{e_1e_2\}\{e_4e_3\}}^{\chi_{e_1}\chi_{e_2} \rightarrow \chi_{e_4}\chi_{e_3}} ({}^{2s+1}S_J) ,
\end{aligned} \tag{5.9}$$

with

$$\eta_s = \begin{cases} 1 & \text{for } s = 0 \\ -1 & \text{for } s = 1 \end{cases} . \tag{5.10}$$

5.2.2 Basis of dimension-8 operators in $\delta\mathcal{L}_{\text{ann}}$

At next-to-next-to-leading order in the non-relativistic expansion in momenta and mass differences,⁵ dimension-8 four-fermion operators contribute to $\delta\mathcal{L}_{\text{ann}}$.⁶ Similar to the compact notation used for the dimension-6 four-fermion operators in (5.7), the contributions from dimension-8 operators can be written as

$$\begin{aligned}
\delta\mathcal{L}_{\text{ann}}^{d=8} = & \sum_{\chi\chi\rightarrow\chi\chi} \frac{1}{4M^2} f_{\{e_1e_2\}\{e_4e_3\}}^{\chi\chi\rightarrow\chi\chi} ({}^1P_1) \mathcal{O}_{\{e_4e_3\}\{e_2e_1\}}^{\chi\chi\rightarrow\chi\chi} ({}^1P_1) \\
& + \sum_{\chi\chi\rightarrow\chi\chi} \sum_{J=0,1,2} \frac{1}{4M^2} f_{\{e_1e_2\}\{e_4e_3\}}^{\chi\chi\rightarrow\chi\chi} ({}^3P_J) \mathcal{O}_{\{e_4e_3\}\{e_2e_1\}}^{\chi\chi\rightarrow\chi\chi} ({}^3P_J) \\
& + \sum_{\chi\chi\rightarrow\chi\chi} \sum_{s=0,1} \frac{1}{4M^2} g_{\{e_1e_2\}\{e_4e_3\}}^{\chi\chi\rightarrow\chi\chi} ({}^{2s+1}S_s) \mathcal{P}_{\{e_4e_3\}\{e_2e_1\}}^{\chi\chi\rightarrow\chi\chi} ({}^{2s+1}S_s) \\
& + \sum_{\chi\chi\rightarrow\chi\chi} \sum_{s=0,1} \sum_{i=1,2} \frac{1}{4M^2} h_{i\{e_1e_2\}\{e_4e_3\}}^{\chi\chi\rightarrow\chi\chi} ({}^{2s+1}S_s) \mathcal{Q}_{i\{e_4e_3\}\{e_2e_1\}}^{\chi\chi\rightarrow\chi\chi} ({}^{2s+1}S_s) . \quad (5.11)
\end{aligned}$$

The $f_{\{e_1e_2\}\{e_4e_3\}}^{\chi\chi\rightarrow\chi\chi}$, $g_{\{e_1e_2\}\{e_4e_3\}}^{\chi\chi\rightarrow\chi\chi}$ and $h_{i\{e_1e_2\}\{e_4e_3\}}^{\chi\chi\rightarrow\chi\chi}$ denote the Wilson coefficients of the corresponding four-fermion operators $\mathcal{O}_{\{e_4e_3\}\{e_2e_1\}}$, $\mathcal{P}_{\{e_4e_3\}\{e_2e_1\}}$ and $\mathcal{Q}_i\{e_4e_3\}\{e_2e_1\}$, whose explicit form for the case of $\chi_{e_1}^0\chi_{e_2}^0 \rightarrow \chi_{e_4}^0\chi_{e_3}^0$ scattering reactions is given in Tab. 5.3.⁷ As before in (5.7), the labels e_i in (5.11) range over $e_i = 1, \dots, n_0$ (resp. $e_i = 1, \dots, n_+$), if the respective field χ_{e_i} in the $\chi_{e_1}\chi_{e_2} \rightarrow \chi_{e_4}\chi_{e_3}$ reaction refers to neutralino- (chargino-) species. The factor $1/4$ in front of the operators in (5.11) is a convenient normalisation of transition matrix elements in the effective theory. In addition, a normalisation factor of $1/M^2$ has been factored out in (5.11), such that the next-to-next-to-leading order Wilson coefficients have the same mass dimension (-2) as the leading-order ones in Sec. 5.2.1. The mass scale M is equal to half the sum of the masses of the χ_{e_i} particles involved in the reaction $\chi_{e_1}\chi_{e_2} \rightarrow \chi_{e_4}\chi_{e_3}$, *i.e.*

$$M = \frac{1}{2} \sum_{i=1}^4 m_{e_i}, \quad (5.12)$$

such that M itself constitutes a process-specific quantity. Note that the operators $\mathcal{Q}_i ({}^{2s+1}S_s)$ have the same structure as the dimension-6 operators $\mathcal{O} ({}^{2s+1}S_s)$ given in

⁵The need for and the details on an expansion in mass differences become most obvious in the MSSM matching calculation that leads to the determination of the Wilson coefficients of the four-fermion operators in $\delta\mathcal{L}_{\text{ann}}$. A corresponding discussion is therefore postponed to Sec. 6.1.2.

⁶Let us remark that we do not consider next-to-leading order contributions to $\delta\mathcal{L}_{\text{ann}}$, corresponding to dimension-7 four-fermion operators, as these encode ${}^1S_0 - {}^3P_0$, ${}^3S_1 - {}^1P_1$ and ${}^3S_1 - {}^3P_1$ transitions which will require the addition of v_{rel} -suppressed potential interactions in the long-range part of the annihilation; we consider only $\mathcal{O}(v_{\text{rel}}^2)$ effects from the short-distance annihilation, and not those arising from subleading non-Coulomb (non-Yukawa) potentials.

⁷In order to ensure the $U(1)_{\text{em}}$ gauge invariance of the NRMSSM, all derivatives ∂ in dimension-8 four-fermion operators \mathcal{O} and \mathcal{P} that act on chargino fields (η_i, ζ_i) have to be replaced by the corresponding covariant derivative $\mathbf{D} = \partial + ie\mathbf{A}$, where \mathbf{A} denotes the spatial components of the photon field A^μ .

$\mathcal{O}^{XX \rightarrow XX}(^1P_1)$	$\xi_{e_4}^\dagger \left(-\frac{i}{2} \overleftrightarrow{\partial}\right) \xi_{e_3}^c \cdot \xi_{e_2}^{c\dagger} \left(-\frac{i}{2} \overleftrightarrow{\partial}\right) \xi_{e_1}$
$\mathcal{O}^{XX \rightarrow XX}(^3P_0)$	$\frac{1}{3} \xi_{e_4}^\dagger \left(-\frac{i}{2} \overleftrightarrow{\partial} \cdot \boldsymbol{\sigma}\right) \xi_{e_3}^c \cdot \xi_{e_2}^{c\dagger} \left(-\frac{i}{2} \overleftrightarrow{\partial} \cdot \boldsymbol{\sigma}\right) \xi_{e_1}$
$\mathcal{O}^{XX \rightarrow XX}(^3P_1)$	$\frac{1}{2} \xi_{e_4}^\dagger \left(-\frac{i}{2} \overleftrightarrow{\partial} \times \boldsymbol{\sigma}\right) \xi_{e_3}^c \cdot \xi_{e_2}^{c\dagger} \left(-\frac{i}{2} \overleftrightarrow{\partial} \times \boldsymbol{\sigma}\right) \xi_{e_1}$
$\mathcal{O}^{XX \rightarrow XX}(^3P_2)$	$\xi_{e_4}^\dagger \left(-\frac{i}{2} \overleftrightarrow{\partial}^{(i\sigma j)}\right) \xi_{e_3}^c \cdot \xi_{e_2}^{c\dagger} \left(-\frac{i}{2} \overleftrightarrow{\partial}^{(i\sigma j)}\right) \xi_{e_1}$
$\mathcal{P}^{XX \rightarrow XX}(^1S_0)$	$\frac{1}{2} \left[\xi_{e_4}^\dagger \xi_{e_3}^c \cdot \xi_{e_2}^{c\dagger} \left(-\frac{i}{2} \overleftrightarrow{\partial}\right)^2 \xi_{e_1} + \xi_{e_4}^\dagger \left(-\frac{i}{2} \overleftrightarrow{\partial}\right)^2 \xi_{e_3}^c \cdot \xi_{e_2}^{c\dagger} \xi_{e_1} \right]$
$\mathcal{P}^{XX \rightarrow XX}(^3S_1)$	$\frac{1}{2} \left[\xi_{e_4}^\dagger \boldsymbol{\sigma} \xi_{e_3}^c \cdot \xi_{e_2}^{c\dagger} \boldsymbol{\sigma} \left(-\frac{i}{2} \overleftrightarrow{\partial}\right)^2 \xi_{e_1} + \xi_{e_4}^\dagger \boldsymbol{\sigma} \left(-\frac{i}{2} \overleftrightarrow{\partial}\right)^2 \xi_{e_3}^c \cdot \xi_{e_2}^{c\dagger} \boldsymbol{\sigma} \xi_{e_1} \right]$
$\mathcal{Q}_1^{XX \rightarrow XX}(^1S_0)$	$(\delta m M) \xi_{e_4}^\dagger \xi_{e_3}^c \cdot \xi_{e_2}^{c\dagger} \xi_{e_1}$
$\mathcal{Q}_1^{XX \rightarrow XX}(^3S_1)$	$(\delta m M) \xi_{e_4}^\dagger \boldsymbol{\sigma} \xi_{e_3}^c \cdot \xi_{e_2}^{c\dagger} \boldsymbol{\sigma} \xi_{e_1}$
$\mathcal{Q}_2^{XX \rightarrow XX}(^1S_0)$	$(\delta \overline{m} M) \xi_{e_4}^\dagger \xi_{e_3}^c \cdot \xi_{e_2}^{c\dagger} \xi_{e_1}$
$\mathcal{Q}_2^{XX \rightarrow XX}(^3S_1)$	$(\delta \overline{m} M) \xi_{e_4}^\dagger \boldsymbol{\sigma} \xi_{e_3}^c \cdot \xi_{e_2}^{c\dagger} \boldsymbol{\sigma} \xi_{e_1}$

Table 5.3: Explicit form of the P -wave (\mathcal{O}) and next-to-next-to-leading order S -wave (\mathcal{P} , \mathcal{Q}_i) four-fermion operators contributing to $\chi_{e_1}^0 \chi_{e_2}^0 \rightarrow \chi_{e_4}^0 \chi_{e_3}^0$ scattering reactions. Each index e_i can take the values $e_i = 1, \dots, n_0$. The P - and next-to-next-to-leading order S -wave four-fermion operators for the remaining neutral, charged and double-charged $\chi_{e_1} \chi_{e_2} \rightarrow \chi_{e_4} \chi_{e_3}$ processes are obtained by replacing the field operators ξ_{e_i} , $i = 1, \dots, 4$ above by those of the respective particle species involved. The quantity $\overleftrightarrow{\partial}$ is a 3-vector whose components are $\partial^i \equiv \partial/\partial x_i$. The action of $\overleftrightarrow{\partial}$ on the two field operators at its left and right is defined as $\xi_{e_b}^{c\dagger} \overleftrightarrow{\partial} \xi_{e_a} \equiv \xi_{e_b}^{c\dagger} (\partial \xi_{e_a}) - (\partial \xi_{e_b}^c)^\dagger \xi_{e_a}$. The symmetric traceless components of a tensor T^{ij} are denoted by $T^{(ij)} = (T^{ij} + T^{ji})/2 - T^{kk} \delta^{ij}/3$. Finally, the mass scale M is defined in (5.12) and the mass differences $\delta m, \delta \overline{m}$ are given in (5.13).

Tab. 5.2, but are proportional to the mass differences

$$\delta m = \frac{m_{e_4} - m_{e_1}}{2}, \quad \delta \overline{m} = \frac{m_{e_3} - m_{e_2}}{2}, \quad (5.13)$$

computed from the masses m_{e_i} in the reaction $\chi_{e_1} \chi_{e_2} \rightarrow \chi_{e_4} \chi_{e_3}$. In order to ensure convergence, the mass differences (5.13) have to be considered as $\mathcal{O}(v_{\text{rel}}^2)$ effects in the non-relativistic expansion of the amplitudes. We discuss this point in context of the matching calculation in Sec. 6.1.2. The mass splittings between the χ^0/χ^\pm species that can be part of the NRMSSM, are therefore limited to be much smaller than m_{LSP} , the mass of the lightest non-relativistic state in the effective theory. This implies in turn

that those neutralino and chargino states in a given MSSM spectrum that have mass splittings of the order m_{LSP} should be decoupled explicitly and integrated out. Since $\delta m = \delta \overline{m} = 0$ for diagonal annihilation reactions $\chi_{e_1} \chi_{e_2} \rightarrow \chi_{e_1} \chi_{e_2}$ (where the absorptive parts of the respective amplitudes are related to the corresponding annihilation cross section), the \mathcal{Q}_i (${}^{2s+1}S_s$) are only relevant for the computation of the off-diagonal rates.

We note that dimension-8 operators $\mathcal{P}({}^3S_1, {}^3D_1)$, which describe ${}^3S_1 \rightarrow {}^3D_1$ transitions, have not been included in $\delta \mathcal{L}_{\text{ann}}^{d=8}$. In the calculation of the tree-level annihilation cross section in the centre-of-mass frame, contributions from these operators vanish, while for the Sommerfeld enhanced annihilation cross section they will require to consider a v_{rel}^2 -suppressed potential interaction in the long-range part of the annihilation in order to compensate for the change in orbital angular momentum in the short-distance part, thus yielding a contribution to the cross section of $\mathcal{O}(v_{\text{rel}}^4)$.

As we have noted in Sec. 5.2.1 we construct $\delta \mathcal{L}_{\text{ann}}$ in such a way that it contains all redundant operators, which arise through interchanging the single-particle field-operators at the first and second (third and fourth) position given a specific four-fermion operator, such that several operators describe one specific scattering reaction with a χ_{e_1} and χ_{e_2} (χ_{e_4} and χ_{e_3}) particle in the initial (final) state. Consequently there are symmetry relations among the Wilson coefficients associated with the subsets of redundant operators in $\delta \mathcal{L}_{\text{ann}}^{d=8}$, similar to the relations for leading-order S -wave coefficients in (5.9). They read

$$\begin{aligned} k_{\{e_2 e_1\}\{e_4 e_3\}}^{\chi_{e_2} \chi_{e_1} \rightarrow \chi_{e_4} \chi_{e_3}} ({}^{2s+1}L_J) &= (-1)^{s+L} k_{\{e_1 e_2\}\{e_4 e_3\}}^{\chi_{e_1} \chi_{e_2} \rightarrow \chi_{e_4} \chi_{e_3}} ({}^{2s+1}L_J) , \\ k_{\{e_1 e_2\}\{e_3 e_4\}}^{\chi_{e_1} \chi_{e_2} \rightarrow \chi_{e_3} \chi_{e_4}} ({}^{2s+1}L_J) &= (-1)^{s+L} k_{\{e_1 e_2\}\{e_4 e_3\}}^{\chi_{e_1} \chi_{e_2} \rightarrow \chi_{e_4} \chi_{e_3}} ({}^{2s+1}L_J) , \end{aligned} \quad (5.14)$$

where $k = f, g$ for P - and next-to-next-to-leading order S -wave coefficients, respectively. Note that (5.14) generalises the leading-order S -wave relations in (5.9). Finally let us note that similar relations as (5.14) apply for the Wilson coefficients h_i , where however an additional exchange of the particles in the definition of the mass differences $\delta m, \delta \overline{m}$ in front of the corresponding operators \mathcal{Q}_i has to be taken into account.

Chapter 6

The hard annihilation reactions

In Chap. 5 we have introduced the NRMSSM, an effective field theory that is designed to describe scattering and annihilation reactions of non-relativistic neutralinos and charginos. Here we will focus on the hard pair-annihilation reactions of non-relativistic χ^0/χ^\pm states in the effective theory, which are encoded in the absorptive part of the Wilson coefficients of four-fermion operators in $\delta\mathcal{L}_{\text{ann}}$, a part of the generic EFT Lagrangian $\mathcal{L}^{\text{NRMSSM}}$. Conceptually this chapter is divided into three parts. The first part comprises Sec. 6.1 and contains the technical details on the calculation of our purely analytic expressions for the absorptive parts of the Wilson coefficients. We describe the steps in the calculation of the coefficients related to leading-order S -wave, P - and next-to-next-to leading order S -wave annihilation processes and collect explicit analytic expressions for the coefficients in terms of the underlying MSSM parameters and couplings in Appendices A.1–A.3. Sec. 6.2 covers the second part, where we provide an extensive discussion on the numerical comparison of the hard (tree-level) annihilation cross sections derived in the NRMSSM with results from the numerical code MADGRAPH [89]. The third part is contained in Sec. 6.3. Here we illustrate in an analytic sample calculation in the pure-wino NRMSSM, how the generic results for the Wilson coefficients, collected in Appendices A.1–A.3, have to be applied in order to obtain all (off-) diagonal hard co-annihilation rates in this scenario.

The structure of the first part is as follows. The matching condition that relates the perturbative $\chi_i\chi_j \rightarrow \chi_l\chi_k$ scattering amplitudes in the NRMSSM with the corresponding amplitudes in the MSSM and thereby allows the determination of the Wilson coefficients in $\delta\mathcal{L}_{\text{ann}}$ in terms of the underlying MSSM parameters and couplings is discussed in Sec. 6.1.1. The matching procedure requires an expansion of the MSSM amplitudes in the non-relativistic external momenta. In addition, as we generically consider processes $\chi_{e_1}\chi_{e_2} \rightarrow \chi_{e_4}\chi_{e_3}$ where the outgoing two-particle states can be different and slightly lighter or heavier than the incoming ones, we have to perform an expansion in mass differences of the states involved. We comment on these expansions in Sec. 6.1.2. Subsequently we give a brief discussion on the gauge used in the calculation in Sec. 6.1.3. Further details on the actual determination through the MSSM matching calculation and the final form of the Wilson coefficients are provided in Sec. 6.1.4, including a master

formula for the Wilson coefficients in terms of coupling and kinematic factors. Results and recipes for the construction of these coupling and kinematic factors, valid in the general MSSM, are collected in Appendices A.1–A.3.

In the second part we discuss the numerical comparison of our non-relativistic approximation to χ^0/χ^\pm pair-annihilation cross sections σv_{rel} with corresponding results produced with MADGRAPH. To this end we select several annihilation processes where the role of the next-to-next-to-leading corrections from our analytic calculation of the annihilation cross section is markedly different. In Sec. 6.2.1 we present two reactions where P - and next-to-next-to-leading S -wave contributions are of the same order. Two S -wave dominated reactions are considered in Sec. 6.2.2, followed by a P -wave dominated process in Sec. 6.2.3. The case of an off-diagonal rate, where no numerical check with MADGRAPH is available, is given in Sec. 6.2.4. As our effective field theory framework allows to describe annihilation rates of “hydrogen-like” $\chi\chi$ states as well, we conclude by comparing results for annihilation reactions of two such “hydrogen-like” states with MADGRAPH generated data in Sec. 6.2.5. The examples of Sec. 6.2 in particular illustrate the importance of separating the different partial-wave contributions to the short-distance annihilation in view of the computation of the Sommerfeld-corrected cross sections, including $\mathcal{O}(v_{\text{rel}}^2)$ corrections to the hard annihilation rates.¹

In the third part we first provide in Sec. 6.3.1 a detailed derivation of the coupling factor expressions needed in the construction of the Wilson coefficients in non-relativistic $\chi_1^+\chi_1^- \rightarrow W^+W^-$ annihilations in the pure-wino NRMSSM. Subsequently the corresponding kinematic factor expressions are derived in Sec. 6.3.2. In both sections we rely on the conventions and notations introduced in Appendices A.1–A.3. Finally, Sec. 6.3.3 contains analytic results for all exclusive tree-level co-annihilation rates in the pure-wino NRMSSM at $\mathcal{O}(v_{\text{rel}}^2)$, that are relevant in the relic abundance calculation in this scenario.

6.1 Matching calculation & Master formula

6.1.1 Matching condition

The Wilson coefficients of the four-fermion operators in $\delta\mathcal{L}_{\text{ann}}$ are determined by the matching condition

$$\begin{aligned} \mathcal{A}(\chi_i\chi_j \rightarrow \chi_l\chi_k) \Big|_{\text{MSSM, perturbative}} &= \sum \frac{1}{4 M^{d-6}} f_{\{e_1e_2\}\{e_4e_3\}}^{(d)\chi\chi\rightarrow\chi\chi}(^{2s+1}L_J) \\ &\times \langle \chi_l\chi_k | \mathcal{O}_{\{e_4e_3\}\{e_2e_1\}}^{(d)\chi\chi\rightarrow\chi\chi}(^{2s+1}L_J) | \chi_i\chi_j \rangle \Big|_{\text{NRMSSM, perturbative}} . \end{aligned} \quad (6.1)$$

¹The investigation of Sommerfeld enhancements in some popular MSSM scenarios is the content of Chap. 9, where we find that Sommerfeld-enhanced P - and next-to-next-to-leading order S -wave corrections to the hard annihilation rates play a subdominant role in the relic abundance calculation as compared to the effect from correctly accounting for off-diagonal (leading-order S -wave) annihilation rates. The latter turns out to be particularly crucial in an accurate calculation of the χ_1^0 relic density including Sommerfeld enhancements, as we discuss in detail in Chap. 9.

Here we have denoted the dimension- d four-fermion operators and their corresponding Wilson coefficients with symbols $\mathcal{O}^{(d)}$ and $f^{(d)}$ in order to make the notation of the matching condition – which in particular implies a summation $\sum_{d \geq 6}$ – simpler. The connection to the notation established in Chap. 5 is obvious. For instance we have the correspondence $\mathcal{O}^{(d=6)}(1S_0) = \mathcal{O}(1S_0)$ and $f^{(d=6)}(1S_0) = f(1S_0)$ as well as $\mathcal{O}^{(d=8)}(1S_0) = \mathcal{P}(1S_0)$ and $f^{(d=8)}(1S_0) = g(1S_0)$. Except for this section (Sec. 6.1), we will always use the notation from Chap. 5 and denote the Wilson coefficients of dimension $d = 6$ and $d = 8$ operators by $f^{(2s+1)S_s}$ and $f^{(2s+1)P_J}$, $g^{(2s+1)S_s}$, $h_i^{(2s+1)S_s}$, respectively. The same applies to the notation for the dimension $d = 6, 8$ four-fermion operators. Recall that the mass scale M , defined in (5.12), is a $\chi_{e_1}\chi_{e_2} \rightarrow \chi_{e_4}\chi_{e_3}$ process-specific quantity. Let us finally note that any Wilson coefficient $f^{(d)}$ in (6.1) generically has mass dimension -2 , independent of the mass dimension d of the corresponding four-fermion operator.

For equation (6.1) to hold, we have to use the same (non-relativistic) normalisation of the incoming and outgoing states in both the full theory and the NRMSSM. Formally this condition is a generalisation and appropriate modification of the matching condition set up in [30], therein used for the determination of the Wilson coefficients of four fermion operators in the NRQCD Lagrangian. Here we will determine the contributions to the Wilson coefficients in $\delta\mathcal{L}_{\text{ann}}$ that describe the tree-level annihilation reactions of χ^0/χ^\pm pairs into exclusive SM and light Higgs two-body final states $X_A X_B$, which we shall denote as $\hat{f}^{(d)\chi\chi \rightarrow X_A X_B \rightarrow \chi\chi}(2s+1)L_J$. The unitarity of the S-matrix at the diagrammatic level establishes a relation among the tree-level annihilation rate for $\chi_i\chi_j \rightarrow X_A X_B$ and the imaginary part of the 1-loop forward-scattering reaction $\chi_i\chi_j \rightarrow X_A X_B \rightarrow \chi_i\chi_j$:

$$\begin{aligned} & \int [\text{dPS}_{AB}] |\mathcal{A}(\chi_i\chi_j \rightarrow X_A X_B)|^2 = 2 \Im [\mathcal{A}(\chi_i\chi_j \rightarrow X_A X_B \rightarrow \chi_i\chi_j)] \quad (6.2) \\ & = 2 \sum \frac{1}{4M^{d-6}} \Im \left[f_{\{e_1 e_2\}\{e_4 e_3\}}^{(d)\chi\chi \rightarrow X_A X_B \rightarrow \chi\chi}(2s+1)L_J \right] \langle \chi_i\chi_j | \mathcal{O}_{\{e_4 e_3\}\{e_2 e_1\}}^{(d)\chi\chi \rightarrow \chi\chi}(2s+1)L_J | \chi_i\chi_j \rangle. \end{aligned}$$

We generalise this relation and define the absorptive part of the (off-) diagonal amplitude $\mathcal{A}(\chi_i\chi_j \rightarrow X_A X_B \rightarrow \chi_l\chi_k)$ as well as the absorptive part of the Wilson coefficients in the following way:

$$\begin{aligned} & \int [\text{dPS}_{AB}] \mathcal{A}(\chi_i\chi_j \rightarrow X_A X_B) \times \mathcal{A}(\chi_l\chi_k \rightarrow X_A X_B)^* \quad (6.3) \\ & = 2 [\mathcal{A}(\chi_i\chi_j \rightarrow X_A X_B \rightarrow \chi_l\chi_k)] |_{\text{absorptive}} \\ & = 2 \sum \frac{1}{4M^{d-6}} \hat{f}_{\{e_1 e_2\}\{e_4 e_3\}}^{(d)\chi\chi \rightarrow X_A X_B \rightarrow \chi\chi}(2s+1)L_J \langle \chi_l\chi_k | \mathcal{O}_{\{e_4 e_3\}\{e_2 e_1\}}^{(d)\chi\chi \rightarrow \chi\chi}(2s+1)L_J | \chi_i\chi_j \rangle, \end{aligned}$$

where we have introduced the notation

$$\hat{f}_{\{ij\}\{lk\}}^{(d)\chi\chi \rightarrow X_A X_B \rightarrow \chi\chi}(2s+1)L_J = f_{\{ij\}\{lk\}}^{(d)\chi\chi \rightarrow X_A X_B \rightarrow \chi\chi}(2s+1)L_J |_{\text{absorptive}}. \quad (6.4)$$

With this definition, the absorptive part of a Wilson coefficient that encodes a $\chi_i\chi_j \rightarrow \chi_i\chi_j$ forward-scattering reaction coincides with its imaginary part. The adjoint of the

four-fermion operators in $\delta\mathcal{L}_{\text{ann}}$ that do not involve mass differences δm , $\delta\bar{m}$ in their definition satisfy

$$\mathcal{O}_{\{e_4e_3\}\{e_2e_1\}}^{(d)\dagger}(^{2s+1}L_J) = \mathcal{O}_{\{e_1e_2\}\{e_3e_4\}}^{(d)}(^{2s+1}L_J), \quad (6.5)$$

which for dimension- d operators with $d = 6, 8$ is easily seen from the explicit expressions in Tab. 5.2 and Tab. 5.3. We can use this relation in order to express the absorptive part of a Wilson coefficient $\hat{f}^{(d)}(^{2s+1}L_J)$, defined through (6.3), in terms of full Wilson coefficients $f^{(d)}(^{2s+1}L_J)$,

$$-i \left(f_{\{e_1e_2\}\{e_4e_3\}}^{(d)\chi\chi\rightarrow\chi\chi}(^{2s+1}L_J) - [f_{\{e_4e_3\}\{e_1e_2\}}^{(d)\chi\chi\rightarrow\chi\chi}(^{2s+1}L_J)]^* \right) = 2 \hat{f}_{\{e_1e_2\}\{e_4e_3\}}^{(d)\chi\chi\rightarrow\chi\chi}(^{2s+1}L_J). \quad (6.6)$$

As a trivial consequence we obtain the following relation between the absorptive parts of the Wilson coefficients under the exchange of the particle labels:

$$\hat{f}_{\{e_1e_2\}\{e_4e_3\}}^{(d)\chi\chi\rightarrow\chi\chi}(^{2s+1}L_J) = \left[\hat{f}_{\{e_4e_3\}\{e_1e_2\}}^{(d)\chi\chi\rightarrow\chi\chi}(^{2s+1}L_J) \right]^*. \quad (6.7)$$

The latter two relations hold for all Wilson coefficients apart from those related to operators that involve mass difference terms δm and $\delta\bar{m}$, as for example the operators $\mathcal{Q}_{i=1,2}$ in Tab. 5.3, in which case an additional exchange of the particles in the definition of the mass differences $\delta m, \delta\bar{m}$ in front of the corresponding operators has to be taken into account.²

We make use of the defining relations to determine the absorptive part of the Wilson coefficients $\hat{f}^{(d=6,8)\chi\chi\rightarrow X_A X_B \rightarrow \chi\chi}$ from the product of the full-theory tree-level annihilation amplitudes integrated over the final state particles' phase-space, as given in the first line of (6.3). Technically this is achieved by considering all 1-loop scattering amplitudes $\chi_i \chi_j \rightarrow X_A X_B \rightarrow \chi_l \chi_k$ of non-relativistic χ^0/χ^\pm pairs $\chi_i \chi_j$ and $\chi_l \chi_k$ with a specific SM or Higgs particle pair $X_A X_B$ in the intermediate state and by applying the Cutkosky rules [90, 91] to the X_A and X_B propagators. The resulting expression coincides with the first line of (6.3). To determine the absorptive part of the Wilson coefficients, the expression has to be expanded in the non-relativistic momenta of the external particles as well as in their mass differences and an appropriate spin-projection has to be performed. Further details on this expansion are provided in the following section.

6.1.2 Expansion in momenta and mass differences in $\delta\mathcal{L}_{\text{ann}}$

Our framework allows us to consider annihilation processes of two particles with similar mass ($m \sim \bar{m}$), but also annihilation reactions of hydrogen-like two particle systems, where one particle is much lighter than the other (though still heavy enough to be considered as non-relativistic). In order to cover both cases we adopt the convention that particles e_1 and e_4 (e_2 and e_3) in the scattering reaction $\chi_{e_1} \chi_{e_2} \rightarrow \chi_{e_4} \chi_{e_3}$ of non-relativistic two-particle states share the same mass scale m (\bar{m}). m and \bar{m} can be but

²Note that if $\delta m, \delta\bar{m}$ are considered as part of the corresponding Wilson coefficients and not the operators $\mathcal{Q}_{i=1,2}$, then (6.7) also holds for the former.

are not necessarily close to each other.³ Further we simplify the notation by replacing the indices (e_1, e_2, e_3, e_4) by $(1, 2, 3, 4)$ throughout this section. With these conventions and assignments, we define

$$\begin{aligned} m_1 &= m - \delta m, & m_2 &= \bar{m} - \delta \bar{m}, \\ m_4 &= m + \delta m, & m_3 &= \bar{m} + \delta \bar{m}, \end{aligned} \quad (6.8)$$

with

$$m = \frac{m_1 + m_4}{2}, \quad \bar{m} = \frac{m_2 + m_3}{2}, \quad (6.9)$$

such that the mass differences read

$$\delta m = \frac{m_4 - m_1}{2}, \quad \delta \bar{m} = \frac{m_3 - m_2}{2}. \quad (6.10)$$

Diagonal scattering reactions $\chi_1\chi_2 \rightarrow \chi_1\chi_2$ imply $m = m_1$ and $\bar{m} = m_2$, and the mass differences δm and $\delta \bar{m}$ obviously vanish in that case. The analytic results for the Wilson coefficients, that we collect in the appendices A.1 and A.2, refer to the definitions (6.8–6.10). If for a given process $\chi_i\chi_j \rightarrow \chi_l\chi_k$ it turns out that the reverse condition, $m_i \sim m_k \sim m$ and $m_j \sim m_l \sim \bar{m}$, is more meaningful given the actual values of the masses, one can make use of the symmetry properties (5.9) to relate the Wilson coefficients for $\chi_i\chi_j \rightarrow \chi_l\chi_k$ to those of $\chi_i\chi_j \rightarrow \chi_k\chi_l$. This would then conform to the prescription above, *i.e.* m would be equal to the average of the mass of the particle associated with field 1 and the mass of the particle associated with field 4, $m = (m_i + m_k)/2$.

In course of the matching calculation there are a few subtleties in the expansion in mass differences and momenta of the MSSM amplitudes, particularly related to off-diagonal reactions. They are related to the fact that the absorptive parts of the Wilson coefficients are obtained by matching amplitudes for the process $\chi_1\chi_2 \rightarrow \chi_4\chi_3$ with on-shell external states. This implies that the energy-conservation relation in the centre-of-mass system,

$$\sqrt{s} = E_1(\vec{p}^2) + E_2(\vec{p}^2) = E_4(\vec{p}'^2) + E_3(\vec{p}'^2), \quad (6.11)$$

with $E_i(\vec{p}^2) = \sqrt{m_i^2 + \vec{p}^2}$ and \vec{p} (\vec{p}') the incoming (outgoing) particles' momentum in the centre-of-mass system, is fulfilled. Using (6.8–6.10) and $M \equiv m + \bar{m}$, the expansion of the energy-conservation relation (6.11) for non-relativistic momenta \vec{p}^2 and \vec{p}'^2 reads

$$\sqrt{s} = M - \delta m - \delta \bar{m} + \frac{\vec{p}^2}{2\mu} + \dots = M + \delta m + \delta \bar{m} + \frac{\vec{p}'^2}{2\mu} + \dots, \quad (6.12)$$

³Let us emphasise at this point, that we include a discussion and numerical comparison of our results applied to hydrogen-like $\chi\chi$ state tree-level annihilation reactions in Sec. 6.2.5.

where $\mu = m\bar{m}/M$ and we have dropped terms of order \vec{p}^4/μ^3 and $(\delta m/M \times \vec{p}^2/\mu)$. This can be rewritten as

$$\frac{\vec{p}'^2}{2\mu} = \frac{\vec{p}^2}{2\mu} - 2\delta m - 2\delta\bar{m} + \dots \quad (6.13)$$

From (6.13) we see that a consistent expansion which treats both \vec{p}^2 and \vec{p}'^2 as small quantities of the same order requires that the mass differences $\delta m, \delta\bar{m}$ are also formally considered of order \vec{p}^2/μ in the expansion of the amplitudes. Let us recall again that only off-diagonal scattering reactions require an expansion in mass differences as in these cases the incoming and outgoing $\chi\chi$ states are different. In contrast we always have $\delta m = \delta\bar{m} = 0$ for diagonal reactions $\chi_1\chi_2 \rightarrow \chi_1\chi_2$.

Taking the expansion in mass differences consistently into account and relying on the conventions established above, we can identify the two distinct energy scales associated with a generic process $\chi_1\chi_2 \rightarrow X_A X_B \rightarrow \chi_4\chi_3$ of non-relativistic two-particles states. The amplitudes are characterised by the hard scales m, \bar{m} , and additionally involve the small scales $(\vec{p}^2/\mu, \vec{p}'^2/\mu, \vec{p} \cdot \vec{p}'/\mu, \delta m, \delta\bar{m}) \sim \mathcal{O}(\mu v^2)$, where v stands for the relative velocity in the two-particle system. In order to obtain the absorptive part of the Wilson coefficients from the perturbative process $\chi_1\chi_2 \rightarrow X_A X_B \rightarrow \chi_4\chi_3$, including the subleading $\mathcal{O}(v^2)$ terms, we therefore proceed with the following steps.

1. Start from the 1-loop scattering amplitude $\chi_1\chi_2 \rightarrow X_A X_B \rightarrow \chi_4\chi_3$ with a SM or Higgs two particle final state $X_A X_B$. The masses of the two pairs $\chi_1\chi_2$ and $\chi_4\chi_3$ have to share the same scale $M = m + \bar{m}$ and the mass differences δm_i , (6.10), have to be of the same order as typical non-relativistic kinetic energies of the pairs. The absorptive part of the 1-loop amplitude is obtained by applying the Cutkosky rules [90,91] to the X_A and X_B propagators. The result is written in terms of the hard and small mass scales introduced above, and expanded in the small scales retaining terms up to $\mathcal{O}(v^2)$.
2. To $\mathcal{O}(v^2)$ the result contains scalar products with at most two powers of \vec{p} and \vec{p}' . For the spin-1 configuration, the scalar products also involve the spin-polarisation vectors \vec{n} and \vec{n}' of the incoming ($\chi_1\chi_2$) and outgoing ($\chi_4\chi_3$) states, respectively. Generically the results for spin-1 incoming and outgoing states takes the form

$$\begin{aligned} & \left\{ c_0({}^3S_1) + c_1({}^3S_1) \delta m + c_2({}^3S_1) \delta\bar{m} + c_3({}^3S_1) \vec{p}^2 + c_4({}^3S_1) \vec{p}'^2 \right\} \vec{n} \cdot \vec{n}' \\ & + c_5({}^3P_0) (\vec{p} \cdot \vec{n}) (\vec{p}' \cdot \vec{n}') + c_6({}^3P_1) [p, n]^k [p', n']^k + c_7({}^3P_2) p^{\{i} n^{j\}} p'^{\{i} n'^{j\}} \\ & + c_8({}^3S_1, {}^3P_1) n^k [p', n']^k + c_9({}^3P_1, {}^3S_1) [p, n]^k n'^k \\ & + c_{10}({}^3S_1, {}^3D_1) p^{\{i} p'^{j\}} n^i n'^j + c_{11}({}^3D_1, {}^3S_1) p^{\{i} p'^{j\}} n^i n'^j, \end{aligned} \quad (6.14)$$

where we have introduced the notation $[a, b]^k \equiv \varepsilon^{ijk} a^i b^j$ and $a^{\{i} b^{j\}} \equiv a^i b^j + a^j b^i - 2\vec{a} \cdot \vec{b} \delta^{ij}/3$, corresponding to $J = 1$ and $J = 2$ Cartesian tensors, respectively. The spin-polarisation vector \vec{n} is introduced by replacing the spinor matrix $[\xi\xi^{\dagger}]_{ij}$ of an incoming two-neutralino state by $\frac{1}{\sqrt{2}} \vec{n} \cdot \vec{\sigma}_{ij}$. Similar replacements apply to

outgoing two-particle states and states involving charginos. Each coefficient c_i is a function of m and \bar{m} . In addition the c_i depend on the masses of internally exchanged particles, that appear in the s -, t - or u -channels of the one-loop MSSM amplitudes as well as on the X_A and X_B masses and coupling factors related to the vertices of the contributing diagrams. The first term, c_0 , gives the leading-order contribution, where all the others count as $\mathcal{O}(v^2)$, according to the scaling rules for non-relativistic particle pair annihilations that we have established above. We have further specified the quantum numbers 3L_J of each term, which matches the angular-momentum configuration of the incoming state, equal to that of the outgoing state except for the c_{8-11} terms (the first quantum number between parentheses refers then to the incoming state, the second to the outgoing one). For spin-0 incoming and outgoing states, the result simplifies to

$$c_0({}^1S_0) + c_1({}^1S_0)\delta m + c_2({}^1S_0)\delta\bar{m} + c_3({}^1S_0)\vec{p}^2 + c_4({}^1S_0)\vec{p}'^2 + c_5({}^1P_1)\vec{p}\cdot\vec{p}'. \quad (6.15)$$

We do not consider the possibility of spin-0 to spin-1 transitions between incoming and outgoing states in the hard annihilation process. These transitions, ${}^3S_1 \rightarrow {}^1P_1$, ${}^3P_{0,1} \rightarrow {}^1S_0$ and ${}^3P_{0,1} \rightarrow {}^1P_1$, in the hard annihilation part of the full forward scattering amplitude are also allowed at $\mathcal{O}(v)$ by angular-momentum conservation. However they require spin-changing potential interactions in the long-range part of the amplitude in order to bring the spin of the two-particle state after annihilation back to the spin of the incoming state. Since the non-relativistic spin-changing potentials carry an additional v -suppression, such transitions are only relevant for the calculation of the annihilation rates at $\mathcal{O}(g^2v^2)$. In this work we ignore $\mathcal{O}(v^2)$ effects that arise from subleading non-Coulomb (non-Yukawa) potentials and include only those from the short-distance annihilation. As similarly the terms c_{8-11} in (6.14) require a change of the orbital angular momentum, that has to be compensated by a potential interaction which is also v -suppressed in the non-relativistic limit, we ignore such terms for our purposes.

3. The Wilson coefficients of the dimension-8 operators with derivatives shall also have the symmetry property (6.7) under the exchange of the incoming and outgoing states. This is ensured by rewriting powers of \vec{p}^2 and \vec{p}'^2 in the expanded expressions for the amplitudes by virtue of the energy-conservation relation (6.12) as

$$\begin{aligned} \vec{p}^2 &= \frac{1}{2}(\vec{p}^2 + \vec{p}'^2) + \frac{2m\bar{m}}{M}(\delta m + \delta\bar{m}) + \dots, \\ \vec{p}'^2 &= \frac{1}{2}(\vec{p}^2 + \vec{p}'^2) - \frac{2m\bar{m}}{M}(\delta m + \delta\bar{m}) + \dots, \end{aligned} \quad (6.16)$$

such that the coefficients multiplying \vec{p}^2 and \vec{p}'^2 become equal.

4. In the last step we identify the Wilson coefficients $\hat{f}^{(d=6,8)}_{\chi_1\chi_2 \rightarrow X_A X_B \rightarrow \chi_4\chi_3}({}^{2s+1}L_J)$ by comparing the expanded expression for the absorptive part of the MSSM ampli-

tude $\mathcal{A}(\chi_1\chi_2 \rightarrow X_A X_B \rightarrow \chi_4\chi_3)$ with the amplitude for the same process computed with the dimension 6 and dimension 8 EFT operators in $\delta\mathcal{L}_{\text{ann}}$.

We provide explicit analytic expressions for the building blocks of (next-to-next-to-) leading-order S - and P -wave coefficients in the appendices A.1 and A.2. The results are given in terms of kinematic and coupling factors, that have to be combined in a particular way in order to obtain the Wilson coefficients. In the next section we add a brief discussion on the gauge used in the matching calculation. Sec. 6.1.4 finally contains the master formula, that allows to determine the absorptive parts of the Wilson coefficients from coupling and kinematic factors. Finally note that the Wilson coefficients refer to inclusive annihilation rates, summed over all accessible final states $X_A X_B$. Our calculation is however performed for individual final states, which are therefore also given separately. While only inclusive neutralino and chargino $\chi\chi$ co-annihilation rates are needed in our application to the χ_1^0 relic abundance calculation, our final-state separated results can be of interest to the calculation of primary decay spectra of (Sommerfeld-enhanced) χ_1^0 dark matter annihilation in the present Universe.

6.1.3 Unitary vs Feynman gauge

The computation of the absorptive parts of the Wilson coefficients for forward-scattering reactions, $\chi_{e_1}\chi_{e_2} \rightarrow X_A X_B \rightarrow \chi_{e_1}\chi_{e_2}$, has been performed using both the unitary and Feynman gauge. The results agree numerically, therefore providing a useful check of our calculation. For the off-diagonal reactions, where the incoming and outgoing states are different, the use of unitary gauge for final states with two massive vector bosons (characterised by the gauge boson mass scale M_V) in the final state introduces enhanced $1/M_V^4$ and $1/M_V^2$ terms, which are proportional to the mass differences between the incoming and outgoing particle species and which must cancel in the final result. Similarly, a cancellation of $1/M_V^2$ enhanced terms in off-diagonal rates with one massive vector boson in the final state has to take place. However, for these cancellations to occur, one has to also expand the SUSY mixing matrices systematically in the gauge boson masses M_V . In the same way, the mass differences between the incoming and outgoing particles have to be expanded in M_V and in the differences of soft SUSY breaking parameters M_1 , M_2 , μ , if these differences are small. The latter expansions must be done differently depending on how many neutralinos and charginos are (nearly) mass-degenerate. The presentation of the results computed with unitary gauge then has to distinguish among many cases and also consider diagonal and off-diagonal terms separately, since for the diagonal terms it is desirable to keep the full mass dependence as well as unexpanded mixing matrices. It is therefore more convenient to use Feynman gauge for the calculation of the off-diagonal reactions, which allows to keep the coupling matrices unexpanded and a more concise presentation of the results. The price for this is that a large number of unphysical final states containing pseudo-Goldstone Higgs and ghost particles has to be included. These states $X_A X_B$ are collected in Tab. 6.1.

$\chi\chi \rightarrow \chi\chi$	VV	VS	SS	ff	$\eta\bar{\eta}$
$\chi^0\chi^0 \rightarrow \chi^0\chi^0$ $\chi^-\chi^+ \rightarrow \chi^-\chi^+$ $\chi^0\chi^0 \rightarrow \chi^-\chi^+$ $\chi^-\chi^+ \rightarrow \chi^0\chi^0$	W^+W^- , ZZ , $\gamma\gamma, Z\gamma$	Zh^0, ZH^0 , $\gamma h^0, \gamma H^0$, ZG^0, ZA^0 , $\gamma G^0, \gamma A^0$, W^+G^-, W^+H^- , W^-G^+, W^-H^+	h^0h^0, h^0H^0, H^0H^0 , G^0h^0, A^0h^0 , G^0H^0, A^0H^0 , G^0G^0, G^0A^0, A^0A^0 , G^+G^-, G^+H^- , H^+G^-, H^+H^-	$u^J\bar{u}^I$, $d^J\bar{d}^I$, $e^J\bar{e}^I$, $\nu^J\bar{\nu}^I$	$\eta^+\bar{\eta}^+$, $\eta^-\bar{\eta}^-$, $\eta^Z\bar{\eta}^Z$
$\chi^0\chi^+ \rightarrow \chi^0\chi^+$	W^+Z , $W^+\gamma$	$ZG^+, \gamma G^+$, $ZH^+, \gamma H^+$, W^+h^0, W^+H^0 , W^+G^0, W^+A^0	G^+h^0, G^+H^0 , H^+h^0, H^+H^0 , G^+G^0, G^+A^0 , H^+G^0, H^+A^0	$u^J\bar{d}^I$, $\nu^J\bar{e}^I$	$\eta^+\bar{\eta}^Z$, $\eta^Z\bar{\eta}^-$, $\eta^+\bar{\eta}^F$, $\eta^F\bar{\eta}^-$
$\chi^+\chi^+ \rightarrow \chi^+\chi^+$	W^+W^+	W^+G^+ , W^+H^+	G^+G^+ , G^+H^+ , H^+H^+		

Table 6.1: Particle pairs $X_A X_B$ in $\chi\chi \rightarrow X_A X_B \rightarrow \chi\chi$ scattering reactions (abbreviated as $\chi\chi \rightarrow \chi\chi$), that we account for in the calculation of the absorptive part of the Wilson coefficients. The pairs are classified according to their type: VV, VS, SS, ff and $\eta\bar{\eta}$. Negatively charged processes, corresponding to the charge-conjugates of the singly or doubly positively charged reactions above are not explicitly written.

6.1.4 A master formula for the Wilson coefficients

In Sec. 6.1.2 we have enumerated the steps in the determination of the absorptive parts of the Wilson coefficients of dimension 6 and 8 operators in $\delta\mathcal{L}_{\text{ann}}$ in terms of the parameters of the underlying full theory, the MSSM. Here we provide further details on the actual diagrams that we have to consider in the MSSM matching calculation. Finally we introduce and discuss our master formula for the absorptive parts $\hat{f}^{(d)(2s+1)L_J}$ of the Wilson coefficients, that expresses the individual $\hat{f}^{(d)(2s+1)L_J}$ in terms of a sum over products of coupling and kinematic factors. With this master formula and given the results on the coupling and kinematic factors collected in Appendices A.1 and A.2, any (next-to-next-to-) leading-order S -wave or P -wave Wilson coefficient $\hat{f}^{(2s+1)S_s}$, $\hat{f}^{(2s+1)P_J}$, $\hat{g}^{(2s+1)S_s}$ or $\hat{h}_i^{(2s+1)S_s}$ related to an (off-) diagonal (tree-level) co-annihilation rate $\chi_{e_1}\chi_{e_2} \rightarrow \chi_{e_4}\chi_{e_3}$ can be determined.

In order to consistently treat off-diagonal rates $\chi_{e_1}\chi_{e_2} \rightarrow \chi_{e_4}\chi_{e_3}$ at the same time as diagonal ones, we refer to the calculation in Feynman gauge throughout in the following. The two-particle final states $X_A X_B$ that we account for can be classified to be of vector-vector (VV), vector-scalar (VS), scalar-scalar (SS), fermion-antifermion (ff) or ghost-anti-ghost ($\eta\bar{\eta}$) type. A list of all considered $X_A X_B$ states, comprising all possible two particle states built from SM gauge bosons, fermions, the MSSM Higgses and finally the

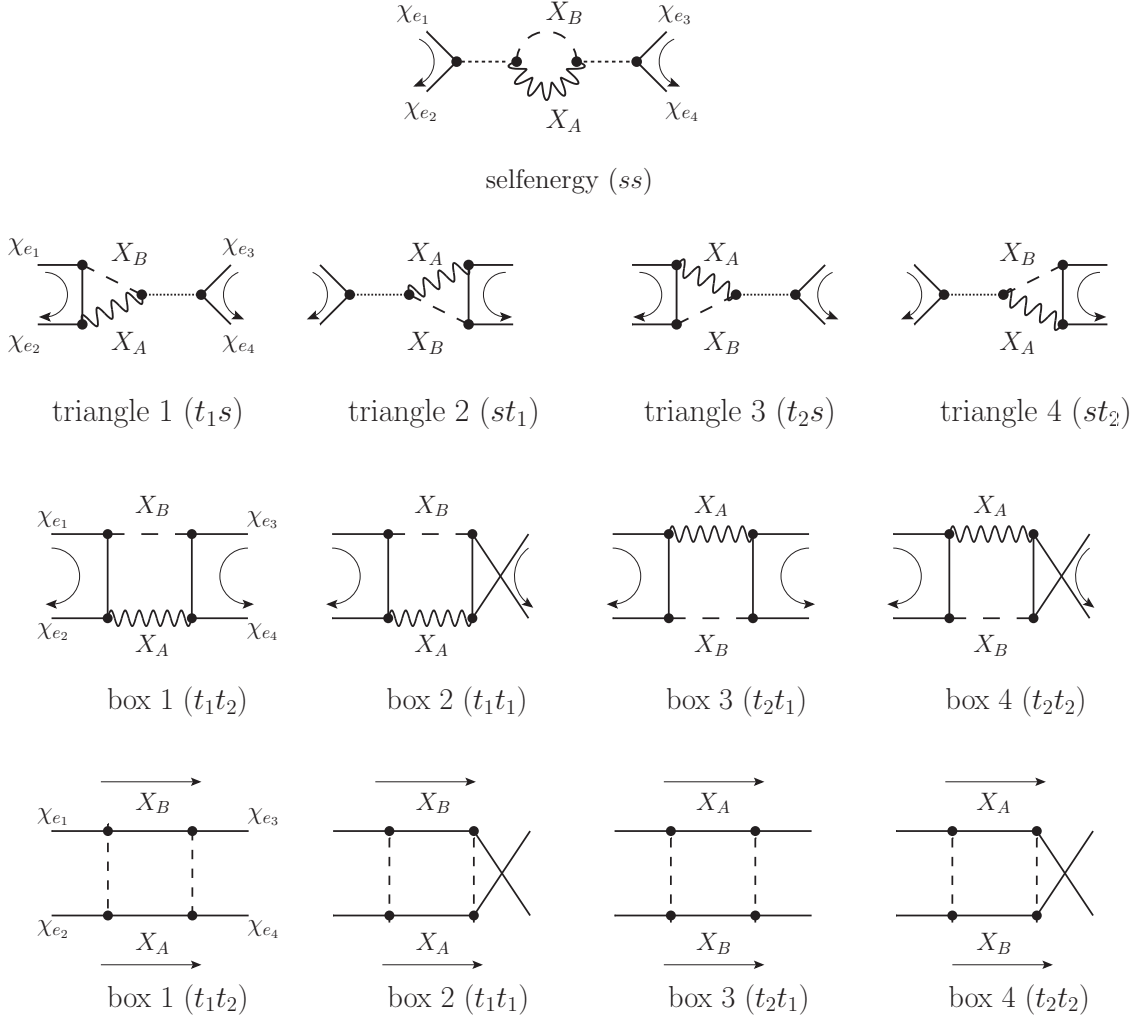


Figure 6.1: Generic one-loop diagrams in $\chi\chi \rightarrow X_A X_B \rightarrow \chi\chi$ reactions. Particles X_A and X_B represent any two-body final state of SM and Higgs particles, which can be produced on-shell in $\chi\chi \rightarrow X_A X_B$ annihilations. The box diagrams in the third line arise in case of $X_A X_B = VV, VS, SS$, while the box amplitudes in the last line refer to the case $X_A X_B = ff$.

ghost states, is given in Tab. 6.1. The determination of the absorptive part of the Wilson coefficients for the processes $\chi_{e_1}\chi_{e_2} \rightarrow X_A X_B \rightarrow \chi_{e_4}\chi_{e_3}$ requires the calculation of a large number of Feynman diagrams. To be able to present the results in an efficient manner it is convenient to make use of the classification in VV -, VS -, SS -, ff - and $\eta\bar{\eta}$ - type $X_A X_B$ particle states and to further subdivide the contributing diagrams according to their topology. In each of the classes under consideration there arise generic 1-loop amplitudes with selfenergy, triangle and box topology shown in Fig. 6.1. The generic selfenergy-diagram as well as the four generic triangle and box diagrams cover all possible kinematic

configurations⁴ that can arise in a $\chi_{e_1}\chi_{e_2} \rightarrow X_A X_B \rightarrow \chi_{e_4}\chi_{e_3}$ 1-loop amplitude. Note that we have assigned specific directions for the fermion flow in each diagram in Fig. 6.1, indicated by the arrows, as it is convenient in the context of calculations involving both Dirac and Majorana fermions, following the Feynman rules for fermion-number violating interactions set out in [92]. The depicted fermion flows establish our convention to arrange the external fermion states $\chi_{e_i}, i = 1, \dots, 4$ in descending order, see Tab. 5.2.

We calculate analytically the absorptive part of any of the contributing selfenergy, triangle and box amplitudes, subject to our convention for the fermion flows and following the steps from Sec. 6.1.2. Thereby we consider generic external Majorana fermions, generic t- and u-channel exchanged Majorana fermions or sfermions, generic $X_A X_B$ states of type VV, VS, SS, ff and $\eta\bar{\eta}$, and hence use generic ‘place-holder’ coupling factors at each vertex. This allows us to determine the generic form of those terms in the contributions to the $\hat{f}^{(d)\chi\chi \rightarrow X_A X_B \rightarrow \chi\chi}(2s+1 L_J)$, that are associated with the kinematics of the $\chi\chi \rightarrow X_A X_B \rightarrow \chi\chi$ reaction, where each of these kinematic terms multiplies a certain combination of the place-holder coupling factors. In particular, these kinematic contributions are generic in the sense that they apply to both the cases of external and internal Majorana and Dirac fermions.

A specific diagram’s contribution to the absorptive part of a particular $\chi_{e_1}\chi_{e_2} \rightarrow X_A X_B \rightarrow \chi_{e_4}\chi_{e_3}$ MSSM 1-loop process is obtained by replacing the generic place-holder coupling factors with their actual expressions in the above described generic Majorana fermion $2 \rightarrow 2$ scattering reactions. Note that by choosing these coupling factors properly, all $\chi_{e_1}\chi_{e_2} \rightarrow X_A X_B \rightarrow \chi_{e_4}\chi_{e_3}$ processes with external and internal Majorana or Dirac fermions can be covered, although the kinematic contributions are calculated referring to the generic Majorana fermion $2 \rightarrow 2$ scattering reaction. Hence, the absorptive part of the Wilson coefficient, which encodes the absorptive part of a $\chi_{e_1}\chi_{e_2} \rightarrow X_A X_B \rightarrow \chi_{e_4}\chi_{e_3}$ scattering reaction, with the incoming and outgoing two-particle states in a $^{2s+1}L_J$ partial-wave configuration, can be written as

$$\begin{aligned}
& \hat{f}_{\{e_1 e_2\}\{e_4 e_3\}}^{(d)\chi_{e_1}\chi_{e_2} \rightarrow X_A X_B \rightarrow \chi_{e_4}\chi_{e_3}}(2s+1 L_J) \\
&= \frac{\pi\alpha_2^2}{M^2} \left(\sum_n \sum_{i_1, i_2} b_{n, i_1 i_2}^{\chi_{e_1}\chi_{e_2} \rightarrow X_A X_B \rightarrow \chi_{e_4}\chi_{e_3}} B_{n, i_1 i_2}^{X_A X_B}(2s+1 L_J) \right. \\
&\quad + \sum_{\alpha=1}^4 \sum_n \sum_{i_1, i_2} c_{n, i_1 i_2}^{(\alpha)\chi_{e_1}\chi_{e_2} \rightarrow X_A X_B \rightarrow \chi_{e_4}\chi_{e_3}} C_{n, i_1 i_2}^{(\alpha)X_A X_B}(2s+1 L_J) \\
&\quad \left. + \sum_{\alpha=1}^4 \sum_n \sum_{i_1, i_2} d_{n, i_1 i_2}^{(\alpha)\chi_{e_1}\chi_{e_2} \rightarrow X_A X_B \rightarrow \chi_{e_4}\chi_{e_3}} D_{n, i_1 i_2}^{(\alpha)X_A X_B}(2s+1 L_J) \right). \quad (6.17)
\end{aligned}$$

⁴The case of four different triangle and four different box diagrams in Fig. 6.1 applies to non-identical particles $X_A \neq X_B$. For identical particles $X_A = X_B$, triangle (box) 1 and 3 as well as triangle (box) 2 and 4 coincide. In this case only one of the identical diagrams must be taken into account to compute the corresponding $\hat{f}^{(d)\chi\chi \rightarrow X_A X_A \rightarrow \chi\chi}$ coefficients. This rule incorporates the symmetry factor of 1/2 in the cross section for identical final-state particles, that one would take into account in the conventional calculation of the tree-level $\chi_{e_1}\chi_{e_2} \rightarrow X_A X_A$ annihilation rate.

Here $\alpha_2 = g_2^2/4\pi$, where g_2 denotes the $SU(2)_L$ gauge coupling. The sums in the first line on the right-hand side of (6.17) collect all contributions from selfenergy amplitudes. Similarly, the second (third) line gives the triangle (box) amplitudes' contributions. We use the index α to enumerate expressions related to the four different triangle and box amplitudes,⁵ according to the labelling of the diagrams in Figs. 6.1. Further, we indicate the kinematic factors of the generic $2 \rightarrow 2$ Majorana fermion scattering amplitudes within a given class and topology with capital letters ($B_{n,i_1i_2}, C_{n,i_1i_2}^{(\alpha)}, D_{n,i_1i_2}^{(\alpha)}$). These are the quantities that include the kinematics of the process and hence encode the $^{2s+1}L_J$ partial-wave specific information. The process-specific coupling factors that multiply the kinematic factors are denoted with lowercase letters ($b_{n,i_1i_2}, c_{n,i_1i_2}^{(\alpha)}, d_{n,i_1i_2}^{(\alpha)}$). Depending on the type of the particles X_A and X_B as well as the topology, there is a fixed number of different coupling-factor expressions that can occur, together with the corresponding kinematic factors. The different contributions are enumerated with the index n in (6.17) above. Finally, in each of the processes there is a certain set of particle species that can be exchanged in the s - or the t -channels of the contributing amplitudes. These are labelled with the indices i_1 and i_2 .

The generic structure of the Wilson coefficients in (6.17) suggests to give the coupling factors and the kinematic factors separately. A recipe for the construction of the coupling factors $b_{n,i_1i_2}, c_{n,i_1i_2}^{(\alpha)}, d_{n,i_1i_2}^{(\alpha)}$ in any of the covered reactions is given in Appendix A.1. Analytic results for the kinematic factors $B_{n,i_1i_2}, C_{n,i_1i_2}^{(\alpha)}, D_{n,i_1i_2}^{(\alpha)}$ for the leading-order 1S_0 and 3S_1 partial-wave configurations as well as the expressions related to 1P_1 partial waves and the combination of spin-1 P -waves, 3P_J , can be found in Appendix A.2. These expressions depend on the masses of the external and internal particles in a particular $\chi_{e_1}\chi_{e_2} \rightarrow X_A X_B \rightarrow \chi_{e_4}\chi_{e_3}$ process. However, the kinematic factors are generic in the sense that their form is the same for all possible external two-body states $\chi_{e_1}\chi_{e_2}$ and $\chi_{e_3}\chi_{e_4}$ of neutralinos or charginos and all $X_A X_B$ particles within one of the classes VV, VS, SS, ff or $\eta\bar{\eta}$.

The coupling and kinematic factors will depend on the supersymmetric particles' mixing matrices and masses, respectively. We adopt the same notation as in [62] and hence introduce the chargino and neutralino mixing matrices Z_{\pm} and Z_N defined via

$$Z_-^T M_{\chi^{\pm}} Z_+ = \begin{pmatrix} m_{\chi_1^+} & \\ & m_{\chi_2^+} \end{pmatrix}, \quad (6.18)$$

$$Z_N^T M_{\chi^0} Z_N = \begin{pmatrix} m_{\chi_1^0} & & & \\ & m_{\chi_2^0} & & \\ & & m_{\chi_3^0} & \\ & & & m_{\chi_4^0} \end{pmatrix}, \quad (6.19)$$

where $M_{\chi^{\pm}}$ and M_{χ^0} denote the chargino and neutralino mass matrices, respectively (for details regarding the mass matrix expressions refer to Chap. 4 or [62]). $m_{\chi_j^+}, j = 1, 2,$

⁵For identical particles $X_A = X_B$ the index α has to be taken from 1 to 2 only, see footnote 4.

and $m_{\chi_i^0}$, with $i = 1, \dots, 4$ indicate the masses in the mass eigenstate basis of charginos and neutralinos, ordered according to increasing mass, respectively.

In order to properly apply the formulae for coupling and kinematic factors, collected in Appendices A.1 and A.2, given a specific MSSM spectrum, it is important to note that the NRMSSM and hence the analytic expressions for the Wilson coefficients explicitly rely on the positivity of all mass parameters. This derives from the fact that the NRMSSM Lagrangian is obtained by extracting the high-energy fluctuations (of the order of the particle mass) from the relativistic fields, which yields the non-relativistic kinetic term \mathcal{L}_{kin} shown in (5.2). For species other than the LSP, the procedure leads to the mass difference terms $(m_i - m_{\text{LSP}})$ in (5.2). If any of the m_i in \mathcal{L}_{kin} is negative, then the corresponding mass difference counts as $\mathcal{O}(m_{\text{LSP}})$, an indication that the parametrisation used to relate the relativistic and non-relativistic fields for that particle species is not the appropriate one. The simplest way to obtain the NRMSSM Lagrangian in case that the mass $m_{\chi_{e_i}}$ of one or several of the external χ_{e_i} particles happens to be negative for a given MSSM spectrum, is to perform a field redefinition of the corresponding MSSM fields that yields mass terms with positive mass parameters. Such a field redefinition affects the chargino and neutralino mixing matrices, which are mapped in the following way:

$$Z_{\pm} \rightarrow \tilde{Z}_{\pm} = Z_{\pm} \cdot \begin{pmatrix} \sqrt{\text{sgn}(m_{\chi_1^+})} & & & \\ & \sqrt{\text{sgn}(m_{\chi_2^+})} & & \\ & & & \\ & & & \end{pmatrix}, \quad (6.20)$$

$$Z_N \rightarrow \tilde{Z}_N = Z_N \cdot \begin{pmatrix} \sqrt{\text{sgn}(m_{\chi_1^0})} & & & & \\ & \sqrt{\text{sgn}(m_{\chi_2^0})} & & & \\ & & & & \\ & & & \sqrt{\text{sgn}(m_{\chi_3^0})} & \\ & & & & \sqrt{\text{sgn}(m_{\chi_4^0})} \end{pmatrix}. \quad (6.21)$$

(We define $\sqrt{-1} = i$.) The redefined mixing matrices \tilde{Z}_{\pm} and \tilde{Z}_N as well as the corresponding positive mass parameters for all MSSM neutralino and chargino fields should be used within the expressions given in Appendices A.1 and A.2.

6.2 Numerical comparison: Tree-level annihilation rates

As first application of the results from the previous section we consider here the tree-level pair-annihilation cross sections of non-relativistic χ^0/χ^{\pm} pairs, expressed in terms of the (next-to-next-to-) leading order S -wave and P -wave Wilson coefficients $\hat{f}^{(d=6,8)}(2s+1 L_J)$. Our focus is the determination of tree-level $\chi\chi$ annihilation rates (in our non-relativistic approximation, including the $\mathcal{O}(v_{\text{rel}}^2)$ corrections from P - and next-to-next-to-leading order S -waves) for generic MSSM scenarios and the comparison to corresponding cross

sections obtained from publicly available numerical codes. In Sec. 6.3, to the contrary, we discuss the application of our analytic results for the coefficients $\hat{f}^{(d=6,8)(2s+1)L_J}$ to obtain purely analytic expressions for (off-) diagonal annihilation rates at $\mathcal{O}(v_{\text{rel}}^2)$ in the simple limiting scenario of the pure-wino NRMSSM.

The expansion of the exclusive, spin-averaged centre-of-mass frame $\chi_{e_1}\chi_{e_2} \rightarrow X_A X_B$ tree-level pair-annihilation cross section in the non-relativistic momentum \vec{p} of the χ_{e_i} particles, written in terms of the Wilson coefficients contained in $\delta\mathcal{L}_{\text{ann}}$, is given by

$$\begin{aligned} \sigma^{\chi_{e_1}\chi_{e_2} \rightarrow X_A X_B} v_{\text{rel}} &= \hat{f}(^1S_0) + 3 \hat{f}(^3S_1) \\ &+ \frac{\vec{p}^2}{M^2} \left(\hat{f}(^1P_1) + \frac{1}{3} \hat{f}(^3P_0) + \hat{f}(^3P_1) + \frac{5}{3} \hat{f}(^3P_2) + \hat{g}(^1S_0) + 3 \hat{g}(^3S_1) \right) + \mathcal{O}(\vec{p}^4). \end{aligned} \quad (6.22)$$

Here $v_{\text{rel}} = |\vec{v}_{e_1} - \vec{v}_{e_2}|$ is the relative velocity of the $\chi_{e_1}\chi_{e_2}$ pair and \vec{v}_{e_i} denotes the velocity of particle χ_{e_i} in the centre-of-mass frame of the annihilation reaction. We have suppressed the superscripts $\chi_{e_1}\chi_{e_2} \rightarrow X_A X_B \rightarrow \chi_{e_1}\chi_{e_2}$ on the Wilson coefficients $\hat{f}^{(d=6,8)}$ in (6.22), where these expressions explicitly refer to the exclusive (tree-level) annihilation rates. Further note that here and in the following we use the notation $\hat{f}^{(2s+1)L_J}$, $\hat{g}^{(2s+1)S_s}$ and $\hat{h}_i^{(2s+1)S_s}$ for the Wilson coefficients $\hat{f}^{(d=6,8)(2s+1)L_J}$, as established in Chap. 5.

In the non-relativistic limit the relation between the relative velocity v_{rel} and the particle momentum \vec{p} in the centre-of-mass frame of the $\chi_{e_1}\chi_{e_2}$ annihilation reaction is approximated by

$$v_{\text{rel}} = |\vec{v}_{e_1} - \vec{v}_{e_2}| = |\vec{p}| \left(\frac{m_{e_1} + m_{e_2}}{m_{e_1} m_{e_2}} + \mathcal{O}(\vec{p}^2) \right). \quad (6.23)$$

Together with (6.22), this relation allows us to express the first two coefficients, a and b , in the Taylor expansion of the $\chi_{e_1}\chi_{e_2} \rightarrow X_A X_B$ centre-of-mass frame annihilation cross section with respect to the relative velocity,

$$\sigma^{\chi_{e_1}\chi_{e_2} \rightarrow X_A X_B} v_{\text{rel}} = a + b v_{\text{rel}}^2 + \mathcal{O}(v_{\text{rel}}^4), \quad (6.24)$$

in terms of the partial-wave separated Wilson coefficients $\hat{f}^{\chi_{e_1}\chi_{e_2} \rightarrow X_A X_B \rightarrow \chi_{e_1}\chi_{e_2}(2s+1)L_J}$ and $\hat{g}^{\chi_{e_1}\chi_{e_2} \rightarrow X_A X_B \rightarrow \chi_{e_1}\chi_{e_2}(2s+1)L_J}$. The coefficient a in the expansion is expressed in terms of the leading-order S -wave Wilson coefficients as

$$a = \hat{f}(^1S_0) + 3 \hat{f}(^3S_1), \quad (6.25)$$

and the coefficient b can be written as the sum $b = b_P + b_S$, where

$$b_P = \frac{\mu_{e_1 e_2}^2}{M^2} \left(\hat{f}(^1P_1) + \frac{1}{3} \hat{f}(^3P_0) + \hat{f}(^3P_1) + \frac{5}{3} \hat{f}(^3P_2) \right), \quad (6.26)$$

$$b_S = \frac{\mu_{e_1 e_2}^2}{M^2} \left(\hat{g}(^1S_0) + 3 \hat{g}(^3S_1) \right), \quad (6.27)$$

and

$$\mu_{e_1 e_2} = \frac{m_{e_1} m_{e_2}}{m_{e_1} + m_{e_2}} \quad (6.28)$$

is the reduced mass of the $\chi_{e_1} \chi_{e_2}$ two-particle state.

The parameters a and b in (6.24) can also be extracted numerically from computer codes that determine the centre-of-mass frame annihilation cross sections. This is done by considering the cross section's behaviour for small relative velocities of the annihilating particle pair and performing a parabola fit to $\sigma^{\chi_{e_1} \chi_{e_2} \rightarrow X_A X_B} v_{\text{rel}}$, which provides the corresponding coefficients a and b . Note, however, that a separation of the coefficient b into its constituent P -wave, (6.26), and next-to-next-to-leading order S -wave, (6.27), contributions cannot be achieved with the sole knowledge of the cross section. Likewise, the separation of the S -wave contributions for the spin singlet and triplet configurations, as performed in (6.25) and (6.27), requires intervention at the amplitude level, which is not straightforward for the publicly available computer codes. In contrast our analytic approach allows us to perform this separation by construction. The separate knowledge of the different $^{2s+1}L_J$ partial-wave contributions to the tree-level co-annihilation rates is indeed essential for a precise determination of Sommerfeld enhanced neutralino co-annihilation cross sections, because the Sommerfeld enhancements depend both on the spin- and orbital angular momentum quantum numbers of the annihilating particle pair. Therefore a consistent treatment of the Sommerfeld enhancement including P -wave effects requires the separate knowledge of all relevant (off-) diagonal tree-level 1S_0 and 3S_1 partial-wave annihilation rates both at leading and next-to-next-to-leading order, as well as the individual (off-)diagonal tree-level 1P_1 and 3P_J partial-wave annihilation rates. In the latter case, the knowledge of the (spin-weighted) sum over the three different 3P_0 , 3P_1 and 3P_2 partial-wave Wilson coefficients,

$$\hat{f}(^3P_J) = \frac{1}{3} \hat{f}(^3P_0) + \hat{f}(^3P_1) + \frac{5}{3} \hat{f}(^3P_2) , \quad (6.29)$$

is sufficient, as long as only leading-order non-relativistic potential interactions between the neutralino and chargino states are taken into account in the full annihilation amplitudes. This is because the leading-order potential interactions depend on the spin ($s = 0, 1$) of the $\chi_{e_a} \chi_{e_b}$ particle pairs taking part in the $\chi_i \chi_j \rightarrow \dots \rightarrow \chi_{e_1} \chi_{e_2} \rightarrow X_A X_B \rightarrow \chi_{e_4} \chi_{e_3} \rightarrow \dots \rightarrow \chi_i \chi_j$ scattering process, but do not discriminate among the three spin-1 P -wave states 3P_J with different total angular momentum $J = 0, 1, 2$. As we discuss in Chap. 7, we will indeed consider only the leading-order potential interactions in our application to non-relativistic χ^0/χ^\pm pair annihilations in the χ_1^0 relic abundance calculation, such that the knowledge of the spin-weighted Wilson coefficient $\hat{f}(^3P_J)$ in (6.29) is sufficient for our purposes. In Appendix A.3 we therefore give analytic results for the kinematic factors related to the spin-weighted coefficients $\hat{f}(^3P_J)$ rather than the separate spin-1 P -wave coefficients $\hat{f}(^3P_0)$, $\hat{f}(^3P_1)$ and $\hat{f}(^3P_2)$. However we have determined the individual kinematic factors, that build the three different spin-1 P -wave coefficients, separately. Results on those are for example included in the electronic supplement, that comes with the publication [32]. Also our numerical code, that allows for

the determination of the (off-) diagonal short-distance annihilation rates in χ^0/χ^\pm pair annihilations and that has been developed as part of this work, contains separate results for the spin-1 P -wave Wilson coefficients $\hat{f}({}^3P_{0,1,2})$.

Recently, Sommerfeld corrections including P -wave effects have been subject of study at 1-loop [93] and with full resummation [94]. In these studies, the next-to-next-to-leading order contributions in the expansion of the relevant (co-)annihilation rates were assumed to be given only by P -waves. While such reasoning is justified when the leading-order S -wave contributions to the annihilation rates are strongly suppressed with respect to the next-to-next-to-leading order coefficients in (6.24), it does not hold for the general case. In particular, P - and next-to-next-to-leading order S -wave terms can come with differing signs, such that a partial compensation of different next-to-next-to-leading order contributions to the annihilation rates may occur. We illustrate this effect in Sec. 6.2.1.

We have performed a dedicated numeric check of our results for the non-relativistically approximated $\chi_{e_1}\chi_{e_2} \rightarrow X_A X_B$ tree-level annihilation cross sections as given in (6.22, 6.24) for all initial state two-particle pairs in Tab. 5.1 into all accessible SM and Higgs two-particle final states. To this end several MSSM spectra have been considered, which we compute using the spectrum calculator **SuSpect** [86] and its implementation of the *phenomenological MSSM*, a model with 27 free parameters. For each spectrum, we obtain the coefficients a and b in (6.25) and (6.26, 6.27) from our analytic calculation, and compare them with the corresponding coefficients extracted purely numerically using **MADGRAPH** [89] to calculate the cross sections. Our results for the coefficient a agree with the corresponding numeric expression extracted from **MADGRAPH** data at per mil level. Similarly, we find agreement of the coefficients b derived with (6.26, 6.27) and extracted from **MADGRAPH** data at 1% up to per mil level, where the level of agreement slightly varies depending on the initial- and final-state particles. In addition, the level of agreement on the parameter b depends on the interval of the v_{rel} variable used for the parabola fit to the **MADGRAPH** data, which for the numbers quoted above is taken as $v_{\text{rel}}/c = [0, 0.4]$. We find that the non-relativistic approximation is reliable for single-particle velocities up to $v_{e_i}/c \sim 0.3$. For such velocities the absolute error of the non-relativistic approximation to $\sigma^{\chi_{e_1}\chi_{e_2} \rightarrow X_A X_B} v_{\text{rel}}$ with respect to the unexpanded $\sigma^{\chi_{e_1}\chi_{e_2} \rightarrow X_A X_B} v_{\text{rel}}$ expression lies within the level of a few percent. Therefore the non-relativistic approximation has an acceptable accuracy for calculations in the early Universe during the time of χ_{e_i} -decoupling, as the mean velocity of the χ_{e_i} in that period was around $v_{e_i}/c \sim 0.2$.

In the following subsections we give several examples for the numerical comparison with **MADGRAPH**. In addition we discuss in detail the impact of the different partial-wave contributions on the corresponding annihilation cross section times relative velocity, $\sigma^{\chi_{e_1}\chi_{e_2} \rightarrow X_A X_B} v_{\text{rel}}$, as obtained from our results. To this end we have selected processes with significantly different S - and P -wave dependence. The **SuSpect**-generated MSSM spectrum, that underlies all results presented in the next sections, contains a wino-like neutralino LSP with mass $m_{\chi_1^0} = 2748.92$ GeV, and an almost mass-degenerate wino-like chargino partner with $m_{\chi_1^\pm} = 2749.13$ GeV.

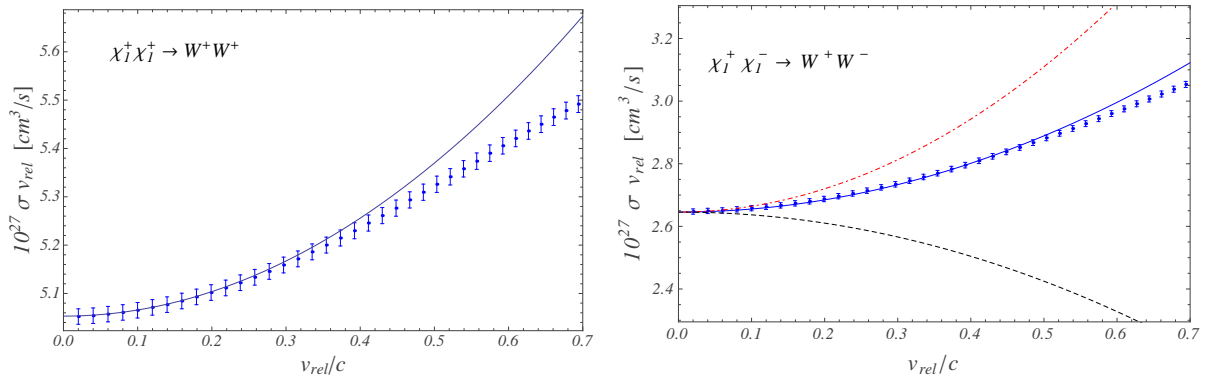


Figure 6.2: *Left plot:* Numeric comparison of the non-relativistic approximation (solid line) to the tree-level annihilation cross section times relative velocity, σv_{rel} , for the $\chi_1^+ \chi_1^+ \rightarrow W^+ W^+$ process with the corresponding unexpanded annihilation cross section produced with MADGRAPH. *Right plot:* Comparison between MADGRAPH data and our non-relativistic approximation (solid line) to σv_{rel} for the $\chi_1^+ \chi_1^- \rightarrow W^+ W^-$ reaction. In addition the dash-dotted red (dashed black) curve represents the constant leading-order term in the non-relativistic expansion of the cross section plus the P -wave (next-to-next-to-leading order S -wave) contribution, $a + b_P v_{\text{rel}}^2$ ($a + b_S v_{\text{rel}}^2$). Numeric errors on the MADGRAPH data are given by $\sigma v_{\text{rel}}/\sqrt{N}$, where $N = 10^5$ gives the number of events used in the MADGRAPH calculation of each cross section value.

6.2.1 $\chi_1^+ \chi_1^+ \rightarrow W^+ W^+$ and $\chi_1^+ \chi_1^- \rightarrow W^+ W^-$

We start with the discussion of two exclusive tree-level annihilation cross sections that are particularly relevant in the calculation of the neutralino LSP relic abundance for heavy χ_1^0 dark matter including co-annihilations,⁶ namely the annihilation rate of the double-charged two particle state $\chi_1^+ \chi_1^+$ into the exclusive final state $W^+ W^+$ as well as the exclusive reaction of the neutral two particle state $\chi_1^+ \chi_1^-$ into a pair of oppositely charged W bosons.

The plot on the left-hand side of Fig. 6.2 displays the annihilation cross section times the relative velocity for the double-charged reaction $\chi_1^+ \chi_1^+ \rightarrow W^+ W^+$. For $v_{\text{rel}}/c \lesssim 0.4$ our analytic, non-relativistic approximation nicely reproduces the numeric, unexpanded cross section $\sigma^{\chi_1^+ \chi_1^+ \rightarrow W^+ W^+} v_{\text{rel}}$ determined with MADGRAPH. Furthermore, as the absolute curvature in this reaction is rather small compared to the coefficient a , even the absolute error that one would make in using the non-relativistic approximation instead of the full cross section is only of the order of 2% for $v_{\text{rel}}/c \sim 0.6$. The coefficient b for this reaction, calculated using (6.26, 6.27), is given by $1.27 \cdot 10^{-27} \text{ cm s}$. Its P - and S -wave contributions are of the same order and read $2.95 \cdot 10^{-27} \text{ cm s}$ and $-1.68 \cdot 10^{-27} \text{ cm s}$, respectively. Obviously they enter with opposite sign and partially cancel each other.

⁶A heavy χ_1^0 dark matter candidate, that explains all the observed cold dark matter as thermal relic is typically either wino- or higgsino-like or a wino-higgsino mixture. In these cases the two gauge boson final states $X_A X_B = VV$ give dominant contributions to the inclusive $\chi\chi$ co-annihilation cross sections in the χ_1^0 relic abundance calculation.

Such partial compensation of the P - and next-to-next-to-leading order S -wave contributions to the cross section can be seen explicitly in the right hand side plot in Fig. 6.2. The plot displays the $\chi_1^+ \chi_1^- \rightarrow W^+ W^-$ tree-level annihilation rate, where the solid blue line corresponds to the non-relativistic approximation to the tree-level annihilation cross section, $\sigma^{\chi_1^+ \chi_1^- \rightarrow W^+ W^-} v_{\text{rel}}$, and the points correspond to the full tree-level result obtained with MADGRAPH. The deviation between our approximation and the MADGRAPH data is at one percent level for $v_{\text{rel}}/c \sim 0.6$ and in the per mil regime for smaller relative velocities. In addition the composition of the non-relativistic approximation to $\sigma^{\chi_1^+ \chi_1^- \rightarrow W^+ W^-} v_{\text{rel}}$ out of P - and next-to-next-to-leading order S -wave contributions can be directly read off from Fig. 6.2: the dash-dotted red line represents the contribution $a + b_P v_{\text{rel}}^2$ to (6.24), while the dashed black line is $a + b_S v_{\text{rel}}^2$. While both b_P and b_S are roughly of the same order of magnitude, the summed P -wave contributions enter with a positive sign ($b_P c^2 = 1.86 \cdot 10^{-27} \text{ cm}^3 \text{ s}^{-1}$), whereas the summed next-to-next-to-leading order S -wave contributions come with a negative weight, $b_S c^2 = -0.88 \cdot 10^{-27} \text{ cm}^3 \text{ s}^{-1}$. It is worth noting that the sum of next-to-next-to-leading order corrections in the $\chi_1^+ \chi_1^- \rightarrow W^+ W^-$ tree-level cross section times relative velocity gives a $\sim 6\%$ correction to the leading-order approximation for $v_{\text{rel}}/c \sim 0.4$. For this relative velocity, the corrections to the leading-order approximation from P -waves only amount to $\sim 11\%$, while those from next-to-next-to-leading order S -wave contributions amount to $\sim -5\%$. Hence, in the light of the expected future experimental precision on the measured dark matter density, it is crucial to take these corrections into account. Further, as generically the Sommerfeld enhancements for each of the contributing partial waves are different, we consistently consider the Sommerfeld enhancements on the different partial-wave contributions to the cross sections separately.

The fact that the P -wave terms in the two examples of Fig. 6.2 contribute with positive sign is generic: the sum of all $^{2s+1}P_J$ partial-wave contributions to any $\chi_{e_1} \chi_{e_2} \rightarrow X_A X_B$ annihilation cross section has to be positive, as it results from the absolute square of the coefficient of the $\mathcal{O}(\mathbf{p})$ terms in the expansion of the annihilation amplitude. Moreover, the separate $^{2s+1}P_J$ partial-wave contributions must also be positive, since different $^{2s+1}P_J$ -wave amplitudes do not interfere in the absolute square of the annihilation amplitude due to total angular-momentum conservation and the additional conservation of spin in the non-relativistic regime. The next-to-next-to-leading order S -wave contributions to the $\chi_{e_1} \chi_{e_2} \rightarrow X_A X_B$ annihilation cross section, however, result from the product of leading-order and next-to-next-to-leading order S -wave contributions in the expansion of the $\chi_{e_1} \chi_{e_2} \rightarrow X_A X_B$ amplitude. There is a priori no reason why this product should be positive, and hence negative next-to-next-to-leading order S -wave contributions to the cross section can occur, as can be explicitly seen in the examples presented in this section.

6.2.2 The S -wave dominated processes $\chi_1^0 \chi_1^+ \rightarrow t\bar{b}, u\bar{d}$

We continue with the discussion of $\chi_1^0 \chi_1^+$ annihilation reactions into exclusive final states built from a pair of fermions. The plot on the left-hand side in Fig. 6.3 depicts the

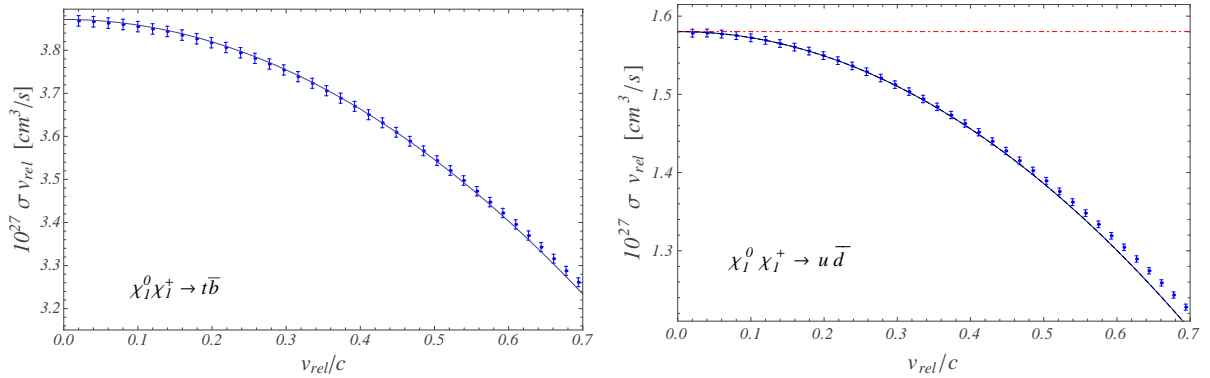


Figure 6.3: *Left plot:* The non-relativistic approximation (solid line) to the tree-level annihilation cross section times relative velocity, σv_{rel} , for the $\chi_1^0 \chi_1^+ \rightarrow t \bar{b}$ process compared to the corresponding unexpanded annihilation cross section produced with MADGRAPH. *Right plot:* Similarly to the left figure, we compare MADGRAPH data and our non-relativistic approximation (solid line) to σv_{rel} for the $\chi_1^0 \chi_1^+ \rightarrow u \bar{d}$ reaction. In addition we show the different partial-wave contributions to the cross section in our non-relativistic approximation: the dash-dotted red (dashed black) curve represents the constant leading-order term in the non-relativistic expansion plus the P -wave (next-to-next-to-leading order S -wave) contribution, $a + b_P v_{\text{rel}}^2$ ($a + b_S v_{\text{rel}}^2$). The numeric errors on the MADGRAPH data are taken to be $\sigma v_{\text{rel}}/\sqrt{N}$, where $N = 10^5$ gives the number of events used in the MADGRAPH calculation of each cross section value.

annihilation reaction $\chi_1^0 \chi_1^+ \rightarrow t \bar{b}$ with (massive) fermionic final states. As it receives significant leading-order S -wave contributions, this annihilation process is also relevant in the neutralino LSP relic abundance calculation including co-annihilation processes. Here it turns out that the b coefficient is S -wave dominated, as the contributions from P -waves are suppressed by five orders of magnitude. Such suppression also arises for the exclusive $u \bar{d}$ final state (generically for all $\chi_1^0 \chi_1^+ \rightarrow f \bar{f}$ reactions). We discuss the reason for this P -wave suppression below. Let us stress here that our analytic results for the Wilson coefficients include the full mass dependence of the final state particles and can be applied to MSSM scenarios with flavour off-diagonal sfermion generation mixing as well.

The right-hand plot in Fig. 6.3 shows results for the S -wave dominated tree-level $\chi_1^0 \chi_1^+ \rightarrow u \bar{d}$ annihilation process, also of importance in the neutralino relic abundance calculation including co-annihilations. Here we display again explicitly the separate contributions from P - and next-to-next-to-leading order S -waves, which makes the dominance of S -wave contributions particularly apparent. The dashed black line, representing the $a + b_S v_{\text{rel}}^2$ contribution to the non-relativistic expansion of the annihilation rate with $b_S c^2 = -0.78 \cdot 10^{-27} \text{ cm}^3 \text{ s}^{-1}$, basically coincides with the solid blue line, which corresponds to the complete non-relativistic approximation (6.24). MADGRAPH produced data for the $\chi_1^0 \chi_1^+ \rightarrow u \bar{d}$ tree-level annihilation rate are shown in addition, illustrating once again the nice agreement of the non-relativistic approximation with the unexpanded

tree-level cross section results for relative velocities up to $v_{\text{rel}}/c \sim 0.6$.

It is worthwhile to understand the suppression of P -waves with respect to the next-to-next-to-leading order S -wave contributions in the $\chi_1^0\chi_1^+ \rightarrow t\bar{b}, u\bar{d}$ processes (generically $\chi_1^0\chi_1^+ \rightarrow f\bar{f}$ for the given MSSM spectrum) as well as the composition of the corresponding coefficients b_S out of their 1S_0 and 3S_1 partial-wave contributions: First note, that in the case of vanishing final state masses, $m_u = m_d = 0$, the contributions to both a and b_S can be attributed solely to 3S_1 partial waves. The absence (or more generally the suppression in m_q/M , $q = u, d$) of 1S_0 partial-wave contributions both in the leading-order coefficient a and in b_S is a helicity suppression effect. The helicity suppression argument applies to all $^{2s+1}L_J$ partial-wave reactions with $J = 0$, as the final state of a massless (left-handed) quark and a massless (right-handed) anti-quark in its centre-of-mass system cannot build a total angular-momentum state $J = 0$. Hence both 1S_0 as well as 3P_0 partial-wave contributions are helicity suppressed.

The suppression of 1P_1 , 3P_1 and 3P_2 partial-wave contributions that proceed through single s -channel gauge boson or Higgs exchange is related to either factors of $\Delta_m = (m_{\chi_1^0} - m_{\chi_1^+})/(m_{\chi_1^0} + m_{\chi_1^+})$ or to vertex couplings that vanish in the exact $SU(2)_L$ symmetric limit. Similarly, contributions from t -channel exchange amplitudes introduce Δ_m factors or coupling factor combinations that lead to vanishing contributions in the $SU(2)_L$ symmetric theory (case of 1P_1 waves), or are additionally suppressed (as it is the case of 3P_1 and 3P_2 partial-wave configurations) by the masses of t -channel exchanged sfermions, since the mass scale of the latter is above 5 TeV in the MSSM scenario considered. Consequently, as the initial two particle state in the reactions $\chi_1^0\chi_1^+ \rightarrow t\bar{b}, u\bar{d}$ consists of two wino-like particles with $|\Delta_m| \sim 4 \cdot 10^{-5}$, the 1P_1 , 3P_1 and 3P_2 partial waves give suppressed contributions to the tree-level annihilation rate.

6.2.3 The P -wave dominated reaction $\chi_2^+\chi_2^- \rightarrow h^0h^0$

An example of a P -wave dominated process is provided in the left plot of Fig. 6.4. It corresponds to the tree-level $\chi_2^+\chi_2^- \rightarrow h^0h^0$ annihilation, wherein S -wave contributions vanish, such that the process is purely P -wave mediated in the non-relativistic regime (the coefficient $b_P c^2$ is given by $9.94 \cdot 10^{-29} \text{ cm}^3 \text{ s}^{-1}$). The absence of S -wave contributions can be explained by CP and total angular-momentum conservation in the $\chi_2^+\chi_2^- \rightarrow h^0h^0$ reaction.⁷ The CP quantum number of the final two-particle state h^0h^0 is given by $CP = (-1)^L = (-1)^J$, as the total angular momentum of a h^0h^0 state coincides with its orbital angular momentum and the parity of such a state is given by $P = (-1)^L$, while its charge conjugation is $C = 1$. In case of the annihilating $\chi_a^+\chi_a^-$ two-particle state the J^{PC} quantum numbers are 0^{-+} for a 1S_0 partial-wave configuration and 1^{--} for a 3S_1 partial-wave state. Hence, for the $\chi_a^+\chi_a^-$ state, $CP = -1$ is realised in case of S -waves for the $J = 0$ configuration, and $CP = +1$ for $J = 1$, which are opposite to

⁷The following reasoning applies to all possible $\chi_a^+\chi_a^- \rightarrow X_A X_B$ annihilation reactions with two CP -even MSSM Higgs particles in the final state, $X_A X_B = h^0 h^0, h^0 H^0, H^0 H^0$. Note that CP is conserved in these reactions if the mixing matrices in the chargino sector are real, which is the case for the scenario we consider.

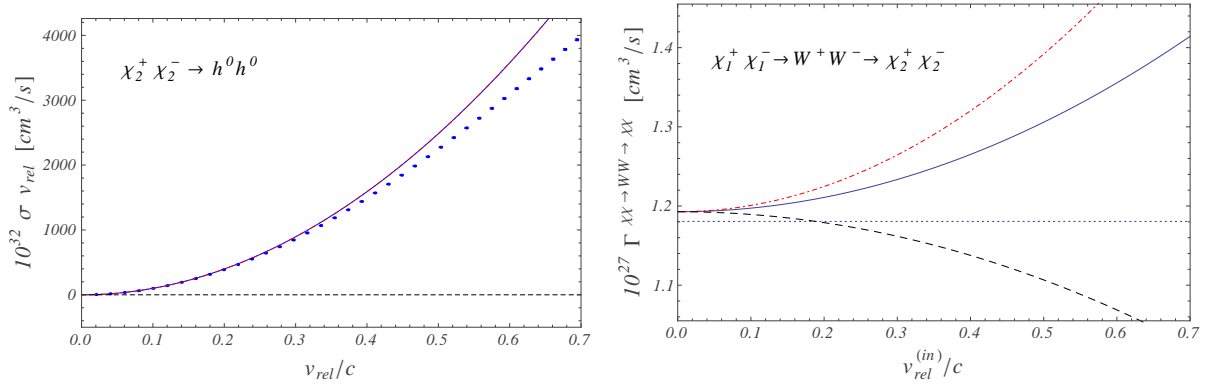


Figure 6.4: *Left plot:* Numeric comparison of the non-relativistic approximation (solid blue curve) to the tree-level annihilation cross section times relative velocity, σv_{rel} , for the P -wave dominated $\chi_2^+ \chi_2^- \rightarrow h^0 h^0$ reaction to data for the corresponding unexpanded annihilation cross section produced with MADGRAPH. Numeric errors on the MADGRAPH data are taken to be $\sigma v_{\text{rel}}/\sqrt{N}$, where $N = 10^5$ gives the number of events used in the MADGRAPH calculation of each cross section value. The dash-dotted red and dashed black lines represent the constant leading-order term plus the P -wave or the next-to-next-to-leading order S -wave contribution, $a + b_P v_{\text{rel}}^2$ or $a + b_S v_{\text{rel}}^2$, respectively. Note that the $a + b_P v_{\text{rel}}^2$ contribution and the non-relativistic approximation coincide, as there are no S -wave contributions in this particular annihilation reaction. *Right plot:* Off-diagonal annihilation rate Γ for the reaction $\chi_1^+ \chi_1^- \rightarrow W^+ W^- \rightarrow \chi_2^+ \chi_2^-$. The solid line includes all contributions to Γ up to next-to-next-to-leading order in the non-relativistic expansion. It is obtained from (6.30) assuming that \mathbf{p} and \mathbf{p}' are parallel to each other. The constant dotted blue line gives the leading-order approximation to Γ . Summing the P - or the (momentum-dependent) next-to-next-to-leading order S -wave contributions to the constant S -wave terms (given by the leading order plus the terms proportional to δm and $\delta \bar{m}$) yields the dash-dotted red or the dashed black line, respectively. The curves are plotted against the relative velocity $v_{\text{rel}}^{(\text{in})}$ of the incoming state $\chi_1^+ \chi_1^-$.

the CP quantum numbers of a $h^0 h^0$ final state with the same total angular momentum. The same reasoning explains the absence of 3P_1 annihilations in any of the processes $\chi_a^+ \chi_a^- \rightarrow X_A X_B$ with $X_A X_B = h^0 h^0, h^0 H^0, H^0 H^0$, as the J^{PC} quantum numbers of the 3P_1 partial-wave configuration of the incoming $\chi_a^+ \chi_a^-$ states are 1^{++} , hence $CP = +1$ for $J = 1$. This is opposite to the CP quantum number of the two CP -even Higgs boson final state with total angular momentum $J = 1$.

Let us finally note that there are also no contributions from 1P_1 partial waves in the process shown in the left plot in Fig. 6.4. This feature is generic to $\chi_a^+ \chi_b^- \rightarrow X_A X_B$ annihilations with identical scalar particles in the final state, $X_A X_B = h^0 h^0, H^0 H^0$. The argument relies on the statistics of the final state identical bosons, and applies to all $\chi_a^+ \chi_b^-$ incoming states and not only to particle-anti-particle states $\chi_a^+ \chi_a^-$: Bose statistics forbids the two identical final state scalars to be in a $J = L = 1$ state, as the corresponding two-particle wave-function for odd total angular momentum J would be

anti-symmetric. This argument can also be used to explain the absence of the $J = 1$ 3S_1 and 3P_1 states in a $\chi_a^+\chi_b^- \rightarrow h^0h^0, H^0H^0$ annihilation reaction.

Generically, if the coefficient a in the expansion (6.24) is suppressed with respect to the coefficient b , the curvature and hence the corresponding non-relativistic annihilation process is P -wave dominated. This property derives from the fact, that the leading-order coefficient a is related to the product of the leading-order S -wave contributions to the tree-level annihilation amplitude with its complex conjugate. As the next-to-next-to-leading order S -wave contributions to the coefficient b result from the product of leading-order with next-to-next-to-leading order S -wave contributions in the annihilation amplitudes, a suppressed coefficient a indicates a small next-to-next-to-leading order S -wave contribution to the coefficient b as well.

6.2.4 The off-diagonal $\chi_1^+\chi_1^- \rightarrow W^+W^- \rightarrow \chi_2^+\chi_2^-$ rate

In order to discuss the importance of the non-relativistic corrections to not only the cross sections but also the off-diagonal annihilation rates, we generalise the definition of the annihilation rates to include off-diagonal reactions. We define the centre-of-mass frame tree-level annihilation rate Γ associated with the (off-) diagonal $\chi_{e_1}\chi_{e_2} \rightarrow X_AX_B \rightarrow \chi_{e_4}\chi_{e_3}$ scattering reaction as the product of the $\chi_{e_1}\chi_{e_2} \rightarrow X_AX_B$ tree-level annihilation amplitude with the complex conjugate of the tree-level amplitude for the $\chi_{e_4}\chi_{e_3} \rightarrow X_AX_B$ annihilation reaction, integrated over the final X_AX_B particles' phase space⁸ and averaged over the spin states of the respective incoming particles χ_{e_i} , $i = 1, \dots, 4$. In the latter spin-average it is assumed that the $\chi_{e_1}\chi_{e_2}$ and $\chi_{e_4}\chi_{e_3}$ pair reside in the same spin state.⁹ The external $\chi_{e_a}\chi_{e_b}$ states are further taken to be non-relativistic normalised in order to match with the definition of the annihilation cross section times relative velocity in case of diagonal reactions $\chi_{e_1}\chi_{e_2} \rightarrow X_AX_B \rightarrow \chi_{e_1}\chi_{e_2}$. In terms of the Wilson coefficients of the four-fermion operators, the expansion of the annihilation rate Γ in the non-relativistic momenta and in the mass differences $\delta m, \delta \bar{m}$, is then given by

$$\begin{aligned} \Gamma^{\chi_{e_1}\chi_{e_2} \rightarrow X_AX_B \rightarrow \chi_{e_4}\chi_{e_3}} &= \hat{f}(^1S_0) + 3 \hat{f}(^3S_1) \\ &+ \frac{\delta m}{M} \left(\hat{h}_1(^1S_0) + 3 \hat{h}_1(^3S_1) \right) + \frac{\delta \bar{m}}{M} \left(\hat{h}_2(^1S_0) + 3 \hat{h}_2(^3S_1) \right) \\ &+ \frac{\mathbf{p} \cdot \mathbf{p}'}{M^2} \left(\hat{f}(^1P_1) + \frac{1}{3} \hat{f}(^3P_0) + \hat{f}(^3P_1) + \frac{5}{3} \hat{f}(^3P_2) \right) \end{aligned} \quad (6.30)$$

⁸ The product of tree-level annihilation amplitudes has to be multiplied with an additional symmetry factor of 1/2 if the final state particles are identical, $X_A = X_B$.

⁹In the calculation of Sommerfeld enhanced $\chi_i\chi_j \rightarrow X_AX_B$ pair-annihilation rates through the imaginary part of the $\chi_i\chi_j \rightarrow \dots \rightarrow \chi_{e_1}\chi_{e_2} \rightarrow X_AX_B \rightarrow \chi_{e_4}\chi_{e_3} \rightarrow \dots \rightarrow \chi_i\chi_j$ forward scattering reaction, the assumption that the incoming and outgoing particle pairs in the $\chi_{e_1}\chi_{e_2} \rightarrow X_AX_B \rightarrow \chi_{e_4}\chi_{e_3}$ short-distance annihilation part have the same spin state implies that just leading-order potential interactions in the $\chi_i\chi_j \rightarrow \dots \rightarrow \chi_{e_1}\chi_{e_2}$ and $\chi_i\chi_j \rightarrow \dots \rightarrow \chi_{e_4}\chi_{e_3}$ scattering reactions are considered, since the long-range potentials are spin-diagonal only at leading order and hence pass the spin-configuration of the incoming $\chi_i\chi_j$ pair to the $\chi_{e_1}\chi_{e_2}$ and $\chi_{e_4}\chi_{e_3}$ pairs. Note that we restrict to the case of leading-order potential interactions in this work, see Sec. 7.

$$\begin{aligned}
& + \frac{\mathbf{p}^2 + \mathbf{p}'^2}{2M^2} \left(\hat{g}(^1S_0) + 3 \hat{g}(^3S_1) \right) \\
& + \mathcal{O} \left((\mathbf{p}^2 + \mathbf{p}'^2)^2, (\mathbf{p} \cdot \mathbf{p}')^2, \mathbf{p}^{(\prime)2} \delta m, \mathbf{p}^{(\prime)2} \delta \bar{m}, \delta m \delta \bar{m} \right),
\end{aligned}$$

where \mathbf{p} and \mathbf{p}' correspond to the momenta of the χ_{e_1} and χ_{e_4} particle, respectively, in the centre-of-mass frame of the reaction. To shorten the notation we have suppressed in (6.30) the label “ $\chi_{e_1}\chi_{e_2} \rightarrow X_A X_B \rightarrow \chi_{e_4}\chi_{e_3}$ ” on the Wilson coefficients \hat{f}, \hat{g} and \hat{h}_i . As we study annihilation rates of non-relativistic $\chi_{e_a}\chi_{e_b}$ particle pairs, the mass differences δm and $\delta \bar{m}$ have to be (at most) of the order of the $\chi_{e_a}\chi_{e_b}$ non-relativistic kinetic energy, as argued in Sec. 6.1.2. Note that the non-relativistic expansion (6.30) incorporates this convention and assumes that $\delta m, \delta \bar{m} \sim \mathcal{O}(\mathbf{p}^2/M)$. In case of diagonal $\chi_{e_1}\chi_{e_2} \rightarrow X_A X_B \rightarrow \chi_{e_1}\chi_{e_2}$ scattering reactions, the definition of the corresponding annihilation rate Γ obviously coincides with the definition of the spin-averaged centre-of-mass frame tree-level $\chi_{e_1}\chi_{e_2} \rightarrow X_A X_B$ annihilation cross section times relative velocity, $\sigma^{\chi_{e_1}\chi_{e_2} \rightarrow X_A X_B} v_{\text{rel}}$, and the expansion in (6.30), with $\mathbf{p}' = \mathbf{p}$, reduces to the non-relativistic expansion of $\sigma^{\chi_{e_1}\chi_{e_2} \rightarrow X_A X_B} v_{\text{rel}}$ as given in (6.22).

As an example for an off-diagonal rate Γ we show in the right-hand plot in Fig. 6.4 the off-diagonal annihilation rate associated with the process $\chi_1^+\chi_1^- \rightarrow W^+W^- \rightarrow \chi_2^+\chi_2^-$, which is relevant, for instance, in the calculation of the (exclusive) Sommerfeld-enhanced $\chi_1^0\chi_1^0 \rightarrow W^+W^-$ and $\chi_1^+\chi_1^- \rightarrow W^+W^-$ co-annihilation cross sections. The mass splitting between the χ_1^\pm and χ_2^\pm charginos is given by 324.18 GeV in the MSSM scenario considered, which results in rather large mass differences, namely $\delta m = \delta \bar{m} = 162.09$ GeV. In this case, the Wilson coefficients h_1 and h_2 , that are proportional to δm and $\delta \bar{m}$, lead to a 1% positive correction to the constant leading-order rate. This positive shift corresponds to the difference between the leading-order approximation to the annihilation rate Γ (first line in (6.30), dotted blue line in the right plot in Fig. 6.4), and the complete non-relativistic result for Γ including next-to-next-to-leading corrections (solid blue line) at zero momentum. The corrections induced by the terms proportional to $\delta m, \delta \bar{m}$ turn out to be somewhat smaller than the naive expectation $\delta m/M = \delta \bar{m}/M = 2.78\%$, but represent nevertheless the dominant next-to-next-to-leading order correction up to $v_{\text{rel}}/c \sim 0.16$. For larger relative velocities, the P - and next-to-next-to-leading order S -wave terms provide larger contributions to the absorptive part of the $\chi_1^+\chi_1^- \rightarrow W^+W^- \rightarrow \chi_2^+\chi_2^-$ scattering amplitude. This is indicated by the dash-dotted red and dashed black curves, which result from the addition of the constant S -wave contributions (first two lines in (6.30)) and the P -wave contributions (third line in (6.30)) or the momentum-dependent S -wave next-to-next-to-leading terms (fourth line in (6.30)), respectively. The correction to the leading-order Γ rate due to the P - and next-to-next-to-leading order S -wave terms amounts to a 7% for $v_{\text{rel}}/c = 0.4$.

Note that no comparison with public numeric codes providing results for (tree-level) $\chi\chi \rightarrow X_A X_B$ annihilation rates is available for the off-diagonal annihilation rates. The calculation of the partial-wave decomposed off-diagonal annihilation rates therefore constitutes one of our main results regarding the hard annihilation reactions in the effective theory. The relevance of off-diagonal annihilation rates in the calculation of Sommerfeld enhanced co-annihilation amplitudes in context of the χ_1^0 relic abundance calculation is in

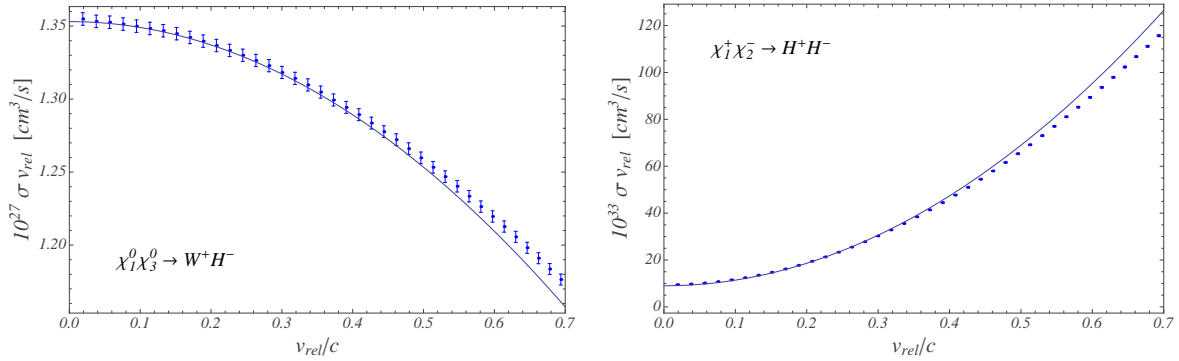


Figure 6.5: Numeric comparison of the non-relativistic approximation (solid line) to σv_{rel} for the two neutral hydrogen-like two-body states $\chi_1^0 \chi_3^0 \rightarrow W^+ H^-$ (left) and $\chi_1^+ \chi_2^- \rightarrow H^+ H^-$ (right) to data produced with MADGRAPH. Again, we take the errors on the MADGRAPH data to be $\sigma v_{rel}/\sqrt{N}$, where $N = 10^5$ gives the number of events used in the MADGRAPH calculation of each cross section value. The process on the right-hand side is dominated by P -wave annihilations. The underlying MSSM spectrum is the same as in the plots in Fig. 6.2 – 6.4, where the masses of the χ_3^0 and χ_2^- are given by $m_{\chi_3^0} = 3061.99$ GeV and $m_{\chi_2^-} = 3073.31$ GeV. The mass of the Higgs particles H^\pm takes the value $m_{H^\pm} = 167.29$ GeV.

particular investigated in Chap. 9. There we discuss in detail the effect on Sommerfeld-enhanced co-annihilation rates when off-diagonal rates are wrongly neglected or correctly included in the calculation.

6.2.5 Annihilation cross sections of “hydrogen-like” $\chi\chi$ states

The plots in Fig. 6.5 show that our results can not only be used to describe pair annihilations of nearly mass-degenerate incoming particles $\chi_{e_1} \chi_{e_2} \rightarrow X_A X_B$, but also apply to annihilations of a non-relativistic “hydrogen-like” $\chi_{e_1} \chi_{e_2}$ two-particle system of non-degenerate-in-mass constituents. We will not investigate such systems further in later chapters. However we like to emphasise with the following two examples, that our results allow to describe the tree-level annihilation reactions of such non-relativistic $\chi\chi$ states as well and to very good accuracy. Let us note that we use the notion “hydrogen-like” to refer to two-particle states with non-degenerate-in-mass constituents, where the mass difference between the two constituents is larger than several 100 GeV.

The plot on the left hand side in Fig. 6.5 corresponds to the pair annihilation of a hydrogen-like $\chi_1^0 \chi_3^0$ state into a $W^+ H^-$ final state, with $m_{\chi_3^0} = 3061.99$ GeV, which is dominated by leading-order S -wave contributions. The curvature is driven negative by the next-to-next-to-leading order S -wave contributions b_S to the coefficient b , given by $b_S c^2 = -5.29 \cdot 10^{-28} \text{ cm}^3 \text{ s}^{-1}$. The P -wave contributions are however of the same order and read $b_P c^2 = 1.30 \cdot 10^{-28} \text{ cm}^3 \text{ s}^{-1}$.

The right plot in Fig. 6.5 again refers to a hydrogen-like incoming two-body system, $\chi_1^+ \chi_2^-$, where the mass of the second chargino is given by $m_{\chi_2^-} = 3073.31$ GeV. In this case

the annihilation $\chi_1^+ \chi_2^- \rightarrow H^+ H^-$ is P -wave dominated: the P -wave contribution b_P to the coefficient b is given by $b_P c^2 = 2.48 \cdot 10^{-31} \text{ cm}^3 \text{ s}^{-1}$. Both the leading and next-to-next-to-leading order S -wave contributions are strongly suppressed and of $\mathcal{O}(10^{-33} \text{ cm}^3/\text{s})$.

6.3 Application of the analytic results at $\mathcal{O}(v_{\text{rel}}^2)$: A pure-wino NRMSSM sample calculation

In this section we illustrate the usage of the analytic kinematic and coupling factor results collected in Appendices A.1–A.3. To this end we consider the idealised pure-wino NRMSSM, which allows to present compact analytic results. First we give a detailed end-to-end calculation of the non-relativistic annihilation cross section for the $\chi_1^+ \chi_1^- \rightarrow W^+ W^-$ reaction including up to $\mathcal{O}(v_{\text{rel}}^2)$ effects. We start from the construction of the coupling factors in this process in Sec. 6.3.1 and continue in Sec. 6.3.2 with the determination of the corresponding kinematic factors and the final approximation to the annihilation cross section. In Sec. 6.3.3 we subsequently provide the results for the Wilson coefficients needed to determine all exclusive (off-) diagonal co-annihilation rates $\chi_{e_1} \chi_{e_2} \rightarrow X_A X_B \rightarrow \chi_{e_4} \chi_{e_3}$ in the decoupling limit of the pure-wino scenario. To the best of our knowledge the analytic results for the P - and $\mathcal{O}(v_{\text{rel}}^2)$ S -wave (off-) diagonal annihilation rates in the pure-wino NRMSSM have not been given before in the literature and were first published in [32]. They can be of interest in the study of next-to-next-to-leading order effects in Sommerfeld-enhanced pure-wino dark matter annihilations in the Early Universe.

Later in Chap. 9 we will compare results on Sommerfeld-enhanced co-annihilation rates in the relic abundance calculation for wino-like χ_1^0 dark matter to corresponding results within the pure-wino NRMSSM. As we will discuss in detail, the knowledge of all off-diagonal rates is crucial for an accurate determination of the χ_1^0 relic abundance including Sommerfeld enhancements. Furthermore we will show that the precise value of the calculated relic density depends on the details of the spectrum, such that results from a study in the pure-wino limit do not directly apply to scenarios with wino-like χ_1^0 . Nevertheless the pure-wino NRMSSM allows to give a clear illustration how the Wilson coefficients are constructed from our analytic results. In addition, generic properties of wino-like χ_1^0 scenarios can be deduced from the pure-wino NRMSSM results.

The pure-wino (toy-)NRMSSM scenario is characterised by the mass-degenerate $SU(2)_L$ fermion triplet states χ_1^0, χ_1^\pm (winos) with mass scale $M_2 > 0$, where the latter denotes the soft SUSY-breaking wino mass.¹⁰ All other SUSY mass parameters includ-

¹⁰As regards the hard annihilation rates, the pure-wino states χ_1^0 and χ_1^\pm can be treated as mass-degenerate: The hard pure-wino $\chi\chi$ annihilation reactions are characterised by the scale $2M_2$. The χ_1^+/χ_1^0 mass splitting, $\delta m_{\chi_1^+} = m_{\chi_1^+} - m_{\chi_1^0} \ll M_2$, is $\mathcal{O}(160 \text{ MeV})$ in the pure-wino limit [80], and therefore gives subleading contributions to the hard rates for $\mathcal{O}(\text{TeV})$ pure-wino states. In the application of our results to generic MSSM scenarios we treat the external state masses in the hard annihilation cross sections exactly – in the pure-wino NRMSSM we use $m_{\chi_1^+} = m_{\chi_1^0} = M_2$. However, as far as the long-range potential interactions and the corresponding Schrödinger equations are concerned, the one-loop

ing the Bino soft mass M_1 and the Higgsino mass parameter μ as well as all sfermion mass parameters are assumed to be much larger than M_2 , namely $M_1, |\mu| \gg M_2$. Consequently all heavier states χ_i^0 , $i = 2, 3, 4$ and χ_2^\pm as well as all sfermion states are treated as completely decoupled. According to the $SU(2)_L$ symmetric limit the $SU(2)_L$ gauge bosons as well as all Standard Model fermions are treated as massless in the hard annihilation rates, in agreement with the complete mass-degeneracy between the non-relativistic states χ_1^0 and χ_1^\pm . The neutralino and chargino mixing matrix entries relevant to the calculation in the pure-wino NRMSSM read

$$\tilde{Z}_{N i 1} = \delta_{i 2}, \quad \tilde{Z}_{\pm i 1} = \delta_{i 1}, \quad (6.31)$$

where the $\tilde{Z}_N, \tilde{Z}_\pm$ derive from the conventionally defined neutralino and chargino mixing matrices Z_N, Z_\pm by accounting for a potentially necessary rotation to positive mass parameters in the NRMSSM, as defined through (6.20, 6.21). Such a rotation does however not affect the above mixing-matrix entries relevant in the pure-wino NRMSSM with $M_2 > 0$. Finally, let us introduce the notation $m_\chi = M_2$ for the only mass parameter present in the annihilation rates of the pure-wino NRMSSM scenario.

6.3.1 Coupling factors

In this section we strongly rely on the generic rules to construct the coupling factors set out in Appendix A.1. In order to follow the discussion below it is therefore recommendable to first read the corresponding chapter in the appendix, where the construction of coupling factors in the generic case is discussed and our notation is established. The application of the generic rules to the coupling factors in the $\chi_1^+ \chi_1^- \rightarrow W^+ W^-$ process in this chapter will then give a nice illustration on the construction of the coupling factors.

In Appendix A.1 we note that each of the coupling factors $b_n, c_n^{(\alpha)}, d_n^{(\alpha)}$ in (6.17) related to a specific $\chi_{e_1} \chi_{e_2} \rightarrow X_A X_B \rightarrow \chi_{e_4} \chi_{e_3}$ reaction is given by a product of two coupling factors associated with the two vertices occurring in the tree-level annihilation amplitude $\mathcal{A}_{\chi_{e_1} \chi_{e_2} \rightarrow X_A X_B}^{(0)}$ and the complex conjugate of another such two-coupling factor product related to the tree-level amplitude $\mathcal{A}_{\chi_{e_4} \chi_{e_3} \rightarrow X_A X_B}^{(0)}$. The building blocks of the $b_n, c_n^{(\alpha)}, d_n^{(\alpha)}$ relevant in $\chi_1^+ \chi_1^- \rightarrow X_A X_B$ annihilation rates are therefore given by the (axial-) vector or (pseudo-) scalar vertex factors in the $\chi_1^+ \chi_1^- \rightarrow X_A X_B$ tree-level annihilation amplitudes. Since our results for the kinematic factors refer to Feynman gauge, in order to determine the annihilation rates into a physical $W^+ W^-$ final state we have to consider $\chi_1^+ \chi_1^-$ annihilations into the exclusive final states $X_A X_B = W^+ W^-, W^+ G^-, W^- G^+, G^+ G^-, \eta^+ \bar{\eta}^+, \eta^- \bar{\eta}^-$, with G^\pm the charged pseudo-Goldstone Higgs and η^\pm the charged ghost particles. In the pure-wino NRMSSM, the only non-vanishing amplitudes are given by the diagrams depicted in Fig. 6.6, which we should compare with the generic

mass splitting between the slightly heavier χ_1^\pm states and the χ_1^0 is accounted for also in the pure-wino NRMSSM. This one-loop mass splitting counts at the same order as the typical non-relativistic kinetic energies in reactions of non-relativistic pure-wino $\chi\chi$ states.

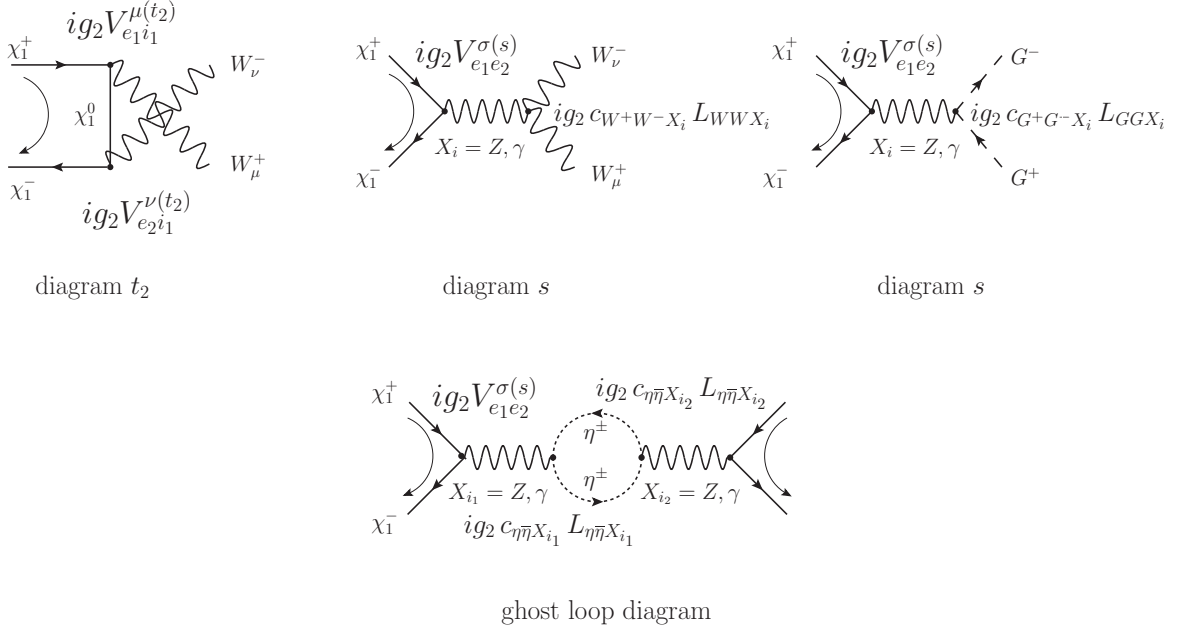


Figure 6.6: Amplitudes contributing to the physical $\chi_1^+ \chi_1^- \rightarrow W^+ W^-$ annihilation reaction in Feynman gauge. Note the fermion flow, that has been fixed to match with the conventions established in Fig. A.1 in Appendix A.1.

$\chi\chi \rightarrow X_A X_B$ diagrams drawn in Fig. A.1 in order to extract the coupling factors in accordance to the conventions established in Appendix A.1. In particular note the fermion flow in the diagrams in Fig. 6.6, which coincides with the convention used in the generic $\chi_{e_1} \chi_{e_2} \rightarrow X_A X_B$ diagrams in Fig. A.1. In the case of diagram t_2 in Fig. 6.6, which contributes both to the box and triangle coupling factors, $d_{n, i_1 i_2}^{(\alpha)}$ and $c_{n, i_1 i_2}^{(\alpha)}$, the vertex factors $V_{ei}^{\rho(t_2)}$ read

$$V_{e_1 i_1}^{\mu(t_2)} = \gamma^\mu (v_{e_1 i_1}^{W*} + a_{e_1 i_1}^{W*} \gamma_5) , \quad V_{e_2 i_1}^{\nu(t_2)} = \gamma^\nu (v_{e_2 i_1}^W + a_{e_2 i_1}^W \gamma_5) , \quad (6.32)$$

where $e_1, e_2 = 1$ as these indices refer to the external states $\chi_{e_1} = \chi_1^+$ and $\chi_{e_2} = \chi_1^-$. In the pure-wino NRMSSM, the only possible t -channel exchanged particle in diagram t_2 is χ_1^0 , therefore $i_1 = 1$. Comparing to the generic vertex factor $V_{ei}^{\rho(d)} = \gamma^\rho (r_{ei}^{(d)} + q_{ei}^{(d)} \gamma_5)$, we identify the expressions that substitute the respective place-holder couplings $r_{ei}^{(d)}$ and $q_{ei}^{(d)}$:

$$\left(\{r_{e_1 i_1}^{(t_2)}, q_{e_1 i_1}^{(t_2)}\}, \{r_{e_2 i_1}^{(t_2)}, q_{e_2 i_1}^{(t_2)}\} \right) \rightarrow \left(\{v_{11}^{W*}, a_{11}^{W*}\}, \{v_{11}^W, a_{11}^W\} \right) . \quad (6.33)$$

Let us obtain first the coupling factors $d_{n, i_1 i_2}^{(\alpha)}$ related to the four box amplitudes shown in the third row of Fig. 6.1. As there is no t -channel exchange diagram t_1 , the only non-vanishing coupling factors $d_{n, i_1 i_2}^{(\alpha)}$ are those with label $\alpha = 4$: $d_{n, i_1 i_2}^{(4)}$ expressions arise

from the product of coupling factors in $\chi_{e_1}\chi_{e_2} \rightarrow X_A X_B$ annihilation diagrams of type t_2 with the complex conjugate of the coupling factors associated with $\chi_{e_4}\chi_{e_3} \rightarrow X_A X_B$ annihilation via diagram type t_2 .¹¹ The constituent coupling factors for the $d_{n,i_1i_2}^{(4)}$ in $\chi_1^+\chi_1^- \rightarrow W^+W^- \rightarrow \chi_1^+\chi_1^-$ scattering are collected in the following table:

$$\begin{aligned} \alpha = 4 : \quad & \left(\{r_{e_1i_1}^{(t_2)}, q_{e_1i_1}^{(t_2)}\}, \{r_{e_2i_1}^{(t_2)}, q_{e_2i_1}^{(t_2)}\}, \{r_{e_3i_2}^{(t_2)*}, q_{e_3i_2}^{(t_2)*}\}, \{r_{e_4i_2}^{(t_2)*}, q_{e_4i_2}^{(t_2)*}\} \right) \\ & \rightarrow \left(\{v_{11}^{W*}, a_{11}^{W*}\}, \{v_{11}^W, a_{11}^W\}, \{v_{11}^{W*}, a_{11}^{W*}\}, \{v_{11}^W, a_{11}^W\} \right). \end{aligned} \quad (6.34)$$

Selecting one element from each of the four subsets and multiplying these selected elements with each other gives rise to the $d_{n,i_1i_2}^{(4)}$. The label n denotes a string of four characters, that indicates which coupling (type r or q) was selected from the i th subset in (6.34). For instance

$$d_{rrrr,11}^{(4)\chi_1^+\chi_1^- \rightarrow W^+W^- \rightarrow \chi_1^+\chi_1^-} = v_{11}^{W*} v_{11}^W v_{11}^{W*} v_{11}^W. \quad (6.35)$$

Turning to the coupling factors in triangle and selfenergy amplitudes, $c_{n,i_1i_2}^{(\alpha)}$ and b_{n,i_1i_2} , they receive contributions from the s -channel diagrams in Fig. 6.6. We proceed in a similar way as done for the diagram t_2 and identify the following coupling factors for the case of single s -channel Z -exchange (first line) and single s -channel γ -exchange (second line):

$$\begin{aligned} V_{11}^{\sigma(s)} &= \gamma^\sigma (v_{11}^Z + a_{11}^Z \gamma_5), & c_{W+W-Z} &= c_W, \\ V_{11}^{\sigma(s)} &= \gamma^\sigma (v_{11}^\gamma + a_{11}^\gamma \gamma_5), & c_{W+W-\gamma} &= s_W. \end{aligned} \quad (6.36)$$

The building blocks for the $b_{n,i_1i_2}, c_{n,i_1i_2}^{(\alpha)}$ and finally these expressions themselves can now be obtained in a similar manner as described for the $d_{n,i_1i_2}^{(\alpha)}$ expressions. However, before proceeding with their explicit construction, significant simplifications can be performed by noting that the pure-wino NRMSSM exhibits a particularly simple coupling structure: the (axial-)vector couplings of χ_1^0 and χ_1^\pm to the Standard Model gauge bosons are given by

$$\begin{aligned} v_{11}^W &= 1, \quad a_{11}^W = 0, & v_{11}^\gamma &= -s_W, \quad a_{11}^\gamma = 0, \\ v_{11}^Z &= -c_W, \quad a_{11}^Z = 0. \end{aligned} \quad (6.37)$$

With the vanishing of all axial-vector couplings the only non-vanishing coupling factor $d_{n,i_1i_2}^{(\alpha)}$ for $\chi_1^+\chi_1^- \rightarrow W^+W^- \rightarrow \chi_1^+\chi_1^-$ in the pure-wino NRMSSM hence reads

$$d_{rrrr,11}^{(4)\chi_1^+\chi_1^- \rightarrow W^+W^- \rightarrow \chi_1^+\chi_1^-} = 1. \quad (6.38)$$

The absence of a t -channel exchange diagram t_1 implies, that only $c_{n,i_1i_2}^{(\alpha)}$ factors with $\alpha = 3, 4$ can be non-vanishing, as these are built from vertex coupling factors associated

¹¹For further conventions on the enumeration label α see Appendix A.1.

with diagram type t_2 and diagram type s , see Fig. 6.1. In the pure-wino NRMSSM, we find the following expressions

$$c_{rrr,1Z}^{(\alpha=3,4)\chi_1^+\chi_1^-\rightarrow W^+W^-\rightarrow\chi_1^+\chi_1^-} = -c_W^2, \quad c_{rrr,1\gamma}^{(\alpha=3,4)\chi_1^+\chi_1^-\rightarrow W^+W^-\rightarrow\chi_1^+\chi_1^-} = -s_W^2, \quad (6.39)$$

and all other $c_{n,i_2}^{(\alpha)}$ vanish. Finally, the non-zero factors b_{n,i_1i_2} read

$$b_{rr,ZZ} = c_W^4, \quad b_{rr,Z\gamma} = b_{rr,\gamma Z} = c_W^2 s_W^2, \quad b_{rr,\gamma\gamma} = s_W^4, \quad (6.40)$$

where we have suppressed the superscript $\chi_1^+\chi_1^-\rightarrow W^+W^-\rightarrow\chi_1^+\chi_1^-$ to shorten the notation. A similar procedure leads to the coupling factors in $\chi_1^+\chi_1^-\rightarrow X_A X_B$ rates with the (unphysical) final states $X_A X_B = G^+G^-, \eta^+\eta^+$ and $\eta^-\eta^-$. We quote the non-vanishing results for the coupling factors related to $\chi_1^+\chi_1^-\rightarrow G^+G^-\rightarrow\chi_1^+\chi_1^-$ reactions:

$$\begin{aligned} b_{rr,ZZ} &= \frac{1}{4} (c_W^2 - s_W^2)^2, & b_{rr,Z\gamma} &= b_{rr,\gamma Z} = \frac{s_W^2}{2} (c_W^2 - s_W^2), \\ b_{rr,\gamma\gamma} &= s_W^4. \end{aligned} \quad (6.41)$$

In case of $\chi_1^+\chi_1^-\rightarrow\eta^+\eta^+\rightarrow\chi_1^+\chi_1^-$ and $\chi_1^+\chi_1^-\rightarrow\eta^-\eta^-\rightarrow\chi_1^+\chi_1^-$ reactions we find in both cases the same result (again suppressing the process-specifying superscripts):

$$b_{rr,ZZ} = c_W^4, \quad b_{rr,Z\gamma} = b_{rr,\gamma Z} = c_W^2 s_W^2, \quad b_{rr,\gamma\gamma} = s_W^4. \quad (6.42)$$

6.3.2 Kinematic factors

As for the coupling factors, the kinematic factors $B_{n,i_1i_2}, C_{n,i_1X}^{(\alpha)}, D_{n,i_1i_2}^{(\alpha)}$ reduce to very simple expressions in the pure-wino NRMSSM. Again we rely in this section on conventions introduced in the appendices, in particular in Appendices A.2 and A.3. For the notation used in the following, the reader is therefore referred to these chapters.

As the hard annihilation reactions in the pure-wino NRMSSM refer to the limit of vanishing $SU(2)_L$ gauge boson masses, the relevant (mass) parameters in any of the $\chi_{e_1}\chi_{e_2}\rightarrow X_A X_B\rightarrow\chi_{e_4}\chi_{e_3}$ scattering reactions with $\chi_{e_a} = \chi_1^0, \chi_1^\pm$ read

$$\begin{aligned} m &= \bar{m} = m_\chi, & M &= 2 m_\chi, & \Delta_{AB} &= 0, \\ \beta &= 1, & P_{Z,\gamma}^s &= 1, & P_{1AB} &= \frac{1}{2}. \end{aligned} \quad (6.43)$$

Further, the rescaled quantity $\hat{m}_{i_1,2}$ in the pure-wino limit reads $\hat{m}_1 = 1/2$ if it refers to the χ_1^0 or χ_1^\pm species and it vanishes if related to Z and γ , $\hat{m}_{Z,\gamma} = 0$. Taking the relations (6.43) into account, we obtain concise analytic results for the kinematic factors relevant in $\chi_1^+\chi_1^-\rightarrow X_A X_B\rightarrow\chi_1^+\chi_1^-$ scattering. These are collected in Tab. 6.2. Note that we have given only those kinematic factors that are associated with non-vanishing coupling factors in the physical $\chi_1^+\chi_1^-\rightarrow W^+W^-\rightarrow\chi_1^+\chi_1^-$ reaction. Assembling and inserting the above results into the master formula (6.17) we find the results for the absorptive part

	1S_0	3S_1	1P_1	3P_J	$^1S_0^{(p^2)}$	$^3S_1^{(p^2)}$
$B_{rr,VV}^{VV}(^{2s+1}L_J)$	0	$-\frac{19}{6}$	0	0	0	$\frac{152}{9}$
$C_{rrr,1V}^{(\alpha=3,4)VV}(^{2s+1}L_J)$	0	$-\frac{4}{3}$	0	0	0	$\frac{64}{9}$
$D_{rrrr,11}^{(4)VV}(^{2s+1}L_J)$	2	$\frac{2}{3}$	$\frac{8}{3}$	$\frac{56}{3}$	$-\frac{32}{3}$	$-\frac{32}{9}$
$B_{rr,VV}^{SS}(^{2s+1}L_J)$	0	$\frac{1}{3}$	0	0	0	$-\frac{16}{9}$
$B_{rr,VV}^{\eta\bar{\eta}}(^{2s+1}L_J)$	0	$-\frac{1}{12}$	0	0	0	$\frac{4}{9}$

Table 6.2: Kinematic factors for partial-wave reactions up to $\mathcal{O}(v_{\text{rel}}^2)$ in the pure-wino NRMSSM, relevant for the determination of the $\chi_1^+\chi_1^- \rightarrow W^+W^-$ annihilation rate. The subscript label V on the kinematic factors B and C above refers to both the cases of Z and γ single s -channel exchange in the (tree-level) annihilation amplitudes. The results for the kinematic factor B in the last line apply to $\eta\bar{\eta} = \eta^+\bar{\eta}^+, \eta^-\bar{\eta}^-$.

of the Wilson coefficients that provide the $\chi_1^+\chi_1^- \rightarrow W^+W^-$ annihilation cross section (6.24). For 3S_1 annihilation we have

$$\begin{aligned}
& \hat{f}_{\{11\}\{11\}}^{\chi_1^+\chi_1^- \rightarrow W^+W^- \rightarrow \chi_1^+\chi_1^-}(^3S_1) \\
&= \frac{\pi\alpha_2^2}{4m_\chi^2} \left(\sum_{n=rr} \sum_{i_1, i_2=Z, \gamma} b_{n, i_1 i_2}^{\chi_1^+\chi_1^- \rightarrow W^+W^- \rightarrow \chi_1^+\chi_1^-} B_{n, i_1 i_2}^{VV}(^3S_1) \right. \\
&\quad + \sum_{\alpha=3,4} \sum_{n=rrr} \sum_{i_1=1, i_2=Z, \gamma} c_{n, i_1 i_2}^{(\alpha)\chi_1^+\chi_1^- \rightarrow W^+W^- \rightarrow \chi_1^+\chi_1^-} C_{n, i_1 i_2}^{(\alpha)VV}(^3S_1) \\
&\quad + \sum_{\alpha=4} \sum_{n=rrrr} \sum_{i_1, i_2=1} d_{n, i_1 i_2}^{(\alpha)\chi_1^+\chi_1^- \rightarrow W^+W^- \rightarrow \chi_1^+\chi_1^-} D_{n, i_1 i_2}^{(\alpha)VV}(^3S_1) \\
&\quad + \sum_{n=rr} \sum_{i_1, i_2=Z, \gamma} b_{n, i_1 i_2}^{\chi_1^+\chi_1^- \rightarrow G^+G^- \rightarrow \chi_1^+\chi_1^-} B_{n, i_1 i_2}^{SS}(^3S_1) \\
&\quad \left. + \sum_{\eta=\eta^\pm} \sum_{n=rr} \sum_{i_1, i_2=Z, \gamma} b_{n, i_1 i_2}^{\chi_1^+\chi_1^- \rightarrow \eta\bar{\eta} \rightarrow \chi_1^+\chi_1^-} B_{n, i_1 i_2}^{\eta\bar{\eta}}(^3S_1) \right) \\
&= \frac{\pi\alpha_2^2}{4m_\chi^2} \left((c_W^4 + c_W^2 s_W^2 + s_W^4) \times \left(-\frac{19}{6} \right) + 2(-c_W^2 - s_W^2) \times \left(-\frac{4}{3} \right) \right)
\end{aligned}$$

$$\begin{aligned}
& + 1 \times \frac{2}{3} + \frac{1}{4} \times \frac{1}{3} - 2 \times \frac{1}{12} \Big) \\
& = \frac{1}{48} \frac{\pi \alpha_2^2}{m_\chi^2}, \tag{6.44}
\end{aligned}$$

where we have summed over all (unphysical) final states in Feynman gauge, $X_A X_B = W^+ W^-, G^+ G^-, \eta^+ \bar{\eta}^+, \eta^- \bar{\eta}^-$, that contribute to the physical $\chi_1^+ \chi_1^- \rightarrow W^+ W^-$ rate in the pure-wino NRMSSM scenario. In case of the 1S_0 annihilation reaction only the pieces related to the $\alpha = 4$ box amplitude contribute, and the only non-vanishing coupling factor $d_{n, i_1 i_2}^{(4)}$ is $d_{rrrr, 11}^{(4)}$ given in (6.38), therefore

$$\begin{aligned}
\hat{f}_{\{11\}\{11\}}^{\chi_1^+ \chi_1^- \rightarrow W^+ W^- \rightarrow \chi_1^+ \chi_1^-} (^1S_0) &= \frac{\pi \alpha_2^2}{4m_\chi^2} d_{rrrr, 11}^{(4) \chi_1^+ \chi_1^- \rightarrow W^+ W^- \rightarrow \chi_1^+ \chi_1^-} D_{rrrr, 11}^{(4) VV} (^1S_0) \\
&= \frac{\pi \alpha_2^2}{2m_\chi^2}. \tag{6.45}
\end{aligned}$$

Finally, the absorptive parts of the $\mathcal{O}(v_{\text{rel}}^2)$ partial-wave Wilson coefficients read

$$\begin{aligned}
\hat{f}_{\{11\}\{11\}}^{\chi_1^+ \chi_1^- \rightarrow W^+ W^- \rightarrow \chi_1^+ \chi_1^-} (^1P_1) &= \frac{2\pi \alpha_2^2}{3m_\chi^2}, & \hat{f}_{\{11\}\{11\}}^{\chi_1^+ \chi_1^- \rightarrow W^+ W^- \rightarrow \chi_1^+ \chi_1^-} (^3P_J) &= \frac{14\pi \alpha_2^2}{3m_\chi^2}, \\
\hat{g}_{\{11\}\{11\}}^{\chi_1^+ \chi_1^- \rightarrow W^+ W^- \rightarrow \chi_1^+ \chi_1^-} (^1S_0) &= -\frac{8\pi \alpha_2^2}{3m_\chi^2}, & \hat{g}_{\{11\}\{11\}}^{\chi_1^+ \chi_1^- \rightarrow W^+ W^- \rightarrow \chi_1^+ \chi_1^-} (^3S_1) &= -\frac{\pi \alpha_2^2}{9m_\chi^2}. \tag{6.46}
\end{aligned}$$

Following (6.24), the non-relativistic expansion of the $\chi_1^+ \chi_1^- \rightarrow W^+ W^-$ annihilation cross section in the pure-wino NRMSSM is given by

$$\begin{aligned}
\sigma^{\chi_1^+ \chi_1^- \rightarrow W^+ W^-} v_{\text{rel}} &= a + (b_P + b_S) v_{\text{rel}}^2 + \mathcal{O}(v_{\text{rel}}^4) \\
&= \frac{9}{16} \frac{\pi \alpha_2^2}{m_\chi^2} + \left(\frac{1}{3} - \frac{3}{16} \right) \frac{\pi \alpha_2^2}{m_\chi^2} v_{\text{rel}}^2 + \mathcal{O}(v_{\text{rel}}^4), \\
&= \frac{9}{16} \frac{\pi \alpha_2^2}{m_\chi^2} + \frac{7}{48} \frac{\pi \alpha_2^2}{m_\chi^2} v_{\text{rel}}^2 + \mathcal{O}(v_{\text{rel}}^4). \tag{6.47}
\end{aligned}$$

The values for the parameters a, b_P and b_S , that one obtains for a pure-wino NRMSSM mass scale $m_\chi = 2748.92 \text{ GeV}$ read $a = 3.06 \cdot 10^{-27} \text{ cm}^3 \text{ s}^{-1}$, $b_P c^2 = 1.81 \cdot 10^{-27} \text{ cm}^3 \text{ s}^{-1}$ and $b_S c^2 = -1.02 \cdot 10^{-27} \text{ cm}^3 \text{ s}^{-1}$. The mass scale m_χ agrees with the neutralino LSP mass of the MSSM scenario introduced in Sec. 6.2. The latter MSSM scenario features a small but non-vanishing Higgsino admixture to the wino-like χ_1^0 and χ_1^\pm : the Higgsino-like neutralino and chargino states are not at all decoupled but reside at the scale of $\sim 2.9 - 3 \text{ TeV}$. Thus we should not expect the results for the wino-like scenario of Sec. 6.2 to be approximated by the pure-wino NRMSSM. This is in fact what the comparison of the parameters a, b_P and b_S for the $\chi_1^+ \chi_1^- \rightarrow W^+ W^-$ annihilation cross section shows: the corresponding parameters in the MSSM scenario investigated in Sec. 6.2 were given

by $a = 2.65 \cdot 10^{-27} \text{ cm}^3 \text{ s}^{-1}$, $b_P c^2 = 1.86 \cdot 10^{-27} \text{ cm}^3 \text{ s}^{-1}$, $b_S c^2 = -0.88 \cdot 10^{-27} \text{ cm}^3 \text{ s}^{-1}$. The results for the S -wave parameters a and b_S in the pure-wino $\chi_1^+ \chi_1^- \rightarrow W^+ W^-$ reaction are a bit larger, which is a consequence of the larger couplings of the pure-wino neutralino and chargino states to the $SU(2)_L$ gauge bosons and the absence of t -channel annihilation into the (unphysical) final state $G^+ G^-$. Due to the non-decoupled higgsino-like neutralino states in the scenario of Sec. 6.2 the latter contribution is present and interferes destructively with the corresponding s -channel exchange contribution also present in the pure-wino NRMSSM limit. This leads to a suppression of the a and b_S cross section parameters in the wino-like scenario of Sec. 6.2 with respect to the pure-wino NRMSSM. On the contrary the parameter b_P turns out to be somewhat larger in the Sec. 6.2 scenario which traces back to the non-vanishing P -wave t -channel annihilations into $G^+ G^-$ final states that are absent in the pure-wino NRMSSM. Note that the $\chi^+ \chi^- \rightarrow W^+ W^-$ annihilation cross section for the Sec. 6.2 scenario in addition exhibits non-vanishing contributions from the (unphysical) $VS = W^\pm G^\mp$ final states not present in the pure-wino NRMSSM. These are however suppressed with respect to the $X_A X_B = W^+ W^-, G^+ G^-$ contributions.

6.3.3 Exclusive pure-wino NRMSSM co-annihilation rates

We conclude the discussion of the short distance (tree-level) annihilation rates in the pure-wino NRMSSM by collecting results for all exclusive (physical) $X_A X_B$ final state contributions to the Wilson coefficients \hat{f}, \hat{g} that determine the (off-) diagonal co-annihilation rates $\chi_{e_1} \chi_{e_2} \rightarrow X_A X_B \rightarrow \chi_{e_4} \chi_{e_3}$ in this scenario. The non-relativistic expansion of the respective exclusive rates can then be obtained from (6.22) and (6.30). For convenience we write the pure-wino NRMSSM Wilson coefficients as

$$\hat{f}^{\chi_{e_1} \chi_{e_2} \rightarrow X_A X_B \rightarrow \chi_{e_4} \chi_{e_3}} ({}^{2s+1}L_J) = \frac{\pi \alpha_2^2}{m_\chi^2} c^{\chi_{e_1} \chi_{e_2} \rightarrow X_A X_B \rightarrow \chi_{e_4} \chi_{e_3}} ({}^{2s+1}L_J) . \quad (6.48)$$

In case of the next-to-next-to-leading order S -wave coefficients we establish a similar notation with \hat{f} replaced by \hat{g} on the l.h.s. of (6.48) and the ${}^{2s+1}L_J = {}^1S_0, {}^3S_1$ label of the factor c on the r.h.s. substituted by ${}^1S_0^{(p^2)}, {}^3S_1^{(p^2)}$. Note that the Wilson coefficients \hat{h}_i always vanish in the hard annihilation rates in the pure-wino NRMSSM due to the complete mass-degeneracy of the χ_1^0 and χ_1^\pm states.

At the beginning of Sec. 6.3 we have already noted, that the calculation of the hard annihilation rates in the pure-wino NRMSSM toy-scenario refers to massless SM gauge bosons and SM fermions. These can hence appear as possible $X_A X_B$ final state particles in the $\chi_{e_1} \chi_{e_2} \rightarrow X_A X_B \rightarrow \chi_{e_4} \chi_{e_3}$ reactions. As far as the Higgs-sector is concerned we present in this section results that refer to the decoupling limit [95] in the underlying MSSM scenario: we assume a SM-like CP -even Higgs boson h^0 in the low-energy spectrum of the theory while the heavier Higgs states A^0, H^0, H^\pm are entirely decoupled ($m_{A^0} \sim m_{H^0} \sim m_{H^\pm} \gg m_\chi \gg 0$). As generically $m_{h^0} < m_Z$ at tree-level in the MSSM, the h^0 is consequently treated as massless in the pure-wino NRMSSM hard annihilation rates. According to their overall charge the (co-)annihilation processes

$\chi_1^+ \chi_1^- \rightarrow \chi_1^+ \chi_1^-$ reactions						
physical final state $X_A X_B$	$c(^1S_0)$	$c(^3S_1)$	$c(^1P_1)$	$c(^3P_{\mathcal{J}})$	$c(^1S_0^{(p^2)})$	$c(^3S_1^{(p^2)})$
$W^+ W^-$	$\frac{1}{2}$	$\frac{1}{48}$	$\frac{2}{3}$	$\frac{14}{3}$	$-\frac{8}{3}$	$-\frac{1}{9}$
ZZ	c_W^4	0	0	$\frac{28}{3} c_W^4$	$-\frac{16}{3} c_W^4$	0
$Z\gamma$	$2 c_W^2 s_W^2$	0	0	$\frac{56}{3} c_W^2 s_W^2$	$-\frac{32}{3} c_W^2 s_W^2$	0
$\gamma\gamma$	s_W^4	0	0	$\frac{28}{3} s_W^4$	$-\frac{16}{3} s_W^4$	0
Zh^0	0	$\frac{1}{48}$	0	0	0	$-\frac{1}{9}$
$q\bar{q}$	0	$\frac{1}{8}$	0	0	0	$-\frac{2}{3}$
$l^+ l^-, \nu\bar{\nu}$	0	$\frac{1}{24}$	0	0	0	$-\frac{2}{9}$
$\sum X_A X_B$	$\frac{3}{2}$	$\frac{25}{24}$	$\frac{2}{3}$	14	-8	$-\frac{50}{9}$
$\chi_1^0 \chi_1^0 \rightarrow \chi_1^0 \chi_1^0$ reactions						
$W^+ W^-$	2	0	0	$\frac{56}{3}$	$-\frac{32}{3}$	0
$\chi_1^0 \chi_1^0 \rightarrow \chi_1^+ \chi_1^-$ and $\chi_1^+ \chi_1^- \rightarrow \chi_1^0 \chi_1^0$ reactions						
$W^+ W^-$	1	0	0	$\frac{28}{3}$	$-\frac{16}{3}$	0

Table 6.3: $c(^{2s+1}L_J)$ factors that enter the contributions to the pure-wino NRMSSM Wilson coefficients in neutral $\chi_{e_1} \chi_{e_2} \rightarrow X_A X_B \rightarrow \chi_{e_4} \chi_{e_3}$ processes with exclusive (physical) final states $X_A X_B$. In case of $\chi_1^+ \chi_1^- \rightarrow X_A X_B \rightarrow \chi_1^+ \chi_1^-$ rates where several two-particle final states $X_A X_B$ are accessible the inclusive result is also given.

can be arranged into three charge-sectors: neutral, positive and double positive charged. The results for the corresponding (double) negative charged reactions are identical to the results for (double) positive charged processes. We collect our results for the factors $c(^{2s+1}L_J)$ in Tables 6.3–6.4.

In case of inclusive leading-order 1S_0 and 3S_1 (co-) annihilations we find agreement between the results of Tables 6.3–6.4 and the corresponding expressions given in [20] for the same scenario. In addition, we reproduce the leading-order 1S_0 wave annihilation rates into the exclusive final states $W^+ W^-$, ZZ , $Z\gamma$ and $\gamma\gamma$ given by the same authors in [19], apart from the $W^+ W^-$ off-diagonal rates, where our findings are a factor of 2 larger. We emphasise once again, that the results for the P - and $\mathcal{O}(v_{\text{rel}}^2)$ S -wave Wilson coefficients are new.

$\chi_1^0 \chi_1^+ \rightarrow \chi_1^0 \chi_1^+$ reactions						
physical final state $X_A X_B$	$c(^1S_0)$	$c(^3S_1)$	$c(^1P_1)$	$c(^3P_J)$	$c(^1S_0^{(p^2)})$	$c(^3S_1^{(p^2)})$
$W^+ Z$	$\frac{1}{2} c_W^2$	$\frac{1}{48}$	$\frac{2}{3} c_W^2$	$\frac{14}{3} c_W^2$	$-\frac{8}{3} c_W^2$	$-\frac{1}{9}$
$W^+ \gamma$	$\frac{1}{2} s_W^2$	0	$\frac{2}{3} s_W^2$	$\frac{14}{3} s_W^2$	$-\frac{8}{3} s_W^2$	0
$W^+ h^0$	0	$\frac{1}{48}$	0	0	0	$-\frac{1}{9}$
$u \bar{d}$	0	$\frac{1}{4}$	0	0	0	$-\frac{4}{3}$
νl^+	0	$\frac{1}{12}$	0	0	0	$-\frac{4}{9}$
$\sum X_A X_B$	$\frac{1}{2}$	$\frac{25}{24}$	$\frac{2}{3}$	$\frac{14}{3}$	$-\frac{8}{3}$	$-\frac{50}{9}$

$\chi_1^+ \chi_1^+ \rightarrow \chi_1^+ \chi_1^+$ reactions						
physical final state $X_A X_B$	$c(^1S_0)$	$c(^3S_1)$	$c(^1P_1)$	$c(^3P_J)$	$c(^1S_0^{(p^2)})$	$c(^3S_1^{(p^2)})$
$W^+ W^+$	1	0	0	$\frac{28}{3}$	$-\frac{16}{3}$	0

Table 6.4: $c(^{2s+1}L_J)$ expressions associated with the pure-wino NRMSSM Wilson coefficients in exclusive single charged $\chi_1^0 \chi_1^+ \rightarrow X_A X_B \rightarrow \chi_1^0 \chi_1^+$ reactions (upper table) and in double charged $\chi_1^+ \chi_1^+ \rightarrow X_A X_B \rightarrow \chi_1^+ \chi_1^+$ processes (lower table). The last line in the upper table is the corresponding inclusive result.

Let us add a further note on an analytic comparison of our results with known expressions in the literature, which refers to exclusive $\chi_{e_1}^0 \chi_{e_1}^0$ tree-level annihilation rates: in [96], the authors have performed a calculation of the neutralino relic abundance in minimal supergravity models. In the appendix, they give a complete summary of all partial-wave separated tree-level helicity amplitudes in $\chi_1^0 \chi_1^0 \rightarrow X_A X_B$ pair annihilations. These comprehensive results for tree-level neutralino LSP pair-annihilation rates are also referenced and (partly) quoted in the (SUSY) particle dark matter reviews [3] and [4], and easily extend to $\chi_{e_1}^0 \chi_{e_1}^0 \rightarrow X_A X_B$ annihilations. Hence, these results allow for an explicit analytic check of our expressions for the different partial-wave contributions to a neutralino $\chi_{e_1}^0 \chi_{e_1}^0 \rightarrow X_A X_B$ annihilation cross section. The partial-wave coefficients that can be cross-checked in that way correspond to 1S_0 -, 3P_0 -, 3P_1 - and 3P_2 -wave $\chi_{e_1}^0 \chi_{e_1}^0 \rightarrow X_A X_B$ annihilation reactions, and the leading-order and next-to-next-to-leading order 1S_0 -wave contributions can be compared separately. Since the results in [96] cover only the case of $\chi_1^0 \chi_1^0 \rightarrow X_A X_B$ reactions, we cannot cross-check our results for 3S_1 and 1P_1 partial wave reactions, which are absent in identical particle pair-annihilations. Our expres-

sions for the partial-wave separated $\chi_{e_1}^0 \chi_{e_1}^0 \rightarrow X_A X_B$ annihilation cross sections into all possible SM and Higgs final states, obtained from (6.22), agree with the corresponding terms derived from the helicity amplitudes in [96]¹². Let us finally note that our results for annihilations into a pair of fermions include the case of flavour-off-diagonal sfermion mixing as well, which is covered in [3] and [4], but was not yet included in [96], wherein only flavour-diagonal right-left sfermion mixing was taken into account, although it is straightforward to extend these results to the general flavour-off-diagonal case.

¹²The only minor discrepancies that we find are related to P -wave contributions: our results for 3P_1 -wave $\chi_{e_1}^0 \chi_{e_1}^0 \rightarrow H^+ H^-$ annihilations correspond to a factor 2 instead of a factor 4 in the second term of Eq. (A27b) in [96]. In the case of 3P_0 -wave $\chi_{e_1}^0 \chi_{e_1}^0 \rightarrow f \bar{f}$ reactions, our results correspond to a factor $\sqrt{2/3}$ instead of a factor $\sqrt{6}$ in the second term in the first line of Eq. (A29b) in [96].

Chapter 7

Long-range potential interactions

The instantaneous but spatially non-local long-range potential interactions that eventually cause the Sommerfeld enhancement of $\chi\chi$ pair-annihilation cross sections in the non-relativistic regime are encoded in the part \mathcal{L}_{pot} of the effective field theory Lagrangian $\mathcal{L}^{\text{NRMSSM}}$ introduced in Sec. 5.1. In (5.3) we have already given the generic form of the contributions to \mathcal{L}_{pot} . Here we explicitly determine the coefficients of the four-fermion operators in \mathcal{L}_{pot} at leading order in the non-relativistic expansion, which are given by Yukawa- and Coulomb-potentials associated with electroweak gauge or Higgs boson mediator particles. The corresponding matching calculation that provides explicit analytical expressions for the potentials in terms of MSSM parameters and couplings is the content of Sec. 7.1, where we use the example of potential Z -boson exchange to illustrate the procedure. Explicit expressions that allow to build all leading-order NRMSSM potentials are collected in Appendix B. In Sec. 7.2 we subsequently discuss the representation of potential interactions as well as hard annihilation reactions in the NRMSSM in terms of corresponding potential and annihilation matrices. This requires the definition of a suitable basis of NRMSSM two-particles states $(\chi\chi)_{I=1,\dots,N}$. The two possible choices, one basis which contains and counts as different the states $\chi_{e_1}\chi_{e_2}$ and $\chi_{e_2}\chi_{e_1}$ with non-identical particles χ_{e_a} and χ_{e_b} , the other where the redundant states $\chi_{e_2}\chi_{e_1}$ are absent, are discussed in Sec. 7.2.1. To complete the presentation of results related to the pure-wino NRMSSM in Sec. 6.3 we finally provide in Sec. 7.2.2 explicit analytic expressions for the potential and annihilation matrices in that scenario, using both the basis with and without redundant $\chi\chi$ states.

7.1 NRMSSM potentials: Matching calculation

In Sec. 2.1 we have discussed ladder diagrams in non-relativistic $\chi\chi \rightarrow \chi\chi$ scattering with light mediator exchange in order to understand the origin of the Sommerfeld enhancement effect starting from amplitudes in the full theory. The enhancement effect could be attributed to particularly large contributions to the individual loop integrals in the ladder diagram that arise in the region where the loop momenta have potential

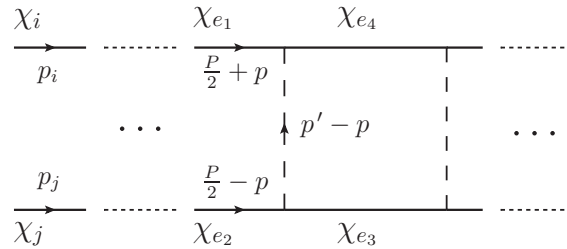


Figure 7.1: Box subgraph of a characteristic diagram with multiple ladder-like exchanges of vector and Higgs bosons among intermediate $\chi\chi$ states. Arrows in this picture indicate the direction of the labelled momenta.

scaling behaviour, see (2.1).¹ Before we enter the actual matching calculation let us first slightly generalise here the discussion of Sec. 2.1 to include the case of potential scattering reactions $\chi_{e_1}\chi_{e_2} \rightarrow \chi_{e_4}\chi_{e_3}$ of two-particle states $\chi_{e_1}\chi_{e_2}$ and $\chi_{e_4}\chi_{e_3}$ that exhibit small mass differences. To this end consider Fig. 7.1 that generalises the example in Sec. 2.1 (Fig. 2.1) to the case of several nearly mass degenerate $\chi_{e_a}\chi_{e_b}$ states. We fix conventions such that in the centre-of-mass system of the initially incoming $\chi_i\chi_j$ pair with individual momenta p_i and p_j and total momentum $P = p_i + p_j = (\sqrt{s}, \vec{0})$ the loop momentum p' that is related to the box with fermions χ_{e_4} and χ_{e_3} is the relative momentum of the $\chi_{e_4}\chi_{e_3}$ pair, $p' = (p_4 - p_3)/2$. This implies that the momentum of the exchanged boson in the $\chi_{e_1}\chi_{e_2} \rightarrow \chi_{e_4}\chi_{e_3}$ scattering reaction is given by the difference of the relative momentum p' of the $\chi_{e_4}\chi_{e_3}$ and the relative momentum p of the $\chi_{e_1}\chi_{e_2}$ pair. For the loop momenta defined in this way the scaling rules in (2.1) apply and the contributions to the loop integrals from potential momenta give rise to enhancements as discussed in Sec. 2.1. In particular we have the following scaling of the 0-component of the momentum p' in the potential region, $p'^0 \sim \vec{p}'^2/m_{\text{LSP}} \ll m_{\text{LSP}}$ and similar for p . At leading order in the expansion of the boson propagator $1/((p' - p)^2 - m_\phi^2)$ in the potential region we therefore obtain the expression $-1/((\vec{p}' - \vec{p})^2 + m_\phi^2)$ with m_ϕ the mass of the exchanged boson. It is this energy-independent propagator which gives rise to the instantaneous but spatially non-local potential interactions. The expression in particular agrees with the corresponding term derived in Sec. 2.1. The important additional feature with respect to the previous discussion is that here the term $(p'^0 - p^0)^2$ that has been dropped at leading order in the potential region expansion of the gauge boson propagator involves contributions proportional to the mass differences squared, $(m_4 - m_1)^2$ or $(m_3 - m_2)^2$. The latter terms are consistently neglected, as mass differences between the NRMSSM states are assumed to be of order $\vec{p}_{ij}^2/m_{\text{LSP}} \sim \mathcal{O}(m_{\text{LSP}}v^2)$ at most, where $p_{ij} = (p_i - p_j)/2$ denotes the incoming $\chi_i\chi_j$ state's relative momentum.

¹Let us recall from Sec. 2.1 that the classification of the loop momentum to be hard, soft, potential or ultra-soft requires a certain canonical routing of the loop momenta in the ladder diagrams, which we use in Fig. 2.1 of Sec. 2.1 and, as well, in Fig. 7.1 of this section.

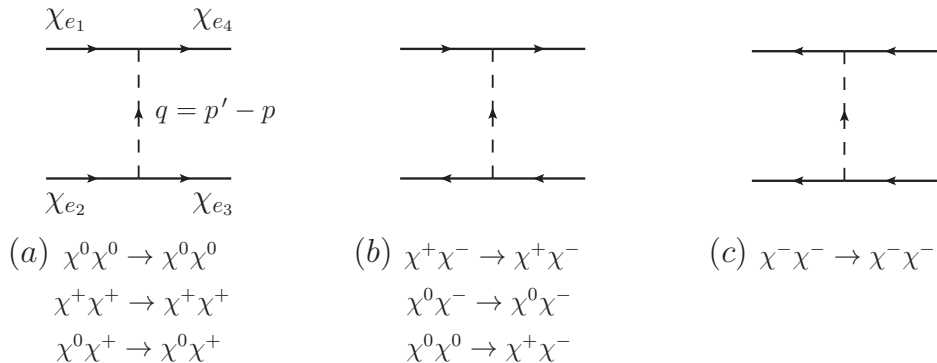


Figure 7.2: The three different tree-level diagrams with t -channel boson exchange that generate the leading-order potential among non-relativistic neutralinos and charginos. According to the arrows in the neutralino/chargino lines that indicate the fermion flow, each diagram contributes only to the scattering processes specified below.

After this generic discussion regarding the form of the propagator of the exchanged potential boson we will now determine the terms in the effective theory Lagrangian that encode the corresponding potential interaction in $\chi_{e_1}\chi_{e_2} \rightarrow \chi_{e_4}\chi_{e_3}$ scattering reactions of NRMSSM neutralino and chargino states.

Similar to the procedure for hard annihilation reactions in Sec. 6.1 we determine the coefficients encoding potential interactions in the NRMSSM by means of a matching calculation of corresponding EFT and MSSM amplitudes. As we are interested in the determination of leading-order potential interactions in the EFT, we have to consider tree-level $\chi_{e_1}\chi_{e_2} \rightarrow \chi_{e_4}\chi_{e_3}$ on-shell scattering amplitudes with gauge boson or Higgs particle exchange in the MSSM, which have to be expanded to leading order in non-relativistic momenta and mass differences, according to the non-relativistic expansion introduced in Sec. 6.1.2. In the following we use the example of Z -boson exchange in $\chi_{e_1}\chi_{e_2} \rightarrow \chi_{e_4}\chi_{e_3}$ tree-level scattering to illustrate the relevant steps in the matching calculation. Results for all possible mediator particles that can be exchanged in the MSSM, comprising the electroweak gauge bosons W^\pm , Z and the photon as well as the Higgs particles – as long as the latter are sufficiently lighter than the NRMSSM neutralino and chargino states (see the discussion in Sec. 2.1) – can be found in Appendix B. Fig. 7.2 comprises the three tree-level diagrams with different fermion flow that generically have to be considered in the matching calculation. The vector (v) or axial-vector (a) interaction vertex of two neutralinos or charginos with the Z -boson that is relevant in our sample calculation of the Z -boson exchange potential can be generically written as

$$g_2 \bar{\chi}_{e_i} [v_{ij}\gamma^\mu + a_{ij}\gamma^\mu\gamma_5] \chi_{e_j} Z_\mu, \quad (7.1)$$

where the two fields $\bar{\chi}_{e_i}\chi_{e_j}$ are either given by $\bar{\chi}_{e_i}^0\chi_{e_j}^0$ or $\bar{\chi}_{e_i}^+\chi_{e_j}^+$. The $\chi\chi Z$ -interaction in the MSSM arises also in case of the hard $\chi_{e_i}\chi_{e_j} \rightarrow X_A X_B$ annihilation reactions discussed

in Chap. 6 and explicit expressions for the vertex factors v_{ij} and a_{ij} are provided in Appendix A.1.2.²

As regards the determination of the leading-order Z -exchange potential we start from the on-shell scattering amplitude in Fig. 7.2(a) and expand the full-theory amplitude in the small relative momenta $\vec{p}, \vec{p}' \sim m_{\text{LSP}} v_{\text{rel}} \sim M_Z$ as well as in $p^0, p'^0 \sim m_{\text{LSP}} v_{\text{rel}}^2$, keeping only the leading-order terms. This implies an expansion of the Dirac bilinears $\bar{u}(p_4)\Gamma u(p_1)\bar{u}(p_3)\tilde{\Gamma}u(p_2)$ associated with the amplitude, where Γ and $\tilde{\Gamma}$ stand for a certain combination of the structures $1_{4\times 4}, \gamma_\mu, \gamma_5, \not{q}$ with $q = p_4 - p_1 = p_2 - p_3$, as well as a corresponding expansion of the Z -boson propagator

$$\frac{-i}{q^2 - M_Z^2} \left(g_{\mu\nu} - \frac{q_\mu q_\nu}{M_Z^2} \right) + \frac{q_\mu q_\nu}{M_Z^2} \frac{-i}{q^2 - \xi M_Z^2}, \quad (7.2)$$

here defined in R_ξ -gauge. At leading order the non-relativistic expansion of the former product of Dirac bilinears is equivalent to the following replacements in the full-theory amplitude:

$$\begin{aligned} \gamma^\mu \otimes \gamma_\mu &\rightarrow \mathbf{1} \otimes \mathbf{1}, \quad \gamma^\mu \gamma_5 \otimes \gamma_\mu \gamma_5 \rightarrow -\sigma^i \otimes \sigma^i, \\ \gamma^\mu \gamma_5 \otimes \gamma_\mu, \quad \gamma^\mu \otimes \gamma_\mu \gamma_5 &\rightarrow 0, \\ \not{q} \otimes \not{q} &\rightarrow -(m_{e_4} - m_{e_1})(m_{e_3} - m_{e_2}) \mathbf{1} \otimes \mathbf{1}, \\ \not{q} \otimes \not{q} \gamma_5, \quad \not{q} \gamma_5 \otimes \not{q}, \quad \not{q} \gamma_5 \otimes \not{q} \gamma_5 &\rightarrow 0. \end{aligned} \quad (7.3)$$

While the expressions on the left-hand side in these replacement rules are understood to act on the four-component spinors associated with the on-shell fields at the upper and lower interaction vertex in Fig. 7.2(a), the right-hand side terms should be understood as matrices acting on the two-component Pauli spinors of the corresponding non-relativistic neutralino or chargino fields. Accordingly, the latter spin operators written in component notation read $\sigma^i \otimes \sigma^i \equiv \sigma_{\alpha_4 \alpha_1}^i \sigma_{\alpha_3 \alpha_2}^i$ and $\mathbf{1} \otimes \mathbf{1} \equiv \delta_{\alpha_4 \alpha_1} \delta_{\alpha_3 \alpha_2}$. Note that as already remarked in Sec. 6.1, the matching procedure implies the use of the non-relativistic normalisation $\bar{u}(p_{e_a})u(p_{e_a}) = 1$ of the four-component spinors. Finally let us point out that the relation in the third line in (7.3) is obtained using the equation of motion for the spinors. The non-relativistic scaling of the corresponding term is discussed below. Using (7.3) the leading-order term in the non-relativistic expansion of amplitude Fig. 7.2(a) with Z -boson exchange is given by

$$\begin{aligned} (\text{Fig.3a})^Z &= \frac{-ig_2^2}{\vec{q}^2 + M_Z^2} \left[\left(1 + \frac{\delta m_{e_4 e_1} \delta m_{e_3 e_2}}{M_Z^2} \right) v_{e_4 e_1}^Z v_{e_3 e_2}^Z \mathbf{1} \otimes \mathbf{1} - a_{e_4 e_1}^Z a_{e_3 e_2}^Z \sigma^i \otimes \sigma^i \right] \\ &+ \frac{ig_2^2}{\vec{q}^2 + \xi M_Z^2} \frac{\delta m_{e_4 e_1} \delta m_{e_3 e_2}}{M_Z^2} v_{e_4 e_1}^Z v_{e_3 e_2}^Z \mathbf{1} \otimes \mathbf{1}. \end{aligned} \quad (7.4)$$

²Similarly, the vertex factors related to $\chi\chi W^\pm$ and $\chi\chi\gamma$ interactions as well as the scalar (s) and pseudo-scalar (p) vertex factors associated with $\chi\chi$ -Higgs three-point interactions can be found in this appendix. All such interactions can arise in potential $\chi_{e_1}\chi_{e_2} \rightarrow \chi_{e_4}\chi_{e_3}$ tree-level scattering reactions and the corresponding vertex factors enter the explicit expressions for the respective potentials from gauge boson (Z, W^\pm, γ) or Higgs particle (h^0, H^0, A^0, H^\pm) exchange collected in Appendix B.

For simplicity this expression refers to the case of $\chi^0\chi^0 \rightarrow \chi^0\chi^0$ or $\chi^+\chi^+ \rightarrow \chi^+\chi^+$ scattering reactions where the type of (axial-)vector couplings at both the upper and lower vertices in Fig. 7.2(a) is the same, namely either related to $\chi^0\chi^0 Z$ or to $\chi^+\chi^- Z$ three-point interactions. The extension to $\chi^0\chi^+ \rightarrow \chi^0\chi^+$ processes where the vector and axial-vector couplings related to both the $\chi^0\chi^0 Z$ and $\chi^+\chi^- Z$ vertex arise is straightforward.

Before we comment on the expression in the first line in (7.4) that involves the product of mass differences, $\delta m_{e_4 e_1} \delta m_{e_3 e_2}$, let us first discuss the term in the second line. This term arises from the ξ -dependent term in the Z -boson propagator in (7.2). Due to gauge invariance it has to cancel against the contribution from Goldstone boson $A_2^0 \equiv G^0$ exchange, where the Goldstone boson mass is given by $m_{G^0} = \xi M_Z^2$. Such cancellation takes place as certain relations among the vector and scalar couplings of the neutralinos and charginos hold within the MSSM: the leading-order contribution in the non-relativistic expansion of the amplitude Fig. 7.2(a) with scalar boson ϕ exchange reads

$$(\text{Fig.3a})^\phi = \frac{ig_2^2}{\vec{q}^2 + m_\phi^2} s_{e_4 e_1}^\phi s_{e_3 e_2}^\phi \mathbf{1} \otimes \mathbf{1} . \quad (7.5)$$

Pseudo-scalar interactions do not survive in (7.5) because at leading order in the non-relativistic expansion the replacements $\mathbf{1} \otimes \gamma_5, \gamma_5 \otimes \mathbf{1}, \gamma_5 \otimes \gamma_5 \rightarrow 0$, relevant in the case of amplitudes with scalar particle exchange, complement among others the replacement rules in (7.3). For a cancellation of the ξ -dependent terms in (7.4) and (7.5) the condition

$$\frac{\delta m_{e_4 e_1} \delta m_{e_3 e_2}}{M_Z^2} v_{e_4 e_1}^Z v_{e_3 e_2}^Z + s_{e_4 e_1}^{G^0} s_{e_3 e_2}^{G^0} = 0 \quad (7.6)$$

must hold, implying that the relations $v_{ij}^Z (m_i - m_j)/M_Z = \pm i s_{ij}^{G^0}$ must be fulfilled. The latter relations can be proven using the explicit expressions of the couplings v^Z and s^{G^0} in terms of mixing matrices and couplings given in Appendix A.1.2, as well as the diagonalisation properties of the mixing matrices. Consequently we can drop the ξ -dependent contributions in (7.4) together with the Goldstone boson G^0 -exchange contributions (7.5). Similar cancellation take, for instance, place in case of potential $\chi_{e_1} \chi_{e_2} \rightarrow \chi_{e_4} \chi_{e_3}$ scattering with W^{+-} and G^{\pm} -exchange, such that we can eventually consider only ξ -independent contributions to the potential interactions that are related to the exchange of physical states, leaving out the case of potential Goldstone bosons in the diagrams of Fig. 7.2.

As regards the $\delta m_{e_4 e_1} \delta m_{e_3 e_2}$ proportional term in the first line of (7.4) – which is related to expressions involving $\not{q} \otimes \not{q}$ in the unexpanded full-theory amplitude – it typically yields a very small contribution, since the effective theory contains only those species that give rise to mass differences $\delta m \sim \mathcal{O}(m_{\text{LSP}} v_{\text{rel}}^2)$. Even for a spectrum with heavy χ_1^0 where $m_{\text{LSP}} v_{\text{rel}}^2 \gg M_Z$ is possible for non-relativistic NRMSSM states, the $\delta m_{e_4 e_1} \delta m_{e_3 e_2}$ proportional term gives $\mathcal{O}(1)$ contributions at most due to suppressed vector couplings. This can be seen in the decoupling limit $m_{\text{LSP}} \rightarrow \infty$. As long as the mass difference $\delta m_{e_a e_b}$ refers to particles χ_{e_a}, χ_{e_b} within the same electroweak multiplet it scales

as $\delta m_{e_a e_b} \sim M_{\text{EW}}^2/m_{\text{LSP}}$, such that the mass difference terms in (7.4) are suppressed as $\delta m_{e_a e_b}/M_Z \sim M_{\text{EW}}/m_{\text{LSP}}$. If to the contrary the particles χ_{e_a}, χ_{e_b} belong to different multiplets, the terms $\delta m_{e_a e_b}/M_Z$ can be large but are multiplied by suppressed couplings $v_{e_a e_b}^Z \sim M_{\text{EW}}/\delta m_{e_a e_b}$ following (7.6). Finally let us note that the axial-vector couplings go to zero in the decoupling limit such that the gauge-independent, off-diagonal terms in square brackets in the first line in (7.4) are in this case given by the pseudo Goldstone boson couplings $-s_{e_4 e_1}^{G^0} s_{e_3 e_2}^{G^0}$.

Instead of performing the same non-relativistic expansion again in order to obtain the leading-order terms for amplitudes (b) and (c) with Z -boson or neutral scalar ϕ exchange in Fig. 7.2 we can derive them directly from the corresponding expressions for amplitude (a) in (7.4) and (7.5). Only certain labels on the vertex factors as well as signs in front of these factors have to be interchanged, where the corresponding replacement rules can be obtained by a simple adaption of the rules 1. and 2. given in Appendix A.1.2: If the fermion flow on a line of diagram (b) or (c) is reversed with respect to amplitude (a) we need to interchange the labels on the corresponding vertex factors (for instance, $X_{e_3 e_2} \rightarrow X_{e_2 e_3}$ to go from (a) to (b)) and change the sign of the corresponding vector coupling. In this way we obtain

$$\begin{aligned}
(\text{Fig.3b})^Z &= \frac{ig_2^2}{\vec{q}^2 + M_Z^2} \left[\left(1 + \frac{\delta m_{e_4 e_1} \delta m_{e_3 e_2}}{M_Z^2}\right) v_{e_4 e_1}^Z v_{e_2 e_3}^Z \mathbf{1} \otimes \mathbf{1} + a_{e_4 e_1}^Z a_{e_2 e_3}^Z \sigma^i \otimes \sigma^i \right] \\
&\quad - \frac{ig_2^2}{\vec{q}^2 + \xi M_Z^2} \frac{\delta m_{e_4 e_1} \delta m_{e_3 e_2}}{M_Z^2} v_{e_4 e_1}^Z v_{e_2 e_3}^Z \mathbf{1} \otimes \mathbf{1} , \\
(\text{Fig.3b})^\phi &= \frac{ig_2^2}{\vec{q}^2 + m_\phi^2} s_{e_4 e_1}^\phi s_{e_2 e_3}^\phi \mathbf{1} \otimes \mathbf{1} , \tag{7.7}
\end{aligned}$$

as well as

$$\begin{aligned}
(\text{Fig.3c})^Z &= \frac{-ig_2^2}{\vec{q}^2 + M_Z^2} \left[\left(1 + \frac{\delta m_{e_4 e_1} \delta m_{e_3 e_2}}{M_Z^2}\right) v_{e_1 e_4}^Z v_{e_2 e_3}^Z \mathbf{1} \otimes \mathbf{1} - a_{e_1 e_4}^Z a_{e_2 e_3}^Z \sigma^i \otimes \sigma^i \right] \\
&\quad + \frac{ig_2^2}{\vec{q}^2 + \xi M_Z^2} \frac{\delta m_{e_4 e_1} \delta m_{e_3 e_2}}{M_Z^2} v_{e_1 e_4}^Z v_{e_2 e_3}^Z \mathbf{1} \otimes \mathbf{1} , \\
(\text{Fig.3c})^\phi &= \frac{ig_2^2}{\vec{q}^2 + m_\phi^2} s_{e_1 e_4}^\phi s_{e_2 e_3}^\phi \mathbf{1} \otimes \mathbf{1} . \tag{7.8}
\end{aligned}$$

Similar expressions for the leading-order contributions to potential $\chi_{e_1} \chi_{e_2} \rightarrow \chi_{e_4} \chi_{e_3}$ scattering processes generated by photon exchange can be obtained from the above Z -boson exchange case by replacing the corresponding vector couplings ($v^Z \rightarrow v^\gamma$), setting the axial-vector couplings as well as the force carrier mass to zero and keeping only the $g_{\mu\nu}$ dependent part of the propagator in (7.2). The expressions related to pseudo-Goldstone boson G^0 exchange in (7.5, 7.7) and (7.8) can generically be applied to neutral Higgs boson (h^0, H^0, A^0) exchange by appropriate replacements of the coupling factors and the boson mass. The case of W^\pm -boson and charged scalar boson (H^\pm, G^\pm) exchange arises

in $\chi^0\chi^0 \rightarrow \chi^\pm\chi^\mp$, $\chi^\pm\chi^\mp \rightarrow \chi^0\chi^0$ and $\chi^0\chi^\pm \rightarrow \chi^\pm\chi^0$ processes. Note that when applying the results in (7.4, 7.5, 7.7, 7.8) to these cases we have – apart from the replacements of masses – to hermitian conjugate the coupling matrices at vertices involving either an initial χ^+ or a final χ^0 . This prescription follows from the fact that we provide the vertex factors for incoming χ_j^0 and outgoing χ_i^+ in the $\chi^0\chi^\pm W^\pm$ and $\chi^0\chi^\pm H_m^\pm$ vertex factors in Appendix A.1.2; our notation therein is such that the first index in the corresponding vector (scalar) and axial-vector (pseudo-scalar) coupling is related to the outgoing χ_i^+ , while the second index refers to the incoming χ_j^0 , see Fig. A.3.

The results provided so far in (7.4, 7.5) as well as in (7.7) and (7.8) refer to the leading-order potentials in momentum-space. The Schrödinger equation that takes into account the resummation of potential gauge and Higgs boson exchange in the ladder diagrams such as Fig. 7.1 (or Fig. 2.1(a) of Sec. 2.1) will however be written in coordinate-space, see Chap. 2 and Chap 8. The corresponding coordinate-space potentials are obtained from the momentum-space expressions above by Fourier transformation

$$V_{\{e_1e_2\}\{e_4e_3\}}^{\chi\chi\rightarrow\chi\chi}(r) = \int \frac{d^3\vec{q}}{(2\pi)^3} e^{i\vec{q}\cdot\vec{x}} i T_{e_1e_2e_4e_3}^{\chi\chi\rightarrow\chi\chi}(\vec{q}^2), \quad (7.9)$$

where $T_{e_1e_2e_4e_3}^{\chi\chi\rightarrow\chi\chi}$ denotes the momentum-space amplitude as given in equations (7.4, 7.5, 7.7, 7.8) and $r \equiv |\vec{x}|$. From the identity

$$\int \frac{d^3\vec{q}}{(2\pi)^3} e^{i\vec{q}\cdot\vec{x}} \frac{1}{\vec{q}^2 + m^2} = \frac{e^{-mr}}{4\pi r}, \quad (7.10)$$

we obtain the well-known Yukawa-type potentials for amplitudes that involve the exchange of a massive mediator with mass m . In case of a massless force carrier, $m = 0$, (7.10) gives the Coulomb potential.³

Before presenting the final form of the leading-order coordinate-space potentials in the NRMSSM we rewrite the spin operator $\sigma^i \otimes \sigma^i$ that appears in the potentials with gauge boson exchange as

$$\sigma^i \otimes \sigma^i = 2(\vec{S}^2 - \vec{s}_1^2 - \vec{s}_2^2) = 2\vec{S}^2 - 3(\mathbf{1} \otimes \mathbf{1}), \quad (7.11)$$

where \vec{s}_1 (\vec{s}_2) denotes the spin operator acting on the particles χ_{e_4} and χ_{e_1} (χ_{e_3} and χ_{e_2}) at the upper (lower) vertices in the diagrams in Fig. 7.2. In the second equality we have replaced $\vec{s}_{1,2}^2$ by $s(s+1)(\mathbf{1} \otimes \mathbf{1}) = 3/4(\mathbf{1} \otimes \mathbf{1})$ for the neutralino and chargino species. \vec{S} denotes the total spin operator acting on the total spin of the incoming and outgoing neutralino and chargino pairs $\chi_{e_a}\chi_{e_b}$, $\vec{S} = \vec{s}_1 + \vec{s}_2 \equiv 1/2(\vec{\sigma} \otimes \mathbf{1} + \mathbf{1} \otimes \vec{\sigma})$. In the basis of eigenstates of total spin of the $\chi_{e_a}\chi_{e_b}$ pairs we can replace \vec{S}^2 by its eigenvalue $S(S+1)(\mathbf{1} \otimes \mathbf{1}) = 2S(\mathbf{1} \otimes \mathbf{1})$ for $S = 0, 1$, where in particular $\mathbf{1} \otimes \mathbf{1}$ is the identity operator. Eventually, referring to the basis of total spin we can write the leading-order coordinate-space potentials in the NRMSSM in the generic form

$$V_{\{e_1e_2\}\{e_4e_3\}}^{\chi\chi\rightarrow\chi\chi}(r) = (a_{e_1e_2e_4e_3} - (3 - 4S)b_{e_1e_2e_4e_3}) \frac{e^{-m_X r}}{r}, \quad (7.12)$$

³Let us note that the $+i\epsilon$ prescription in the gauge boson propagators of the full theory provides the necessary regularisation for the $m = 0$ case in (7.10).

for exchange of a gauge boson X with mass m_X among the incoming and outgoing pairs $\chi_{e_1}\chi_{e_2}$ and $\chi_{e_4}\chi_{e_3}$. The coefficient $b_{e_1e_2e_4e_3}$ is solely built from a product of two axial-vector couplings as can be seen from the terms involving $\sigma^i \otimes \sigma^i$ in the momentum-space potentials in (7.4, 7.7, 7.8), together with the relation (7.11). Consequently, $b_{e_1e_2e_4e_3}$ vanishes for the case of leading-order potentials from scalar boson and photon exchange. A spin-dependence of a generic leading-order potential (7.12) thus arises only in presence of corresponding non-vanishing axial-vector couplings. We collect explicit expressions for all leading-order NRMSSM potentials from electroweak gauge boson, photon and light Higgs exchange in Appendix B.

7.2 Matrix representation of NRMSSM potentials

Both the labels on the potentials $V_{\{e_1e_2\}\{e_4e_3\}}^{\chi\chi\rightarrow\chi\chi}(r)$ that arise as coefficients of the four-fermion operators in \mathcal{L}_{pot} as well as the labels on the Wilson coefficients $\hat{f}_{\{e_1e_2\}\{e_4e_3\}}^{\chi\chi\rightarrow\chi\chi}$ of the four-fermion operators in $\delta\mathcal{L}_{\text{ann}}$ refer to two-particle states $\chi_{e_1}\chi_{e_2}$ and $\chi_{e_4}\chi_{e_3}$. By analysis of the perturbative expansion of the $\chi_i\chi_j \rightarrow X_AX_B$ annihilation amplitude with ladder-like gauge and Higgs boson exchanges in the non-relativistic limit, we will show later in Sec. 8.2 that the amplitude can be written as a product of potentials (7.12) times non-relativistic two-particle propagators related to the corresponding intermediate $\chi_{e_a}\chi_{e_b}$ pairs, integrated over corresponding loop momenta and finally multiplied by an appropriate short-distance Wilson coefficient \hat{f} encoding the actual hard annihilation. All parts in this amplitude expression refer to $\chi_{e_a}\chi_{e_b}$ two-particle states rather than the individual χ_{e_a} and χ_{e_b} particles. The annihilation reactions including the Sommerfeld enhancement – arising due to the presence of long-range potential interactions which require a consistent resummation of all amplitudes with potential ladder exchanges – are therefore conveniently described using a basis of two-particle states. Considering such a two-particle state basis it is convenient to speak of potential matrices as well as annihilation matrices instead of their components, the potential interactions (7.12) and the absorptive parts of the Wilson coefficients \hat{f} discussed in Chap. 6: the entries of the matrices are related to a corresponding specific potential or Wilson coefficient \hat{f} referring to the $2 \rightarrow 2$ scattering reaction of two-particle basis states $\chi_{e_1}\chi_{e_2} \rightarrow \chi_{e_4}\chi_{e_3}$.

In context of the heuristic discussion of Sommerfeld enhancements and the corresponding Schrödinger equation for certain toy scenarios in Chap. 2 we started already from a two-particle state basis. In the NRMSSM we now have to construct the two-particle state basis from the individual neutralino and chargino species in the effective theory. There are two options, one where states $\chi_{e_a}\chi_{e_b}$ and $\chi_{e_b}\chi_{e_a}$ built from non-identical particles are considered as different, the other where the redundant second state is not considered. Depending on the convention chosen there are certain combinatorial factors that have to be taken into account when building from the potentials $V_{\{e_1e_2\}\{e_4e_3\}}^{\chi\chi\rightarrow\chi\chi}(r)$ and absorptive parts of Wilson coefficients $\hat{f}_{\{e_1e_2\}\{e_4e_3\}}^{\chi\chi\rightarrow\chi\chi}$ the corresponding potential and annihilation matrices. We discuss the two bases and the implications for the potential and annihilation matrices in Sec. 7.2.1. Subsequently we provide as an

example in Sec. 7.2.2 the potential and annihilation matrices in the pure-wino NRMSSM.

7.2.1 The two possibles bases of $\chi\chi$ states in the NRMSSM

In the discussion of NRMSSM two-particle states we generically have to take five different (electric) charge sectors into account, as two-particle states built from neutralino and chargino species can have electric charge $Q = 0, \pm 1, \pm 2$. In each charge sector Q we encounter a certain total number $N_{|Q|}$ of different two-particle states,⁴ which depends on the choice of the two-particle state basis. In the following we discuss two different choices for such basis, termed “method-1” and “method-2” basis, in turn.

In case of n_0 neutralino and n_+ chargino states in the NRMSSM we encounter n_0^2 neutralino pairs, $\chi^0\chi^0$, and $2n_+^2$ neutral $\chi^\pm\chi^\mp$ states, where we counted as different the states $\chi_{e_a}\chi_{e_b}$ and $\chi_{e_b}\chi_{e_a}$ for non-identical species χ_{e_a}, χ_{e_b} , that arise from interchanging the particles at the first and second position in the $\chi\chi$ state. Consequently we obtain $N_0 = n_0^2 + 2n_+^2$ neutral two-particle states. Similarly, the charge $Q = \pm 1$ sectors comprise $N_1 = 2n_0n_+$ two-particle states and in case of $Q = \pm 2$ we have $N_2 = n_+^2$. If for a given MSSM spectrum the masses of the four neutralino and the two chargino species are, for instance, so close to each other that all these species have to be taken into account in the NRMSSM, we confront $n_0 = 4$ and $n_+ = 2$. This implies that potential scattering and annihilation reactions between $N_0 = 24$ neutral two-particle states have to be considered in the $Q = 0$ sector. Correspondingly, the single and double charged sectors involve $N_1 = 16$ and $N_2 = 4$ interacting $\chi\chi$ states. Written explicitly we have to consider in this “ $n_0 = 4$ and $n_+ = 2$ ” example the $N_0 = 24$ neutral states

$$\begin{aligned} &\chi_1^0\chi_1^0, \chi_1^0\chi_2^0, \chi_1^0\chi_3^0, \chi_1^0\chi_4^0, \chi_2^0\chi_1^0, \chi_2^0\chi_2^0, \chi_2^0\chi_3^0, \chi_2^0\chi_4^0, \chi_3^0\chi_1^0, \dots, \chi_4^0\chi_4^0, \\ &\chi_1^+\chi_1^-, \chi_1^+\chi_2^-, \chi_2^+\chi_1^-, \chi_2^+\chi_2^-, \chi_1^-\chi_1^+, \chi_1^-\chi_2^+, \chi_2^-\chi_1^+, \chi_2^-\chi_2^+, \end{aligned} \quad (7.13)$$

as well as the following $N_1 = 16$ states in the two charge $Q = \pm 1$ sectors,

$$\begin{aligned} &\chi_1^0\chi_1^\pm, \chi_1^0\chi_2^\pm, \chi_2^0\chi_1^\pm, \chi_2^0\chi_2^\pm, \chi_3^0\chi_1^\pm, \chi_3^0\chi_2^\pm, \chi_4^0\chi_1^\pm, \chi_4^0\chi_2^\pm, \\ &\chi_1^\pm\chi_1^0, \chi_2^\pm\chi_1^0, \chi_1^\pm\chi_2^0, \dots, \chi_2^\pm\chi_4^0, \end{aligned} \quad (7.14)$$

and finally the $N_2 = 4$ states in the $Q = \pm 2$ charge sectors,

$$\chi_1^\pm\chi_1^\pm, \chi_1^\pm\chi_2^\pm, \chi_2^\pm\chi_1^\pm, \chi_2^\pm\chi_2^\pm. \quad (7.15)$$

The entirety of all $N_0 + 2N_1 + 2N_2 = 64$ states in (7.13 – 7.15) defines the “method-1 basis” of two-particles states in our “ $n_0 = 4$ and $n_+ = 2$ ” example. The adaption to the case of $n_0 \leq 4$ and $n_+ \leq 2$ neutralino and chargino species in the NRMSSM is straightforward. Note that the order of states in each charge sector in (7.13 – 7.15) is of course a matter of convention. By using the method-1 basis of two-particle states

⁴Note that our notation implies $|Q| = 0, 1, 2$; the total number of states in the single-positive and single-negative, $Q = \pm 1$, (double-positive and double-negative, $Q = \pm 2$) charge sector obviously agrees and is denoted by N_1 (N_2).

in the NRMSSM – that is by treating $\chi_{e_a}\chi_{e_b}$ and $\chi_{e_b}\chi_{e_a}$ for non-identical particles χ_{e_a} and χ_{e_b} as different – we can in the construction of potential and annihilation matrices directly use the expressions for potentials and Wilson coefficients as derived in Sec. 7.1 and Chap. 6: In the calculation of $\chi_i\chi_j \rightarrow X_A X_B$ annihilation amplitudes with ladder-like exchanges there are no additional combinatorial factors to be taken into account in front of potentials V or Wilson coefficients \hat{f} as long as we consider and sum over all method-1 basis states that are part of the same charge sector as the annihilating $\chi_i\chi_j$ pair.

The “method-2 basis” that we discuss next has the advantage that it contains less two-particle states than the corresponding method-1 basis. In return the potentials and annihilation matrices to be used in the calculation of $\chi_i\chi_j \rightarrow X_A X_B$ annihilation rates in the method-2 basis have to be calculated from the method 1 expressions (directly related to the potentials taken from Sec. 7.1 and Wilson coefficients from Chap. 6) by accounting for certain combinatorial factors and combinations of different method-1 matrix entries. The method-2 basis is built from all $\chi\chi$ states that differ pairwise with respect to the individual particle content. This implies that only one of the states $\chi_{e_a}\chi_{e_b}$ and $\chi_{e_b}\chi_{e_a}$ for different particle species $\chi_{e_{a,b}}$ is considered as a basis state, the other is redundant and ignored. While this prescription is still ambiguous as it is not specified which two-particle state should be dropped, we define the method-2 basis such that it contains only those neutral two-particle states $\chi_{e_a}^0\chi_{e_b}^0$ with $e_a \leq e_b$, where the individual particles $\chi_{e_{a,b}}^0$ are part of the n_0 NRMSSM neutralino species. Further all neutral states $\chi_{e_a}^+\chi_{e_b}^-$ built from the n_+ NRMSSM chargino states are part of the basis, while states $\chi_{e_b}^-\chi_{e_a}^+$ are not. In the single-charged sectors $Q = \pm 1$ we include states $\chi_{e_a}^0\chi_{e_b}^\pm$ in the method-2 basis and accordingly neglect the redundant states $\chi_{e_b}^\pm\chi_{e_a}^0$. Finally, as in case of two-neutralino states, the $\chi_{e_a}^\pm\chi_{e_b}^\pm$ pairs in the charge $Q = \pm 2$ sectors are part of the basis if $e_a \leq e_b$. With this definition we obtain $\tilde{N}_0 = n_0(n_0 + 1)/2 + n_+^2$ neutral two-particle basis states as well as $\tilde{N}_1 = n_0 n_+$ and $\tilde{N}_2 = n_+(n_+ + 1)/2$ basis states in the charge $Q = \pm 1$ and $Q = \pm 2$ sectors, respectively. The method-2 basis is then given by the entirety of $\tilde{N}_0 + \tilde{N}_1 + \tilde{N}_2$ states. In case of the example with $n_0 = 4$ and $n_+ = 2$ discussed above for method-1, we obtain the following $\tilde{N}_0 = 14$ neutral states in the method-2 basis,

$$\begin{aligned} &\chi_1^0\chi_1^0, \chi_1^0\chi_2^0, \chi_1^0\chi_3^0, \chi_1^0\chi_4^0, \chi_2^0\chi_2^0, \chi_2^0\chi_3^0, \chi_2^0\chi_4^0, \chi_3^0\chi_3^0, \chi_3^0\chi_4^0, \chi_4^0\chi_4^0, \\ &\chi_1^+\chi_1^-, \chi_1^+\chi_2^-, \chi_2^+\chi_1^-, \chi_2^+\chi_2^-, \end{aligned} \quad (7.16)$$

the following $\tilde{N}_1 = 8$ states in each of the two single charged ($Q = \pm 1$) sectors,

$$\chi_1^0\chi_1^\pm, \chi_1^0\chi_2^\pm, \chi_2^0\chi_1^\pm, \chi_2^0\chi_2^\pm, \chi_3^0\chi_1^\pm, \chi_3^0\chi_2^\pm, \chi_4^0\chi_1^\pm, \chi_4^0\chi_2^\pm, \quad (7.17)$$

and finally the $\tilde{N}_2 = 3$ double charged states in the each of the two double-charged ($Q = \pm 2$) sectors,

$$\chi_1^\pm\chi_1^\pm, \chi_1^\pm\chi_2^\pm, \chi_2^\pm\chi_2^\pm. \quad (7.18)$$

The reduction of the number of states contained in the method-2 basis with respect to the corresponding method-1 basis is more significant the larger the numbers n_0 and n_+

of neutralino and chargino states in the NRMSSM. It is in particular maximal for the case $n_0 = 4$ and $n_+ = 2$ considered above.

While, for instance, we have two potential matrix entries corresponding to the scattering reactions $\chi_{e_1}\chi_{e_2} \rightarrow \chi_{e_4}\chi_{e_3}$ and $\chi_{e_1}\chi_{e_2} \rightarrow \chi_{e_3}\chi_{e_4}$ in method-1, where the latter is the so-called ‘‘crossed’’ contribution which differs from the former for $\chi_{e_3} \neq \chi_{e_4}$, we encounter only one potential matrix entry in case of method-2, as one of the states $\chi_{e_4}\chi_{e_3}$ or $\chi_{e_4}\chi_{e_3}$ is absent in the corresponding basis. For the following discussion let us denote a state in the method-2 basis by $(\chi\chi)_{e_1e_2}$ in order to distinguish it from a method-1 basis state, which we will still write as $\chi_{e_1}\chi_{e_2}$. We obtain the potential matrix entries $V_{\{.. \}\{.. \}}^{(\chi\chi) \rightarrow (\chi\chi)}$ in the method-2 basis from the method-1 entries $V_{\{.. \}\{.. \}}^{\chi\chi \rightarrow \chi\chi}$ in the following way:

$$\begin{aligned}
e_1 \neq e_2 \text{ and } e_4 \neq e_3 : \quad & V_{\{e_1e_2\}\{e_4e_3\}}^{(\chi\chi) \rightarrow (\chi\chi)} = V_{\{e_1e_2\}\{e_4e_3\}}^{\chi\chi \rightarrow \chi\chi} + (-1)^{L+S} V_{\{e_1e_2\}\{e_3e_4\}}^{\chi\chi \rightarrow \chi\chi}, \\
e_1 \neq e_2 \text{ and } e_4 = e_3 : \quad & V_{\{e_1e_2\}\{e_4e_4\}}^{(\chi\chi) \rightarrow (\chi\chi)} = \sqrt{2} V_{\{e_1e_2\}\{e_4e_4\}}^{\chi\chi \rightarrow \chi\chi}, \\
e_1 = e_2 \text{ and } e_4 \neq e_3 : \quad & V_{\{e_1e_1\}\{e_4e_3\}}^{(\chi\chi) \rightarrow (\chi\chi)} = \sqrt{2} V_{\{e_1e_1\}\{e_4e_3\}}^{\chi\chi \rightarrow \chi\chi}, \\
e_1 = e_2 \text{ and } e_4 = e_3 : \quad & V_{\{e_1e_1\}\{e_4e_4\}}^{(\chi\chi) \rightarrow (\chi\chi)} = V_{\{e_1e_1\}\{e_4e_4\}}^{\chi\chi \rightarrow \chi\chi}.
\end{aligned} \tag{7.19}$$

Note that the labels $\{e_1e_2\}$ and $\{e_4e_3\}$ on the method-2 potential entries obviously have to refer to states $(\chi\chi)_{e_1e_2} \equiv \chi_{e_1}\chi_{e_2}$ and $(\chi\chi)_{e_4e_3} \equiv \chi_{e_4}\chi_{e_3}$ contained in the method-2 basis. The factor $(-1)^{L+S}$ in front of the method-1 potential entry associated with the crossed diagram in the first line of (7.19) arises from the product $(-1) \times (-1)^L \times (-1)^{S+1}$: the first factor (-1) is associated with Wick ordering and the exchange of $e_3 \leftrightarrow e_4$ leads to a change of sign in the relative momentum that translates into the factor $(-1)^L$ as well as to a factor $(-1)^{S+1}$ in the spin wave function. In addition to the rules in (7.19) there is a further prescription to be considered in the construction of the method-2 potential entries that is related to the fact that two identical spin-1/2 particles χ_{e_a} cannot form a two-particle state $(\chi\chi)_{e_ae_a} = \chi_{e_a}\chi_{e_a}$ with odd $L+S$, *i.e.* with quantum numbers 3S_1 and 1P_1 in the case at hand. Entries that refer to such a $(\chi\chi)_{e_ae_a}$ state in the method-2 potentials have to be set to zero. In this way we prevent that a non-zero annihilation amplitude for a forbidden partial-wave state of two-identical particles is obtained through a transition to an intermediate allowed state, such as for example $(\chi^0\chi^0)_{11} \rightarrow (\chi^+\chi^-)_{11} \rightarrow X_A X_B$, where the $\chi_1^+\chi_1^-$ pair can but the $\chi_1^0\chi_1^0$ pair cannot form a 3S_1 or 1P_1 state. In method-1 there is no such additional prescription needed as a priori certain cancellations between different contributions to a forbidden annihilation amplitude of identical particles are effective: For instance, in addition to the term $\chi_1^0\chi_1^0 \rightarrow \chi_1^+\chi_1^- \rightarrow X_A X_B$ in the above example there is a corresponding contributions from $\chi_1^0\chi_1^0 \rightarrow \chi_1^-\chi_1^+ \rightarrow X_A X_B$. The symmetry properties of the Wilson coefficients – encoding the hard $\chi_1^\pm\chi_1^\mp \rightarrow X_A X_B$ annihilations – under exchange of the particle labels, (5.9, 5.14), then guarantee the mutual compensation of the two contributions for reactions with odd $L+S$ in method-1. Contrary to the potentials in method-1, the just described prescription together with the rules in (7.19) implies that the method-2 potentials depend already at leading order in the non-relativistic expansion on the orbital angular momentum L .

Similar to the case of potential matrices let us introduce the notation $\Gamma_{\{.. \}\{.. \}}^{\chi\chi \rightarrow \chi\chi(2S+1)L_J}$

to denote an annihilation matrix entry corresponding to the method-1 two-particle state basis, while $\Gamma_{\{\dots\}\{\dots\}}^{(\chi\chi)\rightarrow(\chi\chi)}(2^{S+1}L_J)$ denotes the corresponding expression referring to the method-2 basis. In case of the method-1 basis the annihilation matrix entries are directly obtained from the absorptive parts of the Wilson coefficients \hat{f} that we presented and discussed in Chap. 6: $\Gamma_{mn}^{\chi\chi\rightarrow\chi\chi}(2^{S+1}L_J) \equiv \hat{f}_{mn}^{\chi\chi\rightarrow\chi\chi}(2^{S+1}L_J)$, where the labels m, n are compound two-particle indices $m, n \equiv \{e_a e_b\}$ and can refer to all possible $\chi_{e_a} \chi_{e_b}$ method-1 basis states. However, similar to the case of the potential matrix entries related to the method-2 basis, there are certain additional factors that have to be accounted for in the construction of the corresponding method-2 annihilation matrices. An annihilation matrix entry that refers to the absorptive part of the hard $(\chi\chi)_{e_1 e_2} \rightarrow (\chi\chi)_{e_4 e_3} \equiv (\chi\chi)_m \rightarrow (\chi\chi)_n$ (off-) diagonal forward scattering reaction of method-2 basis states in a $2^{S+1}L_J$ wave configuration is given by the product $\Gamma_{mn}^{\chi\chi\rightarrow\chi\chi}(2^{S+1}L_J) \equiv (1/\sqrt{2})^{n_{id}} \times \hat{f}_{mn}^{\chi\chi\rightarrow\chi\chi}(2^{S+1}L_J)$, with $n_{id} = 1, 2$ if the states $(\chi\chi)_{e_1 e_2}$ or/and $(\chi\chi)_{e_4 e_3}$ are built from identical particles and $n_{id} = 0$ otherwise.

7.2.2 Pure-wino NRMSSM potential & annihilation matrices

In order to provide an explicit example for the construction of the potential and annihilation matrices related to the method-1 and method-2 bases described in the preceding section, we give here the corresponding expressions for the neutral sector of the pure-wino NRMSSM introduced in Sec. 6.3.

From the results for the potentials in Appendix B we obtain the following expression for both the Spin-0 and Spin-1 potential matrices in the $Q = 0$ sector within method-1:

$$V_{Q=0}^{(1)}(r) = \begin{pmatrix} 0 & -\alpha_2 \frac{e^{-M_W r}}{r} & -\alpha_2 \frac{e^{-M_W r}}{r} \\ -\alpha_2 \frac{e^{-M_W r}}{r} & -\frac{\alpha}{r} - \alpha_2 c_W^2 \frac{e^{-M_Z r}}{r} & 0 \\ -\alpha_2 \frac{e^{-M_W r}}{r} & 0 & -\frac{\alpha}{r} - \alpha_2 c_W^2 \frac{e^{-M_Z r}}{r} \end{pmatrix}, \quad (7.20)$$

where the matrix indices ($m, n = 1, 2, 3$) correspond to the following three neutral states $\chi_1^0 \chi_1^0, \chi_1^+ \chi_1^-, \chi_1^- \chi_1^+$ contained in the method-1 pure-wino NRMSSM basis. In applications to MSSM spectra beyond the pure-wino limit we will generically encounter two different method-1 potential matrices, corresponding to the $S = 0$ and $S = 1$ case, respectively. As however axial-vector couplings vanish in the pure-wino NRMSSM and the difference between the Spin-0 and Spin-1 potentials is solely attributed to the latter (see the discussion after (7.12)), there is effectively only one leading-order pure-wino NRMSSM potential matrix, (7.20), within method-1.

According to the rules in (7.19) and the prescription given in the paragraph following these rules, the L - and S -dependent leading-order potentials in the $Q = 0$ sector within method-2 read

$$V_{Q=0, \text{even } L+S}^{(2)}(r) = \begin{pmatrix} 0 & -\sqrt{2} \alpha_2 \frac{e^{-M_W r}}{r} \\ -\sqrt{2} \alpha_2 \frac{e^{-M_W r}}{r} & -\frac{\alpha}{r} - \alpha_2 c_W^2 \frac{e^{-M_Z r}}{r} \end{pmatrix}, \quad (7.21)$$

$$V_{Q=0,\text{odd } L+S}^{(2)}(r) = \begin{pmatrix} 0 & 0 \\ 0 & -\frac{\alpha}{r} - \alpha_2 c_W^2 \frac{e^{-M_Z r}}{r} \end{pmatrix}, \quad (7.22)$$

and the matrix indices ($m, n = 1, 2$) now refer to the two neutral method-2 basis states $(\chi^0 \chi^0)_{11} = \chi_1^0 \chi_1^0$, $(\chi^+ \chi^-)_{11} = \chi_1^+ \chi_1^-$.

From the results for the absorptive parts of the Wilson coefficients in the pure-wino NRMSSM in Sec. 6.3 we immediately obtain the annihilation matrices within method-1. Let us first introduce the following 3×3 matrices

$$A_{\text{even } L+S} = \begin{pmatrix} 2 & 1 & 1 \\ 1 & \frac{3}{2} & \frac{3}{2} \\ 1 & \frac{3}{2} & \frac{3}{2} \end{pmatrix}, \quad A_{\text{odd } L+S} = \begin{pmatrix} 0 & 0 & 0 \\ 0 & 1 & -1 \\ 0 & -1 & 1 \end{pmatrix}. \quad (7.23)$$

Referring to the same ordering of basis states as for the corresponding method-1 potential matrix (7.20), the leading-order S -wave annihilation matrices are then given by

$$\Gamma^{(1)}[\hat{f}({}^1S_0)] = \frac{\pi\alpha_2^2}{m_\chi^2} A_{\text{even } L+S}, \quad \Gamma^{(1)}[\hat{f}({}^3S_1)] = \frac{25}{24} \frac{\pi\alpha_2^2}{m_\chi^2} A_{\text{odd } L+S}. \quad (7.24)$$

The respective $\mathcal{O}(v_{\text{rel}}^2)$ annihilation matrices read

$$\begin{aligned} \Gamma^{(1)}\left[\frac{\hat{f}({}^1P_1)}{M^2}\right] &= \frac{1}{6} \frac{\pi\alpha_2^2}{m_\chi^4} A_{\text{odd } L+S}, & \Gamma^{(1)}\left[\frac{\hat{f}({}^3P_J)}{M^2}\right] &= \frac{7}{3} \frac{\pi\alpha_2^2}{m_\chi^4} A_{\text{even } L+S}, \\ \Gamma^{(1)}\left[\frac{\hat{f}({}^1S_0^{(p^2)})}{M^2}\right] &= -\frac{4}{3} \frac{\pi\alpha_2^2}{m_\chi^4} A_{\text{even } L+S}, & \Gamma^{(1)}\left[\frac{\hat{f}({}^3S_1^{(p^2)})}{M^2}\right] &= -\frac{25}{18} \frac{\pi\alpha_2^2}{m_\chi^4} A_{\text{odd } L+S}. \end{aligned} \quad (7.25)$$

It is nicely seen from (7.23, 7.24, 7.25) that entries in the method-1 annihilation matrices, which differ only in the replacement $\chi_1^+ \chi_1^- \leftrightarrow \chi_1^- \chi_1^+$ as incoming or outgoing state are equal up to a factor $(-1)^{L+S}$, which is related to the symmetry properties of the Wilson coefficients under exchange of labels, see (5.9) and (5.14).

By applying the rules for the construction of the method-2 annihilation matrices from the corresponding method-1 expressions as set out in Sec. 7.2.1 we first deduce the following 2×2 matrices \tilde{A} from the 3×3 matrices A in (7.23),

$$\tilde{A}_{\text{even } L+S} = \begin{pmatrix} 1 & \frac{1}{\sqrt{2}} \\ \frac{1}{\sqrt{2}} & \frac{3}{2} \end{pmatrix}, \quad \tilde{A}_{\text{odd } L+S} = \begin{pmatrix} 0 & 0 \\ 0 & 1 \end{pmatrix}. \quad (7.26)$$

According to the same ordering of basis states as used in the presentation of the corresponding potential matrices in (7.21, 7.22), we then obtain the following method-2 annihilation matrices related to leading-order S -wave processes

$$\Gamma^{(2)}[\hat{f}({}^1S_0)] = \frac{\pi\alpha_2^2}{m_\chi^2} \tilde{A}_{\text{even } L+S}, \quad \Gamma^{(2)}[\hat{f}({}^3S_1)] = \frac{25}{24} \frac{\pi\alpha_2^2}{m_\chi^2} \tilde{A}_{\text{odd } L+S}. \quad (7.27)$$

The latter results together with (7.21, 7.22) have been presented before in [19, 20]. The expressions (7.27) obviously follow from (7.24) by the replacements $A \rightarrow \tilde{A}$. In the same way, replacing $A \rightarrow \tilde{A}$ in (7.25), the corresponding method-2 $\mathcal{O}(v_{\text{rel}}^2)$ annihilation matrices are obtained that have not been given before in the literature.

From the results for the pure-wino NRMSSM Wilson coefficients presented in Sec. 6.3 and the generic expressions for the potential interactions given in Appendix B, the annihilation and potential matrices in the pure-wino NRMSSM within the remaining $Q = \pm 1, \pm 2$ charge sectors can be similarly obtained.

Chapter 8

Sommerfeld enhancement

In this chapter we finally come to the rigorous derivation of the non-relativistic χ^0/χ^\pm pair-annihilation cross section including Sommerfeld enhancements within the non-relativistic effective theory that we have developed in the preceding Chaps. 5 – 7. The structure of this chapter is as follows. In Sec. 8.1 we start from the annihilation cross section in the effective theory written in terms of matrix elements of the four-fermion operators in $\delta\mathcal{L}_{\text{ann}}$ and their corresponding Wilson coefficients. From this we derive a convenient form of this central expression given by a sum over products of Sommerfeld enhancement factors times the corresponding Wilson coefficients encoding the partial-wave dependent hard annihilation rates. The Sommerfeld enhancement factors themselves involve two-particle wave functions in presence of the potential interactions, subject to a certain partial-wave configuration of the incoming particle pair, as well as corresponding Wilson coefficient expressions. In the course of rewriting the cross section we thus provide a refined, rigorous definition of the Sommerfeld enhancement factors first introduced in Chap. 2.

At two points in Sec. 8.1 we make use of relations whose detailed derivation is postponed to later sections. The first point concerns the relation between the operator matrix elements and two-particle wave functions – appearing in the Sommerfeld enhancement factors – that we address in Sec. 8.2: we first establish here the connection between the pair-annihilation matrix element and the Green function associated with the annihilating non-relativistic two-particle state. Elementary scattering theory and the Lippmann-Schwinger equation subsequently provide the link to the two-particle wave functions that are solutions to a corresponding multi-state Schrödinger equation. Eventually a form of the Sommerfeld enhancement factors of use in practical calculations is derived. As all expressions related to the determination of the Sommerfeld factors and non-relativistic pair-annihilation cross sections refer to two-particle states, we can make use of the method-1 and method-2 two-particle state bases introduced in Sec. 7.2.1. In Sec. 8.3 we therefore rewrite the definition of the Sommerfeld factors in terms of quantities associated with the one or the other basis. The equivalence of results on the Sommerfeld factors derived within the two methods is shown in Appendix. C.

It is worth to stress already here that the final expression for the Sommerfeld en-

hancement factors in terms of scattering wave function solutions of a corresponding Schrödinger equation differs slightly with respect to the advanced-guess formula from Chap. 2: if the hermitian potential matrix in the Schrödinger equation is not in addition real-symmetric ($V_{ij} = V_{ji}^* \neq V_{ji}$), the scattering wave function solutions in the Sommerfeld factor formula have to be replaced by their complex conjugates with respect to the expression in Chap. 2.¹ The steps to numerically determine the Sommerfeld factors for a system of coupled scattering states $(\chi\chi)_{i=1,\dots,N}$ by solving a multi-component Schrödinger equation are however easily obtained by adaption of the steps given at the end of Sec. 2.2. It turns out, though, that this method suffers from severe numerical instabilities in the application to χ^0/χ^\pm co-annihilation processes in the general MSSM. The origin of these instabilities is discussed in Sec. 8.4 and an improved method that allows to resolve the issue is introduced.

The second missing derivation of a relation presupposed in Sec. 8.1 is presented in Sec. 8.5, which treats the relation between the matrix elements of the next-to-next-to-leading and the leading-order S -wave four-fermion operators. Eventually, Sec. 8.6 contains the description of a method that allows to perturbatively include the effects from heavier neutralino and chargino states that are not part of the NRMSSM in the last potential loop of ladder-amplitudes prior to the actual pair annihilation.

8.1 Sommerfeld-corrected annihilation rates

In Chap. 5 we have given the generic formula for the inclusive spin-averaged centre-of-mass frame $\chi_i\chi_j$ annihilation cross section in terms of matrix elements of the operators contained in $\delta\mathcal{L}_{\text{ann}}$, see (5.5). Here we start from this equation and explicitly insert the dimension-6 and dimension-8 four-fermion operators from $\delta\mathcal{L}_{\text{ann}}$ in the forward-scattering matrix element. In this way we obtain the following expression for the inclusive $\chi_i\chi_j$ annihilation cross section in the non-relativistic effective theory:

$$\begin{aligned} \sigma^{\chi_i\chi_j \rightarrow \sum X_A X_B} v_{\text{rel}} &= \left(\frac{1}{4} \sum_{s_i, s_j} \right) 2 \Im \langle \chi_i\chi_j | \delta\mathcal{L}_{\text{ann}} | \chi_i\chi_j \rangle \\ &= \frac{1}{8} \sum_{s_i, s_j} \left\{ \left(\hat{f}(^1S_0) + \frac{\delta m}{M} \hat{h}_1(^1S_0) + \frac{\delta \bar{m}}{M} \hat{h}_2(^1S_0) \right) \langle \chi_i\chi_j | \mathcal{O}(^1S_0) | \chi_i\chi_j \rangle \right. \\ &\quad + \left(\hat{f}(^3S_1) + \frac{\delta m}{M} \hat{h}_1(^3S_1) + \frac{\delta \bar{m}}{M} \hat{h}_2(^3S_1) \right) \langle \chi_i\chi_j | \mathcal{O}(^3S_1) | \chi_i\chi_j \rangle \\ &\quad \left. + \frac{\hat{g}(^1S_0)}{M^2} \langle \chi_i\chi_j | \mathcal{P}(^1S_0) | \chi_i\chi_j \rangle + \frac{\hat{g}(^3S_1)}{M^2} \langle \chi_i\chi_j | \mathcal{P}(^3S_1) | \chi_i\chi_j \rangle \right\} \end{aligned}$$

¹In the analysis of Sommerfeld enhancements in the toy scenarios of Chap. 2 we have considered real potentials, such that all results discussed in context of these toy models remain valid. In the MSSM application, though, we generically encounter potential matrices that are not real-symmetric.

$$\begin{aligned}
& + \frac{\hat{f}({}^1P_1)}{M^2} \langle \chi_i \chi_j | \mathcal{O}({}^1P_1) | \chi_i \chi_j \rangle + \frac{3 \hat{f}({}^3P_J)}{M^2} \langle \chi_i \chi_j | \mathcal{O}({}^3P_0) | \chi_i \chi_j \rangle \Big\} \\
& + \text{higher order contributions} . \tag{8.1}
\end{aligned}$$

Again we use $v_{\text{rel}} = |\vec{v}_i - \vec{v}_j|$ to denote the (modulus of the) relative velocity of the annihilating particles χ_i and χ_j in their centre-of-mass frame.² The contributions to (8.1) denoted with ‘higher order’ are related to four-fermion operators in $\delta\mathcal{L}_{\text{ann}}$ with mass dimension 9 and higher, which are suppressed with respect to the dimension-6 and 8 four-fermion operators and therefore safely neglected. The incoming and outgoing states in (8.1) are non-relativistically normalised, which implies that for the free single-particle momentum eigenstates of the NRMSSM neutralinos and charginos the normalisation $\langle \vec{p} | \vec{p}' \rangle = (2\pi)^3 \delta^{(3)}(\vec{p} - \vec{p}')$ holds. We have used a short-hand notation in (8.1), that allows a concise representation of the different contributions: we suppress the labels on the four-fermion operators and their corresponding Wilson coefficients that indicate the specific (off-) diagonal $\chi_{e_1} \chi_{e_2} \rightarrow \chi_{e_4} \chi_{e_3}$ scattering reaction to which these quantities refer. In addition the sum symbol over all such (off-) diagonal $\chi\chi \rightarrow \chi\chi$ reactions, compatible with the charge of the incoming $\chi_i \chi_j$ state, has been omitted. Written in full form the first term in (8.1) for instance reads

$$\frac{1}{8} \sum_{s_i, s_j} \sum_{\chi\chi \rightarrow \chi\chi} \hat{f}_{\{e_1 e_2\}\{e_4 e_3\}}^{\chi\chi \rightarrow \chi\chi} ({}^1S_0) \langle \chi_i \chi_j | \mathcal{O}_{\{e_4 e_3\}\{e_2 e_1\}}^{\chi\chi \rightarrow \chi\chi} ({}^1S_0) | \chi_i \chi_j \rangle . \tag{8.2}$$

In the following we will always omit the sum symbol $\sum_{\chi\chi \rightarrow \chi\chi}$ and imply summation over repeated indices e_i if those appear in an expression. Let us further recall from Sec. 5.2.2 that the quantities M , δm and $\delta \bar{m}$ that come with the dimension-8 four-fermion operators in (8.1) denote $\chi_{e_1} \chi_{e_2} \rightarrow \chi_{e_4} \chi_{e_3}$ process-specific quantities.

In order to obtain the second equality in (8.1) we used the fact that

$$\Im \left[f({}^{2S+1}L_J) \langle \chi_i \chi_j | \mathcal{O}({}^{2S+1}L_J) | \chi_i \chi_j \rangle \right] = \hat{f}({}^{2S+1}L_J) \langle \chi_i \chi_j | \mathcal{O}({}^{2S+1}L_J) | \chi_i \chi_j \rangle , \tag{8.3}$$

which follows from (6.5) and (6.6). A similar relation obviously holds for the next-to-next-to-leading order S -wave operators $\mathcal{P}({}^{2S+1}S_S)$. The forward-scattering matrix elements of the three spin $S = 1$ P -wave operators, $\langle \chi_i \chi_j | \mathcal{O}({}^3P_{J=0,1,2}) | \chi_i \chi_j \rangle$, agree apart from simple spin-weighted factors, as long as only leading-order potential interactions that do not change the spin and orbital angular momentum of the incoming $\chi_i \chi_j$ state are considered in the calculation. Since our analysis is restricted to leading-order potentials we have therefore already expressed the spin $S = 1$ P -wave contributions to the

²As already noted in context of (5.5) (see footnote 4 in Chap. 5) also here we abuse notation to make contact with the common notation used in quarkonium annihilations and write in (8.1) the matrix elements of the operators $\delta\mathcal{L}_{\text{ann}}$, $\mathcal{O}({}^{2S+1}L_J)$ and $\mathcal{P}({}^{2S+1}L_J)$ instead of the corresponding forward-scattering amplitudes. The proper way to write the relation (8.1) would involve the configuration-space integrated quantities, $\int d^4x \delta\mathcal{L}_{\text{ann}}$, $\int d^4x \mathcal{O}({}^{2S+1}L_J)$ and $\int d^4x \mathcal{P}({}^{2S+1}L_J)$ in the forward-scattering matrix elements on the right-hand side instead of the sole operators. The additional factors $(2\pi)^4 \delta^{(4)}(p_{\text{initial}} - p_{\text{final}})$ that then arise when evaluating the matrix elements should however not be included in the relation to the cross section (8.1).

annihilation cross section in (8.1) in terms of the matrix element of the operator $\mathcal{O}({}^3P_0)$ multiplied by $\hat{f}({}^3P_{\mathcal{J}})$, the appropriate spin-weighted sum of the three spin-1 P -wave Wilson coefficients introduced in (6.29).

Note that we immediately obtain the exclusive tree-level annihilation cross sections (6.22) from (8.1), when the matrix elements are evaluated for the perturbative case (neglecting long-range potential interactions contained in \mathcal{L}_{pot}) and when the Wilson coefficients are determined at $\mathcal{O}(\alpha_i^2)$. At this order infrared divergences are absent such that (8.1) applies separately for each exclusive final state $X_A X_B$. Consequently, as we have explicitly used in Chap. 6, the contributions to the Wilson coefficients \hat{f} , \hat{g} and \hat{h}_i from $\chi\chi \rightarrow X_A X_B \rightarrow \chi\chi$ reactions can be given separately and therefore allow to obtain the non-relativistic expansion of the exclusive $\chi_i\chi_j \rightarrow X_A X_B$ tree-level annihilation cross section including $\mathcal{O}(v_{\text{rel}}^2)$ contributions.

Eventually we want to rewrite (8.1) such that the non-relativistic expansion of the $\chi_i\chi_j$ pair-annihilation cross section is expressed in terms of a sum over products of Wilson coefficients – encoding the short-distance annihilations – and their corresponding partial-wave dependent Sommerfeld enhancement factors, which are related to the long-range effects. To this end we proceed in three steps. First we express the matrix elements of the operators in terms of non-relativistic wave-functions and their derivatives evaluated at the origin, a procedure well known from quarkonium physics. Subsequently we provide the definition of the Sommerfeld enhancement factors in terms of Wilson coefficients and the non-relativistic wave-functions, which refines the corresponding definition in Chap. 2. From this we finally obtain the desired expression for the $\chi_i\chi_j$ pair-annihilation cross section, that explicitly involves the Sommerfeld enhancement factors.

In the first step we start from the matrix elements of the four-fermion operators and insert the operator $|0\rangle\langle 0|$ that projects onto the NRMSSM vacuum state, the Fock space state that involves no neutralinos and charginos. For instance, the matrix element of the dimension-6 operator $\mathcal{O}({}^1S_0)$ is with this insertion written as

$$\begin{aligned} \langle \chi_i\chi_j | \mathcal{O}_{\{e_4e_3\}\{e_2e_1\}}^{XX \rightarrow XX}({}^1S_0) | \chi_i\chi_j \rangle &= \langle \chi_i\chi_j | \chi_{e_4}^\dagger \chi_{e_3}^c | 0 \rangle \langle 0 | \chi_{e_2}^{c\dagger} \chi_{e_1} | \chi_i\chi_j \rangle \\ &= \left[\langle \xi_j^{c\dagger} \xi_i \rangle \left(\psi_{e_4e_3,ij}^{(0,0)} + \psi_{e_3e_4,ij}^{(0,0)} \right) \right]^* \langle \xi_j^{c\dagger} \xi_i \rangle \left(\psi_{e_1e_2,ij}^{(0,0)} + \psi_{e_2e_1,ij}^{(0,0)} \right). \end{aligned} \quad (8.4)$$

Note that the relation in the first line is exact at the level of terms that we include in $\mathcal{L}_{\text{kin}} + \mathcal{L}_{\text{pot}}$. With the second equality in (8.4) we define $\psi_{e_a e_b, ij}^{(L=0, S=0)}$, the $\chi_{e_a} \chi_{e_b}$ -component of a scattering wave function related to the incoming $\chi_i \chi_j$ state with centre-of-mass energy \sqrt{s} , orbital angular momentum $L = 0$ and total spin $S = 0$, evaluated for zero relative distance and normalised to the free scattering solution. The quantities ξ_i, ξ_j denote the two-component Pauli spinors of the incoming particles and we use the notation $\langle \dots \rangle$ to indicate the trace in spin space. The relation between the matrix element $\langle 0 | \chi_{e_2}^{c\dagger} \chi_{e_1} | \chi_i \chi_j \rangle$ and the wave functions in (8.4) is generalised in the following way to the case of ${}^{2S+1}L_J$ partial-wave reactions:

$$\langle 0 | \chi_{e_2}^{c\dagger} \Gamma K \left[-\frac{i}{2} \overleftrightarrow{\boldsymbol{\partial}} \right] \chi_{e_1} | \chi_i \chi_j \rangle = \langle \xi_j^{c\dagger} \Gamma \xi_i \rangle K[\vec{p}] \left(\psi_{e_1e_2,ij}^{(L,S)} + (-1)^{L+S} \psi_{e_2e_1,ij}^{(L,S)} \right), \quad (8.5)$$

where $\Gamma = 1_{2 \times 2}$ in case of total spin $S = 0$ and $\Gamma = \vec{\sigma}$ for $S = 1$. Further, K denotes a polynomial in relative momentum $\vec{p} = \vec{p}_{ij}$ of the incoming $\chi_i \chi_j$ pair (or, accordingly, derivatives in position space) corresponding to a given angular momentum L . Generically, the multi-component wave-function $\vec{\psi}_{ij}^{(L,S)}$ encodes the effect of all (off-) diagonal potential interactions that involve the incoming non-relativistic $\chi_i \chi_j$ pair in a $^{2S+1}L_J$ partial-wave state as well as all possible further (intermediate) neutralino and chargino NRMSSM two-particle states with the same charge and within the same partial-wave configuration. In the perturbative case, where the potential interactions in \mathcal{L}_{pot} are neglected, the wave functions reduce to $\psi_{e_a e_b, ij}^{(L,S)} \rightarrow \delta_{e_a i} \delta_{e_b j}$. This can be checked explicitly by direct calculation of the matrix elements of the operators in the perturbative case, which in particular leads to the result for the tree-level annihilation cross section in (6.22). The explicit determination of the wave functions from the matrix elements on the left-hand side in (8.5) is postponed to Sec. 8.2. Here we use the relation (8.5) to express the spin-averaged annihilation cross section (8.1) in terms of the non-relativistic wave functions,

$$\begin{aligned}
& \sigma^{\chi_i \chi_j \rightarrow \sum X_A X_B} v_{\text{rel}} \\
&= \left[\psi_{e_4 e_3, ij}^{(0,0)} \right]^* \left(\hat{f}(^1S_0) + \frac{\delta m}{M} \hat{h}_1(^1S_0) + \frac{\delta \bar{m}}{M} \hat{h}_2(^1S_0) + \hat{g}_\kappa(^1S_0) \right) \psi_{e_1 e_2, ij}^{(0,0)} \\
&+ 3 \left[\psi_{e_4 e_3, ij}^{(0,1)} \right]^* \left(\hat{f}(^3S_1) + \frac{\delta m}{M} \hat{h}_1(^3S_1) + \frac{\delta \bar{m}}{M} \hat{h}_2(^3S_1) + \hat{g}_\kappa(^3S_1) \right) \psi_{e_1 e_2, ij}^{(0,1)} \\
&+ \vec{p}_{ij}^2 \left[\psi_{e_4 e_3, ij}^{(1,0)} \right]^* \frac{\hat{f}(^1P_1)}{M^2} \psi_{e_1 e_2, ij}^{(1,0)} + \vec{p}_{ij}^2 \left[\psi_{e_4 e_3, ij}^{(1,1)} \right]^* \frac{\hat{f}(^3P_J)}{M^2} \psi_{e_1 e_2, ij}^{(1,1)}, \quad (8.6)
\end{aligned}$$

where we have used the spin sums

$$\frac{1}{2} \sum_{s_i, s_j} \langle \xi_j^{c\dagger} \xi_i \rangle \langle \xi_j^{c\dagger} \xi_i \rangle^* = 1, \quad \frac{1}{2} \sum_{s_i, s_j} \langle \xi_j^{c\dagger} \sigma^k \xi_i \rangle \langle \xi_j^{c\dagger} \sigma^\ell \xi_i \rangle^* = \delta_{k\ell}, \quad (8.7)$$

as well as the symmetry properties (5.9, 5.14) of the Wilson coefficients. The relative momentum \vec{p}_{ij} of the two non-relativistic particles χ_i and χ_j in the $\chi_i \chi_j$ two-particle state is related to the available centre-of-mass energy \sqrt{s} by

$$\vec{p}_{ij}^2 = 2\mu_{ij} (\sqrt{s} - M_{ij}) + \mathcal{O}(\vec{p}_{ij}^4), \quad (8.8)$$

with μ_{ij} the reduced and M_{ij} the total mass of the two-particle system. In addition we use in (8.6) the following relation between the matrix elements of the next-to-next-to-leading and the leading-order S -wave operators $\mathcal{P}(^{2S+1}S_S)$ and $\mathcal{O}(^{2S+1}S_S)$,

$$\frac{\hat{g}(^{2S+1}S_S)}{M^2} \langle \chi_i \chi_j | \mathcal{P}(^{2S+1}S_S) | \chi_i \chi_j \rangle = \hat{g}_\kappa(^{2S+1}S_S) \langle \chi_i \chi_j | \mathcal{O}(^{2S+1}S_S) | \chi_i \chi_j \rangle, \quad (8.9)$$

with

$$\hat{g}_{\kappa \{e'_1 e'_2\} \{e'_4 e'_3\}}(^{2S+1}S_S) = \frac{\hat{g}_{\{e_1 e_2\} \{e_4 e_3\}}(^{2S+1}S_S)}{2M^2} \left(\kappa_{e_1 e_2, e'_1 e'_2}^* \delta_{e_4 e_3, e'_4 e'_3} + \delta_{e_1 e_2, e'_1 e'_2} \kappa_{e_4 e_3, e'_4 e'_3} \right) \quad (8.10)$$

and the parameter κ defined as

$$\kappa_{e_1 e_2, e'_1 e'_2} = \vec{p}_{e_1 e_2}^2 \delta_{e_1 e_2, e'_1 e'_2} + 2 \mu_{e_1 e_2} \alpha_2 \sum_a m_{\phi_a} c_{e_1 e_2, e'_1 e'_2}^{(a)}. \quad (8.11)$$

The sum in the second term in (8.11) runs over all potential scattering reactions $\chi_{e'_1} \chi_{e'_2} \rightarrow \chi_{e_1} \chi_{e_2}$ arising from ϕ_a -mediator exchange. The corresponding coefficients $c_{e_1 e_2, e'_1 e'_2}^{(a)}$ are collected in Tab. B.1. The definition for the relative momentum $\vec{p}_{e_1 e_2}^2$ in (8.11) follows from (8.8). The derivation of relation (8.9) is postponed to Sec. 8.5. Let us however note here, that the simpler form $\langle \chi \chi | \mathcal{P}^{(2S+1)S_S} | \chi \chi \rangle = \vec{p}^2 \langle \chi \chi | \mathcal{O}^{(2S+1)S_S} | \chi \chi \rangle$ familiar from NRQCD applications to heavy quarkonium is obtained from (8.9 – 8.11), when the theory contains just one single two-particle state and the exchanged bosons ϕ_a are massless.

As second step in our derivation of a $\chi_i \chi_j$ cross section formula involving products of Sommerfeld enhancement factors and Wilson coefficients, we provide now the definition of the Sommerfeld enhancement factor for an incoming $\chi_i \chi_j$ state with centre-of-mass energy \sqrt{s} , spin S and orbital angular momentum L . The enhancement factor is associated with Wilson coefficients (or suitable combinations of Wilson coefficients) \hat{f} , that encode the corresponding short-distance annihilations subject to the given total spin S and orbital angular momentum L , and defined by the ratio

$$S_{ij}[\hat{f}^{(2S+1)L_J}] = \frac{\left[\psi_{e_4 e_3, ij}^{(L,S)} \right]^* \hat{f}_{\{e_1 e_2\}\{e_4 e_3\}}^{\chi\chi \rightarrow \chi\chi} ({}^{2S+1}L_J) \psi_{e_1 e_2, ij}^{(L,S)}}{\hat{f}_{\{ij\}\{ij\}}^{\chi\chi \rightarrow \chi\chi} ({}^{2S+1}L_J)|_{\text{LO}}}. \quad (8.12)$$

This definition has to be understood such that according to the expressions in the expansion of the cross section (8.6), for instance, the combinations $\hat{f}({}^1P_1)/M^2$ and $\hat{f}({}^3P_J)/M^2$ appear as arguments of the corresponding S_{ij} . In case of leading-order S -waves the arguments are simply given by $\hat{f}({}^1S_0)$ and $\hat{f}({}^3S_1)$. It is worth to recall at this point that the mass scale M that comes with the Wilson coefficients of dimension-8 operators in $\delta\mathcal{L}_{\text{ann}}$ derives from the masses of the particles $\chi_{e_{i=1,\dots,4}}$ to which the respective Wilson coefficient \hat{f} refers. With the subscript “LO” in the denominator of (8.12) we indicate that only that contribution to $\hat{f}({}^{2S+1}L_J)$ that is leading order in the coupling α_2 , $\mathcal{O}(\alpha_2^2)$, should be kept in the corresponding expressions. As far as our application is concerned, this prescription is only relevant to us for the case of enhancement factors associated with next-to-next-to-leading order S -wave annihilations, $S_{ij}[\hat{g}_\kappa({}^{2S+1}S_S)]$, where we have to set the α_2 proportional term in κ to zero, so that $\hat{g}_\kappa^{\chi\chi \rightarrow \chi\chi} ({}^{2S+1}S_S)|_{\text{LO}} = \vec{p}_{ij}^2 / M_{ij}^2 \hat{g}_{\{ij\}\{ij\}}^{\chi\chi \rightarrow \chi\chi} ({}^{2S+1}S_S)$. However note that definition (8.12) generically allows to incorporate the higher-order (hard) radiative corrections to the short-distance part of the annihilation into the Sommerfeld factor. Though not explicitly indicated in (8.12) it is important to note that the Sommerfeld enhancement factors depend on the available centre-of-mass energy \sqrt{s} or, equivalently, the relative velocity v_{rel} of the incoming $\chi_i \chi_j$ state.

As third and final step, using the definition (8.12), we parametrise the non-relativistic expansion of the inclusive $\chi_i \chi_j$ pair-annihilation cross section in (8.1) in terms of Som-

merfeld enhancement factors and Wilson coefficients:

$$\begin{aligned}
\sigma^{\chi_i \chi_j \rightarrow \sum X_A X_B} v_{\text{rel}} &= S_{ij} [\hat{f}_h(1S_0)] \hat{f}_{\{ij\}\{ij\}}^{\chi\chi \rightarrow \chi\chi}(1S_0) + S_{ij} [\hat{f}_h(3S_1)] 3 \hat{f}_{\{ij\}\{ij\}}^{\chi\chi \rightarrow \chi\chi}(3S_1) \\
&+ \frac{\vec{p}_{ij}^2}{M_{ij}^2} \left(S_{ij} [\hat{g}_\kappa(1S_0)] \hat{g}_{\{ij\}\{ij\}}^{\chi\chi \rightarrow \chi\chi}(1S_0) + S_{ij} [\hat{g}_\kappa(3S_1)] 3 \hat{g}_{\{ij\}\{ij\}}^{\chi\chi \rightarrow \chi\chi}(3S_1) \right. \\
&\left. + S_{ij} \left[\frac{\hat{f}(1P_1)}{M^2} \right] \hat{f}_{\{ij\}\{ij\}}^{\chi\chi \rightarrow \chi\chi}(1P_1) + S_{ij} \left[\frac{\hat{f}(3P_J)}{M^2} \right] \hat{f}_{\{ij\}\{ij\}}^{\chi\chi \rightarrow \chi\chi}(3P_J) \right), \quad (8.13)
\end{aligned}$$

where in addition to the spin-weighted sum $\hat{f}(3P_J)$ of spin $S = 1$ P -wave Wilson coefficients defined in (6.29), we introduced the following combinations of Wilson coefficients

$$\begin{aligned}
\hat{f}_h(1S_0) &= \hat{f}(1S_0) + \frac{\delta m}{M} \hat{h}_1(1S_0) + \frac{\delta \bar{m}}{M} \hat{h}_2(1S_0), \\
\hat{f}_h(3S_1) &= \hat{f}(3S_1) + \frac{\delta m}{M} \hat{h}_1(3S_1) + \frac{\delta \bar{m}}{M} \hat{h}_2(3S_1). \quad (8.14)
\end{aligned}$$

The non-relativistic expansion of the inclusive $\chi_i \chi_j$ tree-level annihilation cross section is recovered from (8.13) by setting all Sommerfeld enhancement factors to one. In this case the cross section formula contains only those Wilson coefficients that refer to diagonal $\chi_i \chi_j \rightarrow \chi_i \chi_j$ reactions. Wilson coefficients related to off-diagonal rates – in particular the coefficients $\hat{h}_{i=1,2}$ that vanish for diagonal reactions – can only enter the Sommerfeld enhancement factors. This is why the symbols \hat{f}_h appear only as arguments of the factors S_{ij} in (8.13).

8.2 NR matrix-elements & the Schrödinger equation

In this section we provide the missing derivation of the relation between the matrix elements and wave functions in (8.5). We proceed in three steps: first a relation between the matrix elements and corresponding momentum space two-particle Green functions is established. Second, we move to the corresponding coordinate-space Green functions and, third, use elementary scattering theory to obtain an expression involving scattering wave functions instead of the Green functions.

The non-relativistic matrix element in (8.5) systematically includes long-range potential interactions, which cannot be treated perturbatively but require a resummation up to all orders. We have noted in Chap. 2 that the corresponding contributions to the matrix element are obtained from a resummation of the potential region contributions to ladder diagrams such as Fig. 8.1. To extract the relevant expressions from the full theory ladder diagrams we can perform similar replacements as in Sec. 2.1, (2.5, 2.6), for the (ladder bar) fermion and (ladder rung) boson propagators. Let us recall however that compared to Chap. 2 we consider here the case of several nearly mass degenerate fermion states, where the corresponding mass differences shall be of the same order as the non-relativistic kinetic energy of the external states. We write the on-shell momenta

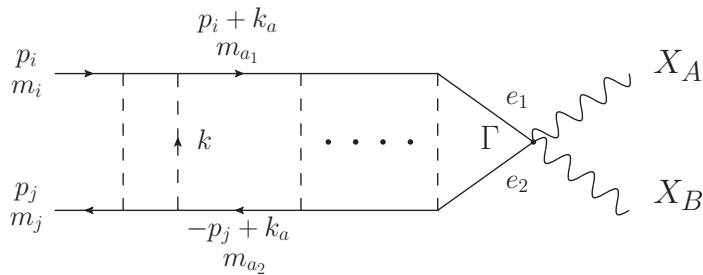


Figure 8.1:

p_i and p_j of incoming NRMSSM states χ_i and χ_j in Fig. 8.1 as

$$\vec{p}_i = \frac{\mu_{ij}}{m_j} \vec{P} + \vec{p}, \quad \vec{p}_j = \frac{\mu_{ij}}{m_i} \vec{P} - \vec{p}, \quad (8.15)$$

where μ_{ij} denotes the reduced mass of the $\chi_i\chi_j$ pair and \vec{P} and \vec{p} are its total and relative momentum, respectively. The latter fulfil $|\vec{P}|, |\vec{p}| \ll \mu_{ij}$ such that the centre-of-mass energy in the non-relativistic $\chi_i\chi_j$ annihilation reaction is given by

$$\sqrt{s} = m_i + m_j + \mathcal{E} \equiv 2m_{\text{LSP}} + E, \quad \mathcal{E} = \frac{\vec{p}^2}{2\mu_{ij}}, \quad (8.16)$$

where we have neglected higher-order terms in the non-relativistic expansion. The variable E introduced above measures the available non-relativistic kinetic energy with respect to the reference scale $2m_{\text{LSP}}$ given by two times the mass $m_{\text{LSP}} = m_{\chi_1^0}$ of the lightest neutralino state. The introduction of such common scale will prove useful in the following. Since we allow for small mass differences among the NRMSSM neutralino and chargino states χ_i, χ_j , with $m_i + m_j - 2m_{\text{LSP}} \sim m_{\text{LSP}}v^2$, both energies \mathcal{E} and E scale as $E \sim \mathcal{E} \sim m_{\text{LSP}}v^2$.

The potential region expansion that we now perform on the full theory ladder-diagram expression again refers to canonical routing of momenta as indicated in Fig. 8.1. We noted in Chap. 2 and discussed in detail in Chap. 7 that the potential region expansion of the boson propagators associated with the ladder rungs in Fig. 8.1 leads to potential interactions between the fermion pairs in the ladder bars. Let us in particular consider the loop that involves the two states χ_{a_1} and χ_{a_2} with masses m_{a_1} and m_{a_2} as well as the exchanged boson with four-momentum k . We denote the corresponding loop momentum with k_a . It is worth to note that the boson momentum k is given by the difference of the loop momentum k_a and the loop momentum of the previous loop in the ladder diagram. The potential interaction associated with the exchanged boson depends only on the spatial components of its four-momentum, \vec{k} , but not on k^0 . Since this generically applies to all boson mediated potential interactions, it is eventually possible to perform the integration over the zero-components of the loop-momenta. In particular, after a consistent potential region expansion of the χ_{a_1} and χ_{a_2} propagators, neglecting

systematically all higher order contributions, we obtain

$$\begin{aligned} & \int \frac{dk_a^0}{2\pi} \frac{2m_{a_1}}{(p_i + k_a)^2 - m_{a_1}^2 + i\epsilon} \frac{2m_{a_2}}{(-p_j + k_a)^2 - m_{a_2}^2 + i\epsilon} \\ &= \frac{-i}{E - [M_a - 2m_{\text{LSP}}] - \frac{(\vec{p} + \vec{k}_a)^2}{2\mu_a}}. \end{aligned} \quad (8.17)$$

In the potential region expansion of the propagator denominators in the first line we treated the mass differences between the states along the upper or lower fermion line in the diagram Fig. 8.1 as small, $m_{a_1} - m_i \sim m_{a_2} - m_j \sim m_{\text{LSP}}v^2$. However we do not require that the mass differences $m_{a_2} - m_{a_1}$ and $m_j - m_i$ are small.³ Further note that within our leading-order approximation we can equivalently substitute the reduced mass μ_a of the $\chi_{a_1}\chi_{a_2}$ pair in the kinetic energy term in the denominator of (8.17) by μ_{ij} or $m_{\text{LSP}}/2$, or any other NRMSSM two-particle state reduced mass.

After the systematic potential region expansion of the full-theory ladder diagrams and subsequent integration over the zero-components of the loop momenta we obtain an expression given by products of two-particle propagators (8.17) associated with $\chi_{a_1}\chi_{a_2}$ pairs times corresponding momentum-space potential interactions from boson exchange. This potential region contribution to the full theory amplitude agrees with the non-relativistic matrix element including the non-perturbative potential interactions, such that we can write

$$\begin{aligned} & \langle 0 | \chi_{e_2}^{c\dagger} \Gamma K \left[-\frac{i}{2} \overleftrightarrow{\mathcal{D}} \right] \chi_{e_1} | \chi_i \chi_j \rangle = \langle \xi_j^{c\dagger} \Gamma \xi_i \rangle \\ & \times \lim_{\hat{E} \rightarrow E} (-1) \left(\hat{E} - \frac{\vec{p}^2}{2\mu_{ij}} \right) \int \frac{d^3\vec{q}}{(2\pi)^3} K[\vec{q}] \left(\tilde{G}^{ie}(\vec{p}, \vec{q}; \hat{E}) + (-1)^{L+S} \tilde{G}^{i\bar{e}}(\vec{p}, \vec{q}; \hat{E}) \right), \end{aligned} \quad (8.18)$$

where we have introduced the compound index notation with index i referring to the $\chi_i\chi_j$ states and index e (\bar{e}) associated with the state $\chi_{e_1}\chi_{e_2}$ ($\chi_{e_2}\chi_{e_1}$). This compound notation will be used frequently below. The function \tilde{G} in (8.18) is given by

$$\begin{aligned} \tilde{G}^{ab}(\vec{p}, \vec{q}; E) &= -\frac{\delta^{ab}}{E - [M_a - 2m_{\text{LSP}}] - \frac{\vec{p}^2}{2\mu_a}} (2\pi)^3 \delta^{(3)}(\vec{p} - \vec{q}) \\ &+ \frac{1}{E - [M_a - 2m_{\text{LSP}}] - \frac{\vec{p}^2}{2\mu_a}} iH^{ab}(\vec{p}, \vec{q}; E) \frac{1}{E - [M_b - 2m_{\text{LSP}}] - \frac{\vec{q}^2}{2\mu_b}} \end{aligned} \quad (8.19)$$

and

$$H^{ab}(\vec{p}, \vec{q}; E) = i \sum_{n=0}^{\infty} \int \left[\prod_{i=1}^n \frac{d^3\vec{k}_i}{(2\pi)^3} \right] \hat{V}^{aa_1}(\vec{k}_1) \frac{1}{E - [M_{a_1} - 2m_{\text{LSP}}] - \frac{(\vec{p} + \vec{k}_1)^2}{2\mu_{a_1}}}$$

³This implies that the formalism can be applied to hydrogen-like two-particle states with mutual boson exchange as well. In our application to the χ_1^0 relic abundance calculation including χ^0/χ^\pm co-annihilations, however, we necessarily encounter $m_{e_j} - m_{e_j} \sim m_{\text{LSP}}v^2$ for all states in the set of nearly mass degenerate NRMSSM neutralino and chargino states.

$$\times \hat{V}^{a_1 a_2}(\vec{k}_2 - \vec{k}_1) \dots \frac{1}{E - [M_{a_n} - 2m_{\text{LSP}}] - \frac{(\vec{p} + \vec{k}_n)^2}{2\mu_{a_n}}} \hat{V}^{a_n b}(\vec{q} - \vec{p} - \vec{k}_n). \quad (8.20)$$

The $n = 0$ contribution to the sum in (8.20) involves no integration and we have to additionally set $\vec{k}_0 = 0$ as well as $a_0 = a$. Let us discuss the individual terms arising on the right-hand side of (8.18) in the following, starting with the function \tilde{G} . The first contribution to \tilde{G} , explicitly written in (8.19), accounts for the bare two-particle propagator with no potential boson exchanges. A term with given n in H^{ab} , (8.20), then refers to a corresponding $(n + 1)$ -loop ladder diagram involving $(n + 1)$ potential boson exchanges, where the momentum-space potentials $\hat{V}^{ab}(\vec{k})$ that we derived in Chap. 7 comprise the potential propagators of the exchanged bosons together with the coupling factors from the two corresponding vertices. In (8.18) we have further used that applying the on-shell conditions for the external spinors the Dirac structures in the numerator of the full theory ladder diagrams can be reduced in the potential region to the expression $\xi_j^{c\dagger} \Gamma \xi_i$ with two-component spinors $\xi_{i,j}$. The 2×2 matrix Γ is either given by $\Gamma = \mathbf{1}$ or $\vec{\sigma}$, in which case either the total spin $S = 0$ or 1 momentum-space potentials have to be used in the above equations. Eventually this will cause the spin S dependence of the wave functions $\psi_{e_1 e_2, ij}^{(L, S)}$. The dependence on the orbital angular momentum L enters through the polynomial $K[\vec{q}]$ in (8.18) with $K = 1$ in the (leading-order) $L = 0$ case and $K = \vec{q}$ for $L = 1$. The limiting procedure $\hat{E} \rightarrow E$ is required in (8.18) as the factor $[\hat{E} - \vec{p}^2 / (2\mu_{ij})]$ vanishes for $\hat{E} = E$, while the function $\tilde{G}^{ab}(\vec{p}, \vec{q}; \hat{E})$ is singular at $\hat{E} = E$. The latter singularity is associated with scattering states with relative-momentum kinetic energy E . Finally note that the integration over \vec{q} in (8.18) refers to the last loop integration before annihilation of the states $\chi_{e_1} \chi_{e_2}$ and $\chi_{e_2} \chi_{e_1}$.

The function $\tilde{G}^{ab}(\vec{p}, \vec{q}; E)$ is the momentum space Green function of a corresponding Schrödinger operator. By explicit calculation one easily checks that the following Lippmann-Schwinger equation for $\tilde{G}^{ab}(\vec{p}, \vec{q}; E)$ holds,

$$\left(\frac{\vec{p}^2}{2\mu_a} - [E - M_a + 2m_{\text{LSP}}] \right) \tilde{G}^{ab}(\vec{p}, \vec{q}; E) + \int \frac{d^3 \vec{k}}{(2\pi)^3} \hat{V}^{ac}(\vec{k}) \tilde{G}^{cb}(\vec{p} - \vec{k}, \vec{q}; E) = \delta^{ab} (2\pi)^3 \delta^{(3)}(\vec{p} - \vec{q}). \quad (8.21)$$

In our second step we now move to the corresponding configuration space Green function $G^{ab}(\vec{r}, \vec{r}'; E)$ that is related to (8.19) by Fourier transformation. Accordingly, it fulfils the Schrödinger equation

$$\left(-\frac{\vec{\nabla}^2}{2\mu_a} - E \right) G^{ab}(\vec{r}, \vec{r}'; E) + V^{ac}(r) G^{cb}(\vec{r}, \vec{r}'; E) = \delta^{ab} \delta^{(3)}(\vec{r} - \vec{r}'), \quad (8.22)$$

where we have introduced the coordinate-space potential

$$V^{ac}(r) = \hat{V}^{ac}(r) + \delta^{ac} [M_a - 2m_{\text{LSP}}] \quad (8.23)$$

that includes effects from mass-differences between the co-annihilating NRMSSM two-particle states with respect to the common mass scale $2m_{\text{LSP}}$ set by the lightest pair, $\chi_1^0\chi_1^0$. In addition we used already that the potentials that we consider in the NRMSSM are spherically symmetric, $\hat{V}(\vec{r}) = \hat{V}(r)$.

In our last step we establish the connection between the Green function $G^{ab}(\vec{r}, \vec{r}'; E)$ and corresponding scattering wave functions by making use of relations from elementary scattering theory. To this end we define the matrix-valued Green operators

$$G(\hat{E}) = \frac{1}{H - \hat{E} - i\epsilon}, \quad G_0(\hat{E}) = \frac{1}{H_0 - \hat{E} - i\epsilon}. \quad (8.24)$$

H and H_0 denote the interacting and the free Hamiltonian of the Schrödinger problem with the momentum eigenstates

$$H|\vec{p}+, a\rangle = \frac{\vec{p}^2}{2\mu_a}|\vec{p}+, a\rangle, \quad H_0|\vec{p}, a\rangle = \frac{\vec{p}^2}{2\mu_a}|\vec{p}, a\rangle. \quad (8.25)$$

The dimensionality of the operators G, G_0 is related to the number of two-particle NRMSSM basis states $(\chi\chi)_a = \chi_{a_1}\chi_{a_2}$ in a given charge sector. Therefore the momentum eigenstates in (8.25) also carry a corresponding compound index a that indicates a specific basis state $\chi_{a_1}\chi_{a_2}$. The states $|\vec{p}+, a\rangle$ refer to exact stationary scattering solutions of the interacting Hamiltonian, whereas states $|\vec{p}, a\rangle$ correspond to plane wave solutions of the respective free system where long-range potential interactions are neglected. Note that in the latter case the coordinate space potentials (8.23) are solely given by mass difference terms. The representation of the stationary scattering states $|\vec{p}+, a\rangle$ in the basis of corresponding plane wave states is given by the momentum-space wave function $[\tilde{\psi}_E(\vec{q})]_{ab} = \langle \vec{q}, a | \vec{p}+, b \rangle$. Further, we obtain from the Lippmann-Schwinger equation the relation $|\vec{p}+, a\rangle = GG_0^{-1}|\vec{p}, a\rangle$. Using the defining relation (8.5) for the wave functions $\psi_{e_1e_2, ij}^{(L,S)}$ as well as (8.18) we can thus derive

$$\begin{aligned} K[\vec{p}] \psi_{e_1e_2, ij}^{(L,S)} &= \lim_{\hat{E} \rightarrow E} (-1) \left(\hat{E} - \frac{\vec{p}^2}{2\mu_{ij}} \right) \int \frac{d^3\vec{q}}{(2\pi)^3} K[\vec{q}] \underbrace{\tilde{G}^{ie}(\vec{p}, \vec{q}; \hat{E})}_{\langle \vec{p}, i | G(\hat{E}) | \vec{q}, e \rangle} \\ &= \lim_{\hat{E} \rightarrow E} \int \frac{d^3\vec{q}}{(2\pi)^3} K[\vec{q}] \underbrace{\langle \vec{p}, i | \left(\frac{\vec{p}^2}{2\mu_{ij}} - \hat{E} \right) G(\hat{E}) | \vec{q}, e \rangle}_{\langle \vec{p}, i | G_0^{-1}(\hat{E})} = \int \frac{d^3\vec{q}}{(2\pi)^3} K[\vec{q}] [\tilde{\psi}_E(\vec{q})]_{ei}^*. \end{aligned} \quad (8.26)$$

From the comparison with (8.5) and using that $K[\vec{q}] = 1$ ($K[\vec{q}] = \vec{q}$) for orbital angular momentum $L = 0$ ($L = 1$) we finally obtain

$$\psi_{e_1e_2, ij}^{(0,S)} = [\psi_E(0)]_{e_1e_2, ij}^* \quad \text{and} \quad \vec{p}\psi_{e_1e_2, ij}^{(1,S)} = -i [\vec{\nabla}\psi_E(0)]_{e_1e_2, ij}^*. \quad (8.27)$$

The coordinate-space wave function $\psi_E(\vec{r})_{e_1e_2, ij}$ evaluated at zero relative distance in (8.27) carries two compound indices, ij and e_1e_2 . The index ij refers to the incoming

$\chi_i\chi_j$ pair described by the incoming plane wave two-particle state $|\vec{p}, i\rangle$ with kinetic energy E in the centre-of-mass frame of the annihilation reaction. Consequently, the compound index e_1e_2 indicates the component of the full scattering wave function with incoming $\chi_i\chi_j$ pair that refers to the $\chi_{e_1}\chi_{e_2}$ state. The latter e_1e_2 component is picked out (at $\vec{r} = 0$) by the annihilation operator that defines $\psi_{e_1e_2,ij}^{(L,S)}$ through (8.5). The coordinate space scattering wave functions $[\psi_E(\vec{r})]_{a,ij}$ are obtained as solutions of the matrix Schrödinger equation

$$\left(\left[-\frac{\vec{\nabla}^2}{2\mu_a} - E \right] \delta^{ab} + V^{ab}(r) \right) [\psi_E(\vec{r})]_{b,ij} = 0 \quad (8.28)$$

with the matrix-valued coordinate-space potentials obtained from (8.23). The initial condition for a solution $\psi_E(\vec{r})_{b,ij}$ has to be chosen such that the asymptotic incoming state refers to the $\chi_i\chi_j$ pair. Due to our assumption on the mass splittings between the NRMSSM states to be of $\mathcal{O}(m_{\text{LSP}}v^2)$, we can replace the reduced mass μ_a in (8.28) by the reduced mass $m_{\text{LSP}}/2$ in the lightest NRMSSM two-particle system $\chi_1^0\chi_1^0$. The difference is an $\mathcal{O}(v^2)$ effect which we consistently neglect in the part of the annihilation rates that is associated with the long-range effects. Let us recall that we have performed the same approximation in Sec. 2.2, see (2.9, 2.11) and the corresponding discussion therein. Consequently, we have to determine within our non-relativistic approximation the wave functions $[\psi_E(\vec{r})]_{a,ij}$ that are solutions of the Schrödinger equation

$$\left(\left[-\frac{\vec{\nabla}^2}{m_{\text{LSP}}} - E \right] \delta^{ab} + V^{ab}(r) \right) [\psi_E(\vec{r})]_{b,ij} = 0, \quad (8.29)$$

with initial conditions chosen such that $[\psi_E(\vec{r})]_{b,ij}$ refers to the asymptotic incoming states $\chi_i\chi_j$.

It is important to note that the relation among the wave functions $\psi_{e_1e_2,ij}^{(L,S)}$ and $[\psi_E(0)]_{e_1e_2,ij}$ in (8.27) involves a complex conjugation. Using (8.27) in the refined definition of the Sommerfeld factor in (8.12), we therefore conclude that the advanced-guess Sommerfeld enhancement formula from Chap. 2, (2.8, 2.33), was correct up to complex conjugation of the scattering wave function appearing therein.⁴ While this has consequences for the enhancement formulae, we can however directly use all results from Chap. 2 that are related to the scattering solution wave functions $[\psi_E(\vec{r})]_{b,i}$.⁵ Taking

⁴Let us mention that the appearance of the complex conjugated scattering wave function $[\tilde{\psi}_E(\vec{q})]_{ei}^*$ in (8.26) is related to the convention used for the left and right states in the definition of the Green function (8.19). When using the opposite convention we would end up with a wave function $[\tilde{\psi}_E(\vec{q})]_{ei}$ in (8.26), but with V^{ba} instead of V^{ab} in the corresponding Schrödinger equation (8.29). Note that the solutions $\psi_E(\vec{r})$ and $[\psi_E(\vec{r})]^*$ are identical for real-symmetric potentials, such that the correct result for the Sommerfeld enhancement factor would be obtained even if the conventions for the Green function and the potential were not consistently taken care of: this is the case for the toy model results in Chap. 2. In the MSSM, however, we encounter in general complex-hermitian potential matrices.

⁵Within the NRMSSM we have established the convention to use lowercase letters for the compound

the normalisation convention for $\psi^{(L,S)}$ noted in context of its definition in (8.5) into account, we derive the following relation from (2.31) and (2.32),

$$\psi_{e,i}^{(L,S)} = \frac{(2L+1)!!}{(L+1)!} [\chi_L^{(L+1)}(0)]_{eb}^* \frac{[M_L^{-1}]_{bi}^*}{k_i^{L+1}}. \quad (8.30)$$

χ_L denotes the regular L -th partial wave solution to the radial Schrödinger equation related to (8.29). The wave numbers k_i are given by

$$k_i = \sqrt{m_{\text{LSP}} (E + i\epsilon - \delta M_i)}, \quad (8.31)$$

where $\delta M_i = M_i - 2m_{\text{LSP}}$ is the mass splitting of the two-particle state $(\chi\chi)_i$ with respect to the state $\chi_1^0\chi_1^0$. As E measures the non-relativistic kinetic energy with respect to the scale $2m_{\text{LSP}}$, the definition (8.31) agrees with (2.16). Finally, the definition of M_L is obtained from (2.20). Using (2.42), we eventually obtain the relation

$$\psi_{e_1 e_2, ij}^{(L,S)} = i^{-L} (2L-1)!! \frac{[T_L^T]_{ei}}{k_i^L}, \quad (8.32)$$

which expresses $\psi^{(L,S)}$ in terms of the transpose of the coefficient matrix T_L associated with the large r behaviour of the singular radial solutions, see (2.37).

With these preparations we can rewrite the Sommerfeld enhancement factor (8.12) using the matrix T_L as

$$\begin{aligned} S_i[\hat{f}^{(2S+1)L_J}] &= \left(\frac{(2L-1)!!}{k_i^L} \right)^2 \frac{[T_L^*]_{ie'} \hat{f}_{ee'}^{\chi\chi \rightarrow \chi\chi}(2S+1L_J) [T_L^T]_{ei}}{\hat{f}_{ii}^{\chi\chi \rightarrow \chi\chi}(2S+1L_J)|_{\text{LO}}} \\ &= \left(\frac{(2L-1)!!}{k_i^L} \right)^2 \frac{[T_L]_{ie} \hat{f}_{ee'}^{\chi\chi \rightarrow \chi\chi}(2S+1L_J) [T_L^\dagger]_{e'i}}{\hat{f}_{ii}^{\chi\chi \rightarrow \chi\chi}(2S+1L_J)|_{\text{LO}}}. \end{aligned} \quad (8.33)$$

In the second line we have just reordered the factors in the numerator. With the latter rewriting we arrive at our final expression for the Sommerfeld enhancement factors, that allows for the following clear reading from left to right: The ie component of the first matrix factor in the numerator, $[T_L]_{ie}$, is associated with the e -state component of the (L partial-wave) scattering wave function at the origin that refers to incoming two-particle state i . This matrix component is multiplied with the Wilson coefficient $\hat{f}_{ee'}$ encoding the absorptive part of the forward scattering reactions from state e to state e' . Finally, the factor $[T_L^\dagger]_{e'i}$ is associated with the complex conjugate of the e' states' component of the wave function referring to incoming state i . This notation has the advantage that all

indices denoting the two particle channels, $(\chi\chi)_i$, opposed to capital letters, $(\chi\chi)_I$, in Chap. 2. In the latter chapter the notation $\psi(\vec{r})_{JI}$ was used to refer to scattering solutions of a corresponding matrix Schrödinger equation with incoming two-particle state $(\chi\chi)_I$, where the label J used to indicate the component of the wave function related to the two-particle state $(\chi\chi)_J$. Here, the same quantity is denoted with $[\psi_E(\vec{r})]_{j,i}$, where according to our notation the compound index i is associated with the incoming pair $(\chi\chi)_i$ and the index j picks the component corresponding to the $(\chi\chi)_j$ state.

quantities appear in the same order, from left to right, as in the diagrammatic pictures for the corresponding processes such as Fig. 5.1. The matrix T_L can be determined by following the first two steps proposed at the end of Sec. 2.2. In Sec. 8.4 we discuss the issue of numerical instabilities associated with the strategy of Sec. 2.2 and present an improved method for solving the problem. Before, we replace in the next section the Wilson coefficients that appear in the definition (8.12) and in the conveniently rewritten form (8.33) of the Sommerfeld enhancement factors by appropriate annihilation matrices introduced in Sec. 7.2.

8.3 Sommerfeld factors in the method-1 and 2 bases

In Sec. 7.2 we have argued that pair-annihilation processes of non-relativistic neutralino and chargino states including long-range potential interactions can be described by two-particle propagators (as explicitly seen in the previous section), two-particle state potential interactions and the final hard two-particle annihilation reaction, such that the use of a two-particle states basis is obvious. Correspondingly we introduced potential and annihilation matrices subject to the so-called method-1 or method-2 two-particle state bases, see Sec. 7.2.1. Here we come back to these bases and present a form of the Sommerfeld enhancement factors defined in (8.12), that involves the matrix representations of potential scattering and annihilation reactions introduced in Sec. 7.2.

Let us first note that the derivation in Sec. 8.1 – and therefore in particular the definition of the Sommerfeld enhancement factors (8.12) as well as the final form of the cross section (8.13) – can be directly related to the method-1 two-particle state basis: The definition of the operators in the parts \mathcal{L}_{pot} and $\delta\mathcal{L}_{\text{ann}}$ of the NRMSSM Lagrangian is such, that all redundant operators that arise when interchanging the labels $e_1 \leftrightarrow e_2$ or/and $e_4 \leftrightarrow e_3$ of a given specific operator are again part of \mathcal{L}_{pot} or $\delta\mathcal{L}_{\text{ann}}$, respectively. This implies that the intermediate states $\chi_{e_a}\chi_{e_b}$ and $\chi_{e_b}\chi_{e_a}$ of non-identical species $\chi_{e_a,b}$ can arise and are in particular treated as different in the calculation of the $\chi_i\chi_j$ state's forward scattering amplitude (8.1). In (8.5) this can, for instance, be seen explicitly as both the wave function components $\psi_{e_1e_2,ij}^{(L,S)}$ and $\psi_{e_2e_1,ij}^{(L,S)}$ appear. According to the definition of the annihilation matrices Γ in method-1 at the end of Sec. 7.2.1 we can therefore immediately rewrite the definition of the Sommerfeld enhancement factors given in (8.12) to

$$S_i[\hat{f}^{(2S+1)}L_J] = \frac{\left[\psi_{bi}^{(L,S)}\right]^* \Gamma_{cb}[\hat{f}^{(2S+1)}L_J] \psi_{ci}^{(L,S)}}{\Gamma_{ii}[\hat{f}^{(2S+1)}L_J]|_{\text{LO}}}, \quad (8.34)$$

where the wave functions are determined from (8.27) and (8.29), and the potential matrix in the Schrödinger equation should obviously refer to the method-1 basis. The indices in (8.34) are compound two-particle indices labelling the method-1 basis states; the label i , for example, refers to the two indices ij that denote the incoming two-particle state $\chi_i\chi_j$. The expression corresponding to (8.33) that involves the matrix T_L as well as the

annihilation matrix $\Gamma[\hat{f}^{(2S+1)L_J}]$ reads

$$S_i[\hat{f}^{(2S+1)L_J}] = \left(\frac{(2L-1)!!}{k_i^L} \right)^2 \frac{[T_L]_{ie} \Gamma_{ee'}[\hat{f}^{(2S+1)L_J}] [T_L^\dagger]_{e'i}}{\Gamma_{ii}[\hat{f}^{(2S+1)L_J}]|_{\text{LO}}}. \quad (8.35)$$

Similar to the replacements of all (off-) diagonal Wilson coefficients by the corresponding entries of method-1 annihilation matrices in (8.34, 8.35), we can further substitute the Wilson coefficients $\hat{f}_{\{ij\}\{ij\}}^{\chi\chi \rightarrow \chi\chi}$ and $\hat{g}_{\{ij\}\{ij\}}^{\chi\chi \rightarrow \chi\chi}$ in the non-relativistic expansion of the $\chi_i\chi_j$ annihilation cross section (8.13) by the diagonal entries in the corresponding method-1 annihilation matrices Γ . In this way the cross section is expressed in terms of quantities that solely refer to the method-1 basis.

In Appendix C we show by means of an example that using method-2 potentials and annihilation matrices in the calculation of the right-hand side of (8.34, 8.35) yields the same expression as in the method-1 calculation. Equation (8.34) therefore generically provides the definition of the Sommerfeld enhancement factors using either method-1 or method-2 potentials and annihilation matrices. As the CPU time for the determination of the Sommerfeld factors significantly increases the larger the number of two-particle states to be treated in the corresponding Schrödinger equation, it is often advantageous to calculate the factors using method-2 expressions. It has to be noted in that case, though, that contrary to the method-1 calculation the expansion of the cross section (8.13) is not simply expressed in terms of the Sommerfeld factors times the corresponding diagonal entries of the method-2 annihilation matrices. The latter involve certain prefactors with respect to the Wilson coefficients, see the definition in Sec. 7.2.1, which have to be taken into account when rewriting (8.13) in terms of method-2 quantities.

8.4 Solution of the Schrödinger equation: improved method

At the end of Sec. 2.2 a strategy was proposed that in principle allows for the numerical determination of the Sommerfeld enhancement factors in an N two-particle state model through the calculation of the matrix $\chi_l(r)$.⁶ This matrix contains in its columns the N regular linearly independent basis solutions to the system's radial Schrödinger equation subject to initial conditions at the origin, see (2.50). From $\chi_l(r)$ the matrix $U_l(r)$, (2.45), related to $\chi_l(r)$ and its derivative, is constructed and subsequently inverted. In the asymptotic limit $r \rightarrow \infty$ the expression $U_l^{-1}(r)$ approaches the constant matrix T_l^\dagger , (2.46), which finally determines the Sommerfeld enhancement factors (8.33, 8.35). In our practical applications where the Schrödinger equation is solved up to some finite r_∞ (and the stability of the obtained $U_l^{-1}(r_\infty)$ against varying and increasing r_∞ is

⁶In Chap. 2 we have used the lowercase letter l in order to refer to the orbital angular momentum quantum number of a $\chi\chi$ state, while we have established the notation with capital letter L in the NRMSSM. Since in this section we refer to results from Chap. 2, we adopt the lower case notation here. In the remaining sections of this chapter we return to the capital letter notation.

checked), severe numerical instabilities occur in the determination of the Sommerfeld factors. These are related to the behaviour of the radial wave function solutions encoded in $\chi_l(r)$, eventually implying that the inversion of the matrix $U_l(r_\infty)$ cannot be performed. We describe the origin of the instabilities next and subsequently present an improved method that solves the issue.

The numerical instabilities are associated with the presence of kinematically closed two-particle channels. As we allow for scenarios with N two-particle states $(\chi\chi)_a$ that are not necessarily mass-degenerate to a high degree, the condition for channel a to be closed, $2m_{\text{LSP}} + m_{\text{LSP}}v^2 - M_a < 0$, is easily fulfilled either for sufficiently low LSP velocity v or for states with larger⁷ mass splittings $\delta M_a = M_a - 2m_{\text{LSP}}$. For a qualitative discussion of the origin of the numeric instability let us consider the radial Schrödinger equation (2.23) for a system with (at least) one kinematically closed channel. The components in the matrix-valued function of regular basis solutions, $\chi_l(r)$, which refer to a kinematically open channel have an asymptotically oscillating behaviour in the limit $r \rightarrow \infty$. Contrarily, the components that refer to a kinematically closed channel b involve an exponentially growing contribution for $r \rightarrow \infty$, which is proportional to $e^{\kappa_b r}$ with $\kappa_b = \sqrt{m_{\text{LSP}}[M_b - (2m_{\text{LSP}} + E)]}$. Due to the strong exponential growth in the limit of large r we can already expect a strong growth of the ‘closed-channel’ components of $\chi_l(r)$ for intermediate ranges of r . When the system of coupled differential equations (2.23) is integrated a numerical problem arises from the fact that the closed-channel solutions mix into the differential equations for the open-channel solutions through off-diagonal potentials. The strong growth of the closed-channel solutions can cause them to entirely dominate the right-hand side of the differential equations (2.23) already for moderate r and eventually linear independence of solutions with different initial conditions is lost due to limited numerical accuracy. As soon as the columns of $\chi_l(r_\infty)$ become linearly dependent, an inversion of the related matrix $U_l(r_\infty)$ becomes impossible and therefore the Sommerfeld enhancement factors that require the knowledge of $U^{-1}(r_\infty)$ cannot be obtained.

A rough criterion for the described numerical issue to appear can be derived by considering explicitly the product $V(r)_{ab} \chi_{lbi}(r)$ of the off-diagonal potential-matrix entry $V(r)_{ab}$ with the closed-channel component solution $\chi_{lbi}(r)$, that mixes into the differential equation for an open-channel component $\chi_{lai}(r)$ in (2.23). The potentials in the off-diagonals of the matrix $V(r)$ are of Yukawa-type, proportional to $e^{-M_{\text{EW}}r}/r$, where M_{EW} denotes the mass scale of the electroweak gauge bosons and light Higgses that mediate the potential scattering. As the solution $\chi_{lbi}(r)$ involves an (asymptotic) exponentially growing component, the product of the off-diagonal potential with $\chi_{lbi}(r)$ will involve a contribution proportional to $e^{(\kappa_b - M_{\text{EW}})r}/r$. If the exponent is positive this contribution

⁷In wino- or higgsino-like χ_1^0 scenarios the $(\chi\chi)_a$ states are highly mass-degenerate within some 100 MeV or only a few GeV, respectively. Our aim is to cover also those cases where the mass splittings become larger, of the order of some 10 to even some 100 GeV. Note that the mass splittings cannot be too large, as our approach requires that all $(\chi\chi)_a$ states, that are treated exactly in the Schrödinger equations, are non-relativistic for a given available centre-of-mass energy $\sqrt{s} = 2m_{\text{LSP}} + m_{\text{LSP}}v^2$. If the splittings become large, however, the Sommerfeld effect is less relevant as well.

can start to dominate the right-hand side of the Schrödinger equation (2.23) for the open-channel solution $\chi_{l ai}(r)$ in the range of intermediate r . The condition for a positive exponent reads

$$M_b - (2 m_{\text{LSP}} + m_{\text{LSP}} v^2) > \frac{M_{\text{EW}}^2}{m_{\text{LSP}}}, \quad (8.36)$$

and is easily satisfied in our case as we are interested in scenarios with $m_{\text{LSP}} \gg M_{\text{EW}}$, unless the states $(\chi\chi)_a$ included in the calculation are very degenerate within a few GeV or even less.

Instead of calculating $U_l^{-1}(r_\infty)$ by matrix-inversion we will now propose an improved method that allows to obtain $U^{-1}(r_\infty)$ in another way, thereby solving the issue of numerical instabilities in the calculation of the Sommerfeld enhancement factors. We apply this new method, which is based on an adaptation of the reformulation of the Schrödinger equation problem described in [97], in the numerical calculation of Sommerfeld enhanced χ^0/χ^\pm (co-) annihilation rates throughout this thesis. In order to review the relevant steps of [97] and to describe the essential points in our adaptation to the Sommerfeld enhancement factor determination, let us start from the radial Schrödinger equation (2.23) for a system of N coupled states $(\chi\chi)_a$ and rewrite it in terms of the dimensionless variable $x = m_{\text{LSP}} v r$,

$$[\chi_l''(x)]_{ai} = \left(\frac{l(l+1)}{x^2} \delta_{ab} + \left[\frac{V(x)}{E} - \mathbf{1} \right]_{ab} \right) [\chi_l(x)]_{bi}, \quad (8.37)$$

with $E = m_{\text{LSP}} v^2$. It is convenient to separate the asymptotically non-vanishing, constant part of $V(x)$ by defining $V(x) = V_{\text{inf}} + \hat{V}(x)$ where V_{inf} is diagonal and contains the constant mass splittings while $\hat{V}(x \rightarrow \infty) \rightarrow 0$. Further the matrix $\chi_l(x)$ specifically refers in the following to the matrix that contains the N regular radial wave-function solutions in its columns, subject to the initial conditions given in (2.50). Our first step in following [97] consists in the ansatz⁸

$$[\chi_l(x)]_{ai} = f_a(x) \alpha_{ai}(x) - g_a(x) \beta_{ai}(x) \quad (\text{no sum over } a), \quad (8.38)$$

where the $2N$ functions f_a, g_a are known analytic solutions of simplified decoupled second order differential equations and $\alpha(x)$ and $\beta(x)$ denote matrix-valued x -dependent functions (hence ‘variable phases’). In our application as well as in [97] the functions f_a, g_a are solutions to the N decoupled free Schrödinger equations

$$h_a''(x) = \left(\frac{l(l+1)}{x^2} - \hat{k}_a^2 \right) h_a(x), \quad (8.39)$$

with $h_a = f_a, g_a$, and the dimensionless wave numbers $\hat{k}_a = \sqrt{1 - \delta M_a/E}$. We choose the free solutions f_a, g_a as the following linear combinations of regular $\sqrt{x} J_{l+1/2}(x)$ and

⁸For a better readability we suppress the label l that specifies the partial-wave state on the functions f_a, g_a, α_{ai} and β_{ai} throughout this section.

irregular $\sqrt{x}Y_{l+1/2}(x)$ Bessel functions,

$$f_a(x) = \sqrt{\frac{\pi x}{2}} J_{l+1/2}(\hat{k}_a x), \quad g_a(x) = -\sqrt{\frac{\pi x}{2}} \left(Y_{l+1/2}(\hat{k}_a x) - iJ_{l+1/2}(\hat{k}_a x) \right). \quad (8.40)$$

From the asymptotic behaviour of the Bessel functions in the limit $r \rightarrow 0$ we obtain

$$f_a(x \rightarrow 0) \rightarrow \sqrt{\frac{\pi}{2}} \frac{(\hat{k}_a/2)^{l+1/2}}{\Gamma(l + \frac{3}{2})} x^{l+1}, \quad g_a(x \rightarrow 0) \rightarrow \sqrt{\frac{1}{2\pi}} \frac{\Gamma(l + 1/2)}{(\hat{k}_a/2)^{l+1/2}} x^{-l}, \quad (8.41)$$

which allows to check that the Wronskian of each of the N pairs f_a, g_a of free solutions is normalised to one,

$$f'_a(x) g_a - f_a(x) g'_a = 1 \quad (\text{no sum over } a). \quad (8.42)$$

With the ansatz (8.38) we have doubled the set of unknown functions. This artificially introduced freedom is eliminated by imposing the conditions

$$f_a(x) \alpha'_{ab}(x) - g_a(x) \beta'_{ab}(x) = 0 \quad (\text{no sum over } a). \quad (8.43)$$

From the above definitions we can now obtain a set of coupled first order differential equations for the matrix-valued functions $\alpha(x)$ and $\beta(x)$,

$$\alpha'_{ai}(x) = g_a \frac{\hat{V}_{ab}}{E} (f_b(x) \alpha_{bi}(x) - g_b(x) \beta_{bi}(x)), \quad (8.44)$$

$$\beta'_{ai}(x) = f_a \frac{\hat{V}_{ab}}{E} (f_b(x) \alpha_{bi}(x) - g_b(x) \beta_{bi}(x)). \quad (8.45)$$

As these equations couple different components of $\alpha(x)$ and $\beta(x)$ the second step following [97] is the introduction of the matrix-valued function $\tilde{M}(x)$ defined through $\beta_{ai}(x) = \tilde{M}_{ab}(x) \alpha_{bi}(x)$. The first order differential equations for the components of \tilde{M} ,

$$\tilde{M}'_{ab}(x) = (f_a \delta_{an} - \tilde{M}_{an} g_n) \frac{\hat{V}_{nm}}{E} (f_m \delta_{mb} - g_m \tilde{M}_{mb}), \quad (8.46)$$

couple different components of $\tilde{M}(x)$ but do no longer involve components of the matrix $\alpha(x)$. Instead of solving the set of differential equations for \tilde{M} and subsequently for $\alpha(x)$ yet another pair of matrix-valued functions is now defined through

$$\tilde{N}_{ab} = f_a g_a \delta_{ab} - g_a \tilde{M}_{ab} g_b, \quad \tilde{\alpha}_{ai} = \frac{\alpha_{ai}}{g_a}, \quad (8.47)$$

that satisfy the first-order differential equations

$$\tilde{N}'_{ab} = \delta_{ab} + \left(\frac{g'_a}{g_a} + \frac{g'_b}{g_b} \right) \tilde{N}_{ab} - \tilde{N}_{ac} \frac{\hat{V}_{cd}}{E} \tilde{N}_{db}, \quad (8.48)$$

$$\tilde{\alpha}'_{ai} = Z_{ab} \tilde{\alpha}_{bi} \quad \text{with} \quad Z_{ab} \equiv -\frac{g'_a}{g_a} \delta_{ab} + \frac{\hat{V}_{ac}}{E} \tilde{N}_{cb}. \quad (8.49)$$

The initial conditions that we have imposed on $\chi_l(\hat{r})$ for \hat{r} close to zero in (2.50) translate into

$$\tilde{N}_{ab}(\hat{x}) = \frac{\hat{x}}{2l+1} \delta_{ab}, \quad \tilde{\alpha}_{ai}(\hat{x}) = \delta_{ai} \hat{x}^l, \quad (8.50)$$

with dimensionless $\hat{x} = m_{\text{LSP}} v \hat{r}$.

Up to here the described procedure was close to [97]. In the last step we now come back to our starting point, the determination of $U^{-1}(r_\infty)$. By making use of the various functions introduced above we obtain the relation

$$[\chi'_l(x)]_{ai} = \tilde{\alpha}_{ai}(x) + \frac{g'_a}{g_a} [\chi_l(x)]_{ai}, \quad (8.51)$$

which, as we will see in a few lines, allows us to relate $U_l(x \rightarrow \infty)$ to $\tilde{\alpha}(x \rightarrow \infty)$. First recall from the definition

$$\begin{aligned} U_{ai}(x) &= e^{i\hat{k}_a x} \left([\chi'_l(x)]_{ai} - i\hat{k}_a [\chi_l(x)]_{ai} \right) \\ &= e^{i\hat{k}_a x} \tilde{\alpha}_{ai} + e^{i\hat{k}_a x} \left(\frac{g'_a(x)}{g_a(x)} - i\hat{k}_a \right) [\chi_l(x)]_{ai}. \end{aligned} \quad (8.52)$$

The difference $g'_a(x)/g_a(x) - i\hat{k}_a$ vanishes for large x . Specifically for the cases $l = 0, 1$, which are relevant in our application to the NRMSSM, we have

$$\frac{g'_a(x)}{g_a(x)} - i\hat{k}_a = \begin{cases} 0 & l = 0 \\ -\frac{1}{x(1 - i\hat{k}_a x)} & l = 1 \end{cases}. \quad (8.53)$$

This implies that $U_l(x)$ and $\tilde{\alpha}(x)$ are asymptotically trivially related by

$$U_{lai}(x) \stackrel{x \rightarrow \infty}{\simeq} e^{i\hat{k}_a x} \tilde{\alpha}_{ai}(x), \quad (8.54)$$

and the matrix T_l^\dagger that occurs as ingredient in the definition of the Sommerfeld enhancement factor can be obtained from

$$[T^\dagger]_{ai} = [U^{-1}(x_\infty)]_{ai} = e^{-i\hat{k}_i x_\infty} [\tilde{\alpha}^{-1}(x_\infty)]_{ai}, \quad (8.55)$$

for sufficiently large x_∞ . The crucial improvement of the described procedure consists in the important observation that without having first to calculate and then to invert $\tilde{\alpha}(x)$, the matrix $\tilde{\alpha}^{-1}(x)$ can be directly obtained as a solution of the first-order differential equations

$$[\tilde{\alpha}^{-1'}(x)]_{ia} = -[\tilde{\alpha}^{-1}(x)]_{ib} Z_{ba}, \quad [\tilde{\alpha}^{-1}(\hat{x})]_{ia} = \delta_{ia} \hat{x}^{-l}, \quad (8.56)$$

which follow directly from (8.49), where also the definition of Z is given.

To summarise, the following three steps have to be performed in order to determine the Sommerfeld enhancement factors with the improved method:

- (1) Solve the first-order differential equations for \tilde{N}_{ab} in (8.48) with initial conditions specified in (8.50) for every $b = 1, \dots, N$.
- (2) Solve the first-order differential equations (8.56) in order to determine $\tilde{\alpha}^{-1}$.
- (3) Determine T^\dagger from (8.55) for several x_∞ and check (by varying and increasing x_∞) that T^\dagger is independent of x_∞ within a certain target accuracy.

In order to exemplify the need of and the actual improvement due to the ‘improved method’ we consider the Sommerfeld enhancements in the 1S_0 and $^3P_{\mathcal{J}}$ partial-wave annihilations of the $\chi_1^0\chi_1^0$ channel for a MSSM spectrum with wino-like χ_1^0 LSP. The χ_1^0 mass is given by $m_{\chi_1^0} = 2749.4$ GeV and the mass of its wino-like chargino partner reads $m_{\chi_1^\pm} = 2749.61$ GeV. The next-lightest χ^0/χ^\pm state χ_2^0 is bino-like and about 200 GeV heavier, $m_{\chi_2^0} = 2950.25$ GeV. We chose a velocity $v = 0.012$, slightly below the threshold for on-shell production of the $\chi_1^+\chi_1^-$ state. First the S - and P -wave Sommerfeld enhancements $S_{\chi_1^0\chi_1^0}[\hat{f}(^1S_0)]$ and $S_{\chi_1^0\chi_1^0}[\hat{f}(^3P_{\mathcal{J}})]$ are calculated as functions of x_∞ by using the ‘old method’ of Sec. 2.2 and keeping only the two states $\chi_1^0\chi_1^0$ and $\chi_1^+\chi_1^-$ in the Schrödinger equation and annihilation rates. The S -wave (P -wave) $S(x_\infty)$ is given by the dashed red curve in the upper left (right) plot in Fig. 8.2. After rapid variations of $S(x_\infty)$ in the region of small x_∞ – in the S -wave case with a peak structure – the respective functions $S(x_\infty)$ reach a plateau and stay at constant values $S(\infty)$, which determine the actual 1S_0 and $^3P_{\mathcal{J}}$ enhancement factors. If the about 400 GeV heavier and kinematically closed $\chi_1^0\chi_2^0$ state is now included in the Schrödinger equation and annihilation rates, the determination of $S(\infty)$ fails as can be seen from the solid blue curves in both upper plots in Fig. 8.2. For x_∞ slightly larger than 1 both functions $S(x_\infty)$ drop to 0 after a few spikes. A solution for larger x_∞ values where $S(x_\infty)$ should stabilise cannot be obtained. The two lowermost plots in Fig. 8.2 contain the results on $S(x_\infty)$ using the ‘improved method’. $S(x_\infty)$ can now be evolved for sufficiently large x_∞ also when the $\chi_1^0\chi_2^0$ state is included. In case of the 1S_0 wave enhancement in the lower left plot, the solid red and solid blue curves – corresponding to $S(x_\infty)$ for the case of two and three $\chi\chi$ -states in the Schrödinger equation and annihilation rates – cannot be distinguished on the scale of the plot. Indeed the obtained Sommerfeld enhancement values $S(\infty) = 199.59$ for the two $\chi\chi$ -state and $S(\infty) = 199.72$ for the three $\chi\chi$ -state case differ only by a tiny amount. A similar result is obtained in the case of the $^3P_{\mathcal{J}}$ enhancement factor. Also here the two solid red and blue curves for the two and three $\chi\chi$ -state case lie on top of each other and a plateau is reached for $x_\infty > 50$ with $S(x_\infty) \approx 4.31$. In the P -wave case we show in addition in the lower left plot the dashed curve that corresponds to the ‘old-method’ solution for the two $\chi\chi$ -state case. The agreement of all three curves for large x_∞ values is obvious but there is a visible deviation for $x_\infty < 10$. The deviation is due to the fact that the matrices U and α are trivially related only for $x \rightarrow \infty$, see (8.54). This implies that the Sommerfeld factors calculated in the ‘old’ and improved method agree in general only for sufficiently large x_∞ . While the agreement is exact for the S -wave case, the difference vanishes as $1/x_\infty^2$ for P -waves, as can be inferred from (8.53). As with the improved method there is no severe numerical restriction on the

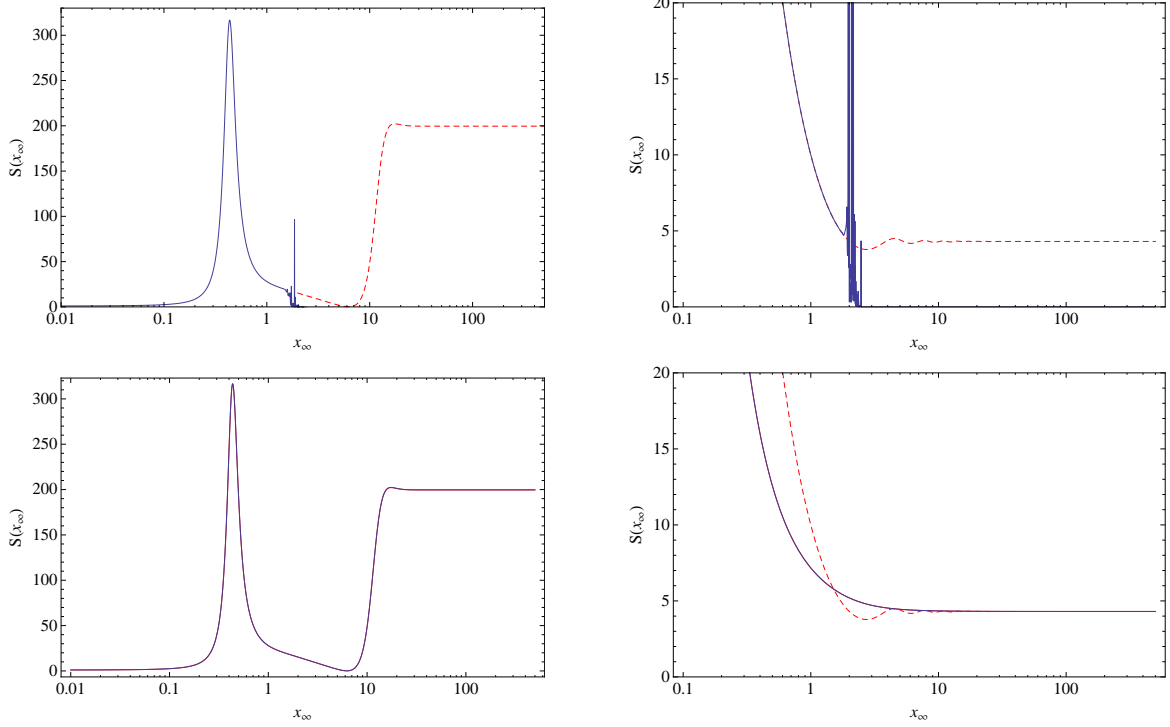


Figure 8.2: Comparison of the performances in determining the Sommerfeld enhancement factors by the method described at the end of Sec. 2.2 and by the improved method from Sec. 8.4. *Upper two plots:* The enhancement factors $S \equiv S_{\chi_1^0 \chi_1^0}[\hat{f}({}^1S_0)]$ (left plot) and $S \equiv S_{\chi_1^0 \chi_1^0}[\hat{f}({}^3P_J)]$ (right plot) as a function of x_∞ for $v = 0.012$ obtained from the prescription given at the end of Sec. 2.2. Relevant details on the corresponding MSSM spectrum with wino-like χ_1^0 are given in the text. The dashed red curves give $S(x_\infty)$ when only the two states $\chi_1^0 \chi_1^0$ and $\chi_1^+ \chi_1^-$ are kept. The solid blue curves result when in addition the state $\chi_1^0 \chi_2^0$ is included. In this case the evaluation fails in both the S - and P -wave case for $x_\infty > 2$ and no reliable result for the enhancements factors is obtained. *Lower two plots:* As in the upper row but now using the improved method to determine the enhancement factors. The solid red and solid blue curves are for the case of two and three $\chi\chi$ -channels in the Schrödinger equation and annihilation matrices and lie on top of each other on the scale of the plots. In addition the dashed red curve in the right plot gives the two $\chi\chi$ -state $S(x_\infty)$ as in the upper left plot.

value of x_∞ , the deviation can always be made sufficiently small. In the chosen wino-like χ_1^0 model this can be nicely seen in the lower left plot. Thus also the P -wave Sommerfeld enhancement factors can be determined within a sufficient accuracy with the improved method.

As the χ_2^0 state in the considered MSSM scenario here is bino-like, it is rather weakly coupled to the wino-like states χ_1^0, χ_1^\pm . It is therefore expected that including the $\chi_1^0 \chi_2^0$

state in the Schrödinger equation and annihilation rates has very little effect on the enhancements of the $\chi_1^0\chi_1^0$ channel as explicitly confirmed by the calculation in the improved method.

8.5 Second-derivative operators

In this section we come back to the derivation of the second relation presupposed in Sec. 8.1, which is (8.9), and that concerns the connection between the matrix elements of next-to-next-to-leading order ($\mathcal{P}_{\{e_4e_3\}\{e_2e_1\}}^{\chi\chi\rightarrow\chi\chi}(^{2S+1}S_S)$) and corresponding leading-order ($\mathcal{O}_{\{e_4e_3\}\{e_2e_1\}}^{\chi\chi\rightarrow\chi\chi}(^{2S+1}S_S)$) S -wave operators. Explicit expressions for the latter operators are collected in Tab. 5.3 and Tab. 5.2, respectively. In order to confirm (8.9) we show that

$$\langle 0|\chi_{e_2}^{c\dagger}\Gamma\left(-\frac{i}{2}\overleftrightarrow{\partial}\right)^2\chi_{e_1}|\chi_i\chi_j\rangle = \kappa_{ee'}^* \langle 0|\chi_{e_2'}^{c\dagger}\Gamma\chi_{e_1'}|\chi_i\chi_j\rangle. \quad (8.57)$$

Labels e, e' are compound indices referring to the two-particle states $\chi_{e_1}\chi_{e_2}$ and $\chi_{e_1'}\chi_{e_2'}$, respectively. The definition of κ has been given in (8.11). For completeness we quote it here again in compound index notation:

$$\kappa_{ee'} = \vec{p}_e^2 \delta_{ee'} + 2\mu_e\alpha_2 \sum_a m_{\phi_a} c_{ee'}^{(a)}. \quad (8.58)$$

Making use of (8.18) and (8.26), we can rewrite the left-hand side in (8.57) as

$$\langle 0|\chi_{e_2}^{c\dagger}\Gamma\left(-\frac{i}{2}\overleftrightarrow{\partial}\right)^2\chi_{e_1}|\chi_i\chi_j\rangle = \langle \xi_j^{c\dagger}\Gamma\xi_i \rangle \int \frac{d^3\vec{q}}{(2\pi)^3} \vec{q}^2 \left([\tilde{\psi}_E(\vec{q})]_{ei}^* + (-1)^S [\tilde{\psi}_E(\vec{q})]_{\bar{e}i}^* \right), \quad (8.59)$$

where the compound index \bar{e} refers to the state $\chi_{e_2}\chi_{e_1}$, while e , as noted before, is used to label the corresponding state $\chi_{e_1}\chi_{e_2}$. In order to simplify the integral on the right-hand side we apply the momentum-space version of the Schrödinger equation (8.28), which leads to

$$\begin{aligned} \int \frac{d^3\vec{q}}{(2\pi)^3} \vec{q}^2 [\tilde{\psi}_E(\vec{q})]_{ei}^* &= 2\mu_e(2m_{\text{LSP}} - M_e + E) \int \frac{d^3\vec{q}}{(2\pi)^3} [\tilde{\psi}_E(\vec{q})]_{ei}^* \\ &\quad - 2\mu_e \int \frac{d^3\vec{q}}{(2\pi)^3} \frac{d^3\vec{k}}{(2\pi)^3} [\hat{V}^{ee'}(\vec{k})]^* [\tilde{\psi}_E(\vec{q} - \vec{k})]_{e'i}^*. \end{aligned} \quad (8.60)$$

The explicit form of the momentum-space potentials, associated with gauge boson and light Higgs particle exchange, is given by

$$\hat{V}^{ee'}(\vec{k}) = 4\pi\alpha_2 \sum_a \frac{c_{ee'}^{(a)}}{k^2 + m_{\phi_a}^2}, \quad (8.61)$$

where m_{ϕ_a} denotes the mass of the exchanged mediator, and the corresponding coefficients $c_{ee'}^{(a)}$ are those collected in Tab. B.1. The sum extends over all gauge boson and

Higgs mediator particles that can be exchanged in a specific $\chi_{e_1}\chi_{e_2} \rightarrow \chi_{e'_1}\chi_{e'_2}$ potential scattering reaction.

We can factorise the two integrations in the second line of (8.60) by performing the shift $\vec{q} \rightarrow \vec{q} + \vec{k}$. Using dimensional regularisation, the linearly divergent integral over momentum \vec{k} can then be evaluated to the finite result

$$\int \frac{d^{d-1}\vec{k}}{(2\pi)^{d-1}} \frac{1}{\vec{k}^2 + m_\phi^2} \stackrel{d \rightarrow 4}{=} -\frac{m_\phi}{4\pi}. \quad (8.62)$$

Consequently, the right-hand side of (8.59) can be rewritten as

$$\begin{aligned} \langle 0 | \chi_{e_2}^{c\dagger} \left(-\frac{i}{2} \overleftrightarrow{\mathcal{D}} \right)^2 \chi_{e_1} | \chi_i \chi_j \rangle &= \langle \xi_j^{c\dagger} \Gamma \xi_i \rangle \int \frac{d^3\vec{q}}{(2\pi)^3} [\tilde{\psi}_E]_{e'i}^*(\vec{q}) \\ &\times \left[2\mu_e(2m_{\text{LSP}} - M_e + E)\delta_{e'e} + 2\mu_e\alpha_2 \sum_a m_{\phi_a} c_{ee'}^{(a)*} \right] + (-1)^S \{e \rightarrow \bar{e}\} \\ &= \langle \xi_j^{c\dagger} \Gamma \xi_i \rangle \int \frac{d^3\vec{q}}{(2\pi)^3} [\tilde{\psi}_E]_{e'i}^*(\vec{q}) \left(\kappa_{ee'}^* + (-1)^S \kappa_{\bar{e}e'}^* \right). \end{aligned} \quad (8.63)$$

In the last equality we have used that the relative momentum associated with the two-particle system $\chi_{e_1}\chi_{e_2}$, \vec{p}_e , is given by $\vec{p}_e^2 = 2\mu_e(2m_{\text{LSP}} - M_e + E)$, such that the term in square brackets in the second line yields $\kappa_{ee'}^*$, see (8.58). Next, let us write the integrand in (8.63) as

$$[\tilde{\psi}_E]_{e'i}^*(\vec{q}) \left(\kappa_{ee'}^* + (-1)^S \kappa_{\bar{e}e'}^* \right) = \kappa_{ee'}^* [\tilde{\psi}_E]_{e'i}^*(\vec{q}) + (-1)^S \kappa_{\bar{e}\bar{e}'}^* [\tilde{\psi}_E]_{\bar{e}'i}^*(\vec{q}), \quad (8.64)$$

where the index over which summation is carried out in the second term on the right-hand side has been renamed from e to \bar{e} . Since the potentials for $\chi_{e_1}\chi_{e_2} \rightarrow \chi_{e'_1}\chi_{e'_2}$ and $\chi_{e_2}\chi_{e_1} \rightarrow \chi_{e'_2}\chi_{e'_1}$ scattering involve the same coupling structure, the relation $c_{ee'}^{(a)} = c_{\bar{e}\bar{e}'}^{(a)}$ holds, which implies $\kappa_{\bar{e}\bar{e}'} = \kappa_{ee'}$. This allows to eventually obtain

$$\langle 0 | \chi_{e_2}^{c\dagger} \left(-\frac{i}{2} \overleftrightarrow{\mathcal{D}} \right)^2 \chi_{e_1} | \chi_i \chi_j \rangle = \kappa_{ee'}^* \langle \xi_j^{c\dagger} \Gamma \xi_i \rangle \int \frac{d^3\vec{q}}{(2\pi)^3} \left([\tilde{\psi}_E]_{e'i}^*(\vec{q}) + (-1)^S [\tilde{\psi}_E]_{\bar{e}'i}^*(\vec{q}) \right). \quad (8.65)$$

The summation in the above expression runs over the two-particle states indicated with the primed labels; while e' (related to $\chi_{e_1}\chi_{e_2}$) is varied, the associated label \bar{e}' (referring to $\chi_{e_2}\chi_{e_1}$) changes accordingly. The right-hand side of (8.65) agrees with the right-hand side in (8.57), such that the latter relation is proven.

With this relation between the matrix elements of next-to-next-to-leading order and leading-order S -wave operators it is possible to define the effective Wilson coefficients \hat{g}_κ , (8.9, 8.10), that come with the matrix elements of corresponding leading-order S -wave operators. Let us finally note that the second term in $\kappa_{ee'}$, (8.58), would be absent, if all exchanged mediator particles would be massless. In the NRMSSM only the potential from photon exchange involves a massless mediator, such that there are typically non-vanishing contributions to the second term related to electroweak gauge boson or Higgs exchange potentials.

In Sec. 2.1 we have argued that ladder amplitudes with exchange of massive mediators give only rise to enhanced radiative corrections, if the mediator mass is much smaller than the masses of the non-relativistic states in the ladder bars. Accordingly, in the NRMSSM only those contributions to the potentials are relevant that arise from gauge boson or Higgs particle ϕ exchange with mass $m_\phi \ll m_{\text{LSP}}$. As can be seen explicitly from the momentum space potential expression $\hat{V}(\vec{k})$ in (8.61), heavy ϕ_b exchange leads to strongly suppressed contributions to the full potential. Effectively, heavy mediator exchange thus results in a suppressed local $(\chi^\dagger\chi)^2$ potential interaction. The dominant contributions to (8.61) arise from light ϕ_a exchange with m_{ϕ_a} scaling as the non-relativistic 3-momentum $|\vec{k}| \sim m_{\text{LSP}}v$. This implies that the contributions to κ related to the light mediators ϕ_a are parametrically of the same order, since $M_e - 2m_{\text{LSP}} \sim E \sim m_{\text{LSP}}v^2$ and $\alpha_2 m_{\phi_a} \sim vm_{\text{EW}} \sim m_{\text{LSP}}v^2$. To the contrary, heavy Higgs boson contributions to the last term in κ can become large, although the corresponding potential interaction itself is irrelevant. The origin of such unphysical power-counting breaking contribution is the linearly divergent integral (8.62). The simplest solution to eliminate such unphysical terms is to decouple heavy Higgs bosons by not including them in the long-range NRMSSM potentials discussed in Chap. 7. The decoupling of the corresponding heavy states gives rise to the above mentioned local interaction terms, which count as $\mathcal{O}(v^2)$ corrections to the NRMSSM long-range potential interactions. As we have neglected $\mathcal{O}(v^2)$ corrections to the expressions associated with the long-range effects throughout, we consistently neglect the local potential interactions from heavy mediator exchange. In practical applications, given a specific MSSM spectrum, we eliminate Higgs boson exchange contributions to the potentials (and thus to κ) if the corresponding Higgs masses fulfil $m_H > 0.5 m_{\text{LSP}}$, unless $m_H < 100$ GeV. Let us remind however, that s -channel exchange of heavy Higgs states is taken into account in the absorptive parts of the Wilson coefficients.

8.6 Approximate treatment of heavy channels

In the preceding sections we have developed a formalism that allows for the calculation of Sommerfeld-corrected co-annihilation rates of non-relativistic, nearly mass-degenerate neutralino and chargino pairs. Consequently, when accounting for Sommerfeld corrections on the neutralino and chargino pair-annihilation cross sections in the χ_1^0 relic abundance calculation, we first have to determine the set of those neutralino and chargino pairs $\chi\chi$ for a given MSSM spectrum, which are nearly mass-degenerate with the lightest such pair, $\chi_1^0\chi_1^0$. For these “light” $\chi\chi$ states Sommerfeld-enhanced annihilation rates are subsequently calculated by means of (8.13) which implies solving corresponding multi-state Schrödinger equations. The latter take the potential and annihilation reactions among the non-relativistic and nearly mass-degenerate light $\chi\chi$ pairs with the same electric charge and within the same partial wave configuration into account.

Given a specific MSSM spectrum, there will be in general several “heavy” $\chi\chi$ pairs that do not fulfil the requirement to be nearly mass-degenerate with the $\chi_1^0\chi_1^0$. These

states cannot be part of the NRMSSM neutralino and chargino two-particle pairs. In principle we should thus exclude them a priori, such that they do not appear in the Schrödinger equations and NRMSSM Wilson coefficients. However when keeping those heavy $\chi\chi$ states in the EFT ladder diagrams there should be little effect on the enhancements of the light $\chi\chi$ channels, as the EFT two-particle propagators (8.17) for heavy states $(\chi\chi)_h$ with masses $M_h \gg 2m_{\text{LSP}}$ cannot go on-shell and therefore do not cause an enhancement effect. Consequently, it is possible to keep these heavy channels as internal states in the series of ladder-diagrams, as long as this does not lead in turn to numerical problems in the solution of the corresponding Schrödinger equations. Since the improved method described in Sec. 8.4 addresses and solves the issue of numerical instabilities associated with closed channels in the solution of the Schrödinger equation, there is from the point of view of numerical accuracy no reason why closed heavy channels could not be included in the potentials and annihilation matrices. In particular, there is the possibility that a heavy $\chi\chi$ state has a larger tree-level annihilation rate than the light two-particle channels, such that the annihilation contributions from the heavy channel can effectively enhance the annihilation rate of a light state. To include such effects it is desirable to keep closed heavy channels in the Schrödinger equations.

However, practical limitations on the number of channels that can be treated exactly in the Schrödinger equations are imposed by CPU time considerations. For example, if for a given MSSM spectrum and non-relativistic scattering energy E the calculation of the factor $S[\hat{f}(^1S_0)]$ for the $\chi_1^0\chi_1^0$ channel within method 2 takes 0.1 s if two channels are included in the corresponding matrix Schrödinger equation, the CPU time increases to 14 s for four included two-particle channels and becomes 5 min for 8 channels. Eventually, including all 14 neutral two-particle channels within method-2, the determination of this specific $S[\hat{f}(^1S_0)]$ takes nearly three hours.⁹ Even for fixed scattering energy there are typically several open channels for which Sommerfeld enhancement factors have to be calculated. Moreover, the determination of the thermally averaged annihilation cross sections entering the relic abundance calculation requires an integral over the scattering energy. In our application to the χ_1^0 relic abundance calculation, CPU considerations therefore restrict the number of two-particle channels that can be treated exactly in the Schrödinger equations.

In order to cover the case of strong annihilation contributions of closed heavy channels to a light channel's annihilation rate we allow that heavy channels appear in the last potential loop before annihilation in the series of ladder-diagrams with incoming light $\chi\chi$ state. However, we neglect heavy channels in all ladder bars apart from the last loop. This is motivated by non-relativistic power-counting, which shows that there is a suppression factor of the order $[E/(M_h - 2m_{\text{LSP}})]^a$ when a light two-particle channel in the ladder-diagram is replaced by a heavy channel, where $a = 1/2$ for the contribution in the last loop before annihilation and $a = 3/2$ for contributions inside the ladder. In the following we describe how the last potential loop contributions of heavy channels can be absorbed into an effective annihilation matrix. In the determination of the Som-

⁹The quoted numbers are strongly model and scattering energy $E = m_{\text{LSP}}v^2$ dependent. They are meant as an example to illustrate the effect of the strong increase in CPU time.

merfeld enhancement factors we thus solve the Schrödinger equations referring to the smaller number of light channels only and use in (8.34, 8.35) the yet to define effective annihilation matrices that include potential one-loop effects from heavy channels.

Let us start by dividing the N two-particle basis states $(\chi\chi)_a$ in a given charge sector into n light states treated exactly in the corresponding Schrödinger equations and $N - n$ heavy states that we only include in the last potential loop.¹⁰ In the following we use the compound index $h = \{h_{e_1} h_{e_2}\}$ to refer to one of the $N - n$ heavy states. Extending (8.18) to include the contribution from a heavy channel in the last potential loop before annihilation, we write

$$\begin{aligned} \langle 0 | \chi_{h_2}^{c\dagger} \Gamma K \left[-\frac{i}{2} \overleftrightarrow{\mathcal{D}} \right] \chi_{h_1} | \chi_i \chi_j \rangle &= \langle \xi_j^{c\dagger} \Gamma \xi_i \rangle \lim_{\hat{E} \rightarrow E} (-1) \left(\hat{E} - \frac{\vec{p}^2}{2\mu_{ij}} \right) \\ &\times \int \frac{d^3 \vec{q}}{(2\pi)^3} \int \frac{d^3 \vec{k}}{(2\pi)^3} K[\vec{q}] \hat{V}^{lh}(\vec{q} - \vec{k}) \frac{1}{E - [M_h - 2m_{\text{LSP}}] - \frac{\vec{q}^2}{2\mu_h}} \tilde{G}^{il}(\vec{p}, \vec{k}; \hat{E}) \\ &+ (-1)^{L+S} \{h \rightarrow \bar{h}\}, \end{aligned} \quad (8.66)$$

where summation over the compound index l that refers to the light states is implied. Further, \tilde{G}^{il} denotes the Green function for the Schrödinger operator associated with the $n \times n$ problem of light states. The momentum-space potential \hat{V}^{lh} encodes the potential scattering from the light states $(\chi\chi)_l$ to the heavy state $(\chi\chi)_h$ that undergoes annihilation. Let us now consider the operator matrix elements similar to (8.66), but this time for all and not only the heavy state operators, multiplied by the corresponding absorptive parts of Wilson coefficients, \hat{f} . Making use of (8.26) and taking the heavy channels in the last loop into account as in (8.66), we obtain

$$\begin{aligned} \hat{f}_{ee'} \langle 0 | \chi_{e_2}^{c\dagger} \Gamma K \left[-\frac{i}{2} \overleftrightarrow{\mathcal{D}} \right] \chi_{e_1} | \chi_i \chi_j \rangle &= 2 \langle \xi_j^{c\dagger} \Gamma \xi_i \rangle \int \frac{d^3 \vec{q}}{(2\pi)^3} [\tilde{\psi}_E]_{li}^*(\vec{q}) \\ &\times \left[\hat{f}_{le'} K[\vec{q}] + \hat{f}_{he'} \int \frac{d^3 \vec{k}}{(2\pi)^3} K[\vec{k}] \hat{V}^{lh}(\vec{k} - \vec{q}) \frac{1}{E - [M_h - 2m_{\text{LSP}}] - \frac{\vec{k}^2}{2\mu_h}} \right], \end{aligned} \quad (8.67)$$

where the index l runs over the n light and the index h over the $N - n$ heavy channels. The equality in (8.67) holds only if heavy channels contribute exclusively to the last loop of the ladder-amplitudes prior to annihilation. The form of the right-hand side in (8.67) suggests to rewrite and appropriately simplify the term in square brackets such that it eventually describes an effective annihilation matrix $\hat{f}_{le'}^{\text{eff}} K[\vec{q}]$. To this end we use the explicit form of the momentum-space potentials (8.61). The integration over

¹⁰Let us recall that we include all neutralino and chargino species in the determination of the relic density; however, for the co-annihilation cross sections of heavy neutralino and chargino pairs we use tree-level instead of Sommerfeld-enhanced rates. Contributions of the heavy channels to the thermally averaged effective rate $\langle \sigma_{\text{eff}} v \rangle$ are strongly Boltzmann-suppressed and thus typically negligible, unless there is a particular enhancement of the corresponding annihilation rate (such as for example in resonant annihilation), that compensates the Boltzmann suppression.

the loop-momentum \vec{k} can then be performed and the expression in square brackets in (8.67) is subsequently written as

$$\hat{f}_{W'}^{\text{eff, right}} = \hat{f}_{W'} + I_{lh} \hat{f}_{h\nu'}, \quad (8.68)$$

where summation over the compound index h referring to the heavy channels is carried out. For a better readability we have suppressed the $^{2S+1}L_J$ wave dependence of the Wilson coefficients $\hat{f} = \hat{f}^{(2S+1)L_J}$ and $\hat{f}^{\text{eff}} = \hat{f}^{\text{eff}(2S+1)L_J}$ in the last equations. The expression I_{lh} in the second term in (8.68) depends on the orbital angular momentum L of the corresponding partial wave configuration and is given by

$$I_{lh} = \alpha_2 \sum_a c_{lh}^{(a)}(-2\mu_h) I_L(2\mu_h(M_h - [2m_{\text{LSP}} + E] - i\epsilon), m_{\phi_a}, \vec{q}^2). \quad (8.69)$$

A dependence on the total spin enters through the coefficients $c^{(a)}$ of the spin-dependent leading-order potentials. In case of leading-order S -wave matrix elements, where $L = 0$ and $K[\vec{q}] = 1$, the function $I_{L=0}$ in (8.69) takes the following form:

$$I_0(y, m, \vec{q}^2) = \frac{i}{2\sqrt{\vec{q}^2}} \ln \frac{i(m^2 - y + \vec{q}^2) + 2m\sqrt{\vec{q}^2}}{i(m^2 - y - \vec{q}^2) + 2\sqrt{y}\vec{q}^2}. \quad (8.70)$$

In the P -wave case with $L = 1$ and $K[\vec{q}] = \vec{q}$ we obtain

$$I_1(y, m, \vec{q}^2) = \frac{\sqrt{y} - m}{2\vec{q}^2} + \frac{i(m^2 - y + \vec{q}^2)}{2(\vec{q}^2)^{3/2}} \ln \frac{i(m^2 - y + \vec{q}^2) + 2m\sqrt{\vec{q}^2}}{i(m^2 - y - \vec{q}^2) + 2\sqrt{y}\vec{q}^2}. \quad (8.71)$$

In (8.68) we have used the superscript label “right” to indicate that with (8.67) we have considered the first half of the corresponding full NRMSSM $\chi_i\chi_j$ forward scattering matrix element. Accounting in the same way for the second half, we eventually arrive at the following effective Wilson coefficients

$$\hat{f}_{W'}^{\text{eff}} = \hat{f}_{W'} + I_{lh} \hat{f}_{h\nu'} + I_{\nu'h}^* \hat{f}_{lh} + I_{lh} I_{\nu'h}^* \hat{f}_{hh'}. \quad (8.72)$$

The expression $\hat{f}_{W'}^{\text{eff}} = \hat{f}_{W'}^{\text{eff}(2S+1)L_J}$ encodes the hard (off-) diagonal tree-level annihilation reaction of light $\chi\chi$ states, $(\chi\chi)_l \rightarrow \sum X_A X_B \rightarrow (\chi\chi)_{\nu'}$, supplemented by potential one-loop corrections that involve the heavy channels $(\chi\chi)_h$ prior to annihilation into the SM and light Higgs particle final states $X_A X_B$. The result $\hat{f}_{W'}^{\text{eff, right}}$ in (8.68) is thus associated with the $(\chi\chi)_l$ tree-level annihilation amplitude plus the potential one-loop correction arising from heavy channels inside the loop before annihilation. If we take the index h in (8.68) to run over all $(\chi\chi)_a$ pairs in the corresponding charge sector and not only the heavy channels, then the expression $\hat{f}_{W'}^{\text{eff, right}}$ is related to the leading-order non-relativistic approximation to the full one-loop annihilation amplitude for incoming $(\chi\chi)_l$ state, which has also been obtained by direct expansion in [93].¹¹

¹¹It can be checked that the loop integrals $I_{S,P}$ defined in [93] are equal to $(2\pi|\vec{q}|) I_{0,1}$. Let us note that

While (8.72) introduces effective Wilson coefficients accounting for potential one-loop corrections from heavy channels, this expression still involves the factors I_{lh} and $I_{l'h}^*$, which in turn imply a dependence on the momentum \vec{q} of the last potential loop before annihilation. In the evaluation of (8.67) the knowledge of the full momentum-space wave function $\tilde{\psi}_E(\vec{q})$ would therefore be needed and not just the corresponding position-space expression and its derivative at the origin. However, we only want to absorb one-loop corrections of heavy channels $(\chi\chi)_h$ with mass-splittings $M_h - 2m_{\text{LSP}} \gg E$ into the effective Wilson coefficients in (8.72). The typical relative momentum \vec{q} over which the last potential-loop integration is carried out scales as $\vec{q}^2 \sim m_{\text{LSP}}v^2$, such that we can expand the integrals I_L in (8.70, 8.71) in $\sqrt{\vec{q}^2}/(M_h - 2m_{\text{LSP}}v^2)$. We keep only the leading-order terms in this expansion, in which case the expressions $I_{0,1}$ simplify to the following momentum independent terms

$$I_0(y, m, \vec{q}^2) \rightarrow \frac{1}{\sqrt{y} + m}, \quad I_1(y, m, \vec{q}^2) \rightarrow \frac{2\sqrt{y} + m}{3(\sqrt{y} + m)^2}. \quad (8.73)$$

Using these approximations in (8.69) we obtain

$$I_{lh|L=0} = -2\mu_h\alpha_2 \sum_a \frac{c_{lh}^{(a)}}{\sqrt{y_h} + m_{\phi_a}}, \quad (8.74)$$

$$I_{lh|L=1} = -2\mu_h\alpha_2 \sum_a c_{lh}^{(a)} \frac{2\sqrt{y_h} + m_{\phi_a}}{3(\sqrt{y_h} + m_{\phi_a})^2}, \quad (8.75)$$

where $y_h = 2\mu_h(M_h - [2m_{\text{LSP}} + E] - i\epsilon)$. Inserting these expressions in the definition (8.72) of the effective Wilson coefficients $\hat{f}_{ll'}^{\text{eff}}$ finally provides us with effective Wilson coefficients that can be used to obtain local effective annihilation matrices, following the prescriptions in Sec. 7.2.1. We will use these effective annihilation matrices in the Sommerfeld factors (8.34, 8.35) in order to incorporate effects from heavy channels in the last potential loop in the annihilation reactions of light incoming $(\chi\chi)_l$ pairs.

The adaption of the above steps to the case of second-derivative S -wave operators is somewhat more involved, since it requires the application of the equation of motion discussed in Sec. 8.5 to the factor $K[\vec{k}^2]$ in (8.67). In writing

$$\vec{k}^2 = 2\mu_h \left(2m_{\text{LSP}} + E - M_h - \left[2m_{\text{LSP}} + E - M_h - \frac{\vec{k}^2}{2\mu_h} \right] \right) \quad (8.76)$$

in [93] additional terms proportional to the mass differences between the incoming and the virtual χ s in the loop are kept in the non-relativistic expansion, originating from the numerator of the full one-loop amplitude. As we separate in our formalism the long-distance from the short-range physics, the latter mass difference terms can contribute to $\mathcal{O}(v^2)$ corrections to the long-distance part – which we neglect – or to $\mathcal{O}(v^2)$ corrections to the short-distance annihilations. We have kept the latter contributions by taking all mass-difference terms $\delta m, \delta \bar{m}$ in the Wilson coefficients into account, see Chaps. 5 and 6. It is worth to add that there are further sources of terms proportional to mass differences that have been neglected in [93] and in our approach. For instance, there is the anti-particle pole contribution in the q^0 -integration of the full amplitude which we neglect as it belongs to a class of $\mathcal{O}(v^2)$ corrections to the long-range interactions. In [93] these corrections from the anti-particle pole have been omitted as well.

and noting the corresponding steps in Sec. 8.5 we finally obtain the following result for the effective Wilson coefficients associated with second-derivative operators:

$$\hat{g}_{\kappa, l'l'}^{\text{eff}} = \hat{g}_{\kappa, l'l'} + \frac{1}{2} \left[I_{lh, D^2} \frac{\hat{g}_{hl'}}{M^2} + I_{l'h, D^2}^* \frac{\hat{g}_{lh}}{M^2} + I_{lh|L=0} I_{l'h', D^2}^* \frac{\hat{g}_{hh'}}{M^2} + I_{lh, D^2} I_{l'h'|L=0}^* \frac{\hat{g}_{hh'}}{M^2} \right]. \quad (8.77)$$

The expression I_{lh, D^2} introduced above reads

$$I_{lh, D^2} = 2\mu_h \alpha_2 \left((2m_{\text{LSP}} + E - M_h)(-2\mu_h) \sum_a \frac{c_{lh}^{(a)}}{\sqrt{y_h} + m_{\phi_a}} + \sum_a m_{\phi_a} c_{lh}^{(a)} \right). \quad (8.78)$$

Note that a dependence on the spin $S = 0, 1$ is implicit through the coefficients $c^{(a)}$ associated with the spin-dependent leading-order potentials (8.61). Further let us note that the mass scale M in each term in (8.77) is defined by the masses of the two $\chi\chi$ pairs specified by the indices of the accompanying Wilson coefficients \hat{g} . For the generic definition of this process-specific mass scale see (5.12).

This concludes the presentation of our EFT set-up, which allows to determine Sommerfeld-enhanced co-annihilation rates of a set of nearly mass-degenerate “light” $\chi\chi$ pairs including effects from heavy channels in the last potential loop before annihilation. In Chap. 9 we apply this formalism to the calculation of the χ_1^0 relic abundance including Sommerfeld enhancements, providing a detailed study for several MSSM benchmark scenarios. In that chapter we will also address the question how the neutralino and chargino two-particle states should be divided into light and heavy channels. If not noted otherwise, the potential one-loop corrections from heavy channels will be included in the analysis by using corresponding effective annihilation matrices obtained from (8.72) and (8.77) in the formula for the Sommerfeld enhancement factors. At the end of Chap. 9 we will additionally discuss the comparison of the relic abundance results when heavy channels are treated approximately in the last potential loop of corresponding co-annihilation rates with the respective result, where those heavy channels are taken into account exactly in the Schrödinger equations. In anticipation of results from Sec. 9.5 let us note that the perturbative treatment of effects from heavy states for the MSSM scenario studied therein gives a very good approximation to the results where the heavy states are considered exactly in the Schrödinger equations. From this we conclude that the approximate treatment of heavy states is often a good approximation to the result from full resummation. However, this does not imply that either of the two, the approximate or exact treatment, is a good approximation to the true one-loop corrections from heavy channels. Generically we cannot expect that we obtain a good approximation to the full one-loop results with heavy internal states, if we use the non-relativistic approximation in the potential region for the latter, because the non-relativistic expansion breaks down for large mass splitting terms $[M_h - 2m_{\text{LSP}}]$. Nevertheless, as noted before, heavy channel loops are at least suppressed by $(E/[M_h - 2m_{\text{LSP}}])^{1/2}$ with respect to the light channel contributions. As the impact of heavy states on the Sommerfeld enhancements of light

$(\chi\chi)_l$ channels is in any case rather small, we decide to include their effect by using the effective Wilson coefficients (8.72, 8.77).

Chapter 9

Benchmark models in the general MSSM

In the preceding chapters we have developed a non-relativistic MSSM effective theory framework, the NRMSSM, that allows to systematically address the calculation of enhanced radiative corrections in pair-annihilation rates of non-relativistic and nearly mass-degenerate neutralino and chargino states in the general MSSM. The focus has been on the construction of the effective theory and on a detailed description of the relevant technical aspects in the NRMSSM calculation of Sommerfeld-enhanced rates. Here we apply the framework to several well-motivated MSSM scenarios with heavy neutralino LSP and investigate in particular the impact of Sommerfeld enhancements on the χ_1^0 relic abundance calculation. The underlying physics effects are analysed in detail in each step of the calculation, which allows to illustrate the general use of our effective theory set-up applicable in the general MSSM. Furthermore, the question of viability of popular MSSM scenarios in light of a consistent treatment of the Sommerfeld effect can be addressed.

We choose to consider three scenarios taken from the set of Snowmass pMSSM benchmark models [98]. These models pass all constraints from so far unsuccessful SUSY searches at the LHC, additional collider, flavour and precision measurement bounds as well as constraints from dark matter direct detection experiments and indirect searches. The neutralino LSP relic abundance within these models, calculated from perturbative annihilation rates, is not larger than the WMAP bound, but can be smaller than the experimentally measured value. The latter allows for the case that neutralino dark matter does not make up all the cosmic cold dark matter. In addition to these benchmark scenarios we investigate the Sommerfeld enhancements in neutralino/chargino co-annihilations in a set of models interpolating between a scenario with almost pure-higgsino χ_1^0 to a wino-like χ_1^0 model. The MSSM spectra for the models on this “higgsino-to-wino” trajectory are generated with DarkSUSY [5]. As our work allows for the first time a consistent study of the Sommerfeld effect on the relic abundance calculation for models with mixed wino-higgsino neutralino LSP we provide an extensive discussion of the Sommerfeld effect in such a scenario.

We start our analysis in Sec. 9.1 with the investigation of a wino-like χ_1^0 benchmark model taken from the set of Snowmass pMSSM benchmark scenarios in [98]. Sec. 9.2 contains the analysis of a corresponding higgsino-like χ_1^0 Snowmass model. In both cases we compare to results obtained in the well-studied “pure” wino and higgsino scenarios where the χ_1^0 is assumed to be part of an unbroken $SU(2)_L$ triplet or two unbroken $SU(2)_L$ doublets. As Sommerfeld enhancements have been studied extensively in the particular case of a pure wino χ_1^0 in the literature, we address the question of the validity of conclusions inferred from these pure wino and higgsino scenarios to wino- and higgsino-like χ_1^0 spectra in the general MSSM. In Sec. 9.3 the effect of Sommerfeld enhancements in co-annihilations of wino-like neutralino and chargino states in a bino-like χ_1^0 pMSSM benchmark scenario is considered. A “higgsino-to-wino” trajectory is defined in Sec. 9.4, by introducing 13 models that interpolate between a higgsino- and wino-like χ_1^0 spectrum while the relic density calculated from perturbative rates is kept fixed. Our discussion here is focused on the spectra and the obtained relic abundances omitting particular details on the Sommerfeld enhanced co-annihilation cross sections. The specific features of the Sommerfeld effect for a mixed wino-higgsino χ_1^0 are subsequently studied in detail in Sec. 9.5, where the selected spectrum is one of the trajectory models of the preceding section.

9.1 Wino-like χ_1^0

Wino-like χ_1^0 dark matter arranges into an approximate $SU(2)_L$ fermion triplet together with the two chargino states χ_1^\pm . In the $SU(2)_L \times U(1)_Y$ symmetric limit the triplet would be assigned zero hypercharge. All states χ_1^0, χ_1^\pm share the same $\mathcal{O}(\text{TeV})$ mass scale, characterised by the wino mass parameter M_2 , $m_\chi \sim |M_2|$. As discussed in Sec. 4.3, electroweak symmetry-breaking introduces a small mass splitting between the neutral and the charged components of the triplet; the tree-level mass splitting happens to be very small, $\mathcal{O}(m_W^4/m_{\text{SUSY}}^3)$, and the one-loop radiative corrections dominate over the tree-level splitting.

A pMSSM scenario with wino-like χ_1^0 is provided by the SUSY spectrum with model ID 2392587 in [98]. A measure for the wino fraction of a given neutralino LSP state is the square of the modulus of the neutralino mixing-matrix entry Z_{N21} . For the Snowmass pMSSM scenario 2392587 the χ_1^0 constitutes a rather pure wino, $|Z_{N21}|^2 = 0.999$, with a mass $m_{\text{LSP}} \equiv m_{\chi_1^0} = 1650.664 \text{ GeV}$. The mass of the chargino partner χ_1^\pm is given by $m_{\chi_1^\pm} = 1650.819 \text{ GeV}$, such that $\delta m = m_{\chi_1^\pm} - m_{\chi_1^0}$ turns out to be 0.155 GeV . Without any modification these values are taken from the spectrum card provided by [98] where the mass parameters refer to the $\overline{\text{DR}}$ -scheme. As the precise sub $\mathcal{O}(\text{GeV})$ -scale $\chi_1^0 \chi_1^\pm$ mass splitting is an essential ingredient in the calculation of the Sommerfeld-enhanced co-annihilation rates we have to assume an accuracy of the given mass spectrum at the level of 10 MeV for our analysis of the Sommerfeld enhancement in the pMSSM scenario to be meaningful. A rigorous analysis of Sommerfeld-enhanced co-annihilation processes in a given model should refer to the on-shell mass spectrum of the neutralino and chargino

states instead of $\overline{\text{DR}}$ -parameters, where a sub-GeV scale precision of the mass parameters requires the consideration of one-loop renormalised quantities. For reference purposes, however, we do not modify the publicly available $\overline{\text{DR}}$ -spectra of [98] for all three pMSSM models discussed here.

In the context of minimal dark matter models [28], wino dark matter is realised as the neutral component of an approximate $SU(2)_L$ triplet state as well. In contrast to MSSM scenarios with wino-like χ_1^0 , the $SU(2)_L$ triplet minimal dark matter models (referred to as “pure-wino” models in the following) consider interactions of the dark matter states with the electroweak gauge bosons only. Two-particle final states in minimal dark matter pair-annihilation reactions are hence given by pairs of SM particles and the SM Higgs boson and all heavier states above the minimal dark matter mass scale are treated as completely decoupled. Such a scenario agrees with the decoupling limit in a MSSM scenario with wino-like χ_1^0 LSP. To the contrary, the wino-like pMSSM model that we consider here features non-decoupled sfermion states at the 2 – 3 TeV scale with non-vanishing couplings of the χ_1^0 and χ_1^\pm to sfermions and to the (heavier) Higgs states, though the latter are suppressed with respect to the couplings to the gauge bosons, because any Higgs- $\chi\chi$ (tree-level) interaction takes place between the gaugino-component of the one and the higgsino-component of the other χ . As the higgsino-like neutralino and chargino states in the pMSSM model under consideration reside at the $\mathcal{O}(3.9 \text{ TeV})$ scale any Higgs- $\chi\chi$ interaction plays a sub-dominant role in our analysis of pair-annihilation reactions of the wino-like χ_1^0 and χ_1^\pm states. Due to the non-decoupled sfermion states though, some annihilation rates in the wino-like χ_1^0 pMSSM scenario are reduced with respect to the pure-wino dark matter case.

In the calculation of the relic abundance we have to take into account all possible two-particle co-annihilation reactions between the (approximate) $SU(2)_L$ triplet states χ_1^0, χ_1^\pm . In addition, in the pMSSM model 2392587, the bino-like χ_2^0 is only about 8% heavier than the χ_1^0 , $m_{\chi_2^0} = 1781.37 \text{ GeV}$. Hence the χ_2^0 is a potentially relevant co-annihilating particle as well. It turns out though, that this state eventually plays no role for the relic abundance, as the corresponding cross sections are strongly suppressed with respect to those of the wino-like particles χ_1^0 and χ_1^\pm due to the much weaker couplings of the bino-like χ^0 to gauge bosons and to the remaining χ^0/χ^\pm states. All remaining heavier particles in the pMSSM scenario lie above the 2 TeV scale, so they are already Boltzmann suppressed and hence practically irrelevant during the χ_1^0 freeze-out.

Sommerfeld enhancements on the co-annihilation rates are taken into account by including in the multi-state Schrödinger equations, discussed in context of the NRMSSM in Chap. 8, all $\chi\chi$ two-particle states with mass smaller than $M_{\text{max}} = 2m_{\chi_1^0} + m_{\chi_1^0}v_{\text{max}}^2$, where we set $v_{\text{max}} = 1/3$. This choice is motivated by the fact that v_{max} roughly corresponds to the χ_1^0 's mean velocity around freeze-out, hence these states are potentially relevant for co-annihilation processes, and can still be produced on-shell in a $\chi_1^0\chi_1^0$ scattering process. The remaining heavier two-particle states with mass above M_{max} are included in the computation of the Sommerfeld enhancement of the lighter states in the last loop before the annihilation, following the method developed in Sec. 8.6. The $\chi\chi$ -channels, whose long-distance interactions are treated exactly, can be classified ac-

ording to their total electric charge. The sector of neutral two-particle states comprises the $\chi_1^0\chi_1^0$ and $\chi_1^+\chi_1^-$ channels. In the pMSSM scenario considered here, this sector contains in addition the $\chi_1^0\chi_2^0$ state. In the single-charged and the double-charged sectors of a pure-wino dark matter scenario there is only one state present in each sector, $\chi_1^0\chi_1^+$ ($\chi_1^0\chi_1^-$) and $\chi_1^+\chi_1^+$ ($\chi_1^-\chi_1^-$), whereas in the pMSSM scenario we have to add in addition a second state with χ_1^0 replaced by χ_2^0 , in agreement with the rule above that defines the channels which enter the Schrödinger equation. Since the bino-like neutralino essentially neither couples to the wino-like particles nor to gauge bosons, and because sfermion states are rather heavy, potential interactions as well as tree-level annihilation reactions involving the bino-like χ_2^0 are strongly suppressed with respect to the corresponding interactions with wino-like particles χ_1^0, χ_1^\pm . As a consequence, χ_2^0 plays essentially no role for Sommerfeld enhancements, and we focus the discussion that follows on the channels built from the wino-like χ_1^0 and χ_1^\pm states only.

In each of the charge sectors long-range interactions due to potential exchange of electroweak gauge bosons, photons and light Higgses are present.¹ Potential W -boson exchange leads to a Yukawa potential interaction that induces transitions between the $\chi_1^0\chi_1^0$ and the $\chi_1^+\chi_1^-$ state in the neutral sector. Hence the part of the neutral sector consisting of the channels $\chi_1^0\chi_1^0$ and $\chi_1^+\chi_1^-$ is characterised by a potential matrix with non-vanishing off-diagonals which are of the same strength as the diagonal entries. As the incoming $\chi_1^0\chi_1^0$ pair cannot build a 3S_1 or 1P_1 state, potential interactions are responsible for transitions between the two neutral states $\chi_1^0\chi_1^0$ and $\chi_1^+\chi_1^-$ in a 1S_0 or 3P_J configuration.

In Fig. 9.1 we plot the enhancement $(\sigma^{\text{SF}v})/(\sigma^{\text{pert}v})$ of annihilation rates including long-range interactions, $\sigma^{\text{SF}v} \equiv \sigma^{\text{SF}}v_{\text{rel}}$, with respect to the perturbative tree-level result, $\sigma^{\text{pert}v} \equiv \sigma^{\text{pert}}v_{\text{rel}}$, for the two-particle states $\chi_1^0\chi_1^0$ and $\chi_1^+\chi_1^-$ in the neutral sector of the model as a function of the velocity v_{LSP} of the incoming χ_1^0 's in their centre-of-mass frame. We define the velocity v_{LSP} by $\sqrt{s} = 2m_{\chi_1^0} + m_{\chi_1^0}v_{\text{LSP}}^2$ with \sqrt{s} the available centre-of-mass energy. The spin-averaged inclusive tree-level annihilation rates $\sigma^{\text{pert}v}$ are calculated in the non-relativistic approximation

$$\sigma^{\text{pert}v} = a + bv^2 + \mathcal{O}(v^4), \quad (9.1)$$

and are obtained from the appropriate sum over the exclusive rates in (6.24) including $\mathcal{O}(v_{\text{rel}}^2)$ effects. In case of the $\chi_1^0\chi_1^0$ state the relation between the relative velocity v and v_{LSP} is given by $v = 2v_{\text{LSP}}$. For $\chi_1^+\chi_1^-$ annihilation reactions the relation is

$$v = 2 \text{Re} \sqrt{m_{\chi_1^0}/m_{\chi_1^+} [v_{\text{LSP}}^2 - 2\delta m/m_{\chi_1^0}]}. \quad (9.2)$$

The coefficients a and b in (9.1) are determined from the absorptive part of partial-wave decomposed Wilson coefficients as discussed in Chap. 6. In case of the Sommerfeld-

¹Potentials from Higgs exchange are negligible compared to the leading contributions from gauge bosons in the pMSSM scenario with wino-like χ_1^0 , again because in any Higgs- $\chi\chi$ vertex the gaugino component of one χ is coupled to the higgsino component of the other χ . In the wino-like χ_1^0 Snowmass model the lowest-lying χ 's relevant for the Sommerfeld effect are rather pure wino-like χ^0 and χ^\pm states with a very small higgsino component.

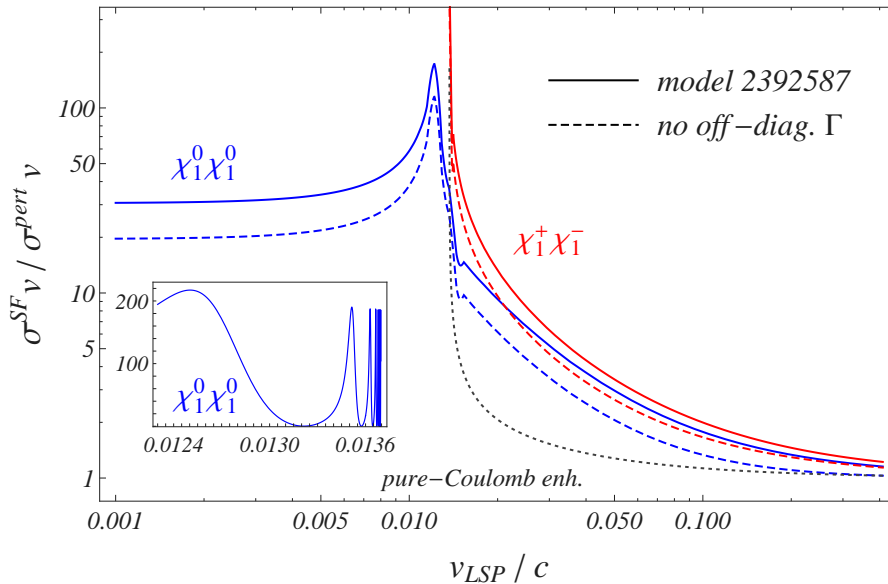


Figure 9.1: The enhancement of the $\chi_1^0\chi_1^0$ and $\chi_1^+\chi_1^-$ annihilation cross sections for Snowmass model 2392587 relative to the perturbative tree-level rate, $(\sigma^{\text{SF}}v)/(\sigma^{\text{pert}}v)$. The solid lines refer to the calculation of the Sommerfeld-enhanced rates with off-diagonal entries in the annihilation matrices Γ properly included. The dashed curves show the enhancement with respect to the perturbative cross sections when off-diagonal annihilation rates are not considered. The dotted curve labelled “pure-Coulomb enh.” shows the enhancement from photon exchange only in the $\chi_1^+\chi_1^-$ channel.

enhanced rates $\sigma^{\text{SF}}v$ each partial wave contribution to the tree-level cross section (9.1) gets multiplied by an enhancement factor related to the two-particle wave-function of the respective incoming state, see (8.13). Unless otherwise stated, Sommerfeld-enhanced results include the one-loop corrections from heavy $\chi\chi$ -states in the last potential loop, following the approximation discussed in Sec. 8.6. The results for the wino-like pMSSM scenario hence include perturbative corrections from heavy $\chi\chi$ -pairs involving the higgsino-like $\chi_{3,4}^0$ and χ_2^\pm particles. The effects of the latter nevertheless amount only to a negligible per mil level deviation on $\sigma^{\text{SF}}v$. This can be traced back to the fact that the higgsino states lie at the rather high mass scale of around 3.9 TeV and thus are basically decoupled. The $(\sigma^{\text{SF}}v)/(\sigma^{\text{pert}}v)$ curves in Fig. 9.1 show some characteristic features, which we describe next. As there is a small mass splitting between the χ_1^0 and the χ_1^\pm , the threshold for the on-shell production of the heavier neutral state $\chi_1^+\chi_1^-$ opens at $v_{\text{LSP}}/c \simeq 0.014$. Well below this threshold, the enhancement for the $\chi_1^0\chi_1^0$ system is velocity-independent and of $\mathcal{O}(10)$. This saturation effect is characteristic for Yukawa-type interactions in the kinematic regime where the relative momentum of the incoming state is well below the mass scale of the mediator: this is the case for the $\chi_1^0\chi_1^0$ state at very small velocities, where off-diagonal Yukawa potentials are generated by W -boson

exchange with $m_{\chi_1^0} v_{\text{LSP}} \ll m_W$. The actual strength of the enhancement is, however, a combined effect of the off-diagonal Yukawa potential from W -exchange that allows for $\chi_1^0 \chi_1^0 \rightarrow \chi_1^+ \chi_1^-$ transitions and the QED Coulomb interaction in the (kinematically closed) $\chi_1^+ \chi_1^-$ channel. At velocities v_{LSP} just below the $\chi_1^+ \chi_1^-$ threshold resonances in the $\chi_1^0 \chi_1^0$ channel can be observed. While the main plot in Fig. 9.1 displays a curve smoothed over this region, we show in the small sub-figure a close-up of the resonance pattern. The existence of resonance enhancements at the threshold of a heavier channel is well-known and has been described for instance in [36]. However, opposed to the pattern in the close-up in Fig. 9.1 no oscillating behaviour was found in [36], as only Yukawa potentials were considered. In fact the oscillatory pattern is related to the photon exchange in the $\chi_1^+ \chi_1^-$ subsystem. Going to even larger velocities, above the $\chi_1^+ \chi_1^-$ threshold, the enhancement in the $\chi_1^0 \chi_1^0$ channel decreases, approaching one as we depart from the non-relativistic regime. Turning to the enhancement in the $\chi_1^+ \chi_1^-$ channel, it shows quite a different behaviour right above its threshold compared to the $\chi_1^0 \chi_1^0$ system at small velocities: instead of approaching a constant value, the enhancement factor for $\chi_1^+ \chi_1^-$ rises increasingly as the velocities of the χ_1^\pm get smaller. Such a behaviour is expected in the presence of long-range Coulomb-potential interactions, where the enhancement does not saturate because the mediator is massless. Indeed, the photon exchange between the charged constituents of the neutral $\chi_1^+ \chi_1^-$ pair dominates the potential interactions in the regime of very small velocities: the Yukawa potentials become very short-ranged and thus negligible compared to the Coulomb-interaction. The dotted (black) curve in Fig. 9.1 displays the enhancement factor in the $\chi_1^+ \chi_1^-$ system arising from Coulomb interactions due to photon exchange only. For small velocities the pure-Coulomb enhancement factor diverges as $1/v_{\chi_1^+}$. The true enhancement curve, that involves all potential interactions affecting the $\chi_1^+ \chi_1^-$ system asymptotically reaches this Coulomb-like behaviour for velocities directly above the $\chi_1^+ \chi_1^-$ threshold.² For larger velocities in the $\chi_1^+ \chi_1^-$ system the presence of the Yukawa potentials leads to a larger enhancement than in case of Coulomb interactions only.

The dashed curves in Fig. 9.1 show the enhancements $(\sigma^{\text{SF}}v)/(\sigma^{\text{pert}}v)$ for the $\chi_1^0 \chi_1^0$ and $\chi_1^+ \chi_1^-$ states when off-diagonal terms in the annihilation matrices are (incorrectly) left out. This can lead to a $\lesssim 30\%$ underestimation of the actual enhancement in the $\chi_1^0 \chi_1^0$ channel. The effect is less pronounced for the $\chi_1^+ \chi_1^-$ channel, as in this case the cross section also gets significant contributions from 3S_1 annihilations and not just from 1S_0 ones. As the 3S_1 sector is purely diagonal, the effect of off-diagonals, relevant in the case of 1S_0 wave annihilations, becomes milder for the spin-averaged total cross section $\sigma^{\text{SF}}v$. It is worth to stress that the overall order of magnitude of the enhancements is $\mathcal{O}(10)$, and becomes $\mathcal{O}(10^2)$ in the resonance region around the $\chi_1^+ \chi_1^-$ threshold.

The quantity that enters the Boltzmann equation for the neutralino number density is the thermally averaged effective annihilation rate $\langle \sigma_{\text{eff}} v \rangle$. Fig. 9.2 shows $\langle \sigma_{\text{eff}} v \rangle$

²Note that in spite of the $\propto 1/v_{\chi_1^+}$ divergence, the enhanced cross sections lead to a finite result in the average over the thermal velocity distribution due to the $v_{\chi_1^+}^2$ term in the integration measure, $\int_{\mathbb{R}^3} d^3 \vec{v}_{\chi_1^+} = \int d\Omega \int_0^\infty dv_{\chi_1^+} v_{\chi_1^+}^2$.

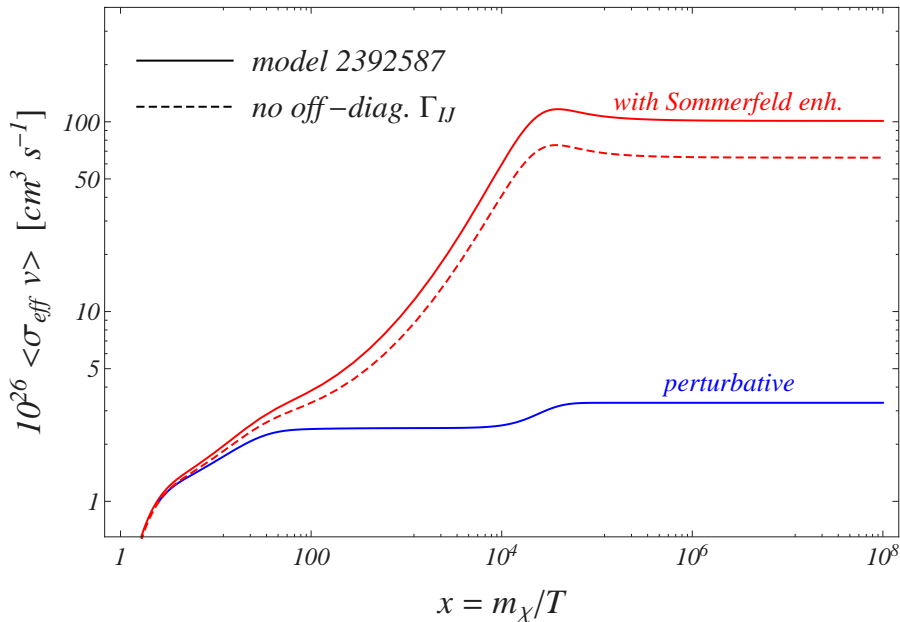


Figure 9.2: The thermally averaged effective annihilation rate $\langle \sigma_{\text{eff}} v \rangle$ as a function of the scaled inverse temperature $x = m_{\chi_1^0}/T$ in case of Snowmass model 2392587. The two upper (red) curves correspond to the Sommerfeld-enhanced annihilation cross sections including (solid line) or neglecting (dashed line) the off-diagonals in the annihilation matrices. The lower (blue) curve represents $\langle \sigma_{\text{eff}} v \rangle$ obtained from perturbative (tree-level) cross sections.

as defined in (3.37) as a function of the inverse scaled temperature $x = m_{\chi_1^0}/T$. The lower solid (blue) curve represents the perturbative (tree-level) annihilation rates while the upper solid and the dashed (red) lines refer to Sommerfeld-enhanced cross sections including and neglecting off-diagonal annihilation rates, respectively. The plot can be divided into several regions with different characteristics. Let us first note that for $x \lesssim 10$ the depicted behaviour of $\langle \sigma_{\text{eff}} v \rangle$ is unphysical. The mean velocity of the annihilating particles in the plasma scales as $\sqrt{1/x}$ and hence is no longer non-relativistic for $x \lesssim 10$ while the results of our framework strictly apply only to non-relativistic $\chi\chi$ pair-annihilations, *i.e.* for $x \gtrsim 10$. Around $x \sim 20$ the annihilation rates of χ_1^0 and χ_1^\pm can no longer maintain chemical equilibrium and the particles start to decouple from the thermal plasma. Hence only the region above $x \sim 20$ is important for the calculation of the relic abundance. Around $x \gtrsim 10^4$ the number densities of the χ_1^\pm are so strongly Boltzmann suppressed with respect to the χ_1^0 number density despite the small mass splitting that the rates of the charginos basically play no role in the effective rate $\langle \sigma_{\text{eff}} v \rangle$, which is then essentially given by $\chi_1^0 \chi_1^0$ annihilations. Note that we can estimate the point of chargino decoupling between $x \sim 10^4 - 10^5$ from the ratio of the Boltzmann distributions $n_{\chi_1^\pm}/n_{\chi_1^0} \propto \exp(-\delta m/m_{\chi_1^0} x)$, taking the $\mathcal{O}(10^{-1} \text{ GeV})$ mass splitting into

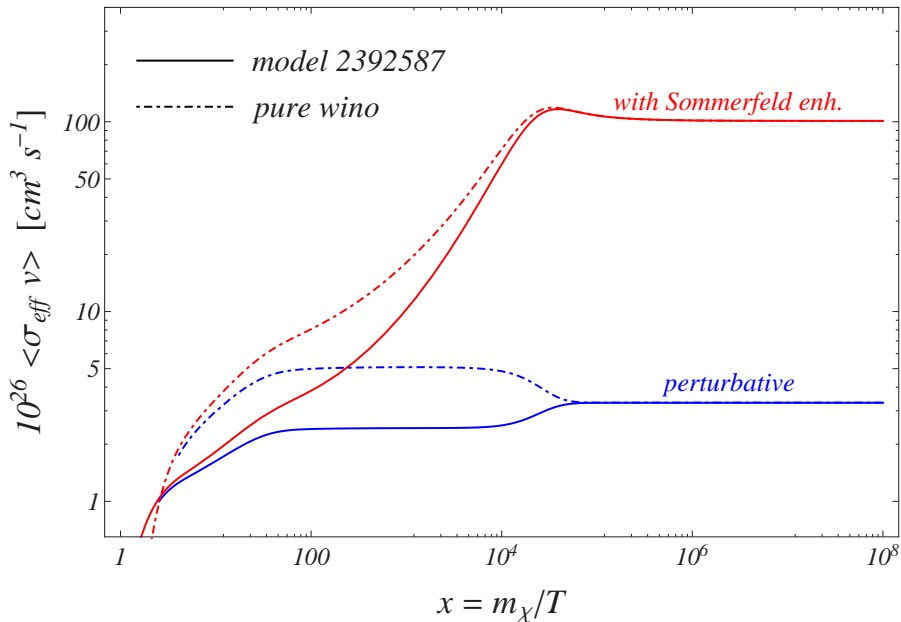


Figure 9.3: Thermally averaged effective annihilation rates $\langle \sigma_{\text{eff}} v \rangle$ as a function of the scaled inverse temperature $x = m_{\chi_1^0}/T$. The two upper (red) curves refer to a calculation with Sommerfeld-enhanced cross sections while the two lower (blue) curves represent the perturbative results. Solid lines correspond to the Snowmass pMSSM scenario 2392587 and dot-dashed curves show the results for the pure-wino scenario.

account. After χ_1^\pm decoupling, $\langle \sigma_{\text{eff}} v \rangle$ including the Sommerfeld enhancements becomes constant, which we can infer from the constant enhancement factor for the $\chi_1^0 \chi_1^0$ system for very low velocities shown in Fig. 9.1. Before χ_1^\pm decoupling, $\langle \sigma_{\text{eff}} v \rangle$ including the Sommerfeld enhancements rises with increasing x due to the contributions from the charginos but also due to the velocity-dependent enhancement on the $\chi_1^0 \chi_1^0$ system itself for larger relative velocities. On the contrary, the perturbatively determined $\langle \sigma_{\text{eff}} v \rangle$ shows a constant behaviour before and after χ_1^\pm decoupling with a rise only around the decoupling region; the contributions that dominate the perturbative cross sections in the non-relativistic regime are the velocity-independent leading-order S -wave terms.

Fig. 9.3 compares the thermally averaged effective rates $\langle \sigma_{\text{eff}} v \rangle$ as calculated from the wino-like pMSSM scenario and from a pure-wino $SU(2)_L$ triplet minimal dark matter model with the same χ_1^0 mass. In the pure-wino model the mass splitting between the χ_1^0 and χ_1^\pm has to be kept in the Schrödinger equation as it is of the same order as the non-relativistic kinetic energy and the potentials. However in the hard annihilation rates the mass splitting is a subleading effect and is neglected; the annihilation matrices in the pure-wino model depend on the χ_1^0 mass only. Let us recall that we have given corresponding analytic expressions for the potential and annihilation matrices in the pure-wino model in Sec. 7.2.2. While the rates for $\chi_1^0 \chi_1^0$ annihilations agree at per mil

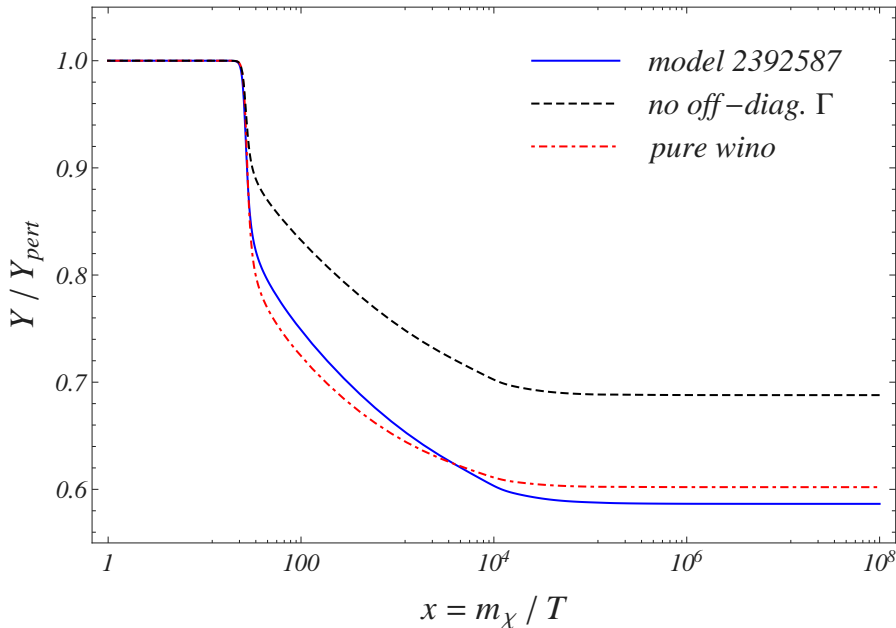


Figure 9.4: The ratios of the yield Y/Y_{pert} as a function of $x = m_{\chi_1^0}/T$, where Y is calculated including the Sommerfeld enhancement on the $\chi\chi$ annihilation rates while Y_{pert} just uses the perturbative ones. The solid (blue) and dashed (black) curves give the results for the Snowmass model 2392587 including and neglecting off-diagonal annihilation rates, respectively. The dot-dashed (red) curve corresponds to $Y/Y_{\text{pert}}(x)$ in the pure-wino model.

level, the cross sections involving χ_1^\pm are generically larger by factors of $\mathcal{O}(1)$ in the pure-wino model as compared to the pMSSM wino-like model. This can be mainly traced back to the destructive interference between t -channel sfermion and s -channel Z (and Higgs-boson) exchange amplitudes in $\chi_1^+\chi_1^- \rightarrow ff$ annihilations in the pMSSM scenario case, while the t -channel sfermion exchange amplitudes are absent in the pure-wino model. In addition the pure-wino case neglects all final state masses which in particular gives rise to larger annihilation rates into the $t\bar{t}$ and electroweak gauge boson final states as compared to the pMSSM scenario, where the non-vanishing masses of all SM particles are taken into account. This accounts for the deviation between the curves in Fig. 9.3 before χ_1^\pm decoupling.

Finally we consider the yield $Y = n/s$, defined in (3.22) as the ratio of the number density n of all co-annihilating particle species divided by the entropy density s in the cosmic co-moving frame. As discussed in Chap. 3, the dependence of the yield on the scaled inverse temperature $x = m_{\chi_1^0}/T$ is governed by the Boltzmann equation (3.28), and the χ_1^0 relic abundance is obtained from the yield today, see (3.31). In Fig. 9.4 we show the ratio of the yield Y calculated from Sommerfeld-enhanced cross sections in both the pMSSM and the pure-wino model to the corresponding results using perturbative

cross sections, Y_{pert} , as a function of x .

First note, that the denominator Y_{pert} in the ratio Y/Y_{pert} differs for the pMSSM and the pure-wino model, which is a consequence of the different effective rates $\langle\sigma_{\text{eff}}v\rangle$, see Fig. 9.3. Further, in case of the pMSSM scenario we show results corresponding to a calculation of Y including and neglecting off-diagonal annihilation rates. Around $x \sim 20$ the yields including Sommerfeld enhancements start to depart from the corresponding perturbative results; the enhanced rates delay the freeze-out of interactions, which leads to a reduction of the yield Y compared to the perturbative result Y_{pert} . The most drastic reduction in Y/Y_{pert} occurs between $x \sim 20$ and $x \sim 10^3$. In this region the enhancement factors on the cross sections are of $\mathcal{O}(10)$ (and not yet $\mathcal{O}(10^2)$ as for very large x), leading to Y/Y_{pert} values that deviate from 1 by a few 10%. For $x \gtrsim 10^5$ the fraction Y/Y_{pert} stays constant, meaning that at these temperatures the particle abundances in both the perturbative and Sommerfeld-enhanced calculation are frozen in. In case of the wino-like model we find that the relic densities calculated from the yield today read $\Omega^{\text{pert}}h^2 = 0.112$ and $\Omega^{\text{SF}}h^2 = 0.066$. Hence taking into account the Sommerfeld effect leads to a reduction of the calculated relic abundance of around 40%. On the other hand, neglecting the off-diagonal annihilations in the calculation of Sommerfeld-enhanced rates overestimates the relic density by 15% compared to the correct $\Omega^{\text{SF}}h^2$. Let us recall that the relic density calculated without corrections from heavy $\chi\chi$ -states in the last potential loop differs from the $\Omega^{\text{SF}}h^2$ value quoted above at most at the per mil level. Due to overall larger hard annihilation rates in the pure-wino model, the calculated relic density including Sommerfeld-enhanced rates turns out to be $\Omega_{\text{pure-w}}^{\text{SF}}h^2 = 0.034$, while the corresponding perturbative result is $\Omega_{\text{pure-w}}^{\text{pert}}h^2 = 0.056$.

A quantification of the theoretical error on such numbers is difficult. In conventional tree-level calculations of annihilation cross sections and the ensuing determination of relic densities neglecting radiative corrections, the results on the relic densities are supposed to be accurate to $\mathcal{O}(5\%)$ in the absence of enhanced corrections due to non-relativistic scattering, large Sudakov logarithms, or, potential strong-interaction effects for quark and gluon final states. The latter two restrictions still apply when the Sommerfeld effect is included. Further, our computation of the Sommerfeld effect itself neglects $\mathcal{O}(v^2)$ corrections to the scattering potentials as well as ordinary, non-enhanced corrections to the short-distance annihilation coefficients. Hence the accuracy of the Sommerfeld-corrected annihilation cross sections and relic densities is presumably again at the $\mathcal{O}(5\%)$ accuracy level at best.

9.2 Higgsino-like χ_1^0

The higgsino-like neutralino χ_1^0 arises as the lightest out of four mass eigenstates $\chi_{1,2}^0, \chi_1^\pm$ related to two $SU(2)_L$ fermion doublets. Note that the hypercharges of the two $SU(2)_L$ doublets are given by $Y = \pm 1/2$ respectively, which ensures the electric neutrality of the χ_1^0 . The common mass scale of the $\chi_{1,2}^0, \chi_1^\pm$ states is set by the $\mathcal{O}(\text{TeV})$ higgsino mass parameter, $m_\chi \sim |\mu|$. Electroweak symmetry breaking introduces a tree-level splitting

between $m_{\chi_1^0}$ and the masses of the three heavier states of $\mathcal{O}(m_Z^2/m_{\text{LSP}}) \sim \mathcal{O}(1 \text{ GeV})$, see the corresponding discussion in Sec. 4.3. This is considerably larger than the tree-level mass splitting in the wino-like χ_1^0 case; in particular loop corrections play a sub-dominant role in the mass splittings of higgsino-like neutralinos and charginos.

As an example of this class of models we consider the Snowmass pMSSM scenario with ID 1627006 [98], that features a higgsino-like χ_1^0 LSP with $m_{\chi_1^0} = 1172.31 \text{ GeV}$ and higgsino fraction $|Z_{31}|^2 + |Z_{41}|^2 = 0.98$. The heavier higgsino-like states χ_1^\pm and χ_2^0 have a mass splitting of $\delta m_{\chi_1^\pm} = 1.8 \text{ GeV}$ and $\delta m_{\chi_2^0} = 9.5 \text{ GeV}$ to the χ_1^0 mass. Again, all pMSSM spectrum parameters are taken without any modification from the corresponding Snowmass (slha) model-file 1627006 provided by [98].

As in Sec. 9.1, it is instructive to compare the pMSSM scenario with higgsino-like χ_1^0 and co-annihilating χ_2^0 and χ_1^\pm to a model with pure-higgsino $\chi_{1,2}^0, \chi_1^\pm$ states and completely decoupled sfermions and heavy Higgses. We refer to the latter scenario as “pure-higgsino” model; such model is also discussed in the context of Minimal Dark Matter [28]. Pure-Higgsino states interact only with the SM gauge bosons W^\pm, Z, γ but not with the Higgs bosons. The accessible final states in $2 \rightarrow 2$ co-annihilation reactions of pure higgsinos are hence given by particle pairs formed out of SM gauge bosons and fermions as well as of the (SM-like) Higgs h^0 , where all these SM particles are taken to be massless, and only SM gauge bosons and higgsinos appear as intermediate states in tree-level annihilations. The co-annihilation rates of the higgsino-like $\chi_{1,2}^0, \chi_1^\pm$ states in the pMSSM scenario 1627006 happen to be larger than the corresponding reactions in the pure-higgsino case. This can be traced back to the presence of non-decoupled sfermion and Higgs states in the higgsino-like χ_1^0 pMSSM model and in particular to non-decoupled wino-like states χ_3^0, χ_2^\pm at the scale of 1.6 TeV.

In the determination of the χ_1^0 relic abundance for this pMSSM scenario including co-annihilations only the higgsino-like states are relevant. Other heavier states are already sufficiently Boltzmann-suppressed during χ_1^0 freeze-out. Hence we neglect the co-annihilations of the lightest sfermion states $\tilde{\tau}_1$ and $\tilde{\nu}_3$, with masses around 1.44 TeV, although we include co-annihilation reactions of all heavier χ^0/χ^\pm states. Yet the latter have basically no effect on the χ_1^0 relic density, as their abundances are already sufficiently suppressed at χ_1^0 decoupling. Obviously, in the pure-higgsino scenario only the co-annihilations between the higgsino-like species $\chi_{1,2}^0, \chi_1^\pm$ are taken into account for the calculation of the relic abundance.

We consider Sommerfeld corrections to all co-annihilation rates between two higgsino-like particles in both the pMSSM scenario 1627006 and the pure-higgsino model by treating all channels built from the states $\chi_{1,2}^0, \chi_1^\pm$ exactly in the corresponding Schrödinger equations. Moreover, the remaining heavier χ^0/χ^\pm two-particle states in the higgsino-like pMSSM scenario are treated perturbatively in the last potential loop according to the method developed in Sec. 8.6. In case of the pure-higgsino model though, all heavier states are considered as completely decoupled. Dividing the co-annihilation reactions into sets corresponding to total electric charge, we identify a neutral sector with the four two-particle states $\chi_1^0\chi_1^0, \chi_1^0\chi_2^0, \chi_2^0\chi_2^0$ and $\chi_1^+\chi_1^-$. The single-positive (negative) charged sector contains the two states $\chi_1^0\chi_1^+, \chi_2^0\chi_1^+$ ($\chi_1^0\chi_1^-, \chi_2^0\chi_1^-$), whereas the double-positive (double-

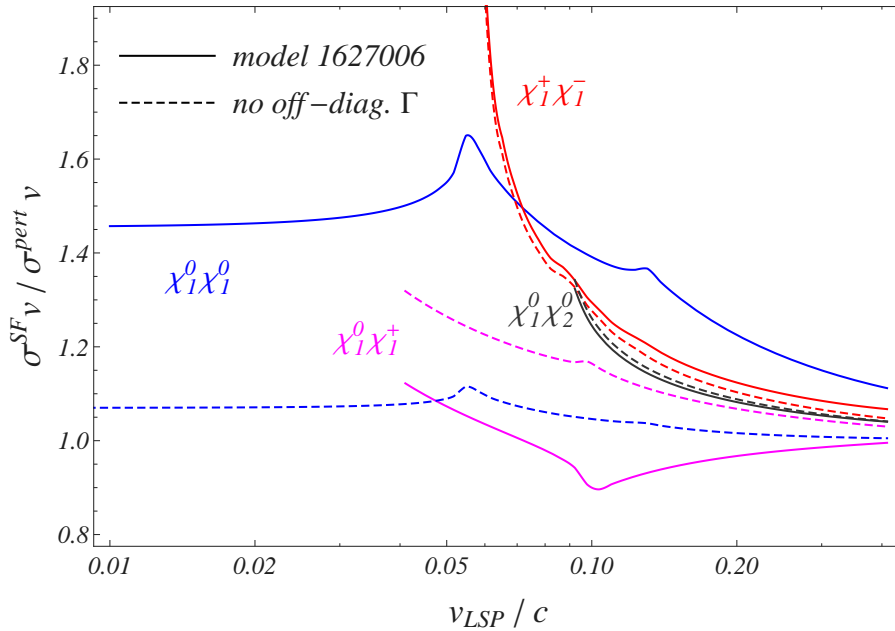


Figure 9.5: Enhancement factors $(\sigma^{\text{SF}}v)/(\sigma^{\text{pert}}v)$ in the four most relevant two-particle channels $\chi_1^0\chi_1^0$, $\chi_1^+\chi_1^-$, $\chi_1^0\chi_2^0$ and $\chi_1^0\chi_1^+$ of Snowmass model 1627006. The enhancement factor for the additionally relevant channel $\chi_1^0\chi_1^-$ agrees with the one for the $\chi_1^0\chi_1^+$ pair. Solid lines refer to the calculation of the Sommerfeld-enhanced rates with off-diagonal terms in the annihilation matrices properly included. Dashed curves show the enhancement when the off-diagonal annihilation rates are neglected.

negative) charged sector features only one two-particle state relevant in co-annihilations with the higgsino-like χ_1^0 dark matter candidate: $\chi_1^+\chi_1^+$ ($\chi_1^-\chi_1^-$). Note that annihilations of the latter double-charged states $\chi_1^+\chi_1^+$ and $\chi_1^-\chi_1^-$ are absent in the pure-higgsino model due to hypercharge conservation in this $SU(2)_L \times U(1)_Y$ symmetric limit, as they have a non-zero hypercharge, namely $Y_{\chi^\pm\chi^\pm} = \pm 1$. In contrast, in the higgsino-like χ_1^0 pMSSM case with broken $U(1)_Y$ symmetry, annihilations of the double-charged channels into a W^+W^+ or W^-W^- pair are possible, though the rates are suppressed by a factor $\sim m_W/m_{\chi_1^0}$ compared to the magnitude of the neutral sector's leading rates.

Fig. 9.5 shows the enhancement $(\sigma^{\text{SF}}v)/(\sigma^{\text{pert}}v)$ of the individual cross sections for those channels that have the most relevant contribution to the relic abundance calculation, that is $\chi_1^0\chi_1^0$, $\chi_1^+\chi_1^-$, $\chi_1^0\chi_2^0$ in the neutral sector, and $\chi_1^0\chi_1^+$ in the single-charged sector ($\chi_1^0\chi_1^-$ gives the same contribution). First note that the enhancements are only of $\mathcal{O}(1)$, opposed to $\mathcal{O}(10^2)$ enhancements in case of the wino-like model in Sec. 9.1. This can be explained due to the larger mass splittings to the next-to-lightest states χ_1^\pm , χ_2^0 in the higgsino-like χ_1^0 case and the fact that the couplings to SM gauge bosons and (light) Higgs particles are generically smaller for higgsinos than for winos. The enhancement of the $\chi_1^0\chi_1^0$ rate as a function of the velocity v_{LSP} shows again the saturated, velocity-

independent behaviour typical for Yukawa type potentials in the low velocity regime well below the thresholds of the heavier two-particle states. As in the wino-model, both the off-diagonal Yukawa potential and the (diagonal) Coulomb potential in the kinematically closed $\chi_1^+\chi_1^-$ channel contribute here to the actual size of the enhancement. At larger velocities, two resonance regions at the thresholds for $\chi_1^+\chi_1^-$ and $\chi_2^0\chi_2^0$ production are visible (the $\chi_2^0\chi_2^0$ channel opens up at $v_{\text{LSP}}/c \simeq 0.127$; the ratio $(\sigma^{\text{SF}}v)/(\sigma^{\text{pert}}v)$ for this channel is very close to 1, and is not shown in Fig. 9.5). One might ask why no resonance at the $\chi_1^0\chi_2^0$ threshold is visible in the $\chi_1^0\chi_1^0$ channel: recall that Fermi-statistics forbids the $\chi_1^0\chi_1^0$ -pair to build the totally symmetric partial-wave configurations 3S_1 and 1P_1 . In case of unbroken $SU(2)_L \times U(1)_Y$ symmetry it turns out, though, that the $\chi_1^0\chi_2^0$ pair can build 3S_1 and 1P_1 configurations but not 1S_0 and 3P_J states. Hence there are no off-diagonal entries in the neutral potential matrices encoding $\chi_1^0\chi_1^0 \rightleftharpoons \chi_1^0\chi_2^0$ interactions in the pure-higgsino limit. Departing from the $SU(2) \times U(1)_Y$ symmetric limit gives rise to $\chi_1^0\chi_2^0$ contributions to the enhancement $(\sigma^{\text{SF}}v)/(\sigma^{\text{pert}}v)$ in the $\chi_1^0\chi_1^0$ channel that are however suppressed by $(m_W/m_{\chi_1^0})^3$ with respect to the leading contributions; this explains why no $\chi_1^0\chi_2^0$ threshold effect is visible in Fig. 9.5. Such restrictions due to non-accessible partial-wave configurations do not exist for the next-to-lightest neutral two-particle state $\chi_1^+\chi_1^-$, and resonances at the thresholds of all co-annihilating neutral $\chi\chi$ -pairs heavier than the $\chi_1^+\chi_1^-$ are visible in the latter channel in Fig. 9.5. Furthermore, note the $1/v_{\chi_1^+}$ Coulomb-type enhancement in the $\chi_1^+\chi_1^-$ channel directly above its threshold caused by potential photon-exchange between the χ_1^+ and χ_1^- . The Coulomb potential surpasses the potentials from massive gauge boson and Higgs exchange at very small velocities in the $\chi_1^+\chi_1^-$ channel, but for moderate velocities both the Coulomb and the (off-)diagonal Yukawa interactions are relevant. Turning to channel $\chi_1^0\chi_2^0$, the corresponding enhancement $(\sigma^{\text{SF}}v)/(\sigma^{\text{pert}}v)$ increases as the velocity decreases. In particular, there is no saturation of the enhancement directly above threshold, because the lighter channels $\chi_1^0\chi_1^0$ and especially $\chi_1^+\chi_1^-$ are always kinematically open and accessible from an on-shell $\chi_1^0\chi_2^0$ state via off-diagonal potential interactions.

The ratio $(\sigma^{\text{SF}}v)/(\sigma^{\text{pert}}v)$ for the charged state $\chi_1^0\chi_1^+$ that is additionally plotted in Fig. 9.5 (lowermost magenta line) shows that the Sommerfeld effect can also produce corrections that reduce the perturbative result. For the channel $\chi_1^0\chi_1^+$ the negative correction arises from the interference of amplitudes where, after multiple electroweak and Higgs boson exchanges, the state that annihilates into the light final state particles is the same as the incoming one, $\chi_1^0\chi_1^+$, with amplitudes where the actual state that annihilates is $\chi_2^0\chi_1^+$. In the EFT formalism such interferences arise from the off-diagonal annihilation terms $\chi_1^0\chi_1^+ \rightarrow \chi_2^0\chi_1^+$ and $\chi_2^0\chi_1^+ \rightarrow \chi_1^0\chi_1^+$, combined with the off-diagonal potential term for $\chi_1^0\chi_1^+ \rightarrow \chi_2^0\chi_1^+$. The dashed magenta curve in Fig. 9.5 refers to the situation where off-diagonal short-distance rates are neglected in the calculation of the Sommerfeld enhanced $\chi_1^0\chi_1^+$ annihilation cross section. It is nicely seen that the destructive interference effect disappears in this case and the ratio $(\sigma^{\text{SF}}v)/(\sigma^{\text{pert}}v)$ is always positive. The enhancement in the $\chi_1^0\chi_1^+$ channel also saturates as its on-shell production threshold is approached. This should be the case as the $\chi_1^0\chi_1^+$ channel is the lightest in the single positive-charged sector, and its behaviour should be similar to

the one of the lightest neutral channel, $\chi_1^0\chi_1^0$, directly above threshold. However, such saturation is not visible in Fig. 9.5 because there we plot the $\chi_1^0\chi_1^+$ cross section as a function of v_{LSP} and not as a function of the relative velocity of the channel, related to the latter by $v^2 = 2(m_{\chi_1^0} + m_{\chi_1^+})/(m_{\chi_1^0}m_{\chi_1^+}) \times (m_{\chi_1^0}v_{\text{LSP}}^2 - 2\delta m)$.³ Let us also mention that the dip in the $\chi_1^0\chi_1^+$ cross section caused by interference effects is located at the velocity where the other state included in the Schrödinger equation for this charge sector, $\chi_2^0\chi_1^+$, opens up.

As we have already noted in context of the $\chi_1^0\chi_1^+$ channel above, the dashed curves in Fig. 9.5 show the results for the corresponding enhancements of the pMSSM scenario 1627006 when off-diagonal annihilation rates are neglected. This disregard would lead to an underestimation of the actual enhancement due to the long-range potential interactions of around 30% in the $\chi_1^0\chi_1^0$ channel. The effect is much milder for the $\chi_1^0\chi_2^0$ and $\chi_1^+\chi_1^-$ pairs and is explained by the contributions of 3S_1 partial-wave annihilations to the cross sections (absent for the identical particle-pair channel $\chi_1^0\chi_1^0$); off-diagonal 3S_1 annihilation rates are suppressed relative to the leading (diagonal) rates by an order of magnitude, due to destructive interference effects between sfermion and gauge boson exchange amplitudes. Hence, as off-diagonals play a minor role in 3S_1 annihilations, their effect in the spin-averaged cross sections $\sigma^{\text{SF}}v$ will also be less pronounced. As the conclusions on the enhancements in case of the pure-higgsino χ_1^0 model are similar to the results in Fig. 9.5 we do not show a corresponding plot here. Let us mention though again, that the hard co-annihilation rates in the pure-higgsino model are a few percent smaller than in the higgsino-like χ_1^0 model. Furthermore, the off-diagonal rates for 3S_1 annihilations in the system of $\chi_1^0\chi_2^0$ and $\chi_1^+\chi_1^-$ states are of the same order of magnitude as the diagonal ones.

Fig. 9.6 shows the thermally averaged effective annihilation rate $\langle\sigma_{\text{eff}}v\rangle$ as a function of the inverse scaled temperature x . The lower solid (blue) curve represents the result using perturbatively calculated rates, while the upper two (red) curves with solid and dashed line style refer to computations with Sommerfeld-enhanced cross sections including and neglecting off-diagonal annihilation rates, respectively. Again the region for $x \lesssim 10$ is unphysical, as the co-annihilating particles' mean velocities are outside the non-relativistic regime. Due to larger mass splittings between the higgsino-like neutralino and chargino states, the decoupling of the heavier states χ_1^\pm and χ_2^0 takes place already around $x \simeq 10^3$. As can be seen from Fig. 9.6, the Sommerfeld effect enhances the thermally averaged effective annihilation cross section by 3% up to 25% with respect to the perturbative result in the region of x around $10 - 10^3$ which is most relevant in the relic abundance calculation. The effect of correctly treating off-diagonal annihilation rates is most essential for large values of x in the range $10^4 - 10^8$, where $\langle\sigma_{\text{eff}}v\rangle$ would be underestimated by around 25% if off-diagonals were neglected in the hard annihilation rates. In the region $x = 10 - 10^3$ the effect of off-diagonal rates is also noticeable, leading to an overestimation of $\langle\sigma_{\text{eff}}v\rangle$ that reaches 6% if off-diagonal rates are not taken into account.

³If the $\chi_1^0\chi_1^+$ cross section behaves as $\sigma^{\text{SF}}v \simeq a + bv^2$ close to threshold, the saturation is visible because of the zero slope of this function at $v = 0$; in terms of v_{LSP} it reads $\sigma^{\text{SF}}v = a + b'(v_{\text{LSP}}^2 - c)$, which does not have a zero slope at the threshold of the channel, $v_{\text{LSP}} = \sqrt{c}$.

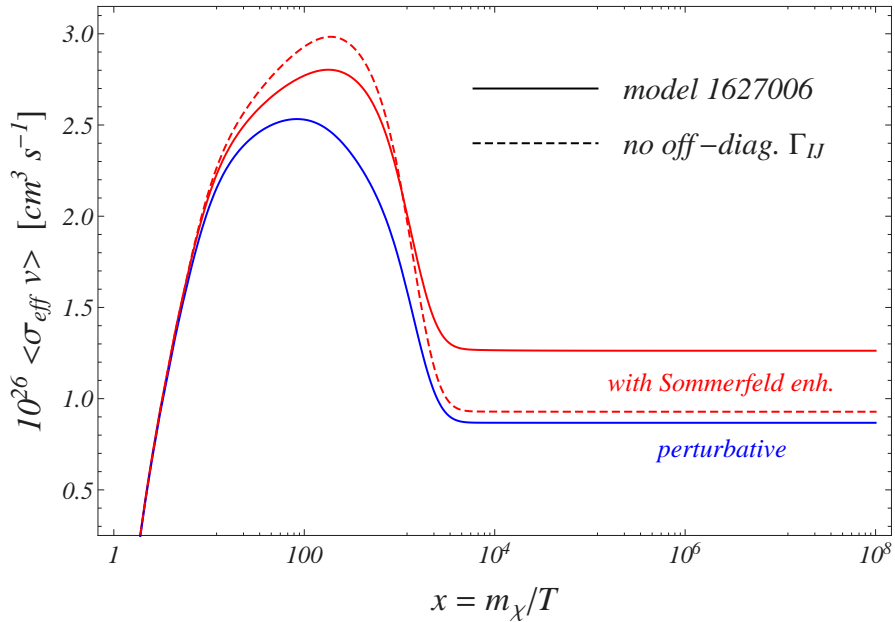


Figure 9.6: The thermally averaged effective annihilation rate $\langle \sigma_{\text{eff}} v \rangle$ as a function of the scaled inverse temperature $x = m_{\chi_1^0}/T$ for the pMSSM Snowmass model 1627006 with higgsino-like χ_1^0 . The upper two (red) curves refer to the Sommerfeld-enhanced cross sections: the solid line includes the off-diagonal annihilation rates while the dashed curve does not. The lowermost (blue) curve corresponds to the perturbative result.

The latter difference with respect to the true result is traced back to the contribution to $\langle \sigma_{\text{eff}} v \rangle$ of the charged $\chi_1^0 \chi_1^\pm$ channel, which in the absence of off-diagonal annihilation terms does not get the negative interference term that lowers the Sommerfeld-corrected cross section, see Fig. 9.5. Once the χ_1^\pm particles are decoupled, the contributions of the channels $\chi_1^0 \chi_1^\pm$ to $\langle \sigma_{\text{eff}} v \rangle$ basically vanish. The much larger enhancement in the $\chi_1^0 \chi_1^0$ cross section when off-diagonal rates are consistently taken into account then explains why the correct $\langle \sigma_{\text{eff}} v \rangle$ result crosses the dashed line for $x \gtrsim 10^3$ in Fig. 9.6.

Finally, Fig. 9.7 shows the ratio Y/Y_{pert} . The solid (blue) and dashed (black) curves refer to calculations within the pMSSM Snowmass model 1627006 with off-diagonal annihilation reactions included and neglected, respectively. The dot-dashed (red) line applies to the pure-higgsino model. The relic abundances that we calculate within the pMSSM Snowmass model read $\Omega^{\text{pert}} h^2 = 0.108$ if perturbative annihilation reactions are considered and $\Omega^{\text{SF}} h^2 = 0.100$ taking Sommerfeld-enhanced rates into account. Accounting for the long-range potential interactions hence leads to a reduction of 8% on the predicted relic density for the pMSSM higgsino-like χ_1^0 model. Neglecting off-diagonal rates in the pMSSM Snowmass model calculation reduces the relic abundance to a value $\Omega^{\text{SF, no-off}} h^2 = 0.096$. This is because the effective thermal average cross section without the off-diagonal rates is larger in the region where chemical decoupling takes place, see

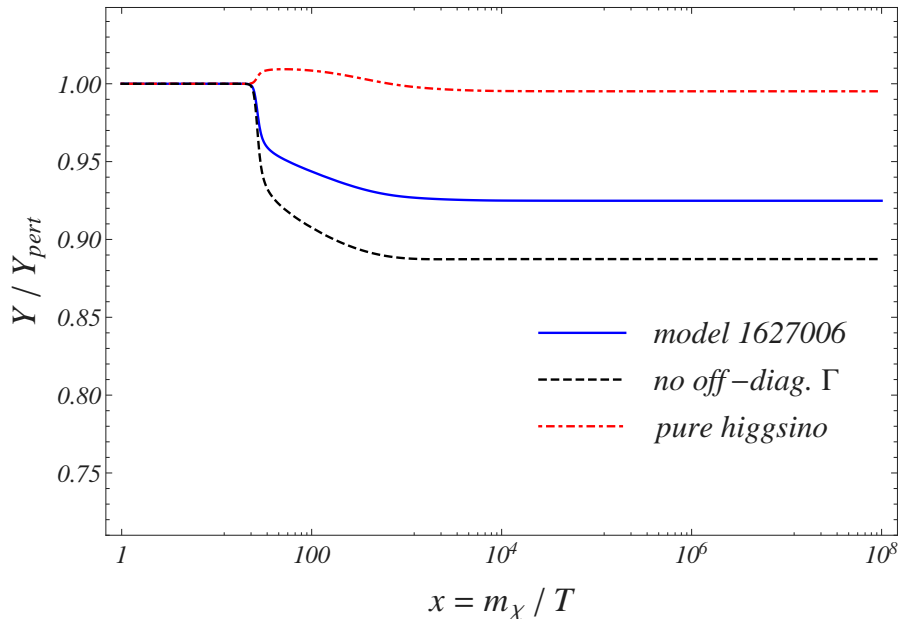


Figure 9.7: The ratio of the yields Y/Y_{pert} , where Y is calculated including Sommerfeld enhancements on the annihilation rates and Y_{pert} uses purely perturbative rates. The solid (blue) line corresponds to the calculation within the pMSSM Snowmass model 1627006 with higgsino-like χ_1^0 , that includes off-diagonal annihilation rates. The dashed (black) line gives the same result but with neglected off-diagonal rates. The dot-dashed curve is the result (with off-diagonal rates) obtained for the pure-higgsino model.

Fig. 9.6. The error on $\Omega^{\text{SF}} h^2$ when disregarding off-diagonal rates therefore amounts to an underestimation of 4% in this case. The Sommerfeld-enhanced rates without the one-loop corrections from heavy $\chi\chi$ -states in the last potential loop before annihilation give a 1% deviation on the final $\Omega^{\text{SF}} h^2$ result. In contrast, the relic abundances in the pure-higgsino model, obtained using perturbative or Sommerfeld-enhanced rates, almost coincide, namely $\Omega_{\text{pure-h}}^{\text{pert}} h^2 = 0.127$ and $\Omega_{\text{pure-h}}^{\text{SF}} h^2 = 0.126$, where the latter result includes the off-diagonal rates. As can be expected, the overall smaller annihilation rates in the pure-higgsino scenario lead to a larger relic abundance than in the higgsino-like pMSSM scenario. The fact that the perturbative yield surpasses the Sommerfeld-corrected one right after chemical decoupling in the pure-higgsino model is explained by the slightly smaller $\langle\sigma_{\text{eff}} v\rangle$ in the Sommerfeld-corrected result in that region of x , which is in turn produced by the Sommerfeld suppression in the charged channels $\chi_1^0\chi_1^\pm$. Overall, there is a strong cancellation between cross section enhancement in the neutral and suppression in the charged channels, leading to an almost vanishing net Sommerfeld correction.

9.3 Light scenario

Light neutralino dark matter with a relic abundance of the order of the observed value is realised for a χ_1^0 with a sizable bino component. The bino is a $SU(2)_L$ singlet with zero hypercharge. As for a pure bino there are no interactions with electroweak gauge bosons nor photons we can already expect that there will be essentially no long-range potential interactions for the bino-like χ_1^0 and hence no Sommerfeld enhancements in $\chi_1^0\chi_1^0$ annihilations. Yet it is interesting to confirm this expectation and to investigate the relevance of Sommerfeld enhancements in possible co-annihilations with (slightly) heavier neutralino and chargino states. As an example for such a bino-like χ_1^0 we chose to study the pMSSM Snowmass model with ID 2178683 that features wino-like NLSP states with masses around 6% heavier than the χ_1^0 state: $m_{\chi_1^0} = 488.8$ GeV, $m_{\chi_2^0} = 516.0$ GeV and $m_{\chi_1^\pm} = 516.2$ GeV.

In the calculation of the χ_1^0 relic abundance we consider co-annihilation reactions among all χ^0/χ^\pm two-particle states, although only the two-particle annihilations between the states $\chi_{1,2}^0, \chi_1^\pm$ are relevant since the higgsino-like states $\chi_{3,4}^0, \chi_2^\pm$ lie at the 2 TeV scale and their abundances are strongly Boltzmann-suppressed at χ_1^0 freeze-out. The lightest sfermions are the $\tilde{\tau}_1$ and $\tilde{\nu}_\tau$ with masses around 770 GeV and we neglect their effect in the relic abundance.

Sommerfeld corrections on the co-annihilation cross sections from all two-particle states built from $\chi_{1,2}^0$ and χ_1^\pm are determined exactly through the solution of the corresponding Schrödinger equations in each charge sector. The outcome for the enhancement $(\sigma^{\text{SF}}v)/(\sigma^{\text{pert}}v)$ in the neutral sector, which entails the two-particle states $\chi_1^0\chi_1^0, \chi_1^0\chi_2^0, \chi_2^0\chi_2^0$ and $\chi_1^+\chi_1^-$, is shown in Fig. 9.8. Solid (dashed) curves correspond to a calculation with (without) off-diagonal annihilation rates in the Sommerfeld-enhanced reactions. Due to the absence of interactions with the electroweak gauge bosons in case of a pure-bino state, the χ_1^0 of the pMSSM Snowmass model 217868 also experiences basically no long-range potential interactions and there is essentially no coupling between the bino-like χ_1^0 and the NLSP χ_2^0 . As a consequence, both the absolute (perturbative as well as Sommerfeld-enhanced) $\chi_1^0\chi_1^0$ and $\chi_1^0\chi_2^0$ annihilation rates are strongly suppressed and there is no enhancement in these reactions; the ratio $(\sigma^{\text{SF}}v)/(\sigma^{\text{pert}}v)$ is equal to one in both cases. As it cannot be inferred from Fig. 9.8, let us note in addition that the absolute $\chi_1^0\chi_1^0$ ($\chi_1^0\chi_2^0$) annihilation cross section is suppressed with respect to the dominant $\chi_2^0\chi_2^0$ and $\chi_1^+\chi_1^-$ rates by four (two) orders of magnitude.

In the subsystem of the neutral wino-like two-particle channels $\chi_2^0\chi_2^0$ and $\chi_1^+\chi_1^-$, the Sommerfeld enhancement due to long-range potential interactions is effective, see the corresponding curves in Fig. 9.8. Note that χ_2^0 and χ_1^\pm co-annihilations should still be relevant in the χ_1^0 relic abundance calculation within the pMSSM scenario 2178683, as the threshold velocities for $\chi_2^0\chi_2^0$ and $\chi_1^+\chi_1^-$ on-shell production are $v_{\chi_1^0} \lesssim 0.34c$ and thus of the order of typical χ_1^0 velocities during thermal freeze-out. This scenario provides an example showing that the criterion established before for including long-distance effects among two-particle states with masses smaller than $M_{\text{max}} = 2m_{\chi_1^0} + m_{\chi_1^0}v_{\text{max}}^2$ and $v_{\text{max}} = 1/3$ should not be considered rigidly. Rather it has to be reassessed according to

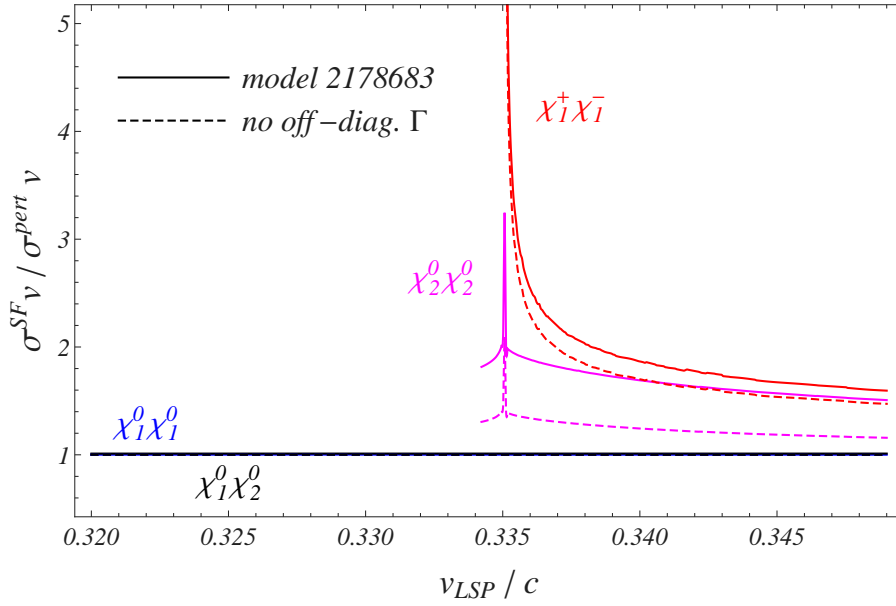


Figure 9.8: $(\sigma^{\text{SF}} v) / (\sigma^{\text{pert}} v)$ for the neutral-sector states in the light scenario (Snowmass model 2178683). Solid (dashed) curves show the enhancement for the case of properly included (wrongly neglected) off-diagonal annihilation rates.

the given MSSM spectra to avoid overlooking interesting effects. Consequently, in order to account for the wino-like subsystem formed by the states $\chi_2^0 \chi_2^0$ and $\chi_1^+ \chi_1^-$ we have set $v_{\text{max}} = 0.34$ in the light scenario. At very small velocities the enhancements in the $\chi_2^0 \chi_2^0$ and $\chi_1^+ \chi_1^-$ channels show the characteristics discussed already for the wino model in Sec. 9.1: In the $\chi_2^0 \chi_2^0$ system we find resonances just below the $\chi_1^+ \chi_1^-$ threshold, smoothed out in Fig. 9.8. The strength of the enhancement below and above this resonance region is a combined effect of the (off-diagonal) Yukawa and the diagonal Coulomb potential interactions in the $\chi_1^+ \chi_1^-$ system. In particular the enhancement is finite below the $\chi_1^+ \chi_1^-$ threshold. To the contrary, the $\chi_1^+ \chi_1^-$ channel shows the typical Coulomb-like $1/v_{\chi_1^+}$ enhancement from the dominating photon-exchange potential at velocities directly above its on-shell production threshold. Opposed to the $\mathcal{O}(10^2)$ enhancements found in Sec. 9.1, the overall enhancements of the neutral wino-like two-particle channels here reach factors of $\mathcal{O}(1)$ only. These less pronounced enhancements result from the lower masses of the wino-like states, since as $m_{\chi_1^0}$ decreases the Yukawa potentials from electroweak gauge boson exchange eventually become short-ranged as compared to the Bohr radius of the system proportional to $(m_{\chi_1^0} \alpha_{\text{EW}})^{-1}$, where $\alpha_{\text{EW}} = g_2^2 / (4\pi)$ and g_2 denotes the $SU(2)_L$ gauge coupling.

Fig. 9.9 displays the effective annihilation cross section $\langle \sigma_{\text{eff}} v \rangle(x)$. The dominance of the wino-like χ_2^0, χ_1^\pm particle annihilation rates by more than three orders of magnitude before their decoupling near $x \sim 100$ is clearly visible. The Sommerfeld enhancement affects only the annihilation of the wino-like particles and thus disappears for $x > 100$.

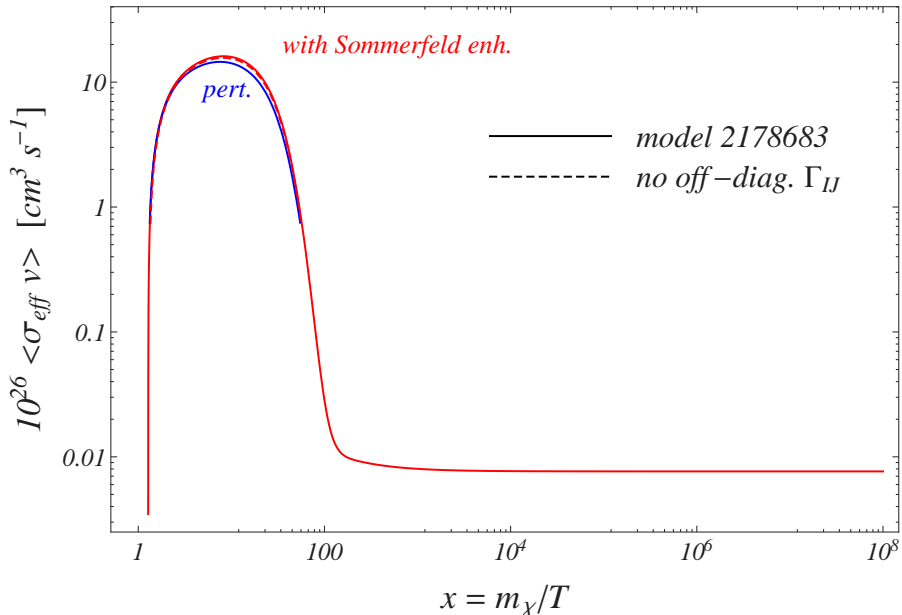


Figure 9.9: The thermally averaged effective rate $\langle \sigma_{\text{eff}} v \rangle(x)$ within the pMSSM Snowmass model 2178683 with Sommerfeld enhancements (upper red curve) and in the perturbative computation (lower blue curve). The result from disregarding off-diagonal rates in the Sommerfeld-enhanced processes is plotted by the dashed line. However the latter curve basically overlays with the upper (red) curve in this plot. This is because the Sommerfeld-enhanced $\langle \sigma_{\text{eff}} v \rangle(x)$ is dominated by the $\chi_2^0 \chi_2^0$ and $\chi_1^+ \chi_1^-$ rates (before χ_2^0 and χ_1^\pm decoupling), and the effect of disregarding off-diagonals in the latter gives a correction of around 10% only, see Fig. 9.8.

Although the Sommerfeld factors for these channels lead to $\mathcal{O}(1)$ enhancements of the cross sections above the threshold near $v_{\text{LSP}} \sim 1/3$, similar in magnitude to the model with wino-like LSP for the same velocities, the thermal average over v_{LSP} dilutes the enhancement, since the cross section for the heavy channels vanishes below the threshold. Nevertheless, the small enhancement visible in Fig. 9.9 occurs precisely in the x range most relevant for freeze-out. The effect of co-annihilations with the wino-like NLSP states therefore leads to a reduction of the yield when taking into account Sommerfeld enhancements with respect to the perturbative case, as is shown in Fig. 9.10. The relic density with perturbative annihilation rates is found to be $\Omega^{\text{pert}} h^2 = 0.120$. There is a $\sim 15\%$ reduction of this result when considering the Sommerfeld-enhanced rates, $\Omega^{\text{SF}} h^2 = 0.102$. The latter sizable reduction of the relic density is attributed purely to the co-annihilating heavier wino states. Note that in the sector of wino-like states the potentials from massive gauge boson and photon exchange are equally important for the Sommerfeld enhancement, while in the $\chi_1^+ \chi_1^-$ system the Coulomb potential dominates over the Yukawa potentials only for very small velocities of the charginos. Neglecting

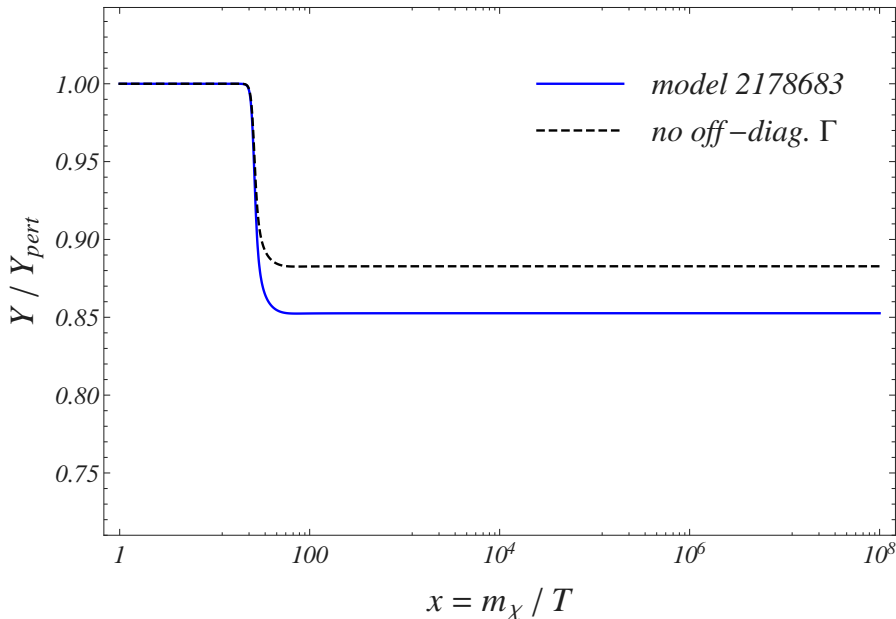


Figure 9.10: The ratio of the yields Y/Y_{pert} , where Y is calculated including the Sommerfeld enhancement on the annihilation rates and Y_{pert} refers to the corresponding perturbative calculation. The solid (blue) line includes off-diagonal rates while in the dashed (black) curve these have been neglected.

the perturbative correction from the heavier $\chi\chi$ -states not included in the Schrödinger equation leads essentially to no difference (below per mil level) in the relic density, as the heavy higgsino-like $\chi_{3,4}^0, \chi_2^\pm$ species lie at the scale of around 2 TeV. If no off-diagonals in the calculation of Sommerfeld-enhanced rates were considered, the relic abundance would be overestimated by 3.5%.

9.4 Higgsino-to-wino trajectory

In case of the wino-like χ_1^0 model of Sec. 9.1 we have seen that the relic abundance including Sommerfeld enhancements on the co-annihilation rates is reduced by about 40% with respect to the result calculated from tree-level annihilation rates. In contrast, the model with higgsino-like χ_1^0 in Sec. 9.2 shows a less strong reduction, which is however still of the order of $\Omega^{\text{SF}} h^2 / \Omega^{\text{pert}} h^2 \approx 0.9$. The difference in the reduction factor $\Omega^{\text{SF}} h^2 / \Omega^{\text{pert}} h^2$ between the wino- and the higgsino-like χ_1^0 model was explained by the smaller Sommerfeld enhancements in the latter case due to larger mass splittings between all co-annihilating particles and the fact that the potential interactions happen to be generically weaker for higgsino-like compared to the wino-like χ_1^0 models. In addition, we observed a Sommerfeld suppression effect in the single-charged sector of the

pure higgsino scenario as well as the higgsino-like Snowmass model. Departing from the scenarios with rather pure wino, higgsino or bino χ_1^0 , we may ask ourselves about the features of a model with χ_1^0 LSP that contains both significant wino and higgsino contributions. It is worth to recall here that previous work in the literature focused on the wino- or higgsino-like χ_1^0 cases only, due to the lack of expression for potentials and annihilation matrices for a generically composed χ_1^0 state. Our results allow for the first time to perform a rigorous study of Sommerfeld enhancements in $\chi\chi$ pair-annihilations within models with mixed gaugino and higgsino composition of the co-annihilating neutralinos and charginos. We find it particular instructive to consider a series of models in the MSSM parameter space that describes the transition from a model with higgsino-like χ_1^0 to a model with primarily wino- χ_1^0 . In the following we will refer to this series of models as models on a “higgsino-to-wino” trajectory. We are interested in the case of reductions of $\Omega^{\text{SF}}h^2$ relative to $\Omega^{\text{pert}}h^2$ by $\gtrsim 10\%$ here and hence will not consider a significant bino-admixture to the χ_1^0 ; as we have seen in Sec. 9.3 the bino-like χ_1^0 itself does not experience any Sommerfeld enhancement. In such a situation a reduction of $\Omega^{\text{SF}}h^2$ can only arise due to co-annihilating particles with Sommerfeld-enhanced rates, see for example the model discussed in Sec. 9.3 with co-annihilating wino-like NLSPs.

In order to define the models for the higgsino-to-wino trajectory, we should note first that the proper choice of the two SUSY parameters μ and M_2 controls the higgsino and wino content of the mass eigenstate χ_1^0 . In order to avoid a bino-admixture to the χ_1^0 state we will choose the parameter M_1 , that controls the neutralinos’ bino-content, to be sufficiently larger than both μ and M_2 throughout this section. Our setup excludes accidental mass degeneracies of the MSSM sfermions with the χ_1^0 , which implies that the actual parameters of the sfermion sector play a minor role in the choice of adequate models on the trajectory. Let us recall that the sfermion sector is irrelevant for Sommerfeld enhancements in our setup, as the latter are caused by potential gauge boson and light Higgs exchange between neutralino and chargino two-particle states prior to the hard annihilation reactions. The sfermion sector parameters only affect the precise value of the hard (tree-level) annihilation rates. The sfermion – basically the stop – sector however controls the value of the Higgs h^0 mass and we will adjust its parameters such that the experimental value for m_{h^0} is reproduced within 2.5% accuracy. Yet matching the precise experimental Higgs mass value is in fact not important to us here, as potential exchange from the h^0 gives always a subleading contribution to the potentials compared to the effects from SM gauge boson exchange.

In order to generate MSSM scenarios on a higgsino-to-wino trajectory we hence make the following choice for MSSM input parameters in the spectrum generation:

- fix a common sfermion mass scale of 9 TeV,
- set the trilinear couplings to $A_t = A_b = 9 \text{ TeV}$,
- fix $m_{A^0} = 500 \text{ GeV}$ and
- choose $\tan\beta = 15$.

All other trilinear couplings are assumed to vanish. The gluino mass parameter M_3 is fixed by $M_3 = \alpha_s / (\sin(\theta_w) \alpha_e) M_2$, but this choice is completely irrelevant to our discussion. To avoid a significant bino-admixture to the χ_1^0 we further restrict to models with $M_1 = 10 M_2$. This leaves us with yet-to-choose parameter pairs in the $\mu - M_2$ plane. We require that the trajectory models allow for an explanation of the observed cosmic cold dark matter in terms of the neutralino relic abundance without including radiative corrections: in order to do so we employ the program DarkSUSY [5] and identify (μ, M_2) pairs such that the DarkSUSY calculated relic density $\Omega^{\text{DS}} h^2$ matches the most accurate determination obtained from the combination of PLANCK, WMAP, BAO and high resolution CMB data, $\Omega_{\text{cdm}} h^2 = 0.1187 \pm 0.0017$ [2]⁴, which we quoted already in Chap. 1. In such a way we define 13 models on the higgsino-to-wino trajectory. The position of these models in the $\mu - M_2$ plane is shown in Fig. 9.11. For each of the 13 models, given the pairs (μ, M_2) as well as the remaining input parameters defined above, we run our code and determine the corresponding relic densities including and neglecting Sommerfeld effects. The comparison between our perturbative results $\Omega^{\text{pert}} h^2$ with the corresponding DarkSUSY expressions $\Omega^{\text{DS}} h^2$ provides a cross-check of our perturbative calculation.

There is one important point to note concerning the MSSM spectrum generation from the SUSY input parameters. The DarkSUSY spectrum calculated from the inputs refers to tree-level $\overline{\text{DR}}$ -parameters. It is well-known and has been noted before in Chap. 4 that the mass splitting between a wino-like neutralino and its chargino partner is dominated by radiative corrections; the leading one-loop contribution to the splitting is of $\mathcal{O}(160 \text{ MeV})$ and dominates over the $\mathcal{O}(1 \text{ MeV})$ tree-level contribution. Both for the calculation of the Sommerfeld enhancements and in the determination of the relic abundance including co-annihilations a precise knowledge of the mass splitting between the χ_1^0 LSP and the NLSP particles is crucial and in a rigorous analysis we should therefore consider the spectra determined with one-loop accuracy. To this end we have been provided by one-loop on-shell renormalised SUSY spectra for all 13 models on the trajectory by a member of the collaboration [83, 84]. The values of the input parameters μ, M_2, \dots are the same as for the corresponding calculation within DarkSUSY with the difference that for the one-loop on-shell spectrum generation these inputs are considered as on-shell parameters and no renormalisation group running of the mass parameters is performed. Hence there are small differences in the values for the masses and mixing-matrix entries between the spectra that we use in our code and the corresponding DarkSUSY spectra. In particular the mass splittings between the χ_1^0 LSP and the NLSPs obtained from the on-shell masses renormalised at one-loop can be significantly different from the splittings derived using tree-level $\overline{\text{DR}}$ -parameters. There exist different renormalisation schemes for on-shell renormalisation in the neutralino/chargino sector [82–85]: for all trajectory models apart from model 8 the on-shell renormalisation has been performed requiring that the values of the two chargino masses as well as the heaviest (in all our models bino-like) neutralino mass at one-loop are given by their tree-level values (“CCN-

⁴Note that the DarkSUSY collaboration claims an error of 5% on the relic densities calculated from their code.

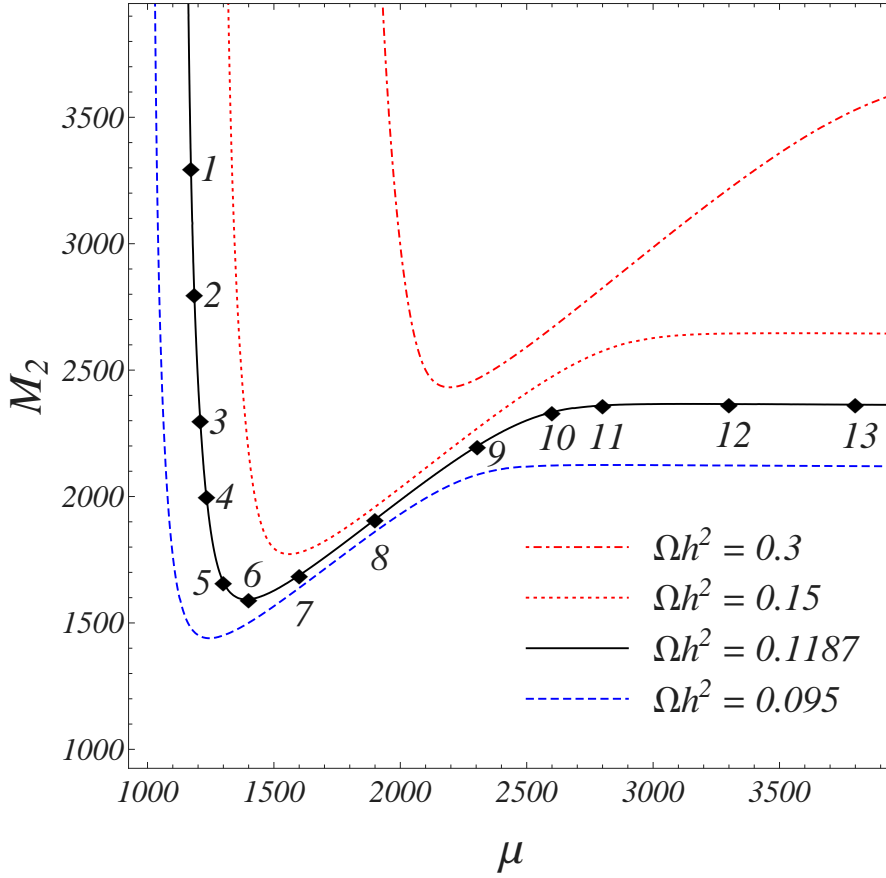


Figure 9.11: The $\mu - M_2$ plane with the 13 models defining the higgsino-to-wino trajectory, indicated with diamonds. All trajectory models lie on the iso-contour for constant relic density $\Omega^{\text{DS}} h^2 = 0.1187$ calculated with DarkSUSY. As reference we also show the iso-contours of constant relic densities $\Omega^{\text{DS}} h^2 = 0.095$ (lowermost contour-line) 0.15 and 0.3 (uppermost iso-contour).

scheme”). Such a scheme works well as long as the two charginos are rather pure wino- and higgsino-like states. As soon as the charginos are (strongly) mixed wino-higgsino states - as in case of our model 8, where the input parameters μ and M_2 happen to be very close to each other - a more suitable scheme is obtained when only one chargino, one lighter neutralino and the heaviest bino-like neutralino mass are fixed to their tree-level value (“CNN scheme”).

For each of the 13 models on the trajectory we list the input parameters μ and M_2 in Tab. 9.1, together with the one-loop renormalised LSP mass $m_{\chi_1^0}$ as well as the one-loop on-shell mass splitting $\delta m_{\chi_1^\pm} = m_{\chi_1^\pm} - m_{\chi_1^0}$. The χ_1^\pm is the NLSP in all models considered in this section. As additional information we give the χ_1^0 's wino fraction $|Z_{N21}|^2$ and collect the results for $\Omega^{\text{SF}} h^2$ including Sommerfeld effects as well as for the suppression $\Omega^{\text{SF}} h^2 / \Omega^{\text{pert}} h^2$ of the former relic density with respect to the perturbative

ID	μ/GeV	M_2/GeV	$m_{\chi_1^0}/\text{GeV}$	$\delta m_{\chi_1^+}/\text{GeV}$	$ Z_{N21} ^2$	$\Omega^{\text{SF}}h^2$	$\frac{\Omega^{\text{SF}}h^2}{\Omega^{\text{pert}}h^2}$
1	1171.925	3300.000	1169.957	0.876	0.001	0.1157	0.974
2	1185.224	2800.000	1169.427	0.958	0.001	0.1129	0.970
3	1208.699	2300.000	1205.096	1.057	0.003	0.1136	0.956
4	1233.685	2000.000	1228.674	1.129	0.006	0.1119	0.943
5	1300.000	1661.705	1289.890	1.203	0.026	0.1074	0.908
6	1400.000	1593.100	1382.390	1.153	0.076	0.1016	0.860
7	1600.000	1688.240	1569.117	0.971	0.203	0.0922	0.776
8	1900.000	1909.355	1844.126	0.601	0.458	0.0791	0.661
9	2304.666	2200.000	2172.690	0.266	0.826	0.0680	0.550
10	2600.000	2333.7034	2320.986	0.183	0.955	0.0503	0.394
11	2800.000	2360.2715	2352.475	0.166	0.982	0.0530	0.412
12	3300.000	2365.830	2362.264	0.158	0.996	0.0635	0.494
13	3800.000	2363.500	2361.254	0.157	0.998	0.0644	0.503

Table 9.1: Information on the models on the higgsino-to-wino trajectory. The first column is the model ID while the second and third column contain the input parameter values for μ and M_2 . The one-loop on-shell renormalised χ_1^0 LSP mass is given in the fourth column and we provide the one-loop mass splitting to the lighter chargino, $\delta m_{\chi_1^+} = m_{\chi_1^+} - m_{\chi_1^0}$ in the fifth column. The χ_1^\pm are the NLSP states in all models considered here. In the sixth column the wino fraction, $|Z_{N21}|^2$, of the χ_1^0 is specified. The second-to-last and the last columns give the relic density including Sommerfeld-enhanced cross sections as well as the suppression factor of the $\Omega^{\text{SF}}h^2$ with respect to the perturbative result $\Omega^{\text{pert}}h^2$. The results including the Sommerfeld enhancements involve corrections from heavier $\chi\chi$ -pairs in the last potential loop.

result. Both $\Omega^{\text{SF}}h^2$ and $\Omega^{\text{pert}}h^2$ are calculated from our programs, and the latter shows small deviations of the order of a few percent from the DarkSUSY value $\Omega^{\text{DS}}h^2 = 0.1187$. As can be read off Tab. 9.1 we can categorise the models on the trajectory to feature either a higgsino-like χ_1^0 with wino fraction below 10% but a higgsino fraction $|Z_{N31}|^2 + |Z_{N41}|^2$ above 0.9 (models 1–6), a mixed wino-higgsino χ_1^0 where both the wino and the higgsino fraction lie within 0.1 – 0.9 (models 7–9) or a predominantly wino-like χ_1^0 with wino fraction above 0.9 (models 10–13). For all models we collect the relic density results $\Omega^{\text{pert}}h^2$ and $\Omega^{\text{SF}}h^2$ in Fig. 9.12. The bars with dotted (black) hatching indicate $\Omega^{\text{pert}}h^2$. Bars with solid-line (red) and dashed (blue) hatching give the corresponding results including Sommerfeld enhancements with and without off-diagonal rates, respectively. In particular for the higgsino-like models 1–6 but also for models 7–9 our relic densities $\Omega^{\text{pert}}h^2$ agree very well with the relic density $\Omega^{\text{DS}}h^2 = 0.1187$ calculated with DarkSUSY for the same set of input parameters. The latter relic density value is indicated by the black horizontal line and the grey horizontal band comprises all values deviating at most by 5% from the $\Omega^{\text{DS}}h^2$ value. For the wino-like models our relic density results deviate by $\lesssim 8\%$ from the corresponding DarkSUSY value.

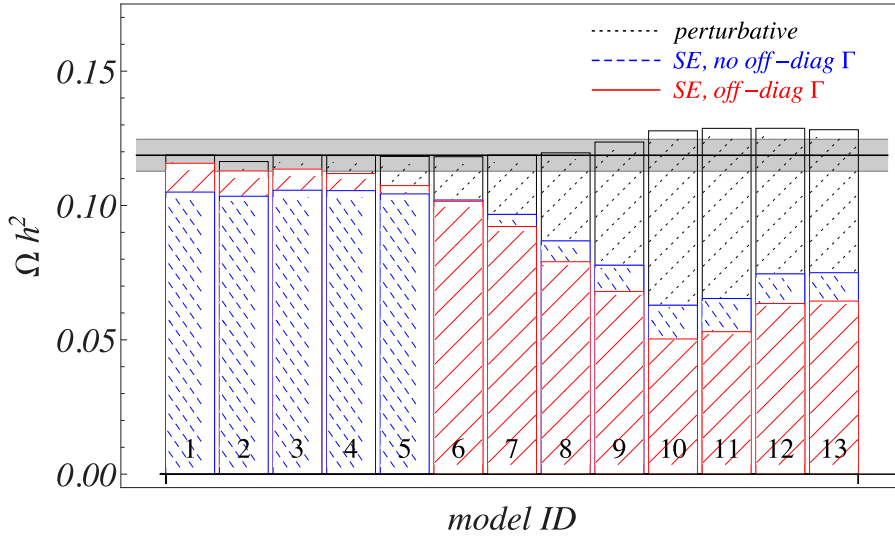


Figure 9.12: Relic densities Ωh^2 for models 1 – 13 on the higgsino-to-wino trajectory calculated with our code. The charts with dotted (black) hatching are the perturbative results $\Omega^{\text{pert}} h^2$. Bars with dashed (blue) and solid-line (red) hatching refer to a calculation with Sommerfeld-enhanced cross sections neglecting and properly including off-diagonal rates, respectively. The grey shaded band comprises Ωh^2 values within 5% around the mean experimental value $\Omega_{\text{cdm}} h^2 = 0.1187$ [2]. The latter value is indicated by the black horizontal line and agrees with the DarkSUSY result for all 13 MSSM models on the trajectory.

Let us discuss the characteristics of the models in the three different classes corresponding to their wino and higgsino admixture in turn. The models 1 – 6, with predominant higgsino composition, resemble the higgsino model of Sec. 9.2. This applies also to the corresponding shapes of the Sommerfeld-enhanced rates $\sigma^{\text{SF}} v$, $\langle \sigma_{\text{eff}} v \rangle$, as well as to the yields Y/Y^{pert} , that we do not show here. The reduction in the relic density when taking the Sommerfeld effect into account ranges from 3% to 14% for trajectory models 1 – 6. Models 1 – 3, with a 3% to 4% reduction are close to a pure-higgsino limit behaviour, whereas models 4 – 6 yield a similar outcome as for the Sec. 9.2 higgsino-like χ_1^0 Snowmass model. The potential interactions among all two-particle states built from the higgsino-like particles $\chi_{1,2}^0, \chi_1^\pm$ have been accounted for exactly by solving the corresponding multi-state Schrödinger equation in models 1 – 6. This is in agreement with the criterion introduced in Sec. 9.1 that considers the long-distance effects among all $\chi\chi$ -states with mass smaller than $M_{\text{max}} = 2m_{\chi_1^0} + m_{\chi_1^0} v_{\text{max}}^2$, where $v_{\text{max}} = 1/3$ is of the order of the χ_1^0 's mean-velocity during freeze-out. Heavier $\chi\chi$ channels enter the calculation through the perturbative corrections to the annihilation rates of the lighter channels treated exactly, and their tree-level co-annihilation rates are also included in the calculation of the χ_1^0 relic density, as done in the previous sections. The effect of neglecting off-diagonal annihilation rates in the determination of $\Omega^{\text{SF}} h^2$ yields an error of

about 9% to 3% for models 1 – 5, underestimating the true result. In case of model 6 the $\Omega^{\text{SF}}h^2$ results obtained when neglecting or correctly including off-diagonal annihilation rates happen to agree. This can be understood from the Sommerfeld suppressions in the two single-charged sectors that arise when correctly accounting for off-diagonal annihilation rates and that can lead to a partial compensation of enhancements encountered in the neutral sector. While there is no suppression effect if off-diagonal annihilation rates are neglected, also the Sommerfeld enhancements in the charge-neutral sector are milder in that case, see for instance Fig. 9.5. Relic density results with and without off-diagonal annihilation rates can therefore accidentally agree, as it happens for model 6. If corrections from heavier states in the last potential loop were not included in the calculation of the relic abundance, the corresponding result would be larger by 2% for model 1 to 6% for model 6 as compared to the $\Omega^{\text{SF}}h^2$ values quoted in Tab. 9.1. As expected, the latter effect gains importance as the mass splitting of the heavier states to the higgsino-like $\chi_{1,2}^0$ and χ_1^\pm becomes smaller; while the wino-like states χ_3^0, χ_2^\pm in model 1 are rather heavy ($m \sim 3.3$ TeV), these states have a mass of about 1.6 TeV in case of model 6.

For models 7 – 9 with mixed wino-higgsino χ_1^0 , where the wino content increases with higher model ID, Fig. 9.12 shows a reduction of $\Omega^{\text{SF}}h^2$ the larger the wino admixture of the χ_1^0 . The ratio $\Omega^{\text{SF}}h^2/\Omega^{\text{pert}}h^2$ ranges from ~ 0.78 for model 7 over ~ 0.66 for model 8 and gives ~ 0.55 in case of model 9. In the region of mixed wino-higgsino χ_1^0 , where the masses of the states $\chi_{1,2,3}^0, \chi_{1,2}^\pm$ lie close to each other, more two-particle states have been considered exactly in the multi-state Schrödinger equation. Precisely, the set of neutral $\chi\chi$ -states considered in the Schrödinger equations for model 7 comprises the seven states $\chi_1^0\chi_1^0, \chi_1^+\chi_1^-, \chi_1^0\chi_2^0, \chi_2^0\chi_2^0, \chi_1^0\chi_3^0, \chi_1^\pm\chi_2^\mp$, while for model 8 the state $\chi_2^0\chi_3^0$ is included in addition, and for model 9 only the six states $\chi_1^0\chi_1^0, \chi_1^+\chi_1^-, \chi_1^0\chi_2^0, \chi_1^0\chi_3^0, \chi_1^\pm\chi_2^\mp$ are treated exactly in the neutral sector. While in the three models 7 – 9 (particularly in the neutral sector), the mutual interaction among a large number of channels is solved through the Schrödinger equations, it is mainly the larger wino fraction of the χ_1^0 that controls the increasing relevance of the Sommerfeld enhancements on the final relic abundance. While the wino fraction of the χ_1^0 in model 7 is 20% it becomes 46% for model 8 and finally reaches 83% in case of model 9. The larger wino admixture of both the χ_1^0 and χ_1^\pm states also manifests itself in the decreasing mass splitting $\delta m_{\chi_1^\pm}$ between these two states, ranging from 0.971 GeV (model 7) over 0.601 GeV (model 8) to only 0.266 GeV (model 9). A larger wino component of the χ_1^0 implies stronger potential interactions between the co-annihilating channels, in particular the $\chi_1^0\chi_1^0$ and $\chi_1^+\chi_1^-$, where the latter is composed of χ_1^\pm states with similar wino fraction as the χ_1^0 . The stronger potential interactions finally lead to a more pronounced Sommerfeld enhancement effect for models with larger wino admixture to the χ_1^0 state. Neglecting off-diagonal annihilation rates would lead to a result enhanced by 5% (model 7), 10% (model 8) and 14% (model 9) with respect to the actual $\Omega^{\text{SF}}h^2$ values given in Tab. 9.1. On the other hand, corrections to the Sommerfeld-enhanced rates from heavy $\chi\chi$ -states in the last potential loop reduce the final relic abundances $\Omega^{\text{SF}}h^2$ for models 7 – 9 by around 2 – 4%. The latter reduction is not as large as for model 6, despite the fact that the mass differences in models 7 – 9 are

smaller. This is simply because there are less heavy channels contributing perturbatively now, as more $\chi\chi$ -states have been considered exactly in the Schrödinger equation.

Finally let us consider the subclass of wino-like χ_1^0 models with IDs 10 – 13. Here we account for Sommerfeld effects on the annihilation rates for $\chi\chi$ -states built from the wino-like χ_1^0 and χ_1^\pm particles. The Schrödinger equations in the neutral sector for models 10 – 13 hence contain the two states $\chi_1^0\chi_1^0$ and $\chi_1^+\chi_1^-$ only. The models can be further subdivided into two groups with different impact of Sommerfeld enhancements: in case of models 10 and 11, $\Omega^{\text{SF}}h^2$ is significantly reduced by around 60% with respect to the result from a perturbative calculation. This happens to be the strongest reduction we find along the trajectory. The reason for the especially pronounced Sommerfeld-enhanced annihilation rates in case of models 10 and 11 can be attributed to the presence of a zero-energy resonance [19] in the $\chi_1^0\chi_1^0$ annihilation channel: as already discussed, for velocities well below the $\chi_1^+\chi_1^-$ threshold the enhancement in the $\chi_1^0\chi_1^0$ system is controlled by the Yukawa potential due to electroweak W -exchange. As any short-ranged potential, a Yukawa-potential features a finite number of bound states. By varying the potential's strength and range it is possible to arrange for the presence of a bound state with (almost) zero binding energy [19] (see also [36]). In the presence of such a (loosely) bound state, the scattering cross section for incoming particles with very low velocities is strongly enhanced. Let us remind that we have discussed such zero-energy resonances associated with Yukawa-type potentials in context of our toy model analyses in Sec. 2.3.2 and Sec. 2.4. The presence of a (loosely) bound-state in models 10 and 11 leads to $\mathcal{O}(10^4)$ enhancements in the $\chi_1^0\chi_1^0$ channel for velocities below the $\chi_1^+\chi_1^-$ threshold and eventually translates into the pronounced reduction of about 60% of the relic density. If off-diagonal annihilation rates were not taken into account, the $\Omega^{\text{SF}}h^2$ result would be larger by about 25% (model 10) and 23% (model 11), thus representing a rather large effect for both models: Off-diagonal annihilation rates are particularly important if the corresponding off-diagonal potential interactions are sufficiently strong. In wino-like χ_1^0 models, the only sector with relevant off-diagonal potential interactions is given by the two neutral states $\chi_1^0\chi_1^0$ and $\chi_1^+\chi_1^-$ in a 1S_0 wave configuration.⁵ For models 10 and 11, where the neutral $\chi_1^0\chi_1^0$ channel experiences particularly large enhancements due to the presence of a (loosely) bound state resonance related to the off-diagonal W -exchange potential, also the impact of off-diagonal annihilation rates is therefore found to be significant. Regarding the corrections from heavier $\chi\chi$ -states treated perturbatively in the last potential loop, they are rather mild: $\Omega^{\text{SF}}h^2$ would be smaller by around 3% without this effect. Compared to model 6, where we found a corresponding 6% reduction in $\Omega^{\text{SF}}h^2$, this suggests that the effect from heavier $\chi\chi$ -states in the last potential loop is most significant if these states are built from wino-like particles. The latter have in overall stronger (off-) diagonal annihilation rates compared to higgsino-like states with similar mass. Let us recall that the effect from heavier $\chi\chi$ -states in the last potential loop was at the per mil level in case of the pMSSM scenarios in Secs. 9.1 and 9.3 and around 1% for the higgsino-like scenario in Sec. 9.2, because heavier states were essentially decoupled

⁵To a lesser extent, as it constitutes higher partial waves, also the 3P_J configurations are important.

in these models, opposed to the case for the models on the higgsino-to-wino trajectory.

At last, for models 12 and 13 we find a reduction of $\Omega^{\text{SF}}h^2$ relative to $\Omega^{\text{pert}}h^2$ of roughly 50% in both cases. This is still larger than the 40% reduction arising in case of the wino-like χ_1^0 pMSSM Snowmass model discussed in Sec. 9.1. To explain this effect note first that although the input value μ differs for models 12 and 13, this does not affect the parameters of the corresponding wino-like sectors. The masses of both χ_1^0 and χ_1^\pm as well as their wino fractions are essentially the same in model 12 and 13, see Tab. 9.1. We can hence expect that the results for the χ_1^0 relic abundance calculation are very similar for both models. The presence of a zero-energy resonance in the $\chi_1^0\chi_1^0$ annihilation channel is still noticeable for models 12, 13 – although it is less pronounced, as increasing the χ_1^0 mass moves us away from the exact resonance region. To conclude with the comparison to the wino-like χ_1^0 pMSSM Snowmass model in Sec. 9.1, recall that the mass of the wino-like χ_1^0 there was $m_{\chi_1^0} = 1650.664 \text{ GeV}$; in that case the Yukawa potential does not exhibit (almost) zero-energy bound states. Consequently no additional strong resonant enhancement takes place, such that in comparison to the wino-like models on the trajectory the Sommerfeld effect on the relic density is less prominent in Sec. 9.1, though still around 40%. Finally the calculated relic density $\Omega^{\text{SF}}h^2$ for both models 12 and 13 is increased by 17% and 16%, respectively, if off-diagonal annihilations are neglected. Not including the one-loop effects from heavy $\chi\chi$ -states increases the corresponding results for $\Omega^{\text{SF}}h^2$ in Tab. 9.1 by 2% in both cases.

9.5 Mixed wino-higgsino χ_1^0

As our framework allows for the first time to investigate Sommerfeld enhancements of $\chi\chi$ co-annihilations in scenarios with a χ_1^0 in an arbitrary wino-higgsino admixture, let us discuss here in more detail the mixed wino-higgsino χ_1^0 trajectory model with ID 8 considered in the previous section. Recall from section 9.4 that the neutral sector of the Schrödinger equation for this model is composed of the eight states $\chi_1^0\chi_1^0$, $\chi_1^+\chi_1^-$, $\chi_1^0\chi_2^0$, $\chi_2^0\chi_2^0$, $\chi_1^0\chi_3^0$, $\chi_1^\pm\chi_2^\mp$, $\chi_2^0\chi_3^0$.

Fig. 9.13 shows the enhancements $(\sigma^{\text{SF}}v)/(\sigma^{\text{pert}}v)$ in the two neutral channels $\chi_1^0\chi_1^0$ and $\chi_1^+\chi_1^-$ with (solid lines) and without (dashed lines) off-diagonal annihilation rates. The characteristic velocity-independent enhancement from the W -exchange Yukawa potential in the low velocity regime of the $\chi_1^0\chi_1^0$ channel is visible, as well as the Coulomb-type $1/v_{\chi_1^+}$ enhancement for the $\chi_1^+\chi_1^-$ system at very low velocities. Long-range potential interactions, although stronger than in case of higgsino-like χ_1^0 models are still weaker than in case of a wino-like set of states χ_1^0, χ_1^\pm ; as a consequence enhancement factors of $\mathcal{O}(1 - 10)$ result. We do not show $(\sigma^{\text{SF}}v)/(\sigma^{\text{pert}}v)$ for the remaining six neutral two-particle states in Fig. 9.13, but the resonance regions below their corresponding on-shell production thresholds can be seen as small enhancements in the $\chi_1^0\chi_1^0$ and $\chi_1^+\chi_1^-$ channels. The threshold for $\chi_1^0\chi_2^0$ production opens at $v_{\text{LSP}}/c \simeq 0.18$ but is hardly visible in the curves for channels $\chi_1^0\chi_1^0$ and $\chi_1^+\chi_1^-$ in Fig. 9.13. We can notice a broader (smoothed-out) resonance region around $v_{\text{LSP}}/c \simeq 0.25$, which comprises the thresholds for the four

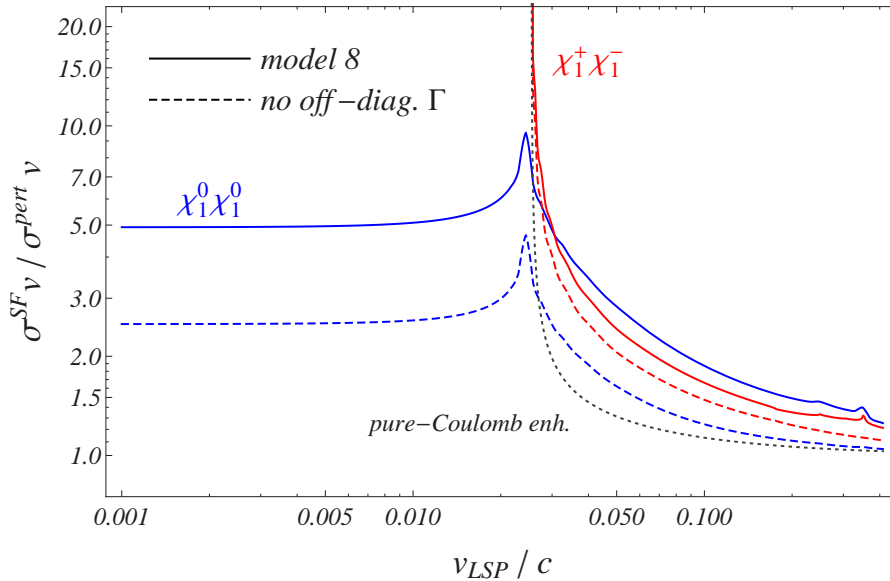


Figure 9.13: Enhancements $(\sigma^{\text{SF}}v)/(\sigma^{\text{pert}}v)$ in the two neutral channels $\chi_1^0\chi_1^0$ and $\chi_1^+\chi_1^-$ of model 8 of the wino-to-higgsino trajectory discussed in Sec. 9.4. Solid (dashed) curves refer to the results with (without) off-diagonal annihilation rates included.

channels $\chi_2^0\chi_2^0$, $\chi_1^0\chi_3^0$ and $\chi_1^\pm\chi_2^\mp$. Finally, the $\chi_2^0\chi_3^0$ threshold shows up at $v_{\text{LSP}}/c \simeq 0.30$. The enhancements for these channels, not shown in Fig. 9.13, are somewhat smaller than for the cases of $\chi_1^0\chi_1^0$ and $\chi_1^+\chi_1^-$. Eventually, at $v_{\text{LSP}}/c \simeq 0.35$ the threshold for on-shell production of the $\chi_3^0\chi_3^0$ state is visible in the $\chi_1^+\chi_1^-$ channel. The $\chi_3^0\chi_3^0$ state is among the heavy states considered perturbatively in the last potential loop for the calculation of the annihilation rates of the channels treated exactly in the neutral sector.

Note that apart from the bino-like χ_4^0 state, which is very heavy ($m_{\chi_4^0} \sim 19$ TeV) and – being bino-like – couples very weakly to the gauge bosons and the other χ^0/χ^\pm species, all χ states in the neutralino/chargino sector are relevant in co-annihilation reactions for the χ_1^0 relic abundance calculation of model 8.

The thermally averaged effective annihilation rates $\langle\sigma_{\text{eff}}v\rangle(x)$ including (upper solid (red) line) and neglecting (dashed red line) off-diagonal rates in the Sommerfeld-enhanced cross sections are depicted in the upper panel of Fig. 9.14. The corresponding perturbative result is given by the lower solid (blue) curve. The perturbative annihilation rates of two-particle states $\chi\chi$ heavier than the $\chi_1^0\chi_1^0$ pair are larger than the perturbative rate of the latter, leading to a drop in the perturbative $\langle\sigma_{\text{eff}}v\rangle(x)$ curve after decoupling of the heavier co-annihilating $\chi\chi$ states. As can be already inferred from Fig. 9.13, the effective rate including Sommerfeld enhancements turns out to be larger than the corresponding perturbative result by factors of at most $\mathcal{O}(1-3)$ in the $x = 10 \dots 10^3$ range relevant to the relic abundance calculation. These enhancements finally give rise to the behaviour of the ratio of yields Y/Y_{pert} shown in the lower panel of Fig. 9.14. Including Sommerfeld

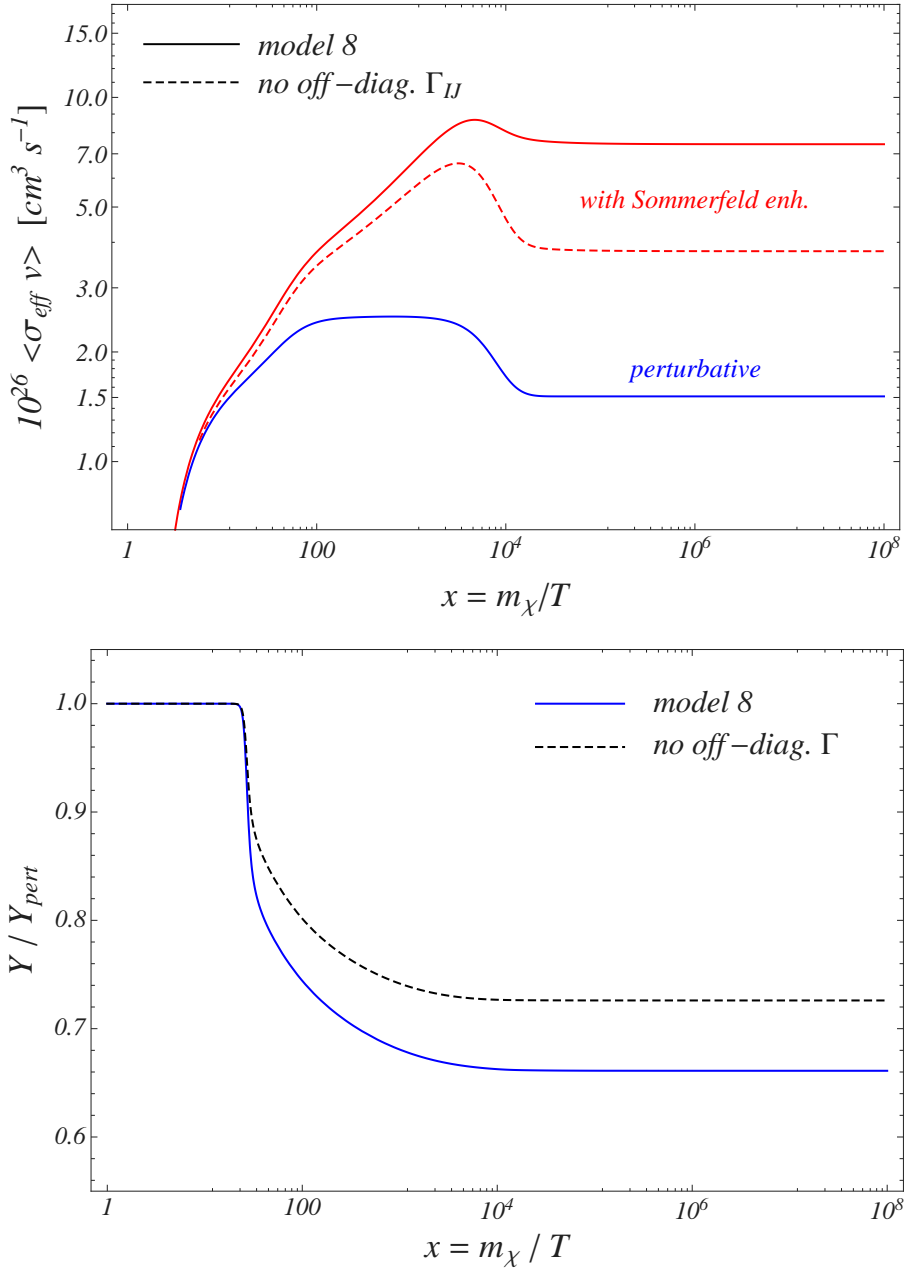


Figure 9.14: *Upper panel:* The effective thermally averaged annihilation rate $\langle \sigma_{\text{eff}} v \rangle(x)$ for trajectory model 8. The two upper (red) curves show the $\langle \sigma_{\text{eff}} v \rangle(x)$ behaviour if Sommerfeld enhancements are taken into account with/without (solid/dashed) off-diagonal rates. The lower solid (blue) curve gives the perturbative result. *Lower panel:* The ratio of the yields Y/Y_{pert} for the trajectory model with ID 8 with off-diagonal rates (solid blue line) and without (dashed black line).

neutral $\chi\chi$ -states	$\chi_1^0\chi_1^0$	$\chi_1^+\chi_1^-$	$\chi_1^0\chi_2^0$	$\chi_2^0\chi_2^0, \chi_1^0\chi_3^0$	$\chi_1^\pm\chi_2^\mp$	$\chi_2^0\chi_3^0$	$\chi_3^0\chi_3^0$	$\chi_2^+\chi_2^-$
$M_{\chi\chi}$ [GeV]	3688	3689	3745	3802	3803	3858	3915	3916
charge ± 1 states	$\chi_1^0\chi_1^\pm$	$\chi_2^0\chi_1^\pm$		$\chi_1^0\chi_2^\pm, \chi_3^0\chi_1^\pm$	$\chi_2^0\chi_2^\pm$		$\chi_3^0\chi_2^\pm$	
$M_{\chi\chi}$ [GeV]	3689	3746		3802	3859		3916	
charge ± 2 states	$\chi_1^\pm\chi_1^\pm$			$\chi_1^\pm\chi_2^\pm$			$\chi_2^\pm\chi_2^\pm$	
$M_{\chi\chi}$ [GeV]	3689			3803			3916	

Table 9.2: $\chi\chi$ -states and corresponding masses $M_{\chi\chi}$ in model 8, ordered according to their electric charge, that are relevant in the calculation of the χ_1^0 relic abundance $\Omega^{\text{SF}}h^2$. Two-particle states involving the bino-like neutralino χ_4^0 are not shown. As their masses $M_{\chi\chi}$ lie above the scale of 20 TeV, they are irrelevant in the calculation of Sommerfeld enhancements to the lighter $\chi\chi$ -channels and in the determination of the χ_1^0 relic abundance. The vertical double lines separate the states with masses below 3762 GeV and above 3893 GeV.

corrections on the co-annihilation rates leads to a reduction of the relic density by 34%. For this model the effect of neglecting off-diagonal rates in the relic abundance calculation turns out to be milder than in the wino-like χ_1^0 models: with the off-diagonal entries we get $\Omega^{\text{SF}}h^2 = 0.0791$ while neglecting these would lead to a value larger by 10%.

It is interesting to analyse the impact on the calculated relic abundance $\Omega^{\text{SF}}h^2$ when the number of channels included in the multi-state Schrödinger equation is changed, or the number of heavier states contributing to corrections from the last potential loop is varied. Let us recall that the results presented so far in this section correspond to calculations where all $\chi\chi$ -states with masses below $M_{\text{max}} = 3893$ GeV are treated exactly in the Schrödinger equation,⁶ while the remaining heavier states are included only at tree-level and in the last loop near the annihilation vertex in the Sommerfeld-corrected rates of the lighter states. Further we have considered δm^2 corrections in the potentials for the channels included in the Schrödinger equation but not in the approximate treatment of the heavier states; these δm^2 corrections are associated with the factors $\lambda^{Z/W}$ in the building blocks for the potential interactions given in Appendix B, Tab. B.1. In order to compare the cases where the number of channels treated in the Schrödinger equation is changed, we neglect these δm^2 corrections in the potentials throughout in the following, so that all cases are computed with the same potential. We calculate $\Omega^{\text{SF}}h^2$ for the cases of $M_{\text{max}} = 3762$ GeV and $M_{\text{max}} = 3893$ GeV, corresponding to $v_{\text{max}} = 0.2$ and $1/3$, as well as for $M_{\text{max}} = \infty$. In the latter case all $\chi\chi$ -channels are taken into account in the Schrödinger equation. To investigate the accuracy of the approximate treatment of heavier states in the last potential loop compared to the case where these

⁶From the definition $M_{\text{max}} = 2m_{\chi_1^0} + m_{\chi_1^0}v_{\text{max}}^2$ the quoted value $M_{\text{max}} = 3893$ GeV for trajectory model 8 is obtained by setting $m_{\chi_1^0} = 1844$ GeV (see Tab. 9.1) and $v_{\text{max}} = 1/3$.

$\Omega^{\text{SF}} h^2$	$M_{\text{max}} = 3762 \text{ GeV}$	$M_{\text{max}} = 3893 \text{ GeV}$	$M_{\text{max}} = \infty$
$M_{\text{cut}} = 3762 \text{ GeV}$	0.0858	—	—
$M_{\text{cut}} = 3893 \text{ GeV}$	0.0817	0.0816	—
$M_{\text{cut}} = \infty$	0.0804	0.0801	0.0801

Table 9.3: Relic abundances $\Omega^{\text{SF}} h^2$ in trajectory model 8 with a different number of channels accounted for in the Schrödinger equation and with a different number of heavy $\chi\chi$ -states treated approximately in the last potential loop. Two-particle channels $\chi\chi$ with masses below M_{max} are included in the Schrödinger equations. One-loop corrections of heavier $\chi\chi$ -channels with masses between M_{max} and M_{cut} are accounted for, while all $\chi\chi$ -channels heavier than M_{cut} are ignored. All results are derived neglecting δm^2 corrections in the potentials.

states are accounted for exactly in the Schrödinger equation, we introduce the variable $M_{\text{cut}} \geq M_{\text{max}}$. $\chi\chi$ -states with a mass larger than M_{cut} are ignored completely. States with mass below M_{max} are included in the Schrödinger equation exactly, while those with mass between M_{max} and M_{cut} are treated approximately through the one-loop corrections in the last potential loop. The relevant $\chi\chi$ -states together with their masses are given in Tab. 9.2, from which the number of exactly and approximately treated states in each charge sector for each of the cases covered in Tab. 9.3 can be read off. The results on $\Omega^{\text{SF}} h^2$ that we obtain for our three choices for M_{max} and for M_{cut} set to $M_{\text{cut}} = 3762 \text{ GeV}$, 3893 GeV and $M_{\text{cut}} = \infty$ are collected in Tab. 9.3.

Let us first discuss the $\Omega^{\text{SF}} h^2$ values on the diagonal of Tab. 9.3, which display the effect of increasing the number of states in the Schrödinger equation while ignoring one-loop corrections from heavier states. Expectedly $\Omega^{\text{SF}} h^2$ decreases the larger M_{max} . There are more $\chi\chi$ -channels for which Sommerfeld enhancements on their individual annihilation cross sections are taken into account. This leads to an increase of the thermally averaged effective rate $\langle\sigma_{\text{eff}}v\rangle$ entering the Boltzmann equation, which in turn decreases the relic abundance. By increasing M_{max} by the steps indicated in Tab. 9.3 the resulting $\Omega^{\text{SF}} h^2$ is reduced by 5% and 2% respectively. The effect on $\Omega^{\text{SF}} h^2$ from more channels in the Schrödinger equations is rather mild as compared to the 33% reduction with respect to the tree-level relic density.⁷ The milder reduction mainly derives from the fact that the Sommerfeld enhancement of the heavier channels' cross sections is less pronounced than in case of the most relevant lighter channels $\chi_1^0\chi_1^0$, $\chi_1^+\chi_1^-$ and $\chi_1^0\chi_1^\pm$. Further, as noted previously, the heavier $\chi\chi$ -channels enter the thermally averaged rate $\langle\sigma_{\text{eff}}v\rangle$ with a Boltzmann suppression factor such that their contribution is generically sub-dominant, unless the individual rates are particularly enhanced. The main effect that leads to the respective 5% and 2% change of $\Omega^{\text{SF}} h^2$ comes from the slight increase of the Sommerfeld-enhanced cross sections of the dominant light channels $\chi_1^0\chi_1^0$, $\chi_1^+\chi_1^-$ and $\chi_1^0\chi_1^\pm$ when more states appear in the potentials of the Schrödinger equations.

⁷Dropping the δm^2 terms in the potential slightly increases the relic density for model 8 from the value quoted in Tab. 9.1, $\Omega^{\text{SF}} h^2 = 0.0791$ to $\Omega^{\text{SF}} h^2 = 0.0801$, which implies $\Omega^{\text{SF}} h^2 / \Omega^{\text{pert}} h^2 = 0.670$.

Let us now consider the reduction of $\Omega^{\text{SF}}h^2$ for fixed M_{max} and increasing M_{cut} . This happens because the effect of heavier channels amounts to a positive correction to the Sommerfeld-enhanced cross sections: the dominant potential interactions are attractive, such that the heavier states in the last potential loop typically give an additional positive contribution. For instance we find a significant reduction of $\Omega^{\text{SF}}h^2$ by 5% from 0.858 to 0.817, when for $M_{\text{max}} = 3762 \text{ GeV}$ the value of M_{cut} is increased from 3762 GeV to 3893 GeV. This indicates that the newly added heavier states in the last loop give a large positive contribution to the Sommerfeld-enhanced cross sections of the $\chi\chi$ -states in the Schrödinger equation. When CPU considerations make the restriction to fewer states treated in the Schrödinger equation necessary, the approximate treatment of heavy channels should give a reasonable approximation to the case where these heavy channels are included fully in the Schrödinger equation. This is nicely confirmed by the numbers shown in Tab.9.3: when the states with mass between 3762 GeV and 3893 GeV are treated approximately, the reduction of $\Omega^{\text{SF}}h^2$ from 0.0858 to 0.0817 is very close to the value 0.0816 obtained from the exact treatment of all states with mass below 3893 GeV. The same observation holds for the comparison between the approximate treatment of all states with masses above 3762 GeV, $\Omega^{\text{SF}}h^2 = 0.0804$, and the exact result $\Omega^{\text{SF}}h^2 = 0.0801$. The agreement becomes even better when the perturbative treatment involves only the heavier channels with mass above 3893 GeV.

Chapter 10

Conclusions

We have studied the impact of Sommerfeld enhancements on co-annihilation rates of non-relativistic and nearly mass-degenerate heavy neutralino and chargino pairs, considering in particular the effect on the χ_1^0 relic abundance calculation.

For a systematic investigation in the general MSSM, where the χ_1^0 is an arbitrary admixture of the electroweak-eigenstate gauginos and higgsinos, we have constructed a non-relativistic effective field theory, the NRMSSM, that is designed to calculate the enhanced radiative corrections to pair-annihilation rates of close-in-mass neutralino and chargino states with small relative velocities. The NRMSSM shares similarities with the NRQCD framework applied to heavy quarkonium annihilation. An important difference is the presence of several heavy neutralino and chargino species with small mass differences in the NRMSSM in contrast to a single heavy quark together with its anti-quark in NRQCD. Further, massive mediator exchange occurs among the heavy neutralino and chargino NRMSSM states, where the mediator particles are given by the electroweak gauge bosons, the photon and the light Higgs bosons subject to the underlying MSSM spectrum. Apart from the photon, which is associated with diagonal Coulomb-type potentials, the mediator particles generate diagonal as well as off-diagonal Yukawa-type potential interactions that allow for potential scattering transitions between two close-in-mass particle pairs built from the NRMSSM neutralino and chargino states.

In the NRMSSM the neutralino and chargino co-annihilation cross sections are obtained from the imaginary part of scattering matrix elements of four-fermion operators. Factorisation of short-distance and long-range effects in the annihilation processes is automatically provided in the effective theory: the short-distance annihilation is encoded in the absorptive parts of the Wilson coefficients of the four-fermion operators, while the matrix-elements of the latter operators contain the long-range effects causing the Sommerfeld enhancements of the full annihilation rate. The weak coupling nature of the involved electromagnetic and electroweak potential interactions allows to explicitly calculate the matrix elements of the four-fermion operators.

Due to the presence of off-diagonal potentials, the NRMSSM short-distance annihilation reactions are characterised by diagonal as well as off-diagonal rates. We have derived purely analytical expressions for all such (off-) diagonal non-relativistic annihilation rates

up to corrections of $\mathcal{O}(v_{\text{rel}}^2)$ and at leading order in the expansion in couplings. The diagonal rates thus reproduce the tree-level annihilation cross sections of non-relativistic neutralino and chargino pairs including the $\mathcal{O}(v_{\text{rel}}^2)$ P - and next-to-next-to-leading order S -wave effects. We have performed a dedicated comparison of our results to numerical data for the pair-annihilation rates obtained with the code MADGRAPH, showing a good reliability of our non-relativistic approximation up to relative velocities of $v_{\text{rel}} \simeq 0.4c$. Our comprehensive results for the (off-) diagonal NRMSSM annihilation rates extend previously known expressions in several aspects. First, off-diagonal short-distance rates in Sommerfeld-enhanced annihilation reactions were only consistently included in the simple limiting scenarios of pure wino and pure higgsino χ_1^0 . Further, the effect of Sommerfeld enhancements on P - and next-to-next-to-leading order S -wave rates has not been considered before. It is worth to mention that a partial-wave separation of the short-distance rates, which is needed for a consistent treatment of the partial-wave dependent Sommerfeld enhancements, is obtained in the NRMSSM by construction, in particular disentangling the $\mathcal{O}(v_{\text{rel}}^2)$ short distance P - and next-to-next-to-leading order S -wave rates.

As regards the potential interactions, we have presented analytic results for all (off-) diagonal leading-order potentials between the NRMSSM neutralino and chargino states, accounting for electroweak gauge boson as well as light Higgs boson exchange. A central expression in our NRMSSM framework is formula (8.13) that gives the Sommerfeld-corrected annihilation rate of a pair $\chi_i\chi_j$ of NRMSSM states including $\mathcal{O}(v_{\text{rel}}^2)$ corrections in the short-distance part; it generalises the non-relativistic approximation to the tree-level annihilation cross section, $\sigma_{\chi_i\chi_j}v_{\text{rel}} = a + bv_{\text{rel}}^2$, by taking Sommerfeld enhancements into account.

The determination of the partial-wave dependent Sommerfeld enhancement factors requires the solution of a multi-state Schrödinger equation containing potential matrices that are related to the (off-) diagonal potential interactions among the NRMSSM states. We have described a novel method to solve the Schrödinger equation in order to obtain the Sommerfeld factors, that is free from numerical instabilities associated with the presence of kinematically closed heavier two-particle channels. In addition we have suggested an approximate treatment of very heavy two-particle states, which are not part of the set of NRMSSM neutralinos and charginos: by introduction of appropriate effective short-distance rates, certain heavy-channel contributions to the annihilation reactions of the NRMSSM states can be incorporated.

As application of our effective theory framework we have presented a detailed investigation of Sommerfeld enhancements in the χ_1^0 relic abundance calculation for several benchmark models with heavy neutralino LSP in the general MSSM. Our analysis is focused on three pMSSM benchmark models with wino-, higgsino- and bino-like χ_1^0 taken from [98]. Since our framework allows for the first time a consistent investigation of Sommerfeld enhancements in neutralino/chargino co-annihilations for χ_1^0 states with arbitrary gaugino and higgsino mixture, we have additionally defined a “higgsino-to-wino” trajectory in the parameter space of the general MSSM. This trajectory is given by a set of 13 DarkSUSY generated spectra interpolating between the cases of a higgsino- to a

wino-like χ_1^0 spectrum. In scenarios with wino-like χ_1^0 we have found sizable 40% to 60% reductions of the relic density when accounting for Sommerfeld-enhanced co-annihilation rates with respect to the calculation with corresponding perturbative cross sections. The reduction is found to be much milder, of the order of 3% to 14%, in case of the studied higgsino-like χ_1^0 models. These results are in agreement with previous investigations in the literature in the pure-wino and pure-higgsino limits. In general the relic abundance obtained including the Sommerfeld effect is reduced the more the stronger the wino admixture to the χ_1^0 . Cases of particular pronounced effects are related to the existence of loosely or zero-energy bound states in the spectrum of the corresponding model. Our investigations show that the precise value of the calculated relic density depends on the particular details of the spectrum, such that results from a study in the pure-wino or pure-higgsino χ_1^0 scenarios do not apply directly. Interestingly, the Sommerfeld enhancements in the co-annihilating sector of a bino-like χ_1^0 can affect the result on $\Omega^{\text{SF}} h^2$ at the 10% level, which is found for the studied benchmark model with bino-like χ_1^0 and slightly heavier wino-like χ^\pm/χ^0 states. The knowledge of precise mass splittings between the co-annihilating neutralinos and charginos is essential in the calculation of Sommerfeld-enhanced rates and will typically require the knowledge of spectra with a one-loop on-shell renormalised neutralino/chargino sector.

With the analyses of Sommerfeld enhancements in neutralino/chargino co-annihilations in several MSSM scenarios we have shown the general features of the enhancement effect and its particular relevance regarding the neutralino relic abundance calculation. Our results imply that Sommerfeld enhancements have to be taken into account when deriving MSSM parameter space constraints on heavy neutralino dark matter from a combination of direct and indirect dark matter searches, collider constraints and the additional requirement to reproduce or at least not overproduce the observed cosmic dark matter abundance in terms of a χ_1^0 relic. Our effective theory framework allows for corresponding future investigations of the parameter space of the general MSSM in view of the relevance of Sommerfeld enhancements in the χ_1^0 relic abundance calculation.

It is worth to stress that the NRMSSM that we have developed in this thesis provides the first – and at the moment the only available – technique to account for Sommerfeld enhancements in neutralino and chargino co-annihilations in the general MSSM with arbitrary χ_1^0 composition. The method can be extended to other WIMP dark matter models provided the necessary model-dependent inputs, that is the potential and annihilation matrices, are known.

Appendix A

Absorptive parts of Wilson coefficients of dimension-6 and 8 operators in $\delta\mathcal{L}_{\text{ann}}$

In this appendix we collect explicit expressions for the coupling and kinematic factors, that are the building blocks entering the master formula (6.17) for the absorptive parts $\hat{f}^{(d=6,8)(2s+1)L_J}$ of the Wilson coefficients related to $\chi_{e_1}\chi_{e_2} \rightarrow X_A X_B \rightarrow \chi_{e_4}\chi_{e_3}$ processes. We discuss the coupling factors in Sec. A.1, where we first present a recipe for the coupling factor construction in Sec. A.1.1. In order to unambiguously fix our conventions we subsequently give in Sec. A.1.2 explicit expressions for the MSSM vertex factors, that appear as constituents of the coupling factors of the Wilson coefficients. As an example, how the recipe of Sec. A.1.1 is applied we finally discuss in Sec. A.1.3 the derivation of coupling factors $c_{n,i_1 V}^{(\alpha)}$, that are related to $\chi_{e_1}^- \chi_{e_2}^+ \rightarrow W^+ G^- \rightarrow \chi_{e_4}^0 \chi_{e_3}^0$ reactions.

Analytic expressions for the kinematic factors arising as constituents of the absorptive parts $\hat{f}^{(2s+1)S_J}$ of leading order S -wave Wilson coefficients are given in Sec. A.2. The subsections A.2.1 – A.2.5 contain the respective results for exclusive final states of type $X_A X_B = VV, VS, SS, ff, \eta\bar{\eta}$. Likewise we present in Sec. A.3 analytic results for the kinematic factors related to coefficients $\hat{f}^{(2s+1)L_J}$ in P -wave reactions, where the subsections A.3.1 – A.3.5 again refer to $X_A X_B = VV, VS, SS, ff, \eta\bar{\eta}$, respectively. While expressions for the kinematic factors for 1P_1 partial-wave configurations are written explicitly, we give in case of the three spin $s = 1$ P -wave configurations $^3P_{J=0,1,2}$ results, that refer to the spin-weighted coefficients introduced in (6.29), namely

$$\hat{f}^{(3P_J)} = \frac{1}{3}\hat{f}^{(3P_0)} + \hat{f}^{(3P_1)} + \frac{5}{3}\hat{f}^{(3P_2)}. \quad (\text{A.1})$$

Results for kinematic factors that arise in next-to-next-to-leading order S -wave coefficients $\hat{g}^{(2s+1)S_s}$ and $\hat{h}_i^{(2s+1)S_s}$ are lengthy and therefore not given explicitly in a separate appendix. Together with the kinematic factors presented here they are collected in the electronic supplement, that comes with [32]. Note that in addition to the kinematic factors for the spin-weighted P -wave coefficients, (A.1), the supplement also contains results related to the three individual spin $s = 1$ P -wave configurations $^3P_{J=0,1,2}$.

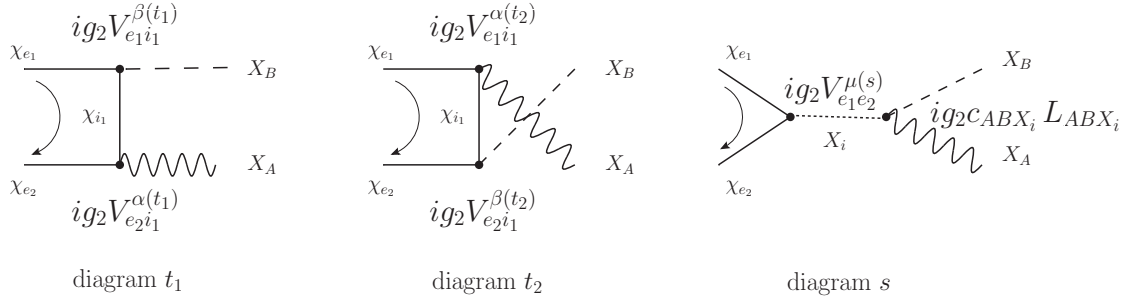


Figure A.1: Generic tree-level amplitudes in $\chi\chi \rightarrow X_A X_B$ annihilations, referring to VV, VS and SS -type final state particles $X_A X_B$. The generic form of s -channel exchange diagrams for $X_A X_B = \eta\bar{\eta}$ final states agrees with the s -channel diagram above. The vertex-factors $V_{ei}^{\rho(d)}$ are defined as $V_{ei}^{\rho(d)} = \gamma^\rho (r_{ei}^{(d)} + q_{ei}^{(d)} \gamma_5)$, if attached to a three-point vertex with a gauge boson (with Lorentz-index ρ), and $V_{ei}^{\rho(d)} = (r_{ei}^{(d)} + q_{ei}^{(d)} \gamma_5)$, if associated with a vertex that involves a scalar particle X_A, X_B or X_i . Here the expression $r_{ei}^{(d)} (q_{ei}^{(d)})$ either denotes a vector or scalar (an axial-vector or pseudo-scalar) type of coupling factor. For the definition of c_{ABX_i} and the Lorentz structures L_{ABX_i} we refer to Tab. A.1 below.

A.1 Coupling factors

A.1.1 Coupling factor construction

By construction, the absorptive part $\hat{f}^{(d)\chi_{e_1}\chi_{e_2} \rightarrow X_A X_B \rightarrow \chi_{e_4}\chi_{e_3}}$ of an individual Wilson coefficient is associated with the product $\mathcal{A}_{\chi_{e_1}\chi_{e_2} \rightarrow X_A X_B}^{(0)} \times (\mathcal{A}_{\chi_{e_4}\chi_{e_3} \rightarrow X_A X_B}^{(0)})^*$ of Born-level annihilation amplitudes $\mathcal{A}^{(0)}$ related to $\chi_{e_i}\chi_{e_j} \rightarrow X_A X_B$ reactions, integrated over the $X_A X_B$ two-particle phase space, see (6.3). Each of the tree-amplitudes $\mathcal{A}_{\chi\chi \rightarrow X_A X_B}^{(0)}$ receives contributions from diagrams with t -channel neutralino or chargino exchange as well as from diagrams with s -channel Higgs-particle or gauge boson exchange, such as the generic diagrams shown in Fig. A.1. In case of fermionic final states $X_A X_B$, instead of neutralino or chargino t -channel exchange, t -channel sfermion-exchange occurs, as depicted in Fig. A.2. Note, that in Fig. A.1 and Fig. A.2 we have established a specific fermion flow, which in particular coincides with the convention for the fermion flow associated with the incoming two particles in the 1-loop amplitudes in Fig. 6.1.

A contribution to the amplitude $\mathcal{A}_{\chi\chi \rightarrow X_A X_B}^{(0)}$ involves a product of two coupling factors, coming from the two vertices in the tree-level diagrams. The generic form of these vertices is indicated in Fig. A.1 and Fig. A.2. It is especially convenient to write all vertex factors in any of the amplitudes contributing to the non-relativistic $\chi\chi \rightarrow X_A X_B \rightarrow \chi\chi$ scattering-processes as a combination of (axial-) vector or (pseudo-) scalar coupling factors, instead of using left- and right-handed couplings, as it is common in calculations related to the MSSM. The reason for that is, that in the non-relativistic limit either the contributions to the annihilation amplitudes involving the axial-vector (pseudo-scalar) coupling will be suppressed with respect to the corresponding contributions related to

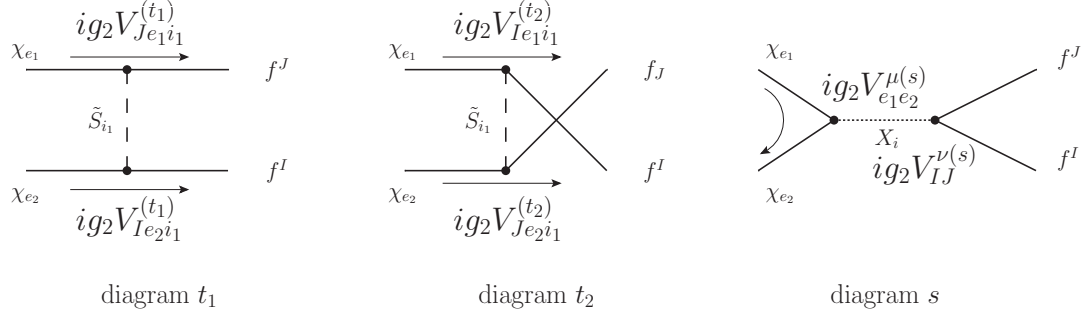


Figure A.2: Generic tree-level amplitudes in $\chi\chi \rightarrow X_A X_B$ annihilations, with $X_A X_B = f^I f^J$. For the definition of $V_{ei}^{\rho(d)}$ see Fig. A.1. The generic vertex factor $V_{Kei}^{(d)}$ is defined as $V_{Kei}^{(d)} = r_{Kei}^{(d)} + q_{Kei}^{(d)}\gamma_5$, such that the $r_{Kei}^{(d)}$ ($q_{Kei}^{(d)}$) denote coupling factors of scalar (pseudo-scalar) type.

the vector (scalar) coupling, or vice versa, such that the use of (axial-) vector and (pseudo-) scalar couplings allows for a clearer understanding of leading and suppressed contributions in the non-relativistic scattering regime that we aim to study.

Each of the coupling factors $b_n, c_n^{(\alpha)}$ and $d_n^{(\alpha)}$ that occur in the master formula (6.17) for the $\hat{f}^{(d)}(2s+1L_J)$, is given by a product of two coupling factors, r or q , arising in an individual diagram in $\mathcal{A}_{\chi_{e_1}\chi_{e_2} \rightarrow X_A X_B}^{(0)}$, and the complex conjugate of another such two-coupling factor product originating from $\mathcal{A}_{\chi_{e_4}\chi_{e_3} \rightarrow X_A X_B}^{(0)}$. In the following, we give a recipe how to construct the coupling factors in (6.17) for a specific $\chi_{e_1}\chi_{e_2} \rightarrow X_A X_B \rightarrow \chi_{e_4}\chi_{e_3}$ reaction, such that taken together with the leading-order S -wave kinematic factors in Sec. A.2 and the P -wave expressions¹ in Sec. A.3, they allow to determine the absorptive part of the corresponding Wilson coefficients $\hat{f}^{(d=6,8)}(2s+1L_J)$:

1. Draw all tree-level diagrams that contribute to $\chi_{e_1}\chi_{e_2} \rightarrow X_A X_B$ and $\chi_{e_4}\chi_{e_3} \rightarrow X_A X_B$ annihilation amplitudes, analogous to the generic diagrams sketched in Fig. A.1 or Fig. A.2. In particular, assign the same fermion flow as indicated for the generic diagrams.
2. Determine the process-specific (axial-) vector and/or (pseudo-) scalar coupling factors, that arise instead of the generic $q_{ei}^{(d)}$ or $r_{ei}^{(d)}$ place-holder expressions at the generic amplitudes' vertex factors. As the $\chi\chi \rightarrow X_A X_B$ processes may involve Majorana as well as Dirac fermions, and the latter involve a conserved fermion-number flow, note the following rules:

- a) If the direction of the fermion-number flow related to a Dirac particle coincides

¹The results on the next-to-next-to-leading order S -wave kinematic factors are quite lengthy. Therefore they are provided in an electronic supplement to [32] rather than written explicitly in an appendix. Note that the electronic supplement collects all leading-order S -wave, P -wave and next-to-next-to-leading order S -wave kinematic factors related to $\chi_{e_1}\chi_{e_2} \rightarrow \chi_{e_4}\chi_{e_3}$ reactions in the NRMSSM.

with the direction of the fermion flow (fixed as in Fig. A.1 and Fig. A.2), the $\chi\chi \rightarrow X_A X_B$ process specific coupling factors at the vertices are directly deduced from the corresponding interaction terms in the underlying Lagrangian. These coupling factors are given later in (A.4–A.10).

- b) Otherwise, if the fermion-number flow is antiparallel to the indicated fermion flow, vector coupling factors at vertices attached to a Dirac fermion line, are given by a factor -1 times the expression for the vector coupling given in (A.4–A.6). Axial-vector, scalar and pseudo-scalar coupling factors are unchanged with respect to case *a*) above.
3. Build all possible two-coupling factor products, including possible signs related to vector couplings, as far as the case in 2b) above applies, that can arise in each single diagram.
 4. Multiply each of the two-coupling factor products, that arise in the $\mathcal{A}_{\chi_{e_1}\chi_{e_2} \rightarrow X_A X_B}^{(0)}$ amplitude, with the complex conjugate of each of the two-coupling factor products, arising in $\mathcal{A}_{\chi_{e_4}\chi_{e_3} \rightarrow X_A X_B}^{(0)}$. As a result, all possible coupling factor combinations that can occur in $\hat{f}^{(d=6,8)}_{\chi_{e_1}\chi_{e_2} \rightarrow X_A X_B \rightarrow \chi_{e_4}\chi_{e_3}}$ are obtained.

Rule 2b) arises in the following way for the case of diagram *s* in Figs. A.1–A.2: according to our convention for the fermion flow in Fig. A.1, we obtain an expression $-\bar{v}(p_1)\Gamma u(p_2)$ for the incoming particles' spinor chain if the case under 2b) applies, where Γ denotes the involved Dirac-matrix structure. The minus sign accounts for our convention for the order of the external fermion states. This expression can be rewritten as

$$-\bar{v}(p_1)\Gamma u(p_2) = \bar{v}(p_2) C \Gamma^T C^{-1} u(p_1) , \quad (\text{A.2})$$

wherein C denotes the charge conjugation matrix. Using

$$C \Gamma^T C^{-1} = \begin{cases} -\Gamma & \text{for } \Gamma = \gamma_\mu , \\ \Gamma & \text{for } \Gamma = 1, \gamma_5, \gamma_\mu \gamma_5 , \end{cases} \quad (\text{A.3})$$

the origin of the minus sign rules for vector couplings under 2b) above becomes obvious. For diagrams with *t*-channel exchange, a similar derivation also confirms rule 2b).

Let us introduce the shorthand $a\tilde{a}$ to indicate the diagrams *a* and \tilde{a} in the $\chi_{e_1}\chi_{e_2} \rightarrow X_A X_B$ and $\chi_{e_4}\chi_{e_3} \rightarrow X_A X_B$ processes, respectively, to which the coupling factors in a specific coupling factor combination are related. Both *a* and \tilde{a} can be given by *s*, t_1 or t_2 , see Figs. A.1–A.2. Coupling factor combinations originating from *ss* lead to the *b* factors, that correspond to the generic selfenergy-amplitude in Fig. 6.1.² We label coupling factor combinations, that originate from $t_1 s$, $s t_1$, $t_2 s$ and $s t_2$ with the superscript $\alpha = 1, \dots, 4$, respectively. These coupling factor combinations, related to one *t*-channel

²Note, that in case of identical particles $X_A = X_B$, all coupling factor expressions *b* have to be multiplied with a symmetry factor 1/2, which incorporates the symmetry factor associated with the selfenergy amplitudes in case of identical particles $X_A = X_B$ in the loop.

and one s -channel exchange diagram give rise to the $c^{(\alpha)}$ expressions in (6.17). The $\alpha = 1, \dots, 4$ label-convention for the specific coupling factor combinations allows to correctly allocate the $c^{(\alpha)}$ to their corresponding generic triangle-amplitude ‘triangle α ’ in Fig. 6.1. Coupling factor combinations originating from $t_1 t_2$, $t_1 t_1$, $t_2 t_1$ and $t_2 t_2$ are labeled with superscript $\alpha = 1, \dots, 4$, and give rise to the $d^{(\alpha)}$ expressions. As in case of the $c^{(\alpha)}$, this convention correctly assigns $d^{(\alpha)}$ expressions to their corresponding ‘box α ’ amplitude in Fig. 6.1.

We introduce the index n in order to label the different coupling factor combinations for a given fixed $a\tilde{a}$. Each individual n is given by a character-string, where the i th character gives the type (r or q) of the coupling factor which is related to the i th vertex in the particular diagram $a\tilde{a}$ in Fig. 6.1. The vertices of box-amplitudes are enumerated according to the respective attached external particles χ_{e_i} , $i = 1, \dots, 4$. In case of selfenergy- and triangle-diagrams with inner vertices our vertex-enumeration convention is from top to bottom and left to right. Vertex factors of type c_{ABX_i} are not specified in the corresponding string n , because the nature of the particles X_A , X_B and X_i involved in the diagram completely characterize that coupling. For triangles with $X_A X_B = VV, VS$ or SS , for example, the index n will range over strings rrr, qqr, \dots , where the characters r or q indicate the type of coupling of the external particles to the $X_A X_B$ pair and to the single s -channel exchanged particle species, see the triangle diagrams in Fig. 6.1.

To further specify the coupling factor combinations for given $a\tilde{a}$ and n , we use the labels i_1 and i_2 to indicate the particle species that are internally exchanged in diagrams a and \tilde{a} . Therewith, the coupling factor combinations $b_{n i_1 i_2}$, $c_{n i_1 i_2}^{(\alpha)}$ and $d_{n i_1 i_2}^{(\alpha)}$ that should enter in (6.17), together with the generic kinematic factor expressions given in App. A.2-A.3 and the electronic supplement to [32], can be unambiguously determined.

A.1.2 (Axial-)vector and (pseudo-)scalar MSSM vertex factors

In order to completely fix our conventions, we summarize in the following the expressions for the (axial-) vector and (pseudo-) scalar coupling factors, that arise in the three-point interactions of charginos and neutralinos with SM and Higgs particles. The definitions of the coupling factors assume that we take χ_i^+ to be the particle and χ_i^- its anti-particle, such that the Dirac fermion number flow, indicated by the arrow on the Dirac fermion line for a chargino, will always refer to the direction of χ_i^+ flow. The latter convention agrees with that of Rosiek [62].

The generic form for the vertex factor, that describes the 3-point interaction of an incoming neutralino χ_j^0 , an outgoing chargino χ_i^+ and either an incoming charged Higgs particle G^+ or H^+ or an incoming W^+ -boson is given in the left-most diagram in Fig. A.3. Note that the gamma matrix γ^μ in the vertex factor has to be omitted in case of interactions with the charged Higgs particles. The specific scalar and pseudo-scalar or vector and axial-vector coupling factors, that have to be replaced for the generic r_{ij} and q_{ij} couplings therein read

$$s_{ij}^{H_m^\pm}(p_{ij}^{H_m^\pm}) = -\frac{1}{2} \left[Z_H^{2m} \left(\tilde{Z}_N^{4j*} \tilde{Z}_+^{1i*} + \frac{1}{\sqrt{2}} \tilde{Z}_+^{2i*} (\tilde{Z}_N^{2j*} + \tan \theta_W \tilde{Z}_N^{1j*}) \right) \right]$$

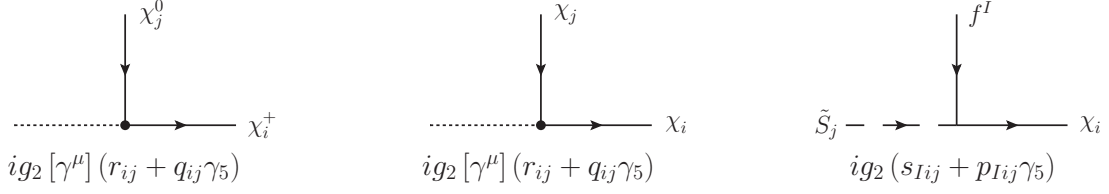


Figure A.3: Generic form of the vertex factors in three-point interactions of neutralinos and charginos with SM and Higgs particles, upon which our definition of the (axial-) vector and (pseudo-) scalar coupling factors given in the text is based.

$$\begin{aligned}
& \pm Z_H^{1m} \left(\tilde{Z}_N^{3j} \tilde{Z}_-^{1i} - \frac{1}{\sqrt{2}} \tilde{Z}_-^{2i} (\tilde{Z}_N^{2j} + \tan \theta_W \tilde{Z}_N^{1j}) \right) \Big], \\
v_{ij}^W &= \frac{1}{2} \left(\tilde{Z}_N^{2j*} \tilde{Z}_-^{1i} + \tilde{Z}_N^{2j} \tilde{Z}_+^{1i*} + \frac{1}{\sqrt{2}} \tilde{Z}_N^{3j*} \tilde{Z}_-^{2i} - \frac{1}{\sqrt{2}} \tilde{Z}_N^{4j} \tilde{Z}_+^{2i*} \right), \\
a_{ij}^W &= \frac{1}{2} \left(\tilde{Z}_N^{2j*} \tilde{Z}_-^{1i} - \tilde{Z}_N^{2j} \tilde{Z}_+^{1i*} + \frac{1}{\sqrt{2}} \tilde{Z}_N^{3j*} \tilde{Z}_-^{2i} + \frac{1}{\sqrt{2}} \tilde{Z}_N^{4j} \tilde{Z}_+^{2i*} \right), \quad (\text{A.4})
\end{aligned}$$

where $H_1^+ \equiv H^+$ and $H_2^+ \equiv G^+$, and the mixing matrices are defined as in Ref. [62]. The generic form of the three point interaction of either two neutralinos or two charginos with an electrically neutral gauge boson or Higgs particle is depicted in the second diagram in Fig. A.3. Again, the gamma-matrix γ^μ has to be omitted in the vertex factor if the corresponding reaction refers to interactions with the neutral Higgs particles. In the case of an incoming χ_j^+ and an outgoing χ_i^+ , the (axial-) vector and (pseudo-) scalar couplings, that encode interactions with the neutral scalar and pseudo-scalar Higgs particles (h^0, H^0, G^0, A^0), the Z -boson or the photon are given by the following expressions:

$$\begin{aligned}
s_{ij}^{H_m^0} (p_{ij}^{H_m^0}) &= -\frac{1}{2\sqrt{2}} \left[Z_R^{1m} \left(\tilde{Z}_-^{2j*} \tilde{Z}_+^{1i*} \pm \tilde{Z}_-^{2i} \tilde{Z}_+^{1j} \right) + Z_R^{2m} \left(\tilde{Z}_-^{1j*} \tilde{Z}_+^{2i*} \pm \tilde{Z}_-^{1i} \tilde{Z}_+^{2j} \right) \right], \\
s_{ij}^{A_m^0} (p_{ij}^{A_m^0}) &= -\frac{i}{2\sqrt{2}} \left[Z_H^{1m} \left(\tilde{Z}_-^{2j*} \tilde{Z}_+^{1i*} \mp \tilde{Z}_-^{2i} \tilde{Z}_+^{1j} \right) + Z_H^{2m} \left(\tilde{Z}_-^{1j*} \tilde{Z}_+^{2i*} \mp \tilde{Z}_-^{1i} \tilde{Z}_+^{2j} \right) \right], \\
v_{ij}^Z &= -\frac{1}{4c_W} \left(\tilde{Z}_-^{1i} \tilde{Z}_-^{1j*} + \tilde{Z}_+^{1i*} \tilde{Z}_+^{1j} + 2(c_W^2 - s_W^2) \delta_{ij} \right), \\
a_{ij}^Z &= \frac{1}{4c_W} \left(\tilde{Z}_+^{1i*} \tilde{Z}_+^{1j} - \tilde{Z}_-^{1i} \tilde{Z}_-^{1j*} \right), \\
v_{ij}^\gamma &= -s_W \delta_{ij}, \\
a_{ij}^\gamma &= 0, \quad (\text{A.5})
\end{aligned}$$

where $H_1^0 \equiv H^0$, $H_2^0 \equiv h^0$ and $A_1^0 \equiv A^0$, $A_2^0 \equiv G^0$. Finally, three-point interactions of an incoming χ_j^0 and an outgoing χ_i^0 with a (pseudo-) scalar Higgs particle or the Z -boson involve the following (axial-) vector or (pseudo-) scalar coupling factors

$$s_{ij}^{(0),H_m^0} (p_{ij}^{(0),H_m^0}) = \frac{1}{4} \left[\left(Z_R^{2m} \tilde{Z}_N^{4i*} - Z_R^{1m} \tilde{Z}_N^{3i*} \right) \left(\tilde{Z}_N^{2j*} - \tan \theta_W \tilde{Z}_N^{1j*} \right) + (i \leftrightarrow j) \right] \pm c.c.,$$

$$\begin{aligned}
s_{ij}^{(0),A^0}(p_{ij}^{(0),A^0}) &= \frac{i}{4} \left[\left(Z_H^{2m} \tilde{Z}_N^{4i*} - Z_H^{1m} \tilde{Z}_N^{3i*} \right) \left(\tilde{Z}_N^{2j*} - \tan \theta_W \tilde{Z}_N^{1j*} \right) + (i \leftrightarrow j) \right] \pm c.c. , \\
v_{ij}^{(0),Z}(a_{ij}^{(0),Z}) &= \frac{1}{4c_W} \left(\tilde{Z}_N^{3i} \tilde{Z}_N^{3j*} - \tilde{Z}_N^{4i} \tilde{Z}_N^{4j*} \mp (i \leftrightarrow j) \right) .
\end{aligned} \tag{A.6}$$

The (axial-) vector and (pseudo-) scalar coupling factors in (A.5) and (A.6), which are all related to interactions with neutral SM and Higgs particles, satisfy

$$\begin{aligned}
v_{ij}^* &= v_{ji} , & a_{ij}^* &= a_{ji} , \\
s_{ij}^* &= s_{ji} , & p_{ij}^* &= -p_{ji} .
\end{aligned} \tag{A.7}$$

as a consequence of the hermiticity of the underlying SUSY Lagrangian.

The generic form of the vertex factor for three-point interactions of a neutralino or chargino with a SM fermion and a sfermion is given in the right-most diagram in Fig. A.3. In case of interactions of an incoming SM fermion f^I with a sfermion \tilde{S}_j and an outgoing neutralino χ_i^0 , the specific (pseudo-) scalar couplings, that have to be replaced for the generic s_{Iij} and p_{Iij} expressions in Fig. A.3 read

$$\begin{aligned}
s_{Iij}^{u\tilde{U}}(p_{Iij}^{u\tilde{U}}) &= \frac{1}{\sqrt{2}} q_u \tan \theta_W \tilde{Z}_N^{1i*} Z_U^{(I+3)j*} - \frac{m_u^I}{2\sqrt{2} \sin \beta M_W} \left(\tilde{Z}_N^{4i*} Z_U^{Ij*} \pm \tilde{Z}_N^{4i} Z_U^{(I+3)j*} \right) \\
&\mp \frac{1}{\sqrt{2}} \left(T_u \tilde{Z}_N^{2i} + (q_u - T_u) \tilde{Z}_N^{1i} \tan \theta_W \right) Z_U^{Ij*} , \\
s_{Iij}^{d\tilde{D}}(p_{Iij}^{d\tilde{D}}) &= \frac{1}{\sqrt{2}} q_d \tan \theta_W \tilde{Z}_N^{1i*} Z_D^{(I+3)j} - \frac{m_d^I}{2\sqrt{2} \cos \beta M_W} \left(\tilde{Z}_N^{3i*} Z_D^{Ij} \pm \tilde{Z}_N^{3i} Z_D^{(I+3)j} \right) \\
&\mp \frac{1}{\sqrt{2}} \left(T_d \tilde{Z}_N^{2i} + (q_d - T_d) \tilde{Z}_N^{1i} \tan \theta_W \right) Z_D^{Ij} , \\
s_{Iij}^{\nu\tilde{\nu}}(p_{Iij}^{\nu\tilde{\nu}}) &= \mp \frac{1}{2\sqrt{2}} \left(\tilde{Z}_N^{2i} - \tilde{Z}_N^{1i} \tan \theta_W \right) Z_\nu^{Ij*} , \\
s_{Iij}^{l\tilde{L}}(p_{Iij}^{l\tilde{L}}) &= \frac{1}{\sqrt{2}} q_l \tan \theta_W \tilde{Z}_N^{1i*} Z_L^{(I+3)j} - \frac{m_l^I}{2\sqrt{2} \cos \beta M_W} \left(\tilde{Z}_N^{3i*} Z_L^{Ij} \pm \tilde{Z}_N^{3i} Z_L^{(I+3)j} \right) \\
&\mp \frac{1}{\sqrt{2}} \left(T_l \tilde{Z}_N^{2i} + (q_l - T_l) \tilde{Z}_N^{1i} \tan \theta_W \right) Z_L^{Ij} .
\end{aligned} \tag{A.8}$$

$I = 1, 2, 3$ denotes the generation index for the fermions, and $j = 1, \dots, 6$ labels the sfermion states ($j = 1, 2, 3$ in case of sneutrinos $\tilde{\nu}_j$). T_f and q_f are defined as

$$\begin{aligned}
T_u &= -T_d = -T_l = \frac{1}{2} , \\
q_u &= \frac{2}{3} , \quad q_d = -\frac{1}{3} , \quad q_l = -1 .
\end{aligned} \tag{A.9}$$

The superscripts $f\tilde{S}$ on the couplings in (A.8) refer to the fermion (f)- and sfermion (\tilde{S})-type involved in the underlying interaction. In case of chargino-fermion-sfermion interactions we find (a sum over repeated indices is implicit)

$$s_{Iij}^{u\tilde{D}}(p_{Iij}^{u\tilde{D}}) = \frac{m_u^I}{2\sqrt{2} \sin \beta M_W} K^{IJ*} \tilde{Z}_+^{2i*} Z_D^{Jj} \pm \frac{m_d^J}{2\sqrt{2} \cos \beta M_W} K^{IJ*} \tilde{Z}_-^{2i} Z_D^{(J+3)j}$$

$X_A X_B X_i$	L_{ABX_i}
$V_\alpha V_\beta V_\mu$	$g^{\alpha\beta}(k_A - k_B)^\mu + g^{\mu\alpha}(k_i - k_A)^\beta + g^{\beta\mu}(k_B - k_i)^\alpha$
$V_\alpha V_\beta S$	$M_W g^{\alpha\beta}$
$V_\alpha S S$	$(k_B - k_i)^\alpha$
$S S V_\mu$	$(k_B - k_A)^\mu$
$S S S$	M_W
$\eta \bar{\eta} V_\mu$	k_B^μ
$\eta \bar{\eta} S$	M_W

Table A.1: The generic form of the Lorentz structures L_{ABX_i} , that are part of the Feynman rule $ig_2 c_{ABX_i} L_{ABX_i}$ for the $X_A X_B X_i$ three-point vertex in Fig A.1. We assume all four-momenta, k_A, k_B, k_i , to be outgoing at the vertex. The case of $X_A X_B X_i = V_\alpha S V_\mu$ is trivially related to the case $V_\alpha V_\beta S$.

$$\begin{aligned}
& \mp \frac{1}{2} K^{IJ*} \tilde{Z}_-^{1i} Z_D^{Jj} , \\
s_{Iij}^{d\tilde{U}}(p_{Iij}^{d\tilde{U}}) &= \frac{m_d^I}{2\sqrt{2} \cos \beta M_W} K^{JI} \tilde{Z}_-^{2i*} Z_U^{Jj*} \pm \frac{m_u^J}{2\sqrt{2} \sin \beta M_W} K^{JI} \tilde{Z}_+^{2i} Z_U^{(J+3)j*} \\
& \mp \frac{1}{2} K^{JI} \tilde{Z}_+^{1i} Z_U^{Jj*} , \\
s_{Iij}^{\nu\tilde{L}}(p_{Iij}^{\nu\tilde{L}}) &= \pm \frac{m_l^I}{2\sqrt{2} \cos \beta M_W} \tilde{Z}_-^{2i} Z_L^{(I+3)j} \mp \frac{1}{2} \tilde{Z}_-^{1i} Z_L^{Ij} , \\
s_{Iij}^{l\tilde{\nu}}(p_{Iij}^{l\tilde{\nu}}) &= \frac{m_l^I}{2\sqrt{2} \cos \beta M_W} \tilde{Z}_-^{2i*} Z_\nu^{Jj*} \mp \frac{1}{2} \tilde{Z}_+^{1i} Z_\nu^{Ij*} . \tag{A.10}
\end{aligned}$$

The coupling factors with $f\tilde{S} = u\tilde{D}, \nu\tilde{L}$ refer to the interaction of an incoming up-type quark (u^I) or neutralino (ν^I) with a \tilde{D}_j - or \tilde{L}_j -sfermion and an outgoing χ_i^+ . In case of $f\tilde{S} = d\tilde{U}, l\tilde{\nu}$, the coupling factors in (A.10) are related to interactions of an incoming down-type quark (d^I) or lepton (l^I) with an \tilde{U}_j - or $\tilde{\nu}_j$ -sfermion and an outgoing χ_i^{+C} (denoting the charge-conjugate field of χ_i^+ , see [62]).

For the specific c_{ABX_i} factors that emerge at the three-point vertex of the $X_A X_B$ particle pair with the single s -channel exchanged particle X_i in Fig. A.1, we refer to the Feynman rules in [62]: a specific c_{ABX_i} is obtained as the factor that multiplies the structure $ig_2 L_{ABX_i}$ in the respective Feynman rule therein. The generic forms of the Lorentz structures L_{ABX_i} are collected in Tab. A.1. Finally, (axial-) vector and (pseudo-) scalar coupling factors r and q of two SM fermions with a gauge or Higgs boson (see Fig. A.2) can be directly taken from the corresponding Feynman rules in [62].

A.1.3 Example: construction of $c_{n,i_1 V}^{(\alpha)}$ in $\chi_{e_1}^- \chi_{e_2}^+ \rightarrow W^+ G^- \rightarrow \chi_{e_4}^0 \chi_{e_3}^0$

In order to illustrate how the above rules should be applied, let us consider an example. Suppose we wish to know the coupling factors $c_{n,i_1 V}^{(\alpha)}$, $\alpha = 1, \dots, 4$, of diagrams with s -channel exchange of a Z -boson for the $\chi_{e_1}^- \chi_{e_2}^+ \rightarrow W^+ G^- \rightarrow \chi_{e_4}^0 \chi_{e_3}^0$ processes. Following the recipe above, we draw all tree-level diagrams for the $\chi_{e_1}^- \chi_{e_2}^+ \rightarrow W^+ G^-$ as well as the $\chi_{e_4}^0 \chi_{e_3}^0 \rightarrow W^+ G^-$ process and assign the same fermion flow as given in the corresponding generic diagrams, Fig. A.1. Referring to that fixed fermion flow, we determine the following vertex factors in the diagrams t_1 and s , associated with tree-level $\chi_{e_1}^- \chi_{e_2}^+ \rightarrow W^+ G^-$ annihilations:

$$\begin{aligned} V_{e_1 i_1}^{\beta(t_1)} &= s_{e_1 i_1}^G + p_{e_1 i_1}^G \gamma_5, & V_{e_2 i_1}^{\alpha(t_1)} &= \gamma^\alpha (-v_{e_2 i_1}^{W^*} + a_{e_2 i_1}^{W^*} \gamma_5), \\ V_{e_1 e_2}^{\mu(s)} &= \gamma^\mu (-v_{e_1 e_2}^Z + a_{e_1 e_2}^Z \gamma_5), & c_{WGZ} &= -\frac{s_W^2}{c_W^2}. \end{aligned} \quad (\text{A.11})$$

The coupling factors are those from (A.4) and (A.5). Note that there is no t -channel exchange diagram t_2 for the above process, as it is forbidden by charge conservation. Further, note that the sign in front of the vector-coupling factor in $V_{e_2 i_1}^{\alpha(t_1)}$ and $V_{e_1 e_2}^{\mu(s)}$ follows from rule 2b) above. In case of diagrams contributing to $\chi_{e_4}^0 \chi_{e_3}^0 \rightarrow W^+ G^-$ we find

$$\begin{aligned} V_{e_4 i_1}^{\beta(t_1)} &= s_{i_1 e_4}^G + p_{i_1 e_4}^G \gamma_5, & V_{e_3 i_1}^{\alpha(t_1)} &= \gamma^\alpha (v_{i_1 e_3}^{W^*} + a_{i_1 e_3}^{W^*} \gamma_5), \\ V_{e_4 i_1}^{\alpha(t_2)} &= \gamma^\alpha (-v_{i_1 e_4}^{W^*} + a_{i_1 e_4}^{W^*} \gamma_5), & V_{e_3 i_1}^{\beta(t_2)} &= s_{i_1 e_3}^G + p_{i_1 e_3}^G \gamma_5, \\ V_{e_4 e_3}^{\mu(s)} &= \gamma^\mu (v_{e_3 e_4}^{(0)Z} + a_{e_3 e_4}^{(0)Z} \gamma_5), & c_{WGZ} &= -\frac{s_W^2}{c_W^2}. \end{aligned} \quad (\text{A.12})$$

To obtain the building blocks for the non-vanishing $c_{n,i_1 V}^{(\alpha)}$ with $\alpha = 1$, one has to combine the coupling factor expressions in the first row of (A.11) (the factors related to diagram t_1 in $\chi_{e_1}^- \chi_{e_2}^+ \rightarrow W^+ G^-$ annihilations) with the coupling factor expressions in the last row of (A.12) (expressions originating from diagram s in $\chi_{e_4}^0 \chi_{e_3}^0 \rightarrow W^+ G^-$), as $\alpha = 1$ refers to the $t_1 s$ product of tree-level diagrams. Similarly, for $\alpha = 2$ and 4, one has to build the combinations of expressions referring to st_1 and st_2 . Therefore, the building-blocks for the non-vanishing $c_{n,i_1 V}^{(\alpha)}$ related to single s -channel $V = Z$ exchange read:

$$\alpha = 1: \quad \{ \{ s_{e_1 i_1}^G, p_{e_1 i_1}^G \}, \{ -v_{e_2 i_1}^{W^*}, a_{e_2 i_1}^{W^*} \}, \{ v_{e_3 e_4}^{(0)Z^*}, a_{e_3 e_4}^{(0)Z^*} \}, \{ -\frac{s_W^2}{c_W^2} \} \}, \quad (\text{A.13})$$

$$\alpha = 2: \quad \{ \{ -v_{e_1 e_2}^Z, a_{e_1 e_2}^Z \}, \{ v_{i_1 e_3}^W, a_{i_1 e_3}^W \}, \{ s_{i_1 e_4}^{G^*}, p_{i_1 e_4}^{G^*} \}, \{ -\frac{s_W^2}{c_W^2} \} \}, \quad (\text{A.14})$$

$$\alpha = 4: \quad \{ \{ -v_{e_1 e_2}^Z, a_{e_1 e_2}^Z \}, \{ s_{i_1 e_3}^{G^*}, p_{i_1 e_3}^{G^*} \}, \{ -v_{i_1 e_4}^W, a_{i_1 e_4}^W \}, \{ -\frac{s_W^2}{c_W^2} \} \}. \quad (\text{A.15})$$

In selecting one element from each of the above given subsets and multiplying the selected elements for fixed α with each other, the $c_{n,i_1 V}^{(\alpha)}$ expressions in $\chi_{e_1}^- \chi_{e_2}^+ \rightarrow W^+ G^- \rightarrow \chi_{e_4}^0 \chi_{e_3}^0$

reactions are obtained. Proceeding in that way, we obtain eight different coupling factor combinations for fixed α , that are labeled with index n . Following our convention for this label, n ranges over $n = rrr, rrq, rqr, qrr, rqq, qrq, qqr, qqq$. The $c_{qqr, i_1 V}^{(2)}$ expression, for example, reads

$$c_{qqr, i_1 V}^{(2)} = -\frac{s_W^2}{c_W^2} a_{e_1 e_2}^Z a_{i_1 e_3}^W s_{i_1 e_4}^{G*} . \quad (\text{A.16})$$

A.2 Kinematic factors at leading order

The kinematic factor expressions that refer to a specific $\chi_{e_1} \chi_{e_2} \rightarrow X_A X_B \rightarrow \chi_{e_4} \chi_{e_3}$ scattering reaction depend on the external particles' mass scales m , \overline{m} and $M = m + \overline{m}$. We remind the reader of our convention (see Sec. 6.1.2)

$$\begin{aligned} m &= \frac{m_{e_1} + m_{e_4}}{2} , & \overline{m} &= \frac{m_{e_2} + m_{e_3}}{2} , \\ \delta m &= \frac{m_{e_4} - m_{e_1}}{2} , & \delta \overline{m} &= \frac{m_{e_3} - m_{e_2}}{2} . \end{aligned} \quad (\text{A.17})$$

Further recall that we expand the scattering amplitudes in δm , $\delta \overline{m}$ and count these quantities as $\mathcal{O}(v^2)$. Hence, for the leading-order S -wave results presented below, the mass differences $\delta m = \delta \overline{m} = 0$, such that there are only two mass scales, m and \overline{m} , left, which characterize the external chargino or neutralino states. The masses of the particles X_A and X_B will be denoted with m_A and m_B . Let us introduce the general notation \widehat{m}_a for the rescaling of any mass m_a in units of the mass scale M ,

$$\widehat{m}_a = \frac{m_a}{M} . \quad (\text{A.18})$$

Define the dimensionless quantities

$$\begin{aligned} \Delta_{AB} &= \widehat{m}_A^2 - \widehat{m}_B^2 , \\ \beta &= \sqrt{1 - 2(\widehat{m}_A^2 + \widehat{m}_B^2) + \Delta_{AB}^2} , \end{aligned} \quad (\text{A.19})$$

where in case that $X_A = X_B$, β is the leading-order term in the expansion of the velocity of the $X_A X_B$ particle pair in the non-relativistic momenta and mass differences. The expansion of single s -channel (gauge or Higgs boson X_i) exchange propagators in δm , $\delta \overline{m}$ and the non-relativistic 3-momenta leads to the following denominator-structure at leading order:

$$P_i^s = 1 - \widehat{m}_i^2 . \quad (\text{A.20})$$

Similarly, the leading-order expansion of t - and u -channel gaugino and sfermion propagators in δm , $\delta \overline{m}$ and the non-relativistic 3-momenta gives rise to the denominator-structures

$$P_{iAB} = \widehat{m} \widehat{m} + \widehat{m}_i^2 - \widehat{m} \widehat{m}_A^2 - \widehat{m} \widehat{m}_B^2 ,$$

$$P_{iBA} = P_{iAB} |_{A \leftrightarrow B} . \quad (\text{A.21})$$

Using the above definitions, the kinematic factors for the leading-order S -wave Wilson coefficients related to the selfenergy-topology in Fig. 6.1 are conveniently written as

$$B_{n,i_1 i_2}^{X_A X_B}(2s+1 S_J) = \frac{\beta}{P_{i_1}^s P_{i_2}^s} \tilde{B}_{n,i_1 i_2}^{X_A X_B}(2s+1 S_J) , \quad (\text{A.22})$$

where the labels i_1 and i_2 refer to the particle species that are exchanged in the left and right s -channel propagator. As generically either gauge boson (V) or Higgs (S) s -channel exchange occurs in the processes under consideration, the combination $i_1 i_2$ is given by $i_1 i_2 = VV, VS, SV, SS$. Kinematic factors arising from the triangle-topologies shown in Fig. 6.1 have the following generic form

$$\begin{aligned} C_{n,i_1 X}^{(\alpha) X_A X_B}(2s+1 S_J) &= \frac{\beta}{P_{i_1 AB} P_X^s} \tilde{C}_{n,i_1 X}^{(\alpha) X_A X_B}(2s+1 S_J) \quad \alpha = 1, 2 \quad , \\ C_{n,i_1 X}^{(\alpha) X_A X_B}(2s+1 S_J) &= \frac{\beta}{P_{i_1 BA} P_X^s} \tilde{C}_{n,i_1 X}^{(\alpha) X_A X_B}(2s+1 S_J) \quad \alpha = 3, 4 \quad . \end{aligned} \quad (\text{A.23})$$

The index i_1 in the above expressions is related to the t - or u -channel exchanged particle species, whereas the subscript-index X indicates the type of the single s -channel exchanged particle-species, $X = V, S$. Finally, kinematic factors associated with the box-topologies of Fig. 6.1 generically read

$$\begin{aligned} D_{n,i_1 i_2}^{(1) X_A X_B}(2s+1 S_J) &= \frac{\beta}{P_{i_1 AB} P_{i_2 BA}} \tilde{D}_{n,i_1 i_2}^{(1) X_A X_B}(2s+1 S_J) , \\ D_{n,i_1 i_2}^{(2) X_A X_B}(2s+1 S_J) &= \frac{\beta}{P_{i_1 AB} P_{i_2 AB}} \tilde{D}_{n,i_1 i_2}^{(2) X_A X_B}(2s+1 S_J) , \\ D_{n,i_1 i_2}^{(3) X_A X_B}(2s+1 S_J) &= \frac{\beta}{P_{i_1 BA} P_{i_2 AB}} \tilde{D}_{n,i_1 i_2}^{(3) X_A X_B}(2s+1 S_J) , \\ D_{n,i_1 i_2}^{(4) X_A X_B}(2s+1 S_J) &= \frac{\beta}{P_{i_1 BA} P_{i_2 BA}} \tilde{D}_{n,i_1 i_2}^{(4) X_A X_B}(2s+1 S_J) . \end{aligned} \quad (\text{A.24})$$

Indices i_1 and i_2 in (A.24) refer to the exchanged particle species in the left and right t - and u -channels of the 1-loop box-amplitudes, respectively.

Throughout this appendix, the labels A and B are related to the particles X_A and X_B . Recall that these are the actual final-state particles in a $\chi_i \chi_j \rightarrow X_A X_B$ (tree-level) annihilation reaction. The overall prefactors in (A.22–A.24) arise from the phase-space integration (β) and from the leading-order expansion of s - or t - and u -channel propagators in the non-relativistic limit.

Finally recall from Appendix A.1.1, that each individual index n in (A.22–A.24) is given by a character string, whose elements indicate the type (r or q) of the corresponding generic coupling structures at the vertices of the respective underlying 1-loop amplitude in Fig. 6.1. In the results that we quote next we only write explicitly the kinematic factors for those n which are non-vanishing.

A.2.1 Kinematic factors for $X_A X_B = VV$

The kinematic factors $\tilde{B}_{n,i_1 i_2}^{VV}$ in case of 1S_0 partial-wave reactions are given by

$$\tilde{B}_{qq,VV}^{VV}(^1S_0) = -\frac{\beta^2}{2} + 3 \Delta_{AB}^2, \quad (\text{A.25})$$

$$\tilde{B}_{qq,VS}^{VV}(^1S_0) = \tilde{B}_{qq,SV}^{VV}(^1S_0) = 3 \hat{m}_W \Delta_{AB}, \quad (\text{A.26})$$

$$\tilde{B}_{qq,SS}^{VV}(^1S_0) = 4 \hat{m}_W^2. \quad (\text{A.27})$$

In case of 3S_1 partial-wave reactions we have

$$\tilde{B}_{rr,VV}^{VV}(^3S_1) = -\frac{9}{2} + \frac{4}{3} \beta^2 - \frac{1}{2} \Delta_{AB}^2. \quad (\text{A.28})$$

Only the kinematic factors $\tilde{B}_{n,i_1 i_2}^{VV}$ given explicitly in (A.25–A.28) with $n = rr, qq$ are non-vanishing. In case of $X_A X_B = VV$, the kinematic factors for the triangle- and box-diagram topologies $\alpha = 3, 4$ are related to the corresponding expressions for diagram-topologies $\alpha = 1, 2$ (see Fig. 6.1). The relations read

$$\begin{aligned} \tilde{C}_{n,i_1 V}^{(3)VV}(^{2s+1}S_J) &= -\tilde{C}_{n,i_1 V}^{(1)VV}(^{2s+1}S_J) |_{A \leftrightarrow B}, \\ \tilde{C}_{n,i_1 V}^{(4)VV}(^{2s+1}S_J) &= -\tilde{C}_{n,i_1 V}^{(2)VV}(^{2s+1}S_J) |_{A \leftrightarrow B}, \\ \tilde{C}_{n,i_1 S}^{(3)VV}(^{2s+1}S_J) &= \tilde{C}_{n,i_1 S}^{(1)VV}(^{2s+1}S_J) |_{A \leftrightarrow B}, \\ \tilde{C}_{n,i_1 S}^{(4)VV}(^{2s+1}S_J) &= \tilde{C}_{n,i_1 S}^{(2)VV}(^{2s+1}S_J) |_{A \leftrightarrow B}, \\ \tilde{D}_{n,i_1 i_2}^{(3)VV}(^{2s+1}S_J) &= \tilde{D}_{n,i_1 i_2}^{(1)VV}(^{2s+1}S_J) |_{A \leftrightarrow B}, \\ \tilde{D}_{n,i_1 i_2}^{(4)VV}(^{2s+1}S_J) &= \tilde{D}_{n,i_1 i_2}^{(2)VV}(^{2s+1}S_J) |_{A \leftrightarrow B}. \end{aligned} \quad (\text{A.29})$$

The minus sign in the relation for the triangle coefficients $\tilde{C}_{n,i_1 V}^{(\alpha)VV}$ in (A.29) arises from interchanging the two gauge bosons X_A and X_B at the internal three-gauge boson vertex. The expressions $\tilde{C}_{n,i_1 V}^{(\alpha)VV}$ for diagram-topologies $\alpha = 1, 2$, that refer to leading-order 1S_0 partial waves read

$$\tilde{C}_{rqq,i_1 V}^{(1)VV}(^1S_0) = \frac{\beta^2}{2} - \frac{3}{2} (\hat{m} - \widehat{\hat{m}}) \Delta_{AB} - \frac{3}{2} \Delta_{AB}^2 + 3 \hat{m}_{i_1} \Delta_{AB}, \quad (\text{A.30})$$

$$\tilde{C}_{qqr,i_1 V}^{(2)VV}(^1S_0) = \tilde{C}_{rqq,i_1 V}^{(1)VV}(^1S_0). \quad (\text{A.31})$$

In case of $\tilde{C}_{n,i_1 V}^{(\alpha)VV}$ expressions related to 3S_1 partial waves and diagram-topologies $\alpha = 1, 2$ we find

$$\tilde{C}_{rrr,i_1 V}^{(\alpha)VV}(^3S_1) = -\frac{5}{6} \beta^2 + (\hat{m} - \widehat{\hat{m}}) \frac{\Delta_{AB}}{2} + \frac{\Delta_{AB}^2}{2} + 3 \hat{m}_{i_1}. \quad (\text{A.32})$$

We deduce the following expressions for $\tilde{C}_{n,i_1 S}^{(\alpha)VV}$ coefficients and diagram topologies $\alpha = 1, 2$:

$$\tilde{C}_{rqq,i_1 S}^{(1)VV}(^1S_0) = \tilde{C}_{qqr,i_1 S}^{(2)VV}(^1S_0) = -\hat{m}_W (\hat{m} - \widehat{\hat{m}} + \Delta_{AB}) + 4 \hat{m}_W \hat{m}_{i_1}. \quad (\text{A.33})$$

There are additional non-vanishing $C_{n,i_1 X}^{(\alpha)VV}$ expressions for $X = V, S$ in both the case of 1S_0 and 3S_1 partial-wave reactions, which are related to the expressions in (A.30–A.33) in the following way:

$$\begin{aligned}\tilde{C}_{qqr, i_1 X}^{(1)VV}(^{2s+1}S_J) &= \tilde{C}_{rqq, i_1 X}^{(2)VV}(^{2s+1}S_J) = \tilde{C}_{rrr, i_1 X}^{(1)VV}(^{2s+1}S_J)|_{m_{i_1} \rightarrow -m_{i_1}} , \\ \tilde{C}_{qrq, i_1 X}^{(1)VV}(^{2s+1}S_J) &= \tilde{C}_{qrq, i_1 X}^{(2)VV}(^{2s+1}S_J) = \tilde{C}_{rqq, i_1 X}^{(1)VV}(^{2s+1}S_J)|_{m_{i_1} \rightarrow -m_{i_1}} .\end{aligned}\quad (\text{A.34})$$

Turning to terms related to box-diagrams, the non-vanishing expressions $\tilde{D}_{n, i_1 i_2}^{(\alpha)VV}$ for $\alpha = 1, 2$ are given by

$$\tilde{D}_{rrrr, i_1 i_2}^{(\alpha)VV}(^1S_0) = \frac{\beta^2}{2} , \quad (\text{A.35})$$

$$\begin{aligned}\tilde{D}_{rqq, i_1 i_2}^{(1)VV}(^1S_0) &= \frac{\beta^2}{2} + (\hat{m} - \hat{\bar{m}})^2 - \Delta_{AB}^2 + 4 \hat{m}_{i_1} \hat{m}_{i_2} \\ &\quad - \hat{m}_{i_1} (\hat{m} - \hat{\bar{m}} - \Delta_{AB}) - \hat{m}_{i_2} (\hat{m} - \hat{\bar{m}} + \Delta_{AB}) ,\end{aligned}\quad (\text{A.36})$$

$$\begin{aligned}\tilde{D}_{rqq, i_1 i_2}^{(2), VV}(^1S_0) &= -\frac{\beta^2}{2} + \left(\hat{m} - \hat{\bar{m}} + \Delta_{AB}\right)^2 + 4 \hat{m}_{i_1} \hat{m}_{i_2} \\ &\quad - (\hat{m}_{i_1} + \hat{m}_{i_2}) (\hat{m} - \hat{\bar{m}} + \Delta_{AB}) ,\end{aligned}\quad (\text{A.37})$$

and

$$\tilde{D}_{rrrr, i_1 i_2}^{(1)VV}(^3S_1) = -\frac{2}{3} \beta^2 - \frac{1}{2} (\hat{m} - \hat{\bar{m}})^2 + \frac{1}{2} \Delta_{AB}^2 + 2 \hat{m}_{i_1} \hat{m}_{i_2} , \quad (\text{A.38})$$

$$\tilde{D}_{rrrr, i_1 i_2}^{(2)VV}(^3S_1) = \frac{2}{3} \beta^2 - \frac{1}{2} \left(\hat{m} - \hat{\bar{m}} + \Delta_{AB}\right)^2 - 2 \hat{m}_{i_1} \hat{m}_{i_2} , \quad (\text{A.39})$$

$$\begin{aligned}\tilde{D}_{rqq, i_1 i_2}^{(1)VV}(^3S_1) &= -\frac{1}{3} \beta^2 - \frac{1}{2} (\hat{m} - \hat{\bar{m}})^2 + \frac{1}{2} \Delta_{AB}^2 - 2 \hat{m}_{i_1} \hat{m}_{i_2} \\ &\quad + \hat{m}_{i_1} (\hat{m} - \hat{\bar{m}} - \Delta_{AB}) + \hat{m}_{i_2} (\hat{m} - \hat{\bar{m}} + \Delta_{AB}) ,\end{aligned}\quad (\text{A.40})$$

$$\begin{aligned}\tilde{D}_{rqq, i_1 i_2}^{(2)VV}(^3S_1) &= -\frac{1}{3} \beta^2 + \frac{1}{2} \left(m - \bar{m} + \hat{\Delta}_{AB}\right)^2 + 2 \hat{m}_{i_1} \hat{m}_{i_2} \\ &\quad - \hat{m}_{i_1} (\hat{m} - \hat{\bar{m}} + \Delta_{AB}) - \hat{m}_{i_2} (\hat{m} - \hat{\bar{m}} + \Delta_{AB}) .\end{aligned}\quad (\text{A.41})$$

The remaining non-vanishing kinematic factors $\tilde{D}_{n, i_1 i_2}^{VV}$ for both spin-0 and spin-1 $\chi\chi$ states are related to the expressions given above by

$$\begin{aligned}\tilde{D}_{qqqq, i_1 i_2}^{(\alpha)VV}(^{2s+1}S_J) &= \tilde{D}_{rrrr, i_1 i_2}^{(\alpha)VV}(^{2s+1}S_J) , \\ \tilde{D}_{rrqq, i_1 i_2}^{(\alpha)VV}(^{2s+1}S_J) &= \tilde{D}_{qqrr, i_1 i_2}^{(\alpha)VV}(^{2s+1}S_J) = \tilde{D}_{rrrr, i_1 i_2}^{(\alpha)VV}(^{2s+1}S_J)|_{\hat{m}_{i_1} \hat{m}_{i_2} \rightarrow -\hat{m}_{i_1} \hat{m}_{i_2}} , \\ \tilde{D}_{qrrq, i_1 i_2}^{(\alpha)VV}(^{2s+1}S_J) &= \tilde{D}_{rqq, i_1 i_2}^{(\alpha)VV}(^{2s+1}S_J)|_{\hat{m}_{i_1, 2} \rightarrow -\hat{m}_{i_1, 2}} , \\ \tilde{D}_{rqrq, i_1 i_2}^{(\alpha)VV}(^{2s+1}S_J) &= \tilde{D}_{rqq, i_1 i_2}^{(\alpha)VV}(^{2s+1}S_J)|_{\hat{m}_{i_2} \rightarrow -\hat{m}_{i_2}} , \\ \tilde{D}_{qrqr, i_1 i_2}^{(\alpha)VV}(^{2s+1}S_J) &= \tilde{D}_{rqq, i_1 i_2}^{(\alpha)VV}(^{2s+1}S_J)|_{\hat{m}_{i_1} \rightarrow -\hat{m}_{i_1}} .\end{aligned}\quad (\text{A.42})$$

The notation in the second line of (A.42) means that the product $\hat{m}_{i_1} \hat{m}_{i_2}$ is replaced, but all other appearances of either \hat{m}_{i_1} or \hat{m}_{i_2} are untouched.

A.2.2 Kinematic factors for $X_A X_B = VS$

We find the following expressions for $\tilde{B}_{n,i_1 i_2}^{VS}$ terms in 1S_0 partial-wave reactions with $i_1 i_2 = VV, VS, SV, SS$:

$$\tilde{B}_{qq,VV}^{VS}(^1S_0) = -\hat{m}_W^2, \quad (\text{A.43})$$

$$\tilde{B}_{qq,VS}^{VS}(^1S_0) = \tilde{B}_{qq,SV}^{VS}(^1S_0) = \frac{\hat{m}_W}{2} (-3 + \Delta_{AB}), \quad (\text{A.44})$$

$$\tilde{B}_{qq,SS}^{VS}(^1S_0) = \frac{\beta^2}{4} - \frac{9}{4} + \frac{3}{2} \Delta_{AB} - \frac{\Delta_{AB}^2}{4}. \quad (\text{A.45})$$

In case of 3S_1 partial-wave processes the corresponding $\tilde{B}_{n,i_1 i_2}^{VS}$ coefficients read

$$\tilde{B}_{rr,VV}^{VS}(^3S_1) = \hat{m}_W^2. \quad (\text{A.46})$$

Kinematic factors $\tilde{C}_{n,i_1 V}^{(\alpha)VS}$, that are related to the four generic triangle-topologies α with gauge boson (V) exchange in the single s -channel (see Fig. 6.1) are given by

$$\tilde{C}_{rqq,i_1 V}^{(1)VS}(^1S_0) = \tilde{C}_{qqr,i_1 V}^{(2)VS}(^1S_0) = -\frac{\hat{m}_W}{2} (\hat{m} - \widehat{\bar{m}} + \Delta_{AB}) - \hat{m}_W \hat{m}_{i_1}, \quad (\text{A.47})$$

$$\tilde{C}_{rqq,i_1 V}^{(3)VS}(^1S_0) = \tilde{C}_{qqr,i_1 V}^{(4)VS}(^1S_0) = \frac{\hat{m}_W}{2} (\hat{m} - \widehat{\bar{m}} - \Delta_{AB}) + \hat{m}_W \hat{m}_{i_1}, \quad (\text{A.48})$$

as well as

$$\tilde{C}_{rrr,i_1 V}^{(1)VS}(^3S_1) = \tilde{C}_{rrr,i_1 V}^{(2)VS}(^3S_1) = -\tilde{C}_{rqq,i_1 V}^{(1)VS}(^1S_0), \quad (\text{A.49})$$

$$\tilde{C}_{rrr,i_1 V}^{(3)VS}(^3S_1) = \tilde{C}_{rrr,i_1 V}^{(4)VS}(^3S_1) = -\tilde{C}_{rqq,i_1 V}^{(3)VS}(^1S_0)|_{\hat{m}_{i_1} \rightarrow -\hat{m}_{i_1}}. \quad (\text{A.50})$$

In case of $\tilde{C}_{n,i_1 S}^{(\alpha)VS}$ expressions we find

$$\begin{aligned} \tilde{C}_{rqq,i_1 S}^{(1)VS}(^1S_0) &= -\frac{\beta^2}{4} - \frac{3}{4} (\hat{m} - \widehat{\bar{m}}) + (\hat{m} - \widehat{\bar{m}} - 3) \frac{\Delta_{AB}}{4} \\ &\quad + \frac{\Delta_{AB}^2}{4} - \frac{\hat{m}_{i_1}}{2} (3 - \Delta_{AB}), \end{aligned} \quad (\text{A.51})$$

$$\tilde{C}_{qqr,i_1 S}^{(2)VS}(^1S_0) = \tilde{C}_{rqq,i_1 S}^{(1)VS}(^1S_0), \quad (\text{A.52})$$

$$\begin{aligned} \tilde{C}_{rqq,i_1 S}^{(3)VS}(^1S_0) &= -\frac{\beta^2}{4} + \frac{3}{4} (\hat{m} - \widehat{\bar{m}}) - (\hat{m} - \widehat{\bar{m}} + 3) \frac{\Delta_{AB}}{4} \\ &\quad + \frac{\Delta_{AB}^2}{4} + \frac{\hat{m}_{i_1}}{2} (3 - \Delta_{AB}), \end{aligned} \quad (\text{A.53})$$

$$\tilde{C}_{qqr,i_1 S}^{(4)VS}(^1S_0) = \tilde{C}_{rqq,i_1 S}^{(3)VS}(^1S_0). \quad (\text{A.54})$$

There are additional non-vanishing kinematic factors for $\tilde{C}_{n,i_1 X}^{(\alpha)VS}$ with $X = V$ or S , related to the corresponding expressions in (A.47–A.54) in the following way:

$$\tilde{C}_{qqr,i_1 X}^{(1)VS}(^{2s+1}S_J) = \tilde{C}_{rqq,i_1 X}^{(2)VS}(^{2s+1}S_J) = -\tilde{C}_{rrr,i_1 X}^{(1)VS}(^{2s+1}S_J)|_{\hat{m}_{i_1} \rightarrow -\hat{m}_{i_1}},$$

$$\begin{aligned}
\tilde{C}_{qqr, i_1 X}^{(3)VS}(^{2s+1}S_J) &= \tilde{C}_{rqq, i_1 X}^{(4)VS}(^{2s+1}S_J) = \tilde{C}_{rrr, i_1 X}^{(3)VS}(^{2s+1}S_J)|_{\hat{m}_{i_1} \rightarrow -\hat{m}_{i_1}} , \\
\tilde{C}_{grq, i_1 X}^{(1)VS}(^{2s+1}S_J) &= \tilde{C}_{grq, i_1 X}^{(2)VS}(^{2s+1}S_J) = -\tilde{C}_{rqq, i_1 X}^{(1)VS}(^{2s+1}S_J)|_{\hat{m}_{i_1} \rightarrow -\hat{m}_{i_1}} , \\
\tilde{C}_{grq, i_1 X}^{(3)VS}(^{2s+1}S_J) &= \tilde{C}_{grq, i_1 X}^{(4)VS}(^{2s+1}S_J) = \tilde{C}_{rqq, i_1 X}^{(3)VS}(^{2s+1}S_J)|_{\hat{m}_{i_1} \rightarrow -\hat{m}_{i_1}} .
\end{aligned} \tag{A.55}$$

The non-vanishing kinematic factors for $X_A X_B = VS$ and the four box-topologies α are given by

$$\begin{aligned}
\tilde{D}_{rqqr, i_1 i_2}^{(1)VS}(^1S_0) &= \frac{1}{4} \beta^2 + \frac{1}{4} (\hat{m} - \widehat{\bar{m}})^2 - \frac{1}{4} \Delta_{AB}^2 + \hat{m}_{i_1} \hat{m}_{i_2} \\
&\quad + \frac{1}{2} \hat{m}_{i_1} (\hat{m} - \widehat{\bar{m}} - \Delta_{AB}) + \frac{1}{2} \hat{m}_{i_2} (\hat{m} - \widehat{\bar{m}} + \Delta_{AB}) ,
\end{aligned} \tag{A.56}$$

$$\begin{aligned}
\tilde{D}_{rqqr, i_1 i_2}^{(2)VS}(^1S_0) &= \frac{1}{4} \beta^2 - \frac{1}{4} (\hat{m} - \widehat{\bar{m}} + \Delta_{AB})^2 - \hat{m}_{i_1} \hat{m}_{i_2} \\
&\quad - \frac{1}{2} (\hat{m}_{i_1} + \hat{m}_{i_2}) (\hat{m} - \widehat{\bar{m}} + \Delta_{AB}) ,
\end{aligned} \tag{A.57}$$

$$\tilde{D}_{rqqr, i_1 i_2}^{(3)VS}(^1S_0) = \tilde{D}_{rqqr, i_1 i_2}^{(1)VS}(^1S_0)|_{A \leftrightarrow B} , \tag{A.58}$$

$$\tilde{D}_{rqqr, i_1 i_2}^{(4)VS}(^1S_0) = \tilde{D}_{rqqr, i_1 i_2}^{(2)VS}(^1S_0)|_{A \leftrightarrow B} . \tag{A.59}$$

In case of 3S_1 partial waves we have

$$\begin{aligned}
\tilde{D}_{rrrr, i_1 i_2}^{(1)VS}(^3S_1) &= -\frac{1}{12} \beta^2 - \frac{1}{4} (\hat{m} - \widehat{\bar{m}})^2 + \frac{1}{4} \Delta_{AB}^2 + \hat{m}_{i_1} \hat{m}_{i_2} \\
&\quad - \frac{1}{2} \hat{m}_{i_1} (\hat{m} - \widehat{\bar{m}} - \Delta_{AB}) + \frac{1}{2} \hat{m}_{i_2} (\hat{m} - \widehat{\bar{m}} + \Delta_{AB}) ,
\end{aligned} \tag{A.60}$$

$$\begin{aligned}
\tilde{D}_{rrrr, i_1 i_2}^{(2)VS}(^3S_1) &= -\frac{1}{12} \beta^2 + \frac{1}{4} (\hat{m} - \widehat{\bar{m}} + \Delta_{AB})^2 + \hat{m}_{i_1} \hat{m}_{i_2} \\
&\quad + \frac{1}{2} (\hat{m}_{i_1} + \hat{m}_{i_2}) (\hat{m} - \widehat{\bar{m}} + \Delta_{AB}) ,
\end{aligned} \tag{A.61}$$

$$\tilde{D}_{rrrr, i_1 i_2}^{(3)VS}(^3S_1) = \tilde{D}_{rrrr, i_1 i_2}^{(1)VS}(^3S_1)|_{\hat{m} \leftrightarrow \widehat{\bar{m}}} , \tag{A.62}$$

$$\tilde{D}_{rrrr, i_1 i_2}^{(4)VS}(^3S_1) = \tilde{D}_{rrrr, i_1 i_2}^{(2)VS}(^3S_1)|_{\hat{m} \leftrightarrow \widehat{\bar{m}}} , \tag{A.63}$$

$$\tilde{D}_{rqqr, i_1 i_2}^{(\alpha)VS}(^3S_1) = \frac{(-1)^\alpha}{6} \beta^2 . \tag{A.64}$$

Relations for the remaining kinematic factors for both 1S_0 and 3S_1 partial-wave reactions read in case of diagram-topologies $\alpha = 1, 2$:

$$\begin{aligned}
\tilde{D}_{qqq, i_1 i_2}^{(\alpha)VS}(^{2s+1}S_J) &= (-1)^\alpha \tilde{D}_{rrrr, i_1 i_2}^{(\alpha)VS}(^{2s+1}S_J)|_{\hat{m}_{i_1,2} \rightarrow -\hat{m}_{i_1,2}} , \\
\tilde{D}_{rrq, i_1 i_2}^{(\alpha)VS}(^{2s+1}S_J) &= (-1)^{\alpha+1} \tilde{D}_{rrrr, i_1 i_2}^{(\alpha)VS}(^{2s+1}S_J)|_{\hat{m}_{i_2} \rightarrow -\hat{m}_{i_2}} , \\
\tilde{D}_{qrr, i_1 i_2}^{(\alpha)VS}(^{2s+1}S_J) &= -\tilde{D}_{rrrr, i_1 i_2}^{(\alpha)VS}(^{2s+1}S_J)|_{\hat{m}_{i_1} \rightarrow -\hat{m}_{i_1}} , \\
\tilde{D}_{qrr, i_1 i_2}^{(\alpha)VS}(^{2s+1}S_J) &= (-1)^\alpha \tilde{D}_{rqqr, i_1 i_2}^{(\alpha)VS}(^{2s+1}S_J)|_{\hat{m}_{i_1,2} \rightarrow -\hat{m}_{i_1,2}} , \\
\tilde{D}_{rqr, i_1 i_2}^{(\alpha)VS}(^{2s+1}S_J) &= (-1)^{\alpha+1} \tilde{D}_{rqqr, i_1 i_2}^{(\alpha)VS}(^{2s+1}S_J)|_{\hat{m}_{i_2} \rightarrow -\hat{m}_{i_2}} ,
\end{aligned}$$

$$\tilde{D}_{qqr, i_1 i_2}^{(\alpha) VS} ({}^{2s+1} S_J) = - \tilde{D}_{rqr, i_1 i_2}^{(\alpha) VS} ({}^{2s+1} S_J) |_{\hat{m}_{i_1} \rightarrow -\hat{m}_{i_1}} . \quad (\text{A.65})$$

The corresponding relations for diagram-topologies $\alpha = 3, 4$ are given by

$$\begin{aligned} \tilde{D}_{qqq, i_1 i_2}^{(\alpha) VS} ({}^{2s+1} S_J) &= (-1)^\alpha \tilde{D}_{rrr, i_1 i_2}^{(\alpha) VS} ({}^{2s+1} S_J) |_{\hat{m}_{i_1, 2} \rightarrow -\hat{m}_{i_1, 2}} , \\ \tilde{D}_{rrq, i_1 i_2}^{(\alpha) VS} ({}^{2s+1} S_J) &= (-1)^\alpha \tilde{D}_{rrr, i_1 i_2}^{(\alpha) VS} ({}^{2s+1} S_J) |_{\hat{m}_{i_2} \rightarrow -\hat{m}_{i_2}} , \\ \tilde{D}_{qqr, i_1 i_2}^{(\alpha) VS} ({}^{2s+1} S_J) &= \tilde{D}_{rrr, i_1 i_2}^{(\alpha) VS} ({}^{2s+1} S_J) |_{\hat{m}_{i_1} \rightarrow -\hat{m}_{i_1}} , \\ \tilde{D}_{qrr, i_1 i_2}^{(\alpha) VS} ({}^{2s+1} S_J) &= (-1)^\alpha \tilde{D}_{rqr, i_1 i_2}^{(\alpha) VS} ({}^{2s+1} S_J) |_{\hat{m}_{i_1, 2} \rightarrow -\hat{m}_{i_1, 2}} , \\ \tilde{D}_{rqr, i_1 i_2}^{(\alpha) VS} ({}^{2s+1} S_J) &= (-1)^\alpha \tilde{D}_{rqr, i_1 i_2}^{(\alpha) VS} ({}^{2s+1} S_J) |_{\hat{m}_{i_2} \rightarrow -\hat{m}_{i_2}} , \\ \tilde{D}_{qqr, i_1 i_2}^{(\alpha) VS} ({}^{2s+1} S_J) &= \tilde{D}_{rqr, i_1 i_2}^{(\alpha) VS} ({}^{2s+1} S_J) |_{\hat{m}_{i_1} \rightarrow -\hat{m}_{i_1}} . \end{aligned} \quad (\text{A.66})$$

A.2.3 Kinematic factors for $X_A X_B = SS$

The non-vanishing $\tilde{B}_{n, i_1 i_2}^{SS}$ terms with $i_1 i_2 = VV, VS, SV, VV$ read

$$\tilde{B}_{qq, VV}^{SS} ({}^1 S_0) = \Delta_{AB}^2 , \quad (\text{A.67})$$

$$\tilde{B}_{qq, VS}^{SS} ({}^1 S_0) = \tilde{B}_{qq, SV}^{SS} ({}^1 S_0) = - \hat{m}_W \Delta_{AB} , \quad (\text{A.68})$$

$$\tilde{B}_{qq, SS}^{SS} ({}^1 S_0) = \hat{m}_W^2 , \quad (\text{A.69})$$

and in case of ${}^3 S_1$ reactions

$$\tilde{B}_{rr, VV}^{SS} ({}^3 S_1) = \frac{\beta^2}{3} . \quad (\text{A.70})$$

As in the case of $X_A X_B = VV$, the kinematic factors for $X_A X_B = SS$ and diagram-topologies $\alpha = 3, 4$ are related to the corresponding expressions that arise from diagram-topologies $\alpha = 1, 2$. This applies to both triangle- and box-topologies (see Fig. 6.1):

$$\begin{aligned} \tilde{C}_{n, i_1 V}^{(3) SS} ({}^{2s+1} S_J) &= - \tilde{C}_{n, i_1 V}^{(1) SS} ({}^{2s+1} S_J) |_{A \leftrightarrow B} , \\ \tilde{C}_{n, i_1 V}^{(4) SS} ({}^{2s+1} S_J) &= - \tilde{C}_{n, i_1 V}^{(2) SS} ({}^{2s+1} S_J) |_{A \leftrightarrow B} , \\ \tilde{C}_{n, i_1 S}^{(3) SS} ({}^{2s+1} S_J) &= \tilde{C}_{n, i_1 S}^{(1) SS} ({}^{2s+1} S_J) |_{A \leftrightarrow B} , \\ \tilde{C}_{n, i_1 S}^{(4) SS} ({}^{2s+1} S_J) &= \tilde{C}_{n, i_1 S}^{(2) SS} ({}^{2s+1} S_J) |_{A \leftrightarrow B} , \\ \tilde{D}_{n, i_1 i_2}^{(3) SS} ({}^{2s+1} S_J) &= \tilde{D}_{n, i_1 i_2}^{(1) SS} ({}^{2s+1} S_J) |_{A \leftrightarrow B} , \\ \tilde{D}_{n, i_1 i_2}^{(4) SS} ({}^{2s+1} S_J) &= \tilde{D}_{n, i_1 i_2}^{(2) SS} ({}^{2s+1} S_J) |_{A \leftrightarrow B} . \end{aligned} \quad (\text{A.71})$$

In case of expressions $\tilde{C}_{n, i_1 V}^{(\alpha) SS}$ for diagram-topologies $\alpha = 1, 2$ we find

$$\tilde{C}_{rq, i_1 V}^{(1) SS} ({}^1 S_0) = \tilde{C}_{qr, i_1 V}^{(2) SS} ({}^1 S_0) = \frac{\Delta_{AB}}{2} (\hat{m} - \hat{\bar{m}} + \Delta_{AB}) + \hat{m}_{i_1} \Delta_{AB} , \quad (\text{A.72})$$

$$\tilde{C}_{rr, i_1 V}^{(1) SS} ({}^3 S_1) = \tilde{C}_{rr, i_1 V}^{(2) SS} ({}^3 S_1) = - \frac{\beta^2}{6} . \quad (\text{A.73})$$

The $\tilde{C}_{n,i_1 S}^{(\alpha)SS}$ expressions with $\alpha = 1, 2$ are given by

$$\tilde{C}_{rqq,i_1 S}^{(1)SS}(^1S_0) = \tilde{C}_{qqr,i_1 S}^{(2)SS}(^1S_0) = -\frac{\widehat{m}_W}{2} (\widehat{m} - \widehat{m} + \Delta_{AB}) - \widehat{m}_W \widehat{m}_{i_1} . \quad (\text{A.74})$$

All other non-vanishing expressions for $\tilde{C}_{n,i_1 X}^{(\alpha)SS}$ with $X = V, S$ and $\alpha = 1, 2$ can be related to the terms in (A.72–A.74) in the following way:

$$\begin{aligned} \tilde{C}_{qqr,i_1 X}^{(1)SS}(^{2s+1}S_J) &= \tilde{C}_{rqq,i_1 X}^{(2)SS}(^{2s+1}S_J) = -\tilde{C}_{rrr,i_1 X}^{(1)SS}(^{2s+1}S_J)|_{\widehat{m}_{i_1} \rightarrow -\widehat{m}_{i_1}} , \\ \tilde{C}_{qrq,i_1 X}^{(1)SS}(^{2s+1}S_J) &= \tilde{C}_{qqr,i_1 X}^{(2)SS}(^{2s+1}S_J) = -\tilde{C}_{rrr,i_1 X}^{(1)SS}(^{2s+1}S_J)|_{\widehat{m}_{i_1} \rightarrow -\widehat{m}_{i_1}} . \end{aligned} \quad (\text{A.75})$$

The expressions $\tilde{D}_{n,i_1 i_2}^{(\alpha)SS}$ for diagram-topologies $\alpha = 1, 2$ and 1S_0 partial waves read

$$\begin{aligned} \tilde{D}_{rqqr,i_1 i_2}^{(1)SS}(^1S_0) &= \frac{1}{4} (\widehat{m} - \widehat{m})^2 - \frac{\Delta_{AB}^2}{4} + \widehat{m}_{i_1} \widehat{m}_{i_2} \\ &\quad + \frac{\widehat{m}_{i_1}}{2} (\widehat{m} - \widehat{m} - \Delta_{AB}) + \frac{\widehat{m}_{i_2}}{2} (\widehat{m} - \widehat{m} + \Delta_{AB}) , \end{aligned} \quad (\text{A.76})$$

$$\begin{aligned} \tilde{D}_{rqqr,i_1 i_2}^{(2)SS}(^1S_0) &= \frac{1}{4} (\widehat{m} - \widehat{m} + \Delta_{AB})^2 + \widehat{m}_{i_1} \widehat{m}_{i_2} \\ &\quad + \frac{1}{2} (\widehat{m}_{i_1} + \widehat{m}_{i_2})(\widehat{m} - \widehat{m} + \Delta_{AB}) . \end{aligned} \quad (\text{A.77})$$

In case of a 3S_1 partial-wave configuration we find

$$\tilde{D}_{rrrr,i_1 i_2}^{(\alpha)SS}(^3S_1) = (-1)^\alpha \frac{\beta^2}{12} . \quad (\text{A.78})$$

The remaining non-vanishing kinematic factors related to both 1S_0 and 3S_1 partial-wave reactions read

$$\begin{aligned} \tilde{D}_{qqqq,i_1 i_2}^{(\alpha)SS}(^{2s+1}S_J) &= \tilde{D}_{rrrr,i_1 i_2}^{(\alpha)SS}(^{2s+1}S_J) , \\ \tilde{D}_{rrqq,i_1 i_2}^{(\alpha)SS}(^{2s+1}S_J) &= \tilde{D}_{qqrr,i_1 i_2}^{(\alpha)SS}(^{2s+1}S_J) = -\tilde{D}_{rrrr,i_1 i_2}^{(\alpha)SS}(^{2s+1}S_J) , \\ \tilde{D}_{qrrq,i_1 i_2}^{(\alpha)SS}(^{2s+1}S_J) &= \tilde{D}_{rqqr,i_1 i_2}^{(\alpha)SS}(^{2s+1}S_J)|_{\widehat{m}_{i_1,2} \rightarrow -\widehat{m}_{i_1,2}} , \\ \tilde{D}_{rqrq,i_1 i_2}^{(\alpha)SS}(^{2s+1}S_J) &= -\tilde{D}_{rqqr,i_1 i_2}^{(\alpha)SS}(^{2s+1}S_J)|_{\widehat{m}_{i_2} \rightarrow -\widehat{m}_{i_2}} , \\ \tilde{D}_{qrqr,i_1 i_2}^{(\alpha)SS}(^{2s+1}S_J) &= -\tilde{D}_{rqqr,i_1 i_2}^{(\alpha)SS}(^{2s+1}S_J)|_{\widehat{m}_{i_1} \rightarrow -\widehat{m}_{i_1}} . \end{aligned} \quad (\text{A.79})$$

A.2.4 Kinematic factors for $X_A X_B = ff$

The non-vanishing $\tilde{B}_{n,i_1 i_2}^{ff}$ terms with $i_1 i_2 = VV, VS, SV, SS$ are given by

$$\tilde{B}_{qqqq,VV}^{ff}(^1S_0) = 1 - \beta^2 + 4 \widehat{m}_A \widehat{m}_B - \Delta_{AB}^2 , \quad (\text{A.80})$$

$$\tilde{B}_{qqqq,VS}^{ff}(^1S_0) = \tilde{B}_{qqqq,SV}^{ff}(^1S_0) = 2 \left(\widehat{m}_A + \widehat{m}_B - (\widehat{m}_A - \widehat{m}_B) \Delta_{AB} \right) , \quad (\text{A.81})$$

$$\tilde{B}_{qqq,SS}^{ff}(^1S_0) = 1 + \beta^2 + 4 \hat{m}_A \hat{m}_B - \Delta_{AB}^2, \quad (\text{A.82})$$

and in case of 3S_1 partial-wave reactions

$$\tilde{B}_{rrrr,VV}^{ff}(^3S_1) = 1 + \frac{\beta^2}{3} + 4 \hat{m}_A \hat{m}_B - \Delta_{AB}^2. \quad (\text{A.83})$$

There are additional non-vanishing terms $\tilde{B}_{n,i_1i_2}^{ff}$ related to the expressions in (A.80–A.83). In case of $i_1i_2 = VV, SS$, the corresponding relations read

$$\tilde{B}_{rqq, i_1i_2}^{ff}(^{2s+1}S_J) = \tilde{B}_{rrrr, i_1i_2}^{ff}(^{2s+1}S_J)|_{\hat{m}_A \hat{m}_B \rightarrow -\hat{m}_A \hat{m}_B}, \quad (\text{A.84})$$

$$\tilde{B}_{qrr, i_1i_2}^{ff}(^{2s+1}S_J) = \tilde{B}_{qqq, i_1i_2}^{ff}(^{2s+1}S_J)|_{\hat{m}_A \hat{m}_B \rightarrow -\hat{m}_A \hat{m}_B}, \quad (\text{A.85})$$

and our notation implies, that the product $\hat{m}_A \hat{m}_B$ has to be replaced, but all other occurrences of \hat{m}_A or \hat{m}_B are untouched. Similarly, in case of $i_1i_2 = VS, SV$, the additional non-vanishing $\tilde{B}_{n,i_1i_2}^{ff}$ terms are given by

$$\tilde{B}_{rqq, i_1i_2}^{ff}(^{2s+1}S_J) = -\tilde{B}_{rrrr, i_1i_2}^{ff}(^{2s+1}S_J)|_{\hat{m}_A \rightarrow -\hat{m}_A}, \quad (\text{A.86})$$

$$\tilde{B}_{qrr, i_1i_2}^{ff}(^{2s+1}S_J) = -\tilde{B}_{qqq, i_1i_2}^{ff}(^{2s+1}S_J)|_{\hat{m}_A \rightarrow -\hat{m}_A}. \quad (\text{A.87})$$

The relations among kinematic factors for diagram topologies $\alpha = 3, 4$ and diagram-topologies $\alpha = 1, 2$ in both the cases of box- and triangle-topologies are given by ($X = V, S$)

$$C_{n, i_1X}^{(3)ff}(^{2s+1}S_J) = C_{n, i_1X}^{(1)ff}(^{2s+1}S_J) |_{A \leftrightarrow B}, \quad (\text{A.88})$$

$$C_{n, i_1X}^{(4)ff}(^{2s+1}S_J) = C_{n, i_1X}^{(2)ff}(^{2s+1}S_J) |_{A \leftrightarrow B}, \quad (\text{A.89})$$

$$D_{n, i_1i_2}^{(3)ff}(^{2s+1}S_J) = D_{n, i_1i_2}^{(1)ff}(^{2s+1}S_J) |_{A \leftrightarrow B}, \quad (\text{A.90})$$

$$D_{n, i_1i_2}^{(4)ff}(^{2s+1}S_J) = D_{n, i_1i_2}^{(2)ff}(^{2s+1}S_J) |_{A \leftrightarrow B}, \quad (\text{A.91})$$

compare to the generic diagrams in Fig. 6.1. The structures $\tilde{C}_{n, i_1V}^{(\alpha)ff}$ for topologies $\alpha = 1, 2$ are given by

$$\begin{aligned} \tilde{C}_{qqq, i_1V}^{(\alpha)ff}(^1S_0) &= \frac{\beta^2}{4} - \frac{1}{4} (1 - 2 \hat{m}_A)(1 - 2 \hat{m}_B) \\ &\quad - (\hat{m}_A - \hat{m}_B) \frac{\Delta_{AB}}{2} - \frac{\Delta_{AB}^2}{4}, \end{aligned} \quad (\text{A.92})$$

and in case of 3S_1 partial-wave reactions the respective expressions read

$$\begin{aligned} \tilde{C}_{rrrr, i_1V}^{(\alpha)ff}(^3S_1) &= -\frac{\beta^2}{12} - \frac{1}{4} (1 + 2 \hat{m}_A)(1 + 2 \hat{m}_B) \\ &\quad + (\hat{m}_A - \hat{m}_B) \frac{\Delta_{AB}}{2} + \frac{\Delta_{AB}^2}{4}. \end{aligned} \quad (\text{A.93})$$

The relations of the additional non-vanishing $\tilde{C}_{n,i_1V}^{(\alpha)ff}$ expressions to the respective terms in (A.92–A.93) read

$$\begin{aligned}
\tilde{C}_{qqrr,i_1V}^{(1)ff}(^{2s+1}S_J) &= \tilde{C}_{rrqq,i_1V}^{(2)ff}(^{2s+1}S_J) = -\tilde{C}_{rrrr,i_1V}^{(1)ff}(^{2s+1}S_J)|_{m_{A,B} \rightarrow -m_{A,B}} , \\
\tilde{C}_{rqqr,i_1V}^{(\alpha)ff}(^{2s+1}S_J) &= \tilde{C}_{rrrr,i_1V}^{(\alpha)ff}(^{2s+1}S_J)|_{m_A \rightarrow -m_A} , \\
\tilde{C}_{qrqr,i_1V}^{(1)ff}(^{2s+1}S_J) &= \tilde{C}_{rqrq,i_1V}^{(2)ff}(^{2s+1}S_J) = -\tilde{C}_{rrrr,i_1V}^{(1)ff}(^{2s+1}S_J)|_{m_B \rightarrow -m_B} , \\
\tilde{C}_{rqrq,i_1V}^{(1)ff}(^{2s+1}S_J) &= \tilde{C}_{qrqr,i_1V}^{(2)ff}(^{2s+1}S_J) = -\tilde{C}_{qqqq,i_1V}^{(\alpha)ff}(^{2s+1}S_J)|_{m_B \rightarrow -m_B} , \\
\tilde{C}_{qrrq,i_1V}^{(\alpha)ff}(^{2s+1}S_J) &= \tilde{C}_{qqqq,i_1V}^{(\alpha)ff}(^{2s+1}S_J)|_{m_A \rightarrow -m_A} , \\
\tilde{C}_{rrqq,i_1V}^{(1)ff}(^{2s+1}S_J) &= \tilde{C}_{qqrr,i_1V}^{(2)ff}(^{2s+1}S_J) = -\tilde{C}_{qqqq,i_1V}^{(\alpha)ff}(^{2s+1}S_J)|_{m_{A,B} \rightarrow -m_{A,B}} . \quad (\text{A.94})
\end{aligned}$$

The terms $\tilde{C}_{n,i_1S}^{(\alpha)ff}$ for $\alpha = 1, 2$ read

$$\begin{aligned}
\tilde{C}_{qqqq,i_1S}^{(\alpha)ff}(^1S_0) &= \frac{\beta^2}{4} + \frac{1}{4} (1 - 2\hat{m}_A)(1 - 2\hat{m}_B) \\
&\quad + (\hat{m}_A - \hat{m}_B) \frac{\Delta_{AB}}{2} - \frac{\Delta_{AB}^2}{4} , \quad (\text{A.95})
\end{aligned}$$

and all remaining non-vanishing $C_{n,i_1S}^{(\alpha)ff}$ terms are obtained from (A.95) in the following way:

$$\begin{aligned}
\tilde{C}_{rqrq,i_1S}^{(1)ff}(^{2s+1}S_J) &= \tilde{C}_{qrqr,i_1S}^{(2)ff}(^{2s+1}S_J) = \tilde{C}_{qqqq,i_1S}^{(\alpha)ff}(^{2s+1}S_J)|_{m_B \rightarrow -m_B} , \\
\tilde{C}_{qrrq,i_1S}^{(\alpha)ff}(^{2s+1}S_J) &= \tilde{C}_{qqqq,i_1S}^{(\alpha)ff}(^{2s+1}S_J)|_{m_A \rightarrow -m_A} , \\
\tilde{C}_{rrqq,i_1S}^{(1)ff}(^{2s+1}S_J) &= \tilde{C}_{qqrr,i_1S}^{(2)ff}(^{2s+1}S_J) = \tilde{C}_{qqqq,i_1S}^{(\alpha)ff}(^{2s+1}S_J)|_{m_{A,B} \rightarrow -m_{A,B}} . \quad (\text{A.96})
\end{aligned}$$

In case of box-diagram topologies $\alpha = 1, 2$, we find the following $\tilde{D}_{n,i_1i_2}^{(\alpha)ff}$ structures for the 1S_0 partial waves:

$$\tilde{D}_{rrrr,i_1i_2}^{(\alpha)ff}(^1S_0) = \frac{1}{8} (1 + 2\hat{m}_B - \Delta_{AB})(1 + 2\hat{m}_A + \Delta_{AB}) , \quad (\text{A.97})$$

$$\tilde{D}_{rrqq,i_1i_2}^{(\alpha)ff}(^1S_0) = \frac{\beta^2}{8} - \frac{1}{2} \hat{m}_A \hat{m}_B . \quad (\text{A.98})$$

For 3S_1 partial-wave configurations we have

$$\tilde{D}_{rrrr,i_1i_2}^{(\alpha)ff}(^3S_1) = (-1)^\alpha \tilde{D}_{rrrr,i_1i_2}^{(\alpha)ff}(^1S_0) , \quad (\text{A.99})$$

$$\tilde{D}_{rrqq,i_1i_2}^{(\alpha)ff}(^3S_1) = (-1)^{\alpha+1} \left(\frac{\beta^2}{24} + \frac{1}{2} \hat{m}_A \hat{m}_B \right) . \quad (\text{A.100})$$

Relations for the remaining non-vanishing kinematic factors related to both 1S_0 and 3S_1 partial-wave processes read in case of diagram topology $\alpha = 1$

$$\tilde{D}_{qqqq,i_1i_2}^{(1)ff}(^{2s+1}S_J) = \tilde{D}_{rrrr,i_1i_2}^{(1)ff}(^{2s+1}S_J)|_{\hat{m}_{A,B} \rightarrow -\hat{m}_{A,B}} ,$$

$$\begin{aligned}
\tilde{D}_{qqrr, i_1 i_2}^{(1)ff}(^{2s+1}S_J) &= \tilde{D}_{rrqq, i_1 i_2}^{(1)ff}(^{2s+1}S_J) , \\
\tilde{D}_{rqqr, i_1 i_2}^{(1)ff}(^{2s+1}S_J) &= \tilde{D}_{qrrq, i_1 i_2}^{(1)ff}(^{2s+1}S_J) = \tilde{D}_{rrqq, i_1 i_2}^{(1)ff}(^{2s+1}S_J)|_{\hat{m}_A \hat{m}_B \rightarrow -\hat{m}_A \hat{m}_B} , \\
\tilde{D}_{rqrq, i_1 i_2}^{(1)ff}(^{2s+1}S_J) &= \tilde{D}_{rrrr, i_1 i_2}^{(1)ff}(^{2s+1}S_J)|_{\hat{m}_A \rightarrow -\hat{m}_A} , \\
\tilde{D}_{qrqr, i_1 i_2}^{(1)ff}(^{2s+1}S_J) &= \tilde{D}_{rrrr, i_1 i_2}^{(1)ff}(^{2s+1}S_J)|_{\hat{m}_B \rightarrow -\hat{m}_B} .
\end{aligned} \tag{A.101}$$

In case of diagram topology $\alpha = 2$, the corresponding relations are given by

$$\begin{aligned}
\tilde{D}_{qqqq, i_1 i_2}^{(2)ff}(^{2s+1}S_J) &= \tilde{D}_{rrrr, i_1 i_2}^{(2)ff}(^{2s+1}S_J)|_{\hat{m}_{A,B} \rightarrow -\hat{m}_{A,B}} , \\
\tilde{D}_{qrrr, i_1 i_2}^{(2)ff}(^{2s+1}S_J) &= \tilde{D}_{rrqq, i_1 i_2}^{(2)ff}(^{2s+1}S_J) , \\
\tilde{D}_{rqqr, i_1 i_2}^{(2)ff}(^{2s+1}S_J) &= \tilde{D}_{rrrr, i_1 i_2}^{(2)ff}(^{2s+1}S_J)|_{\hat{m}_A \rightarrow -\hat{m}_A} , \\
\tilde{D}_{qrrq, i_1 i_2}^{(2)ff}(^{2s+1}S_J) &= \tilde{D}_{rrrr, i_1 i_2}^{(2)ff}(^{2s+1}S_J)|_{\hat{m}_B \rightarrow -\hat{m}_B} , \\
\tilde{D}_{rqrq, i_1 i_2}^{(2)ff}(^{2s+1}S_J) &= \tilde{D}_{qrqr, i_1 i_2}^{(2)ff}(^{2s+1}S_J) = \tilde{D}_{rrqq, i_1 i_2}^{(2)ff}(^{2s+1}S_J)|_{\hat{m}_A \hat{m}_B \rightarrow -\hat{m}_A \hat{m}_B} .
\end{aligned} \tag{A.102}$$

A.2.5 Kinematic factors for $X_A X_B = \eta \bar{\eta}$

In case of $X_A X_B = \eta \bar{\eta}$ one cannot directly construct the coupling factors $b_{n, i_1 i_2}$ using the recipe given in Sec. A.1.1, which is based on considering the $\chi_{e_1} \chi_{e_2} \rightarrow X_A X_B$ and $\chi_{e_4} \chi_{e_3} \rightarrow X_A X_B$ tree-level annihilation amplitudes. In order to obtain the coupling factor expressions $b_{n, i_1 i_2}$, that correspond to the kinematic factors presented below, one should proceed as follows: First extract the (axial-) vector and (pseudo-) scalar coupling factors associated with the interaction of the $\chi_{e_1} \chi_{e_2}$ or $\chi_{e_4} \chi_{e_3}$ pair and the s -channel exchanged particle species. This is done following the steps 1. and 2. in the recipe given in Sec. A.1.1. Next, complex-conjugate the couplings related to the $\chi_{e_4} \chi_{e_3}$ particle pair. In order to determine the couplings to the ghosts, consider the 1-loop amplitude $\chi_{e_1} \chi_{e_2} \rightarrow \eta \bar{\eta} \rightarrow \chi_{e_4} \chi_{e_3}$, similar to the selfenergy-amplitude in Fig. 6.1. Assign a ghost flow to the lower line of the 1-loop amplitude (labeled with X_A in Fig. 6.1), that flows from left to right. Consequently there is a ghost flow from right to left on the upper line, which is labeled with X_B . Assume that the coupling factors at each of the two ghost vertices are generically of the form $ig_2 c_{ABX_i} L_{ABX_i}$, where the Lorentz structures L_{ABX_i} are defined in Tab. A.1. Determine the expressions that replace the generic c_{ABX_i} factors for the specific process under consideration. Now build all possible combinations of two-coupling factor products from the set of the neutralino/chargino couplings to the s -channel exchanged particles (including factors of -1 in front of vector couplings) in the $\chi_{e_1} \chi_{e_2} \rightarrow \eta \bar{\eta} \rightarrow \chi_{e_4} \chi_{e_3}$ reaction, and multiply them by the $c_{ABX_{i_1}}$ and $c_{ABX_{i_2}}$ factors. The convention for the naming of the resulting coupling factor expressions $b_{n, i_1 i_2}$ with subscripts $n = rr, qq$ is the same as in the cases $X_A X_B = VV, VS, SS$, see Sec. A.1.1. The coupling factors $b_{n, i_1 i_2}$ derived in this way correspond to the kinematic factors given below. Note that the mass parameter m_A in the expressions below refers to the mass of the ghost flowing in the lower line, and m_B to the mass of the ghost in the upper line.

The non-vanishing $\tilde{B}_{n, i_1 i_2}^{\eta\bar{\eta}}$ terms with $i_1 i_2 = VV, VS, SV, SS$ read

$$\tilde{B}_{qq, VV}^{\eta\bar{\eta}}(1S_0) = \frac{1}{4} (1 - \Delta_{AB}^2) , \quad (\text{A.103})$$

$$\tilde{B}_{qq, VS}^{\eta\bar{\eta}}(1S_0) = -\frac{\hat{m}_W}{2} (1 + \Delta_{AB}) , \quad (\text{A.104})$$

$$\tilde{B}_{qq, SV}^{\eta\bar{\eta}}(1S_0) = \frac{\hat{m}_W}{2} (1 - \Delta_{AB}) , \quad (\text{A.105})$$

$$\tilde{B}_{qq, SS}^{\eta\bar{\eta}}(1S_0) = -\hat{m}_W^2 . \quad (\text{A.106})$$

Similarly,

$$\tilde{B}_{rr, VV}^{\eta\bar{\eta}}(3S_1) = -\frac{\beta^2}{12} . \quad (\text{A.107})$$

A.3 Kinematic factors at $\mathcal{O}(v^2)$

Throughout this section we rely on the same definitions and conventions for the masses m, \bar{m} , the mass differences $\delta m, \delta \bar{m}$ and the mass ratio \hat{m}_a as established in (A.17) and (A.18) in Sec. A.2. Further, the same definitions for the parameters Δ_{AB} and β , (A.19), are used and parameters P_i^s and P_{iAB}, P_{iBA} are defined through (A.20) and (A.21).

Regarding the presentation of results for the kinematic factors related to dimension-8 operators in $\delta\mathcal{L}_{\text{ann}}$, it is however convenient to use a notation where factors of the leading-order propagator and $(\hat{m} \widehat{\bar{m}})$, as well as the factor β arising from the phase-space integration are pulled out. This implies that the relations (A.22) and (A.23), introduced to clearly arrange the presentation of leading-order S -wave kinematic factor results corresponding to selfenergy- and triangle-diagrams, differ from the corresponding relations, that we now introduce for the kinematic factors related to the dimension-8 operators: For the kinematic factors related to dimension-8 four-fermion operators, that derive from the selfenergy topology we define

$$B_{n, i_1 i_2}^{X_A X_B (2s+1) L_J} = \frac{\beta}{(\hat{m} \widehat{\bar{m}})^2 P_{i_1}^s P_{i_2}^s} \tilde{B}_{n, i_1 i_2}^{X_A X_B (2s+1) L_J} , \quad (\text{A.108})$$

where the labels i_1 and i_2 refer to the particle species that are exchanged in the left and right s -channel propagator of the selfenergy diagram. As before, the combination $i_1 i_2$ is given by $i_1 i_2 = VV, VS, SV, SS$. Note that compared to (A.22) there is an additional factor $(\hat{m} \widehat{\bar{m}})^2$ in the denominator of (A.108). Likewise, we rewrite the kinematic factors of dimension-8 Wilson coefficients arising from the triangle-topologies as

$$\begin{aligned} C_{n, i_1 X}^{(\alpha) X_A X_B (2s+1) L_J} &= \frac{\beta}{\hat{m} \widehat{\bar{m}} P_{i_1 AB} P_X^s} \tilde{C}_{n, i_1 X}^{(\alpha) X_A X_B (2s+1) L_J} & \alpha = 1, 2 \quad , \\ C_{n, i_1 X}^{(\alpha) X_A X_B (2s+1) L_J} &= \frac{\beta}{\hat{m} \widehat{\bar{m}} P_{i_1 BA} P_X^s} \tilde{C}_{n, i_1 X}^{(\alpha) X_A X_B (2s+1) L_J} & \alpha = 3, 4 \quad , \end{aligned} \quad (\text{A.109})$$

such that compared to (A.23) there appears an additional factor $\widehat{m} \widehat{\overline{m}}$ in the denominator. As in (A.23), the index i_1 is related to the t - or u -channel exchanged particle species, and the subscript-index X indicates the type of exchanged particle ($X = V, S$) in the s -channel. Finally, the kinematic factors associated with the box topologies are written in the same form as the correspondent expressions related to leading dimension-6 operators (A.24):

$$\begin{aligned}
D_{n, i_1 i_2}^{(1) X_A X_B} ({}^{2s+1} L_J) &= \frac{\beta}{P_{i_1 AB} P_{i_2 BA}} \tilde{D}_{n, i_1 i_2}^{(1) X_A X_B} ({}^{2s+1} L_J) , \\
D_{n, i_1 i_2}^{(2) X_A X_B} ({}^{2s+1} L_J) &= \frac{\beta}{P_{i_1 AB} P_{i_2 AB}} \tilde{D}_{n, i_1 i_2}^{(2) X_A X_B} ({}^{2s+1} L_J) , \\
D_{n, i_1 i_2}^{(3) X_A X_B} ({}^{2s+1} L_J) &= \frac{\beta}{P_{i_1 BA} P_{i_2 AB}} \tilde{D}_{n, i_1 i_2}^{(3) X_A X_B} ({}^{2s+1} L_J) , \\
D_{n, i_1 i_2}^{(4) X_A X_B} ({}^{2s+1} L_J) &= \frac{\beta}{P_{i_1 BA} P_{i_2 BA}} \tilde{D}_{n, i_1 i_2}^{(4) X_A X_B} ({}^{2s+1} L_J) . \tag{A.110}
\end{aligned}$$

In (A.110) the indices i_1 and i_2 refer to the exchanged particle species in the left and right t - and u -channels of the 1-loop box amplitudes, respectively.

The conventions for the label n are the same as in Sec. A.2 (see Sec. A.1.1 for the corresponding definitions). Again we quote in the following only those kinematic factors with a given label n , that are non-vanishing.

A.3.1 P -wave kinematic factors for $X_A X_B = VV$

The only non-vanishing kinematic factor $\tilde{B}_{n, i_1 i_2}^{VV}$ in case of ${}^1 P_1$ partial-wave reactions is given by

$$\tilde{B}_{qq, VV}^{VV} ({}^1 P_1) = \frac{\Delta_m^2}{24} (8 \beta^2 - 3 \Delta_{AB}^2 - 27) , \tag{A.111}$$

while for the combined ${}^3 P_J$ waves the non-vanishing kinematic factors read

$$\tilde{B}_{rr, VV}^{VV} ({}^3 P_J) = - \frac{\Delta_m^2}{8} (\beta^2 - 6 \Delta_{AB}^2) , \tag{A.112}$$

$$\tilde{B}_{qq, VV}^{VV} ({}^3 P_J) = \frac{1}{12} (8 \beta^2 - 3 \Delta_{AB}^2 - 27) , \tag{A.113}$$

$$\tilde{B}_{rr, VS}^{VV} ({}^3 P_J) = \tilde{B}_{rr, SV}^{VV} ({}^3 P_J) = - \frac{3}{4} \widehat{m}_W \Delta_m \Delta_{AB} , \tag{A.114}$$

$$\tilde{B}_{rr, SS}^{VV} ({}^3 P_J) = \widehat{m}_W^2 . \tag{A.115}$$

As regards kinematic factors related to triangle- and box-topologies in the case $X_A X_B = VV$, the relations (A.29) among the $\alpha = 1(2)$ and $\alpha = 3(4)$ kinematic factors are fulfilled for any ${}^{2s+1} L_J$ configuration (in particular also for the kinematic factors associated with the absorptive part of the next-to-next-to-leading order S -wave Wilson coefficients, $\hat{g}({}^{2s+1} S_s)$ and $\hat{h}_i({}^{2s+1} S_s)$). By virtue of the relations (A.29), we therefore only need to

give here the kinematic factors for diagram-topologies $\alpha = 1, 2$ for both the cases of triangle and box diagram kinematic factors. Starting with the expressions $\tilde{C}_{n, i_1 V}^{(\alpha)VV}$ for 1P_1 partial waves we have

$$\begin{aligned} \tilde{C}_{rqq, i_1 V}^{(1)VV}(^1P_1) &= \frac{3 \hat{m}_{i_1}}{4 \hat{m} \hat{\bar{m}}} \Delta_m + \frac{\beta^2 \Delta_m}{12 P_{i_1 AB}} (\Delta_m - 6 \hat{m}_{i_1} + 2 \Delta_{AB}) \\ &\quad + \frac{\Delta_m}{24 \hat{m} \hat{\bar{m}}} (6 \Delta_m^2 \Delta_{AB} - \Delta_m (5 \beta^2 - 3 \Delta_{AB}^2) - 3 \Delta_{AB}) , \end{aligned} \quad (\text{A.116})$$

$$\tilde{C}_{qqr, i_1 V}^{(2)VV}(^1P_1) = \tilde{C}_{rqq, i_1 V}^{(1)VV}(^1P_1) , \quad (\text{A.117})$$

whereas for the combined 3P_J quantum numbers we find

$$\begin{aligned} \tilde{C}_{rrr, i_1 V}^{(1)VV}(^3P_J) &= \frac{3 \hat{m}_{i_1}}{4 \hat{m} \hat{\bar{m}}} \Delta_m \Delta_{AB} + \frac{\beta^2 \Delta_m}{12 P_{i_1 AB}} (\Delta_m + 2 \Delta_{AB}) \\ &\quad - \frac{\Delta_m}{8 \hat{m} \hat{\bar{m}}} (2 \Delta_m^2 \Delta_{AB} - \Delta_m (\beta^2 - 3 \Delta_{AB}^2) + \Delta_{AB}) , \end{aligned} \quad (\text{A.118})$$

$$\tilde{C}_{rrr, i_1 V}^{(2)VV}(^3P_J) = \tilde{C}_{rrr, i_1 V}^{(1)VV}(^3P_J) , \quad (\text{A.119})$$

$$\begin{aligned} \tilde{C}_{rqq, i_1 V}^{(1)VV}(^3P_J) &= \frac{3 \hat{m}_{i_1}}{2 \hat{m} \hat{\bar{m}}} \Delta_m - \frac{\beta^2}{2 P_{i_1 AB}} \\ &\quad - \frac{1}{12 \hat{m} \hat{\bar{m}}} (5 \beta^2 - 9 + 9 \Delta_m^2 - 3 \Delta_{AB} (\Delta_m + \Delta_{AB})) , \end{aligned} \quad (\text{A.120})$$

$$\tilde{C}_{qqr, i_1 V}^{(2)VV}(^3P_J) = \tilde{C}_{rqq, i_1 V}^{(1)VV}(^3P_J) . \quad (\text{A.121})$$

The coefficients $\tilde{C}_{n, i_1 S}^{(\alpha)VV}(^1P_1)$, corresponding to triangles with a Higgs particle exchanged in the s -channel, vanish for all n . The corresponding expressions related to 3P_J reactions read for diagram topologies $\alpha = 1, 2$

$$\tilde{C}_{rrr, i_1 S}^{(\alpha)VV}(^3P_J) = -\frac{\hat{m}_W \hat{m}_{i_1}}{\hat{m} \hat{\bar{m}}} - \frac{\beta^2 \hat{m}_W}{6 P_{i_1 AB}} + \frac{\hat{m}_W}{4 \hat{m} \hat{\bar{m}}} (\Delta_m \Delta_{AB} + 1) . \quad (\text{A.122})$$

All the remaining non-vanishing kinematic factors $\tilde{C}_{n, i_1 X}^{(\alpha)VV}$ associated with 1P_1 and 3P_J scattering reactions with both $X = V, S$ are related to the above expressions by

$$\begin{aligned} \tilde{C}_{qqr, i_1 X}^{(1)VV}(^{2s+1}P_J) &= \tilde{C}_{rqq, i_1 X}^{(2)VV}(^{2s+1}P_J) = \tilde{C}_{rrr, i_1 X}^{(1)VV}(^{2s+1}P_J)|_{m_{i_1} \rightarrow -m_{i_1}} , \\ \tilde{C}_{qrq, i_1 X}^{(1)VV}(^{2s+1}P_J) &= \tilde{C}_{qqr, i_1 X}^{(2)VV}(^{2s+1}P_J) = \tilde{C}_{rqq, i_1 X}^{(1)VV}(^{2s+1}P_J)|_{m_{i_1} \rightarrow -m_{i_1}} , \end{aligned} \quad (\text{A.123})$$

where these relations hold in particular in case of separate 3P_J , $J = 0, 1, 2$, partial-wave configurations and hence trivially for the combined 3P_J waves. Finally, the terms related to box diagrams give rise to the following non-vanishing coefficients

$$\begin{aligned} &\tilde{D}_{rrrr, i_1 i_2}^{(1)VV}(^1P_1) \\ &= -\frac{\hat{m}_{i_1} \hat{m}_{i_2}}{4 (\hat{m} \hat{\bar{m}})^2} - \frac{\hat{m}_{i_1}}{4 (\hat{m} \hat{\bar{m}})^2} (\Delta_m \Delta_{AB} - 1) \end{aligned}$$

$$\begin{aligned}
& - \frac{1}{48 (\widehat{m} \widehat{\widehat{m}})^2} (\Delta_m^2 (2 \beta^2 - 3 \Delta_{AB}^2) + 3) - \frac{\beta^4}{12 P_{i_1 AB} P_{i_2 BA}} \\
& - \frac{\beta^2}{12 \widehat{m} \widehat{\widehat{m}} P_{i_1 AB}} (\Delta_m \Delta_{AB} + 2 \widehat{m}_{i_2} - 1) + \left\{ A \leftrightarrow B, i_1 \leftrightarrow i_2 \right\}, \tag{A.124}
\end{aligned}$$

$$\begin{aligned}
& \tilde{D}_{rrrr, i_1 i_2}^{(2)VV} ({}^1P_1) \\
& = \frac{\widehat{m}_{i_1} \widehat{m}_{i_2}}{4 (\widehat{m} \widehat{\widehat{m}})^2} - \frac{\widehat{m}_{i_1}}{4 (\widehat{m} \widehat{\widehat{m}})^2} (\Delta_m \Delta_{AB} + 1) \\
& - \frac{1}{48 (\widehat{m} \widehat{\widehat{m}})^2} (\Delta_m^2 (2 \beta^2 - 3 \Delta_{AB}^2) - 6 \Delta_m \Delta_{AB} - 3) + \frac{\beta^4}{12 P_{i_1 AB} P_{i_2 AB}} \\
& - \frac{\beta^2}{12 \widehat{m} \widehat{\widehat{m}} P_{i_1 AB}} (\Delta_m \Delta_{AB} - 2 \widehat{m}_{i_2} + 1) + \left\{ i_1 \leftrightarrow i_2 \right\}, \tag{A.125}
\end{aligned}$$

$$\begin{aligned}
& \tilde{D}_{rqq, i_1 i_2}^{(1)VV} ({}^1P_1) \\
& = \frac{\widehat{m}_{i_1} \widehat{m}_{i_2}}{4 (\widehat{m} \widehat{\widehat{m}})^2} - \frac{1}{48 (\widehat{m} \widehat{\widehat{m}})^2} (12 \Delta_m^4 - \Delta_m^2 (12 - 4 \beta^2 + 3 \Delta_{AB}^2) + 3) \\
& - \frac{\beta^2}{12 \widehat{m} \widehat{\widehat{m}} P_{i_1 AB}} (2 \Delta_m^2 + \Delta_m (2 \widehat{m}_{i_1} - \Delta_{AB}) - 1) \\
& - \frac{\beta^2}{12 P_{i_1 AB} P_{i_2 BA}} (2 \Delta_m^2 - 2 \Delta_m (\widehat{m}_{i_1} + \widehat{m}_{i_2}) + \beta^2 + 8 \widehat{m}_{i_1} \widehat{m}_{i_2} \\
& + 2 (\widehat{m}_{i_1} - \widehat{m}_{i_2}) \Delta_{AB} - 2 \Delta_{AB}^2) + \left\{ A \leftrightarrow B, i_1 \leftrightarrow i_2 \right\}, \tag{A.126}
\end{aligned}$$

$$\begin{aligned}
& \tilde{D}_{rqq, i_1 i_2}^{(2)VV} ({}^1P_1) \\
& = - \frac{\widehat{m}_{i_1} \widehat{m}_{i_2}}{4 (\widehat{m} \widehat{\widehat{m}})^2} - \frac{\beta^2}{12 \widehat{m} \widehat{\widehat{m}} P_{i_1 AB}} (2 \Delta_m^2 - \Delta_m (2 \widehat{m}_{i_1} - \Delta_{AB}) - 1) \\
& - \frac{1}{48 (\widehat{m} \widehat{\widehat{m}})^2} (12 \Delta_m^3 (\Delta_m + \Delta_{AB}) - \Delta_m^2 (12 + 4 \beta^2 - 3 \Delta_{AB}^2) \\
& - 6 \Delta_m \Delta_{AB} + 3) \\
& + \frac{\beta^2}{12 P_{i_1 AB} P_{i_2 AB}} (2 \Delta_m^2 - 2 \Delta_m (\widehat{m}_{i_1} + \widehat{m}_{i_2} - 2 \Delta_{AB}) \\
& - 2 \Delta_{AB} (\widehat{m}_{i_1} + \widehat{m}_{i_2} - \Delta_{AB}) - \beta^2 + 8 \widehat{m}_{i_1} \widehat{m}_{i_2}) \\
& + \left\{ i_1 \leftrightarrow i_2 \right\}. \tag{A.127}
\end{aligned}$$

In case of combined ${}^3P_{\mathcal{J}}$ waves we have

$$\begin{aligned}
& \tilde{D}_{rrrr,i_1i_2}^{(1)VV}({}^3P_{\mathcal{J}}) \\
&= \frac{\widehat{m}_{i_1}\widehat{m}_{i_2}}{2(\widehat{m}\widehat{m})^2} (1 - \Delta_m^2) + \frac{\widehat{m}_{i_1}}{4(\widehat{m}\widehat{m})^2} (2\Delta_m^2 - \Delta_m\Delta_{AB} - 1) \\
&\quad + \frac{1}{48(\widehat{m}\widehat{m})^2} (18\Delta_m^4 + 3\Delta_m^2(\beta^2 - 2\Delta_{AB}^2 - 10) - 4\beta^2 + 6\Delta_{AB}^2 + 12) \\
&\quad + \frac{\beta^2}{12\widehat{m}\widehat{m}P_{i_1AB}} (5\Delta_m^2 + \Delta_m\Delta_{AB} + 2(2\widehat{m}_{i_1} + \widehat{m}_{i_2} - 2)) \\
&\quad + \frac{\beta^2}{12P_{i_1AB}P_{i_2BA}} (3\Delta_m^2 + 4(\beta^2 - 3\widehat{m}_{i_1}\widehat{m}_{i_2}) - 3\Delta_{AB}^2) \\
&\quad + \left\{ A \leftrightarrow B, i_1 \leftrightarrow i_2 \right\}, \tag{A.128}
\end{aligned}$$

$$\begin{aligned}
& \tilde{D}_{rrrr,i_1i_2}^{(2)VV}({}^3P_{\mathcal{J}}) \\
&= \frac{\widehat{m}_{i_1}\widehat{m}_{i_2}}{2(\widehat{m}\widehat{m})^2} (1 + \Delta_m^2) - \frac{\widehat{m}_{i_1}}{4(\widehat{m}\widehat{m})^2} (2\Delta_m^2 + 3\Delta_m\Delta_{AB} + 1) \\
&\quad + \frac{1}{48(\widehat{m}\widehat{m})^2} (18\Delta_m^4 + 12\Delta_m^3\Delta_{AB} - 3\Delta_m^2(\beta^2 - 2\Delta_{AB}^2 + 6) + 12\Delta_m\Delta_{AB} \\
&\quad\quad - 4\beta^2 + 6\Delta_{AB}^2 + 12) \\
&\quad + \frac{\beta^2}{12\widehat{m}\widehat{m}P_{i_1AB}} (3\Delta_m^2 - \Delta_m\Delta_{AB} + 2(2\widehat{m}_{i_1} + \widehat{m}_{i_2} - 2)) \\
&\quad - \frac{\beta^2}{36P_{i_1AB}P_{i_2AB}} (9\Delta_m^2 + 18\Delta_m\Delta_{AB} - 12(\beta^2 - 3\widehat{m}_{i_1}\widehat{m}_{i_2}) + 9\Delta_{AB}^2) \\
&\quad + \left\{ i_1 \leftrightarrow i_2 \right\}, \tag{A.129}
\end{aligned}$$

$$\begin{aligned}
& \tilde{D}_{rqqr,i_1i_2}^{(1)VV}({}^3P_{\mathcal{J}}) \\
&= \frac{\widehat{m}_{i_1}\widehat{m}_{i_2}}{2(\widehat{m}\widehat{m})^2} \Delta_m^2 + \frac{2\widehat{m}_{i_1}}{\widehat{m}\widehat{m}} \Delta_m \\
&\quad + \frac{1}{48(\widehat{m}\widehat{m})^2} (6\Delta_m^4 + 3\Delta_m^2(\beta^2 - 6) - 8\beta^2 + 6\Delta_{AB}^2 + 6) \\
&\quad + \frac{\beta^2}{12\widehat{m}\widehat{m}P_{i_1AB}} (\Delta_m^2 + \Delta_m(2\widehat{m}_{i_1} - 4\widehat{m}_{i_2} - \Delta_{AB}) - 2) \\
&\quad + \frac{\beta^2}{12P_{i_1AB}P_{i_2BA}} (3\Delta_m^2 - 6\Delta_m(\widehat{m}_{i_1} + \widehat{m}_{i_2}) + 2(\beta^2 + 6\widehat{m}_{i_1}\widehat{m}_{i_2}) \\
&\quad\quad + 6(\widehat{m}_{i_1} - \widehat{m}_{i_2})\Delta_{AB} - 3\Delta_{AB}^2) + \left\{ A \leftrightarrow B, i_1 \leftrightarrow i_2 \right\}, \tag{A.130}
\end{aligned}$$

$$\begin{aligned}
& \tilde{D}_{rqq, i_1 i_2}^{(2)VV}({}^3P_{\mathcal{J}}) \\
&= -\frac{\widehat{m}_{i_1} \widehat{m}_{i_2}}{2 (\widehat{m} \widehat{m})^2} \Delta_m^2 - \frac{2 \widehat{m}_{i_1}}{\widehat{m} \widehat{m}} \Delta_m \\
&\quad - \frac{1}{48 (\widehat{m} \widehat{m})^2} (6 \Delta_m^4 - 3 \Delta_m^2 (\beta^2 + 2) + 12 \Delta_m \Delta_{AB} - 8 \beta^2 + 6 \Delta_{AB}^2 + 6) \\
&\quad - \frac{\beta^2}{12 \widehat{m} \widehat{m} P_{i_1 AB}} (3 \Delta_m^2 - \Delta_m (2 \widehat{m}_{i_1} + 4 \widehat{m}_{i_2} - \Delta_{AB}) - 2) \\
&\quad + \frac{\beta^2}{12 P_{i_1 AB} P_{i_2 AB}} (3 \Delta_m^2 - 6 \Delta_m (\widehat{m}_{i_1} + \widehat{m}_{i_2} - \Delta_{AB}) - 2 (\beta^2 - 6 \widehat{m}_{i_1} \widehat{m}_{i_2}) \\
&\quad\quad - 6 (\widehat{m}_{i_1} + \widehat{m}_{i_2}) \Delta_{AB} + 3 \Delta_{AB}^2) + \{i_1 \leftrightarrow i_2\}. \tag{A.131}
\end{aligned}$$

The remaining non-vanishing kinematic factors $\tilde{D}_{n, i_1 i_2}^{(\alpha)VV}$ for diagram topologies $\alpha = 1, 2$ are related to the expressions given above by

$$\begin{aligned}
\tilde{D}_{qqq, i_1 i_2}^{(\alpha)VV}({}^{2s+1}L_J) &= \tilde{D}_{rrrr, i_1 i_2}^{(\alpha)VV}({}^{2s+1}L_J)|_{m_{i_1, 2} \rightarrow -m_{i_1, 2}}, \\
\tilde{D}_{rrq, i_1 i_2}^{(\alpha)VV}({}^{2s+1}L_J) &= \tilde{D}_{rrrr, i_1 i_2}^{(\alpha)VV}({}^{2s+1}L_J)|_{m_{i_2} \rightarrow -m_{i_2}}, \\
\tilde{D}_{qrr, i_1 i_2}^{(\alpha)VV}({}^{2s+1}L_J) &= \tilde{D}_{rrrr, i_1 i_2}^{(\alpha)VV}({}^{2s+1}L_J)|_{m_{i_1} \rightarrow -m_{i_1}}, \\
\tilde{D}_{qrrq, i_1 i_2}^{(\alpha)VV}({}^{2s+1}L_J) &= \tilde{D}_{rqq, i_1 i_2}^{(\alpha)VV}({}^{2s+1}L_J)|_{m_{i_1, 2} \rightarrow -m_{i_1, 2}}, \\
\tilde{D}_{rqrq, i_1 i_2}^{(\alpha)VV}({}^{2s+1}L_J) &= \tilde{D}_{rqq, i_1 i_2}^{(\alpha)VV}({}^{2s+1}L_J)|_{m_{i_2} \rightarrow -m_{i_2}}, \\
\tilde{D}_{qrq, i_1 i_2}^{(\alpha)VV}({}^{2s+1}L_J) &= \tilde{D}_{rqq, i_1 i_2}^{(\alpha)VV}({}^{2s+1}L_J)|_{m_{i_1} \rightarrow -m_{i_1}}, \tag{A.132}
\end{aligned}$$

where these relations hold for the kinematic factors related to any ${}^{2s+1}L_J$ partial-wave reaction.

A.3.2 P -wave kinematic factors for $X_A X_B = VS$

The only non-vanishing kinematic factor expression associated with 1P_1 partial-wave reactions and related to selfenergy diagrams reads

$$\tilde{B}_{qq, VV}^{VS}({}^1P_1) = \frac{\widehat{m}_W^2}{4} \Delta_m^2. \tag{A.133}$$

In case of combined ${}^3P_{\mathcal{J}}$ waves we have

$$\tilde{B}_{rr, VV}^{VS}({}^3P_{\mathcal{J}}) = -\frac{\widehat{m}_W^2}{4} \Delta_m^2, \tag{A.134}$$

$$\tilde{B}_{qq, VV}^{VS}({}^3P_{\mathcal{J}}) = \frac{\widehat{m}_W^2}{2}, \tag{A.135}$$

$$\tilde{B}_{rr, VS}^{VS}({}^3P_{\mathcal{J}}) = \tilde{B}_{rr, SV}^{VS}({}^3P_{\mathcal{J}}) = \frac{\widehat{m}_W}{8} \Delta_m (3 - \Delta_{AB}), \tag{A.136}$$

$$\tilde{B}_{rr,SS}^{VS}(^3P_J) = \frac{1}{16} (\beta^2 - 9 + 6 \Delta_{AB} - \Delta_{AB}^2). \quad (\text{A.137})$$

The non-vanishing kinematic factors $\tilde{C}_{n,i_1V}^{(\alpha)VS}$ related to the four generic triangle topologies with gauge boson exchange V in the single s -channel read

$$\tilde{C}_{rqq,i_1V}^{(1)VS}(^1P_1) = \frac{\hat{m}_W \hat{m}_{i_1}}{4 \hat{m} \hat{m}} \Delta_m^2 + \frac{\hat{m}_W \Delta_m}{8 \hat{m} \hat{m}} (\Delta_m^2 + \Delta_m - 1 + \Delta_{AB}) + \frac{\beta^2 \hat{m}_W \Delta_m}{12 P_{i_1AB}}, \quad (\text{A.138})$$

$$\tilde{C}_{qqr,i_1V}^{(2)VS}(^1P_1) = \tilde{C}_{rqq,i_1V}^{(1)VS}(^1P_1), \quad (\text{A.139})$$

$$\begin{aligned} \tilde{C}_{rqq,i_1V}^{(3)VS}(^1P_1) &= -\frac{\hat{m}_W \hat{m}_{i_1}}{4 \hat{m} \hat{m}} \Delta_m^2 - \frac{\hat{m}_W \Delta_m}{8 \hat{m} \hat{m}} (\Delta_m^2 - \Delta_m - 1 + \Delta_{AB}) \\ &\quad - \frac{\beta^2 \hat{m}_W \Delta_m}{12 P_{i_1BA}}, \end{aligned} \quad (\text{A.140})$$

$$\tilde{C}_{qqr,i_1V}^{(4)VS}(^1P_1) = \tilde{C}_{rqq,i_1V}^{(3)VS}(^1P_1). \quad (\text{A.141})$$

In case of combined 3P_J wave reactions the kinematic factors $\tilde{C}_{n,i_1V}^{(\alpha)VS}$ read

$$\tilde{C}_{rrr,i_1V}^{(1)VS}(^3P_J) = \tilde{C}_{rrr,i_1V}^{(2)VS}(^3P_J) = -\tilde{C}_{rqq,i_1V}^{(1)VS}(^1P_1), \quad (\text{A.142})$$

$$\tilde{C}_{rrr,i_1V}^{(3)VS}(^3P_J) = \tilde{C}_{rrr,i_1V}^{(4)VS}(^3P_J) = -\tilde{C}_{rqq,i_1V}^{(3)VS}(^1P_1)|_{\hat{m}_{i_1} \rightarrow -\hat{m}_{i_1}}, \quad (\text{A.143})$$

$$\begin{aligned} \tilde{C}_{rqq,i_1V}^{(1)VS}(^3P_J) &= \tilde{C}_{qqr,i_1V}^{(2)VS}(^3P_J) \\ &= \frac{\hat{m}_W \hat{m}_{i_1}}{2 \hat{m} \hat{m}} + \frac{\hat{m}_W}{4 \hat{m} \hat{m}} (\Delta_m \Delta_{AB} + 1) - \frac{\beta^2 \hat{m}_W}{6 P_{i_1AB}}, \end{aligned} \quad (\text{A.144})$$

$$\begin{aligned} \tilde{C}_{rqq,i_1V}^{(3)VS}(^3P_J) &= \tilde{C}_{qqr,i_1V}^{(4)VS}(^3P_J) \\ &= -\frac{\hat{m}_W \hat{m}_{i_1}}{2 \hat{m} \hat{m}} - \frac{\hat{m}_W}{4 \hat{m} \hat{m}} (\Delta_m \Delta_{AB} - 1) - \frac{\beta^2 \hat{m}_W}{6 P_{i_1BA}}. \end{aligned} \quad (\text{A.145})$$

Turning to $\tilde{C}_{n,i_1S}^{(\alpha)VS}$ factors we find that all kinematic factors corresponding to the 1P_1 configuration vanish. Kinematic factors $\tilde{C}_{n,i_1S}^{(\alpha)VS}$ in combined 3P_J partial-wave reactions read

$$\begin{aligned} \tilde{C}_{rrr,i_1S}^{(1)VS}(^3P_J) &= \frac{1}{16 \hat{m} \hat{m}} (\beta^2 - 3 + (4 - \Delta_{AB}) \Delta_{AB} + (\Delta_m^2 + \Delta_m)(3 - \Delta_{AB})) \\ &\quad + \frac{\hat{m}_{i_1} \Delta_m}{8 \hat{m} \hat{m}} (3 - \Delta_{AB}) + \frac{\beta^2}{24 P_{i_1AB}} (\Delta_m + 3 + 2 \hat{m}_{i_1}), \end{aligned} \quad (\text{A.146})$$

$$\tilde{C}_{rrr,i_1S}^{(2)VS}(^3P_J) = \tilde{C}_{rrr,i_1S}^{(1)VS}(^3P_J), \quad (\text{A.147})$$

$$\begin{aligned} \tilde{C}_{rrr,i_1S}^{(3)VS}(^3P_J) &= -\frac{1}{16 \hat{m} \hat{m}} (\beta^2 - 3 + (4 - \Delta_{AB}) \Delta_{AB} + (\Delta_m^2 - \Delta_m)(3 - \Delta_{AB})) \\ &\quad + \frac{\hat{m}_{i_1} \Delta_m}{8 \hat{m} \hat{m}} (3 - \Delta_{AB}) + \frac{\beta^2}{24 P_{i_1BA}} (\Delta_m - 3 - 2 \hat{m}_{i_1}), \end{aligned} \quad (\text{A.148})$$

$$\tilde{C}_{rrr,i_1S}^{(4)VS}(^3P_J) = \tilde{C}_{rrr,i_1S}^{(3)VS}(^3P_J). \quad (\text{A.149})$$

The additional non-vanishing kinematic factor expressions $\tilde{C}_{n,i_1 X}^{(\alpha)VS}$ with $X = V, S$ are related to the above given expressions via (A.55) (where the label $^{2s+1}S_J$ in the latter equations should be replaced by $^{2s+1}L_J$, indicating that the relations hold for both the expressions related to dimension-6 and 8 terms in $\delta\mathcal{L}_{\text{ann}}$).

Finally, kinematic factors $\tilde{D}_{n,i_1 i_2}^{(\alpha)}$ for 1P_1 partial-wave reactions are given by

$$\begin{aligned}
\tilde{D}_{rrrr, i_1 i_2}^{(\alpha)VS}({}^1P_1) &= \frac{\beta^2}{24 (\widehat{m} \widehat{m})^2} , \\
\tilde{D}_{rqqr, i_1 i_2}^{(1)VS}({}^1P_1) &= -\frac{\Delta_m}{8 (\widehat{m} \widehat{m})^2} ((\Delta_m^2 - 1 + \Delta_{AB}) (\widehat{m}_{i_1} + \widehat{m}_{i_2}) - \Delta_m (\widehat{m}_{i_1} - \widehat{m}_{i_2})) \\
&\quad - \frac{\widehat{m}_{i_1} \widehat{m}_{i_2}}{4 (\widehat{m} \widehat{m})^2} \Delta_m^2 - \frac{1}{48 (\widehat{m} \widehat{m})^2} (\Delta_m^2 (3 \Delta_m^2 - 9 + 6 \Delta_{AB}) \\
&\quad\quad\quad - \beta^2 + 3 - 3 (2 - \Delta_{AB}) \Delta_{AB}) \\
&\quad - \frac{\beta^2}{24 \widehat{m} \widehat{m} P_{i_1 AB}} (\Delta_m (\Delta_m + 2 \widehat{m}_{i_2} - 2) - 1 - 2 \widehat{m}_{i_1}) \\
&\quad - \frac{\beta^2}{24 \widehat{m} \widehat{m} P_{i_2 BA}} (\Delta_m (\Delta_m + 2 \widehat{m}_{i_1} + 2) - 1 + 2 \widehat{m}_{i_2}) \\
&\quad - \frac{\beta^2}{12 P_{i_1 AB} P_{i_2 BA}} (\Delta_m (\Delta_m + 2 \widehat{m}_{i_1} + 2 \widehat{m}_{i_2}) + \beta^2 + 4 \widehat{m}_{i_1} \widehat{m}_{i_2} \\
&\quad\quad\quad - (2 \widehat{m}_{i_1} - 2 \widehat{m}_{i_2} + \Delta_{AB}) \Delta_{AB}) , \tag{A.150}
\end{aligned}$$

$$\begin{aligned}
\tilde{D}_{rqqr, i_1 i_2}^{(2)VS}({}^1P_1) &= \frac{\widehat{m}_{i_1} \Delta_m}{8 (\widehat{m} \widehat{m})^2} (\Delta_m^2 + \Delta_m - 1 + \Delta_{AB}) + \frac{\widehat{m}_{i_1} \widehat{m}_{i_2}}{8 (\widehat{m} \widehat{m})^2} \Delta_m^2 \\
&\quad + \frac{1}{96 (\widehat{m} \widehat{m})^2} (3 (\Delta_m^2 + \Delta_m - 1) (\Delta_m^2 + \Delta_m - 1 + 2 \Delta_{AB}) - \beta^2 + 3 \Delta_{AB}^2) \\
&\quad + \frac{\beta^2}{24 \widehat{m} \widehat{m} P_{i_1 AB}} (\Delta_m (\Delta_m + 2 \widehat{m}_{i_2}) - 2 \widehat{m}_{i_1} - 1) \\
&\quad - \frac{\beta^2}{24 P_{i_1 AB} P_{i_2 AB}} \left((\Delta_m + 2 (\widehat{m}_{i_1} + \widehat{m}_{i_2} + \Delta_{AB})) \Delta_m - \beta^2 + 4 \widehat{m}_{i_1} \widehat{m}_{i_2} \right. \\
&\quad\quad\quad \left. + (2 (\widehat{m}_{i_1} + \widehat{m}_{i_2}) + \Delta_{AB}) \Delta_{AB} \right) + \{i_1 \leftrightarrow i_2\} , \tag{A.151}
\end{aligned}$$

$$\tilde{D}_{rqqr, i_1 i_2}^{(3)VS}({}^1P_1) = \tilde{D}_{rqqr, i_1 i_2}^{(1)VS}({}^1P_1)|_{\widehat{m}_{i_1} \leftrightarrow \widehat{m}_{i_2}} , \tag{A.152}$$

$$\tilde{D}_{rqqr, i_1 i_2}^{(4)VS}({}^1P_1) = \tilde{D}_{rqqr, i_1 i_2}^{(2)VS}({}^1P_1)|_{\widehat{m} \leftrightarrow \widehat{m}, \widehat{m}_{i_1,2} \rightarrow -\widehat{m}_{i_1,2}} . \tag{A.153}$$

The kinematic factor expressions $\tilde{D}_{n,i_1 i_2}^{(\alpha)}$ related to ${}^3P_{\mathcal{J}}$ partial-wave reactions read

$$\begin{aligned}
& \tilde{D}_{rrrr,i_1 i_2}^{(1)VS}({}^3P_{\mathcal{J}}) \\
&= \frac{\Delta_m}{8 (\widehat{m} \widehat{\widehat{m}})^2} ((\widehat{m}_{i_1} - \widehat{m}_{i_2}) (\Delta_m^2 + \Delta_{AB} - 1) - (\widehat{m}_{i_1} + \widehat{m}_{i_2}) \Delta_m) - \frac{\widehat{m}_{i_1} \widehat{m}_{i_2}}{4 (\widehat{m} \widehat{\widehat{m}})^2} \Delta_m^2 \\
&+ \frac{1}{48 (\widehat{m} \widehat{\widehat{m}})^2} ((3 \Delta_m^2 + 4 \beta^2 - 9 + 6 \Delta_{AB}) \Delta_m^2 - 3 (\beta^2 - (1 - \Delta_{AB})^2)) \\
&- \frac{\beta^2}{24 \widehat{m} \widehat{\widehat{m}} P_{i_1 AB}} ((\Delta_m + 2 (2 \widehat{m}_{i_1} + \widehat{m}_{i_2} + \Delta_{AB} + 1)) \Delta_m + 2 \widehat{m}_{i_1} + 1) \\
&- \frac{\beta^2}{24 \widehat{m} \widehat{\widehat{m}} P_{i_2 BA}} ((\Delta_m - 2 (2 \widehat{m}_{i_2} + \widehat{m}_{i_1} + \Delta_{AB} + 1)) \Delta_m + 2 \widehat{m}_{i_2} + 1) \\
&+ \frac{\beta^2}{12 P_{i_1 AB} P_{i_2 BA}} (3 \Delta_m (\Delta_m + 2 (\widehat{m}_{i_1} - \widehat{m}_{i_2})) - 12 \widehat{m}_{i_1} \widehat{m}_{i_2} + \beta^2 \\
&\quad - 3 \Delta_{AB} (2 (\widehat{m}_{i_1} + \widehat{m}_{i_2}) + \Delta_{AB})) , \tag{A.154}
\end{aligned}$$

$$\begin{aligned}
& \tilde{D}_{rrrr,i_1 i_2}^{(2)VS}({}^3P_{\mathcal{J}}) \\
&= - \frac{\widehat{m}_{i_1} \Delta_m}{8 (\widehat{m} \widehat{\widehat{m}})^2} (\Delta_m (\Delta_m + 1) + \Delta_{AB} - 1) - \frac{\widehat{m}_{i_1} \widehat{m}_{i_2}}{8 (\widehat{m} \widehat{\widehat{m}})^2} \Delta_m^2 \\
&- \frac{1}{96 (\widehat{m} \widehat{\widehat{m}})^2} ((3 \Delta_m^2 + 6 \Delta_m - 4 \beta^2 - 3 + 6 \Delta_{AB}) \Delta_m^2 \\
&\quad + 6 \Delta_m (\Delta_{AB} - 1) - 3 (\beta^2 - (1 - \Delta_{AB})^2)) \\
&- \frac{\beta^2}{24 \widehat{m} \widehat{\widehat{m}} P_{i_1 AB}} (\Delta_m (3 \Delta_m + 2 (2 \widehat{m}_{i_1} + \widehat{m}_{i_2} + \Delta_{AB})) - 2 \widehat{m}_{i_1} - 1) \\
&+ \frac{\beta^2}{24 P_{i_1 AB} P_{i_2 AB}} (3 \Delta_m (\Delta_m + 2 (\widehat{m}_{i_1} + \widehat{m}_{i_2} + \Delta_{AB})) + 12 \widehat{m}_{i_1} \widehat{m}_{i_2} - \beta^2 \\
&\quad + 3 \Delta_{AB} (2 (\widehat{m}_{i_1} + \widehat{m}_{i_2}) + \Delta_{AB})) + \{i_1 \leftrightarrow i_2\} , \tag{A.155}
\end{aligned}$$

$$\tilde{D}_{rrrr,i_1 i_2}^{(3)VS}({}^3P_{\mathcal{J}}) = \tilde{D}_{rrrr,i_1 i_2}^{(1)VS}({}^3P_{\mathcal{J}})|_{\widehat{m}_{i_1} \leftrightarrow \widehat{m}_{i_2}} , \tag{A.156}$$

$$\tilde{D}_{rrrr,i_1 i_2}^{(4)VS}({}^3P_{\mathcal{J}}) = \tilde{D}_{rrrr,i_1 i_2}^{(2)VS}({}^3P_{\mathcal{J}})|_{\widehat{m} \leftrightarrow \widehat{\widehat{m}}} , \tag{A.157}$$

$$\begin{aligned}
& \tilde{D}_{rqqr,i_1 i_2}^{(1)VS}({}^3P_{\mathcal{J}}) \\
&= - \frac{1}{4 (\widehat{m} \widehat{\widehat{m}})^2} ((\widehat{m}_{i_1} + \widehat{m}_{i_2}) \Delta_m \Delta_{AB} - \widehat{m}_{i_1} + \widehat{m}_{i_2}) - \frac{\widehat{m}_{i_1} \widehat{m}_{i_2}}{2 (\widehat{m} \widehat{\widehat{m}})^2} \\
&+ \frac{1}{24 (\widehat{m} \widehat{\widehat{m}})^2} (\Delta_m^2 (\beta^2 - 3 \Delta_{AB}^2) + 3) + \frac{\beta^2}{12 \widehat{m} \widehat{\widehat{m}} P_{i_1 AB}} (\Delta_m \Delta_{AB} + 2 \widehat{m}_{i_2} - 1)
\end{aligned}$$

$$- \frac{\beta^2}{12 \widehat{m} \widehat{\overline{m}} P_{i_2 BA}} (\Delta_m \Delta_{AB} + 2 \widehat{m}_{i_1} + 1) + \frac{\beta^4}{6 P_{i_1 AB} P_{i_2 BA}} , \quad (\text{A.158})$$

$$\begin{aligned} & \tilde{D}_{rqqr, i_1 i_2}^{(2)VS}({}^3P_J) \\ &= \frac{\widehat{m}_{i_1}}{4 (\widehat{m} \widehat{\overline{m}})^2} (\Delta_m \Delta_{AB} + 1) + \frac{\widehat{m}_{i_1} \widehat{m}_{i_2}}{4 (\widehat{m} \widehat{\overline{m}})^2} \\ & \quad - \frac{1}{48 (\widehat{m} \widehat{\overline{m}})^2} (\Delta_m^2 (\beta^2 - 3 \Delta_{AB}^2) - 6 \Delta_m \Delta_{AB} - 3) + \frac{\beta^4}{12 P_{i_1 AB} P_{i_2 AB}} \\ & \quad - \frac{\beta^2}{12 \widehat{m} \widehat{\overline{m}} P_{i_1 AB}} (\Delta_m \Delta_{AB} + 2 \widehat{m}_{i_2} + 1) + \left\{ i_1 \leftrightarrow i_2 \right\} , \end{aligned} \quad (\text{A.159})$$

$$\tilde{D}_{rqqr, i_1 i_2}^{(3)VS}({}^3P_J) = \tilde{D}_{rqqr, i_1 i_2}^{(1)VS}({}^3P_J)|_{\widehat{m}_{i_1} \leftrightarrow \widehat{m}_{i_2}} , \quad (\text{A.160})$$

$$\tilde{D}_{rqqr, i_1 i_2}^{(4)VS}({}^3P_J) = \tilde{D}_{rqqr, i_1 i_2}^{(2)VS}({}^3P_J)|_{\widehat{m} \leftrightarrow \widehat{\overline{m}}, \widehat{m}_{i_1,2} \rightarrow -\widehat{m}_{i_1,2}} . \quad (\text{A.161})$$

Note that relation (A.156) implies that the denominator structures $P_{i_1 AB}$ and $P_{i_2 BA}$ in the kinematic factor corresponding to diagram topology $\alpha = 1$ have to be replaced by $P_{i_2 AB}$ and $P_{i_1 BA}$ respectively, in order to arrive at the kinematic factor related to diagram topology $\alpha = 3$. Likewise, in (A.157) the replacement rule for the kinematic factor for diagram-topology $\alpha = 2$ implies the replacement of $P_{i_1 AB}$ and $P_{i_2 AB}$ by $P_{i_1 BA}$ and $P_{i_2 BA}$, respectively. Similar replacements are needed to obtain the $\alpha = 3, 4$ kinematic factors from the $\alpha = 1, 2$ expressions with $n = rqqr$ using (A.160) and (A.161). The relations among kinematic factors in (A.156–A.157) and (A.160–A.161) also hold for the individual kinematic factors related to 3P_J partial-wave reactions with $J = 0, 1, 2$.

The remaining non-vanishing kinematic factors $\tilde{D}_{n, i_1 i_2}^{(\alpha)}$ for diagram topologies $\alpha = 1, 2$ and $\alpha = 3, 4$ derive from the above given expressions using the relations (A.65) and (A.66), valid for $\tilde{D}_{n, i_1 i_2}^{(\alpha)VS}({}^{2s+1}L_J)$ expressions related to any ${}^{2s+1}L_J$ partial-wave reaction.

A.3.3 P -wave kinematic factors for $X_A X_B = SS$

In case of $X_A X_B = SS$ the only non-vanishing kinematic factor $\tilde{B}_{n, i_1 i_2}^{SS}$ in 1P_1 partial-wave scattering reactions reads

$$\tilde{B}_{qq, VV}^{SS}({}^1P_1) = \frac{\beta^2}{12} \Delta_m^2 , \quad (\text{A.162})$$

while the corresponding kinematic factors for combined 3P_J reactions read

$$\tilde{B}_{rr, VV}^{SS}({}^3P_J) = \frac{1}{4} \Delta_m^2 \Delta_{AB}^2 , \quad (\text{A.163})$$

$$\tilde{B}_{qq, VV}^{SS}({}^3P_J) = \frac{\beta^2}{6} , \quad (\text{A.164})$$

$$\tilde{B}_{rr, VS}^{SS}({}^3P_J) = \tilde{B}_{rr, SV}^{SS}({}^3P_J) = \frac{\widehat{m}_W}{4} \Delta_m \Delta_{AB} , \quad (\text{A.165})$$

$$\tilde{B}_{rr,SS}^{SS}(^3P_{\mathcal{J}}) = \frac{\widehat{m}_W^2}{4}. \quad (\text{A.166})$$

The kinematic factors for diagram topologies $\alpha = 3(4)$ and $\alpha = 1(2)$ obey in both the cases of triangle and box diagrams the relations (A.71), that generically apply for the respective kinematic factors related to a given $^{2s+1}L_J$ partial-wave configuration, including kinematic factors related to coefficients $\hat{g}(^{2s+1}S_s)$ and $\hat{h}_i(^{2s+1}S_s)$. Expressions for certain triangle- or box-topology related kinematic factors, that we do not write explicitly below, can therefore be obtained from the relations (A.71).

In case of 1P_1 waves we find the following expressions for kinematic factors $\tilde{C}_{n,i_1V}^{(\alpha)SS}$ and diagram topologies $\alpha = 1, 2$:

$$\tilde{C}_{rqq,i_1V}^{(1)SS}(^1P_1) = \tilde{C}_{qqr,i_1V}^{(2)SS}(^1P_1) = \frac{\beta^2}{24 \widehat{m} \widehat{\overline{m}}} \Delta_m^2 - \frac{\beta^2 \Delta_m}{12 P_{i_1AB}} (\Delta_m + 2\widehat{m}_{i_1} + \Delta_{AB}). \quad (\text{A.167})$$

In case of combined $^3P_{\mathcal{J}}$ reactions the corresponding expressions read

$$\begin{aligned} \tilde{C}_{rrr,i_1V}^{(1)SS}(^3P_{\mathcal{J}}) &= \tilde{C}_{rrr,i_1V}^{(2)SS}(^3P_{\mathcal{J}}) \\ &= -\frac{\widehat{m}_{i_1}}{4 \widehat{m} \widehat{\overline{m}}} \Delta_m \Delta_{AB} - \frac{\Delta_m \Delta_{AB}}{8 \widehat{m} \widehat{\overline{m}}} (\Delta_m \Delta_{AB} + 1) + \frac{\beta^2 \Delta_m \Delta_{AB}}{12 P_{i_1AB}}, \end{aligned} \quad (\text{A.168})$$

$$\tilde{C}_{rqq,i_1V}^{(1)SS}(^3P_{\mathcal{J}}) = \tilde{C}_{qqr,i_1V}^{(2)SS}(^3P_{\mathcal{J}}) = \frac{\beta^2}{12 \widehat{m} \widehat{\overline{m}}}. \quad (\text{A.169})$$

Turning to kinematic factors $\tilde{C}_{n,i_1S}^{(\alpha)SS}$ with $\alpha = 1, 2$ we find

$$\begin{aligned} \tilde{C}_{rrr,i_1S}^{(1)SS}(^3P_{\mathcal{J}}) &= \tilde{C}_{rrr,i_1S}^{(2)SS}(^3P_{\mathcal{J}}) \\ &= -\frac{\widehat{m}_W}{8 \widehat{m} \widehat{\overline{m}}} (\Delta_m \Delta_{AB} + 1) - \frac{\widehat{m}_W}{4 \widehat{m} \widehat{\overline{m}}} \widehat{m}_{i_1} + \frac{\beta^2}{12 P_{i_1AB}} \widehat{m}_W, \end{aligned} \quad (\text{A.170})$$

and, as in the case of leading-order 1S_0 and 3S_1 kinematic factors, the remaining non-vanishing expressions for $\tilde{C}_{n,i_1X}^{(\alpha)SS}$ with both $X = V, S$ and $\alpha = 1, 2$ that are associated with 1P_1 and $^3P_{\mathcal{J}}$ (as well as the separate $^3P_J, J = 0, 1, 2$) partial-wave configurations, derive from the above given expressions using (A.75). Finally, the box-diagram related kinematic factors $\tilde{D}_{n,i_1i_2}^{(\alpha)SS}$ for diagram topologies $\alpha = 1, 2$ are given by

$$\begin{aligned} \tilde{D}_{rqqr,i_1i_2}^{(1)SS}(^1P_1) &= -\frac{\beta^2 \Delta_m^2}{96 (\widehat{m} \widehat{\overline{m}})^2} + \frac{\beta^2 \Delta_m}{24 \widehat{m} \widehat{\overline{m}} P_{i_1AB}} (\Delta_m + 2 \widehat{m}_{i_1} + \Delta_{AB}) \\ &\quad - \frac{\beta^2}{24 P_{i_1AB} P_{i_2BA}} (\Delta_m^2 + 2 \Delta_m (\widehat{m}_{i_1} + \widehat{m}_{i_2}) \\ &\quad \quad \quad + (2 \widehat{m}_{i_1} + \Delta_{AB}) (2 \widehat{m}_{i_2} - \Delta_{AB})) \\ &\quad + \left\{ A \leftrightarrow B, i_1 \leftrightarrow i_2 \right\}, \end{aligned} \quad (\text{A.171})$$

$$\begin{aligned}
\tilde{D}_{rqq, i_1 i_2}^{(2)SS}({}^1P_1) &= \frac{\beta^2 \Delta_m^2}{96 (\widehat{m} \widehat{\bar{m}})^2} - \frac{\beta^2 \Delta_m}{24 \widehat{m} \widehat{\bar{m}} P_{i_1 AB}} (\Delta_m + 2 \widehat{m}_{i_1} + \Delta_{AB}) \\
&+ \frac{\beta^2}{24 P_{i_1 AB} P_{i_2 AB}} (\Delta_m^2 + 2 \Delta_m (\widehat{m}_{i_1} + \widehat{m}_{i_2} + \Delta_{AB}) \\
&\quad + (2 \widehat{m}_{i_1} + \Delta_{AB}) (2 \widehat{m}_{i_2} + \Delta_{AB})) \\
&+ \left\{ i_1 \leftrightarrow i_2 \right\} . \tag{A.172}
\end{aligned}$$

For the combined 3P_J reactions we have

$$\begin{aligned}
\tilde{D}_{rrrr, i_1 i_2}^{(1)SS}({}^3P_J) &= \frac{\widehat{m}_{i_1} \widehat{m}_{i_2}}{8 (\widehat{m} \widehat{\bar{m}})^2} - \frac{\widehat{m}_{i_1}}{8 (\widehat{m} \widehat{\bar{m}})^2} (\Delta_m \Delta_{AB} - 1) \\
&+ \frac{\beta^2}{24 \widehat{m} \widehat{\bar{m}} P_{i_1 AB}} (\Delta_m \Delta_{AB} - 2 \widehat{m}_{i_2} - 1) + \frac{\beta^4}{24 P_{i_1 AB} P_{i_2 BA}} \\
&- \frac{1}{32 (\widehat{m} \widehat{\bar{m}})^2} (\Delta_m^2 \Delta_{AB}^2 - 1) + \left\{ A \leftrightarrow B, i_1 \leftrightarrow i_2 \right\} , \tag{A.173}
\end{aligned}$$

$$\begin{aligned}
\tilde{D}_{rrrr, i_1 i_2}^{(2)SS}({}^3P_J) &= \frac{\widehat{m}_{i_1} \widehat{m}_{i_2}}{8 (\widehat{m} \widehat{\bar{m}})^2} + \frac{\widehat{m}_{i_1}}{8 (\widehat{m} \widehat{\bar{m}})^2} (\Delta_m \Delta_{AB} + 1) \\
&- \frac{\beta^2}{24 \widehat{m} \widehat{\bar{m}} P_{i_1 AB}} (\Delta_m \Delta_{AB} + 2 \widehat{m}_{i_2} + 1) + \frac{\beta^4}{24 P_{i_1 AB} P_{i_2 AB}} \\
&+ \frac{1}{32 (\widehat{m} \widehat{\bar{m}})^2} (\Delta_m \Delta_{AB} + 1)^2 + \left\{ i_1 \leftrightarrow i_2 \right\} , \tag{A.174}
\end{aligned}$$

$$\tilde{D}_{rqq, i_1 i_2}^{(\alpha)SS}({}^3P_J) = (-1)^\alpha \frac{\beta^2}{24 (\widehat{m} \widehat{\bar{m}})^2} . \tag{A.175}$$

The remaining non-vanishing kinematic factors can be related to the above given expressions by making use of the following relations among $\tilde{D}_{n, i_1 i_2}^{(\alpha)SS}$ kinematic factors with different labels n :

$$\begin{aligned}
\tilde{D}_{qqqq, i_1 i_2}^{(\alpha)SS}({}^{2s+1}L_J) &= \tilde{D}_{rrrr, i_1 i_2}^{(\alpha)SS}({}^{2s+1}L_J) |_{\widehat{m}_{i_1,2} \rightarrow -\widehat{m}_{i_1,2}} , \\
\tilde{D}_{rrqq, i_1 i_2}^{(\alpha)SS}({}^{2s+1}L_J) &= -\tilde{D}_{rrrr, i_1 i_2}^{(\alpha)SS}({}^{2s+1}L_J) |_{\widehat{m}_{i_2} \rightarrow -\widehat{m}_{i_2}} , \\
\tilde{D}_{qqrr, i_1 i_2}^{(\alpha)SS}({}^{2s+1}L_J) &= -\tilde{D}_{rrrr, i_1 i_2}^{(\alpha)SS}({}^{2s+1}L_J) |_{\widehat{m}_{i_1} \rightarrow -\widehat{m}_{i_1}} , \\
\tilde{D}_{qrrq, i_1 i_2}^{(\alpha)SS}({}^{2s+1}L_J) &= \tilde{D}_{rqq, i_1 i_2}^{(\alpha)SS}({}^{2s+1}L_J) , |_{\widehat{m}_{i_1,2} \rightarrow -\widehat{m}_{i_1,2}} , \\
\tilde{D}_{rqrq, i_1 i_2}^{(\alpha)SS}({}^{2s+1}L_J) &= -\tilde{D}_{rqq, i_1 i_2}^{(\alpha)SS}({}^{2s+1}L_J) |_{\widehat{m}_{i_2} \rightarrow -\widehat{m}_{i_2}} , \\
\tilde{D}_{qrqr, i_1 i_2}^{(\alpha)SS}({}^{2s+1}L_J) &= -\tilde{D}_{rqq, i_1 i_2}^{(\alpha)SS}({}^{2s+1}L_J) |_{\widehat{m}_{i_1} \rightarrow -\widehat{m}_{i_1}} . \tag{A.176}
\end{aligned}$$

Note that these relations hold among the kinematic factors associated with any of the Wilson coefficients $\hat{f}({}^{2s+1}L_J)$, $\hat{g}({}^{2s+1}S_s)$ and $\hat{h}_i({}^{2s+1}S_s)$.

A.3.4 P -wave kinematic factors for $X_A X_B = ff$

The relevant kinematic factors $\tilde{B}_{n,i_1 i_2}^{ff}$, related to the selfenergy diagram topology with a fermion-fermion final state, read

$$\tilde{B}_{qqqq, VV}^{ff}(^1P_1) = \frac{\Delta_m^2}{12} (\beta^2 + 3 - 12 \hat{m}_A \hat{m}_B - 3 \Delta_{AB}^2) , \quad (\text{A.177})$$

for the 1P_1 partial-wave configuration, and

$$\tilde{B}_{rrrr, VV}^{ff}(^3P_J) = -\frac{\Delta_m^2}{4} (\beta^2 - 1 + 4 \hat{m}_A \hat{m}_B + \Delta_{AB}^2) , \quad (\text{A.178})$$

$$\tilde{B}_{rrrr, VS}^{ff}(^3P_J) = \tilde{B}_{rrrr, SV}^{ff}(^3P_J) = -\frac{\Delta_m}{2} (\hat{m}_A - \hat{m}_B - (\hat{m}_A + \hat{m}_B) \Delta_{AB}) , \quad (\text{A.179})$$

$$\tilde{B}_{rrrr, SS}^{ff}(^3P_J) = \frac{1}{4} (\beta^2 + 1 - 4 \hat{m}_A \hat{m}_B - \Delta_{AB}^2) , \quad (\text{A.180})$$

$$\tilde{B}_{qqqq, VV}^{ff}(^3P_J) = \frac{1}{6} (\beta^2 + 3 - 12 \hat{m}_A \hat{m}_B - 3 \Delta_{AB}^2) , \quad (\text{A.181})$$

for the 3P_J case. In the case that the s -channel exchanged particles are of the same type ($i_1 i_2 = VV, SS$), the additional non-vanishing kinematic factors are related to the expressions (A.177)–(A.181) as

$$\tilde{B}_{rqq, i_1 i_2}^{ff}(^{2s+1}P_J) = \tilde{B}_{rrrr, i_1 i_2}^{ff}(^{2s+1}P_J)|_{\hat{m}_A \hat{m}_B \rightarrow -\hat{m}_A \hat{m}_B} , \quad (\text{A.182})$$

$$\tilde{B}_{qrrq, i_1 i_2}^{ff}(^{2s+1}P_J) = \tilde{B}_{qqqq, i_1 i_2}^{ff}(^{2s+1}P_J)|_{\hat{m}_A \hat{m}_B \rightarrow -\hat{m}_A \hat{m}_B} , \quad (\text{A.183})$$

where the notation for the replacement rule applies to the term $\hat{m}_A \hat{m}_B$, but all other occurrences of \hat{m}_A or \hat{m}_B shall be left untouched. Similarly, in case of s -channel particles of different type ($i_1 i_2 = VS, SV$), the additional non-vanishing $\tilde{B}_{n, i_1 i_2}^{ff}$ terms are given by

$$\tilde{B}_{rqq, i_1 i_2}^{ff}(^{2s+1}P_J) = -\tilde{B}_{rrrr, i_1 i_2}^{ff}(^{2s+1}P_J)|_{\hat{m}_A \rightarrow -\hat{m}_A} , \quad (\text{A.184})$$

$$\tilde{B}_{qrrq, i_1 i_2}^{ff}(^{2s+1}P_J) = -\tilde{B}_{qqqq, i_1 i_2}^{ff}(^{2s+1}P_J)|_{\hat{m}_A \rightarrow -\hat{m}_A} . \quad (\text{A.185})$$

The relations (A.91) among kinematic factors for diagram topologies $\alpha = 3(4)$ and diagram topologies $\alpha = 1(2)$ for both the cases of box and triangle diagrams are valid among kinematic factors associated with any $^{2s+1}L_J$ partial wave (in particular also for $\hat{g}(^{2s+1}S_s)$ and $\hat{h}_i(^{2s+1}S_s)$ associated kinematic factors). Therefore we give only non-vanishing kinematic factors related to triangle- and box-topologies $\alpha = 1, 2$ in the following.

The structures $C_{n, i_1 V}^{(\alpha) ff}(^{2s+1}P_J)$ that we obtain for diagram topologies $\alpha = 1, 2$ read

$$C_{qqq, i_1 X}^{(\alpha) ff}(^1P_1) = \frac{\Delta_m}{48 \hat{m} \hat{\bar{m}}} \left(6 (\hat{m}_A + \hat{m}_B) \Delta_{AB} - 6 (\hat{m}_A - \hat{m}_B) \right. \\ \left. - \Delta_m (\beta^2 + 3 - 12 \hat{m}_A \hat{m}_B - 3 \Delta_{AB}^2) \right)$$

$$+ \frac{\beta^2 \Delta_m}{12 P_{i_1 AB}} (\widehat{m}_A - \widehat{m}_B - \Delta_{AB}) , \quad (\text{A.186})$$

and, for the combined ${}^3P_{\mathcal{J}}$ partial-wave reactions,

$$\begin{aligned} C_{rrrr, i_1 X}^{(\alpha) ff}({}^3P_{\mathcal{J}}) &= \frac{\Delta_m}{16 \widehat{m} \widehat{\overline{m}}} \left(-2 (\widehat{m}_A + \widehat{m}_B) \Delta_{AB} + 2 (\widehat{m}_A - \widehat{m}_B) \right. \\ &\quad \left. + \Delta_m (\beta^2 - 1 + 4 \widehat{m}_A \widehat{m}_B + \Delta_{AB}^2) \right) \\ &\quad - \frac{\beta^2 \Delta_m}{12 P_{i_1 AB}} (\widehat{m}_A - \widehat{m}_B + \Delta_{AB}) , \end{aligned} \quad (\text{A.187})$$

$$\begin{aligned} C_{rrrq, i_1 X}^{(1) ff}({}^3P_{\mathcal{J}}) &= \frac{1}{24 \widehat{m} \widehat{\overline{m}}} \left(6 (\widehat{m}_A + \widehat{m}_B - (\widehat{m}_A - \widehat{m}_B) \Delta_{AB}) \Delta_m \right. \\ &\quad \left. + \beta^2 + 3 + 12 \widehat{m}_A \widehat{m}_B - 3 \Delta_{AB}^2 \right) \\ &\quad - \frac{\beta^2}{6 P_{i_1 AB}} (1 - \widehat{m}_A + \widehat{m}_B) , \end{aligned} \quad (\text{A.188})$$

$$C_{rrrq, i_1 X}^{(2) ff}({}^3P_{\mathcal{J}}) = C_{rrrq, i_1 X}^{(1) ff}({}^3P_{\mathcal{J}}) . \quad (\text{A.189})$$

The following relations for the additional non-vanishing $C_{n, i_1 V}^{(\alpha) ff}$ hold:

$$\begin{aligned} \tilde{C}_{rrrq, i_1 V}^{(1) ff}({}^1P_1) &= \tilde{C}_{rrqr, i_1 V}^{(2) ff}({}^1P_1) = -\tilde{C}_{qqqq, i_1 V}^{(\alpha) ff}({}^1P_1)|_{m_B \rightarrow -m_B} , \\ \tilde{C}_{qrrq, i_1 V}^{(\alpha) ff}({}^1P_1) &= \tilde{C}_{qqqq, i_1 V}^{(\alpha) ff}({}^1P_1)|_{m_A \rightarrow -m_A} , \\ \tilde{C}_{rrqq, i_1 V}^{(1) ff}({}^1P_1) &= \tilde{C}_{qqrr, i_1 V}^{(2) ff}({}^1P_1) = -\tilde{C}_{qqqq, i_1 V}^{(\alpha) ff}({}^1P_1)|_{m_{A,B} \rightarrow -m_{A,B}} , \\ \tilde{C}_{qqrr, i_1 V}^{(1) ff}({}^3P_{\mathcal{J}}) &= \tilde{C}_{rrqq, i_1 V}^{(2) ff}({}^3P_{\mathcal{J}}) = -\tilde{C}_{rrrr, i_1 V}^{(1) ff}({}^3P_{\mathcal{J}})|_{m_{A,B} \rightarrow -m_{A,B}} , \\ \tilde{C}_{qrrq, i_1 V}^{(\alpha) ff}({}^3P_{\mathcal{J}}) &= -\tilde{C}_{rrrq, i_1 V}^{(1) ff}({}^3P_{\mathcal{J}})|_{m_{A,B} \rightarrow -m_{A,B}} . \end{aligned} \quad (\text{A.190})$$

Turning to the expressions $C_{n, i_1 S}^{(\alpha) ff}$, we find that all kinematic factors in case of 1P_1 reactions vanish, as it has to be due to total angular-momentum conservation. The non-vanishing kinematic factors in combined ${}^3P_{\mathcal{J}}$ reactions read ($\alpha = 1, 2$)

$$\begin{aligned} \tilde{C}_{rrrr, i_1 S}^{(\alpha) ff}({}^3P_{\mathcal{J}}) &= \frac{1}{16 \widehat{m} \widehat{\overline{m}}} \left(2 (-\widehat{m}_A + \widehat{m}_B + (\widehat{m}_A + \widehat{m}_B) \Delta_{AB}) \Delta_m \right. \\ &\quad \left. + \beta^2 + 1 - 4 \widehat{m}_A \widehat{m}_B - \Delta_{AB}^2 \right) \\ &\quad - \frac{\beta^2}{12 P_{i_1 AB}} (1 + \widehat{m}_A + \widehat{m}_B) , \end{aligned} \quad (\text{A.191})$$

$$\tilde{C}_{qqrr, i_1 S}^{(1) ff}({}^3P_{\mathcal{J}}) = \tilde{C}_{rrqq, i_1 S}^{(2) ff}({}^3P_{\mathcal{J}}) = \tilde{C}_{rrrr, i_1 S}^{(1) ff}({}^3P_{\mathcal{J}})|_{m_{A,B} \rightarrow -m_{A,B}} . \quad (\text{A.192})$$

In case of 1P_1 partial-wave reactions the kinematic factors $\tilde{D}_{n, i_1 i_2}^{(\alpha) ff}$ for $\alpha = 1, 2$ read

$$\tilde{D}_{rrrr, i_1 i_2}^{(1) ff}({}^1P_1)$$

$$\begin{aligned}
&= \frac{1}{384 (\widehat{m} \widehat{\overline{m}})^2} \left(\beta^2 (1 + \Delta_m^2) - (3 - 12 \widehat{m}_A \widehat{m}_B - 3 \Delta_{AB}^2) (1 - \Delta_m^2) \right) \\
&\quad + \frac{\beta^2}{48 \widehat{m} \widehat{\overline{m}} P_{i_1 AB}} \left(1 + \widehat{m}_A + \widehat{m}_B + \Delta_m (\widehat{m}_A - \widehat{m}_B + \Delta_{AB}) \right) \\
&\quad - \frac{\beta^2}{48 P_{i_1 AB} P_{i_2 BA}} (1 + 2 \widehat{m}_A + \Delta_{AB}) (1 + 2 \widehat{m}_B - \Delta_{AB}) \\
&\quad + \left\{ A \leftrightarrow B, i_1 \leftrightarrow i_2 \right\}, \tag{A.193}
\end{aligned}$$

$$\begin{aligned}
&\tilde{D}_{rrrr, i_1 i_2}^{(2)ff} ({}^1 P_1) \\
&= \frac{1}{384 (\widehat{m} \widehat{\overline{m}})^2} \left(\beta^2 (\Delta_m^2 - 1) + (3 - 12 \widehat{m}_A \widehat{m}_B - 3 \Delta_{AB}^2) (\Delta_m^2 + 1) \right. \\
&\quad \left. - 12 \Delta_m (\widehat{m}_A - \widehat{m}_B - (\widehat{m}_A + \widehat{m}_B) \Delta_{AB}) \right) \\
&\quad - \frac{\beta^2}{48 \widehat{m} \widehat{\overline{m}} P_{i_1 AB}} \left(1 + \widehat{m}_A + \widehat{m}_B - \Delta_m (\widehat{m}_A - \widehat{m}_B + \Delta_{AB}) \right) \\
&\quad + \frac{\beta^2}{48 P_{i_1 AB} P_{i_2 AB}} (1 + 2 \widehat{m}_A + \Delta_{AB}) (1 + 2 \widehat{m}_B - \Delta_{AB}) + \left\{ i_1 \leftrightarrow i_2 \right\}, \tag{A.194}
\end{aligned}$$

$$\begin{aligned}
&\tilde{D}_{rrqq, i_1 i_2}^{(1)ff} ({}^1 P_1) \\
&= \frac{1}{192 (\widehat{m} \widehat{\overline{m}})^2} \left(\beta^2 - 3 + 3 \Delta_{AB}^2 + 12 \Delta_m (\widehat{m}_A - \widehat{m}_B - (\widehat{m}_A + \widehat{m}_B) \Delta_{AB}) \right. \\
&\quad \left. - \Delta_m^2 (\beta^2 + 3 + 24 \widehat{m}_A \widehat{m}_B - 3 \Delta_{AB}^2) \right) \\
&\quad + \frac{\beta^2}{48 \widehat{m} \widehat{\overline{m}} P_{i_1 AB}} \left(1 + \widehat{m}_A + \widehat{m}_B - \Delta_m (\widehat{m}_A - \widehat{m}_B + \Delta_{AB}) \right) \\
&\quad + \frac{\beta^2}{48 \widehat{m} \widehat{\overline{m}} P_{i_2 BA}} \left(1 - \widehat{m}_A - \widehat{m}_B - \Delta_m (\widehat{m}_A - \widehat{m}_B - \Delta_{AB}) \right) \\
&\quad - \frac{\beta^2}{24 P_{i_1 AB} P_{i_2 BA}} (\beta^2 - 4 \widehat{m}_A \widehat{m}_B), \tag{A.195}
\end{aligned}$$

$$\begin{aligned}
&\tilde{D}_{rrqq, i_1 i_2}^{(2)ff} ({}^1 P_1) \\
&= - \frac{1}{192 (\widehat{m} \widehat{\overline{m}})^2} \left(\beta^2 - 3 + 3 \Delta_{AB}^2 + \Delta_m^2 (\beta^2 + 3 + 24 \widehat{m}_A \widehat{m}_B - 3 \Delta_{AB}^2) \right) \\
&\quad - \frac{\beta^2}{48 \widehat{m} \widehat{\overline{m}} P_{i_1 AB}} \left(1 + \widehat{m}_A + \widehat{m}_B + \Delta_m (\widehat{m}_A - \widehat{m}_B + \Delta_{AB}) \right) \\
&\quad - \frac{\beta^2}{48 \widehat{m} \widehat{\overline{m}} P_{i_2 AB}} \left(1 - \widehat{m}_A - \widehat{m}_B - \Delta_m (\widehat{m}_A - \widehat{m}_B - \Delta_{AB}) \right)
\end{aligned}$$

$$+ \frac{\beta^2}{24 P_{i_1 AB} P_{i_2 AB}} (\beta^2 - 4 \widehat{m}_A \widehat{m}_B) . \quad (\text{A.196})$$

The corresponding expressions for combined ${}^3P_{\mathcal{J}}$ partial-wave reactions are

$$\tilde{D}_{rrrr, i_1 i_2}^{(1)ff}({}^3P_{\mathcal{J}}) = -3 \tilde{D}_{rrrr, i_1 i_2}^{(1)ff}({}^1P_1) + \frac{\beta^2}{24 (\widehat{m} \widehat{m})^2} (1 + \Delta_m^2) , \quad (\text{A.197})$$

$$\tilde{D}_{rrrr, i_1 i_2}^{(2)ff}({}^3P_{\mathcal{J}}) = 3 \tilde{D}_{rrrr, i_1 i_2}^{(2)ff}({}^1P_1) + \frac{\beta^2}{24 (\widehat{m} \widehat{m})^2} (1 - \Delta_m^2) , \quad (\text{A.198})$$

$$\tilde{D}_{rrqq, i_1 i_2}^{(1)ff}({}^3P_{\mathcal{J}}) = \tilde{D}_{rrqq, i_1 i_2}^{(1)ff}({}^1P_1) - \frac{\widehat{m}_A \widehat{m}_B}{2 (\widehat{m} \widehat{m})^2} - \frac{\beta^2}{3 P_{i_1 AB} P_{i_2 BA}} 2 \widehat{m}_A \widehat{m}_B , \quad (\text{A.199})$$

$$\tilde{D}_{rrqq, i_1 i_2}^{(2)ff}({}^3P_{\mathcal{J}}) = -\tilde{D}_{rrqq, i_1 i_2}^{(2)ff}({}^1P_1) - \frac{\widehat{m}_A \widehat{m}_B}{2 (\widehat{m} \widehat{m})^2} - \frac{\beta^2}{3 P_{i_1 AB} P_{i_2 AB}} 2 \widehat{m}_A \widehat{m}_B . \quad (\text{A.200})$$

The following relations can be used to obtain the remaining non-vanishing $\tilde{D}_{n, i_1 i_2}^{(\alpha)ff}$ expressions in case of diagram topology $\alpha = 1$. Note that they hold for any ${}^{2s+1}L_J$ partial-wave configuration.

$$\begin{aligned} \tilde{D}_{qqqq, i_1 i_2}^{(1)ff}({}^{2s+1}L_J) &= \tilde{D}_{rrrr, i_1 i_2}^{(1)ff}({}^{2s+1}L_J)|_{m_{A,B} \rightarrow -m_{A,B}} , \\ \tilde{D}_{qrrr, i_1 i_2}^{(1)ff}({}^{2s+1}L_J) &= \tilde{D}_{rrqq, i_1 i_2}^{(1)ff}({}^{2s+1}L_J)|_{m_{A,B} \rightarrow -m_{A,B}} , \\ \tilde{D}_{rqqr, i_1 i_2}^{(1)ff}({}^{2s+1}L_J) &= \tilde{D}_{rrqq, i_1 i_2}^{(1)ff}({}^{2s+1}L_J)|_{m_A \rightarrow -m_A} , \\ \tilde{D}_{qrrq, i_1 i_2}^{(1)ff}({}^{2s+1}L_J) &= \tilde{D}_{rrqq, i_1 i_2}^{(1)ff}({}^{2s+1}L_J)|_{m_B \rightarrow -m_B} , \\ \tilde{D}_{rqrq, i_1 i_2}^{(1)ff}({}^{2s+1}L_J) &= \tilde{D}_{rrrr, i_1 i_2}^{(1)ff}({}^{2s+1}L_J)|_{m_A \rightarrow -m_A} , \\ \tilde{D}_{qrqr, i_1 i_2}^{(1)ff}({}^{2s+1}L_J) &= \tilde{D}_{rrrr, i_1 i_2}^{(1)ff}({}^{2s+1}L_J)|_{m_B \rightarrow -m_B} . \end{aligned} \quad (\text{A.201})$$

In case of diagram topology $\alpha = 2$ analogous relations exist:

$$\begin{aligned} \tilde{D}_{qqqq, i_1 i_2}^{(2)ff}({}^{2s+1}L_J) &= \tilde{D}_{rrrr, i_1 i_2}^{(2)ff}({}^{2s+1}L_J)|_{m_{A,B} \rightarrow -m_{A,B}} , \\ \tilde{D}_{qrrr, i_1 i_2}^{(2)ff}({}^{2s+1}L_J) &= \tilde{D}_{rrqq, i_1 i_2}^{(2)ff}({}^{2s+1}L_J)|_{m_{A,B} \rightarrow -m_{A,B}} , \\ \tilde{D}_{rqqr, i_1 i_2}^{(2)ff}({}^{2s+1}L_J) &= \tilde{D}_{rrqq, i_1 i_2}^{(2)ff}({}^{2s+1}L_J)|_{m_A \rightarrow -m_A} , \\ \tilde{D}_{qrrq, i_1 i_2}^{(2)ff}({}^{2s+1}L_J) &= \tilde{D}_{rrqq, i_1 i_2}^{(2)ff}({}^{2s+1}L_J)|_{m_B \rightarrow -m_B} , \\ \tilde{D}_{rqrq, i_1 i_2}^{(2)ff}({}^{2s+1}L_J) &= \tilde{D}_{rrrr, i_1 i_2}^{(2)ff}({}^{2s+1}L_J)|_{m_A \rightarrow -m_A} , \\ \tilde{D}_{qrqr, i_1 i_2}^{(2)ff}({}^{2s+1}L_J) &= \tilde{D}_{rrrr, i_1 i_2}^{(2)ff}({}^{2s+1}L_J)|_{m_B \rightarrow -m_B} . \end{aligned} \quad (\text{A.202})$$

A.3.5 P -wave kinematic factors for $X_A X_B = \eta \bar{\eta}$

In order to properly construct the coupling factors that go along the kinematic factors $\tilde{B}_{n, i_1 i_2}^{\eta \bar{\eta}}$ presented below, we refer the reader to the rules set up in A.2.5.

For 1P_1 partial-wave processes, there is only one non-vanishing kinematic factor with ghosts in the final state:

$$\tilde{B}_{qq,VV}^{\eta\bar{\eta}}({}^1P_1) = -\frac{\beta^2}{48} \Delta_m^2 . \quad (\text{A.203})$$

The corresponding kinematic factors in combined ${}^3P_{\mathcal{J}}$ partial-wave processes read

$$\tilde{B}_{rr,VV}^{\eta\bar{\eta}}({}^3P_{\mathcal{J}}) = \frac{\Delta_m^2}{16} (1 - \Delta_{AB}^2) , \quad (\text{A.204})$$

$$\tilde{B}_{qq,VV}^{\eta\bar{\eta}}({}^3P_{\mathcal{J}}) = -\frac{\beta^2}{24} , \quad (\text{A.205})$$

$$\tilde{B}_{rr,VS}^{\eta\bar{\eta}}({}^3P_{\mathcal{J}}) = \frac{\hat{m}_W}{8} \Delta_m (1 + \Delta_{AB}) , \quad (\text{A.206})$$

$$\tilde{B}_{rr,SV}^{\eta\bar{\eta}}({}^3P_{\mathcal{J}}) = -\frac{\hat{m}_W}{8} \Delta_m (1 - \Delta_{AB}) , \quad (\text{A.207})$$

$$\tilde{B}_{rr,SS}^{\eta\bar{\eta}}({}^3P_{\mathcal{J}}) = -\frac{\hat{m}_W^2}{4} . \quad (\text{A.208})$$

Appendix B

Explicit expressions for the MSSM potentials in \mathcal{L}_{pot}

This appendix contains explicit expressions for all leading-order non-relativistic potential interactions that can arise between MSSM neutralino and chargino two-particle states. In Tab. B.1 we provide the coefficients of the Yukawa terms $e^{-m_{X_i}r}/r$ generated by the exchange of boson X_i ($X_i = Z, W^\pm, \gamma, H_m^0, A_1^0, H^\pm$) in tree-level $\chi_{e_1}\chi_{e_2} \rightarrow \chi_{e_4}\chi_{e_3}$ scattering processes of NRMSSM two-particle state $\chi_{e_a}\chi_{e_b}$.¹ The complete leading order potential in $\chi_{e_1}\chi_{e_2} \rightarrow \chi_{e_4}\chi_{e_3}$ scattering is obtained as the sum of the coefficients in Tab. B.1 multiplied by the corresponding $e^{-m_{X_i}r}/r$ terms. As we have pointed out in Sec. 7.1, the contribution from the pseudo-scalar Goldstone boson ($G^0 \equiv A_2^0$) does not have to be considered, since it cancels against a gauge-dependent piece of the Z -exchange potential, which has been consistently dropped in Tab. B.1. A similar cancellation occurs between the potential from exchange of the charged pseudo-Goldstone bosons $G^\pm \equiv H_2^\pm$ and the gauge dependent part of the W^\pm -exchange potential. Accordingly the potential from G^\pm -exchange does not have to be considered and the contributions from W^\pm -exchange in Tab. B.1 comprise only the corresponding gauge-independent terms. The coefficients are written in terms of the (axial-) vector and (pseudo-) scalar coupling factors defined in Appendix A.1.2.

¹Note that we use the common notation $H_1^0 = H^0$ and $H_2^0 = h^0$.

	$\frac{\alpha_2 e^{-M_Z r}}{r}$	$\frac{\alpha_2 e^{-M_W r}}{r}$	$\frac{\alpha_2}{r}$	$\frac{\alpha_2 e^{-m_\phi r}}{r}$	$\frac{\alpha_2 e^{-M_{H^\pm} r}}{r}$
$\chi_{e_1}^0 \chi_{e_2}^0 \rightarrow \chi_{e_4}^0 \chi_{e_3}^0$	$\lambda^Z v_{e_4 e_1}^{(0),Z} v_{e_3 e_2}^{(0),Z}$ $+\lambda_S a_{e_4 e_1}^{(0),Z} a_{e_3 e_2}^{(0),Z}$	0	0	$-s_{e_4 e_1}^{(0),\phi} s_{e_3 e_2}^{(0),\phi}$	0
$\chi_{e_1}^+ \chi_{e_2}^- \rightarrow \chi_{e_4}^+ \chi_{e_3}^-$	$-\lambda^Z v_{e_4 e_1}^Z v_{e_3 e_2}^Z$ $+\lambda_S a_{e_4 e_1}^Z a_{e_3 e_2}^Z$	0	$-v_{e_4 e_1}^\gamma v_{e_2 e_3}^\gamma$	$-s_{e_4 e_1}^\phi s_{e_2 e_3}^\phi$	0
$\chi_{e_1}^0 \chi_{e_2}^0 \rightarrow \chi_{e_4}^+ \chi_{e_3}^-$	0	$-\lambda^W v_{e_4 e_1}^{W} v_{e_3 e_2}^{W*}$ $+\lambda_S a_{e_4 e_1}^W a_{e_3 e_2}^{W*}$	0	0	$-s_{e_4 e_1}^{H^+} s_{e_3 e_2}^{H^{+*}}$
$\chi_{e_1}^0 \chi_{e_2}^0 \rightarrow \chi_{e_4}^- \chi_{e_3}^+$	0	$-\lambda^W v_{e_4 e_1}^{W*} v_{e_3 e_2}^W$ $+\lambda_S a_{e_4 e_1}^{W*} a_{e_3 e_2}^W$	0	0	$-s_{e_4 e_1}^{H^{+*}} s_{e_3 e_2}^{H^+}$
$\chi_{e_1}^0 \chi_{e_2}^+ \rightarrow \chi_{e_4}^0 \chi_{e_3}^+$	$\lambda^Z v_{e_4 e_1}^{(0),Z} v_{e_3 e_2}^Z$ $+\lambda_S a_{e_4 e_1}^{(0),Z} a_{e_3 e_2}^Z$	0	0	$-s_{e_4 e_1}^{(0),\phi} s_{e_3 e_2}^\phi$	0
$\chi_{e_1}^0 \chi_{e_2}^- \rightarrow \chi_{e_4}^0 \chi_{e_3}^-$	$-\lambda^Z v_{e_4 e_1}^{(0),Z} v_{e_2 e_3}^Z$ $+\lambda_S a_{e_4 e_1}^{(0),Z} a_{e_2 e_3}^Z$	0	0	$-s_{e_4 e_1}^{(0),\phi} s_{e_2 e_3}^\phi$	0
$\chi_{e_1}^0 \chi_{e_2}^+ \rightarrow \chi_{e_4}^+ \chi_{e_3}^0$	0	$\lambda^W v_{e_4 e_1}^W v_{e_2 e_3}^{W*}$ $+\lambda_S a_{e_4 e_1}^W a_{e_2 e_3}^{W*}$	0	0	$-s_{e_4 e_1}^{H^+} s_{e_2 e_3}^{H^{+*}}$
$\chi_{e_1}^0 \chi_{e_2}^- \rightarrow \chi_{e_4}^- \chi_{e_3}^0$	0	$\lambda^W v_{e_4 e_1}^{W*} v_{e_2 e_3}^W$ $+\lambda_S a_{e_4 e_1}^{W*} a_{e_2 e_3}^W$	0	0	$-s_{e_4 e_1}^{H^{+*}} s_{e_2 e_3}^{H^+}$
$\chi_{e_1}^+ \chi_{e_2}^+ \rightarrow \chi_{e_4}^+ \chi_{e_3}^+$	$\lambda^Z v_{e_4 e_1}^Z v_{e_3 e_2}^Z$ $+\lambda_S a_{e_4 e_1}^Z a_{e_3 e_2}^Z$	0	$v_{e_4 e_1}^\gamma v_{e_3 e_2}^\gamma$	$-s_{e_4 e_1}^\phi s_{e_3 e_2}^\phi$	0
$\chi_{e_1}^- \chi_{e_2}^- \rightarrow \chi_{e_4}^- \chi_{e_3}^-$	$\lambda^Z v_{e_1 e_4}^Z v_{e_2 e_3}^Z$ $+\lambda_S a_{e_1 e_4}^Z a_{e_2 e_3}^Z$	0	$v_{e_1 e_4}^\gamma v_{e_3 e_2}^\gamma$	$-s_{e_1 e_4}^\phi s_{e_2 e_3}^\phi$	0

Table B.1: Potentials that describe the non-relativistic interactions among chargino and neutralino pairs in the MSSM at leading order in the non-relativistic expansion. The potential from neutral scalar exchange ϕ has to be summed over the “physical” neutral Higgs bosons, $\phi = H^0, h^0, A^0$. The expressions obtained from the table correspond to the potential entries in method-1. The potentials for the channels not shown are obtained trivially by interchanging indices (like $\chi^- \chi^+ \rightarrow \chi^+ \chi^-$ or $\chi^+ \chi^0 \rightarrow \chi^0 \chi^+$) or are vanishing (like $\chi^- \chi^+ \rightarrow \chi^+ \chi^-$). We have introduced the variable $\lambda_S \equiv (3 - 4S)$ as well as $\lambda^{Z/W} = 1 + \delta m_{e_4 e_1} \delta m_{e_3 e_2} / M_{Z/W}^2$.

Appendix C

Equivalence between method-1 and method-2

In this appendix we show by means of an example, that in the formula for the Sommerfeld enhancement factors in (8.34), written in terms of annihilation matrices and wave functions (resulting as solutions of matrix-valued Schrödinger equations with corresponding potential matrices) we can use either potential and annihilation matrices referring to the method-1 basis or the corresponding method-2 expressions; the outcome will be the same.

Instead of considering (8.34) it is more convenient for the following analysis to refer to the equivalent formula (8.35), where the T matrices encode the corresponding information on the wave functions. For the definition of the T matrix see Chap. 2.

Let us first recall from Sec. 7.2 that the method-1 two-particle basis treats as different the states $\chi_{e_a}\chi_{e_b}$ and $\chi_{e_b}\chi_{e_a}$ with non-identical species χ_{e_a} and χ_{e_b} . In method-2 however, the second, redundant state $\chi_{e_b}\chi_{e_a}$ – describing the same physical particle pair as the first state $\chi_{e_a}\chi_{e_b}$ – is left out. We can therefore already expect that the redundancy of certain states in the method-1 basis translates into the corresponding solutions of the Schrödinger equation and eventually the Sommerfeld enhancement factors, while in the method-2 calculation redundant solutions will be automatically absent.

We consider here the simple example of a system consisting of three method-1 basis states. The first state shall be composed out of identical particles. The second and third basis states involve two different individual particle species but are redundant with respect to the physical particle content. The corresponding method-2 basis thus contains only two states, the one with the two identical particles, and one of the two other redundant method-1 states. We can think of this system as the neutral two-particle sector of the pure-wino NRMSSM: the method-1 basis states then correspond to the three states $\chi_1^0\chi_1^0$, $\chi_1^+\chi_1^-$ and $\chi_1^-\chi_1^+$, while in method-2 we encounter the two neutral basis states $(\chi^0\chi^0)_{11} \equiv \chi_1^0\chi_1^0$ and $(\chi^+\chi^-)_{11} \equiv \chi_1^+\chi_1^-$, see Sec. 7.2.2. Referring to this situation we establish the generic notation $\chi_1\chi_1$, $\chi_2\chi_3$ and $\chi_3\chi_2$ for the three method-1 basis states, with the obvious correspondence between χ_1 and χ_1^0 as well as similarly between $\chi_{2,3}$ and χ_1^\pm . The method-2 basis then contains the states $(\chi\chi)_{11} = \chi_1\chi_1$ and

$(\chi\chi)_{23} = \chi_2\chi_3$.¹ For these basis states we discuss now in turn the determination of the corresponding Sommerfeld factors (8.35) in $\chi_1\chi_1$ and $\chi_2\chi_3$ pair-annihilation reactions relying on potential and annihilation matrices corresponding to method-1 and method-2.

The multi-component Schrödinger equation written with respect to the method-1 two-particle state basis in our example becomes a 3×3 matrix differential equation. The corresponding leading-order potential matrices for total spin $s = 0, 1$ generically read

$$V_s^{(1)}(r) = \begin{pmatrix} V_{11}^s & V_{12}^s & V_{12}^s \\ V_{21}^s & V_{22}^s & V_{23}^s \\ V_{21}^s & V_{23}^s & V_{22}^s \end{pmatrix}, \quad (\text{C.1})$$

where the first, second or third row (or column) refers to the $\chi_1\chi_1$, $\chi_2\chi_3$ or $\chi_3\chi_2$ state, respectively. For instance, the component V_{12}^s is given by the leading-order spin- s potential in $\chi_1\chi_1 \rightarrow \chi_2\chi_3$ scattering. It is worth to recall from Sec. 7.1 that a difference between the spin-0 and spin-1 potentials can only arise in case of non-vanishing axial-vector couplings. As in the pure-wino NRMSSM all axial-vector couplings vanish, we encountered the same potential matrix for both cases $s = 0, 1$ in that scenario, see Sec. 7.2.2. Here we will consider the generic case where $V_{s=0}^{(1)}(r)$ and $V_{s=1}^{(1)}(r)$ are not necessarily equal. In (C.1) we have used that the potential matrix entries V_{12}^s and V_{13}^s are the same. This is because the scattering reactions $\chi_1\chi_1 \rightarrow \chi_2\chi_3$ and $\chi_1\chi_1 \rightarrow \chi_3\chi_2$ give the same amplitudes: while the exchange of $\chi_2\chi_3$ by $\chi_3\chi_2$ corresponds to crossing the lines of the χ_2 and χ_3 in the corresponding diagram, the amplitudes remain the same due to the identical particle nature of the incoming $\chi_1\chi_1$ state. The same reasoning obviously applies to V_{21}^s and V_{31}^s . Further we have taken into account that $V_{32}^s = V_{23}^s$ as well as $V_{22}^s = V_{33}^s$, which follows from the fact that the amplitudes related to the corresponding reactions differ only by a relabelling of the respective internal vertices. Finally note that the hermiticity of the underlying MSSM Lagrangian, from which the potential interactions in the NRMSSM derive, implies the relation $V_{ab}^s = V_{ba}^{s*}$.

In order to determine the Sommerfeld factors we have to construct the matrices T in (8.35) involving certain basis solutions of the corresponding radial Schrödinger equation subject to a certain orbital angular momentum L and spin s . The radial Schrödinger equation in (2.23) can be written as

$$\left[D^{(L)} \mathbf{1} + V_s^{(1)}(r) \right] \vec{u}^{(L,s)}(r) = 0, \quad (\text{C.2})$$

¹The explicit composition of the two-particle basis states in terms of single particle constituents is to a certain extent arbitrary for our purposes here. The essential point is not the single particle content but the properties of the two-particle system. For instance, without reference to the neutral sector of the pure-wino NRMSSM we could have chosen as well the notation $\chi_1\chi_1$, $\chi_1\chi_2$, $\chi_2\chi_1$ for the three method-1 basis states. Accordingly, the method-2 basis states would then be denoted by $\chi_1\chi_1$ and $\chi_1\chi_2$. However, with the above convention for the composition of the two-particle basis states out of individual particles $\chi_{1,2,3}$, the contact to the neutral sector of the pure-wino NRMSSM discussed in Sec. 6.3 and Sec. 7.2.2 becomes most apparent.

where we have introduced the L -dependent differential operator

$$D^{(L)} = \frac{1}{m_{\text{LSP}}} \left[-\frac{d^2}{dr^2} + \frac{L(L+1)}{r^2} - m_{\text{LSP}} E \right]. \quad (\text{C.3})$$

The matrix T is related to the three linear independent regular solutions $\vec{u}^{(i)(L,S)}(r)$, $i = 1, 2, 3$, to (C.2), see Chap. 2 and in particular (2.42). To determine the regular solutions, the structure of the potential matrix (C.1) suggests to first transform to a block-diagonal Schrödinger equation with potential matrix $\tilde{V}_s^{(1)}(r)$ defined by

$$\tilde{V}_s^{(1)} = \mathcal{R} \cdot V_s^{(1)} \cdot \mathcal{R}^\dagger = \begin{pmatrix} V_{11}^s & \sqrt{2} V_{11}^s & 0 \\ \sqrt{2} V_{11}^s & V_{22} + V_{33} & 0 \\ 0 & 0 & V_{22} - V_{33} \end{pmatrix}. \quad (\text{C.4})$$

The constant, L - and s -independent 3×3 matrix \mathcal{R} is given by

$$\mathcal{R} = \begin{pmatrix} 1 & 0 & 0 \\ 0 & \frac{1}{\sqrt{2}} & \frac{1}{\sqrt{2}} \\ 0 & \frac{1}{\sqrt{2}} & -\frac{1}{\sqrt{2}} \end{pmatrix}, \quad (\text{C.5})$$

Note that $\mathcal{R} = \mathcal{R}^\dagger = \mathcal{R}^{-1}$. Let us denote the three linear independent regular solutions of the corresponding block-diagonal Schrödinger equation by $\vec{\tilde{u}}^{(i)(L,s)} = \mathcal{R} \cdot \vec{u}^{(i)(L,s)}$. In order to simplify the notation, we drop in the following the indices L and s on the wave functions. However, it has to be kept in mind that we generically obtain different regular solutions $\vec{u}^{(i=1,2,3)}(r)$ and $\vec{\tilde{u}}^{(i=1,2,3)}(r)$ for different pairs (L, s) . Further we promote to the matrix notation established in Chap. 2, where the regular solution vectors $\vec{\tilde{u}}^{(i)}$ or $\vec{u}^{(i)}$ of the corresponding Schrödinger equation appear in the columns of 3×3 matrices \tilde{u} and u . Due to the block-diagonal form of the Schrödinger equation for $\vec{\tilde{u}}$, the solution matrices obtain the generic form

$$\tilde{u} = \begin{pmatrix} \tilde{u}_{11} & \tilde{u}_{12} & 0 \\ \tilde{u}_{21} & \tilde{u}_{22} & 0 \\ 0 & 0 & \tilde{u}_{33} \end{pmatrix}, \quad u = \mathcal{R}^\dagger \cdot \tilde{u} = \begin{pmatrix} \tilde{u}_{11} & \tilde{u}_{12} & 0 \\ \frac{1}{\sqrt{2}} \tilde{u}_{21} & \frac{1}{\sqrt{2}} \tilde{u}_{22} & \frac{1}{\sqrt{2}} \tilde{u}_{33} \\ \frac{1}{\sqrt{2}} \tilde{u}_{21} & \frac{1}{\sqrt{2}} \tilde{u}_{22} & -\frac{1}{\sqrt{2}} \tilde{u}_{33} \end{pmatrix}. \quad (\text{C.6})$$

We can now use relation (2.42) to determine the matrix T from the product of matrices $u^{(L+1)}$ and M^{-1} . Without having to know the explicit form of the entries we infer from

(C.6), that the matrices $u^{(L+1)}$ and M^{-1} must have the generic structure

$$[u_L^{(L+1)}(0)] = \begin{pmatrix} \tilde{U}_{11} & \tilde{U}_{12} & 0 \\ \frac{\tilde{U}_{21}}{\sqrt{2}} & \frac{\tilde{U}_{22}}{\sqrt{2}} & \frac{\tilde{U}_{33}}{\sqrt{2}} \\ \frac{\tilde{U}_{21}}{\sqrt{2}} & \frac{\tilde{U}_{22}}{\sqrt{2}} & -\frac{\tilde{U}_{33}}{\sqrt{2}} \end{pmatrix}, \quad M = \begin{pmatrix} M_{11} & M_{12} & 0 \\ \frac{M_{21}}{\sqrt{2}} & \frac{M_{22}}{\sqrt{2}} & \frac{M_{33}}{\sqrt{2}} \\ \frac{M_{21}}{\sqrt{2}} & \frac{M_{22}}{\sqrt{2}} & -\frac{M_{33}}{\sqrt{2}} \end{pmatrix}. \quad (\text{C.7})$$

Similarly this also applies to the generic structure of matrices $\tilde{u}^{(L+1)}$ and \tilde{M} that follows from \tilde{u} in (C.6). Note that we use capital letters to denote the $(L+1)$ -th derivatives of the respective components of matrices \tilde{u} and u . The final ingredient for the determination of the Sommerfeld factors is the corresponding method-1 annihilation matrix, which depends on the (L, s) quantum numbers and has the generic form

$$\Gamma^{(1)}[{}^{2s+1}L_J] = \begin{pmatrix} \frac{1+(-1)^{s+L}}{2} \Gamma_{11} & \frac{1+(-1)^{s+L}}{2} \Gamma_{12} & \frac{1+(-1)^{s+L}}{2} \Gamma_{12} \\ \frac{1+(-1)^{s+L}}{2} \Gamma_{21} & \Gamma_{22} & (-1)^{s+L} \Gamma_{22} \\ \frac{1+(-1)^{s+L}}{2} \Gamma_{21} & (-1)^{s+L} \Gamma_{22} & \Gamma_{22} \end{pmatrix}, \quad (\text{C.8})$$

as can be verified using the symmetry properties (5.9, 5.14) of the underlying Wilson coefficients. Further recall that $\Gamma_{ab} = \Gamma_{ba}^*$. For later convenience it is worth to note that the transformed annihilation matrices $\tilde{\Gamma}^{(1)} = \mathcal{R} \cdot \Gamma^{(1)} \cdot \mathcal{R}^\dagger$ have the following generic form, distinguishing the cases where $L + s$ is even or odd,

$$\tilde{\Gamma}_{\text{even}}^{(1)}[{}^{2s+1}L_J] = \begin{pmatrix} \Gamma_{11} & \sqrt{2} \Gamma_{12} & 0 \\ \sqrt{2} \Gamma_{21} & 2 \Gamma_{22} & 0 \\ 0 & 0 & 0 \end{pmatrix}, \quad \tilde{\Gamma}_{\text{odd}}^{(1)}[{}^{2s+1}L_J] = \begin{pmatrix} 0 & 0 & 0 \\ 0 & 0 & 0 \\ 0 & 0 & 2 \Gamma_{22} \end{pmatrix}. \quad (\text{C.9})$$

In (C.8, C.9) we suppress the labels L and s on the matrix entries $\Gamma_{ab} = \Gamma_{ab}({}^{2s+1}L_J)$. To avoid confusion let us therefore note that although the expression Γ_{22} appears in both matrices in (C.9) it does not denote the same term. In the first case the Γ_{22} refers to the $(2, 2)$ entry in a corresponding matrix $\Gamma^{(1)}({}^{2s+1}L_J)$ where $L + s$ is even. In the second case the entry Γ_{22} is associated with a matrix $\Gamma^{(1)}({}^{2s+1}L_J)$ with odd $L + s$.

It is now easy to obtain the Sommerfeld factors from (8.35). Up to a global prefactor given by $[(2L+1)!/((L+1)!k_a^{(L+1)})]^2$, the enhancement factors in annihilation reactions of the basis states $a = 1$ ($\chi_1\chi_1$) and $a = 2$ ($\chi_2\chi_3$) subject to a ${}^{2s+1}L_J$ partial-wave reaction with $L + s = \text{even}$ are given by

$$S_1^{\text{even}} = \left| \frac{M_{22} \tilde{U}_{11} - M_{21} \tilde{U}_{12}}{M_{12} M_{21} - M_{11} M_{22}} \right|^2 + 2 \left| \frac{M_{22} \tilde{U}_{21} - M_{21} \tilde{U}_{22}}{M_{12} M_{21} - M_{11} M_{22}} \right|^2 \frac{\Gamma_{22}}{\Gamma_{11}}$$

$$\begin{aligned}
& + 2\sqrt{2} \operatorname{Re} \left[\frac{(M_{22} \tilde{U}_{21} - M_{21} \tilde{U}_{22})(M_{22} \tilde{U}_{11} - M_{21} \tilde{U}_{12})^* \Gamma_{12}}{|M_{12} M_{21} - M_{11} M_{22}|^2} \frac{\Gamma_{12}}{\Gamma_{11}} \right], \\
S_2^{\text{even}} &= \left| \frac{M_{12} \tilde{U}_{21} - M_{11} \tilde{U}_{22}}{M_{12} M_{21} - M_{11} M_{22}} \right|^2 + \frac{1}{2} \left| \frac{M_{12} \tilde{U}_{11} - M_{11} \tilde{U}_{12}}{M_{12} M_{21} - M_{11} M_{22}} \right|^2 \frac{\Gamma_{11}}{\Gamma_{22}} \\
& + \sqrt{2} \operatorname{Re} \left[\frac{(M_{12} \tilde{U}_{21} - M_{11} \tilde{U}_{22})(M_{12} \tilde{U}_{11} - M_{11} \tilde{U}_{12})^* \Gamma_{12}}{|M_{12} M_{21} - M_{11} M_{22}|^2} \frac{\Gamma_{12}}{\Gamma_{22}} \right], \tag{C.10}
\end{aligned}$$

whereas for annihilation reactions of $^{2s+1}L_J$ states where $L + s$ is odd we obtain

$$\begin{aligned}
S_1^{\text{odd}} &= 0, \\
S_2^{\text{odd}} &= \left| \frac{\tilde{U}_{33}}{M_{33}} \right|^2. \tag{C.11}
\end{aligned}$$

The enhancement factors for the third method-1 basis state $\chi_3\chi_2$ agree with the corresponding expressions for the second state, $\chi_2\chi_3$; this should be the case since both states are physically equivalent. We observe that the enhancement factors for even $L + s$ do not depend on the matrix entries \tilde{U}_{33} and M_{33} : only those wave function solutions that are associated with the upper 2×2 matrix in the block-diagonal Schrödinger equation with potential (C.4) determine the enhancement factors in (C.10). To the contrary, the non-vanishing enhancement factor for odd $L + s$ in (C.11) depends only on the wave-function associated with the 1×1 block in the block-diagonal Schrödinger equation. The factor S_1^{odd} vanishes as two-particle configurations with $L + s = \text{odd}$ are totally symmetric while a state of two identical particles such as $\chi_1\chi_1$ has to be totally antisymmetric.

Let us now turn to method-2 and construct the corresponding potential and annihilation matrices. For the former we obtain, using the rules set out in Sec. 7.2.1 and thus distinguishing even and odd $L + s$,

$$V_{s,\text{even}}^{(2)}(r) = \begin{pmatrix} V_{11}^s & \sqrt{2} V_{12}^s \\ \sqrt{2} V_{21}^s & V_{22}^s + V_{23}^s \end{pmatrix}, \quad V_{s,\text{odd}}^{(2)}(r) = \begin{pmatrix} 0 & 0 \\ 0 & V_{22}^s - V_{23}^s \end{pmatrix}. \tag{C.12}$$

In case of the annihilation matrices we have

$$\Gamma_{\text{even}}^{(2)} [^{2s+1}L_J] = \begin{pmatrix} \frac{1}{2} \Gamma_{11} & \frac{1}{\sqrt{2}} \Gamma_{12} \\ \frac{1}{\sqrt{2}} \Gamma_{21} & \Gamma_{22} \end{pmatrix}, \quad \Gamma_{\text{odd}}^{(2)} [^{2s+1}L_J] = \begin{pmatrix} 0 & 0 \\ 0 & \Gamma_{22} \end{pmatrix}. \tag{C.13}$$

For given orbital angular momentum L and spin s with $L + s$ even, the potential matrix $V_s^{(2)}$ agrees with the upper 2×2 block in the corresponding $\tilde{V}_s^{(1)}$ in (C.4). Similarly the annihilation matrices $\Gamma_{\text{even}}^{(2)}$ correspond, up to a global factor of 2, to the upper 2×2 block of $\tilde{\Gamma}_{\text{even}}^{(1)}$ in (C.9). From (C.6) we therefore obtain immediately the generic form of

the method-2 matrices $[u_L^{(L+1)}(0)]$ and M for even $L + s$:

$$[u_L^{(L+1)}(0)]_{\text{even}} = \begin{pmatrix} \tilde{U}_{11} & \tilde{U}_{12} \\ \tilde{U}_{21} & \tilde{U}_{22} \end{pmatrix}, \quad M_{\text{even}} = \begin{pmatrix} M_{11} & M_{12} \\ M_{21} & M_{22} \end{pmatrix}. \quad (\text{C.14})$$

The functions that appear for given L and s in the components of the matrices in (C.14) are the same as the \tilde{U}_{ab} and M_{ab} functions with $a, b = 1, 2$ in the corresponding method-1 matrices in (C.7).

In order to obtain the method-2 matrices $[u_L^{(L+1)}(0)]$ and M for the case of odd $L + s$ we can use the correspondence of method-2 potential and annihilation matrix entries to the associated method-1 expressions as well. Here we find that for given (L, s) the non-vanishing entry in the potential matrix $V_{s, \text{odd}}^{(2)}$ in (C.12) agrees with the lower 1×1 block of the corresponding matrix $\tilde{V}_s^{(1)}$ in (C.4). Likewise, the non-vanishing entry in the annihilation matrix $\Gamma_{\text{odd}}^{(2)}$ in (C.13) agrees up to a factor of 2 with the entry in the lower 1×1 block of the associated block-diagonal $\tilde{\Gamma}_{\text{odd}}^{(1)}$ in (C.9). For given (L, s) with odd $L + s$ we thus obtain the generic form of the matrices $[u_L^{(L+1)}(0)]$ and M

$$[u_L^{(L+1)}(0)]_{\text{odd}} = \begin{pmatrix} 0 & 0 \\ 0 & \tilde{U}_{33} \end{pmatrix}, \quad M_{\text{odd}} = \begin{pmatrix} 0 & 0 \\ 0 & M_{33} \end{pmatrix}, \quad (\text{C.15})$$

where the function \tilde{U}_{33} is the $(L + 1)$ -th derivative of the function \tilde{u}_{33} , which appears in the lower 1×1 block of the corresponding block-diagonal method-1 matrix \tilde{u} in (C.6), and M_{33} is derived from this function \tilde{u}_{33} as well.

It is now straightforward to determine for given (L, s) the Sommerfeld enhancement factors related to pair-annihilation reactions of the first ($a = 1, (\chi\chi)_{11}$) and second ($a = 2, (\chi\chi)_{23}$) method-2 basis state. The results agree with the respective expressions for the Sommerfeld factors in (C.10) and (C.11), which were derived using method-1.

Bibliography

- [1] **Particle Data Group** Collaboration, K. Olive *et al.*, *Chin.Phys.* **C38** (2014) 090001.
- [2] **Planck Collaboration** Collaboration, P. Ade *et al.*, arXiv:1303.5076 [astro-ph.CO].
- [3] G. Jungman, M. Kamionkowski, and K. Griest, *Phys.Rept.* **267** (1996) 195–373, arXiv:hep-ph/9506380 [hep-ph].
- [4] G. Bertone, D. Hooper, and J. Silk, *Phys.Rept.* **405** (2005) 279–390, arXiv:hep-ph/0404175 [hep-ph].
- [5] P. Gondolo, J. Edsjo, P. Ullio, L. Bergstrom, M. Schelke, *et al.*, *JCAP* **0407** (2004) 008, arXiv:astro-ph/0406204 [astro-ph].
- [6] G. Belanger, F. Boudjema, P. Brun, A. Pukhov, S. Rosier-Lees, *et al.*, *Comput.Phys.Commun.* **182** (2011) 842–856, arXiv:1004.1092 [hep-ph].
- [7] J. Ellis, *Nucl.Phys.* **A827** (2009) 187C–198C, arXiv:0902.0357 [hep-ph].
- [8] D. Hooper, arXiv:0901.4090 [hep-ph].
- [9] M. Cahill-Rowley, R. Cotta, A. Drlica-Wagner, S. Funk, J. Hewett, *et al.*, arXiv:1305.6921 [hep-ph].
- [10] M. Cahill-Rowley, R. Cotta, A. Drlica-Wagner, S. Funk, J. Hewett, *et al.*, arXiv:1405.6716 [hep-ph].
- [11] B. Herrmann and M. Klasen, *Phys.Rev.* **D76** (2007) 117704, arXiv:0709.0043 [hep-ph].
- [12] B. Herrmann, M. Klasen, and K. Kovarik, *Phys.Rev.* **D79** (2009) 061701, arXiv:0901.0481 [hep-ph].
- [13] B. Herrmann, M. Klasen, and K. Kovarik, *Phys.Rev.* **D80** (2009) 085025, arXiv:0907.0030 [hep-ph].

- [14] J. Harz, B. Herrmann, M. Klasen, K. Kovarik, and Q. L. Boulc'h, *Phys.Rev.* **D87** (2013) no. 5, 054031, [arXiv:1212.5241](#).
- [15] B. Herrmann, M. Klasen, K. Kovarik, M. Meinecke, and P. Steppeler, *Phys.Rev.* **D89** (2014) 114012, [arXiv:1404.2931](#) [hep-ph].
- [16] N. Baro, F. Boudjema, and A. Semenov, *Phys.Lett.* **B660** (2008) 550–560, [arXiv:0710.1821](#) [hep-ph].
- [17] N. Baro, F. Boudjema, and A. Semenov, *Phys.Rev.* **D78** (2008) 115003, [arXiv:0807.4668](#) [hep-ph].
- [18] N. Baro, F. Boudjema, G. Chalons, and S. Hao, *Phys.Rev.* **D81** (2010) 015005, [arXiv:0910.3293](#) [hep-ph].
- [19] J. Hisano, S. Matsumoto, M. M. Nojiri, and O. Saito, *Phys.Rev.* **D71** (2005) 063528, [arXiv:hep-ph/0412403](#) [hep-ph].
- [20] J. Hisano, S. Matsumoto, M. Nagai, O. Saito, and M. Senami, *Phys.Lett.* **B646** (2007) 34–38, [arXiv:hep-ph/0610249](#) [hep-ph].
- [21] M. Drees, J. Kim, and K. Nagao, *Phys.Rev.* **D81** (2010) 105004, [arXiv:0911.3795](#) [hep-ph].
- [22] A. Hryczuk, R. Iengo, and P. Ullio, *JHEP* **1103** (2011) 069, [arXiv:1010.2172](#) [hep-ph].
- [23] A. Hryczuk, *Phys.Lett.* **B699** (2011) 271–275, [arXiv:1102.4295](#) [hep-ph].
- [24] A. Hryczuk and R. Iengo, *JHEP* **1201** (2012) 163, [arXiv:1111.2916](#) [hep-ph].
- [25] J. Fan and M. Reece, *JHEP* **1310** (2013) 124, [arXiv:1307.4400](#) [hep-ph].
- [26] T. Cohen, M. Lisanti, A. Pierce, and T. R. Slatyer, *JCAP* **1310** (2013) 061, [arXiv:1307.4082](#).
- [27] A. Hryczuk, I. Cholis, R. Iengo, M. Tavakoli, and P. Ullio, *JCAP* **1407** (2014) 031, [arXiv:1401.6212](#) [astro-ph.HE].
- [28] M. Cirelli, A. Strumia, and M. Tamburini, *Nucl.Phys.* **B787** (2007) 152–175, [arXiv:0706.4071](#) [hep-ph].
- [29] N. Arkani-Hamed, D. P. Finkbeiner, T. R. Slatyer, and N. Weiner, *Phys.Rev.* **D79** (2009) 015014, [arXiv:0810.0713](#) [hep-ph].
- [30] G. T. Bodwin, E. Braaten, and G. P. Lepage, *Phys.Rev.* **D51** (1995) 1125–1171, [arXiv:hep-ph/9407339](#) [hep-ph].

- [31] M. Beneke, C. Hellmann, and P. Ruiz-Femenia, *JHEP* **1303** (2013) 148, [arXiv:1210.7928 \[hep-ph\]](#).
- [32] C. Hellmann and P. Ruiz-Femenia, *JHEP* **1308** (2013) 084, [arXiv:1303.0200 \[hep-ph\]](#).
- [33] M. Beneke, C. Hellmann, and P. Ruiz-Femenia, [arXiv:1411.6924 \[hep-ph\]](#).
- [34] M. Beneke, C. Hellmann, and P. Ruiz-Femenia, [arXiv:1411.6930 \[hep-ph\]](#).
- [35] M. Beneke and V. A. Smirnov, *Nucl.Phys.* **B522** (1998) 321–344, [arXiv:hep-ph/9711391 \[hep-ph\]](#).
- [36] T. R. Slatyer, *JCAP* **1002** (2010) 028, [arXiv:0910.5713 \[hep-ph\]](#).
- [37] R. Iengo, *JHEP* **0905** (2009) 024, [arXiv:0902.0688 \[hep-ph\]](#).
- [38] S. Cassel, *J.Phys.* **G37** (2010) 105009, [arXiv:0903.5307 \[hep-ph\]](#).
- [39] S. Hannestad and T. Tram, *JCAP* **1101** (2011) 016, [arXiv:1008.1511 \[astro-ph.CO\]](#).
- [40] J. L. Feng, M. Kaplinghat, and H.-B. Yu, *Phys.Rev.* **D82** (2010) 083525, [arXiv:1005.4678 \[hep-ph\]](#).
- [41] F. Brau and F. Buisseret, *Phys.Rev.* **C76** (2007) 065212, [arXiv:0706.4012 \[hep-ph\]](#).
- [42] K. L. McDonald, *JHEP* **1207** (2012) 145, [arXiv:1203.6341 \[hep-ph\]](#).
- [43] Z. Zhang, [arXiv:1307.2206 \[hep-ph\]](#).
- [44] B. W. Lee and S. Weinberg, *Phys.Rev.Lett.* **39** (1977) 165–168.
- [45] J. Bernstein, L. S. Brown, and G. Feinberg, *Phys.Rev.* **D32** (1985) 3261.
- [46] R. J. Scherrer and M. S. Turner, *Phys.Rev.* **D33** (1986) 1585.
- [47] M. Srednicki, R. Watkins, and K. A. Olive, *Nucl.Phys.* **B310** (1988) 693.
- [48] K. Griest and D. Seckel, *Phys.Rev.* **D43** (1991) 3191–3203.
- [49] P. Gondolo and G. Gelmini, *Nucl.Phys.* **B360** (1991) 145–179.
- [50] E. W. Kolb and M. S. Turner, *Front.Phys.* **69** (1990) 1–547.
- [51] T. Bringmann and S. Hofmann, *JCAP* **0407** (2007) 016, [arXiv:hep-ph/0612238 \[hep-ph\]](#).

- [52] J. B. Dent, S. Dutta, and R. J. Scherrer, *Phys.Lett.* **B687** (2010) 275–279, [arXiv:0909.4128 \[astro-ph.CO\]](#).
- [53] J. Edsjo and P. Gondolo, *Phys.Rev.* **D56** (1997) 1879–1894, [arXiv:hep-ph/9704361 \[hep-ph\]](#).
- [54] M. Hindmarsh and O. Philipsen, *Phys.Rev.* **D71** (2005) 087302, [arXiv:hep-ph/0501232 \[hep-ph\]](#).
- [55] H. Georgi and S. Glashow, *Phys.Rev.Lett.* **32** (1974) 438–441.
- [56] H. E. Haber and G. L. Kane, *Phys.Rept.* **117** (1985) 75–263.
- [57] S. P. Martin, *Adv.Ser.Direct.High Energy Phys.* **21** (2010) 1–153, [arXiv:hep-ph/9709356 \[hep-ph\]](#).
- [58] M. Drees, R. Godbole, and P. Roy.
- [59] I. J. Aitchison, [arXiv:hep-ph/0505105 \[hep-ph\]](#).
- [60] D. Z. Freedman and A. Van Proeyen.
- [61] J. Gunion and H. E. Haber, *Nucl.Phys.* **B272** (1986) 1.
- [62] J. Rosiek, *Phys.Rev.* **D41** (1990) 3464, [arXiv:hep-ph/9511250 \[hep-ph\]](#).
Erratum: *ibid.* vol. 387, p. 830 (1997).
- [63] G. R. Farrar and P. Fayet, *Phys.Lett.* **B76** (1978) 575–579.
- [64] M. Dine and A. E. Nelson, *Phys.Rev.* **D48** (1993) 1277–1287, [arXiv:hep-ph/9303230 \[hep-ph\]](#).
- [65] M. Dine, A. E. Nelson, and Y. Shirman, *Phys.Rev.* **D51** (1995) 1362–1370, [arXiv:hep-ph/9408384 \[hep-ph\]](#).
- [66] M. Dine, A. E. Nelson, Y. Nir, and Y. Shirman, *Phys.Rev.* **D53** (1996) 2658–2669, [arXiv:hep-ph/9507378 \[hep-ph\]](#).
- [67] G. Giudice and R. Rattazzi, *Phys.Rept.* **322** (1999) 419–499, [arXiv:hep-ph/9801271 \[hep-ph\]](#).
- [68] L. Randall and R. Sundrum, *Nucl.Phys.* **B557** (1999) 79–118, [arXiv:hep-th/9810155 \[hep-th\]](#).
- [69] L. Girardello and M. T. Grisaru, *Nucl.Phys.* **B194** (1982) 65.
- [70] R. Barbieri, S. Ferrara, and C. A. Savoy, *Phys.Lett.* **B119** (1982) 343.
- [71] A. H. Chamseddine, R. L. Arnowitt, and P. Nath, *Phys.Rev.Lett.* **49** (1982) 970.

- [72] S. Choi, M. Guchait, J. Kalinowski, and P. Zerwas, *Phys.Lett.* **B479** (2000) 235–244, [arXiv:hep-ph/0001175](#) [hep-ph].
- [73] S. Choi, J. Kalinowski, G. A. Moortgat-Pick, and P. Zerwas, *Eur.Phys.J.* **C22** (2001) 563–579, [arXiv:hep-ph/0108117](#) [hep-ph].
- [74] J. F. Gunion and H. E. Haber, *Phys.Rev.* **D37** (1988) 2515.
- [75] H.-C. Cheng, B. A. Dobrescu, and K. T. Matchev, *Nucl.Phys.* **B543** (1999) 47–72, [arXiv:hep-ph/9811316](#) [hep-ph].
- [76] D. Pierce and A. Papadopoulos, *Phys.Rev.* **D50** (1994) 565–570, [arXiv:hep-ph/9312248](#) [hep-ph].
- [77] D. Pierce and A. Papadopoulos, *Nucl.Phys.* **B430** (1994) 278–294, [arXiv:hep-ph/9403240](#) [hep-ph].
- [78] G. F. Giudice and A. Pomarol, *Phys.Lett.* **B372** (1996) 253–258, [arXiv:hep-ph/9512337](#) [hep-ph].
- [79] A. Lahanas, K. Tamvakis, and N. Tracas, *Phys.Lett.* **B324** (1994) 387–396, [arXiv:hep-ph/9312251](#) [hep-ph].
- [80] D. M. Pierce, J. A. Bagger, K. T. Matchev, and R.-j. Zhang, *Nucl.Phys.* **B491** (1997) 3–67, [arXiv:hep-ph/9606211](#) [hep-ph].
- [81] A. Chatterjee, M. Drees, S. Kulkarni, and Q. Xu, *Phys.Rev.* **D85** (2012) 075013, [arXiv:1107.5218](#) [hep-ph].
- [82] S. Heinemeyer, F. von der Pahlen, and C. Schappacher, *Eur.Phys.J.* **C72** (2012) 1892, [arXiv:1112.0760](#) [hep-ph].
- [83] A. Bharucha, S. Heinemeyer, F. von der Pahlen, and C. Schappacher, *Phys.Rev.* **D86** (2012) 075023, [arXiv:1208.4106](#) [hep-ph].
- [84] A. Bharucha, A. Fowler, G. Moortgat-Pick, and G. Weiglein, *JHEP* **1305** (2013) 053, [arXiv:1211.3134](#) [hep-ph].
- [85] T. Fritzsche, T. Hahn, S. Heinemeyer, H. Rzehak, and C. Schappacher, [arXiv:1309.1692](#) [hep-ph].
- [86] A. Djouadi, J.-L. Kneur, and G. Moultaka, *Comput.Phys.Commun.* **176** (2007) 426–455, [arXiv:hep-ph/0211331](#) [hep-ph].
- [87] B. Allanach and M. Bernhardt, *Comput.Phys.Commun.* **181** (2010) 232–245, [arXiv:0903.1805](#) [hep-ph].
- [88] W. Porod and F. Staub, *Comput.Phys.Commun.* **183** (2012) 2458–2469, [arXiv:1104.1573](#) [hep-ph].

- [89] J. Alwall, M. Herquet, F. Maltoni, O. Mattelaer, and T. Stelzer, *JHEP* **1106** (2011) 128, [arXiv:1106.0522 \[hep-ph\]](#).
- [90] R. Cutkosky, *J.Math.Phys.* **1** (1960) 429–433.
- [91] G. 't Hooft and M. Veltman, *NATO Sci.Ser.B* **4** (1974) 177–322.
- [92] A. Denner, H. Eck, O. Hahn, and J. Kublbeck, *Nucl.Phys.* **B387** (1992) 467–484.
- [93] M. Drees and J. Gu, *Phys.Rev.* **D87** (2013) no. 6, 063524, [arXiv:1301.1350 \[hep-ph\]](#).
- [94] J. Chen and Y.-F. Zhou, *JCAP* **1304** (2013) 017, [arXiv:1301.5778 \[hep-ph\]](#).
- [95] J. F. Gunion and H. E. Haber, *Phys.Rev.* **D67** (2003) 075019, [arXiv:hep-ph/0207010 \[hep-ph\]](#).
- [96] M. Drees and M. M. Nojiri, *Phys.Rev.* **D47** (1993) 376–408, [arXiv:hep-ph/9207234 \[hep-ph\]](#).
- [97] S. Ershov, J. Vaagen, and M. Zhukov, *Phys.Rev.* **C84** (2011) 064308.
- [98] M. W. Cahill-Rowley, J. L. Hewett, A. Ismail, M. E. Peskin, and T. G. Rizzo, [arXiv:1305.2419 \[hep-ph\]](#).
<http://www.slac.stanford.edu/~aismail/snowmass/index.html>.

Acknowledgements

I am grateful to my advisor Martin Beneke for his supervision in the last years and the many valuable and encouraging discussions. Further, I would like to thank Martin Beneke and Pedro Ruiz-Femenia for the fruitful collaboration on the dark matter project. In addition, I want to thank Pedro Ruiz-Femenia for careful reading of the manuscript of this thesis and many helpful comments.

I thank Jan Piclum for his comments on parts of the manuscript as well as for a lot of useful discussions. Furthermore I would like to thank the members of the Theoretical Particle Physics Department T31 at the Technische Universität München for the encouraging and pleasant working atmosphere.

Finally, I am particularly grateful to the Deutsche Telekom Stiftung and to the Studienstiftung des deutschen Volkes for their generous ideationally and financial support.

Annihilation matrices in pair annihilations of non-relativistic neutralinos and charginos: documentation of the numerical program

Charlotte Hellmann

26.02.2015

Abstract

We provide a documentation of the numerical code that determines the partial-wave separated annihilation matrix expressions in non-relativistic neutralino and chargino pair-annihilation reactions in the general MSSM.

Contents

1	Introduction	2
2	Generic structure of the code	3
3	Part 1: Building the partial wave coefficients	6
3.1	Kinematic factors	6
3.1.1	Selfenergy topologies	7
3.1.2	Triangle topologies	9
3.1.3	Box topologies	10
3.2	Coupling factors	11
3.2.1	Selfenergy diagrams	11
3.2.2	Triangle diagrams	14
3.2.3	Box diagrams	15
3.3	Partial wave coefficients: generic routine	15
3.3.1	The function <code>PartialWaveCoefficient[...]</code>	16
3.3.2	Auxiliary functions in <code>partialwavecoefficients.m</code>	18
3.4	Partial wave coefficients: physical reactions	19
3.4.1	Listing internally exchanged states	19
3.4.2	The function <code>pwc[...]</code> related to the physical exclusive process	22
4	Part 2: Building the annihilation matrices	23
4.1	Enumeration convention for $\chi\chi$ states	24
4.2	The choice of the mass expansion	25
4.3	Inclusive reactions: the final partial wave coefficients	26
4.4	Symmetry factors and symmetry relations	28
4.5	Chopping numerically small annihilation matrix entries	29
4.6	Calculation of the annihilation matrices	29
5	Comparison to the publications' nomenclature	32
5.1	Kinematic and coupling factors	32
5.2	Annihilation matrices	33

1 Introduction

We provide a documentation of the numerical code that allows to calculate the annihilation matrices in pair-annihilation reactions of non-relativistic neutralino and chargino pairs including $\mathcal{O}(v_{\text{rel}}^2)$ effects in the non-relativistic expansion and at leading order in the expansion in the couplings. The annihilation matrices are built from the absorptive parts of Wilson coefficients of four-fermion operators. The latter encode the hard annihilation reactions of non-relativistic neutralinos and charginos in the NRMSSM, an effective field theory designed to determine the enhanced radiative corrections in neutralino/chargino co-annihilation processes.

The construction of the NRMSSM is described in detail in [1–4] as well as in the preceding thesis. The first two publications [1,2]¹ cover the determination of the Wilson coefficients encoding the hard annihilation reactions, while the third focuses on the technical aspects in the calculation of the Sommerfeld enhancements. In [4] a dedicated discussion of several MSSM benchmark scenarios in view of the impact of Sommerfeld enhancements in the χ_1^0 relic abundance is given. For the underlying physics and technical aspects of the calculation we refer the reader to [1–3]. This documentation deals exclusively with the numerical code that determines the annihilation matrices.

The outline of this documentation is as follows. Sec. 2 contains a general overview on the structure of the code, which can be divided into two main parts with respective extensive substructure. Part 1 of the code refers to elementary functions and building blocks related to the construction of the partial wave separated Wilson coefficients. Consequently, part 2 deals with the construction of annihilation matrices, thereby relying on functions that are the subject-matter of part 1.

The first part of the code is described in detail in Sec. 3. Starting with the basic building blocks, Sec. 3.1 and Sec. 3.2 cover the hard-coded kinematic and coupling factors. The generic functions that allow to determine a specific exclusive final state contribution to the absorptive part of a Wilson coefficient from the kinematic and coupling factors are then described in Sec. 3.3. In Sec. 3.4 a description of necessary hard-coded information is given that allows to determine partial wave coefficient contributions related to scattering reactions with exclusive physical final states.

The second part of the code is the subject-matter of Sec. 4 and deals with the functions determining the annihilation matrices, which are related to non-relativistic neutralino and chargino pair-annihilation reactions. Sec. 4.1 introduces the enumeration convention for the neutralino and chargino pairs ($\chi\chi$ pairs) that we have chosen in both the numerical "annihilation matrix" and "Sommerfeld enhancement" programs.² The enumeration convention for the $\chi\chi$ pairs fixes the position (row and column) where the contributions from a specific $\chi\chi$ annihilation reaction appear in the annihilation matrices. The question which version of the hard-coded kinematic factors should be chosen for

¹All conventions and definitions in [1,2] and the thesis agree, such that regarding the contents of [1,2] the reader may refer to Chaps. 5 and 6 of the thesis as well.

²This documentation deals exclusively with the piece of the code determining the short-distance annihilation matrices, that is the "annihilation matrix" program.

a specific annihilation reaction as regards the expansion in mass differences is addressed in Sec. 4.2. Subsequently, in Sec. 4.3, we introduce the functions that determine the absorptive parts of the proper Wilson coefficients, referring to the inclusive annihilation reactions. The issue of symmetry factors and relations among certain Wilson coefficient functions defined in the code is the content of Sec. 4.4. The following Sec. 4.5 introduces a convenient function that allows to sets to zero annihilation matrix entries that are very small compared to the leading annihilation matrix entries. The functions that determine the final annihilation matrix expressions are described in Sec. 4.6.

For the sake of clarity, those expressions are summarised in Sec. 5, whose definition or nomenclature in the numerical program is slightly different with respect to the definition or naming established in [1–4].

2 Generic structure of the code

The numeric code is designed to calculate all diagonal and off-diagonal hard annihilation rates in co-annihilation reactions of non-relativistic and nearly mass-degenerate neutralino and chargino pairs including $\mathcal{O}(v_{\text{rel}}^2)$ corrections in the non-relativistic expansion. While in the current version of the code the final expressions for the annihilation matrices refer to the respective inclusive annihilation rates, all contributing exclusive rates are determined in intermediate steps.³ By appropriate and easily implementable modifications in the current version of the code it is therefore possible to obtain annihilation matrices referring to exclusive final states.

The code relies on the explicit calculation of the absorptive parts of the (partial-wave separated) Wilson coefficients of four fermion operators in the NRMSSM at leading order, $\mathcal{O}(\alpha_2^2)$, in the expansion in the couplings. We use $\alpha_2 = g_2^2/4\pi$ where g_2 denotes the $SU(2)_L$ gauge coupling. For the explicit form of the four-fermion operators we refer the reader to [1, 2] or to the thesis. According to the latter references, the Wilson coefficients corresponding to the four-fermion operators can be written in terms of a sum over products of kinematic and coupling factors. Schematically, the absorptive part of a Wilson coefficient \hat{f} can therefore be obtained from a suitable set of kinematic and coupling factors as

$$\hat{f} = \sum \text{coupling factor} \times \text{kinematic factor} . \quad (1)$$

The definition of the four-fermion operators and their Wilson coefficients as given in [1, 2] and the thesis and as underlying the numerical code described herein is the same. Therefore the expression for a Wilson coefficient can be unambiguously obtained either following the prescriptions given in [1, 2] or from the code described hereafter. However, the definition of the kinematic and the coupling factors is *not* identical in [1, 2] and the numerical code. For instance, in the convention of [1, 2] a sign can be associated with a

³Let us note that the calculated hard annihilation rates refer to the annihilation reactions at tree-level, such that exclusive rates are infrared safe and can be given separately.

specific kinematic factor appearing in the sum (1). In the conventions of the numerical code, the sign can be absent in front of the kinematic factor but will then be attributed to the corresponding coupling factor. As a consequence, the expression for the Wilson coefficient stays always the same. Such difference between kinematic and coupling factor expressions in [1, 2] and the numerical code originates from the fact that the reference processes used in the determination of the kinematic and coupling factors for [1, 2] and in the code are different. The reader should be aware of this difference, implying that intermediate results obtained from expressions in [1, 2] or from the numerical code cannot be used interchangeably. The end result, which is the Wilson coefficient, is unambiguous, also in case of exclusive final state reactions.

Once more, to make the above explicit, note the following: [1, 2] and the thesis contain explicit analytic results for the kinematic factors associated with leading order 1S_0 - and 3S_1 -wave Wilson coefficients as well as analytic results for the kinematic factors related to 1P_1 and 3P_J partial-wave annihilations. The 3P_J -wave Wilson coefficients are a suitable linear combination of the respective three corresponding P -wave coefficients associated with spin $S = 1$, see [2] or eq. (6.29) in the thesis. The code uses an equivalent set of kinematic factors calculated in the same way as the corresponding expressions in [1, 2] and the thesis. However, the kinematic factors given in [1, 2] and Appendix A of the thesis are not identical to the kinematic factors used in the code. In both cases we used a certain reference process $\chi_{e_1}\chi_{e_2} \rightarrow X_A X_B \rightarrow \chi_{e_4}\chi_{e_3}$ to determine the kinematic and coupling factors that built the Wilson coefficients. For instance, in case of final states $X_A X_B$ built from two gauge bosons, the kinematic factors used in the code rely on the reference process $\chi_{e_1}^0\chi_{e_2}^0 \rightarrow W^+W^- \rightarrow \chi_{e_4}^0\chi_{e_3}^0$. To the contrary, we used the reference process $\chi_{e_1}\chi_{e_2} \rightarrow VV \rightarrow \chi_{e_4}\chi_{e_3}$, where χ_{e_i} denote generic Majorana fermions and V a generic gauge boson in the calculation referring to [1, 2]. Similar small differences exist for the other processes. Results on the kinematic and coupling factors can therefore not be used interchangeably in the code and the publications. Each calculation is however self-consistent and the final results on the Wilson coefficients encoding physical rates are identical. A list of reference processes underlying the results for the kinematic and coupling factors used in the numerical code is provided at the end of Sec. 3.1. Taking these reference processes into account and following the generic steps for the kinematic and coupling factor construction described in [1, 2] or Chap. 6 and Appendix A of the thesis, the reader can reproduce the kinematic and coupling factors expressions that are hard-coded in the numerical code.

Conceptually the code is divided into two parts where the first refers to the determination of the Wilson coefficients and the second is subsequently associated with the construction of the annihilation matrices from the former results. Part 1 and part 2 rely on different `Mathematica` “.m” files introduced in the following.

1. a. Within part 1, the following `Mathematica` “.m” file contains hard-coded results for the kinematic factors used in the code:

`kinfactors_Code.m` .

This includes all results referring to box, triangle and selfenergy diagrams. We discuss the structure of the kinematic factors in Sec. 3.1.

b. The corresponding hard-coded coupling factor results are collected in the three files

```
couplingFactors_boxes.m,
couplingFactors_triangles.m,
couplingFactors_selfenergies.m.
```

A closer description of the above files is given in Sec. 3.2.

c. The generic routines that build the different box-, triangle- and selfenergy-diagram contributions to a Wilson coefficient from the kinematic and coupling factors are contained in

```
partialwavecoefficients.m
```

and will be discussed in more detail in Sec. 3.3.

d. In order to build the specific $\chi_{e_1}\chi_{e_2} \rightarrow X_A X_B \rightarrow \chi_{e_4}\chi_{e_3}$ contribution to a certain Wilson coefficient that refers to the inclusive $\chi_{e_1}\chi_{e_2} \rightarrow \sum X_A X_B \rightarrow \chi_{e_4}\chi_{e_3}$ reaction, we have to further specify which particles are exchanged internally in the s -, t - or u -channels of the respective selfenergy, triangle or box diagrams. This is needed because the kinematic and coupling factor expressions are still generic in the sense that they use place-holder masses and indices referring to a certain neutralino or chargino state. The latter have to be set to the corresponding particle masses and indices when a specific Wilson coefficient is determined. For each possible exclusive reaction the information on the internally exchanged particles in the box, triangle and selfenergy amplitudes is collected in the files

```
scatteringchannels_boxes.m,
scatteringchannels_triangles.m,
scatteringchannels_self.m.
```

When building the Wilson coefficients with the help of the functions defined in `partialwavecoefficients.m`, the information encoded in the latter files is used. The nomenclature of the hard-coded lists in the above `scatteringchannels_xxx.m` files is given in Sec. 3.4. In addition, this section contains the description of the functions written in

```
partialwavecoefficients_channels.m,
```

which contain the definition of the Wilson coefficient contributions referring to exclusive physical tree-level annihilation reactions $\chi_{e_1}\chi_{e_2} \rightarrow X_A X_B \rightarrow \chi_{e_4}\chi_{e_3}$.

- Part 2 of the code, dealing with the construction of the annihilation matrices, is based on the functions collected in the file

`annihilationmatrices_vx.m`

where `x` is a place-holder for the version number. The current version is `x=7`. Details on the functions and definitions related to this part are given in Sec. 4.

3 Part 1: Building the partial wave coefficients

3.1 Kinematic factors

As described in [1, 2] and in the preceding thesis in Sec. 6.1.4, the Wilson coefficient of a NRMSSM four-fermion operator is given by a sum over products of kinematic and coupling factors. The numerical code comes with hard-coded expressions for the kinematic and coupling factors that refer to all relevant box, triangle and selfenergy amplitudes. As stated in Sec. 2 above, the conventions underlying the definitions of kinematic and coupling factors are different in [1, 2] and the code, while the outcome for the partial-wave coefficients agrees. We discuss the structure of the code's kinematic factor expressions in this section and subsequently describe in Sec. 3.2 the form of the corresponding coupling factors.

Within the numerical code, the hard-coded kinematic factor expressions are collected in the file `kinfactors_Code.m`. Also the nomenclature in the code differs slightly from the one in the publications. The code's kinematic factors referring to a selfenergy topology have the generic structure

$$\text{kE}[n, \text{"chi chi -> (i1) -> XA XB -> (i2) -> chi chi"}, \{2s+1\}\text{LJ}, \text{mci}, \text{alpha}]. \quad (2)$$

In case of triangle topologies the following nomenclature is used

$$\text{kD}[n, \text{"chi -> (X) -> XA XB -> chi chi"}, \{2s+1\}\text{LJ}, \text{mci}, \text{alpha}], \quad (3)$$

and box topologies are referred to as

$$\text{kC}[n, \text{"chi chi -> XA XB -> chi chi"}, \{2s+1\}\text{LJ}, \text{mci}, \text{alpha}]. \quad (4)$$

In the above expressions the terms `XA XB`, `{2s+1}LJ` and `mci` denote place-holders that can be set to the following values

- `XA XB` refers to the type of particles X_A and X_B in the final state of a $\chi\chi \rightarrow X_A X_B$ annihilation reaction. Both X_A and X_B can be given by a vector boson (V), scalar (S), fermion (f) or a ghost (η). Taking all possible two-particle final state combinations into account the argument `XA XB` in the code can be given the values

$$\text{XA XB} = \begin{cases} V V & (VV \text{ final state}) \\ V S & (VS \text{ final state}) \\ S S & (SS \text{ final state}) \\ f \text{ fbar} & (ff \text{ final state}) \\ gh \text{ gh} & (\eta\bar{\eta} \text{ final state}). \end{cases}$$

- $\{2s+1\}$ LJ specifies the partial wave configuration and is given by one of the following strings

$$\{2s+1\}\text{LJ} = \begin{cases} "1S0", "3S1", & \text{for leading order } S\text{-wave coefficients,} \\ "1P1", "3P_x", & \text{for } {}^1P_1 \text{ and the combined } {}^3P_J \text{ coefficients,} \\ "3P0", "3P1", "3P2", & \text{for the individual } {}^3P_{J=0,1,2} \text{ coefficients,} \\ "1S0, p2", "3S1, p2", & \text{for } p^2 \text{ proportional nnlo } S\text{-wave coeff.,} \\ "1S0, dm", "3S1, dm", & \text{for } \delta m \text{ proportional } S\text{-wave coeff.,} \\ "1S0, dmb", "3S1, dmb", & \text{for } \delta \bar{m} \text{ proportional } S\text{-wave coeff..} \end{cases}$$

Let us recall that the absorptive part of a 3P_J Wilson coefficient \hat{f} is obtained from the spin-1 P -wave Wilson coefficients by the following linear combination

$$\hat{f}({}^3P_J) = \frac{1}{3}\hat{f}({}^3P_0) + \frac{1}{3}\hat{f}({}^3P_1) + \frac{5}{3}\hat{f}({}^3P_2) . \quad (5)$$

The corresponding kinematic factor expressions obviously obtain from the same linear combination.

- `mci` specifies which expansion in mass differences is chosen. It can be set to the two values `mci = mc1, mc2`. For a discussion on the two possible expansions in mass differences we refer the reader to [1,2] or Sec. 6.1.2 in the thesis.

The further arguments of the kinematic factors `kE[...]`, `kD[...]` and `kC[...]` above differ for differing topology. We discuss these arguments for each topology in turn in Sec. 3.1.1 – 3.1.3

In order to determine the kinematic factor expressions used in the numerical code we have calculated the box, triangle and selfenergy amplitudes in processes $\chi_{e_1}^0 \chi_{e_2}^0 \rightarrow X_A X_B \rightarrow \chi_{e_4}^0 \chi_{e_3}^0$ with $X_A X_B$ given by

$$\begin{aligned} W^+ W^- & \text{ serving as reference for } VV \text{ final states,} \\ W^+ G^- & \text{ for } VS \text{ final states,} \\ G^+ G^- & \text{ for } SS \text{ final states,} \\ u^I \bar{u}^J & \text{ for } SS \text{ final states.} \end{aligned} \quad (6)$$

Here the superscripts I, J indicate the family index for the SM up-type quarks. The steps to be followed in the calculation of the code's kinematic factors can be found in [1] or Sec. 6.1.2 – 6.1.4 of the thesis. In the latter also the reference processes used in the calculation of the kinematic factors in [1,2] and the thesis are given.

3.1.1 Selfenergy topologies

The generic form of a selfenergy diagram in $\chi\chi \rightarrow X_A X_B \rightarrow \chi\chi$ scattering is given in Fig. 1. In case of the kinematic factors `kE[...]` related to such selfenergy topology the arguments `n`, `i1`, `i2`, and `alpha` can get the following inputs:

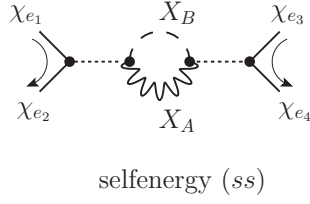


Figure 1: Generic selfenergy diagram in $\chi\chi \rightarrow X_A X_B \rightarrow \chi\chi$ reactions, with X_A and X_B representing any two-body final state of SM and Higgs particles. The shorthand *ss* notation indicates that the selfenergy amplitude corresponds to two *s*-channel exchange tree-level diagrams that are associated with $\chi_{e1}\chi_{e2} \rightarrow X_A X_B$ and $\chi_{e4}\chi_{e3} \rightarrow X_A X_B$ annihilations, respectively. (Also see Fig. 9, 10 in paper I and Fig. A.1, A.2 in the thesis).

- **n** refers to a character string that contains information on the type of couplings at the vertices of the selfenergy diagram. It can be set to

$$\mathbf{n} = \text{"rr"}, \text{"pp"} \quad \text{for } X_A X_B = V V, V S, S S, \text{ gh gh}.$$

The first (second) character in this two-character string refers to the type of coupling at the vertex that involves the incoming $\chi_{e1}\chi_{e2}$ pair (the outgoing $\chi_{e4}\chi_{e3}$ pair) in the selfenergy diagram referring to the $\chi_{e1}\chi_{e2} \rightarrow X_A X_B \rightarrow \chi_{e4}\chi_{e3}$ reaction. While **r** indicates a coupling of either vector or scalar type, the character **p** refers to a coupling of axial-vector or pseudo-scalar type. The couplings of the intermediate particles in the selfenergy amplitude are fixed once **XA XB** and **i1, i2** are specified and therefore do not need to be indicated in the string **n**. However in case of selfenergy diagrams with $X_A X_B = f\bar{f}$ the type of coupling of the final state fermions $X_A X_B$ to the *s*-channel exchanged particles needs to be specified. In this case

$$\mathbf{n} = \text{"rr rr"}, \text{"rr pp"}, \text{"pp rr"}, \text{"pp pp"} \quad \text{for } X_A X_B = f \bar{f}.$$

Here, the character **r** or **p** at the first (second) position in the string indicates the type of coupling of the incoming $\chi_{e1}\chi_{e2}$ (outgoing $\chi_{e4}\chi_{e3}$) pair to the respective *s*-channel exchanged particle. Similarly, the character at the third (fourth) position in the string **n** refers to the type of coupling between the final state fermions $X_A X_B$ and the particle exchanged in the left (right) single *s*-channel. As before and throughout the character **r** is used to refer to a vector or scalar coupling and **p** indicates a coupling of axial-vector or pseudo-scalar type.

- **i1, i2** are given by either **V** or **S**. These inputs denote the particle species – vector boson *V* or scalar *S* – that is exchanged in the left (**i1**) or right (**i2**) single *s*-channel of the corresponding selfenergy amplitude.

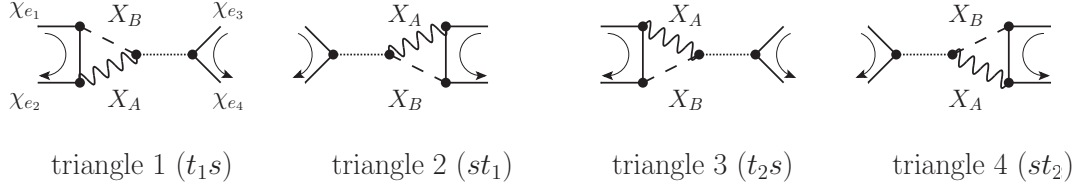


Figure 2: Generic triangle diagrams in $\chi\chi \rightarrow X_A X_B \rightarrow \chi\chi$ reactions, with X_A and X_B representing any two-body final state of SM and Higgs particles. The shorthand $a\tilde{a}$ notation, with $a, \tilde{a} = s, t_1, t_2$, is used in order to indicate the tree-level diagrams a and \tilde{a} in the $\chi_{e_1}\chi_{e_2} \rightarrow X_A X_B$ and $\chi_{e_4}\chi_{e_3} \rightarrow X_A X_B$ processes, respectively, to which the left-hand or right-hand part of the triangle diagrams are related (see Fig. 9, 10 in paper I or Fig. A.1, A.2 in the thesis for further details).

- **alpha** is used to label selfenergy diagrams with different type of particle species exchanged in the two single s -channels, that is

$$\text{alpha} = \begin{cases} 1 & \text{for } i1, i2 = V, \\ 2 & \text{for } i1 = V, i2 = S, \\ 3 & \text{for } i1 = S, i2 = V, \\ 4 & \text{for } i1, i2 = S. \end{cases}$$

Having specified $i1$ and $i2$, the value of **alpha** is immediately obtained.

3.1.2 Triangle topologies

The generic form of the triangle diagrams relevant in $\chi\chi \rightarrow X_A X_B \rightarrow \chi\chi$ scattering is given in Fig. 2, where also our enumeration convention for these diagrams is established. As regards the kinematic factor expressions $\text{kD}[\dots]$ in the code that are related to these triangle topologies, the arguments **n**, **X** and **alpha** can have the following values:

- **n** is a character string containing the information on the type of couplings at the vertices of the respective triangle diagram. It can take the values

$$\mathbf{n} = \text{"rr r", "pp r", "rp p", "pr p"} \quad \text{if } X_A X_B = V V, V S, S S,$$

and in case of $X_A X_B = f \bar{f}$

$$\mathbf{n} = \text{"rr r", "pp r", "rp p", "pr p", "rr p", "pp r", "rp r", "pr r"}.$$

If **alpha** = 1,2, the two characters at the first and second position in each string indicate the type of couplings at the first and second vertex in the corresponding triangle amplitude, where we have enumerated the vertices from top to bottom and left to right. The last character then refers to the type of coupling at the vertex with the outgoing $\chi_{e_4}\chi_{e_3}$ pair. For **alpha** = 3,4 the first (second) character in the string

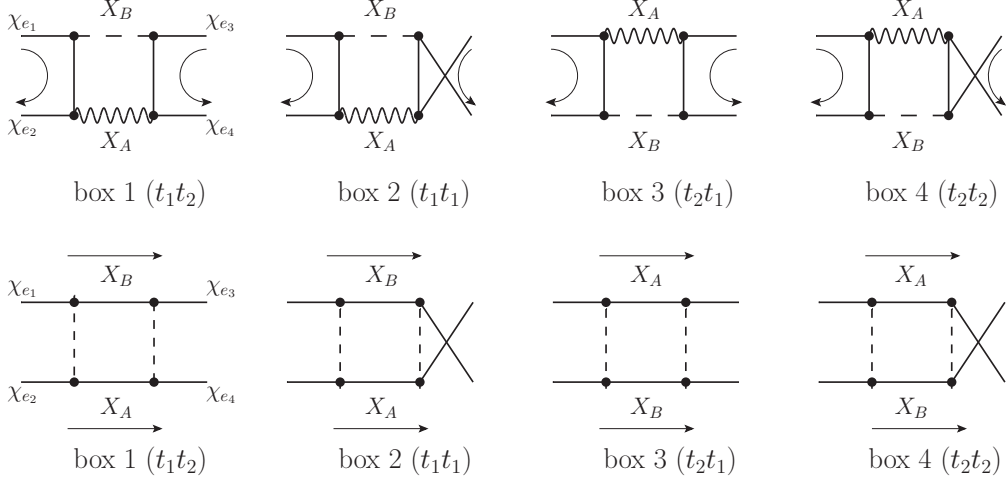


Figure 3: Generic box diagrams in $\chi\chi \rightarrow X_A X_B \rightarrow \chi\chi$ reactions, with X_A and X_B representing any two-body final state of SM and Higgs particles. The box-amplitudes in the first line refer to $X_A X_B = VV, VS, SS$ while the box-amplitudes in the second line apply to $X_A X_B = ff$. The shorthand $a\tilde{a}$ notation, with $a, \tilde{a} = t_1, t_2$, indicates the tree-level diagrams a and \tilde{a} in the $\chi_{e_1}\chi_{e_2} \rightarrow X_A X_B$ and $\chi_{e_4}\chi_{e_3} \rightarrow X_A X_B$ processes, respectively, to which the box diagrams are related. For further details on the tree-level amplitudes we again refer the reader to Fig. 9, 10 in [1] and Fig. A.1, A.2 in the thesis.

\mathbf{n} refers to the coupling with attached external χ_{e_4} (χ_{e_3}). Consequently the last character then indicates the type of coupling at the vertex with the incoming $\chi_{e_1}\chi_{e_2}$ pair. Note that the characters in the string \mathbf{n} refer only to the couplings involving the external fermionic χ_{e_i} states. This information together with the knowledge of the s -channel exchanged particle is sufficient to fix the type of coupling between the latter and the final state $X_A X_B$ pair.

- \mathbf{X} denotes the particle species (vector boson V or scalar particle S) exchanged in the single s -channel of the respective triangle diagram,

$$\mathbf{X} = \mathbf{V}, \mathbf{S}.$$

- \mathbf{alpha} labels the specific triangle diagram and can take the values

$$\mathbf{alpha} = 1, 2, 3, 4.$$

The enumeration convention for the triangle diagrams, which specifies the respective label \mathbf{alpha} can be read off Fig. 2.

3.1.3 Box topologies

Finally let us come to box amplitudes. Fig. 3 collects all corresponding diagrams relevant in $\chi\chi \rightarrow X_A X_B \rightarrow \chi\chi$ reactions. The arguments \mathbf{n} and \mathbf{alpha} of the kinematic factors

`kC[...]` related to these box amplitudes read as follows:

- `n` is a four-character string where the i th character refers to the coupling at the i th vertex of the box amplitude. Here the vertices of the box amplitudes are enumerated according to the respective attached external particles $\chi_{e_i}, i = 1, \dots, 4$. The string `n` can take the form

`n = "rrrr", "pppp", "rrpp", "pprr", "rppr", "prrr", "rprp", "prpr" .`

- `alpha` labels the four box diagrams,

`alpha = 1,2,3,4,`

where our enumeration convention for the box diagrams can be read off Fig. 3.

3.2 Coupling factors

When the three files `couplingFactors_boxes.m`, `couplingFactors_triangles.m` and `couplingFactors_selfenergies.m` are loaded in a `Mathematica` session, coupling factor expressions will be constructed that together with the corresponding kinematic factors described in the previous section will finally allow to build the absorptive part \hat{f} of Wilson coefficients related to a specific $\chi_{e_1}\chi_{e_2} \rightarrow X_A X_B \rightarrow \chi_{e_4}\chi_{e_3}$ reaction. In this section we discuss the nomenclature of the coupling factors used in the numerical code and describe the functions that determine these expressions from specific hard-coded lists. The latter contain the coupling factors that occur at each vertex of a specific box, triangle or selfenergy amplitude.

3.2.1 Selfenergy diagrams

Coupling factors corresponding to selfenergy diagrams have the generic form

`eC[n, "chi chi -> (i1) -> XA XB -> (i2) -> chi chi", alpha] .` (7)

The arguments `n` and `alpha` of the expression `eC[...]` take the same values as the corresponding arguments of the kinematic factors `kE[...]`, which are given in Sec. 3.1 and Sec. 3.1.1. In contrast to the generic kinematic factors, however, the additional argument `"chi chi -> (i1) -> XA XB -> (i2) -> chi chi"` of the coupling factors specifies the exact particle species involved in the respective selfenergy diagram. This implies that the sub-string `chi` refers to either species χ^0, χ^+ or χ^- and therefore can take the following values

`chi = chi0, chi+, chi-.`

Both `i1` and `i2` refer to the s -channel exchanged species and being an argument of the process specific coupling factors generically can be given by the photon (γ), the electroweak gauge bosons (Z, W^\pm) and the MSSM Higgs particles ($h^0, H^0, G^0, A^0, H^\pm, G^\pm$),

`i1,i2 = gamma, Z, W+, W-, h0, H0, G0, A0, H+, H-, G+, G-.`

type of final state	possible values of the coupling factors' argument XA XB
V V	W+ W-, Z Z, gamma gamma, Z gamma, W+ Z, W+ gamma, W- Z, W- gamma, W+ W+
V S	Z h0, Z H0, Z G0, Z A0, gamma h0, gamma H0, gamma G0, gamma A0, W+ G-, W+ H-, W- G+, W- H+, Z G+, Z H+, gamma G+, gamma H+, W+ h0, W+ H0, W+ G0, W+ A0, Z G-, Z H-, gamma G-, gamma H-, W- h0, W- H0, W- G0, W- A0, W+ G+, W+ H+, W- G-, W- H-
S S	h0 h0, h0 H0, H0 H0, G0 h0, A0 h0, G0 H0, A0 H0, G0 G0, G0 A0, A0 A0, G+ G-, G+ H-, H+ G-, H+ H-, G+ h0, G+ H0, H+ h0, H+ H0, G+ G0, G+ A0, H+ G0, H+ A0, G- h0, G- H0, H- h0, H- H0, G- G0, G- A0, H- G0, H- A0, G+ G+, G+ H+, H+ H+, G- G-, G- H-, H- H-
f fbar	u ubar, d dbar, nu nubar, l lbar, u dbar, nu lbar, d ubar, l nubar
gh gh	gh+ ghbar+, gh- ghbar-, ghZ ghbarZ gh+ ghbarZ, ghZ ghbar-, gh+ ghbarF, ghF ghbar- gh- ghbarZ, ghZ ghbar+, gh- ghbarF, ghF ghbar+

Table 1: Values for the argument XA XB in the coupling factors `eC[...]`, `dC[...]` and `cC[...]`.

The proper value depends on the specific diagram under consideration. Finally, the substring XA XB refers to the possible Standard Model (SM) and Higgs two-particle final states. Tab. 1 contains a list of its possible values. Note that at this point we also have to include two-particle states XA XB that involve unphysical states such as pseudo-Goldstone bosons and ghosts. This is because our calculation refers to Feynman gauge; see [1] or Sec. 6.1.3 of the thesis for a discussion on this choice of gauge. The final absorptive parts of the Wilson coefficients, referring to physical annihilation reactions will obviously be given by the appropriate sum over all corresponding physical and unphysical final states.

The coupling factors `eC[...]` are given by a product of four corresponding couplings associated with the four vertices of a given selfenergy diagram. Once the file `couplingFactors_selfenergies.m` is loaded in a `Mathematica` session, these four-coupling products are constructed automatically from predefined lists. For instance the coupling factor `eC[...]` in $\chi_{e_1}^0 \chi_{e_2}^0 \rightarrow W^+ W^- \rightarrow \chi_{e_4}^0 \chi_{e_3}^0$ scattering that is related to the selfenergy diagram with Z exchange in both single s -channels and which involves vector

couplings of the external $\chi_{e_1}^0\chi_{e_2}^0$ and $\chi_{e_4}^0\chi_{e_3}^0$ pairs, is then given by

$$\begin{aligned} & \text{eC}["\text{rr}", "chi0 chi0 -> (Z) -> W+ W- -> (Z) -> chi0 chi0", 1] \\ & = cW^2 \text{vOZ}[\text{e1},\text{e2}] \text{vOZ}[\text{e3},\text{e4}] = cW^2 \text{vOZ}[\text{e1},\text{e2}] \text{vOZ}[\text{e4},\text{e3}]^* . \end{aligned} \quad (8)$$

Here cW denotes the cosine of the electroweak mixing angle.⁴ The factors $\text{vOZ}[\text{e1},\text{e2}]$ and $\text{vOZ}[\text{e3},\text{e4}]$ denote the vector couplings of the external neutralino pairs $\chi_{e_1}^0\chi_{e_2}^0$ and $\chi_{e_4}^0\chi_{e_3}^0$ to the intermediate Z boson, respectively. They are kept as symbolic expressions as long as their arguments ei with $i = 1, \dots, 4$ are not set to integer values and if no `slha` MSSM spectrum card is read in. Only for integer-valued arguments these couplings are later expressed in terms of mixing matrix entries and angles. The definition of $\text{vOZ}[\text{i},\text{j}]$ agrees with the definition of $v_{ij}^{(0,Z)}$ given in Appendix A of [1] and Appendix A.1 of the thesis. In the numeric code the definition of $\text{vOZ}[\text{i},\text{j}]$ in terms of mixing matrices and angles is given at the end of the `couplingFactors_boxes.m` file, where also all other relevant coupling factors involving the external χ_{e_i} states are given. As in case of $\text{vOZ}[\text{i},\text{j}]$ and $v_{ij}^{(0,Z)}$, their nomenclature derives directly from the nomenclature of the couplings in [1], Appendix A or the thesis, Appendix A.1. Further definitions of coupling factors that refer to interactions of the final state pair $X_A X_B$ with the s -channel exchanged states can be found at the end of the file `couplingFactors_selfenergies.m`.

In order to work with the numerical code it is, in principle, sufficient to have at hand the final coupling factor expressions as given in the example above. Let us nevertheless say a few words on the internal determination of these expressions: The `couplingFactors_selfenergies.m` file contains predefined lists that contain, for each possible selfenergy diagram, the occurring coupling factors. The list related to the above example, for instance, reads

$$\begin{aligned} & \text{listSelfenergy}["chi0 chi0 -> (Z) -> W+ W- -> (Z) -> chi0 chi0",1] \\ & = \{\{\text{vOZ}[\text{e1},\text{e2}], \text{aOZ}[\text{e1},\text{e2}]\}, \{\text{vOZ}[\text{e3},\text{e4}], \text{aOZ}[\text{e3},\text{e4}]\}, \{\text{cWWZ}\}, \{\text{cWWZ}\}\}; \end{aligned} \quad (9)$$

The factor cWWZ is a place-holder for the vertex factor related to the three-point interaction of the two W -bosons and the Z . It is assigned to the proper vertex factor at the end of `couplingFactors_selfenergies.m`. In order to obtain the `eC[...]` expressions from lists such as the one written above, an element from each sub-list has to be chosen and multiplied with the chosen elements from the three other sub-lists. This is automatized with the help of two simple functions,

$$\begin{aligned} & \text{GenerateSelfenergyCouplingFactors}[\dots], \\ & \text{GenerateSelfenergyCouplingFactorsffbar}[\dots], \end{aligned} \quad (10)$$

which can be found in the file `couplingFactors_selfenergies.m`. The procedure is similar to the coupling factor construction described in [1], Appendix A.2 and the thesis,

⁴At this stage in the code the experimental value is not yet assigned to cW ; this will only happen if an `slha`-formatted MSSM spectrum file is read in a `Mathematica` session. We come back to this point of assigning numerical values to the parameters in later sections.

Appendix A.1.1. However let us stress that the generic reference processes used to determine kinematic and coupling factors that are used in the numerical code differ from those presented in [1, 2] and in the thesis. For that reason there can be sign differences between the kinematic and coupling factors derived in [1, 2] and the thesis and the corresponding expressions used in the code.

3.2.2 Triangle diagrams

Coupling factors related to triangle amplitudes generically read

$$\text{dC}[\mathbf{n}, \text{"chi chi } \rightarrow (\text{X}) \rightarrow \text{XA XB } \rightarrow \text{chi chi"}, \alpha], \quad (11)$$

where the arguments \mathbf{n} and α can take the same values as the corresponding arguments of the kinematic factors $\text{kD}[\dots]$ described in Sec. 3.1 and Sec. 3.1.2. The sub-strings in the additional argument "chi chi \rightarrow (X) \rightarrow XA XB \rightarrow chi chi" refer to the actual particle species involved in the triangle diagram under consideration. As noted in Sec. 3.2.1 the sub-string chi can take the values

$$\text{chi} = \text{chi0}, \text{chi+}, \text{chi-}.$$

The place-holder X in the argument "chi chi \rightarrow (X) \rightarrow XA XB \rightarrow chi chi" of the coupling factors $\text{dC}[\dots]$ refers to the specific s -channel exchanged particle and therefore can take the values

$$\text{X} = \text{gamma}, \text{Z}, \text{W+}, \text{W-}, \text{h0}, \text{H0}, \text{G0}, \text{A0}, \text{H+}, \text{H-}, \text{G+}, \text{G-}.$$

The possible values for the place-holder XA XB referring to the final state particles in a neutralino/chargino pair-annihilation reaction have been collected in Tab. 1.

Similar to the case of the coupling factors $\text{eC}[\dots]$ related to selfenergy diagrams, the coupling factors $\text{dC}[\dots]$ are automatically constructed from predefined lists once the file `couplingFactors_triangles.m` is loaded in `Mathematica`. For example, the coupling factor with $\mathbf{n} = \text{"rr r"}$ related to the triangle diagram with $\alpha = 1$ and single s -channel Z exchange in the reaction $\chi_{e_1}^0 \chi_{e_1}^0 \rightarrow W^+ W^- \rightarrow \chi_{e_1}^0 \chi_{e_1}^0$ is then given by

$$\begin{aligned} &\text{dC}[\text{"rr r"}, \text{"chi0 chi0 } \rightarrow (\text{Z}) \rightarrow \text{W+ W- } \rightarrow \text{chi0 chi0"}, 1] \\ &= \text{cW} \text{v0Z}[\mathbf{e1}, \mathbf{e2}] \text{v0Z}[\mathbf{e4}, \mathbf{e3}]^* \text{vW}[\mathbf{e2}, \mathbf{i1}]^*. \end{aligned} \quad (12)$$

While the labels \mathbf{ei} refer to the external $\chi_{e_i}^0$ states, the label $\mathbf{i1}$ is related to the $\chi_{i_1}^+$ states that can be exchanged in the t -channel of the triangle diagram. The predefined list from which the above expression is obtained reads

$$\begin{aligned} &\text{listTriangle}[\text{"chi0 chi0 } \rightarrow (\text{Z}) \rightarrow \text{W+ W- } \rightarrow \text{chi0 chi0"}, 1] \\ &= \{ \{ \text{vW}[\mathbf{e1}, \mathbf{i1}], \text{aW}[\mathbf{e1}, \mathbf{i1}] \}, \{ \text{CC}[\text{vW}[\mathbf{e2}, \mathbf{i1}]], \text{CC}[\text{aW}[\mathbf{e2}, \mathbf{i1}]] \}, \\ &\quad \{ \text{v0Z}[\mathbf{e3}, \mathbf{e4}], \text{a0Z}[\mathbf{e3}, \mathbf{e4}] \}, \{ \text{cWWZ} \} \}, \end{aligned} \quad (13)$$

and the function that builds the corresponding factors $\text{dC}[\dots]$ from this list is named

$$\text{GenerateTriangleCouplingFactors}[\dots]. \quad (14)$$

It can be found as well in the corresponding file `couplingFactors_triangles.m`.

3.2.3 Box diagrams

The form of coupling factors associated with box diagrams is given by

$$cC[n, "chi chi \to XA XB \to chi chi", alpha]. \quad (15)$$

Similar to the case of selfenergy and triangle diagrams described in the preceding sections, the arguments `n` and `alpha` in the coupling factors `cC[...]` take the same values as the corresponding kinematic factors `kC[...]` discussed in Sec. 3.1 and Sec. 3.1.3. Again, the sub-strings `chi` in the additional argument `"chi chi \to XA XB \to chi chi"` of `cC[...]` take the values

$$chi = chi0, chi+, chi-.$$

The possible values of the sub-string `XA XB` are collected in Tab. 1.

When the file `couplingFactors_boxes.m` is loaded all relevant `cC[...]` factors are generated with the help of the function

$$\text{GenerateBoxCouplingFactors}[...] \quad (16)$$

from predefined lists, such as for example

$$\begin{aligned} & \text{listBox}["chi0 chi0 \to W+ W- \to chi0 chi0", 1] \\ & = \{ \{vW[e1, i1], aW[e1, i1]\}, \{CC[vW[e2, i1]], CC[aW[e2, i1]]\}, \\ & \quad \{CC[vW[e3, i2]], CC[aW[e3, i2]]\}, \{vW[e4, i2], aW[e4, i2]\} \}. \quad (17) \end{aligned}$$

The labels `ei` refer to the external states $\chi_{e_i}^0$, while labels `ia` with `a = 1, 2` are associated with the internally exchanged chargino states $\chi_{i_a}^\pm$, which occur in the t -channels of the corresponding box diagram. From the above list we obtain for example the following coupling factor `cC[...]` referring to the reaction $\chi_{e_1}^0 \chi_{e_2}^0 \to W^+ W^- \to \chi_{e_4}^0 \chi_{e_3}^0$ that is related to the box diagram labelled with `alpha = 1` and that refers to `n = "rrrr"`:

$$\begin{aligned} & cC["rrrr", "chi0 chi0 \to W+ W- \to chi0 chi0", 1] \\ & = vW[e1, i1] vW[e2, i1]^* vW[e3, i2]^* vW[e4, i2]. \quad (18) \end{aligned}$$

The neutralino-chargino W^\pm vector coupling `vW[i, j]` is evaluated only for integer arguments `i, j` and otherwise left as it stands above. Its definition in terms of mixing matrix entries and angles is given at the end of `couplingFactors_boxes.m`.

3.3 Partial wave coefficients: generic routine

In this section we describe functions provided in the file `partialwavecoefficients.m`, which allow to determine the absorptive part of a specific partial wave coefficient in the NRMSSM. Kinematic and coupling factor expressions have to be loaded in advance in `Mathematica` and an `slha`-formatted MSSM spectrum card has to be read in, before the

respective coefficients can be calculated.⁵ In Sec. 3.3.1 we first discuss the central function `PartialWaveCoefficient[...]` that allows to determine the coefficients. Sec. 3.3.2 then contains a summary on further auxiliary functions needed in building the partial wave coefficient expressions.

3.3.1 The function `PartialWaveCoefficient[...]`

The function `PartialWaveCoefficient[...]` allows to determine the contribution to the absorptive part of a partial wave coefficient that is associated with a specific exclusive $\chi_{e_1}\chi_{e_2} \rightarrow X_A X_B \rightarrow \chi_{e_4}\chi_{e_3}$ reaction. Let us recall that the actual coefficient is determined from the inclusive reaction. The inclusive result is obtained from a different function discussed in Sec. 4.3.

`PartialWaveCoefficient[...]` has the following arguments

$$\text{PartialWaveCoefficient}[\text{Process}, \{\text{p1}, \text{p2}\}, \{\text{p3}, \text{p4}\}, \{\text{pA}, \text{pB}\}, \text{Wave}, \text{mci}]. \quad (19)$$

- The first argument, `Process`, is given by a string that specifies the exclusive reaction $\chi_{e_1}\chi_{e_2} \rightarrow X_A X_B \rightarrow \chi_{e_4}\chi_{e_3}$. It has to have the same form as the strings that appear as arguments in the coupling factors `cC[...]` referring to box diagrams, see Sec. 3.2.3. For example, if a partial wave coefficient associated with the reaction $\chi_1^0\chi_1^0 \rightarrow W^+W^- \rightarrow \chi_1^0\chi_1^0$ shall be evaluated, the argument `Process` is given by the string

`"chi0 chi0 -> W+ W- -> chi0 chi0"`.

The possible strings that are viable arguments are easily built from the generic form

`"chi chi -> XA XB -> chi chi"`

by using Tab. 1 to identify the possible values of `XA XB` and choosing the value for `chi` out of the set of values `chi = chi0, chi+, chi-` according to the exclusive process $\chi_{e_1}\chi_{e_2} \rightarrow X_A X_B \rightarrow \chi_{e_4}\chi_{e_3}$ under consideration.

- The arguments `p1, p2, p3` and `p4` refer to the particle species $\chi_{e_1}, \chi_{e_2}, \chi_{e_3}$ and χ_{e_4} in the process. Each argument `pa` with `a = 1, 2, 3, 4`, can take the values

$$\text{pa} = \begin{cases} \text{Neu}[i] & \text{if } \chi_{e_a} = \chi_i^0, \quad i = 1, \dots, 4, \\ \text{Cha}[j] & \text{if } \chi_{e_a} = \chi_j^0, \quad j = 1, 2, \end{cases}$$

and has to be adjusted according to the particle species χ_{e_a} in the reaction. In the above example of $\chi_1^0\chi_1^0 \rightarrow W^+W^- \rightarrow \chi_1^0\chi_1^0$ scattering we would have to set all `pa` with `a=1, 2, 3, 4` to `Neu[1]`.

⁵In order to read such a MSSM spectrum card we use the same file, `readLHA.m`, as in the Sommerfeld-enhancement part of the code. This file contains the function `ReadMSSMInput[filename]`, where the input `filename` must be an slha formatted MSSM spectrum card. In order to adjust the nomenclature slightly to the annihilation matrix code, one has to load the file `readSUSYparameters.m` after calling `ReadMSSMInput[filename]`. In this way only certain names for masses and couplings are adjusted. For details on the nomenclature we refer the reader to the self-explanatory file `readSUSYparameters.m`.

- The values of `pA` (`pB`) are given by the values of `XA` and `XB`, which can be read of Tab. 1, where however all signs have to be dropped. In our exclusive scattering reaction example $\chi_1^0\chi_1^0 \rightarrow W^+W^- \rightarrow \chi_1^0\chi_1^0$, for instance, `pa` and `pb` have to be set to `pa = pb = W`.
- The possible inputs for `Wave` specify the partial wave configuration and agree with those specified under `{2s+1}LJ` in Sec. 3.1.
- The possible values for `mci` are `mci = mc1,mc2` and indicate the underlying expansion in mass differences, see the corresponding paragraph in Sec. 3.1.

To summarise, we obtain in our $\chi_1^0\chi_1^0 \rightarrow W^+W^- \rightarrow \chi_1^0\chi_1^0$ exclusive process example from

```
PartialWaveCoefficient["chi0 chi0 -> W+ W- -> chi0 chi0",
                      {Neu[1],Neu[1]},{Neu[1],Neu[1]},{W,W},mc2,"1S0,p2"]
```

the contribution to the next-to-next-to-leading order 1S_0 Wilson coefficient associated with $\chi_1^0\chi_1^0 \rightarrow W^+W^- \rightarrow \chi_1^0\chi_1^0$ scattering. This corresponds to the next-to-next-to-leading order 1S_0 -wave contribution to the $\chi_1^0\chi_1^0 \rightarrow W^+W^-$ annihilation cross section. As a side remark let us recall that in case of identical particle annihilation $\chi_{e_1} = \chi_{e_2}$ and further $\chi_{e_1}\chi_{e_2} = \chi_{e_4}\chi_{e_3}$ the choice of either mass expansion option `mc1` or `mc2` gives the same result for the coefficient, see [1,2] or Sec. 5 and 6 in the thesis.

The absorptive part of any Wilson coefficient of a NRMSSM four fermion operator is obtained from the sum of contributions related to box, triangle and selfenergy diagrams. Accordingly, the function `PartialWaveCoefficient[...]` calls three individual functions that have the same arguments as the former and that separately evaluate the contributions from box, triangle and selfenergy diagrams. These functions are named

$$\text{BoxCoefficient}[\text{Process}, \{p1,p2\}, \{p3,p4\}, \{pA, pB\}, \text{Wave}, \text{mci}], \quad (20)$$

$$\text{TriangleCoefficient}[\text{Process}, \{p1,p2\}, \{p3,p4\}, \{pA, pB\}, \text{Wave}, \text{mci}], \quad (21)$$

$$\text{SelfCoefficient}[\text{Process}, \{p1,p2\}, \{p3,p4\}, \{pA, pB\}, \text{Wave}, \text{mci}]. \quad (22)$$

The type of diagrams that appear in case of a final state fermion pair $X_AX_B = ff$ differs slightly from the case of final states built from gauge or Higgs bosons. In particular, as can be inferred from Sec. 3.1 and Sec. 3.2, the number of kinematic and coupling factor expression is larger for $X_AX_B = ff$. Therefore there is a separate function

$$\text{PartialWaveCoefficientFermions}[...], \quad (23)$$

that covers the case of reactions where $X_AX_B = ff$ and which, in addition to the unchanged function `BoxCoefficient[...]`, calls

$$\text{TriangleCoefficientFermions}[...] \quad , \quad (24)$$

$$\text{SelfCoefficientFermions}[...]. \quad (25)$$

The arguments of the above functions are as in `PartialWaveCoefficient[...]`. However, there is one subtlety regarding the nomenclature of fermion final state parameters `pA,pB`:

<code>uQuark[I]</code>	denotes the up-type quark of the I th family, u^I ,
<code>dQuark[I]</code>	denotes the down-type quark of the I th family, d^I ,
<code>neutrino[I]</code>	denotes the neutrino of the I th family, ν^I ,
<code>lepton[I]</code>	denotes the lepton of the I th family, l^I .

(26)

For example, in case of the reaction $\chi_1^0 \chi_1^+ \rightarrow t\bar{b} \rightarrow \chi_1^+ \chi_1^0$ the values of `pa,pB` inside the above functions have to be set to `pa = uQuark[3]` and `pB = dQuark[3]`.

3.3.2 Auxiliary functions in `partialwavecoefficients.m`

In order to determine the exclusive final state contribution of a certain partial wave coefficient with the function `PartialWaveCoefficient[...]`, the terms in the generic kinematic factors and the coupling factor expressions have to be set to numerical values. To this end a `slha`-formatted MSSM spectrum card has to be read in the `Mathematica` session. Once the MSSM spectrum is read in, all values for the masses, angles and mixing matrices are available and only have to be assigned according to the $\chi_{e_1} \chi_{e_2} \rightarrow X_A X_B \rightarrow \chi_{e_4} \chi_{e_3}$ reaction under consideration.

For each exclusive scattering reaction we can generically distinguish between the set of external particles and the internally exchanged (virtual) states. The former set of states contains the χ_{e_i} , $i = 1, \dots, 4$ species as well as the on-shell accessible final states X_A, X_B . The function `PartialWaveCoefficient[...]` calls the subroutine

$$\text{SetExternalVar}[p1, p2, p3, p4, pA, pB, mci]. \quad (27)$$

This function assigns numerical values to the process specific external mass parameters M, m, \bar{m} and $\delta m, \delta \bar{m}$ (denoted by `M,m,mbar` and `dm, dmbar` in the numerical code) as well as m_A, m_B (given by `mA,mB` in the program). Let us recall from [1, 2] and from the thesis that the mass parameters M, m, \bar{m} depend on the choice of the mass expansion option, `mci`, where

$$\begin{aligned} m &= \frac{1}{2} (m_{e_1} + m_{e_3}), & \bar{m} &= \frac{1}{2} (m_{e_2} + m_{e_4}) & \text{for } mci = mc1, \\ m &= \frac{1}{2} (m_{e_1} + m_{e_4}), & \bar{m} &= \frac{1}{2} (m_{e_2} + m_{e_3}) & \text{for } mci = mc2, \end{aligned} \quad (28)$$

and similarly also for δm and $\delta \bar{m}$. Further, `SetExternalVar[...]` also extracts the labels e_i of the external χ_{e_i} states that refer to a specific neutralino or chargino species. For instance, if the argument `p1` of the `SetExternalVar` function is `Neu[1]`, the value of `e1` is set to `e1 = 1`. Note that the argument `e1` is the same as the one appearing in the coupling factors.⁶

⁶As noted in Sec. 3.2 the coupling factors `cC[...]`, `dC[...]` and `eC[...]` can be assigned numerical values only if all the arguments `ea` with `a=1,2,3,4` and `ib` with `b=1,2` (indices `ib` refer to the internally exchanged particle states) related to the individual couplings at each vertex are set to integer values.

While the parameters related to the external states χ_{e_i} and X_A, X_B can be assigned once and for all their corresponding numerical values, the case of the intermediate states is more involved as typically a summation over several internally exchanged states in each diagram has to be taken into account. For instance, in the four box diagrams labelled with $\alpha = 1, \dots, 4$ and related to $\chi_1^0 \chi_1^0 \rightarrow W^+ W^- \rightarrow \chi_1^0 \chi_1^0$, in each of the two t -channels both chargino species χ_j^+ , $j = 1, 2$ can be exchanged. Consequently, each of the box topologies α in this case actually represents four different diagrams: the intermediately exchanged chargino species can be given by $\chi_1^+ \chi_1^+, \chi_1^+ \chi_2^+, \chi_2^+ \chi_1^+$ and $\chi_2^+ \chi_2^+$ where the first (second) element in each tuple refers to the chargino species exchanged in the left (right) t -channel. In each case the masses of the t -channel exchanged species and their corresponding label have to be set accordingly in order to determine the numerical value of the kinematic and coupling factor expressions. This is taken care of by a `Do[]`-loop in `PartialWaveCoefficient[...]`, which calls elements from predefined lists containing all possible tuples of internally exchanged particles related to each of the diagrams in Fig. 1–3.

At this stage the only missing point before a numerical value for a specific partial wave coefficient can be given is the introduction of predefined lists that, for each possible process, contain the information on the internally exchanged particle species. We discuss the structure of these lists in the next section.

3.4 Partial wave coefficients: physical reactions

3.4.1 Listing internally exchanged states

When the function `PartialWaveCoefficient[...]` is called for a specific exclusive reaction, it accesses predefined lists collected in the files `scatteringchannels_box.m`, `scatteringchannels_triangles.m` and `scatteringchannels_self.m`, which summarise the relevant information on the internally exchanged particles in each contributing diagram. Each of the latter `scatteringchannels_xxx.m` files generically contains two types of lists. In the following we discuss their form for each of the three relevant topologies in turn.

The file `scatteringchannels_box.m` summarises the following two types of lists:

$$\begin{aligned} & \text{BoxSubProcess}[\text{Process}], \\ & \text{tChannelBox}[\text{Process}, \text{alpha}]. \end{aligned} \tag{29}$$

In both cases the argument `Process` specifies the exclusive reaction under consideration. Accordingly, it takes the same values as in the function `PartialWaveCoefficient[...]`, see Sec. 3.3. The argument `alpha` refers to the label of the box diagram according to our counting scheme, see Fig. 3 and Sec. 3.1 and 3.2. For each possible $\chi_{e_1} \chi_{e_2} \rightarrow X_A X_B \rightarrow \chi_{e_4} \chi_{e_3}$ process `BoxSubProcess[Process]` is given by a hard-coded list with two elements. The purpose of the list is to provide the arguments for the coupling and kinematic factors that have to be multiplied with each other, respectively, when building the Wilson coefficients. Consequently, the form of the two elements of each

list is dictated by the nomenclature that we have chosen for the kinematic and coupling factor expressions: The first element is given by the process-specifying string that occurs in the coupling factor expressions related to the reaction, while the second element is the string arising as argument in the corresponding kinematic factor term. In case of all processes $\chi_{e_1}^0 \chi_{e_2}^0 \rightarrow W^+ W^- \rightarrow \chi_{e_4}^0 \chi_{e_3}^0$, irrespective which neutralino species with labels e_i are involved, we have, for instance,

$$\begin{aligned} & \text{BoxSubProcess}["\text{chi0 chi0} \rightarrow W^+ W^- \rightarrow \text{chi0 chi0}"] \\ & = \{ "\text{chi0 chi0} \rightarrow W^+ W^- \rightarrow \text{chi0 chi0}", "\text{chi chi} \rightarrow V V \rightarrow \text{chi chi}" \}. \end{aligned} \quad (30)$$

The elements of the lists `tChannelBox[...]` are given by sublists with two elements, where the first (second) element gives the particle species exchanged in the left (right) t -channel of a contributing box amplitude with label `alpha`. In our $\chi_{e_1}^0 \chi_{e_2}^0 \rightarrow W^+ W^- \rightarrow \chi_{e_4}^0 \chi_{e_3}^0$ example – for all the box diagrams with labels $\alpha = 1, 2, 3, 4$ – the t -channel exchanged species are given by the two chargino species $\chi_{1,2}^+$. Consequently the corresponding `tChannelBox[...]` list reads, for all `alpha=1,2,3,4`,

$$\begin{aligned} & \text{tChannelBox}["\text{chi0 chi0} \rightarrow W^+ W^- \rightarrow \text{chi0 chi0}", \text{alpha}] \\ & = \{ \{ \text{Cha}[\text{1}], \text{Cha}[\text{1}] \}, \{ \text{Cha}[\text{1}], \text{Cha}[\text{2}] \}, \{ \text{Cha}[\text{2}], \text{Cha}[\text{1}] \}, \{ \text{Cha}[\text{2}], \text{Cha}[\text{2}] \} \}. \end{aligned} \quad (31)$$

The lists provided in `scatteringchannels_triangles.m` are named

$$\begin{aligned} & \text{TriangleSubProcess}[\text{Process}], \\ & \text{tsChannelTriangles}[\text{SubProcess}, \text{alpha}], \end{aligned} \quad (32)$$

and have a similar form as the lists related to box diagrams described above. The possible arguments `Process` of the expressions `TriangleSubProcess[...]` are identical to the arguments of `BoxSubProcess[...]`. The lists that are obtained when calling a specific `TriangleSubProcess[Process]` are built from several sub-lists, where each of the latter contains as first element a sub-process specifying string occurring as element of a corresponding coupling factor expression. The respective second argument is the string corresponding to the related kinematic factor. Under a “sub-process specifying string” we understand a string that explicitly contains the s -channel exchanged particle species. For triangle diagrams in the example scattering process $\chi_{e_1}^0 \chi_{e_2}^0 \rightarrow W^+ W^- \rightarrow \chi_{e_4}^0 \chi_{e_3}^0$ we have

$$\begin{aligned} & \text{TriangleSubProcesses}["\text{chi0 chi0} \rightarrow W^+ W^- \rightarrow \text{chi0 chi0}"] \\ & = \{ \{ "\text{chi0 chi0} \rightarrow (\text{H0}) \rightarrow W^+ W^- \rightarrow \text{chi0 chi0}", \\ & \quad \quad \quad "\text{chi chi} \rightarrow (\text{S}) \rightarrow V V \rightarrow \text{chi chi}" \}, \\ & \quad \{ "\text{chi0 chi0} \rightarrow (\text{h0}) \rightarrow W^+ W^- \rightarrow \text{chi0 chi0}", \\ & \quad \quad \quad "\text{chi chi} \rightarrow (\text{S}) \rightarrow V V \rightarrow \text{chi chi}" \}, \\ & \quad \{ "\text{chi0 chi0} \rightarrow (\text{Z}) \rightarrow W^+ W^- \rightarrow \text{chi0 chi0}", \end{aligned}$$

$$\text{"chi chi -> (V) -> V V -> chi chi"}\}. \quad (33)$$

The argument `SubProcess` in a list `tsChannelTriangle[SubProcess, alpha]` can take the values provided by the first elements of the sub-lists in `TriangleSubProcess[...]`. The corresponding `tsChannelTriangle[...]` lists contain sub-lists where the first (second) element gives a particle exchanged in the t -channel (s -channel) of the corresponding triangle diagram with label `alpha`. Again, for our explicit $\chi_{e_1}^0 \chi_{e_2}^0 \rightarrow W^+ W^- \rightarrow \chi_{e_4}^0 \chi_{e_3}^0$ example we have for all `alpha=1,2,3,4`,

$$\begin{aligned} &\text{tsChannelTriangle["chi0 chi0 -> (H0) -> W+ W- -> chi0 chi0", alpha]} \\ &= \{\{\text{Cha}[1], \text{H0}\}, \{\text{Cha}[2], \text{H0}\}\}. \end{aligned} \quad (34)$$

According to the sub-lists in the corresponding `TriangleSubProcess[...]` for our example there are in addition two further `tsChannelTriangle[...]`, where the s -channel exchanged state is given by a h^0 or a Z boson.

The structure of the lists contained in `scatteringchannels_self.m` follows immediately from the above discussed cases. Here the nomenclature for the lists is

$$\begin{aligned} &\text{SelfSubProcesses[Process]}, \\ &\text{ssChannelSelf[SubProcess]}. \end{aligned} \quad (35)$$

The argument `Process` of the first type of lists takes the same values as in the corresponding box and triangle diagram related cases: `Process` is a place-holder for a string specifying the exclusive $\chi_{e_1} \chi_{e_2} \rightarrow X_A X_B \rightarrow \chi_{e_4} \chi_{e_3}$ scattering reaction. The elements of a certain `SelfSubProcesses[Process]` list are again sub-lists that contain as elements the process specifying strings related to coupling and corresponding kinematic factors. For instance we have

$$\begin{aligned} &\text{SelfSubProcesses["chi0 chi0 -> W+ W- -> chi0 chi0"]} \\ &= \{\{\text{"chi0 chi0 -> (Z) -> W+ W- -> (Z) -> chi0 chi0"}, \\ &\quad \text{"chi chi -> (V) -> V V -> (V) -> chi chi"}, 1\}, \\ &\quad \{\text{"chi0 chi0 -> (Z) -> W+ W- -> (H0) -> chi0 chi0"}, \\ &\quad \text{"chi chi -> (V) -> V V -> (S) -> chi chi"}, 2\}, \\ &\quad \{\dots\}, \dots \}. \end{aligned} \quad (36)$$

The enumeration index that occurs as third element of the sub-lists is the label `alpha` related to selfenergy topologies which we introduced in Sec. 3.1.1. The possible arguments of `ssChannelSelf[...]` are now given by the respective first sub-elements of `SelfSubProcess[...]`, and the latter lists contain as elements pairs $\{i1, i2\}$ of all possible s -channel exchanged particles $i1, i2$. For instance

$$\begin{aligned} &\text{ssChannelSelf["chi0 chi0 -> (Z) -> W+ W- -> (Z) -> chi0 chi0"]} = \{Z, Z\}, \\ &\text{ssChannelSelf["chi0 chi0 -> (Z) -> W+ W- -> (H0) -> chi0 chi0"]} = \{Z, \text{H0}\}, \end{aligned}$$

... , (37)

where we do not write explicitly the remaining seven lists related to the selfenergy topology in $\chi_{e_1}^0 \chi_{e_1}^0 \rightarrow W^+ W^- \rightarrow \chi_{e_4}^0 \chi_{e_3}^0$ scattering.

3.4.2 The function `pwc[...]` related to the physical exclusive process

We have noted before in Sec. 3.3 that the function `PartialWaveCoefficient[...]` determines the contribution to the absorptive part of a Wilson coefficient that arises from a specific exclusive $X_A X_B$ final state.⁷ As our calculation refers to Feynman gauge, we have to sum over a certain set of final states $X_A X_B$ to arrive at corresponding contributions from physical final states. In order to immediately have at hand a function that gives the exclusive physical final state contribution to the Wilson coefficients, the function `pwc[...]` (abbreviating `partialwavecoefficient`) is introduced in the file `partialwavecoefficients_channels.m`. It has the form

$$\text{pwc}[\text{Process}, \{\text{e1}, \text{e2}\}, \{\text{e3}, \text{e4}\}, \text{Wave}, \text{mci}], \quad (38)$$

where the arguments can take the following values:

- `Process` is a string indicating the exclusive physical reaction

`"chi chi -> XA XB -> chi chi"`

where all sub-strings `chi` and `XA XB` have to be adjusted according to the exclusive reaction under consideration. Note in particular, that the generic species of the external states (neutralino, `chi0`, or chargino, `chi+`, `chi-`) is fixed by this string.

- `e1`, `e2`, `e3`, `e4` denote the labels e_i of the external states χ_{e_i} in the physical $\chi_{e_1} \chi_{e_2} \rightarrow X_A X_B \rightarrow \chi_{e_4} \chi_{e_3}$ reaction.⁸ As the particle species type of each χ_{e_i} , either being a neutralino or a chargino, is already determined by the argument `Process`, only the labels `ei` need to be specified as additional inputs here.

⁷Let us recall in addition from Sec. 3.3 that in case of an exclusive final state built of a fermion pair the corresponding function is named `PartialWaveCoefficientFermions[...]`.

⁸A caveat has to be added here, related to the use of the functions `pwc[...]`: These functions currently contain no internal query if a given final state $X_A X_B$ is on-shell accessible in $\chi_{e_1} \chi_{e_2} \rightarrow X_A X_B$ and $\chi_{e_4} \chi_{e_3} \rightarrow X_A X_B$ reactions. However an absorptive part is only present in $\chi_{e_1} \chi_{e_2} \rightarrow X_A X_B \rightarrow \chi_{e_4} \chi_{e_3}$ scattering, if X_A and X_B can simultaneously go on-shell. Consequently, the result for a `pwc[...]` should be zero, if the state $X_A X_B$ cannot be produced on-shell in the corresponding $\chi_{e_1} \chi_{e_2} \rightarrow X_A X_B$ and $\chi_{e_4} \chi_{e_3} \rightarrow X_A X_B$ annihilations. But when calling `pwc[...]`, the hard coded analytic results for the underlying kinematic factors are called, which rely on a calculation under the assumption that $X_A X_B$ can be produced on-shell. Therefore, in the current version of the code, the user himself has to make sure that $X_A X_B$ is on-shell accessible when using `pwc[...]` and if $X_A X_B$ is not on-shell accessible he has to set the result for the exclusive contribution to the partial wave coefficient to zero by hand. Let us note that in the case of the determination of the inclusive reactions, referring to the absorptive parts of the Wilson coefficients, described in Sec. 4.3 it is taken care of that only those $X_A X_B$ exclusive final state contributions are considered that are on-shell accessible.

- `Wave` takes the same values as in the function `PartialWaveCoefficient[...]`, see Sec. 3.3 and Sec. 3.1 for the possible values.
- `mci` can be either set to `mc1` or `mc2`, specifying the mass expansion option, see again Sec. 3.3 and Sec. 3.1.

Let us imagine we wish to determine the contribution to the leading order 3S_1 partial wave coefficient in $\chi_1^0\chi_2^0 \rightarrow \chi_1^0\chi_2^0$ scattering that arises from a physical W^+W^- exclusive final state, and we chose the mass expansion `mc2`. In this case we have to call

$$\text{pwc}["\text{chi0 chi0} \rightarrow W^+ W^- \rightarrow \text{chi0 chi0}", \{1, 2\}, \{2, 1\}, "3S1", \text{mc2}]. \quad (39)$$

Note the order in which the indices `ei` of the external states χ_{e_i} are given: according to ascending i , while we denote the scattering reaction itself by $\chi_{e_1}\chi_{e_2} \rightarrow \chi_{e_4}\chi_{e_3}$. That is, the indices of the particles with labels e_3 and e_4 appear in the opposite order. This nomenclature goes back to the conventions that we have chosen for the order of indices on the four-fermion operators in [1, 2] and in the thesis. It implies, in particular, that a certain partial wave contribution to the exclusive pair annihilation cross section of two non-identical states $\chi_{e_1}\chi_{e_2}$, which is related to the absorptive part in $\chi_{e_1}\chi_{e_2} \rightarrow \chi_{e_1}\chi_{e_2}$ scattering, is obtain from `pwc[...]` by setting the arguments $\{\mathbf{e1}, \mathbf{e2}\}, \{\mathbf{e3}, \mathbf{e4}\}$ to $\{\mathbf{e1}, \mathbf{e2}\}, \{\mathbf{e2}, \mathbf{e1}\}$. Therefore the output of our above example is proportional to the leading order 3S_1 wave contribution to the exclusive $\chi_1^0\chi_2^0 \rightarrow W^+W^-$ annihilation cross section.

The file `scatteringchannels_channels.m` contains the definition of all functions `pwc[Process, ...]` with differing arguments `Process` that are related to possible exclusive physical $\chi_{e_1}\chi_{e_2} \rightarrow X_A X_B \rightarrow \chi_{e_4}\chi_{e_3}$ reactions arising in neutralino and chargino scattering reactions. In case of fermionic final states $X_A X_B$ the colour factor of $N_c = 3$ is taken into account in the definition of the corresponding `pwc[...]`.

4 Part 2: Building the annihilation matrices

In this section we describe the functions that finally allow to obtain the annihilation matrices encoding hard $\chi_{e_1}\chi_{e_2} \rightarrow \sum X_A X_B \rightarrow \chi_{e_4}\chi_{e_3}$ pair-annihilation reactions. These annihilation matrices are an input to the Sommerfeld enhancement part of the code. Collecting and representing the hard $\chi_{e_1}\chi_{e_2} \rightarrow \sum X_A X_B \rightarrow \chi_{e_4}\chi_{e_3}$ rates in matrix form requires the introduction of an enumeration convention for the $\chi_{e_a}\chi_{e_b}$ two-particle states. Sec. 4.1 summarises our enumeration convention for the two-particle states $\chi_{e_a}\chi_{e_b}$ in each of the charge sectors referring to neutral, single- or double-charged $\chi_{e_a}\chi_{e_b}$ pairs. In Sec. 4.2 we comment on the choice to be made for the mass expansion option, either `mc1` or `mc2`. While in the first part of the code, discussed in Sec. 3, we have described functions that allow to obtain partial wave separated contributions to the NRMSSM four-fermion operators arising from exclusive (physical) final states, we finally introduce in Sec. 4.3 functions that determine the full absorptive part of the Wilson coefficients related to inclusive reactions. Symmetry factors and symmetry relations between certain

$(\chi\chi)_I$ state	method-1 label	method-2 label	$(\chi\chi)_I$ state	method-1 label	method-2 label
$\chi_1^+ \chi_1^+$	1	1	$\chi_2^+ \chi_1^+$	3	-
$\chi_1^+ \chi_2^+$	2	2	$\chi_2^+ \chi_2^+$	4	3

Table 2: Enumeration scheme within method-1 and method-2 for double positive charged $(\chi\chi)_I$ states. The same conventions hold for double negative charged states.

partial wave coefficients are discussed in Sec. 4.4. Compared to the order of magnitude of leading entries in the annihilation matrices, certain entries can be numerically very small and can be set to zero for our purposes; a corresponding function that addresses this issue is discussed in Sec. 4.5. The functions that determine the annihilation matrices are finally given in Sec. 4.6

It is worth to note here that all functions described in the following are introduced and defined in the file `annihilationmatrices_vx.m`, where `x` denotes the version number, which is currently `x=7`.

4.1 Enumeration convention for $\chi\chi$ states

The entries of the annihilation matrices encode the absorptive part of partial wave separated $\chi_{e_1}\chi_{e_2} \rightarrow \chi_{e_4}\chi_{e_3}$ scattering reactions. As they refer to two-particle scatterings we can first divide all possible pairs built from the neutralino and chargino states into sets of neutral, single positive (single negative) and double positive (double negative) $\chi\chi$ states. In the following we will consider $\chi_{e_a}\chi_{e_b}$ pairs rather than individual χ_{e_a} and χ_{e_b} states and therefore introduce a single label I to refer to the pair $\chi_{e_a}\chi_{e_b} \equiv (\chi\chi)_I$. Let us note that we generically consider all possible $\chi\chi$ pairs as external states in the annihilation matrices. This implies that not only those $(\chi\chi)_I$ pairs built from NRMSSM states are considered, but also those $(\chi\chi)_K$ pairs that are too heavy to be part of the NRMSSM. As described in [3] as well as in Sec. 8.6 of the thesis, the effect of heavy $\chi\chi$ states – not being part of the NRMSSM set of $\chi\chi$ states – is taken into account in the last loop prior to the hard annihilation reaction in the ladder-diagrams accounting for the Sommerfeld enhancement effect. One input in the corresponding calculation are the perturbative hard annihilation rates involving the heavy $\chi\chi$ states. Therefore also these rates are determined in the annihilation matrix part of the code.

Within a given charge sector – neutral, single positive (single negative) or double positive (double negative) – the IJ entry of an annihilation matrix Γ_{IJ} encodes the absorptive part of the inclusive $(\chi\chi)_J \rightarrow (\chi\chi)_I$ scattering reaction. Note the order of states in the reaction: the columns (rows) of Γ contain all processes with one fixed incoming (outgoing) state. In each charge sector the J th column (I th row) of the annihilation matrices Γ refers to the incoming (outgoing) two-particle state with enumeration label J (I) according to the enumeration convention of the states summarised in Tabs. 2–4. Note that this enumeration convention obviously has to agree with the one set up in the "Sommerfeld-enhancement part" of the code. Further recall from [3] or Sec. 8.3 of

$(\chi\chi)_I$ state	method-1 label	method-2 label	$(\chi\chi)_I$ state	method-1 label	method-2 label
$\chi_1^0\chi_1^+$	1	1	$\chi_1^0\chi_2^+$	5	5
$\chi_2^0\chi_1^+$	2	2	$\chi_2^0\chi_2^+$	6	6
$\chi_3^0\chi_1^+$	3	3	$\chi_3^0\chi_2^+$	7	7
$\chi_4^0\chi_1^+$	4	4	$\chi_4^0\chi_2^+$	8	8

Table 3: Enumeration scheme within method-1 and method-2 for single positive charged $(\chi^0\chi^+)_I$ states. The same conventions hold for single negative charged states $(\chi^-\chi^0)_I$.

$(\chi\chi)_I$ state	method-1 label	method-2 label	$(\chi\chi)_I$ state	method-1 label	method-2 label
$\chi_1^0\chi_1^0$	1	1	$\chi_4^0\chi_1^0$	13	-
$\chi_1^0\chi_2^0$	2	2	$\chi_4^0\chi_1^0$	14	-
$\chi_1^0\chi_3^0$	3	3	$\chi_4^0\chi_1^0$	15	-
$\chi_1^0\chi_4^0$	4	4	$\chi_4^0\chi_1^0$	16	10
$\chi_2^0\chi_1^0$	5	-	$\chi_1^+\chi_1^-$	17	11
$\chi_2^0\chi_2^0$	6	5	$\chi_1^+\chi_2^-$	18	12
$\chi_2^0\chi_3^0$	7	6	$\chi_2^+\chi_1^-$	19	13
$\chi_2^0\chi_4^0$	8	7	$\chi_2^+\chi_2^-$	20	14
$\chi_3^0\chi_1^0$	9	-	$\chi_1^-\chi_1^+$	21	-
$\chi_3^0\chi_2^0$	10	-	$\chi_1^-\chi_2^+$	22	-
$\chi_3^0\chi_3^0$	11	8	$\chi_2^-\chi_1^+$	23	-
$\chi_3^0\chi_4^0$	12	9	$\chi_2^-\chi_2^+$	24	-

Table 4: Enumeration scheme within method-1 and method-2 for neutral $(\chi\chi)_I$ states.

the thesis that the Sommerfeld factors can be calculated within two different methods; method 1 counts and treats as different the two particle states $\chi_{e_1}\chi_{e_2}$ and $\chi_{e_2}\chi_{e_1}$ for non identical particles χ_{e_1} and χ_{e_2} , while in method 2 the second, redundant state is omitted. For the explicit definition of method 1 and method 2 we refer the reader to [3] or Sec. 7.2 and 8.3 of the thesis.

4.2 The choice of the mass expansion

Recall from [1, 2] or Sec. 6.1.2 of the thesis that our analytic results for the kinematic factors refer to two different expansions in mass differences. As discussed in several of the subsections of Sec. 3 we use the labels `mc1` and `mc2` in the numerical code to refer to and to distinguish expressions referring to the one or the other expansion. As we have noted before, option `mc2` is suited to reproduce the partial wave separated contributions to (exclusive as well as inclusive) $(\chi\chi)_J$ pair-annihilation rates. Since the diagonal entries of any annihilation matrix are proportional to these pair-annihilation rates, all diagonal

entries of the annihilation matrices rely on a calculation using `mc2` kinematic factors.

However, in case of off-diagonal annihilation matrix entries referring to reactions $(\chi\chi)_J \rightarrow (\chi\chi)_I$ with $J \neq I$ it is a priori not clear whether `mc1` or `mc2` expressions should be chosen in the calculation. Generically the mass differences $\delta m, \delta\bar{m}$ should be small for the mass expansion to be consistent, see the discussion in [1] or Sec. 6.1.2 of the thesis. In order to decide which expansion `mc1` should be chosen in the evaluation of off-diagonal entries Γ_{JI} in the code we introduce functions that address this question based on the given MSSM neutralino and chargino mass spectrum. These functions, in case of neutral $\chi_{e_1}\chi_{e_2} \rightarrow \chi_{e_4}\chi_{e_3}$ two-particle state scatterings, are named

$$\begin{aligned}
\text{Mcinnnn}[\mathbf{e1}, \mathbf{e2}, \mathbf{e3}, \mathbf{e4}] & \text{ for } \chi_{e_1}^0\chi_{e_2}^0 \rightarrow \chi_{e_4}^0\chi_{e_3}^0 \text{ reactions,} \\
\text{Mcinccc}[\mathbf{e1}, \mathbf{e2}, \mathbf{e3}, \mathbf{e4}] & \text{ for } \chi_{e_1}^0\chi_{e_2}^0 \rightarrow \chi_{e_4}^-\chi_{e_3}^+ \text{ reactions,} \\
\text{Mciiccnn}[\mathbf{e1}, \mathbf{e2}, \mathbf{e3}, \mathbf{e4}] & \text{ for } \chi_{e_1}^-\chi_{e_2}^+ \rightarrow \chi_{e_4}^0\chi_{e_3}^0 \text{ reactions,} \\
\text{Mciicccc}[\mathbf{e1}, \mathbf{e2}, \mathbf{e3}, \mathbf{e4}] & \text{ for } \chi_{e_1}^-\chi_{e_2}^+ \rightarrow \chi_{e_4}^-\chi_{e_3}^+ \text{ reactions,}
\end{aligned} \tag{40}$$

while in single charged reactions the corresponding functions are named

$$\begin{aligned}
\text{Mcinccn}[\mathbf{e1}, \mathbf{e2}, \mathbf{e3}, \mathbf{e4}] & \text{ for } \chi_{e_1}^0\chi_{e_2}^+ \rightarrow \chi_{e_4}^0\chi_{e_3}^+ \text{ reactions,} \\
\text{Mciicnc}[\mathbf{e1}, \mathbf{e2}, \mathbf{e3}, \mathbf{e4}] & \text{ for } \chi_{e_1}^-\chi_{e_2}^0 \rightarrow \chi_{e_4}^-\chi_{e_3}^0 \text{ reactions.}
\end{aligned} \tag{41}$$

In case of double charged reactions the function `Mciicccc` [e1, e2, e3, e4] introduced in (40) can be used. The four arguments `ei`, `i=1,2,3,4` of all these functions are the labels of the external χ_{e_i} states, respectively. The reason why so many different functions are introduced is related to these arguments: if we have only the information on the label but have to deal with particle masses, we need an additional information on the involved particle species (neutralino or chargino).

The output of all functions given in (40) and (41) is either `mc1` or `mc2`. Which output is returned should be related to the value of the mass differences $\delta m, \delta\bar{m}$ calculated for both expansion options `mc1` and `mc2`, respectively, given a specific underlying MSSM spectrum; the mass expansion `mc1` where the mass differences are smaller should be chosen. This is because the smaller the mass differences the better the convergence of the expansion of the perturbative $\chi\chi \rightarrow X_A X_B \rightarrow \chi\chi$ rates in mass differences δm and $\delta\bar{m}$. The currently implemented criterion reads as follows: if particle χ_{e_1} is lighter (heavier) than χ_{e_2} and at the same time particle χ_{e_4} is lighter (heavier) than χ_{e_3} , then option `mc2` is chosen and the output of the corresponding functions in (40) and (41) is `mc2`. Otherwise the output of the above function is set to `mc1`.

The `Mcixxxx[...]` functions will appear inside some of the functions described in the following that determine the full partial wave coefficients.

4.3 Inclusive reactions: the final partial wave coefficients

In order to build the full partial wave coefficients referring to inclusive reactions from their respective exclusive $X_A X_B$ final state contributions⁹ we have to decide – based

⁹Recall that the functions `pwc[...]` providing the contributions to the absorptive parts of the Wilson coefficients from exclusive (tree-level) reactions $\chi_{e_1}\chi_{e_2} \rightarrow X_A X_B \rightarrow \chi_{e_4}\chi_{e_3}$ are described in Sec. 3.4.2.

on the given MSSM spectrum – which $X_A X_B$ final states are on-shell accessible in a $\chi_{e_a} \chi_{e_b} \rightarrow X_A X_B$ annihilation reaction. Obviously, the heavier the states χ_{e_a} and χ_{e_b} the more final states $X_A X_B$ will be accessible on-shell. However, our currently implemented criterion to treat a $X_A X_B$ state as viable final state in a $\chi_{e_a} \chi_{e_b} \rightarrow X_A X_B$ annihilation reaction related to $\chi_{e_1} \chi_{e_2} \rightarrow X_A X_B \rightarrow \chi_{e_4} \chi_{e_3}$ scattering – and hence our criterion to take into account an exclusive final state in the construction of the annihilation matrices – is based on the lightest two-particle state $\chi_1^0 \chi_1^0$. The reason for this is related to the Sommerfeld enhancements that shall eventually be calculated using the annihilation matrix results provided by the code, and reads as follows: Off-diagonal potential scattering can convert an incoming $\chi_1^0 \chi_1^0$ pair to another neutral $\chi_{e_a} \chi_{e_b}$ state that eventually undergoes pair annihilation. The latter annihilation reaction is encoded in the annihilation matrices. Therefore we have to take care that in Sommerfeld enhanced reactions with initially incoming $\chi_1^0 \chi_1^0$ states only those $X_A X_B$ final states are considered in the inclusive partial wave coefficients, encoded in the annihilation matrices, that are accessible for the $\chi_1^0 \chi_1^0$ pair. Our criterion is therefore such, that all $X_A X_B$ final states that cannot be produced on-shell in $\chi_1^0 \chi_1^0 \rightarrow X_A X_B$ processes are excluded as exclusive final states for any partial wave coefficient. Even more, in our NRMSSM effective theory set-up, the on-shell accessible final state particles $X_A X_B$ should not be non-relativistic, otherwise we would have to consider them among the set of non-relativistic states of the theory and even co-annihilation rates of such additional non-relativistic states could be relevant. Therefore we establish the following criterion to account for a $X_A X_B$ final state in the numerical code: If the sum of masses $m_A + m_B$ is smaller than half the mass of the $\chi_1^0 \chi_1^0$ pair a corresponding flag is set to 1 in the code, otherwise the flag is set to 0. The full partial wave coefficients are obtained from the sum over all $X_A X_B$ state contributions, where each contribution is multiplied by the corresponding flag. Consequently only those final state contributions are taken into account for the full partial wave coefficient that fulfill the above stated criterion related to the $\chi_1^0 \chi_1^0$ mass. Note that the flags are introduced in the file `annihilationmatrices_vx.m` as well.

The following functions determine the absorptive parts of the full partial-wave coefficients related to $\chi_{e_1} \chi_{e_2} \rightarrow \chi_{e_4} \chi_{e_3}$ scattering, taking only those exclusive $X_A X_B$ final state contributions into account that are on-shell accessible in $\chi_1^0 \chi_1^0 \rightarrow X_A X_B$ annihilations:

$$\begin{aligned}
\text{pwcFullnnnnALT}[\{\mathbf{e1}, \mathbf{e2}, \mathbf{e4}, \mathbf{e3}\}, \text{Wave}, \text{mci}] & \text{ for } \chi^0 \chi^0 \rightarrow \chi^0 \chi^0 \text{ reactions,} \\
\text{pwcFullccccALT}[\{\mathbf{e1}, \mathbf{e2}, \mathbf{e4}, \mathbf{e3}\}, \text{Wave}, \text{mci}] & \text{ for } \chi^- \chi^+ \rightarrow \chi^- \chi^+ \text{ reactions,} \\
\text{pwcFullnnccALT}[\{\mathbf{e1}, \mathbf{e2}, \mathbf{e4}, \mathbf{e3}\}, \text{Wave}, \text{mci}] & \text{ for } \chi^0 \chi^0 \rightarrow \chi^- \chi^+ \text{ reactions,} \quad (42)
\end{aligned}$$

are the functions relevant for neutral scattering reactions. The absorptive parts of the Wilson coefficients in off-diagonal $\chi^- \chi^+ \rightarrow \chi^0 \chi^0$ scattering can be obtained from the corresponding $\chi^0 \chi^0 \rightarrow \chi^- \chi^+$ expressions. Note the order of arguments `e4` and `e3` that now appear in the same order as in $\chi_{e_1} \chi_{e_2} \rightarrow \chi_{e_4} \chi_{e_3}$. The values that all the arguments of the `pwcFullxxxxALT[...]` functions can take should be obvious from the preceding sections. In case of single charged reactions we have the corresponding functions

$$\text{pwcFullnccn}[\{\mathbf{e1}, \mathbf{e2}, \mathbf{e4}, \mathbf{e3}\}, \text{Wave}, \text{mci}] \text{ for } \chi^0 \chi^+ \rightarrow \chi^0 \chi^+ \text{ reactions,}$$

$$\text{pwcFullcncnc}[\{\mathbf{e1}, \mathbf{e2}, \mathbf{e4}, \mathbf{e3}\}, \text{Wave}, \text{mci}] \quad \text{for } \chi^- \chi^0 \rightarrow \chi^- \chi^0 \text{ reactions.} \quad (43)$$

Finally, for double charged reactions the corresponding full partial wave coefficients are obtained with functions

$$\begin{aligned} & \text{pwcFullcpcpALT}[\{\mathbf{e1}, \mathbf{e2}, \mathbf{e4}, \mathbf{e3}\}, \text{Wave}, \text{mci}] \quad \text{for } \chi^+ \chi^+ \rightarrow \chi^+ \chi^+ \text{ reactions,} \\ & \text{pwcFullcmcmALT}[\{\mathbf{e1}, \mathbf{e2}, \mathbf{e4}, \mathbf{e3}\}, \text{Wave}, \text{mci}] \quad \text{for } \chi^- \chi^- \rightarrow \chi^- \chi^- \text{ reactions.} \end{aligned} \quad (44)$$

Note that `mci` appears as an argument of all the above functions. There is a version `pwcFullxxxx[...]` of these function – in case of neutral and double-charged reactions without the ending `ALT`¹⁰ – where the appropriate `mci` value to be used in the calculation of a partial wave coefficient is internally determined inside the function with the help of the `Mcixxxx[...]` functions described in Sec. 4.2.

4.4 Symmetry factors and symmetry relations

Certain entries of the annihilation matrices have to refer to reactions $\chi^+ \chi^- \rightarrow \chi^0 \chi^0$ instead of $\chi^- \chi^+ \rightarrow \chi^0 \chi^0$ and to $\chi^0 \chi^0 \rightarrow \chi^+ \chi^-$ instead of $\chi^0 \chi^0 \rightarrow \chi^- \chi^+$. Similarly there are entries related to $\chi^- \chi^+ \rightarrow \chi^+ \chi^-$, $\chi^+ \chi^- \rightarrow \chi^- \chi^+$ or $\chi^+ \chi^- \rightarrow \chi^+ \chi^-$ scattering instead of $\chi^- \chi^+ \rightarrow \chi^- \chi^+$. The respective Wilson coefficients that are not determined by the functions given in Sec. 4.3 can be obtained from the latter by making use of certain symmetry properties of the Wilson coefficients under exchange of labels. For the corresponding relations see for instance eq. (8) in [1] or eq. (5.9) and eq. (5.14) in the thesis.

In the code we introduce the parameter `SymFac[Wave]` that, depending on the argument `Wave`, is either given by 1 or -1 and that agrees with the parameter η in eq. (9) of [1] and eq. (5.10) in the thesis. This allows to finally introduce the following functions

$$\begin{aligned} & \text{pwcFullnnmpALT}[\mathbf{e1}, \mathbf{e2}, \mathbf{e3}, \mathbf{e4}, \text{Wave}, \text{mci}] \quad \text{for } \chi_{e_1}^0 \chi_{e_2}^0 \rightarrow \chi_{e_4}^+ \chi_{e_3}^- \text{ reactions,} \\ & \text{pwcFullpmmpALT}[\mathbf{e1}, \mathbf{e2}, \mathbf{e3}, \mathbf{e4}, \text{Wave}, \text{mci}] \quad \text{for } \chi_{e_1}^+ \chi_{e_2}^- \rightarrow \chi_{e_4}^+ \chi_{e_3}^- \text{ reactions,} \end{aligned} \quad (45)$$

derived from corresponding functions `pwcFullxxxxALT[...]` in Sec. 4.3. For details of the relations to the Sec. 4.3 functions we refer the reader to the part of the code where the definitions of the above functions are given as well as to the relevant paragraphs in [1] or Chap. 5 of the thesis.

The annihilation matrices used in the "Sommerfeld-enhancement part" of the code shall already involve the spin-summed inclusive annihilation reactions. For that reason we further introduce certain spin-weight parameters in the code, named `SpinSum[Wave]`. These will multiply the appropriate partial wave coefficients when building the annihilation matrices from the latter. In our case `SpinSum[Wave]` takes always the value 1 apart from the case of 3S_1 partial wave reactions where it is given by 3.

¹⁰The ending `ALT` denotes "alternative" and was introduced in case of annihilation matrices related to neutral and double charged reactions in course of the code development.

4.5 Chopping numerically small annihilation matrix entries

Due to small numerical inaccuracies in the calculation of the partial wave coefficients some of the annihilation matrix entries that should be exactly zero happen to be non-vanishing. In addition there are further entries that are non-vanishing but strongly suppressed with respect to the leading entries.¹¹ Within the part of the code that determines the Sommerfeld enhancement factors both these types of strongly suppressed entries can potentially cause numerical problems. For that reason we introduce a function that sets all those annihilation matrix entries to zero that are smaller by a certain factor than the leading entry. The relevant function is named

$$\text{chopRoutineALT}[\text{Matrix}, \text{Wave}]. \quad (46)$$

Its first argument `Matrix` will in our application be an annihilation matrix and the second argument specifies the partial wave configuration of that annihilation matrix. The output of `chopRoutineALT[Matrix, Wave]` is the input `Matrix` where however all those entries that are by a certain amount smaller than the leading matrix-entry are set to zero: In case of leading order S -wave related annihilation matrices those entries are set to zero that are smaller than the leading entry by a factor of 10^{-12} . For the case of all P - and next-to-next-to-leading order S -wave matrices the factor is chosen to be 10^{-8} .

4.6 Calculation of the annihilation matrices

Now we have all functions available that allow to determine the annihilation matrices. Particularly relevant for the determination of the respective matrix entries are the functions `pwcFullxxxxALT[...]`, `pwcFullnccn[...]` and `pwcFullcnnc[...]` discussed in Sec. 4.3 that give as output the absorptive parts of the full, partial wave separated Wilson coefficients; apart from possible spin weight factors, the latter determine the respective annihilation matrix entries. Our last step is therefore the construction of the matrices Γ from their individual components Γ_{IJ} related to $(\chi\chi)_J \rightarrow (\chi\chi)_I$ scattering. Let us recall that our specific enumeration convention for the states $(\chi\chi)_I$ in each charge sector is given in Sec. 4.1, see in particular Tabs. 2–4 therein.

We provide the following functions that give as output the partial wave specific annihilation matrices in each charge sector corresponding to the method-1 enumeration convention:¹²

$$\text{GammaNeutralALT}[\text{Wave}] \quad \text{for neutral } \chi\chi \rightarrow \chi\chi \text{ reactions,}$$

¹¹The typical order of magnitude of such numerically strongly suppressed annihilation matrix entries is $10^{-25} \text{ GeV}^{-2}$ in case of leading order S -wave matrices while the corresponding leading entries are typically of $\mathcal{O}(10^{-10} - 10^{-12} \text{ GeV}^{-2})$. In case of P - and next-to-next-to-leading order S -wave annihilation matrices, the corresponding numerically strongly suppressed entries are typically smaller than $\mathcal{O}(10^{-25} \text{ GeV}^{-4})$ while leading entries are typically of $\mathcal{O}(10^{-16} - 10^{-18} \text{ GeV}^{-4})$. The order of magnitude of annihilation matrix entries obviously depends on the underlying MSSM spectrum and the above quoted numbers are rather given as a rough guideline for the orders of magnitude to expect.

¹²The "Sommerfeld-enhancement part" of the code requires method-1 annihilation matrices as an input. In the latter part of the code, the corresponding method-2 matrices are then subsequently constructed from the method-1 expressions.

<code>GammaOpALT[Wave]</code>	for $\chi^0\chi^+ \rightarrow \chi^0\chi^+$ reactions,	
<code>GammaOpALT[Wave]</code>	for $\chi^-\chi^0 \rightarrow \chi^-\chi^0$ reactions,	
<code>GammappALT[Wave]</code>	for $\chi^+\chi^+ \rightarrow \chi^+\chi^+$ reactions,	
<code>GammammALT[Wave]</code>	for $\chi^-\chi^- \rightarrow \chi^-\chi^-$ reactions.	(47)

The possible values of the single arguments `Wave` agree with the possible $\{2s+1\}$ LJ values specified in Sec. 3.1.

Let us say a few words on the internal construction of the annihilation matrix output performed by the above functions. First recall that the annihilation matrices are hermitian such that in their construction it is possible to calculate just one triangle – either the upper or the lower – of the corresponding matrix and to subsequently obtain the full matrix from this triangle matrix using the hermiticity requirement. Moreover the annihilation matrices in the neutral sector and the two double charged sectors contain redundant informations as not all states in the method-1 enumeration convention correspond to physically different states (for instance, the states $\chi_1^0\chi_2^0$ and $\chi_2^0\chi_1^0$ are physically equivalent). In case of annihilation matrices related to neutral and double charged reactions the steps that are performed inside the functions `GammaNeutralALT[...]` and `GammappALT[...]`, `GammammALT[...]` are the following

- As first intermediate step start to create the upper triangle of the matrix $\tilde{\Gamma}^T$, where $\tilde{\Gamma}$ is the matrix related to the proper annihilation matrix Γ that takes only those method-1 states $(\chi\chi)_I$ into account that also appear in the method-2 set of states. Annihilation matrix entries appearing in Γ that we leave out in this way do not need to be calculated explicitly as we can obtain their value easily from calculated expressions in $\tilde{\Gamma}$ using symmetry relations; for the latter see the discussion and the cited references in Sec. 4.4. It is convenient to consider the transpose of $\tilde{\Gamma}$ here as its entry $\tilde{\Gamma}_{IJ}^T$ encodes a $(\chi\chi)_I \rightarrow (\chi\chi)_J$ scattering processes and in the calculation of the upper triangle we only need to consider reactions with $I \leq J$; the restriction to the method-1 states that are also present in method-2 then implies that we can a priori fix the mass expansion to be used in the calculation of the `pwcFullxxxxALT[...]` annihilation matrix entries to either `mc1` or `mc2`. All states $(\chi\chi)_I \equiv \chi_{I_a}\chi_{I_b}$ that appear in the method-2 enumeration convention are built such that the mass of the first state χ_{I_a} is smaller than the mass of the second state χ_{I_b} , $m_{I_a} < m_{I_b}$. Consequently, following our criterion set out in Sec. 4.2, the value of `mc1` can be fixed a priori and does not depend on any specific MSSM mass spectrum. Therefore we do not need to call the functions `Mcixxxx[...]` here.
- In the next step use the hermiticity requirement to construct the full matrix $\tilde{\Gamma}^T$. At this point we take care of possible spin-weight factors to be incorporated in the final annihilation matrix expressions, using the function `SpinSum[Wave]` described in Sec. 4.4.
- Determine the full method-1 annihilation matrix Γ^T expression from $\tilde{\Gamma}^T$ by making use of symmetry relations between redundant entries that have to be added

when constructing Γ^T from $\tilde{\Gamma}^T$. At this point no further call of the functions `pwcFullxxxxALT[...]` is required as all numerical values – apart from possible signs – have been already determined as entries of $\tilde{\Gamma}$. Symmetry factors are implemented using `SymFac[Wave]`, see Sec. 4.4 for the latter function.

- In the last step transpose the obtained Γ^T expression to arrive at the final method-1 annihilation matrix. The latter annihilation matrix is then given as output of the `GammaNeutralALT[...]`, `GammappALT[...]` and `GammammALT[...]` functions. This output can be called with

$$\begin{aligned}
\text{AnnMatrix[Wave]} & \quad \text{in the neutral sector,} \\
\text{AnnMatrixcpcp[Wave]} & \quad \text{in the double positively charged sector,} \\
\text{AnnMatrixcmcm[Wave]} & \quad \text{in the double negatively charged sector.} \quad (48)
\end{aligned}$$

The latter expressions should be written to a `.m` file which can then be read in the "Sommerfeld-enhancement part" of the code.

The procedure to determine the annihilation matrices in the single charged sectors, used within the functions `GammaOpALT[...]`, `GammamOALT[...]`, is very similar to the one described above. Note however that in case of the single charged sectors the number of states within method-1 and method-2 agrees and we do not have to construct a reduced matrix $\tilde{\Gamma}$ first but can directly determine Γ . There is another small difference in the construction of the single charged annihilation matrices with respect to the above listed steps: here we cannot a priori decide which mass expansion `mci` has to be chosen for a certain annihilation matrix entry: this has to be determined based on the specific MSSM spectrum.¹³ Therefore we have to use the functions `pwcFullxxxx[...]` without the ending `ALT` here, which internally determine the mass expansion to be used. Consequently the steps are in this case:

- Build the upper triangle of the annihilation matrix Γ^T , where the entries are determined with the help of functions `pwcFullxxxx[...]`.
- Using the hermiticity of the full annihilation matrix Γ subsequently determine Γ^T from the corresponding upper-triangle matrix. At this point incorporate spin-weight factors for the annihilation rates using the function `SpinSum[Wave]`.
- Transpose the result from the last step to obtain the numerical expression for the respective annihilation matrix Γ , which is then the output of the functions `GammaOpALT[...]` and `GammamOALT[Wave]`. This output can be called with

$$\begin{aligned}
\text{AnnMatrixcpn[Wave]} & \quad \text{in the single positively charged sector,} \\
\text{AnnMatrixcmn[Wave]} & \quad \text{in the single negatively charged sector,} \quad (49)
\end{aligned}$$

¹³As an example consider the state $\chi_2^0\chi_1^+$: here it is not a priori clear if $m_{\chi_2^0} < m_{\chi_1^+}$. If the spectrum has a bino-like LSP and wino-like NLSP states, the latter relation holds. However, in case of a wino-like LSP the NLSP state will be the χ_1^+ , such that $m_{\chi_1^+} < m_{\chi_2^0}$.

and is conveniently written to a `.m` file for future use in the part of the program that determines the Sommerfeld-enhanced annihilation rates.

5 Comparison to the publications' nomenclature

For some of the expressions in the numerical code we have used a differing nomenclature than the one established in the publications [1–4] and in the thesis. For clarity and in order to avoid confusions we list in this section, especially in Tab. 5, all the quantities that are affected by such renaming when going from the expressions used in the code to the notation in the publications [1–4] and the thesis.

5.1 Kinematic and coupling factors

- Note that all expressions for the **kinematic factors in the publications and the thesis** refer to **mass expansion mc2**.
- Further let us stress again that even for $m_{ci} = m_{c2}$ a particular kinematic factor expression provided with the code **can differ with respect to a global sign** from the corresponding kinematic factor given in [1, 2] and the Appendix A of the thesis: as stated in Sec. 2 and Sec. 3.1 above this difference arises because we use different reference processes for the determination of the respective kinematic and coupling factors. For the reference processes used in the calculation of the kinematic factors in the program see Sec. 3.1.
- The same kind of difference with respect to a global sign arises in the comparison of the corresponding coupling factor expressions.

When comparing the nomenclature for the kinematic and coupling factor expression collected in Tab. 5, the latter difference has to be kept in mind; that is, **the correspondence is not one-to-one** but there **can be** – but not necessarily are in every case – **different global signs** associated with individual kinematic and coupling factor expressions.

In order to understand the origin of such global signs it might be useful to familiarise with the steps in the calculation of kinematic and coupling factors set out in [1, 2] and in the thesis. The significance but also the – to a certain extent existing – arbitrariness in the choice of the reference processes underlying the calculation should become clear. Comparing then, for instance, the coupling factors obtained for a specific diagram in $\chi_{e_1}\chi_{e_2} \rightarrow VV \rightarrow \chi_{e_4}\chi_{e_3}$ scattering, referring to generic Majorana fermions χ_{e_i} and generic vector bosons V , with the coupling factors obtained for the same diagram but referring to external neutralinos $\chi_{e_i}^0$ and a W^+W^- final state, the origin of global signs can be understood.

5.2 Annihilation matrices

As described in Sec. 4.6 we determine annihilation matrices $\Gamma^{(2s+1)L_J}$ in the numerical program, which refer to a method-1 set of states, see Tab. 2–4. Recall that according to (48) and (49) the numerical matrices can be called with

$$\Gamma[\text{Wave}] = \text{AnnMatrix}[\text{Wave}], \text{AnnMatrixcpn}[\text{Wave}], \dots \quad (50)$$

The relation of these matrices to the matrices $[\hat{f}^{(2s+1)L_J}]^{(1)}$ in [3] is given by transposition:

$$\Gamma[\{2s+1\}LJ]^T = [\hat{f}^{(2s+1)L_J}]^{(1)}. \quad (51)$$

Finally let us recall that within the numerical annihilation matrix program we determine solely the method-1 annihilation matrices, corresponding to $[\hat{f}^{(2s+1)L_J}]^{(1)}$. Expressions that are related to $[\hat{f}^{(2s+1)L_J}]^{(2)}$ are not determined within this part of the code, also see footnote 12. In the transition from the method-1 to the method-2 annihilation matrices certain prefactors ($\sqrt{2}$ or 2) have to be taken into account in front of certain annihilation matrix entries, which is taken care of in the Sommerfeld enhancement part of the code. For further details on calculations relying on either the method-1 or the method-2 bases of $\chi\chi$ states we refer the reader to [3] or alternatively Sec. 7.2, 8.3 and Appendix C of the thesis.

References

- [1] M. Beneke, C. Hellmann, and P. Ruiz-Femenia, *JHEP* **1303** (2013) 148, [arXiv:1210.7928 \[hep-ph\]](#).
- [2] C. Hellmann and P. Ruiz-Femenia, *JHEP* **1308** (2013) 084, [arXiv:1303.0200 \[hep-ph\]](#).
- [3] M. Beneke, C. Hellmann, and P. Ruiz-Femenia, [arXiv:1411.6924 \[hep-ph\]](#).
- [4] M. Beneke, C. Hellmann, and P. Ruiz-Femenia, [arXiv:1411.6930 \[hep-ph\]](#).